



Long Span Buoyancy Bridge with Submerged Cable Anchoring

Final Report

T. Yip, 1511122

Master of Science
Thesis

Version 2
Status: Final Report
August 6, 2015

A Master Thesis Report
Submitted to the
Faculty of Civil Engineering and Geosciences

By

Christine Yip | 1511122
Christine.tt.yip@gmail.com

Delft University of Technology
Faculty of Civil Engineering and Geosciences
Stevinweg 1
2628 CN Delft
Netherlands

Thesis Committee:

Prof. Ir. F.S.K. Bijlaard (chairman), Professor at Delft University of Technology, Faculty of Civil Engineering and Geosciences, Department of Design and Construction, Structural and Building Engineering, Steel Structures

Ir. R. Abspoel, Assistant Professor at Delft University of Technology, Faculty of Civil Engineering and Geosciences, Department of Design and Construction, Structural and Building Engineering, Steel Structures

MSc. A. Gozzi, Structural Engineer at Iv-Consult, Section of Steel Structures

Dr. Ir. P.C.J. Hoogenboom, at Delft University of Technology, Faculty of Civil Engineering and Geosciences, Department of Design and Construction, Section Structural Mechanics

Ir. L.J.M. Houben (secretary), at Delft University of Technology, Faculty of Civil Engineering and Geosciences, Department of Structural Engineering, Road and Railway Engineering

Ir. W.M. Visser, Manager Structural Design at Iv-Consult, Section of Steel Structures

PREFACE

This MSc thesis report is part of the MSc program Structural Engineering at Delft University of Technology. It contains my knowledge about the buoyancy bridge concept, which I gained during the last 9 months.

During these months, I have never gotten bored of this topic. I have found much enjoyment in discussing and thinking about the challenges with Prof.Ir. F.S.K. Bijlaard, Ir. R. Abspoel and Dr.Ir. P.C.J. Hoogenboom of the graduation committee. Therefore, I would like to thank my committee members for their time and advices.

I am thankful to Wouter Visser for giving me the opportunity to take part in such a fun project involving such a unique bridge.

I would also like to thank Andrea Gozzi for his time and patience during our many lively discussions about the project. I always learn something from him during these discussions, whether it is from his engineering knowledge or his critical attitude.

Furthermore, I want to thank Zwarts & Jansma Architects for their input. It was very interesting to create the forms of parts of the bridge together with them.

Besides my supervisors, I also had family, friends and colleagues who often volunteered to listen to my stories about this project. I would like to thank them all for their support.

All the people mentioned above have contributed to the end result, which I proudly present to you in the next pages.

Delft, 6 August 2015,

Christine Yip

SUMMARY

The purpose of this MSc thesis is to find a feasible concept for a circa 4500 m long buoyancy bridge, which is located at the Sognefjord in Norway. The concept should be structurally and aesthetically competitive.

In contrast to bridges on shore with fixed supports, a buoyancy bridge is supported on floating pontoons. As result, loads will cause the buoyancy bridge to displace, and displacements will in turn cause internal forces in the structure. For these reasons, the environmental loads on buoyancy bridges are usually minimized by placing the bridge girder as low as possible above the water level (small wind load) and by using small spans (small bending moment and shear force on the bridge girder).

In this study, the limits within civil engineering will be tested by trying to find new possibilities for a buoyancy bridge, which consists of 20 spans of 200 m and a large central main span of 465 m. Furthermore, the bridge deck will elevate up to 80 m above water level. This span and elevation are required at the 1000 m deep Sognefjord to create a large fairway clearance. A buoyancy bridge with these properties is unprecedented.

For the buoyancy bridge concept in this study, a whole new approach has been made. 22 long, slim cylindrical shaped pontoons are used, which provide upward buoyancy forces and restoring moments to limit the rotations of the structure. The slim shape of the pontoons will lead to smaller water loads. The radii and lengths of the pontoons vary respectively from 12 to 20 m and from 115 to 202 m.

For common buoyancy bridges, the relative position of the pontoons is maintained by the superstructure. However in this case, the dimensions of the cylindrical pontoons are so large, that a superstructure with plausible dimensions will not be able to restrain the movements of the massive pontoons. Therefore, an anchoring system, consisting of 2 main cables with diameters of 1200 mm and 44 cables of 350 mm, has been designed to maintain the relative positions of the pontoons as much as possible.

From the top view, the anchoring system looks like two mirrored horizontal suspension systems, which restrain the displacements in the direction parallel to the fjord. The displacement due to the maximum combined wind and water load is approximately 6 m for the circa 4500 m long bridge.

Separate lattice bridge girders with a width and height of respectively 24 and 25 m are designed, which have hinged like supports, except in the plane transversal to the superstructure. In this plane, the rotation of the bridge girder around its longitudinal axis is coupled to the rotation of the pontoons, and therefore limited by the restoring moment of the pontoon. Furthermore, the torsional rigidity of the lattice girder varies along its length. This way, a light-weight and flexible bridge girder is possible, which is capable of following the rotations instead of trying to restrain them. For the piers, a form study has been done.

The concept gives rise to a lot of new possibilities, but it also has limitations. The results of this study are only valid when the recommended erection method is used. Different erection methods will induce different forces into the structure. This can affect the capacity and the displacements of the structure. Therefore, the structural design and the erection design should be defined together.

This study provides the first steps to the design of the buoyancy bridge. Much more investigation is needed before the proposed concept can be deemed reliable. The global main structure is considered in this study, but no detailed calculations are done. Designs of several important parts, i.e. the connections, the supports, the piers, etc. should be done in next studies. Also, second order effects, eccentricity, dynamic effects, fatigue, impact loads and more should be investigated.

Although the design only have a concept value, this study shows that a structurally and aesthetically competitive buoyancy bridge for the Sognefjord is feasible and it is recommended to conduct further investigations on this promising buoyancy bridge concept.

LIST OF CONTENTS

Preface	i
Summary	ii
1. Introduction.....	1
1.1 Background and Topic	1
1.2 Problem Statement.....	2
1.3 Problem Analysis.....	2
1.3.1 State of the Art Buoyancy Bridges.....	2
1.3.2 Current Development: Master Thesis Research Done Previously.....	6
1.4 Target and Objectives	7
1.5 Research Questions	7
1.5.1 Main Question	7
1.5.2 Sub Questions.....	7
1.6 Methodological Approach	7
1.7 Overview Report	9
2. Design Information	10
2.1 Coordinate System.....	10
2.2 Design Input and Set-up	10
2.3 Main Differences Previous Buoyancy Bridge Concept and New Concept	13
2.3.1 Anchoring System changed to a Horizontally Suspended Anchoring System	13
2.3.2 Arch Action by Prestressing the Horizontal Arch Omitted	14
2.4 Boundary Condition: Cross-Section Sognefjord.....	15
2.5 Assumptions	16
2.5.1 Bridge Deck assumed Non-Contributing to Torsional Stability	16
2.5.2 Wind Load	16
2.5.3 Wave Load	18
2.5.4 Current Load.....	19
2.5.5 Tides	19
2.5.6 Mass Density and Salinity.....	19
2.5.7 Temperature, Snow and Ice	19
2.5.8 Traffic Load.....	20
2.6 Requirements	21
2.6.1 Design Life Span	21

2.6.2	Functional Requirement for Car Traffic	21
2.6.3	Functional Requirement for Ship Traffic leads to Large Mid-Fjord Span	22
2.6.4	Safety Requirement for Vertical Alignment Road	22
2.6.5	Serviceability Requirements for Displacements and Accelerations	22
2.7	Limitations	24
2.7.1	Considering Only Static Effects for Sufficient Approximation	24
2.7.2	Effects due to Seismic Activity Not Considered.....	24
2.7.3	Marine Growth not Regarded	24
2.7.4	Effect of Passing Ships not Regarded	24
2.7.5	Accidental Loading not Regarded.....	24
2.7.6	No Fatigue Calculations	25
3.	To Design the Substructure: Methods and Assumptions	26
3.1	Starting Points.....	26
3.2	Method Pontoon Design: Mainly Ballast Stabilized	26
3.3	Principle Modeling Restoring Moment as Rotational Spring.....	28
3.4	Method Anchoring System Design.....	30
3.4.1	Anchoring System Design: Erection Method of Great Importance	30
3.4.2	Modeling the Erection Method in Scia Engineer	32
3.4.3	Scia Engineer Modeling Details	34
3.4.4	Anchoring System Design Process.....	35
3.5	Close Interrelation between Pontoon and Anchoring System Design.....	36
4.	Example Substructure	39
4.1	Introduction	39
4.2	Lay-Out Anchoring System with pontoons	39
4.3	Anchoring Cable Properties	41
4.4	Pontoon Properties.....	42
4.5	Load Capacity.....	44
4.6	Displacements and Rotations	44
4.7	Modeling the Anchoring System.....	46
4.7.1	Coordinate System	46
4.7.2	No Superstructure Modeled.....	46
4.7.3	Supports at the pontoons.....	46
4.7.4	Position of pontoons in Scia Engineer Model.....	47
4.8	Recommendations Anchoring System	48

4.8.1	Protection against Corrosion.....	48
4.8.2	Synthetic Fiber Rope vs Steel Cable	49
5.	More Insight and Reccomendations about Anchoring System	51
5.1	More Additional Pretensioning Leads to Fainter S-shape of the Pontoon Locations.....	51
5.2	Self-Weight Anchoring System Influences Pontoon Sizes, Water Loads and Overturning Moment	52
5.3	Wide versus Narrow Anchoring System	54
6.	Proposed Substructure: Anchoring at Water Level.....	56
6.1	Purpose.....	56
6.2	Overview Substructure	56
6.3	Anchoring Cable Properties	59
6.4	Pontoon Properties.....	60
6.4.1	General Properties	60
6.4.2	Eccentric Ballasting in x-z Plane.....	62
6.4.3	Eccentric Ballasting in y-z Plane	62
6.4.4	Recommendation: Investigate Option to Use Water as Ballast	62
6.5	Load Capacity.....	62
6.6	Displacements and Rotations	63
6.6.1	Coordinate System	63
6.6.2	Displacements in x-direction are Small	63
6.6.3	Displacements in y-direction to be Resisted by Bridge Girder	64
6.6.4	Displacements in z-direction to be Resisted by Bridge Girder	64
6.6.5	Rotations around y-axis within Limits	64
6.6.6	Rotations around z-axis Very Small	64
7.	Starting Point Superstructure: Design Philosophy and Boundary Conditions	65
7.1	Coordinate System.....	65
7.2	Design Philosophy: Flexible and Light Superstructure.....	65
7.3	Hinged Bridge Girder Parts for Flexibility	65
7.4	Material: Steel Grade S460 for Efficiency	66
7.5	Aesthetics: Singular, Dynamic Clean Line	66
7.6	Assumption Pontoon Dimensions for Design Superstructure	66
7.7	Straight Bridge Girders and Minimum Bridge Deck Width	67
7.8	Piers: Form Finding Study	67

7.9	Internal Forces Acting on the Bridge Part at Main Span	68
8.	To Design the Superstructure: Process and Methods	69
8.1	Collaboration with Architects to Find a Functional and Aesthetic Superstructure	69
8.2	Estimation Superstructure Height for Architects	69
8.3	Bridge Type: Lattice Girder Bridge	70
8.3.1	Lattice Girder Bridge like the Echinghen Viaduct	70
8.3.2	Composite Girder vs. Steel Girder	70
8.3.3	Sketches of Possible Lattice Girder Bridges	71
8.4	Supports at Bridge Piers/Pylons	73
8.4.1	Support Layout	73
8.4.2	Deformations	74
8.5	Form Study Piers/Pylons	76
9.	Proposed Superstructure	78
9.1	Superstructure Overview	78
9.2	Bridge Piers/Pylons	79
9.3	Lattice Bridge Girders	79
9.3.1	Lattice Structure	79
9.3.2	Varying Torsional Rigidity along the Girder	81
9.3.3	Circular Hollow Section Members	82
9.3.4	High Strength Steel S460	82
9.3.5	Supports	82
9.4	Unity Checks	84
9.5	Displacements and Rotations	86
9.6	Total Self-Weight of Bridge Girder	87
10.	Conclusion Feasibility Study: The Possibilities and Limitations	88
10.1	The Buoyancy Bridge Concept for Sognefjord is Feasible	88
10.2	Substructure: pontoons and Anchoring System	88
10.3	Superstructure: Lattice Bride Girders	88
10.4	Underestimation of Superstructure Weight in this Study can be Easily Adjusted	89
10.5	Limitations	89
10.6	Not Considered Factors: To be Further Investigated	90
10.7	Recommendations	91

11. References	92
ANNEX A: State of the Art Buoyancy Bridges	A-1
A.1 Current Buoyancy Bridges	A-1
A.2 Modern Separate Pontoon Bridges	A-2
A.3 No Buoyancy Bridge with this Span and Elevation exists	A-6
ANNEX B: Buoyancy Bridge Concept from Previous Study	B-1
B.1 Buoyancy Bridge Concept from Previous Study.....	B-1
B.2 Characteristics of Bridge Concept by Hermans (2014)	B-1
B.2.1 Desire for Flexible and Slender Bridge Design.....	B-1
B.2.2 Bridge S-Shaped in Top View.....	B-3
B.2.3 Pontoon Distance of 200 meters in Side Spans.....	B-4
B.2.4 Continuous Box-Tendon Girder Design in the Superstructure	B-4
B.2.5 Torsional Supports at Pontoons	B-4
B.2.6 Side Anchoring System with Four Anchored Pontoons and Arch Action	B-5
B.2.7 Prestressed Anchoring Tendons.....	B-6
B.2.8 Cylindrical Pontoon Elements with Ballast.....	B-6
B.3 Complications Encountered for the Extreme Buoyancy Bridge Concept	B-7
B.3.1 Slenderness and Flexibility leads to excessive Displacements	B-7
B.3.2 Required Clearance at Mid-Fjord Span not Achieved	B-7
B.3.3 Design Mid-Fjord Span Insufficient: Extensive Vertical Deflections and Difficult Detailing	B-7
B.3.4 Continuous System: Low Robustness and Difficult Construction.....	B-8
B.3.5 Anchoring System: Lateral Displacements exceed Limits and Unfavorable for Bridge Girder.....	B-8
B.3.6 Prestressing the Horizontal Arch has no Structural Contribution.....	B-8
B.3.7 Anchoring System: Anchoring Four Pontoons leads to Unfavorable Effects	B-9
B.3.8 No Satisfying Joint Design Obtained Yet	B-9
ANNEX C: Verification Calculation Method Rotational Stiffness Pontoons	C-1
ANNEX D: Verification Restoring Moment Calculation	D-1
ANNEX E: Pontoon Properties and Loads Calculation File	E-1
ANNEX F: Introduction Modeling Cables in SCIA Engineer	F-1
F.1 SCIA Engineer Settings	F-1
F.2 Structure Input and Computational Results	F-1
F.3 Analytical Results Matching the Computational Results	F-3
ANNEX G: Erection Method Involving De-ballasting	G-1

ANNEX H:	Erection Method with Anchoring Cables at Water Level at Start	H-1
ANNEX I:	Cable Length Check for Avoiding Mechanical Pretensioning	I-1
ANNEX J:	Computational Model Substructure Example 1 (Fixed Supports).....	J-1
J.1	Assumptions Model 1	J-1
J.2	Input.....	J-2
J.2.1	Coordinates Anchoring System	J-2
J.2.2	Material Properties	J-4
J.2.3	SCIA Engineer Input Options	J-4
J.3	Results and Evaluation.....	J-5
J.3.1	Deformed Structure	J-5
J.3.2	Reaction Forces	J-6
J.3.3	Forces and Stresses: Lateral cables not loaded to Full Capacity	J-7
J.3.4	Displacement of Nodes	J-8
J.3.5	Equilibrium Check.....	J-9
J.4	Conclusion.....	J-9
ANNEX K:	Computational Model Substructure Example 2 (Adjusted Prestressing).....	K-1
K.1	Assumptions Model 2	K-1
K.2	Input.....	K-1
K.2.1	Supports	K-1
K.2.2	Reduced Submerged Cable Weight.....	K-2
K.2.3	Adjustment Pretensioning Lateral Anchoring Cables	K-2
K.3	Results and Evaluation.....	K-5
K.3.1	Deformed Structure	K-5
K.3.2	Total Vertical Resultant Force Reduced	K-6
K.3.3	Displacement of Nodes	K-7
K.3.4	Forces and Stresses	K-9
K.4	Conclusions.....	K-9
ANNEX L:	Verification Restoring Moment Calculation.....	L-1
ANNEX M:	Pontoon Properties and Loads Calculation File.....	M-1
ANNEX N:	Estimating External Loads: Calculation File.....	N-1
ANNEX O:	Computational Model Substructure Example 3 (with Loads)	O-1
O.1	Assumptions Model 3	O-1
O.2	Input.....	O-1

O.3	Results and Evaluation	O-3
O.3.1	Deformed Structure	O-3
O.3.2	Displacement of Nodes	O-4
O.3.3	Total Vertical Resultant Force Check.....	O-7
O.3.4	Forces and Stresses	O-7
O.4	Conclusions	O-7
ANNEX P:	Computational Modeling: More Variations Anchoring Cables	P-1
ANNEX Q:	Computational Model Substructure example 4 (with Springs)	Q-1
Q.1	Input in Scia Engineer	Q-1
Q.1.1	Modeling the Anchoring System	Q-1
Q.1.2	Coordinates	Q-2
Q.1.3	Anchoring Cables and Pylon Properties	Q-4
Q.1.4	Supports	Q-4
Q.1.5	Loads	Q-5
Q.1.6	Other Scia Engineer Input Options	Q-7
Q.2	Results.....	Q-7
Q.2.1	Deformed Structures of Different Load Cases.....	Q-7
Q.2.2	Displacements	Q-11
Q.2.3	Internal Forces and Stresses.....	Q-12
Q.3	Evaluation/Verification of the Model	Q-13
Q.3.1	Reaction forces in x-direction.....	Q-13
Q.3.2	Reaction forces in z-direction.....	Q-14
Q.3.3	Effect of the Rotational Spring	Q-15
Q.3.4	Effect of Varying the Prestressing Force	Q-15
ANNEX R:	Computational Model Substructure Example 5	R-1
R.1	Input in Scia Engineer	R-1
R.1.1	Modeling the Anchoring System	R-1
R.1.2	Coordinates	R-3
R.1.3	Anchoring Cables and Pylon Properties	R-4
R.1.4	Supports	R-4
R.1.5	Loads and Load Cases.....	R-5
R.1.6	Other Scia Engineer Input Options	R-8
R.2	Results.....	R-8
R.2.1	Deformed Structures of Different Load Cases.....	R-8
R.2.2	Displacements	R-12
R.2.3	Rotations	R-15

R.2.4	Internal Forces and Stresses.....	R-16
R.3	Evaluation/Verification of the Model	R-17
R.3.1	Reaction forces in x-direction.....	R-17
R.3.2	Reaction forces in z-direction.....	R-18
R.3.3	Effect of the Rotational Spring	R-19
R.3.4	Effect of Additional Prestressing Force	R-19
R.3.5	Effect of adding members between rotation center and cable attachment nodes.....	R-21
R.3.6	Effect of External Forces.....	R-22
ANNEX S:	Calculation File Pontoon Properties and Loads for Model 5	S-1
ANNEX T:	Rotational Stiffness along Bridge Girder	T-1
ANNEX U:	Load Cases.....	U-1
ANNEX V:	Aesthetical Design Guidelines from the Architects	V-1
ANNEX W:	Required Bridge Deck Width	W-1
ANNEX X:	Internal Forces and Rotations of Superstructure	X-1
ANNEX Y:	Sketches with Height Estimation of Different Superstructure Types.....	Y-1
ANNEX Z:	For Architects - Feasibility Bridge Girder Height of 12 meters.....	Z-1
ANNEX AA:	For Architects - Feasibility Composite Box Girder	AA-1
ANNEX BB:	Sketches of Possible Superstructures	BB-1
ANNEX CC:	Supports at Bridge Piers/Pylons – Dimensions and Displacements (First Estimation)	CC-1
ANNEX DD:	For Architects – Recommendation Supports (Location and Dimensions)	DD-1
ANNEX EE:	Idea Exchange with Architects - Superstructure	EE-1
ANNEX FF:	Sketches Final Proposed Superstructure	FF-1
ANNEX GG:	Modeling the Final Superstructure in Scia Engineer	GG-1
GG.1	Lattice Girder at Main Span Governing.....	GG-1
GG.2	Input.....	GG-1
GG.2.1	Global Dimensions of Lattice Girder.....	GG-1
GG.2.2	Varying Torsional Rigidity.....	GG-4
GG.2.3	Material: High Strength Steel S460	GG-4

GG.2.4 Member Dimensions	GG-5
GG.2.5 Supports	GG-6
GG.2.6 Loads	GG-6
GG.3 Results.....	GG-8
GG.3.1 Unity Checks	GG-8
GG.3.2 Displacements	GG-10
GG.3.3 Total Self-Weight of Lattice Structure.....	GG-11
GG.4 Conclusion and Evaluation.....	GG-11

1. INTRODUCTION

1.1 Background and Topic

The Norwegian Ministry of Transport and Communications has commissioned the project Coastal Highway E39 to investigate the potential of eliminating all ferries along the western corridor (E39). This western corridor, Norway's coastal highway E39 of almost 1100 km long, is part of the European trunk road system and it contains eight ferry connections, the highest number of ferries for a single road in Europe. Eliminating all ferry connections reduces the travel time by 7-9 hours, to a total of 12-13 hours, which is expected to have positive effect on the trade and industry, regional employment and settlement patterns of Norway [1].

The eight ferry connections along the route, which can be seen in Figure 1-1, are wide and deep fjord crossings that require massive investments and longer spanning structures than previously installed in Norway. Some of them are already replaced by fixed links, except for the more challenging ones. Of all fjords, Sognefjord is considered the most difficult and challenging to cross. The average depth of the other fjords is about 490 meters. But with its width of almost 4000 meters, the vast depths of up to 1300 meters and the 200-300 meters of bottom deposits above the rock, Sognefjord is the pilot site for developing new concepts for extreme bridges.

Furthermore, for the fixed link to accommodate expected traffic situations in 2040, a large fairway clearance is needed for vessels, preferably at the middle of the fjord. The clearance will require a width of 400 meters, a height of 70 meters and a draught of 20 meters, which will lead to a large span and bridge elevation at the middle of the fjord. To give an impression, an elevation of 70 meters means that the bridge deck will be placed at the same height as the roof of an 18-storeys building. To accomplish such wide and high clearance at the middle of the fjord, the design of the bridge will be even more challenging.

For a project of such magnitude and complexity, the necessary professional skills and sufficient capacity within civil engineering are required. Thus, engineering firm Iv-Consult and architect firm Zwarts & Jansma Architects have expressed their interest in participating together in the further detailing and development of this new concept for extreme bridging.

The topic of this Master thesis research is to explore the structural engineering possibilities for a fixed link crossing the extreme Sognefjord. Due to the vast depths, large width and soft bottom of the fjord, it is cost-effective to develop a floating (buoyancy) bridge concept. It will be a step to advancement in civil engineering, since a floating bridge with a span and elevation this high is unprecedented.



FIGURE 1-1 PROJECT COASTAL HIGHWAY E39 [17]

1.2 Problem Statement

Engineering firm Iv-Consult and architect firm Zwarts & Jansma Architects have expressed their interest in participating together in the further detailing and development of a new concept for an extreme buoyancy bridge for project Coastal Highway E39, commissioned by NPRA. However, no feasible solution has been found yet for the development of a structurally and aesthetically competitive concept for the buoyancy bridge with this unprecedented span and elevation. This will be explained in the next section, 1.3 Problem Analysis.

1.3 Problem Analysis

In the next sections, the state of the art of buoyancy bridges and the development of the buoyancy bridge concept will be discussed to illustrate the challenge to find a structurally and aesthetically competitive concept for the buoyancy bridge at Sognefjord.

1.3.1 State of the Art Buoyancy Bridges

Introduction

Where the water crossing is wide and deep, buoyancy bridges become a very cost-effective bridge type. For a site where the water is 2 - 5 km wide, 30 - 60 meters deep and a soft bottom extending another 30 – 60 meters, a floating bridge is estimated to cost 3 – 5 times less than a long span fixed bridge [2]. However, extra attention should be paid to wind, waves and currents.

The concept of a floating bridge takes advantage of the natural law of buoyancy of water to support the dead and live loads. There is no need for conventional piers or foundations. However, an anchoring or structural system is needed to maintain transverse and longitudinal alignments of the bridge.

Floating bridges have been built since time immemorial. Ancient bridges were generally built for military operations. In the present, there are around 12 floating bridges in use for public vehicular traffic. These are listed in Table 1-1. Floating bridges can be classified into two types, namely the continuous pontoon floating bridge (CPF) and the separate pontoon floating bridge (SPFB). A continuous pontoon floating bridge consists of individual pontoons joined together to form a continuous structure. This leads to large horizontal wave and wind actions and large horizontal movements on the bridge, which needs to be restraint. A separate pontoon floating bridge consists of individual pontoons, acting as supports at a certain interval. Examples for both types of floating bridges are shown in Figure 1-2.



FIGURE 1-2 CONTINUOUS PONTOON FLOATING BRIDGE (LEFT) AND SEPARATE PONTOON FLOATING BRIDGE (RIGHT) [25]

TABLE 1-1 FLOATING BRIDGES WHICH ARE CURRENTLY IN USE BY PUBLIC VEHICULAR TRAFFIC

Floating Bridge	Country	Type
Berbice Bridge	Guyana	SPFB
Bergøysund Floating Bridge	Norway	SPFB
Brookfield Floating Bridge	USA	CPFB
Demerara Harbour Bridge	Guyana	SPFB
Governor Albert D. Rosellini Bridge	USA	CPFB
Homer M. Hadley Memorial Bridge	USA	CPFB
Hood Canal Bridge	USA	CPFB
Lacey V. Murrow Memorial Bridge	USA	CPFB
Nordhordland Bridge	Norway	SPFB
William R. Bennet	Canada	CPFB
Yumenai Bridge	Japan	SPFB
New SR520 Bridge (being built)	USA	CPFB

Continuous Pontoon Floating Bridges (CPFB) vs. Separate Pontoon Floating Bridges (SPFB)

In Table 1-1 it can be seen, that all floating bridges in the USA have continuous pontoons. These bridges all cross modest water depths of 60-100 meters, which allows easy anchoring for the large horizontal forces on the continuous pontoons. Achieving horizontal anchoring at the Sognefjord is more complex, since the fjord is more than 1 km deep.

An advantage of the continuous pontoon bridge is the omission of a superstructure. However, due to the required elevation of 70 meters and span of more than 400 meters of the bridge girder near the middle of the fjord, a superstructure is required anyway for the buoyancy bridge at Sognefjord.

Moreover, previous study shows, that a separate pontoon floating bridge is in general cheaper than continuous pontoon floating bridges [3]. More factors and characteristics of both floating bridge types were taken into account and it was concluded that the separate pontoon floating bridge is more suitable for the bridge concept of Sognefjord. More explanation can be found in "*Buoyancy aided crossing for bridging extreme widths*", Annex A, by R.T.H. Hermans.

Modern Separate Pontoon Floating Bridges

Of the bridges listed in Table 1-1, five of them are of the separate pontoon type. These bridges were analyzed extensively in ANNEX A: State of the Art Buoyancy Bridges, since the bridge concept for this feasibility study is also a separate pontoon floating bridge. In the following, an overview of the analysis is shown. In Figure 1-3, the five existing separate floating bridges are shown. The characteristics of these bridges are compared to the required characteristics of the buoyancy bridge at Sognefjord in Table 1-2.

Berbice bridge (Guyana) [4]



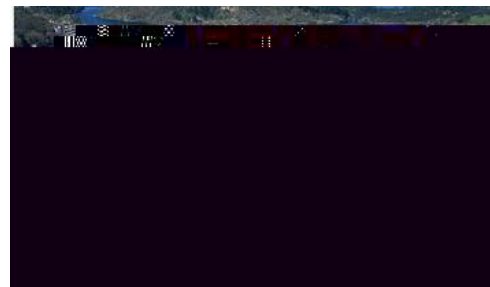
Bergøysund floating bridge (Norway) [5]



Demerara harbour bridge (Guyana) [6]



Nordhordland bridge (Norway) [7]



Yumemai bridge (Japan) [8], [9]



FIGURE 1-3 SEPERATE PONTOON BRIDGES, MORE INFORMATION IN TABLE 1-1

TABLE 1-2 COMPARISON CHARACTERISTICS EXISTING SPFB AND BRIDGE CONCEPT SOGNEFJORD

	Berbice bridge	Bergøy-sund floating bridge	Demerara harbour bridge	Nordhord-land bridge	Yumemai bridge	Bridge concept Sognefjord
Country	Guyana	Norway	Guyana	Norway	Japan	Norway
Year of completion	2008	1992	1978	1994	2001	-
Length (m)	1550	931	2010	1610	410	3507
Longest span (m)	40	106	77	113	280	430
Anchoring system	sideways	none	sideways	none	mooring piles	-
Elevation above water (m)	5	6	5	5,5	26	75
Fairway clearance width x height (m)	40 x 12	106 x 6	77,4 x ∞	172 x 32	200 x ∞	400 x 70
Fairway solution	Elevated bridge deck and retractable part	Between pontoons	Retractable section at midspan	Elevated part by cable-stayed bridge section with one tower near shore	Whole bridge can be swung around pivot axis near one end of girder	Between pontoons

No Buoyancy Bridge Exists with Scale of the Bridge for Sognefjord

As can be seen in Table 1-2, none of the existing floating bridges can be compared to the required characteristics for the buoyancy bridge at Sognefjord.

No retractable bridge part allowed

Three of the separate pontoon floating bridges shown above, facilitate the passing of larger vessels by using retractable parts. In these cases, the vehicular traffic on the bridge will be halted and bridge parts will be retracted, so large vessels will be able to pass the bridge. Since the purpose of the Norwegian Ministry of Transport and Communication to commission the Coastal Highway E39 project was to reduce the travel time by improving the flow of the traffic, replacing the ferry connection with a movable bridge is not considered to be the most effective solution. Therefore, implementing movable bridge parts (like the Berbice Bridge, Demerara Bridge and Yumemai Bridge) to provide the required fairway clearance, is not an option for the bridge concept at Sognefjord.

High elevated height leads to large wind loads

The exclusion of the option to install movable bridge parts, results in a very high elevated height of 70 meters of the bridge girder at the mid-fjord span. The bridge deck elevation of 26 meters of the

Yumemai Bridge is the highest existing bridge deck elevation of a floating bridge. This height is still far smaller than the requirement for the new bridge concept at Sognefjord. A bridge with much larger heights leads to many additional complications. Just as normal bridges with conventional piers and foundations, buoyancy bridges are susceptible to wind load. However, wind load has a much larger influence on the design of buoyancy bridge than a conventional bridge, since it is much more difficult to restrain the displacements and rotations for a buoyancy bridge. The larger the height, the larger the wind load is. The buoyancy bridge at the Sognefjord will require new solutions to resist these large loads.

Unprecedented span

All maximum span widths of the existing buoyancy bridges are much smaller than the required span width of 430 meters for the mid-fjord span at Sognefjord. Currently, the Yumemai Bridge has the largest span between pontoons in the world: a main span of 280 meters.

Great water depth

Because of the large span and elevation of the bridge deck, the magnitude of the loads, which the buoyancy bridge will be subjected to, will entirely be on a new scale compared to the design loads of the existing bridges. Special attention should be paid to the horizontal loads. Usually, the horizontal forces of buoyancy bridges are resisted by an anchoring system or by other supporting structures. In case of the Yumemai Bridge, mooring piles are applied, which reach the canal floor at a depth of 12 meters. For the Sognefjord, which has a water depth up to 1000 meters, the use of mooring piles is obviously not the most efficient solution. Even the design of (sideway) anchoring systems will require special attention.

These facts, which are discussed above, show that new technological alternatives and concepts must be sought for the extreme bridging at Sognefjord.

1.3.2 Current Development: Master Thesis Research Done Previously

Project Coastal Highway E39 contains technological challenges for the crossing of fjords. For this reason, engineering firm Iv-Consult and architect firm Zwarts & Jansma Architects have requested Master students of Delft University of Technology to create general and cutting-edge knowledge through studies and research. Prior to this research, MSc R.T.H. Hermans has contributed to the generation of a feasible concept. He has done extensive studies and research (2014) about the environment of Sognefjord and the design requirements of the Norwegian Public Roads Administration (NPRA) for the fixed link. His extensive literature search will also be gratefully used for this research.

Besides his study about the environment and requirements for the bridge, Hermans also investigated different possibilities for the superstructure, anchoring system and pontoon elements, followed by a proposition of a bridge concept. This concept for the bridge, however, does not comply with the requirements. It was concluded that this concept was not feasible. The buoyancy bridge concept from the research of Hermans (2014) is shown in Figure B-2. The full study is reported in *"Buoyancy aided crossing for bridging extreme widths"*, 2014, by R.T.H. Hermans.

The most important results of the research of Hermans (2014) are summarized in ANNEX B: Buoyancy Bridge Concept from Previous Study. In this section the concept of Hermans is described, while focusing on the characteristics and complications that lead to an infeasible solution. Nevertheless, the effort and extensive research of Hermans provide many useful insights that contribute the development of a new bridge concept in this thesis.

1.4 Target and Objectives

The purpose is to develop a structurally and aesthetically competitive concept for the buoyancy bridge, which fulfills requirements regarding strength, stability, serviceability and functionality.

1.5 Research Questions

1.5.1 Main Question

Is a structurally and aesthetically competitive concept for the buoyancy bridge at Sognefjord feasible?

1.5.2 Sub Questions

- What are the properties of a substructure that restrains the movements of the pontoons as much as possible?
- What kind of bridge girder will be designed for the main and side spans, and how will this girder be supported?

1.6 Methodological Approach

The purpose of this research is to develop a structurally and aesthetically competitive concept for the buoyancy bridge, which fulfills all requirements regarding strength, stability, serviceability and functionality. To achieve this goal, the approach, which is described in the following, will be used. A schematizing of the approach is shown in Figure 1-4.

Step 1 Preparation: work plan and literature search

The first step is to prepare for the research. A good understanding of the current development of the bridge concept is essential. For this, the report of the previous research about the buoyancy bridge by Hermans (2014) is studied thoroughly. Other literature search about the project Coastal Highway E39 and about the state of the art also helped to gain knowledge about this subject. A good awareness of the requirements for the buoyancy bridge at Sognefjord is obtained during this phase. After good understanding and insight was gained, a work plan was drafted.

Step 2 Build scale model

Once it is decided on the concept of the anchoring system, a scale model can be built and tested. The purpose of this scale model is to increase the sense of the designer for the behavior of anchoring system. This will facilitate the design of the system.

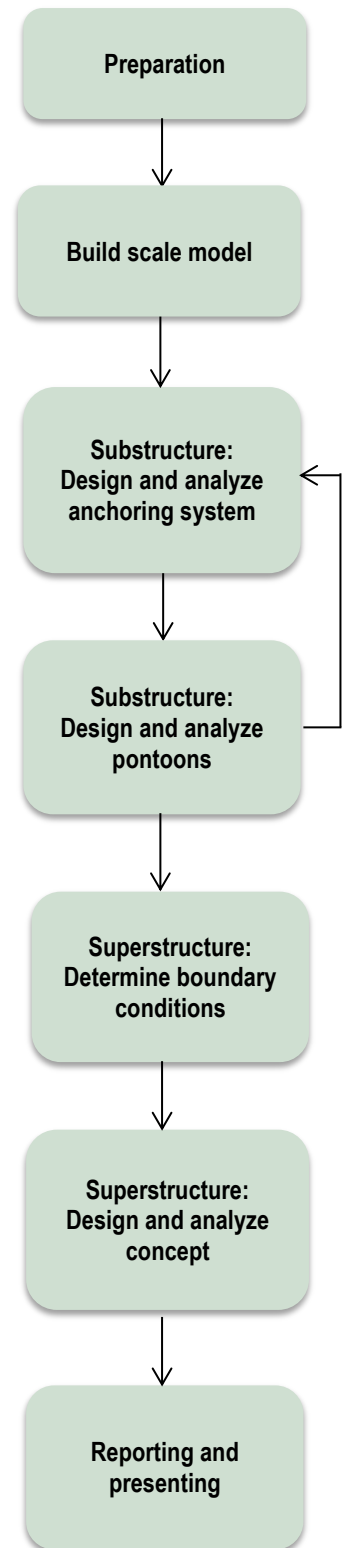


FIGURE 1-4 RESEARCH APPROACH

Step 3 Substructure: design and analyze anchoring system

In general, the superstructure of a separate pontoon floating bridge must be of sufficient strength and stiffness to resist horizontal and vertical forces and to maintain the relative position of the pontoons. However, if an anchoring system was designed, which maintains the relative position of the pontoons as much as possible, the required strength and stiffness of the superstructure will be smaller.

The purpose of this research is to develop a structurally and aesthetically competitive concept of the buoyancy bridge. Since in general, slender bridge superstructures are considered to be more aesthetically pleasing, an anchoring system will first be designed, which will maintain the relative position of the pontoons as much as possible without the contribution of the bridge superstructure.

This will be done by using structural analysis software Scia Engineer, by making analytical calculations and by building a scale model. During this phase and all other design phases, the erection method will be kept in mind. This will be done very roughly, since very careful analysis and calculations are often required to obtain detailed instructions for the erection process. An in-depth analysis will not be included in this study. See chapter 3.4 for more detailed information about the design of the anchoring system.

Step 4 Substructure: design and analyze pontoons

The substructure consists of the anchoring system and the pontoons. For the design of the pontoons, there should be good understanding about the buoyancy and restoring moment generation. More information about this is described in chapter 3.3. More in-depth information about the design of the pontoons is given in chapter 3.2.

Both the designs of the anchoring system and pontoons occur simultaneously, iterations are needed. This is described in chapter 3.5.

Step 5 Superstructure: determine boundary conditions

In this study, first a substructure will be designed which maintains the relative positions and rotations of the pontoons as much as possible. This substructure will give rise to the requirements of the superstructure. Before a new concept for the superstructure can be created, first the boundary conditions should be clearly defined.

Step 6 Superstructure: design and analyze superstructure

With the boundary conditions known, new concepts for the superstructure of the buoyancy bridge will be brainstormed. The effects, which the bridge superstructure must be able to resist, will be taken into account and also the erection method will be kept in mind. It is important to regard the behavior of the entire bridge structure and to have a good understanding of how the choices will affect the other bridge parts. The stiffness's of the connections between bridge parts will be defined for the bridge concepts. Rough schematizations and sketches of new concepts will be created.

Hereafter, structural analysis of the concept can be done by analytical calculations and by using the structural analysis software Scia Engineer.

Step 7 Wrapping Up: presentation and reporting

In the last phase, the conclusions, recommendations and limitations of this research will be reported and presented.

The design of the bridge superstructure and substructure are related. To arrive at a final design, iterations will be needed. For this feasibility study however, a concept will be developed which will indicate the possible global system and the order of magnitude of the buoyancy bridge. No iterations will be done to obtain a detailed design.

1.7 Overview Report

The required design information to design a new bridge concept are summarized the next chapter.

Hereafter, chapter 3 to 6 will be about the substructure. Chapter 3 describes the design method of the substructure, including information about the modeling of the substructure in Scia Engineer. Because the erection method greatly influences the design, the erection method is also discussed and presented in this section (method 3 in section 3.4.1). In chapter 4, an example of a substructure is given to provide a better understanding about the substructure. In chapter 5 more insight and recommendations for the design of the substructure is given and the final proposed substructure is presented in chapter 6.

In chapter 7 to 9, information about the superstructure concept can be found. In chapter 7, the starting points and the boundary conditions for the design of the superstructure are given. The design process is described in chapter 8. Since this part of the bridge is not submerged, but clearly in view above water, information from interactions with the architects can also be found in these sections. The final proposed superstructure concept is presented in chapter 9.

Chapter 10 concludes this report. In this chapter, the conclusion, recommendations and limitations of this study can be found.

The references to used information sources can be found in chapter 11. The documents in Annex A to Annex GG provides extra (in-depth) information.

2. DESIGN INFORMATION

In this chapter the design information will be shown, which will serve as the input for the design of the buoyancy bridge. These include the coordinate system, the design input for the anchoring system, the main difference between the anchoring system of the old infeasible concept of Hermans (2014) (presented in Annex B) and the new anchoring system. Furthermore, this chapter also includes the boundary conditions, the design assumptions, the design requirements and the limitations of the buoyancy bridge concept.

2.1 Coordinate System

The coordinate system is as shown in Figure 2-1.

The x-axis is in the same direction as the bridge deck width.

The y-axis is in the same direction as the bridge girder.

The z-axis is orthogonal to the bridge deck.

The x-y plane is also referred to as the horizontal plane or lateral plane.

The x-z plane is also referred to as the cross-sectional plane.

The y-z plane is also referred to as the vertical plane.

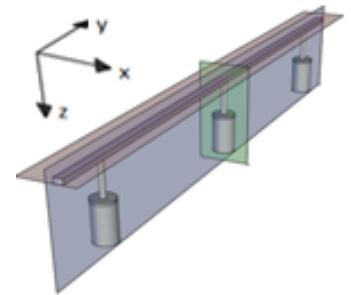
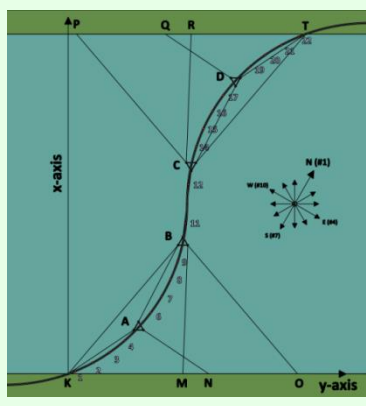
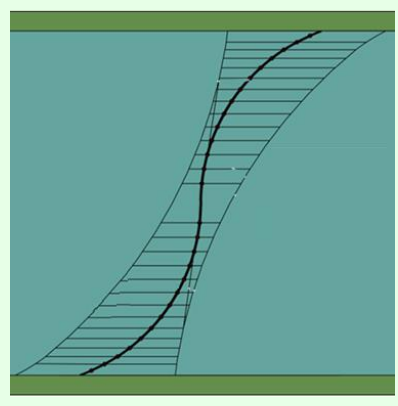


FIGURE 2-1 COORDINATE SYSTEM


2.2 Design Input and Set-up

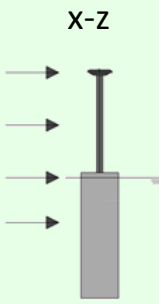
Since this is a project of such magnitude and complexity, a lot of complications arose during the previous research. The previous bridge concept developed by Hermans (2014) is described in section B.2 of ANNEX B: Buoyancy Bridge Concept from Previous Study. This design, however, came with quite some remarks and questionable feasibility, which are indicated in section B.3. Since this concept is found to exceed service and strength limits, a new bridge concept will be generated. In Table 2-1, an overview will be given of the old concept and the expected new bridge concept.

TABLE 2-1 COMPARISON OLD AND NEW BRIDGE CONCEPT

Plane (See Figure 2-1)	Old Bridge Concept	New Bridge Concept
X-Y	 <p>A horizontal cable-stayed anchoring system is used, where four pontoons are anchored.</p>	 <p>All pontoons are anchored in a horizontal suspension anchoring system. The prestressing of the</p>

	<p>Horizontal deflections exceed limits severely in case it is assumed that the horizontal load is resisted by the anchoring tendons alone (bridge girder contribution 0%). Therefore, it was recommended to increase the prestressing in the anchoring tendons and to add bridge girder contribution.</p> <p>Furthermore, to increase the stiffness of the bridge girder in the horizontal plane, the arches of the S-shape are prestressed. This contribution, however, proved to be very small, while introducing a lot of complications in the system (extra stresses in the bridge girder, vulnerability to instability and large anchoring forces.)</p> <p>The bridge girder contribution depends on the ratio between the stiffness of the bridge girder and the stiffness of the anchoring system.</p> <p>The stiffness of the bridge girder is determined by the rotational stiffness provided by the buoyancy of the pontoon, the additional stiffness of the prestressed arch and the stiffness of the connection of the arch to pylon.</p>	<p>horizontal S-shape is omitted.</p> <p>Consequences:</p> <ul style="list-style-type: none"> - As result of anchoring all pontoons instead of only four pontoons, the deflection will be smaller. As result, the bridge girder contribution might not be needed. Then, the bridge girder parts can be continuously or simply supported in the horizontal plane. - The prestressing of the arches in the horizontal plane is omitted. This way, the longitudinal stresses in the bridge girder will decrease, the girder will be less vulnerable to instability and since bridge girder contribution might not even be needed, this also relieves the anchoring tendons. Moreover, the contribution to the stiffness by prestressing the arch proved to be very limited due to the small drape. - Since all pontoons are anchored now, the bridge girder does not have to transfer lateral loads from non-anchored bridge parts to anchored pontoons. The required rotational stiffness of anchored pontoons decreases drastically, resulting in much smaller sizes for anchored pontoons and also in the decrease of total concrete pontoon volume. However, the required material for the anchoring system increases.
	<p>Restraining of rotation around z-axis at the connections between bridge girder sections:</p> <p>$\varphi_{z,anch\ pontoon} \rightarrow$ flexible</p> <p>$\varphi_{z,non-anch\ pont} \rightarrow$ stiff</p> <p>Restraining of displacement of the global bridge structure in y-direction:</p>	<p>Restraining of rotation around z-axis at the connections between bridge girder sections:</p> <p>$\varphi_z \rightarrow ?$</p> <p>Restraining of displacement of the global bridge structure in y-direction:</p> <p>$u_x \rightarrow$ stiff</p>

	$u_{x,anch\ pontoon} \rightarrow$ stiff $u_{x,non-anch\ pont} \rightarrow$ flexible	
	<p>A system with simply supported beams is preferred over a system with a continuous beam. Then, the pontoon movement will induce less effect on the bridge girder.</p> <p>At the mid-fjord span, the deflections are too large, so a continuous girder is used to provide extra stiffness. The bridge deck has a 100% contribution.</p> <p>Since in this concept the horizontal arch is prestressed, a fixed longitudinal connection (continuous system) is required to obtain arch action (φ_x fixed). So even though simply supported beams are suitable for the side spans (deflections are within the limits), the continuous beam is executed over the whole bridge.</p>	<p>As explained above in the description for the x-y plane, the prestressing of the horizontal arch will be omitted. As result, φ_x is not required to be fixed anymore and a choice between a continuous and simply supported system becomes possible.</p> <p>Mid-fjord span: a system will be chosen where either</p> <ul style="list-style-type: none"> - the bridge girder will be simply supported between the two pylons at the mid-fjord span, <p>or</p> <ul style="list-style-type: none"> - a system will be created, where the bridge girder between the mid-fjord span and also (a few) side spans will be continuous. <p>Side span: the remaining side spans, if applicable, can be chosen to be simply supported beams (bridge girder contribution $\approx 0\%$).</p> <p>A slender execution is then possible, while the deflections also stay within the limits. A system with simply supported beams has advantages when regarding pontoon movement.</p>
	<p>Restraining of rotation around y-axis at the connections between bridge girder sections:</p> <p>$\varphi_x \rightarrow$ stiff</p>	<p>Restraining of rotation around y-axis at the connections between bridge girder sections:</p> <p>$\varphi_x \rightarrow ?$</p>

	Restraining of displacement of the global bridge structure in x-direction: $u_y \rightarrow$ stiff	Restraining of displacement of the global bridge structure in x-direction: $u_y \rightarrow$ stiff
	<p>The torsional stability is $\approx 100\%$ provided by the restoring moment of the pontoon.</p> <p>The contribution of the bridge deck is $\approx 0\%$.</p> <p>(This is the case for pontoon sizes with a radius of 15 meters, a metacentric height of 1 meter and a span of 200 meters.)</p> <p>Consequence: anchored pontoons are very big to provide the required rotational stiffness.</p>	<p>Assumption:</p> <ul style="list-style-type: none"> - bridge deck contribution $\approx 0\%$ - torsional stability $\approx 100\%$ provided by pontoons <p>Consequence:</p> <p>If finally, the bridge girder appears to be contributing to the torsional stability, it will have positive consequences for the design of the pontoons: the required size of the pontoons might decrease.</p>
	<p>Restraining of rotation around y-axis at the connection between the bridge girder and the pylon:</p> <p>$\varphi_y \rightarrow$ stiff</p> <p>Restraining of displacement of the global bridge structure in z-direction:</p> <p>$u_z \rightarrow$ stiff</p>	<p>Restraining of rotation around y-axis at the connection between the bridge girder and the pylon:</p> <p>$\varphi_y \rightarrow$ stiff</p> <p>Restraining of displacement of the global bridge structure in z-direction:</p> <p>$u_z \rightarrow$ stiff</p>

2.3 Main Differences Previous Buoyancy Bridge Concept and New Concept

2.3.1 Anchoring System changed to a Horizontally Suspended Anchoring System

In the concept design from the previous research, only four pontoons were anchored in a cable stayed anchoring system. As discussed in chapter B.1, anchoring only four pontoons leads to uncertainties, it requires more pontoon material, it leads to stability issues due to rotation and vertical movement from non-anchored pontoons and it requires heavy, prestressed tendons, which are difficult to install.

Because of these complications, the anchoring system will be changed, so all pontoons are anchored. By anchoring all pontoons instead of four, it will not be necessary anymore for the lateral forces on the non-anchored pontoons to be transferred to the anchored ones by beam action. This way, less stresses need to be transferred by the bridge girder and the torsional stability issues will decrease, which will lead to the possibility of a more slender bridge girder.

Furthermore, anchoring all pontoons will have a positive effect on materials saving of the pontoon, both the concrete and ballast material. However, the material for the anchoring system will increase.

As all pontoons are to be anchored, a horizontal suspension anchoring system, as shown in Figure 2-2, becomes more efficient [3]. Another advantage of the suspension anchoring system is that it is less prone to colliding tendons.

Furthermore, with this new anchoring system, it is possible to realize a superstructure system with simply supported beams, instead of one continuous beam. A system with simply supported beams leads to a more predictable and favorable behavior regarding pontoon movement response.

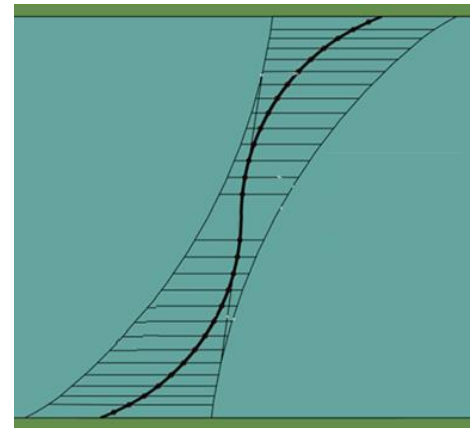


FIGURE 2-2 HORIZONTAL SUSPENSION ANCHORING SYSTEM [3]

2.3.2 Arch Action by Prestressing the Horizontal Arch Omitted

In chapter B.3.6 from ANNEX B: Buoyancy Bridge Concept from Previous Study, it was explained that prestressing the arch for the S-shape at altitude in the top view does not have a structural contribution. When only making use of a part of the arch, the drape appears to be too small to have a contribution to the stiffness. When the whole arch is used, it becomes prone to instability. Furthermore, to achieve arch action by prestressing, undesired consequences for the bridge girder arise. Arch action leads to torsion and longitudinal forces. Since it was decided that a slender bridge deck is of utmost importance, the arch action will be omitted for the development of a new concept.

Besides relieving the bridge deck from stresses, the omission of prestressing the horizontal arch will also relieve both the longitudinal and lateral tendons of the anchoring system. The relief of the forces in the lateral tendons can be explained as follows: The lateral loading on the bridge structure can be resisted by the anchoring system alone, or it can be resisted by the anchoring system in combination with a contribution of the bridge deck. In the second case with bridge deck contribution, the deflections will be less. The contribution of the bridge deck to the lateral resistance is decided by the ratio between the bridge deck stiffness and anchoring tendon stiffness. For example, a completely flexible bridge deck with no stiffness will be non-contributing and a fully fixed bridge deck will be fully contributing. A specific ratio between the stiffnesses of the bridge deck and anchoring tendon is desired to allow the prestressing of the S-shape of the bridge girder to have an effect, while not inducing too many stresses in the bridge girder. As a result, large stiffness of the anchoring system and large forces in the anchoring tendons are required.

To incorporate arch action in the bridge girder by prestressing the ties between anchored pontoons, longitudinally fixed joints between the bridge girder and the pylons are necessary. This results in the implementation of a continuous beam over the whole bridge and it takes away the option of a system with simply supported systems. A system with simply supported beams, however, has a more favorable behavior regarding the response to pontoon movements.

Through research [3, p. 94], it was proven that longitudinal forces in the bridge girder are larger than the lateral forces induced by lateral loading by a factor up to four. This leads to complications for the transfer of these forces from bridge deck level to the anchoring tendon. By omitting the arch action by prestressing, the longitudinal forces in the bridge girder will decrease, resulting in a smaller required capacity for the joint between the bridge deck and pylons.

By decreasing the longitudinal forces, the required buoyant rotational stiffness for transferring the longitudinal loads will also be smaller. A cylindrical pontoon shape is the most efficient when the lateral and longitudinal forces are equal.

2.4 Boundary Condition: Cross-Section Sognefjord

The buoyancy bridge will be located in Norway, along the coastal highway E39, between Lavik and Oppedal, as shown in Figure 2-4. As can be seen, the current E39 crosses the Sognefjord with a ferry connection between Lavik and Oppedal.

The cross-section of the Sognefjord at the location around the crossing is shown in Figure 2-3. The crossing is around 3700 meters wide and 1250 meters deep. At the bottom of the Sognefjord, the soil consists of 200-300 meters clay. The steep inclined parts at the sides consists of rock [3].

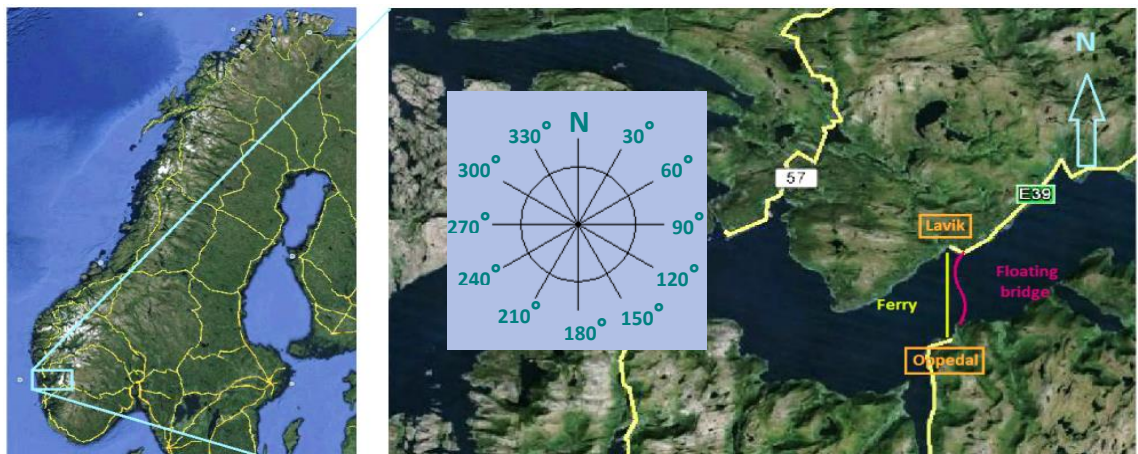


FIGURE 2-4 LOCATION CROSSING SOGNEFJORD

Side : Oppedal

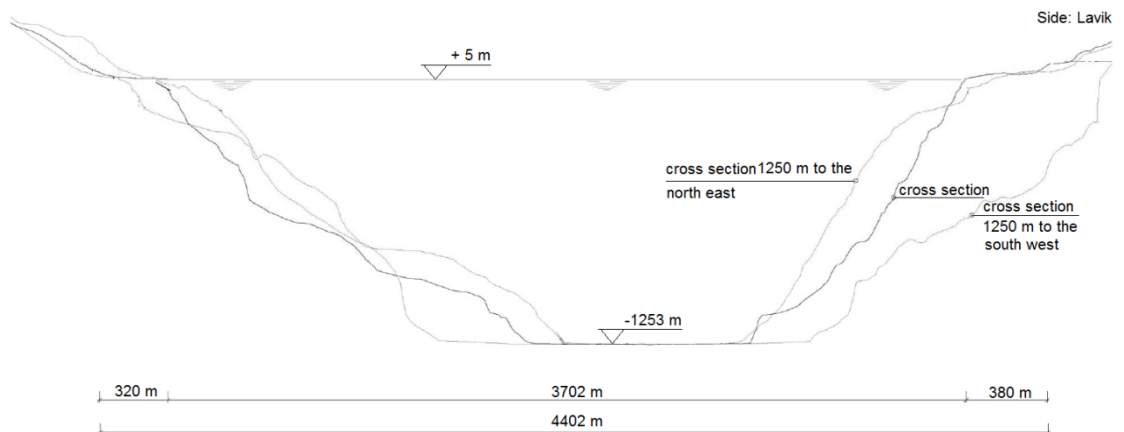


FIGURE 2-3 CROSS-SECTION SOGNEFJORD AT CROSSING [10]

2.5 Assumptions

2.5.1 Bridge Deck assumed Non-Contributing to Torsional Stability

The overturning moment can be compensated by several counteracting mechanisms. The first one is the buoyancy of the pontoon. Rotation of the element with a positive metacentric height causes a restoring moment. The bridge girder can also compensate the overturning moment by transferring the moment to the shore using the torsional rigidity of the girder.

A model as shown in Figure 2-5 can be used to investigate the resistance against lateral loads. Here, the rotational stiffness of the bridge girder is modeled as $k_{r,BG}$, the bending stiffness of the bridge girder against lateral forces as k_{BG} , the stiffness of the anchoring system against lateral movement as k_{AN} and the rotational stiffness caused by the buoyancy of the pontoon $k_{r,BU}$. Using this model, the resistance of the bridge concept of Hermans (2014), which was presented in chapter B.1, against lateral loads was investigated.

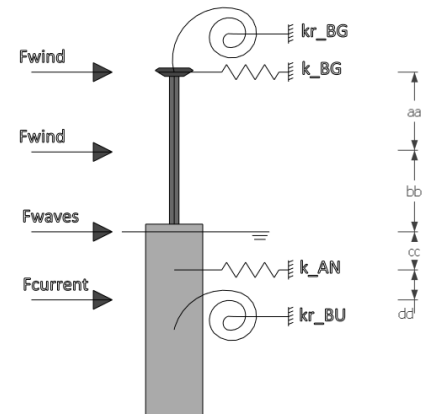


FIGURE 2-5 MODEL FOR RESISTANCE AGAINST LATERAL LOADS [3]

The input variables for investigating the lateral resistance were: the girder properties as shown in Figure B-7, a pontoon radius of 15 meters, a pontoon distance of 200 meters, a required ballast height to obtain a metacentric height of 1 meter (the same metacentric height used for ships) and a horizontal suspension anchoring system. For a bridge structure with these properties, results showed that the buoyancy restoring moment stiffness is the only significant variable which can limit the rotations to meet the requirements. The bending and rotational stiffness of the bridge deck showed to have too small effects to be capable of making a difference.

For the new bridge concept, it will be assumed that the new bridge contribution will also be negligible to limit the rotations in the sectional plane, as shown in Figure 2-5. This assumption is based on the expectation, that the new bridge girder will have a comparable slenderness as the bridge girder from the bridge concept of Hermans (2014). Beside the slenderness of the bridge girder, also the pontoon shape, pontoon size, pontoon distance and the ballast height are all expected to be on the same scale as in the previous concept. Consequently, the dimensions of the pontoons are much larger than the dimensions of the bridge girder. It is assumed that the bridge girder will not provide enough stiffness to resist the effects on the substructure (pontoons and anchoring system).

In case the bridge girder does contribute to the torsional resistance, it will be beneficent to the design of the pontoon, as the required buoyancy restoring moment stiffness of the pontoon will be smaller.

2.5.2 Wind Load

The wind load is a very important factor for the design of a buoyancy bridge. The basis of design is a one in 100 years storm, as is often the basis in offshore engineering. The vicinity of mountains causes a reduced wind effect and the wind majorly flows in fjord direction. For the design a 10-minute wind speed of 35 m/s at a reference height of 10 meters is used. The accordingly hourly mean wind velocity is 32 m/s for a similar return period. The wind direction with maximum wind speed ranges from 180 – 240 degrees relative to the north [3], see Figure 2-6. Different wind speed and directions are shown for winds with different return periods (Rp).

In previous research [3], the wind profile at Sognefjord is obtained by expanding the wind speed at the reference height into a profile along the z-axis. In Figure 2-7 the wind speed is shown as a function of the elevation above the sea surface. The directions are shown in Figure 2-4. Wind profiles from the Norwegian code [10] and Dutch Eurocode [11] were used. It is decided to apply the Logarithmic wind profile from the Norwegian code [10, p. 16], since this profile coincides with the profile based on the Eurocode.

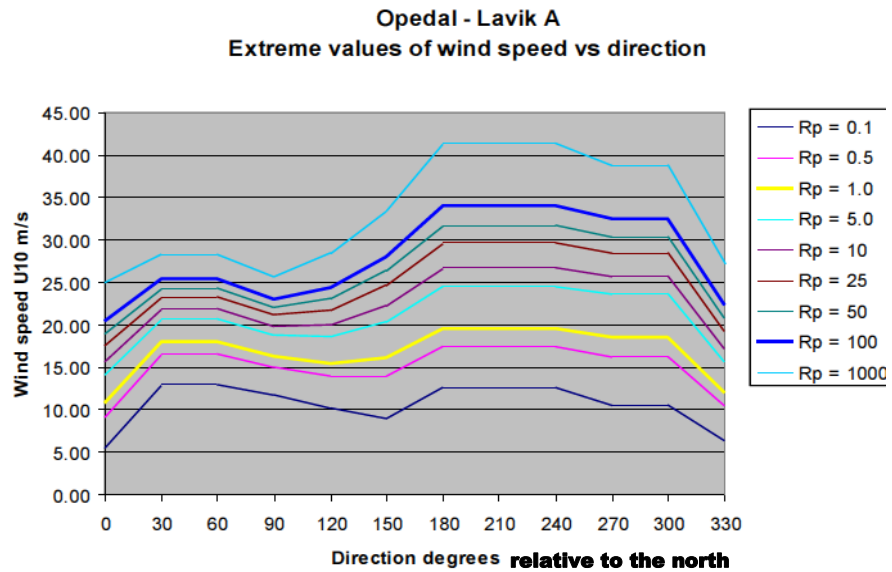


FIGURE 2-6 WIND SPEED AND DIRECTION [10]

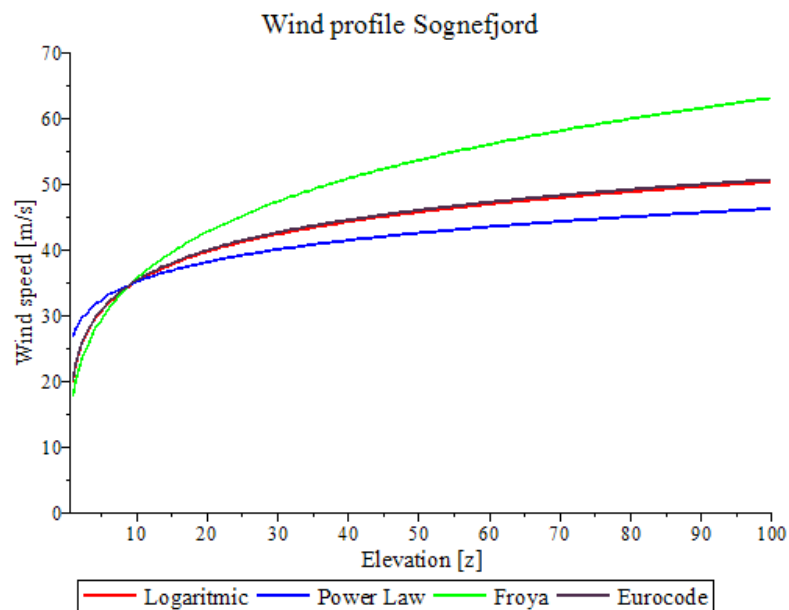


FIGURE 2-7 WIND PROFILE SOGNEFJORD [3]

2.5.3 Wave Load

Besides wind load, effects induced by waves are also very important for buoyancy bridges. The waves in the Sognefjord are assumed to consist of wind waves, swell waves and land slide induced waves. In previous research, the characteristics for the waves were investigated. These are summarized in Table 2-2. In Figure 2-8, the extreme values of wind wave height for different directions are shown. For more information on the acquisition of the wave characteristics, see the study of Hermans, 2014, chapter 4.3.2.

TABLE 2-2 CHARACTERISTICS FOR WAVES AT SOGNEFJORD

Parameter		Wind waves			Swell wave	Land slide
		North side	Mid-fjord	South side		
Sign. Wave height	H_s [m]	2,22	2,34	2,13	0,1	0,2
Spectral top period	T_p [s]	4,6	4,8	4,8	13-14	85
Direction	[°]	180	240	270		
Max. Single wave height	H_{max} [m]	4,55	4,79	4,36	0,2	0,2
Wave length	λ [m]	33	36	36	250	

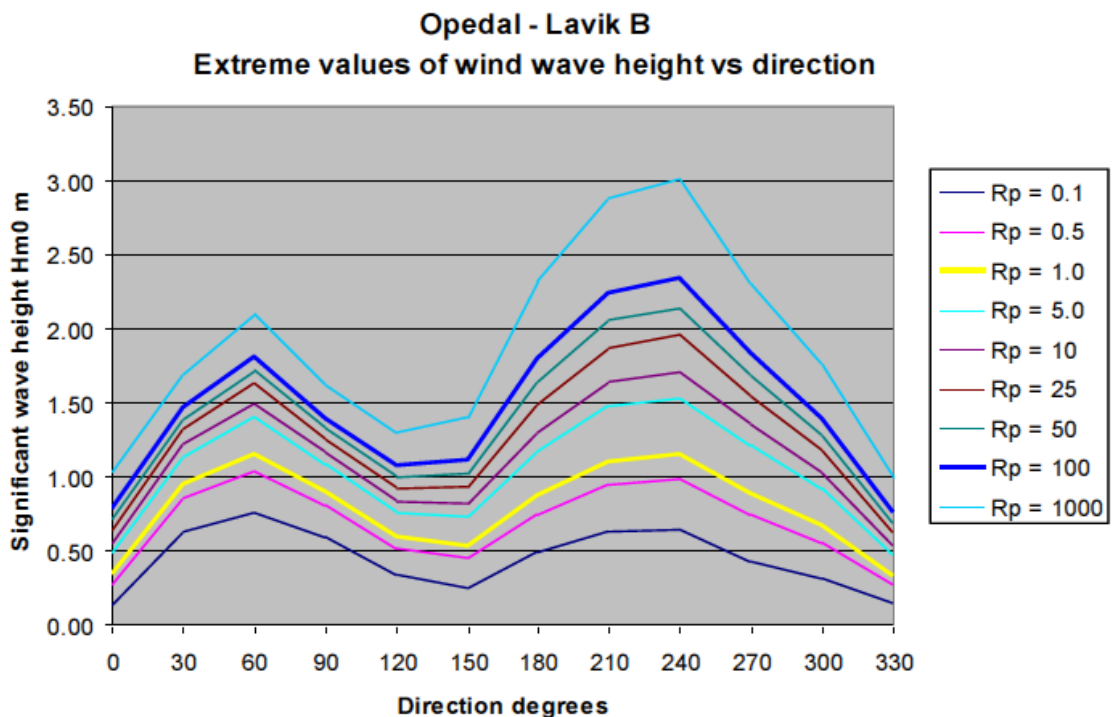


FIGURE 2-8 WIND WAVE HEIGHT FOR DIFFERENT DIRECTION DEGREES [25, P. 13]

2.5.4 Current Load

Currents in the fjord are also of importance for the design of the buoyancy bridge. The characteristics for the currents in the Sognefjord are given in Table 2-3 [12, p. 25].

TABLE 2-3 CHARACTERISTICS CURRENT SOGNEFJORD

Water depth [m]	Velocity outward [m/s]	Mean velocity [m/s]	Velocity inward [m/s]
Mid-fjord			
0-10	-1,06	-0,53	1,27
30	-0,55	0,26	0,48
75	-0,44	0,26	0,39
Shore line			
0-10	-0,86	-0,52	0,96
30	-0,49	0,25	0,43
75	-0,38	0,25	0,33

2.5.5 Tides

Tidal effect is assumed to cause a change in water level over the full fjord's width. For floating structures, this will yield a load on the bridge parts at the shores, where floating elements are connected to the land. The tides at Sognefjord for a 100-years return period is shown in Table 2-4 [13, p. 17].

2.5.6 Mass Density and Salinity

The mean seawater density is 1015 kg/m^3 . To account for salinity, a general 1,0% variation in the seawater density shall be applied. The specific weight is then $9858 - 10055 \text{ N/m}^3$ [3].

TABLE 2-4 TIDE EFFECTS AT SOGNEFJORD

	Parameter	Highest sea level [m]	Lowest sea level [m]
Normal	Lowest astronomical tide (LAT)	0.00	0.00
	Mean Sea level (MSL)	+1,20	+1,20
	Highest astronomical tide (HAT)	+2,39	+2,39
Design	Return period of 1 year	+2,61	-0,10
	Return period of 10 years	+2,88	-0,27
	Return period of 20 years	+2,97	-0,32
	Return period of 100 years	+3,05	-0,38

2.5.7 Temperature, Snow and Ice

The estimated air and water temperature for the Sognefjord are given in Table 2-5. The design values for the air temperature are retrieved from Eurocode 1991-1-5, for a return period of 50 years.

TABLE 2-5 TEMPERATURES AT SOGNEFJORD

	T_{min} [°C]	T_{max} [°C]
Air temperature at water surface	-20	32
Water temperature at water surface	0	20

The values indicate that additional load due to snow and ice will occur. The characteristic snow load on the ground for the crossing site is $2,5 \text{ kN/m}^2$ [3, p. 50]. The effect of snow will be neglected, because the traffic load is expected to be larger than the snow load and it is assumed that traffic load will not occur simultaneously with the governing snow load. Snow load on the pontoons will also be neglected, since it is expected that the load due to snow will be negligible compared to the self-weight of the pontoons.

In addition to snow falling in calm conditions, the effects of wind can also be considered. Wind may cause redistribution of snow, and in some cases, it also causes a partial removal of snow. Eurocode 1 does not cover additional wind loads due to the presence of snow.

In former feasibility studies and researches, the occurrence of ice in the fjord is not considered. The same assumption will be made for this preliminary study of the buoyancy bridge. However, it is recommended to check the effects due to ice in further development stages, since the formation of ice would induce unfavorable effects on the pontoons and anchoring system.

2.5.8 Traffic Load

In practice, a highway bridge is loaded in a very complex way by vehicles of varying sizes and groupings. In order to simplify the design process, this real loading is typically simulated by two basic imposed loads: a uniformly distributed load and an axle load, as shown in Figure 2-9, representing an extreme condition of normal usage.

In previous research, a load model was proposed for the buoyancy bridge. This model is based on Load Model 1 (LM1) of the Eurocode [14] and the Norwegian National Annex. A new load model was proposed, because LM1 is considered conservative for spans above 200 meters. As will be explained in chapter 2.6.3, at the middle of the bridge structure, clearance for the fairway of at least 400 meters in the width is required. This leads to a main span, which greatly exceeds 200 meters. For this reason, new load values were found after consulting the Norwegian National Annex and different feasibility studies. The proposed traffic [3] is shown in Table 2-6.

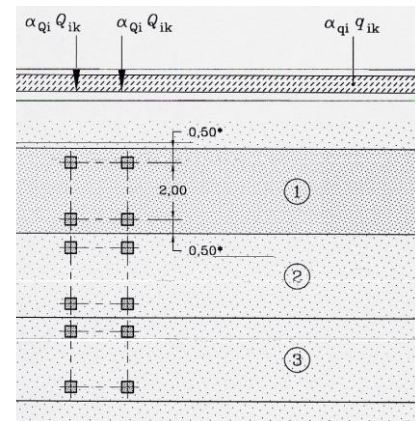


FIGURE 2-9 TRAFFIC LOAD MODEL

Horizontal loads caused by braking and acceleration forces of vehicles are normally taken into account by a longitudinal force [14]. The characteristic values, which also include dynamic effects, are given to be negligible of radii above 1500 meters. The radius of the horizontal arch of the bridge concept is 1.866 meters, as was shown in Table B-1. Therefore, the horizontal loads are neglected.

TABLE 2-6 PROPOSED VERTICAL TRAFFIC LOAD

Load Type	Area	Number of Lanes	Area per lane (m ² /m)	Load (kN/m)	Load (kN)
Uniformly Distributed Load	Traffic lane	2	3,5	35	-
	Pedestrian	1	3,5	3,5	-
Axle load	Traffic lane	2	-	-	1.200

2.6 Requirements

2.6.1 Design Life Span

The design life span of the fixed link shall be 100 years. Easily replaceable parts are allowed to have a shorter design life time of minimal 20 years.

2.6.2 Functional Requirement for Car Traffic

The fixed link is to provide enough capacity to meet requirements for the traffic situation in 2040. The proposed road section in Figure 2-10 fullfills the design basis and requirements [13]:

Annual average daily traffic : 4000 vehicles
 Design speed : 80 km/h
 Road class : S4, single lane in each direction
 Clearance height : 4,8 m

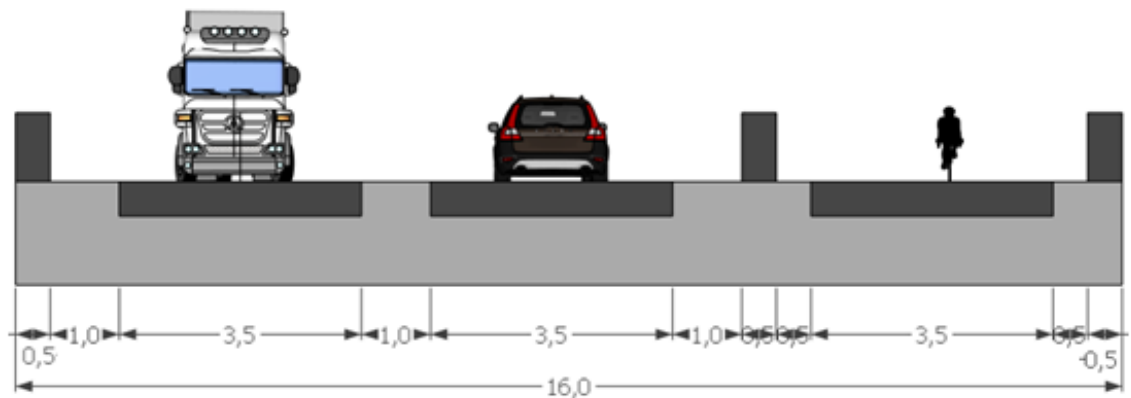


FIGURE 2-10 PROPOSED ROAD SECTION FOR BRIDGE CONCEPT [3]

Another requirement set by Zwarts & Jansma Architects, is to generate a new bridge concept, which will allow vehicle traffic flow without stoppage. This way, the travel time will improve the most compared to the current situation with ferry connections. This implies, that a bridge concept with movable bridge parts, which delays traffic, is not an option.

2.6.3 Functional Requirement for Ship Traffic leads to Large Mid-Fjord Span

At the middle of the crossing, a ship passage, big enough for large cruise ships should be realized. The clearance requirements are:

- Ship clearance in the fairway at the middle of the crossing
 - Width passage : 400 m
 - Height passage : 70 m
 - Draught : 20 m
- Clearance outside the fairway
 - Height : 8 m
 - Draught : 15 m

To fulfill this clearance requirement, a large distance has to be spanned at the middle of the crossing, which leads to one of the biggest challenges for this study.

2.6.4 Safety Requirement for Vertical Alignment Road

For the vehicle safety on the road class S4, there are requirements for the vertical alignment of the road [3]:

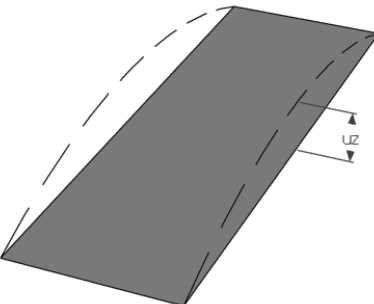
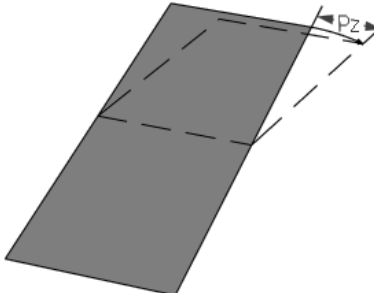
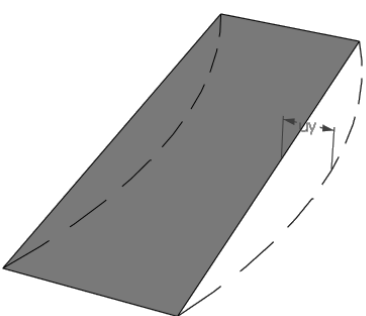
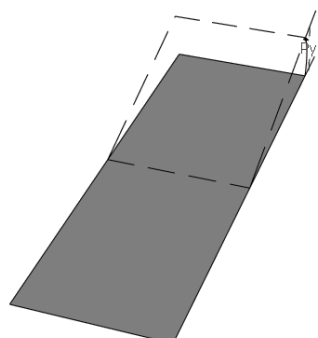
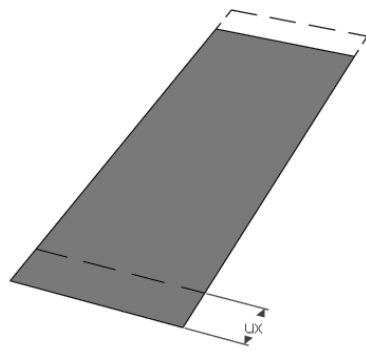
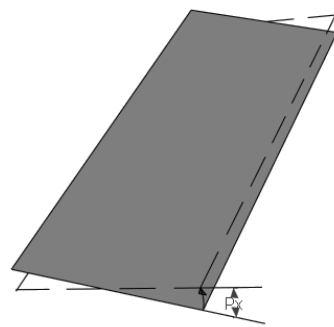
- Maximum gradient : 5%
- Minimal crest radius : 4200 m
- Minimal sag radius : 2100 m

2.6.5 Serviceability Requirements for Displacements and Accelerations

The buoyancy bridge is assumed to be a flexible structure, where movement will occur. As long as the rate in which the movements occur, large movements should also be acceptable. If the movement happens with little acceleration, the force will be very small. But a rapid rate of acceleration could result in a significant force, so the magnitude of the forces depends on the rates of acceleration. For this reason, acceleration limits for the bridge movement were determined in previous research [3].

Besides acceleration, displacement also influences the comfort and safety for users. The displacement and acceleration limits are shown in Table 2-7.

TABLE 2-7 DISPLACEMENTS AND ACCELERATION LIMITS FOR BRIDGE CONCEPT

Vertical deflection u_z		Lateral plane rotation ϕ_z	
	$u_z \leq L/350$ [m]		$\phi_z \leq 0,030$ [rad] or 1,72°
	$a_z \leq 0,7$ [m/s ²]		$\zeta_z \leq 0,050$ [rad/s ²]
Lateral deflection u_y		Vertical plane rotation ϕ_x	
	$u_y \leq L/350$ [m]		Break: $\phi_x \leq 0,025$ [rad] or 1,43°
	$a_y \leq 0,5$ [m/s ²]		Straight: $\phi_x \leq 0,050$ [rad] Or 2,84°
	Not considered		$\phi_y \leq 0,044$ [rad] or 2,52°
	$a_x \leq 0,5$ [m/s ²]		$\zeta_y \leq 0,107$ [rad/s ²]

2.7 Limitations

2.7.1 Considering Only Static Effects for Sufficient Approximation

Although dynamic wave and wind interactions pose threats to the usability of the buoyancy bridge, results from the research of Hermans [3] show that these effects are rather small. It is therefore assumed that considering only the static effects in this primary stage will be sufficient to reach a good approximation for the behavior and design concept.

A buoyancy bridge of this length and expected slenderness is a structure sensitive to wind. In further research stages, it should be given a more sophisticated treatment. It might involve wind tunnel testing and include the influence of the surroundings.

Long anchoring cables subjected to dynamic current and wave loading might be subjected to dynamic movement. This has a strong relation to the prestressing force, since the prestressing force influences the stiffness and Eigen frequencies. The possible dynamic behavior is not further taken into account in this study.

2.7.2 Effects due to Seismic Activity Not Considered

The seismic activity at this location has a return period of 10 000 years of about 3 m/s^2 [15]. However, since this bridge is floating, it is not in direct contact to the ground. This will reduce, if not eliminate the forced accelerations due to seismic activity. Bridge parts which are connected to the shore will be susceptible to seismic activity, but these bridge parts will not be regarded in this study.

In this preliminary study for the bridge concept, the effects due to waves, induced by seismic activity, is also not considered. This is an important aspect in further design phases.

2.7.3 Marine Growth not Regarded

Marine growth may influence the buoyancy of the bridge. Marine growth is assumed to develop on structural elements in the submerged parts and splash zone which extend to 3 meters below and 0,5 meters above the mean water line. This influence is however neglected in this study for the preliminary concept.

2.7.4 Effect of Passing Ships not Regarded

Ships that pass under the bridge will exert forces on the pontoons due to water movement. These movements involve return current, water level depression, ship wakes and propeller wash. These forces are however considered to be negligible compared to the environmental load. Furthermore, it is expected that the dynamic effects due to the passing of vessels will be negligible due to the small wave lengths compared to the pontoon's dimensions [3].

2.7.5 Accidental Loading not Regarded

Accidental actions may occur as a result of accidental situations. These situations include fire, impact or explosion. It is very difficult to quantify these effects. In many cases, it may be preferable to avoid the problem, for instance, by providing crash barriers to avoid collision from vehicles.

A possible collision between a vessel and a pontoon is an important issue. Modeling the effect of the collision requires careful modeling of plastic deformations of the vessel, the pontoon and the corresponding deformation of the bridge structure. This will not be regarded in this study.

2.7.6 No Fatigue Calculations

No fatigue calculations are done besides the static strength calculations in this study. Fatigue calculations are however very important, since fatigue damage is expected due to traffic load, environmental load, effects of passing ships, etc. Therefore, fatigue calculations should be done in further development stages of the bridge concept.

3. TO DESIGN THE SUBSTRUCTURE: METHODS AND ASSUMPTIONS

As discussed in chapter 1.6, first the substructure will be designed, which will maintain the (relative) displacements and rotations of the pontoons as much as possible. The methods and assumptions, which are used to design the substructure, are explained below. Also the information about the modeling of the substructure in Scia Engineer, can be found in this chapter.

3.1 Starting Points

For the buoyance bridge concept, a few starting points for the input are given below:

- the target bridge deck position (S-shape from the top view, see section B.2.2);
- the cylindrical pontoons shapes (see section B.2.8);
- the elevation of the bridge deck, resulting from the required clearance height of 70 meters above water level at mid span (see chapter 2.6.3);
- estimation of the main span at the middle of the fjord, resulting from the required clearance width of at least 400 meters (see chapter 2.6.3);
- roughly the layout of the anchoring system (see chapter 2.3.1);
- no stiffness and strength contribution of the bridge girder;

With these starting points, the design of the substructure can commence. The substructure consists of two parts: the anchoring cables and the pontoons. These two are interrelated, which leads to an iterative design process.

3.2 Method Pontoon Design: Mainly Ballast Stabilized

The main function of the pontoons is to provide the upwards buoyancy force (to resist all vertical loads on the bridge) and to provide a restoring bending moment (M_R) when rotation occurs. The cylindrical shape of the pontoons is comparable to floating spar platforms in the offshore, see Figure 3-1. The mechanism of the restoring moment of a cylindrical shaped pontoon is explained in Figure 3-2.

Because the effect of area moment of inertia is negligible compared to weight-buoyancy effect for vertical cylinders with deep draughts, the cylindrical pontoons are mainly ballast stabilized [16]. Therefore, during the design of the pontoons, all properties are assumed and the ballast is chosen as variable. With other words, as result of vertical loads, certain pontoon draughts/lengths are required. Apart from the ballast, all vertical loads are assumed. Then, the pontoon length can be expressed as a function of the ballast. For an overview of the pontoon design process, see Figure 3-3.

The rotational stiffness k_R is also expressed as a function of the ballast. The other properties which influence the rotational properties are all known and they are shown in Figure 3-3 with α . Then, the ballast can be decided by calculating the required restoring moment M_R when the pontoon is rotated by an angle φ due to external loads. The method of how this rotational stiffness of the pontoons is calculated is validated ANNEX C: Verification Calculation Method Rotational Stiffness Pontoons. In ANNEX D: Verification Restoring Moment Calculation, an example is given of the calculation of the restoring moment of a pontoon, and it is compared to the result of the mathematics software Maple.

With the calculated ballast height, the pontoon length can also be calculated and



FIGURE 3-1 OFFSHORE SPAR STRUCTURE

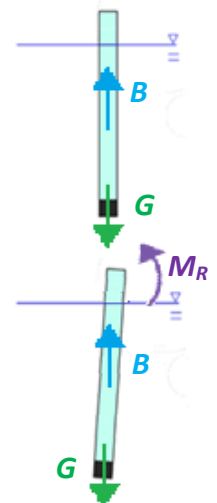


FIGURE 3-2 RESTORING MOMENT OF CYLINDRICAL PONTOON

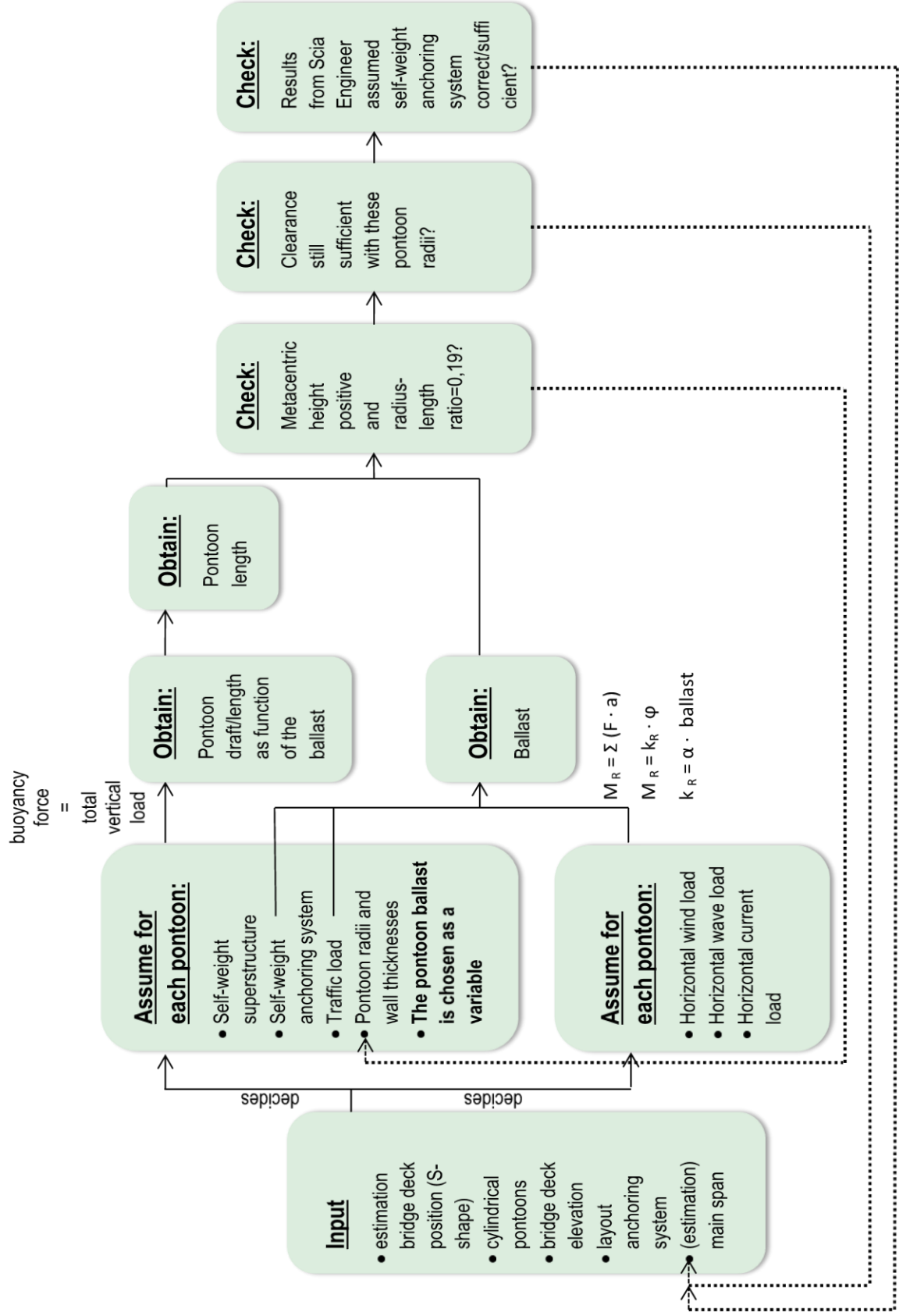


FIGURE 3-3 OVERVIEW PONTOON DESIGN PROCESS

pontoons can also be decided. For static stability, the metacentric heights must be positive. For dynamic stability, a metacentric height should be chosen which leads to a natural oscillation period of the pontoons that is much larger than the period of the water movements [17]. Deciding on the metacentric height (by varying the radius of the pontoon) becomes an issue of selecting a short, “fat” or a long “skinny” pontoon. In this feasibility study however, only static calculations will be done. Therefore, a conventional radius-draught ratio of existing offshore spar structures is used for the design of the pontoons. This ratio is approximately 0,4. In later design phases, the dynamic effects should be checked as well.

To obtain a radius-draught ratio of approximately 0,4 for every pontoon, the pontoon radii are adjusted. The calculation process is repeated until the desired radius-draught ratio is obtained for every pontoon (iteration).

Now the pontoons have new radii, the clearance width should be checked. In case the radii of the pontoons of the main span at the middle of the fjord have become so large that the clearance width requirement does not suffice anymore, the main span should then be enlarged. After changing the main span, the whole calculation process should be repeated again, since the vertical and horizontal loads on the pontoons are influenced by the span.

After the pontoon properties are obtained, which complies with positive metacentric heights, radius-draught ratios of approximately 0,4 and a sufficient clearance width, the resulting properties can be used to model the substructure in Scia Engineer and to test the effects. The calculated rotational stiffness of the pontoons and the calculated external (wave and current) loads (which depend on the dimensions of the pontoons) will be used in Scia Engineer. The modeling in Scia Engineer is further explained in chapter 3.4.

After the substructure (anchoring system and pontoons) is modeled in Scia Engineer, it can be investigated what part of the self-weight of the anchoring system is resisted by each pontoon. This might differ (significantly) from the initially assumed value. The pontoon properties should then be corrected and calculated again. The self-weight of the anchoring system is an important factor, since it is 31% of the total vertical loads acting on the pontoons (self-weight of the pontoons excluded). Again, iterations should be done to obtain pontoon properties which fulfill all requirements. The process should also be repeated in case results show that the strength of the anchoring cables is insufficient and consequently larger cables must be used. Then, the part of the self-weight of the anchoring cables acting on the pontoons will also change and an iteration process will follow again until all requirements are fulfilled.

These calculations were done in the mathematics software Maple. The calculations and descriptions are shown in ANNEX E: Pontoon Properties and Loads Calculation File.

3.3 Principle Modeling Restoring Moment as Rotational Spring

In Figure 3-2, it is shown how the restoring moment of the pontoon is generated. This restoring moment can be modeled as a rotational spring, as illustrated in Figure 3-4.

The rotational spring stiffness kr_{bu} can be considered as a linear spring for small rotations. It can be calculated with the equation below [17].

$$kr_{bu} = B \cdot MG$$

with

B = buoyancy force

MG = metacentric height

The metacentric height can be calculated with the equation below [17].

$$MG = \frac{I}{V_S} + GB$$

with

I = area moment of inertia relative to the y-axis (I_{yy}) of the plane intersected by the waterline

V_S = submerged volume of the pontoon

GB = Distance between center of gravity (green dots in figure) and center of buoyancy (blue dots in figure)

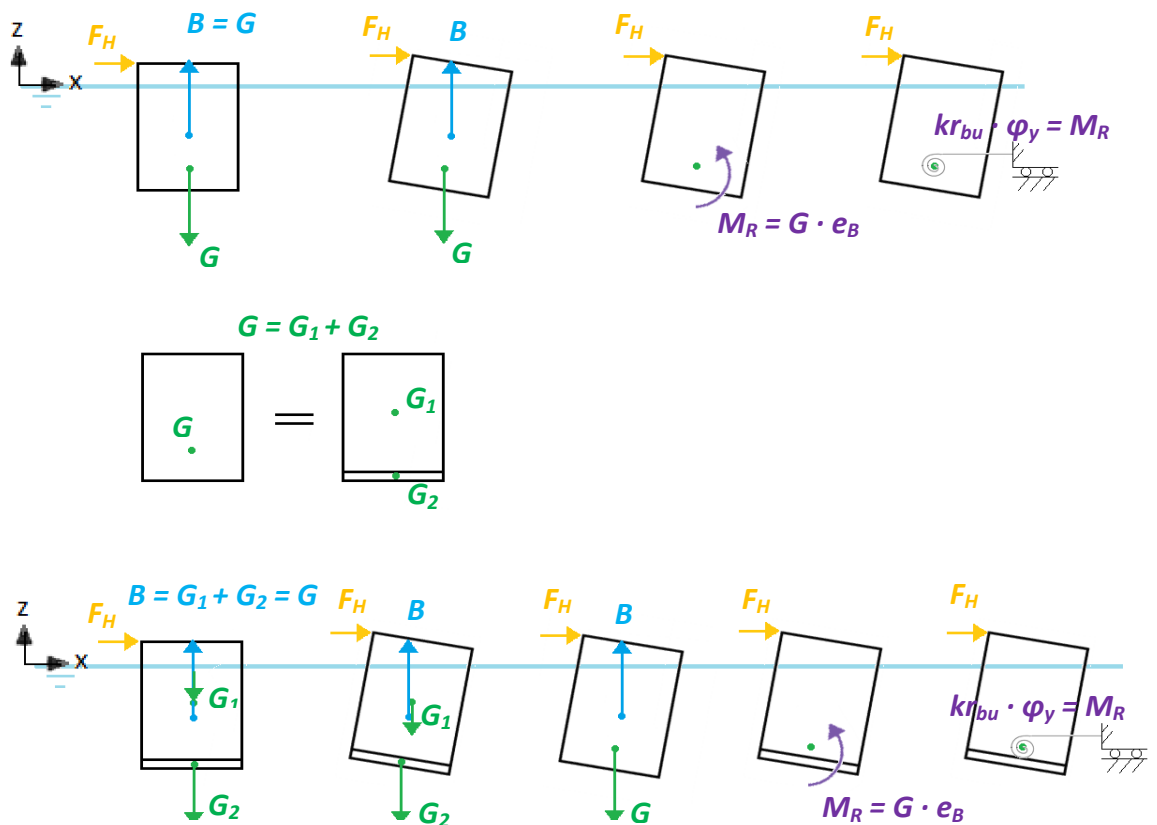


FIGURE 3-4 RESTORING MOMENT GENERATED BY THE SELF-WEIGHT OF (ALL PARTS OF) THE PONTOON

As can be seen in Figure 3-4, the restoring moment is generated by the force couple (the total self-weight and the buoyancy force).

3.4 Method Anchoring System Design

3.4.1 Anchoring System Design: Erection Method of Great Importance

The anchoring system is analyzed with the help of the structural analysis software Scia Engineer. Before modeling, good understanding of cable analysis should be obtained. Some basic knowledge about it is summarized in ANNEX F: Introduction Modeling Cables in SCIA Engineer.

For analyzing the anchoring system in Scia Engineer, there must already be a good idea present about the erection. For the erection of the buoyancy bridge, it is preferred not to use mechanical pretensioning for the anchoring cables, but to induce tension in the cables by using the self-weight of the cables, the self-weight of the pontoons and the buoyancy of the pontoons alone. This way, good use is made of the buoyancy property of the pontoons during the erection phase, besides the use phase.

Since the tension in the anchoring cables is only to be caused by the self-weight of the structure and not by mechanical pretensioning, the input method of the model into Scia Engineer is of great importance. In this case, the erection method should then also be simulated in Scia Engineer to obtain the resulting tension in the anchoring cables.

Few erection methods were considered, which are described below in short. Erection method 3 is used for the proposed anchoring system.

Erection Method 1: Submerged anchoring of main cables and involving de-ballasting and mechanical pretensioning

This erection method involves anchoring the main cables under water. Extra temporary ballast is added in the pontoons to make the pontoons sink to a lower position. Thereafter, the transversal anchoring cables are connected to the pontoons which will cause the pontoons to sink to an even lower position. (See chapter 4.2 for definition 'transversal cable' and explanation about the layout of the anchoring system). By removing the temporary ballast again ("de-ballasting"), the pontoon will rise again, stretching the anchoring cables and thus increasing the tension in the cables.

This erection method was applied in the modeling of the example substructure, illustrated in chapter 4. This substructure was modeled to obtain a better understanding and sense about the system. To investigate the influence, also mechanical pretensioning was used in this example.

This erection method is however considered not to be the most efficient and practical method, since the main cables are to be anchored below water level. Moreover, as explained earlier, it is desired to avoid mechanical tensioning.

Erection Method 2: Anchoring of main cables at water level and involving de-ballasting

This erection method is similar to execution method 2. However, in this case, the main anchoring cables are not supported (100 meters) under water, but at water level for practical reasons. Moreover, no mechanical pretensioning is applied. This will facilitate the erection.

This erection method is described and investigated extensively in ANNEX G: Erection Method Involving De-ballasting. Results showed that this method was not effective, see the Annex for the results.

Erection Method 3: Anchoring of main cables at water level (recommended)

This method is proposed for the erection of the buoyancy bridge. Therefore, this is also the erection method which is modeled in Scia Engineer for the proposed anchoring system, see chapter 6. The erection phases for this method are illustrated in Figure 3-5. The phases in the figure can be explained as follows:

0. The pontoons are constructed. At the fabrication site, the bottom part of the pontoons can be fabricated first. For now it is proposed to use concrete pontoons. This bottom part will have the shape of a caisson which is able to float on the water. Step by step, the upper parts of the pontoon will be casted as well and ballast will be added in the pontoon. However, not the whole amount of the final ballast will be added. Only a part of the ballast will be placed into the pontoons, so that the connection points between the pontoons and anchoring cables are located exactly at water level.

An advantage is that this fabrication can take place on/near site. Then, the pontoons can be transported over water to the final positions.

1. The finished pontoons are brought into position as shown in the top view in Figure 3-6. The anchoring cables will be placed at water surface in a configuration close to the top view shown in Figure 3-6 (some cables are slightly curved, instead of straight as shown the figure. See ANNEX I: Cable Length Check for Avoiding Mechanical Pretensioning for comparison cable length and cable spans). The main cables are anchored at water level at shore. The transversal cables are connected to the main cables and the pontoons. The cables are brought into this position on water surface by using temporary buoyancy elements. At the middle of the fjord, the cables will sag into the water to create a clearance of 400 meters wide and 20 meters deep for passing vessels. However, to simplify the modeling in this preliminary study, it is assumed that all anchoring cables are located at water level in this phase, including the cables at the middle of the fjord. The anchoring cables will be connected to the pontoons in this phase.
2. Hereafter, the temporary buoyancy elements are removed, causing the anchoring system to sink into the water. Due to the self-weight of the anchoring cables, the pontoons will also sink to a certain depth. This vertical displacement is different for every pontoon, it varies from 0,7 to 3,3 meters.
3. In this phase, extra ballast will be added to the pontoons. The amount of ballast varies for each pontoon and should be determined separately. The purpose is to add such an amount of ballast to the pontoons, so that at the end of the next phase, the connection points between the anchoring cables and pontoons will be located at approximately 15 meters below water level.
4. In this phase, the superstructure is installed on top of the pontoons. After the installation, it is expected that the pontoons will have sunk again and the connection points between the anchoring cables and the pontoons will be located at approximately 15 meters below water level.
5. In practice, the connection points will seldom end up at exactly 15 meters at the end of phase 4. Therefore, the last part of the final ballast will be added in this phase to regulate the pontoon elevation in water. Ballast will be added to the pontoons until each of them are positioned in the water in such a way that at the end of the erection, the connection points between the pontoon and anchoring cables are located at 20 meters below water.

This erection method was investigated thoroughly. This sub study is included in ANNEX H: Erection Method with Anchoring Cables at Water Level at Start.

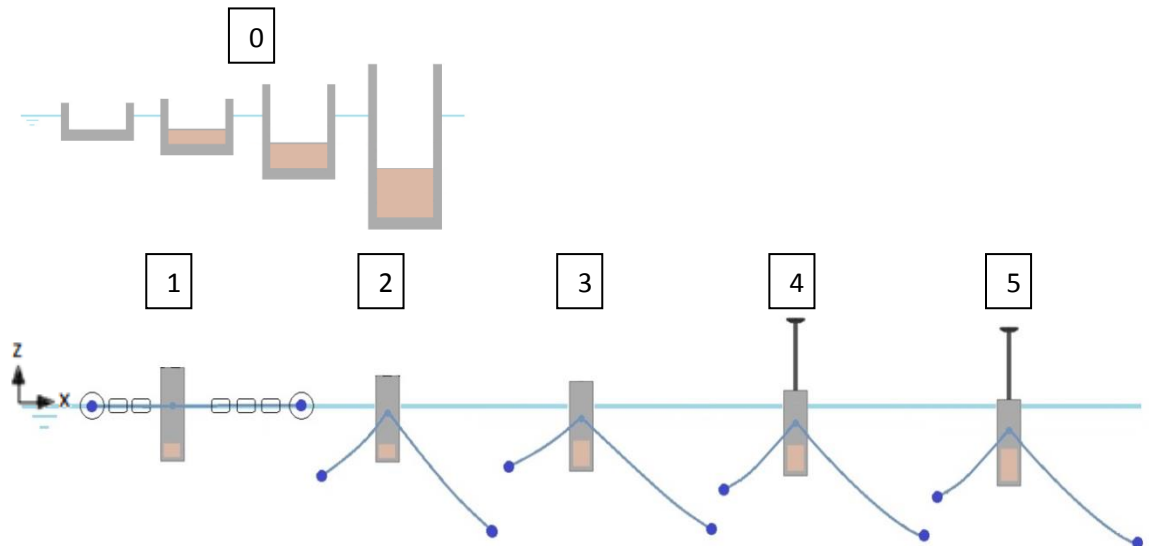


FIGURE 3-5 ERECTION METHOD 3: ERECTION PHASES

Recommendation: It is assumed that the ballast has a density of 2000 kg/m^3 . However, water could also be used as ballast, since sufficient water is available at the site. A disadvantage is that the density of water is lower than 2000 kg/m^3 . This will probably lead to larger pontoon sizes. This option can be further investigated.

3.4.2 Modeling the Erection Method in Scia Engineer

Special attention is paid to modeling the substructure into Scia Engineer. Since the tension in the anchoring cables is only to be caused by the self-weight of the structure and not by mechanical pretensioning, the modeling method is of great importance. Every different way of modeling will lead to a different final configuration of the substructure due to self-weight and to different values for the tension in the anchoring cables, consequently resulting in a different transversal stiffness of the buoyancy bridge against horizontal loads in the direction along the fjord.

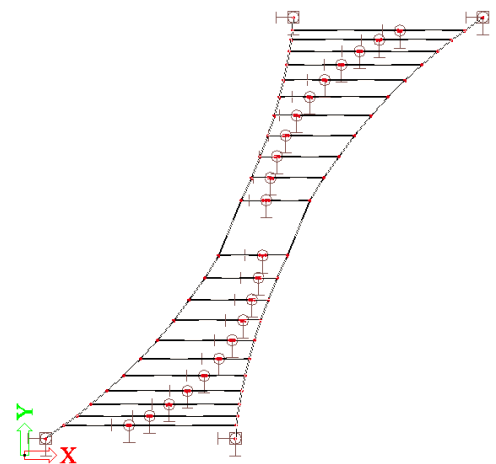


FIGURE 3-6 POSITIONING CABLES AT WATER SURFACE AT ERECTION PHASE 1

Erection method 3 from the previous section is modeled as will be illustrated and described in the following. The erection phases in Figure 3-7 coincides with the phases shown in the previous section (3.4.1).

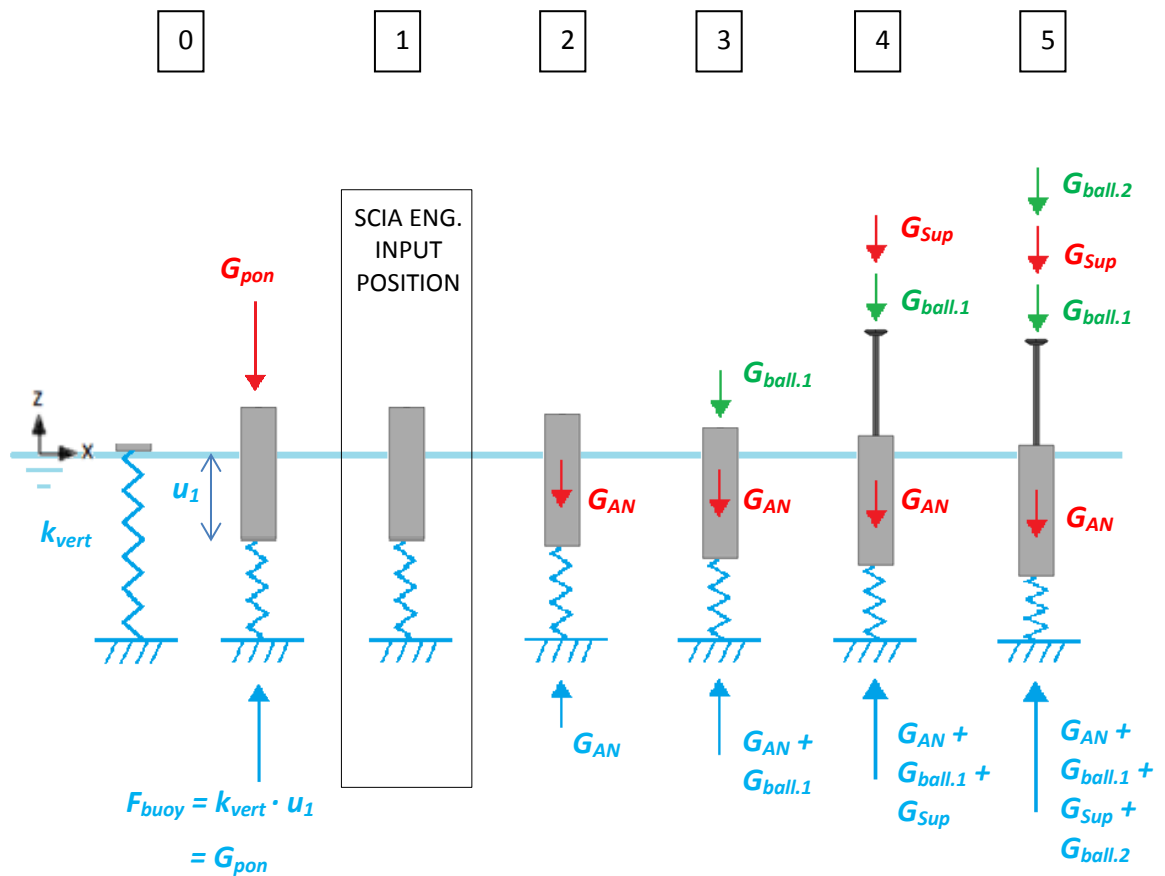


FIGURE 3-7 MODELING THE ERECTION PHASES IN SCIA ENGINEER

The origin of the coordinate system is located at the same height as the water level.

k_{vert} = spring stiffness which represents the buoyancy of the pontoon

$$= \rho_w \cdot g \cdot \pi \cdot r_{pontoon}^2$$

G_{pon} = self-weight of the pontoon including a part of the final ballast. Due to the self-weight, the pontoon sinks to a certain depth. This is taken into account in the Scia Engineer model by modeling the pontoon at that certain depth with respect to the water level.

G_{AN} = self-weight of the anchoring system

$G_{ball.1}$ = self-weight of the ballast which will be added to the pontoons in erection phase 3. This part of the ballast varies for each pontoon. At the end of phase 4, the connection point between the anchoring cables and the pontoons will be positioned at 15 meters below water level due to the self-weight of this part of the ballast, the self-weight of the anchoring system and the self-weight of the superstructure.

G_{Sup} = self-weight of the bridge superstructure (pylons and bridge girder)

$G_{ball.2}$ = self-weight of the ballast which will be added in the last erection phase. The purpose of applying this ballast is to regulate the vertical position of the pontoon. At the end of erection

phase 5, the connection point between the pontoons and anchoring cables should be at 20 meters below water level for every pontoon. (Example: in case the connection point already appears to be located at 20 meters below water level, then $G_{ball,2} = 0$.)

At the end of erection phase 5, the completed structure is modeled. Hereafter, the external loads can be applied to the model to investigate the effects.

3.4.3 Scia Engineer Modeling Details

Nodes and Members in Scia Engineer

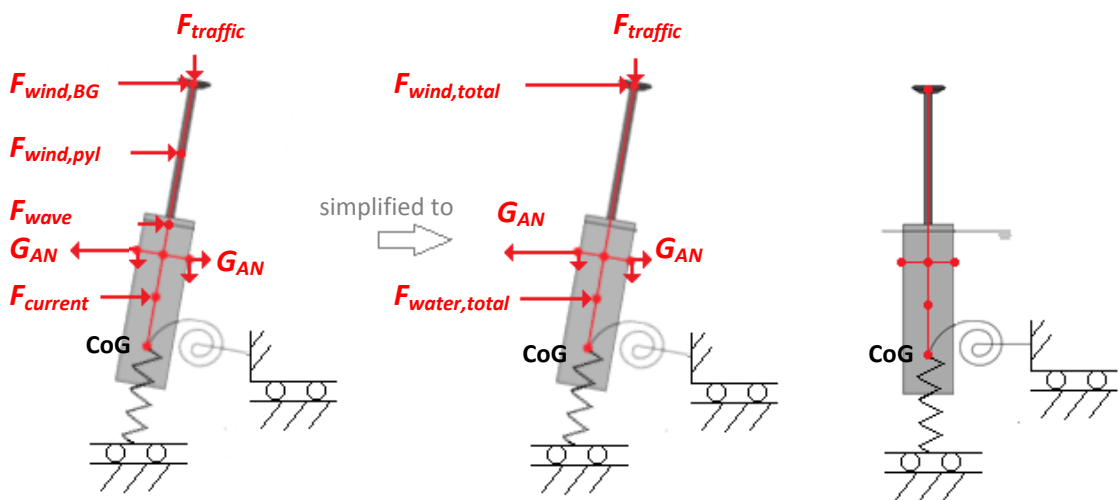


FIGURE 3-8 APPLIED EXTERNAL LOADS TO INVESTIGATE THE ROTATIONS IN SCIA ENGINEER

The nodes and members which are modeled in Scia Engineer are shown in Figure 3-8. As can be seen, a simplification of the loads has been made. All wind loads are concentrated into one point at the bridge girder (BG) and the wave load and current load are concentrated at one point as well.

It can also be seen that the self-weight of the superstructure and substructure are not inserted into the model to check the rotation of the pontoon. Only the loads shown in Figure 3-8 are inserted to check the rotations. This is because of the fact that the self-weight of the structure does not have a negative impact on the second order effects.

As was explained before in section 3.3 and in Figure 3-4, the restoring moment is generated by the force couple consisting of G (total self-weight) and B (buoyancy force). The restoring moment has a positive impact on the second order effects. Since it is considered that the self-weight of the structure and the buoyancy force have a restoring effect, the second order effects of these loads are not modeled when investigating the rotations.

Self-Weight of Structure taken into Account for Vertical Displacements

As could be seen in Figure 3-7, the self-weight of the superstructure and parts of the ballast should be taken into account to investigate the vertical displacements during the erection phases. To investigate the effects of these self-weights on the vertical displacement, these loads are applied at the center of gravity (CoG). This way, the effect of the self-weight of the superstructure and parts of the ballast on the vertical displacements can be investigated without affecting the rotations.

Modeling of the Erection Phases is Simplified

The modeling of the erection phases was shown in Figure 3-7. The nodes, members and supports of the Scia Engineer model could be seen in Figure 3-8. It should be noted, that the rotational spring stiffness is actually not constant for the erection phases. As was explained earlier in section 3.3 and Figure 3-4, the rotational spring stiffness is determined by the force couple total self-weight and buoyancy force. However, the self-weight of the structure changes during the erection. At erection phase 1, only the self-weight of the pontoon and part of the final ballast are present. At phase 3, 4 and 5, self-weight of the superstructure and parts of the ballast are added. In reality, the rotational stiffness is different in these phases. However, to simplify the modeling in this preliminary study, this effect is neglected. In further design phases, the erection should be modeled more in detail.

Asymmetric Ballasting to Compensate Rotational Symmetric Anchoring System

Due to the self-weight of the anchoring cables, the pontoons rotate. This can be seen in Figure 5-4, where the rotations of an example substructure are shown when it is subjected to its self-weight. When horizontal environmental loads are added as well, the rotations become even larger, exceeding the allowed rotation of the bridge deck, see Figure 4-12 for the rotations of the example substructure when loaded by self-weight and horizontal loads.

For the proposed substructure in chapter 6, it is assumed that this eccentricity is compensated by applying ballast in such a way, that the rotations due to the self-weight of the substructure will be equal to (approximately) zero mrad.

3.4.4 Anchoring System Design Process

The top view of the anchoring system was shown in Figure 3-6. This anchoring system will provide the buoyancy bridge resistance against displacements along the direction of the fjord (x-direction). The design of the anchoring system is mainly done with the use of the structural analysis software Scia-Engineer. To input the anchoring system into Scia Engineer, several assumptions are made. Results are then evaluated and the input is then adjusted accordingly. In Figure 3-9, the anchoring design process is shown.

For the input in Scia Engineer, the following assumptions are made: the cable spans, the cable dimensions, the spring stiffness's and the anchoring cable elevations, which depend on the erection method. This inputted model will then be subjected to several load cases, including a load case with only the self-weight of the structure and load cases with also external loads (wind, water, traffic). The magnitude of these external loads are approximated by calculations made in Maple, see ANNEX E: Pontoon Properties and Loads Calculation File.

These load cases will cause a certain configuration of the anchoring cables, stresses in the cables and of course, displacements and rotations will occur. The resulting stresses should not exceed the capacity of the cables for any load case. The displacements and rotations of the pontoons should also be evaluated. In case the stresses and displacements are too large, the cable dimensions can be adjusted; larger cables can then be used. By using larger cables, the stresses in the cables will decrease. Due to the larger dimensions, the self-weight of the anchoring cables will increase, which will result in a larger tension force. With more tension in the anchoring system, the displacements will be limited.

Enlarging the anchoring cables must however be done with care. Larger anchoring cables will increase the load on the pontoons. Larger pontoons will be needed then, which will consequently lead to larger water loads acting on the pontoons. Therefore, iterations are done to reach a suitable cable size. Different models of the anchoring system can be seen in Annex I, J, L, M, N, and O.

The purpose is to design an anchoring system which requires no mechanical pretensioning to facilitate the erection. This is the case if the initial cable lengths are larger than the cable spans. If the initial cable length is smaller than the span, then it is needed to mechanically pretension the cable. The input should then be varied again to obtain an anchoring system which requires no mechanical pretensioning. The cable length check for the proposed substructure in chapter 6 is included in ANNEX I: Cable Length Check for Avoiding Mechanical Pretensioning. For the proposed substructure, indeed no mechanical pretensioning is needed.

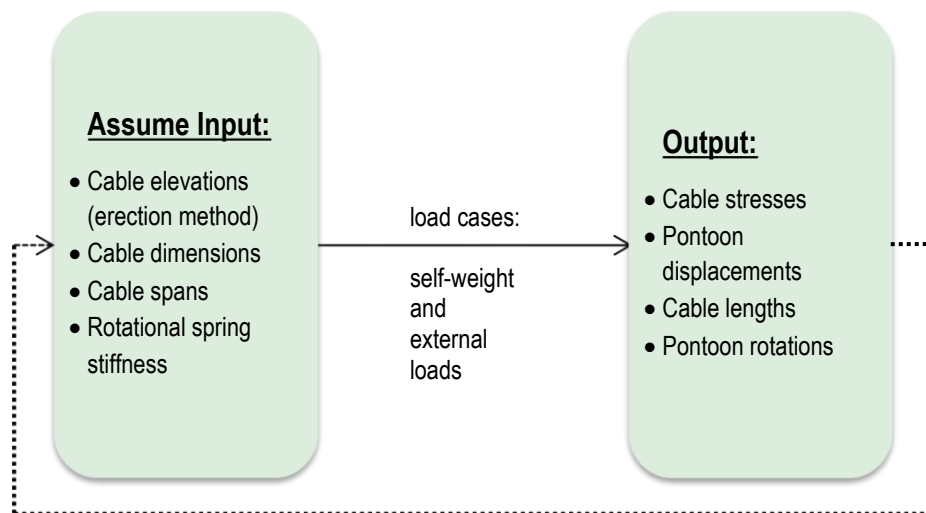


FIGURE 3-9 DESIGN PROCESS ANCHORING SYSTEM

3.5 Close Interrelation between Pontoon and Anchoring System Design

Although the pontoon and anchoring system designs were discussed separately in the previous sections (respectively section 3.2 and 3.4), the design of these two parts are closely related. This is shown in Figure 3-10.

The output from the calculation file for the pontoon design (see ANNEX E: Pontoon Properties and Loads Calculation File) are used for the design of the anchoring system. For example, the rotational spring stiffness of the pontoons is inputted in the model in Scia Engineer to design the anchoring system. Hereafter, the model in Scia Engineer is subjected to loads, which are also calculated in the Maple calculation file (the loads are dependent on the pontoon sizes and the estimated superstructure size). Hereafter, the results from Scia Engineer from the anchoring system design are to be used for the pontoon design again. For instance, the self-weight of the anchoring system influences the design of the pontoons. The heavier the anchoring cables are, the larger the pontoons have to be. An iteration process follows for the design of the pontoons and anchoring system.

In Scia Engineer, certain positions of the pontoons and cables were inputted. These positions are approximately the positions of the pontoon and cables in erection phase 1 (see Figure 3-6). Due to the self-weight, the pontoons and cables displace. Hereafter, the structure will be loaded by external loads (which are calculated in Maple). Therefore, the loads which are calculated in Maple, should be based

on the configuration of the structure, which is already loaded by its self-weight. These positions of the displaced pontoons due to self-weight are obtained by modeling in Scia Engineer. So for an accurate calculation, iterations should be made. However, since the pontoon displacements are relatively small compared to the dimensions of the structure, this iteration is not done for the preliminary study. For the calculations in Maple, it is assumed that the pontoons are positioned in the target S-shape. The small differences between the positioning of the pontoons inputted in the Maple calculations and in the model of Scia Engineer are neglected.

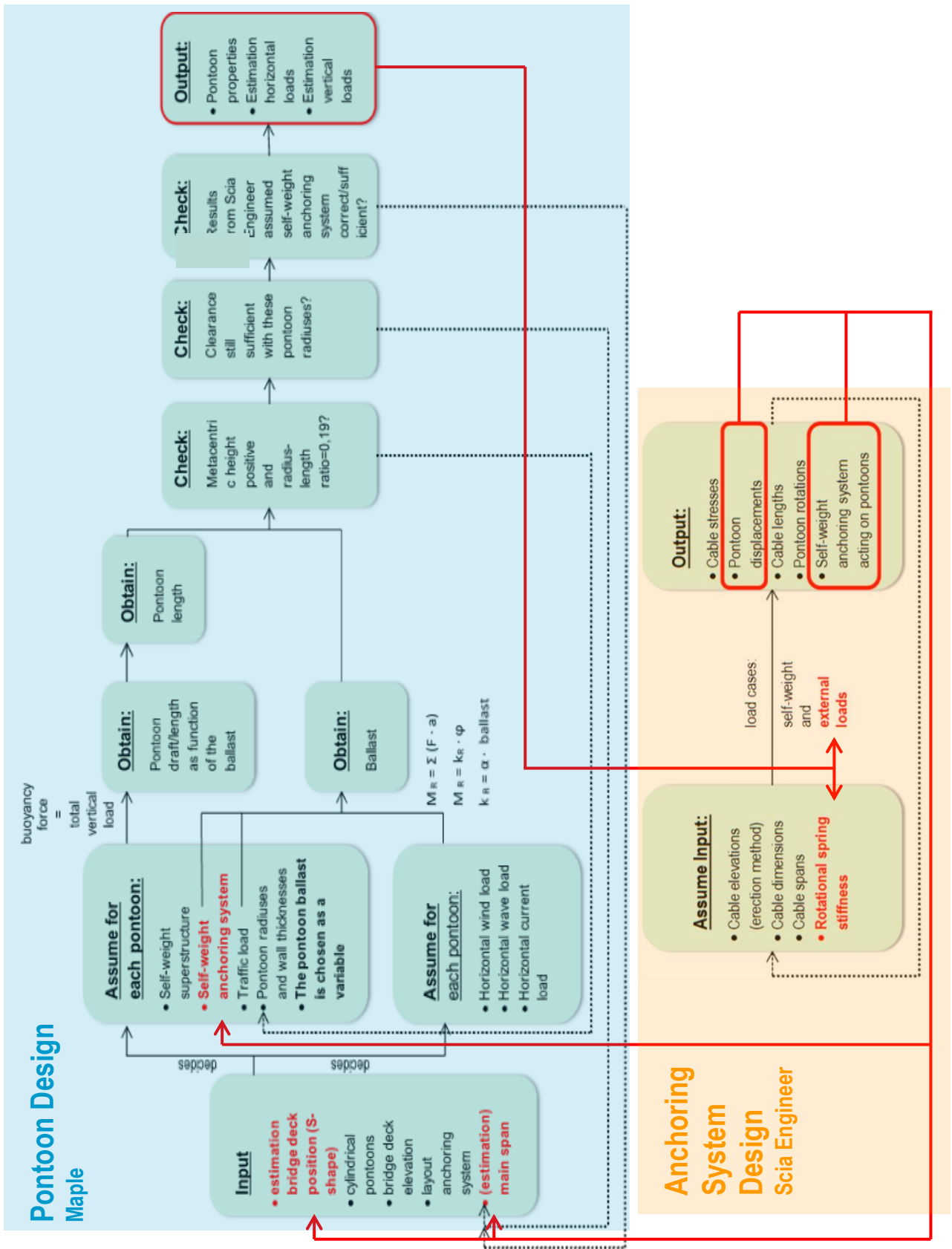


FIGURE 3-10 INTERRELATED PONTOON AND ANCHORING SYSTEM DESIGN

4. EXAMPLE SUBSTRUCTURE

In chapter 3, the design method of the substructure was explained. In this section, an example of a possible substructure is presented. By reviewing the properties and results of this example, good understanding and feeling about the behavior of the substructure can be obtained. This example differs slightly from the proposed substructure. The proposed substructure is presented in chapter 6.

4.1 Introduction

In general, the superstructure of a separate pontoon floating bridge must be of sufficient strength and stiffness to resist horizontal and vertical forces and to maintain the relative position of the pontoons. However, if an anchoring system was designed, which maintains the relative position of the pontoons as much as possible, the required strength and stiffness of the superstructure will be smaller.

For the new buoyancy bridge concept, a horizontal suspension anchoring system will be used. By anchoring all pontoons, the stresses on the bridge superstructure will be minimized, allowing a slender superstructure. The complete argumentation for this type of anchoring system can be found in chapter 2.3.1.

In sections Annex I to Annex N, different properties of the anchoring system are researched with the use of the structural analysis software Scia Engineer. In Annex F, an introduction to modeling cables in Scia Engineer is given. The analysis of this example of the anchoring system is reported in ANNEX R: Computational Model Substructure Example 5. In this annex the properties, input data for the modeling, computational results, strength checks and validation checks can be found.

In this chapter, the discoveries which were found during the research about the anchoring system, are shown. These include the properties of the anchoring cables, the pontoons, the load capacity of the anchoring system and recommendations.

4.2 Lay-Out Anchoring System with pontoons

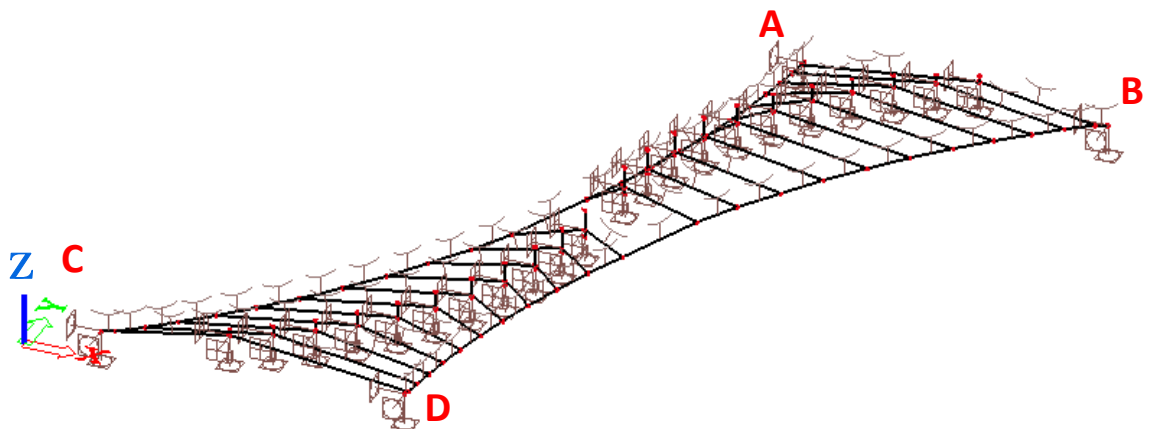


FIGURE 4-1 ANCHORING SYSTEM MODELED IN SCIA ENGINEER

The model of the anchoring system is shown in Figure 4-1. The two main cables are fixed from shore (AB) to shore (CD) at 120 meters below water level, which is located at +5 meters above NAP; one

main cable is fixed from A to C and the other is fixed from B to D. The distance between the shores is 3507 meters.

44 lateral anchoring cables are attached between the main cables and 22 pontoons, which are placed in an S-shape from the top view. A top view is shown in Figure 4-2. The superstructure of the buoyancy bridge will be placed on top of these pontoons. The anchoring system is rotational symmetric.

All lateral anchoring cables are attached to the pontoons at 20 meters below water level. The main span in the input position of the model is 430 meters.

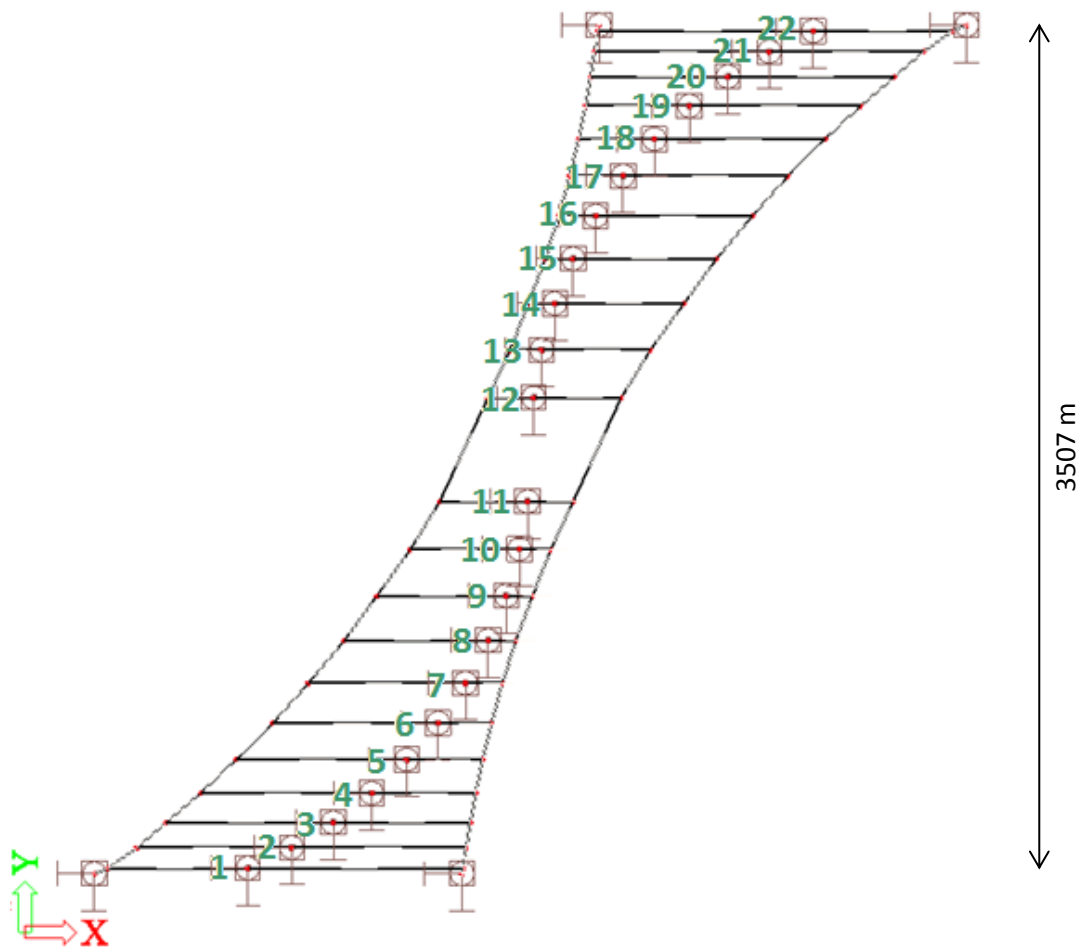


FIGURE 4-2 TOP VIEW ANCHORING SYSTEM WITH PONTOON NUMBERING

Optional: omit the pontoons and lateral anchoring cables near the shore

The maximum water depth at the middle of the fjord is 1248 meters (see Figure 2-3 for a cross-section of the Sognefjord at the location of the buoyancy bridge). Due to this vast water depth and soft bottom, supporting the bridge structure on buoyancy elements is probably an efficient solution. However, near the shores, the water depths are smaller and rock bottoms are present. For instance, the distance from the shore to the first pontoon is 23 meters. At this distance, the water depth is still small. It is possible that at this location, supporting the bridge structure on foundations in the rock

might be economically more favorable than using buoyancy elements. In the next design phases, this could be investigated. In case the pontoons near the shore will be replaced by columns founded on rock, the lateral anchoring cables near the shores connected to those removed pontoons can then also be removed. It is expected that removing the pontoons and lateral anchoring cables near the shore will have little effect on the rest of the anchoring system.

4.3 Anchoring Cable Properties

Cable Properties and Dimensions

Steel Y1860 anchoring cables are used with material properties shown below.

Y1860

Tensile strength : 1860 N/mm²
 Modulus of Elasticity : 195 000 N/mm²
 Reduced unit mass in water : 7850 – 1015 = 6835 kg/m³

Diameter main anchoring cable : 1200 mm
 Diameter lateral anchoring cable : 350 mm

It is assumed that the lateral anchoring cables are attached to the outsides of the pontoons.

Cable Lengths

The cable lengths are given in Table 4-1. The numbering of the cable members is specified in Figure 4-3.

TABLE 4-1 ANCHORING CABLE PROPERTIES

Anchoring cable	Length (m)
main	4205
B72	361
B73	200
B74	445
B75	152
B76	528
B77	138
B78	587
B79	141
B80	640
B81	170
B82	674
B83	228
B84	697
B85	314
B86	699
B87	426
B88	682
B89	561
B90	632
B91	713
B92	569
B93	881

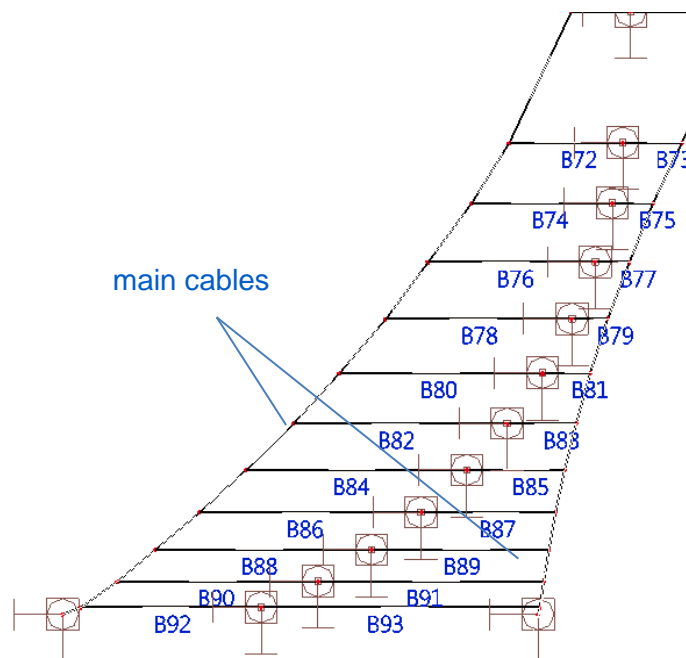


FIGURE 4-3 NUMBERING OF HALF OF THE LATERAL ANCHORING CABLES AT THE BOTTOM

Prestressing in the Anchoring Cables

The anchoring cables are prestressed by their own self-weight. An additional tensioning force of $24,6 \cdot 10^3 \text{ kN}$ is also applied to the main anchoring cables (see R.3.4). This leads to the internal forces in the cables, which are shown in Table 4-2. To facilitate the construction, additional pretensioning in the lateral anchoring cables is avoided.

TABLE 4-2 INTERNAL TENSION FORCES IN THE ANCHORING CABLES

	Internal tension force due to self-weight (kN)	Additional tensioning force (kN)	Internal tension force due to self-weight and additional pretensioning (kN)
main cable	$662,8 \cdot 10^3$	$24,6 \cdot 10^3$	$687,4 \cdot 10^3$
lateral cable	$50,8 \cdot 10^3$	0	$51,8 \cdot 10^3$

4.4 Pontoon Properties

The concrete pontoons are cylindrical shaped, containing ballast, as shown in Figure 4-4. The pontoon length, thickness of the bottom, ballast height and anchoring depth (from the top of the pontoon) are different for every pontoon. These values are shown in Table 4-3. Since the system is rotationally symmetric, the properties of half of the pontoons are given in the table. The pontoon numbering is shown in Figure 4-2.

The following properties are the same for every pontoon:

Pontoon radius	: 15 meters
Thickness top	: 1,0 meter
Thickness sides	: 1,5 meters
Density concrete	: 2500 kg/m^3
Density ballast	: 2000 kg/m^3

It should be remarked, that the properties in Table 4-3 are based on the superstructure from previous studies [3]. Since a new superstructure for the buoyancy bridge will be designed, it is expected that the final (required) pontoon properties, which will belong to the final proposed superstructure, will be different. However, to obtain an estimation about the loads on the pontoons, these pontoon dimensions and properties were used.

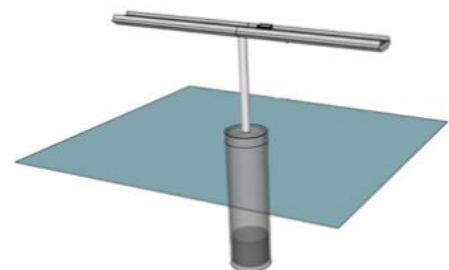


FIGURE 4-4 LAY-OUT PONTOON [3]

TABLE 4-3 PONTOON DIMENSIONS

Pontoon number	Length (m)	h_{ballast} (m)	t_{bottom} (m)	$d_{\text{anchoring}}$ (m)
1	43	6,7	1,86	23,8
2	70	13,6	2,40	24,3
3	79	16,1	2,59	24,4
4	90	19,1	2,80	24,5
5	99	21,6	2,98	24,6
6	110	24,5	3,19	24,7
7	118	26,8	3,35	24,8
8	129	30,2	3,58	24,8
9	124	28,4	3,48	24,9
10	143	34,2	3,86	24,9
11	181	44,3	4,63	25,6

4.5 Load Capacity

The proposed anchoring system is designed to be able to resist the following loads:

- self-weight anchoring system
- self-weight pontoons
- self-weight superstructure
- vertical traffic load
- horizontal wind load
- wave and current load
- Bending moment due to eccentric traffic

The total values for these loads are given in Table 4-4. (The loads acting on each pontoon can be found in the more detailed section R.1.5 from ANNEX R: Computational Model Substructure Example 5.) The calculation of these loads can be found in ANNEX S: Calculation File Pontoon Properties and Loads.

TABLE 4-4 TOTAL LOADS THE ANCHORING SYSTEM CAN RESIST

	Total load	Proportion per direction
Self-weight anchoring system	$0,77 \cdot 10^6$ kN	4 %
Self-weight pontoons	$15,1 \cdot 10^6$ kN	87 %
Self-weight superstructure	$1,43 \cdot 10^6$ kN	8 %
Vertical traffic load	$0,79 \cdot 10^5$ kN	1 %
Total vertical loads	$17,4 \cdot 10^6$ kN	100 %
Horizontal wind load	$62,0 \cdot 10^6$ kN	73 %
Wave and current load	$22,4 \cdot 10^6$ kN	27 %
Total horizontal loads	$84,4 \cdot 10^6$ kN	100 %
Bending moment due to eccentric traffic	$472 \cdot 10^3$ kNm	

4.6 Displacements and Rotations

The deformed structure by self-weight is shown in Figure 4-5 and Figure 4-6.

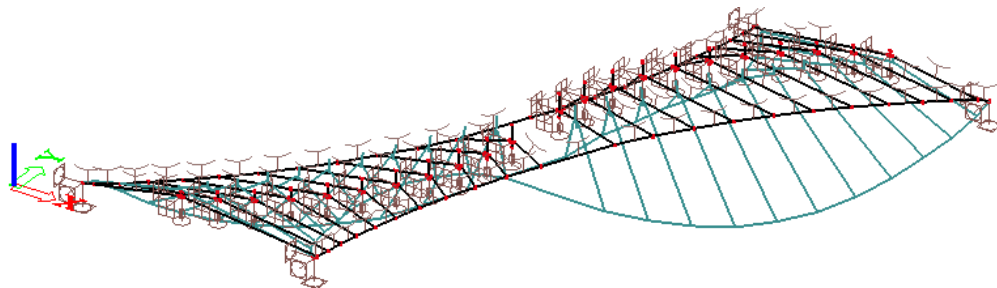


FIGURE 4-5 DEFORMED ANCHORING SYSTEM IN 3D

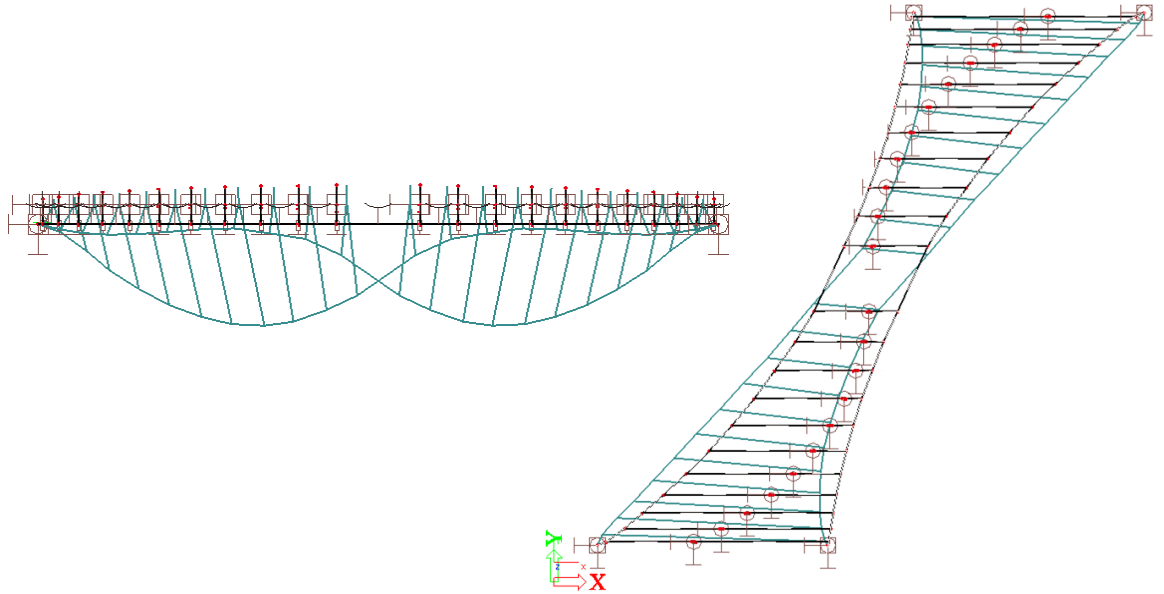


FIGURE 4-6 DEFORMED ANCHORING SYSTEM IN Y-Z PLANE (LEFT) AND X-Y PLANE (RIGHT)

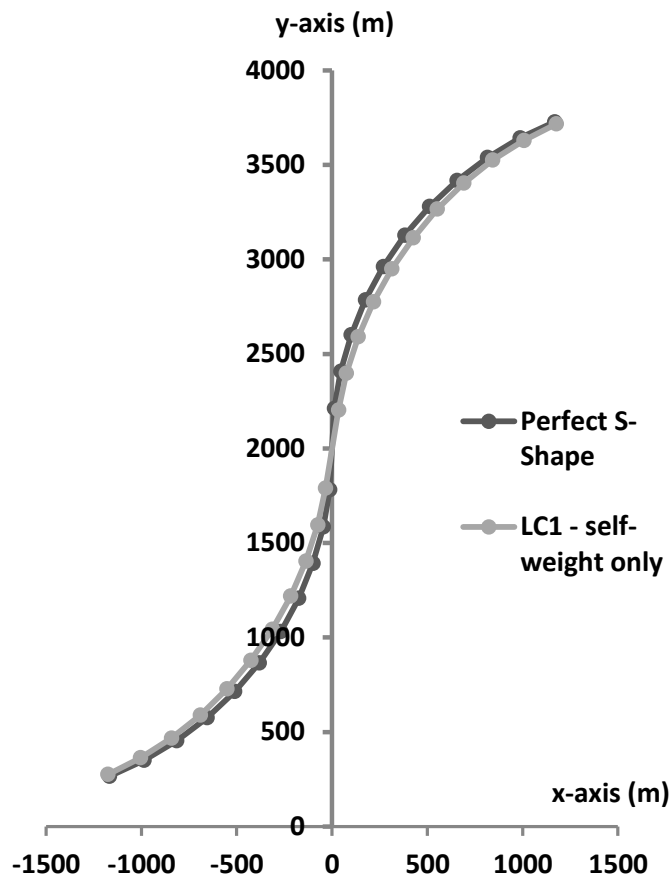


FIGURE 4-7 PONTOON DISPLACEMENTS

The displacements of the pontoons due to the self-weight are shown in Figure 4-7. This displacement is the initial shape of the pontoon locations.

When the structure is loaded by all horizontal loads in x-direction and the bending moment due to eccentric traffic, all given in the previous section 4.5, then the pontoons will displace from the initial shape. This displacement in x-direction is shown in Figure 4-8. The maximum displacement is 13,5 meters at the pontoons in the middle of the fjord.

When the loads are arranged in such a way, that it causes the maximum rotation around the y-axis, the rotations of the pontoons at bridge deck level are as shown in Figure 4-12. The maximum rotation is 95 mrad. If the bridge deck will be rigidly fixed to the pontoon and pylons, the bridge deck will also rotate 95 mrad. However, the serviceability rotation limit is 44 mrad (see Table 2-7). A solution will have to be found to limit the rotations of the bridge deck.

For more detailed results and information about the loads and load cases, see ANNEX R: Computational Model Substructure Example 5.

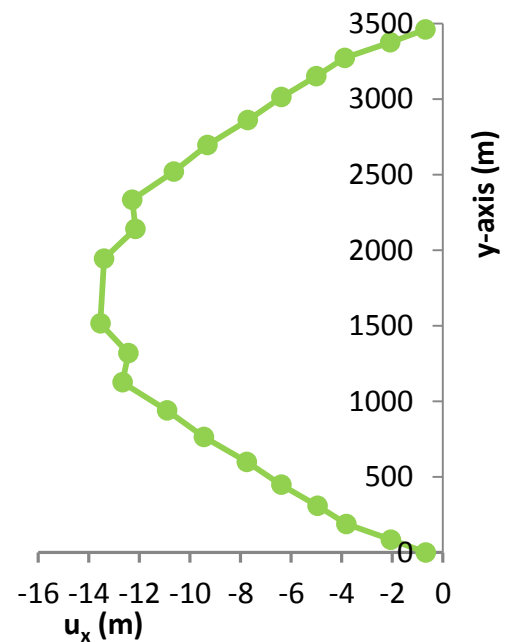


FIGURE 4-8 DISPLACEMENTS FROM THE INITIAL SHAPE OF THE PONTOONS DUE TO HORIZONTAL LOADS

4.7 Modeling the Anchoring System

The anchoring system is the product of a research, for which the process is disclosed in Annex D to K. A summary of the most important modeling choices is given in this section.

4.7.1 Coordinate System

The coordinate system is as shown in Figure 4-9.

The x-axis is in the same direction as the bridge deck width.
 The y-axis is in the same direction as the bridge girder.
 The z-axis is orthogonal to the bridge deck.

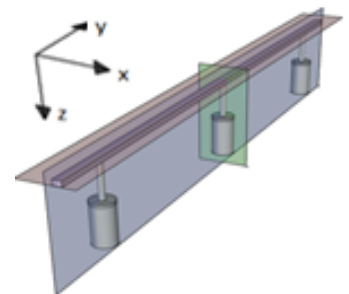


FIGURE 4-9 COORDINATE SYSTEM

4.7.2 No Superstructure Modeled

In general, the superstructure of a separate pontoon floating bridge must be of sufficient strength and stiffness to resist horizontal and vertical forces and to maintain the relative position of the pontoons. However, if an anchoring system was designed, which maintains the relative position of the pontoons as much as possible, the required strength and stiffness of the superstructure will be smaller. Therefore, in the modeling only the anchoring system is modeled to investigate the effects of this system.

4.7.3 Supports at the Pontoons

In reality, the pontoon elements will be floating on the water. The displacements and rotations of the pontoons are not rigid, but free or flexible. In the model of Scia Engineer, the supports at the pontoons are modeled as shown in . The supports are located at the center of rotation of the pontoons.

The varying vertical displacements of the floating pontoon are modeled as a linear vertical spring (k_{vert}). Since all pontoons have the same radius, the springs are equal for all pontoons. For the exact value of the spring, see section R-4 of ANNEX R: Computational Model Substructure Example 5.

The restraints for the horizontal displacements in x- and y-directions of the pontoons are free. So actually, the horizontal displacements will only be restrained by the anchoring cables.

Besides displacements, rotations can also occur, for instance rotations around the x- and y-axis. The overturning moments which cause these rotations are compensated by the restoring moment of the pontoons. This phenomenon is explained in section B.2.8. In Scia Engineer this restoring moment of the buoyancy element is modeled as a rotational spring (k_{rot}). Every pontoon has a different length, different ballast height and consequently, also a different value for the rotational spring. For the calculation of the rotational spring, see ANNEX S: Calculation File Pontoon Properties and Loads. The values of all rotational springs are given in Table R-2.

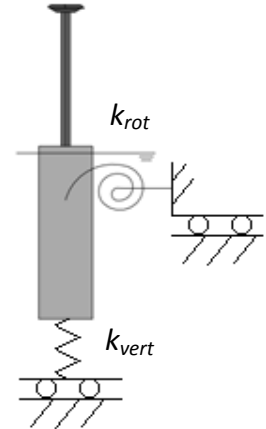


FIGURE 4-10 SUPPORTS AT PONTOON

4.7.4 Position of pontoons in Scia Engineer Model

The schematization for the positioning of the Scia Engineer model, illustrated in , can be explained as follows.

1. The pontoon is floating on water. The buoyancy of the pontoon can be modeled as a vertical spring with stiffness k_{vert} . For the exact value of the spring, see section R-4 of ANNEX R: Computational Model Substructure Example 5.
2. The pontoon is loaded in z-direction. This vertical load consists of the self-weight of the pontoon, the pontoon ballast, the bridge superstructure and also the self-weight of extra ballast, which will be used to adjust the elevation of the pontoon. This vertical load is shown as

$$F_{SW} + F_{extra\ ballast}$$

Due to this loading, the pontoon displaces u_{tot} in z-direction. The buoyancy force is then:

$$F_{buoy} = k_{vert} \cdot u_1$$

Due to equilibrium of forces:

$$F_{buoy} = F_{SW} + F_{extra\ ballast}$$

3. The elevation of step 2 is inputted for the model in Scia Engineer. This is the initial position of the Scia Engineer model. Since F_{buoy} is equal to $F_{SW} + F_{extra\ ballast}$, these two forces do not influence the displacements in z-direction from the initial position.
4. Anchoring cables are added and the pontoon is subjected to the self-weight of the anchoring cables (F_{AN}). Due to this load, the pontoon displaces u_2 in z-direction.

5. The connection between the anchoring cables and the pontoon is designed to be 20 meters below water level when the whole bridge structure is subjected to its own self-weight, including the self-weight of the anchoring cables. Since extra ballast was added in step 2 as well, the pontoon has sunk deeper into the water and the connection is also at more than 20 meters below water level. To bring the connection up to 20 meters below water, the extra ballast will have to be removed from the pontoon again. This is also shown in the figure.

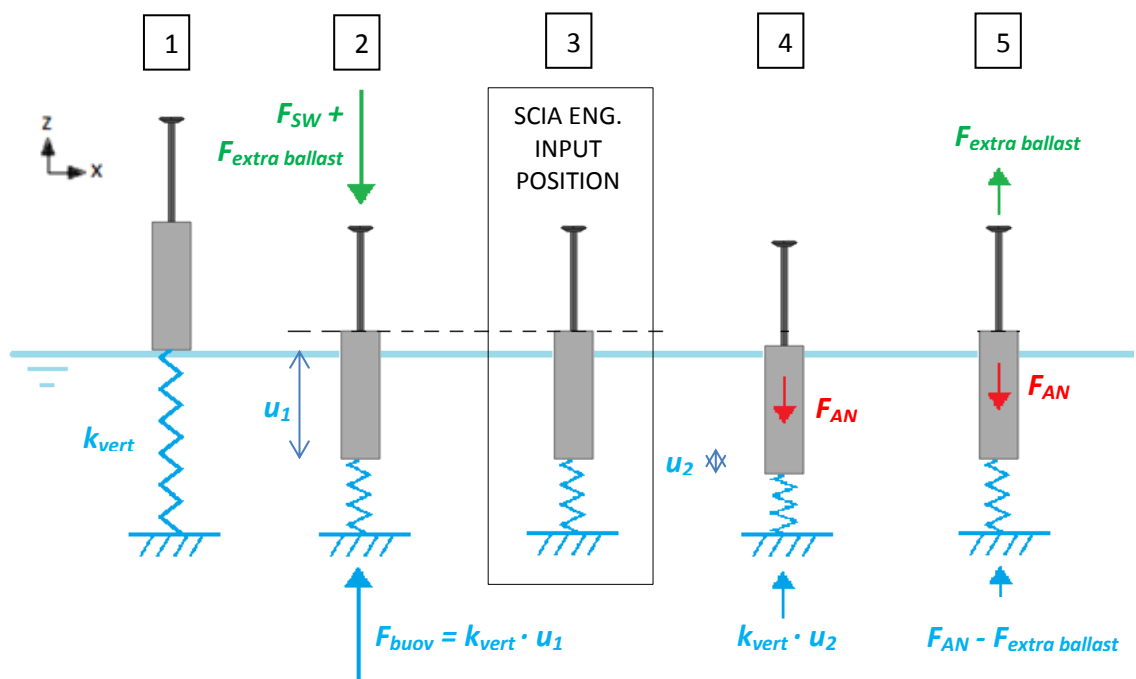


FIGURE 4-11 POSITION OF PONTOON

In this modeling, the extra ballast is chosen to be equal to load caused by the self-weight of the anchoring cables. Because of this, the pontoon elevation of step 2, 3 and 4 are at the same level. This does not necessarily have to be the case. The load caused by extra ballast can also be more or less than the load caused by the self-weight of the anchoring system.

4.8 Recommendations Anchoring System

4.8.1 Protection against Corrosion

Since steel anchoring cables are used under water, measures must be taken against corrosion. A few options are coating, the use of sacrificial/galvanic anodes or metals, etc.

4.8.2 Synthetic Fiber Rope vs Steel Cable

Since the steel anchoring cables are ‘hanging’ to the floating pontoons, the self-weight of the anchoring system has a significant influence on the size of the pontoons. The total weight of the anchoring system is $777 \cdot 10^3$ kN. Part of this weight is resisted by the four anchoring supports of the main cables at the shores (A, B, C and D in Figure 4-1). The remaining weight of $593 \cdot 10^3$ kN is being resisted by the buoyancy force of the pontoons (see Table Q-3 for buoyancy forces). Since the total required pontoon size is dependent on the self-weight of the anchoring system, a heavier anchoring system will consequently increase the total required pontoon volume. Subsequently, the total wave and current loads acting on the pontoon will increase due to the larger pontoon sizes.

For this reason, the use of fiber ropes instead of steel cables for the anchoring system can be considered. Synthetic fiber ropes is a recent development which has a much lower weight than steel, for the same breaking load and a higher elasticity [19, p. 1.8]. In fact, synthetic fiber ropes has such a density, that it floats on water. Common wire ropes used in off-shore mooring lines are six strand and spiral strand, but more products are available on the market.

In Table 4-5, a comparison can be seen between the cases when the self-weight of the anchoring system is equal to zero and the case when steel anchoring cables are used. It can be seen that when the self-weight of the anchoring system is equal to zero, the required pontoon and ballast material will decrease by almost 20%. This will be the advantage of using synthetic fiber rope. Another advantage is the high resistance against corrosion.

However, since fiber ropes float, attention should be paid to the required draught clearance for passing ships. Extra ballast weight could be added to the relevant locations to obtain the required draught clearance. Furthermore, in general fiber ropes have low redundancy. This should be taken into account.

The costs of synthetic fiber ropes can however be high. In further design stages, the (economical) benefits of synthetic fiber ropes versus steel cables can be investigated. Since the wave and current load increase due to the self-weight of the steel anchoring system is relatively small (8,2%), the use of steel anchoring cables is maintained for now. More about the relation between the self-weight of the anchoring, the pontoon sizes and water load can be found in chapter 5.2

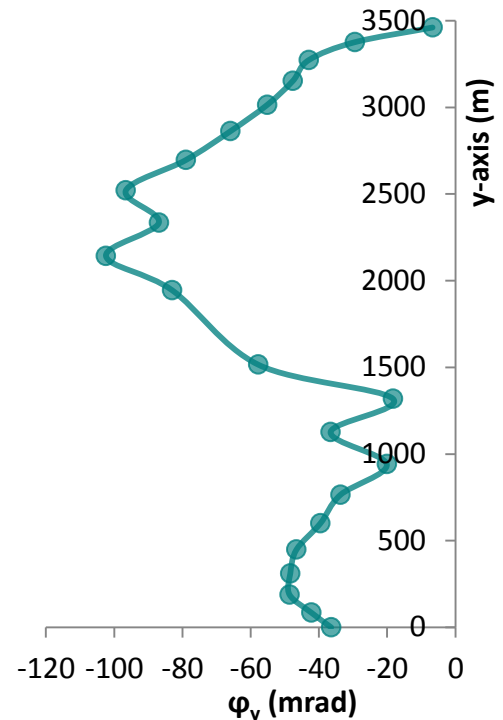


FIGURE 4-12 ROTATION AROUND Y-AXIS OF THE PONTOONS AT BRIDGE DECK LEVEL

TABLE 4-5 COMPARISON REQUIRED PROPERTIES ANCHORING SYSTEMS

	Not taking into account self-weight of anchoring system	Taking into account self-weight of anchoring system	Increase
$G_{\text{anch system}}$ (kN)	0	$778 \cdot 10^3$	-
$G_{\text{pontoon+ballast}}$ (kN)	$11,44 \cdot 10^6$	$13,76 \cdot 10^6$	20%
$L_{\text{pontoon,11}}$ (m)	140	168	20%
$\Sigma F_{\text{wave+current SLS}}$ (kN)	$18,13 \cdot 10^3$	$19,62 \cdot 10^3$	8,2%

5. MORE INSIGHT AND RECCOMENDATIONS ABOUT ANCHORING SYSTEM

In the chapter 3, an anchoring system was proposed. This anchoring system was the product of a research for which the process is disclosed in Annex D to K. During this research, there were several discoveries that provide more insight into the behavior of the anchoring system. These are discussed in this chapter.

5.1 More Additional Pretensioning Leads to Fainter S-shape of the Pontoon Locations

During the design and optimization of the anchoring system, different prestressing forces in the anchoring cables were investigated. It could be concluded, that larger prestressing forces in the cables lead to smaller displacements due to horizontal loads. This is an advantage, since the purpose is to design an anchoring system which maintains the relative position of the pontoons as much as possible. This way, the required strength and stiffness of the superstructure, and consequently also the dimensions, will then be smaller.

However, allowing larger prestressing forces in the cables also had a disadvantage. The S-shape, in which the pontoons are to be placed, will become fainter as larger prestressing forces are applied. This is illustrated in Figure 5-1. The dark line presents the perfect S-shape. However, due to self-weight and pretensioning, which causes a certain tension force in the cables, the positions of the pontoons move and the global S-shape, in which the pontoon were placed, becomes fainter. This is illustrated by the light grey line in the figure. As the tension force in the cables become larger, for instance due to additional applied prestressing, the S-shape of the pontoon locations will become even fainter.

For the proposed anchoring system in chapter 3, an additional pretensioning force is chosen for the main anchoring cable, so due to the self-weight and initial pretensioning, the maximum displacement in x-direction is 45,3 meters at pontoons 7 and 16. This is also shown in Figure 5-1 (for values of all pontoons, see Annex R.2.2). The radii of the perfect S-shape was allowable for the road. This means, that the fainter S-shape due to self-load and initial pretensioning also suffices.

In case the anchoring system is loaded by horizontal loads, the pontoons displaces maximal 13,5 meters more in the direction of the load. This causes little change in the overall S-shape of the pontoon locations.

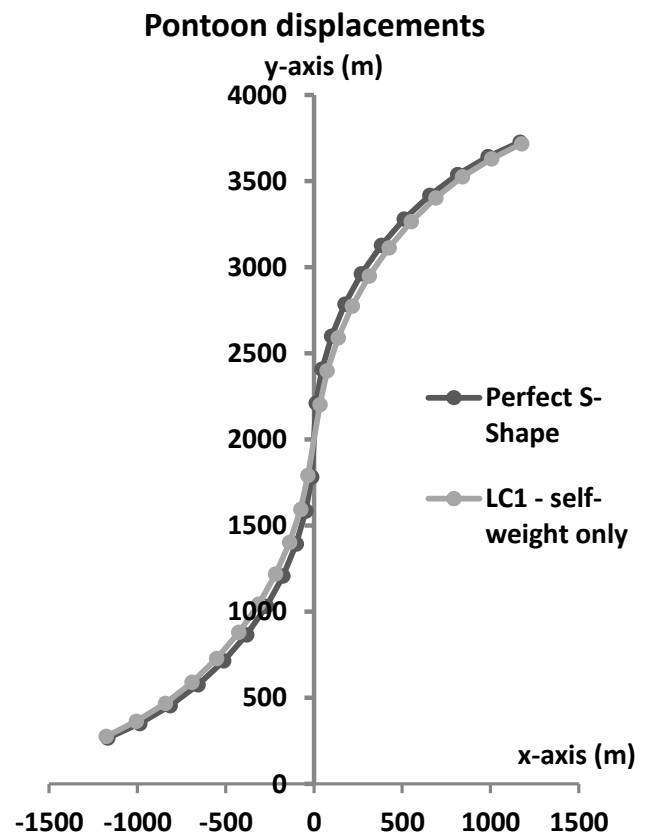


FIGURE 5-1 PONTOON DISPLACEMENTS

5.2 Self-Weight Anchoring System Influences Pontoon Sizes, Water Loads and Overturning Moment

In previous research [3], the self-weight of the anchoring system was neglected. However, in this research, it is decided not to neglect this despite of the fact that it is only 4% of the total vertical loads, see Table 5-1.

As can be seen in the table, the largest vertical load is the self-weight of the pontoons. The pontoons provide upward buoyancy forces for the structure to resist almost all the vertical loads. Therefore, the size and self-weight of the pontoons are calculated by taking into account the remaining vertical loads: the self-weight of the anchoring system, the self-weight of the superstructure and the vertical traffic load. The ratio between these loads is 4 : 8 : 1. Now it seems that the self-weight of the anchoring system does have a significant influence on the size of the pontoons.

For instance, a heavier anchoring system will lead to an increase of the total required pontoon volume. Consequently, the total wave and current loads acting on the pontoon will increase due to the larger pontoon sizes. This relation is shown in Figure 5-2. For every 100 000 kN the self-weight of the anchoring system increase, the pontoon size increases by 2,6% and the water load increases by 1,1%. Hence, the difference between neglecting and taking into account the self-weight of the anchoring system ($774 \cdot 10^3$ kN) is an increase of 20% in pontoon size and an increase of 8% of the water load, acting on the larger pontoons. This information can be used for further considerations of, for instance, using other (lighter) materials for the anchoring cables.

TABLE 5-1 VERTICAL LOADS

	Total load	Proportion
Self-weight anchoring system	$0,77 \cdot 10^6$ kN	4 %
Self-weight pontoons	$15,1 \cdot 10^6$ kN	87 %
Self-weight superstructure	$1,43 \cdot 10^6$ kN	8 %
Vertical traffic load	$0,079 \cdot 10^6$ kN	1 %
Total vertical loads	$17,4 \cdot 10^6$ kN	100 %

Influence self-weight anchoring system on pontoon size and water load

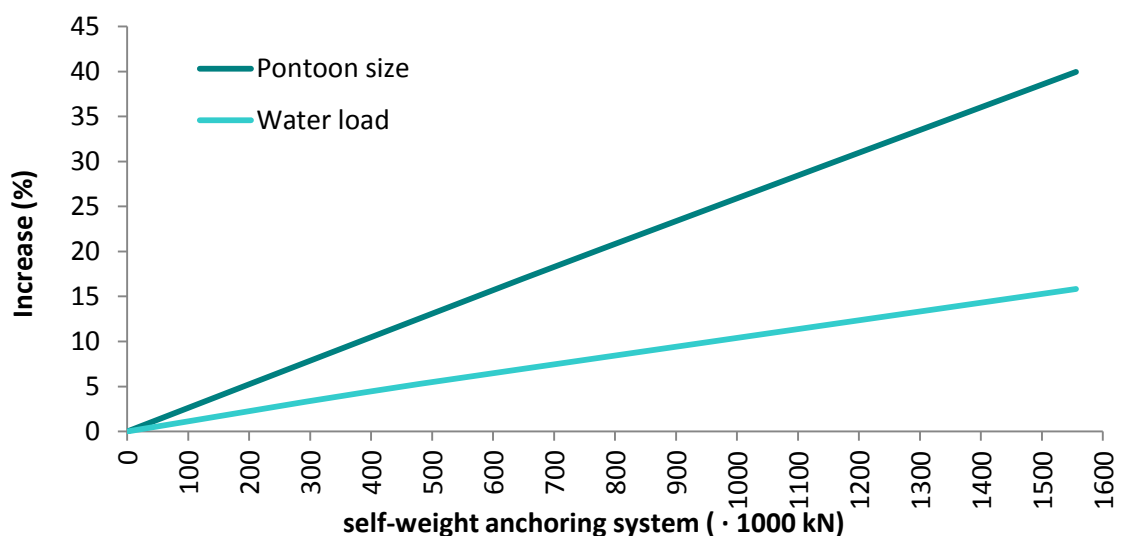


FIGURE 5-2 INFLUENCE SELF-WEIGHT ANCHORING SYSTEM ON PONTOON SIZE AND WATER LOAD

Besides the influence on the pontoon size and water load, the self-weight of the anchoring system also influences the overturning moment, as shown in Figure 5-3.

The overturning moment caused by the anchoring system depends on the magnitude of the two downward forces caused by the two attached lateral anchoring cables, and on the lever arm between the rotation center of the pontoon and the two attachment locations of the lateral anchoring cables.

The lever arm can be adjusted in later design stages, so it is easier to construct. Currently, the lever arm is assumed to be equal to the pontoon radius. It is possible that the attachment locations can be placed inside the pontoon, which will favorably lead to a smaller lever arm. For now, the more disadvantageous lever arm, equal to the pontoon radius, will be used.

Since the lever arms at both sides of the pontoon are equal, the anchoring system leads to an overturning moment in case the downward forces caused by both the lateral anchoring cables at both sides are not equal. Since the anchoring system is not symmetrical, these downward forces are never exactly equal. This is confirmed by the results, shown with a grey line in Figure 5-4. Here, the rotations are shown when the proposed anchoring system is solely loaded by its own self-weight. It can be seen, that the self-weight causes overturning moments, which consequently lead to rotations.

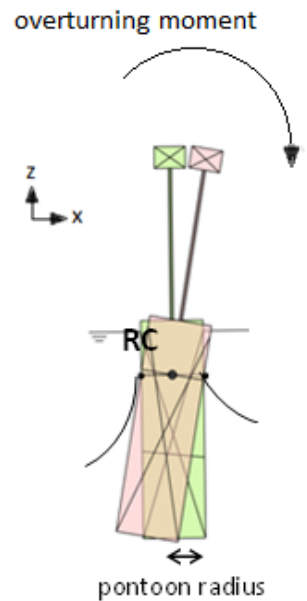


FIGURE 5-3 OVERTURNING MOMENT

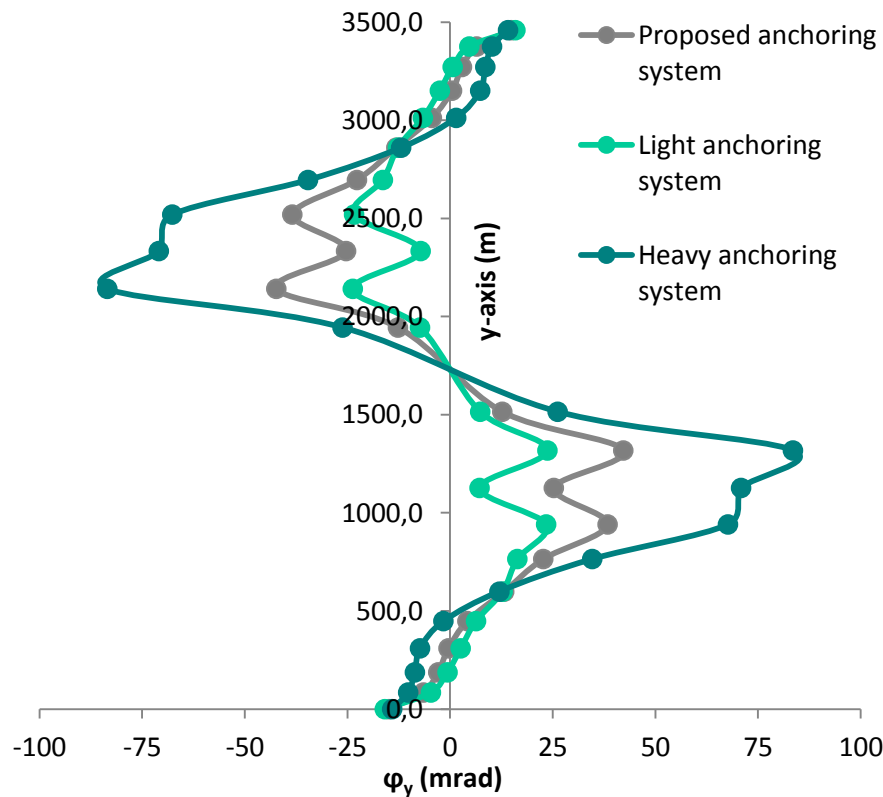


FIGURE 5-4 ROTATION Φ_Y AT BRIDGE DECK LEVEL FOR ANCHORING SYSTEMS WITH DIFFERENT SELF-WEIGHTS

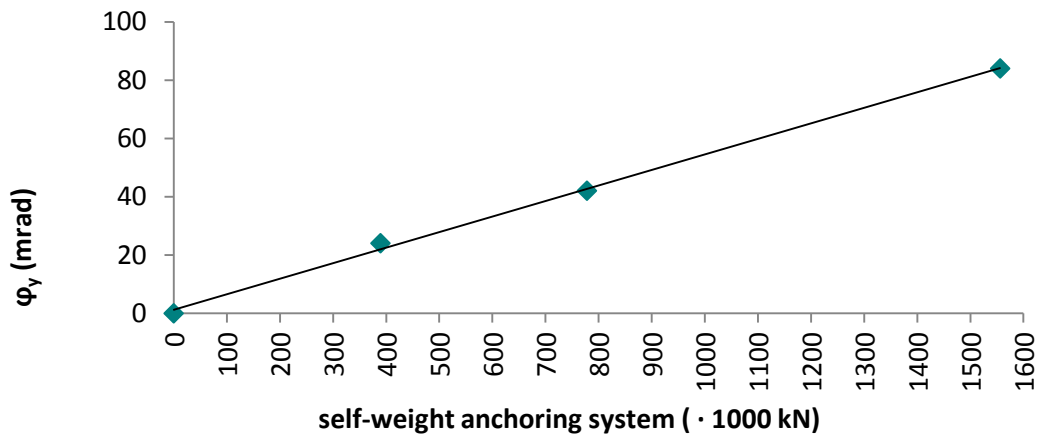


FIGURE 5-5 RELATION SELF-WEIGHT ANCHORING SYSTEM AND OVERTURNING ROTATION

Moreover, in Figure 5-4, the comparison between the proposed anchoring system and both a lighter and heavier anchoring system can be seen. The tension force in the cables are comparable for all these systems (not that it matters much, pretensioning has little influence on the overturning rotation). The comparison shows that heavier the anchoring system, the larger the rotation. This is logical, since a heavy anchoring system causes larger downward loads on the pontoons. Consequently the overturning moment is larger, leading to larger overturning rotations.

This relation is also shown in Figure 5-5. It shows that for every 100 000 kN increase of the self-weight of the anchoring system, the maximum overturning rotation increases by 6,2 mrad.

Due to these relations between the self-weight of the anchoring system and the required pontoon size, acting water loads and overturning rotations, it can be concluded that an anchoring system with smaller weight is more favorable.

Another solution would be to use asymmetric ballasting to compensate the eccentricity due to the self-weight of the anchoring system, see 3.4.3. This is applied for the proposed anchoring system in chapter 6.

5.3 Wide versus Narrow Anchoring System

The influence of a wider anchoring system has been investigated. A wider variant of the proposed anchoring system has been modeled and researched. See Figure 5-6 for both the anchoring systems. For the wide anchoring system, all lateral anchoring cables are elongated by approximately 100 meters; all x-coordinates of the cable ends are shifted 100 meters outwards compared to the narrow system (see section Q-2 for the coordinates of the narrow system).

Because of the longer lengths of the lateral anchoring cables, the angle between the cable and the pontoon will be larger and less steep.

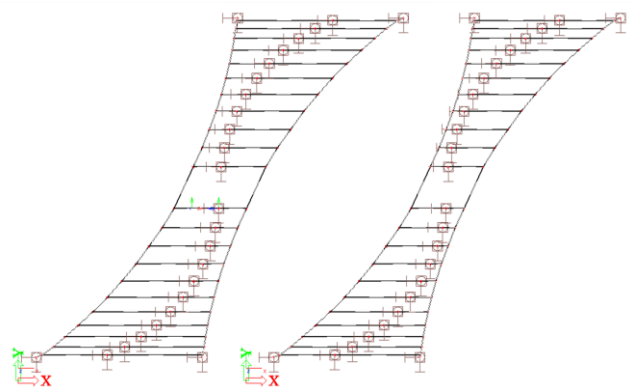


FIGURE 5-6 WIDE (LEFT) AND NARROW (RIGHT) ANCHORING SYSTEM

This way, the wider anchoring system might prove to be more efficient to restrain displacements in x-direction. The truth about this hypothesis has been investigated.

A wide and narrow anchoring system has been modeled. In both the systems, the prestressing forces are comparable (not exactly the same), see Table 5-2.

Results show, that when loaded only by self-weight, the S-shape of the pontoon locations are sustained comparably by both systems.

When horizontal loads are applied, the pontoons move from the initial shape due to self-weight. These displacements in x- and y-direction are shown in Figure 5-7. It can be seen that in x-direction due to the horizontal loads, the pontoons of the wider anchoring system displace more from the initial shape than the ones of the narrower system.

As for the displacements in y-direction due to the horizontal loads in x-direction, the maximum occurring displacement is the smallest for the narrow anchoring system.

Therefore, a narrow anchoring system shows smaller displacements while simultaneously also having a smaller self-weight. Subsequently, this has advantageous consequences for the pontoon sizes, water loads and overturning moment, as was discussed in previous section 5.2. For these reasons, the proposed anchoring system in chapter 3 is based on the narrow anchoring system from this section.

TABLE 5-2 DIFFERENT PROPERTIES WIDE AND NARROW ANCHORING SYSTEM

	Wide Anchoring System	Narrow Anchoring System
Self-weight anchoring system (kN)	$811 \cdot 10^3$	$781 \cdot 10^3$
Maximum internal force in main anchoring cable (kN)	$531 \cdot 10^3$	$530 \cdot 10^3$
Maximum internal force in lateral anchoring cable (kN)	$43 \cdot 10^3$	$59 \cdot 10^3$

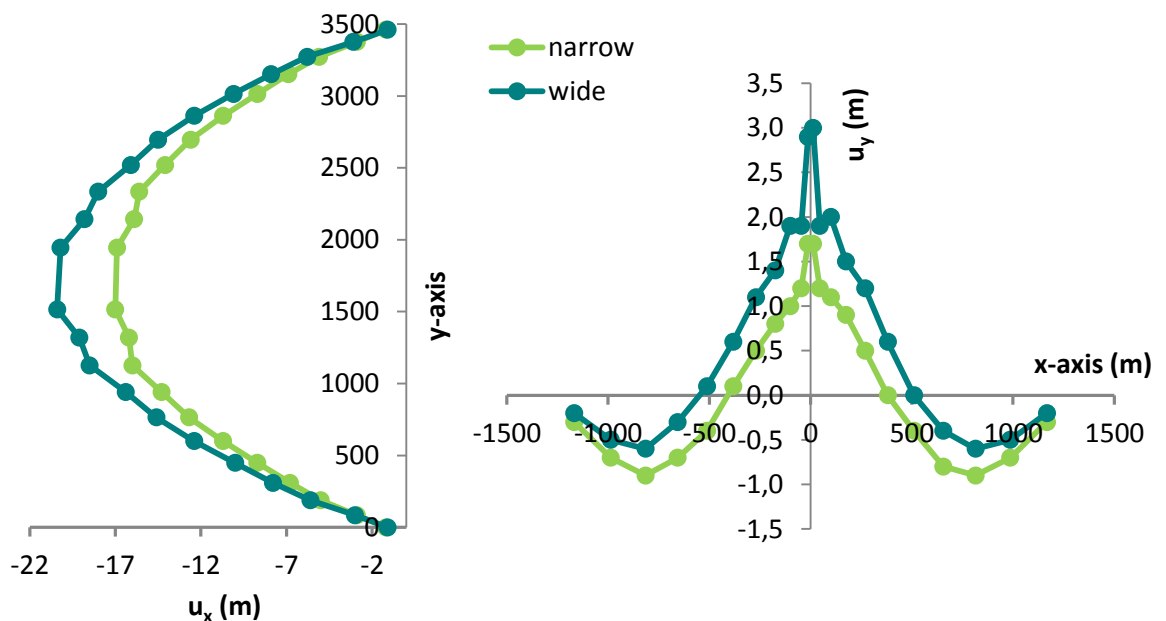


FIGURE 5-7 DISPLACEMENTS OF WIDE AND NARROW ANCHORING SYSTEMS IN X- (LEFT) AND Y-DIRECTION (RIGHT)

6. PROPOSED SUBSTRUCTURE: ANCHORING AT WATER LEVEL

In the previous section, an example for the anchoring system was presented. For that example, the supports of the main anchoring cables were located at 120 meters below water level. Placing the supports at water level however, will facilitate the execution of the bridge. The execution method is described in chapter 3.4.1 (erection method 3). Therefore, a new anchoring system is proposed. In this section, the proposed anchoring system for the buoyancy bridge is presented.

6.1 Purpose

In general, the superstructure of a separate pontoon floating bridge is of sufficient strength and stiffness to resist external loads and to maintain the relative position of the pontoons. However, the purpose of this anchoring system concept is to maintain the relative position of the pontoons as much as possible. Then, the required strength and stiffness of the superstructure will be lower, resulting in a more slender superstructure.

6.2 Overview Substructure

A top view of the anchoring system is shown in Figure 6-1. The two main cables (red) are fixed from shore to shore at water level. The diameter of the main cables is 1200 mm. The distance between the shores is 3507 meters.

44 transversal anchoring cables (yellow) are attached between the main cables and 22 pontoons, which are placed in an S-shape from the top view. The superstructure of the bridge will be placed on top of these pontoons. The diameter of the transversal cables is 350 mm. The anchoring system is rotational symmetric.

As can be seen in the side view (Figure 6-2) and the 3D perspective (Figure 6-3), all pontoons and pylons have different lengths. The length varies from 77 to 138 meters. The pontoons also have varying radii, from 15 to 26 meters.

Note that on the pictures a simple bridge girder has been placed on top of the pylons for visualization. However, the superstructure must yet be designed.

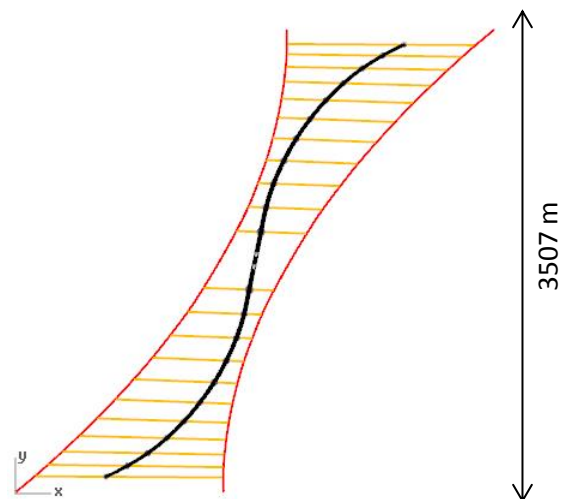


FIGURE 6-1 TOP VIEW ANCHORING SYSTEM

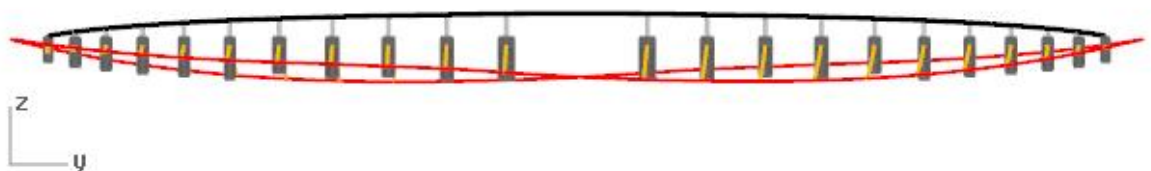


FIGURE 6-2 SIDE VIEW ANCHORING SYSTEM

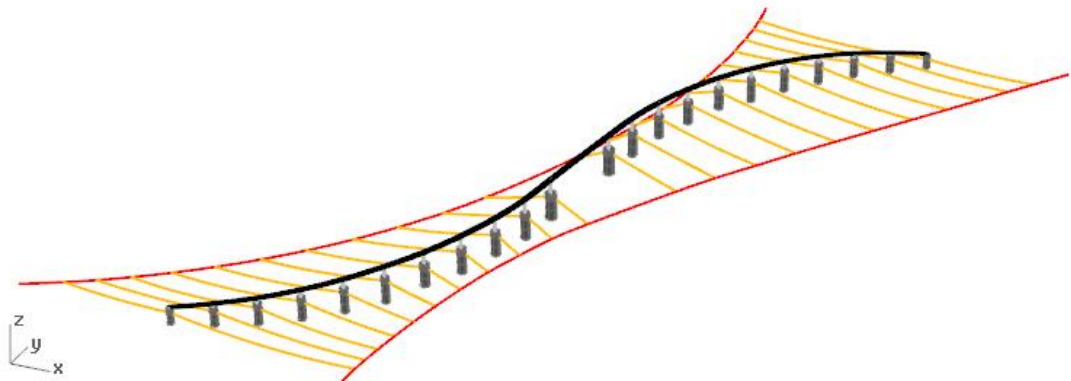


FIGURE 6-3 3D PERSPECTIVE ANCHORING SYSTEM

The anchoring cables are all submerged and the pontoons are for a large part submerged, as can be seen in Figure 6-4. The top of the pontoons are located above water level.

Again, simple pylons and bridge girder are shown in the visualization, the superstructure is however not designed yet.

At the middle of the bridge, a main span is present of 464 meters. The bridge girder will have to be placed at such an elevation above water level so that the fairway clearance height will be at least 70 meters.

The pontoons adjacent to this main span have a radius of 26 meters. This leads to a clearance width of 412 meters.

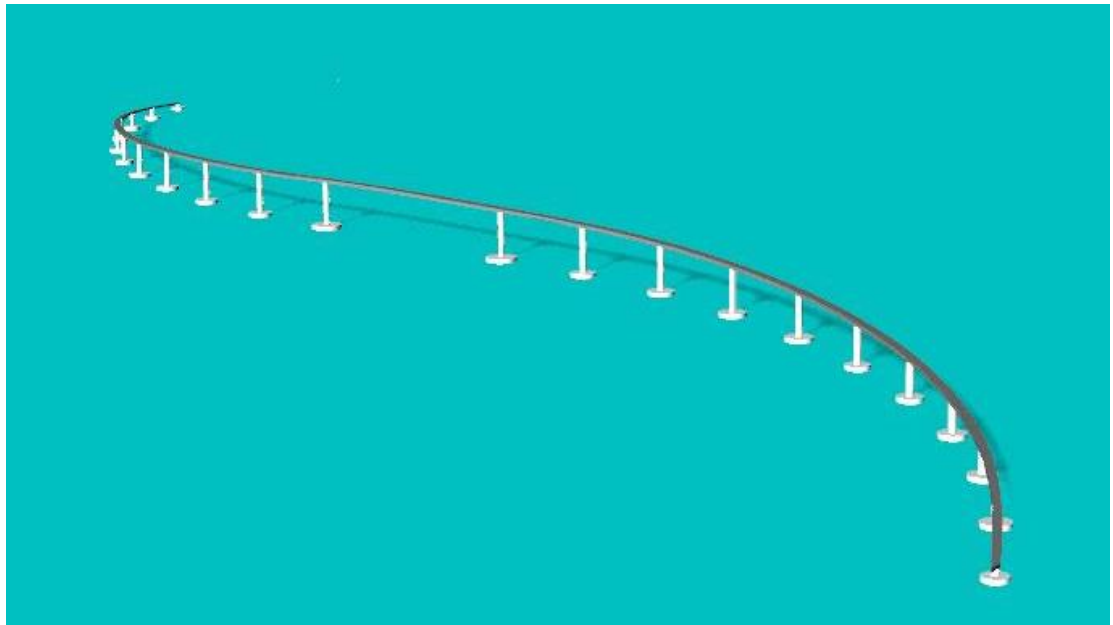


FIGURE 6-4 3D PERSPECTIVE WITH WATER SURFACE SHOWN

In Figure 6-5, it can be seen that the anchoring system is submerged under the water surface. The fairway clearance depth should be at least 20 meters. In Figure 6-6, this boundary is shown as a red

surface. It can be seen that besides small parts of the main and transversal cables near the shore, all cables are submerged more than 20 meters below water level. Since the main anchoring cables are supported at the shores at water level, for a distance of approximately 160 meters from the shore, the anchoring cables are located above the clearance depth.

The design methods for this substructure, including assumptions, modeling details and erection method are described in chapter 3.

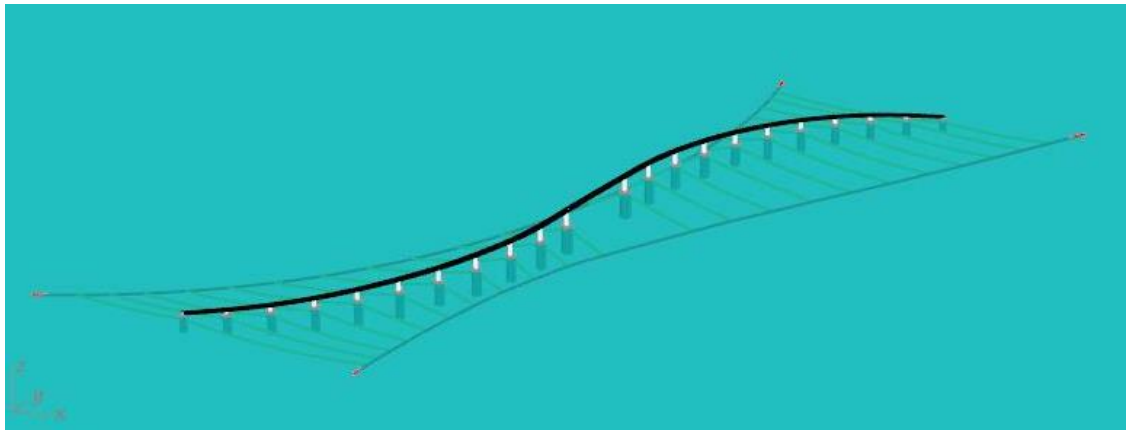


FIGURE 6-5 SUBMERGED ANCHORING SYSTEM

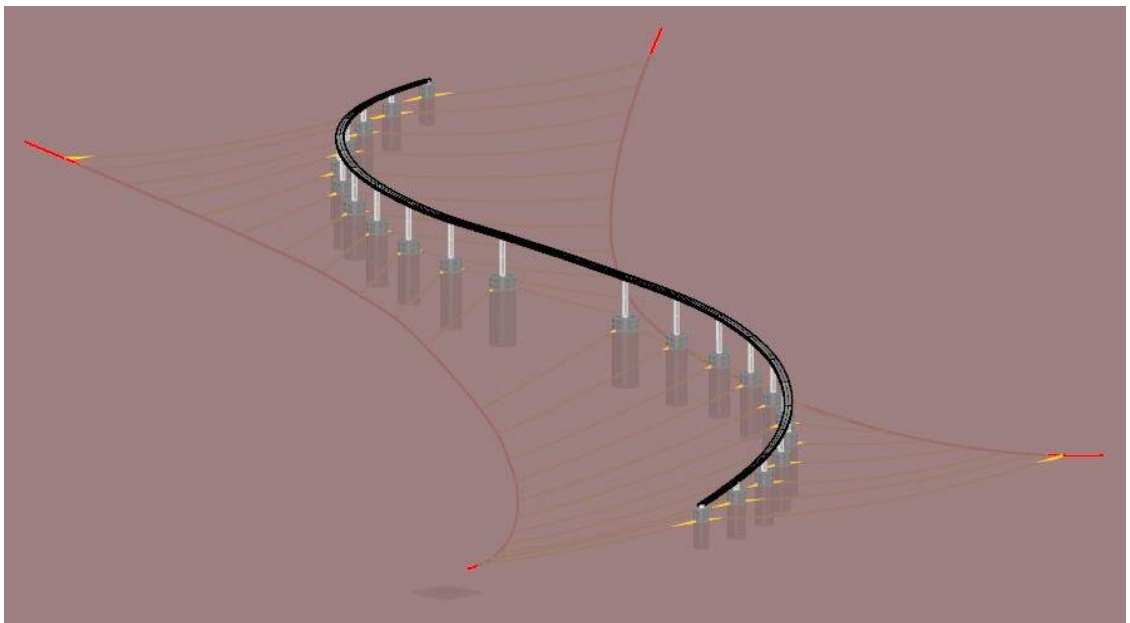


FIGURE 6-6 REQUIREMENT: CLEARANCE DEPTH OF 20 METERS (SHOWN BY RED SURFACE)

6.3 Anchoring Cable Properties

Cable Properties and Dimensions

Y1860

Tensile strength : 1860 N/mm²

Modulus of Elasticity : 195 000 N/mm²

Reduced unit mass in water : 7850 – 1015 = 6835 kg/m³

Diameter main anchoring cable : 1200 mm

Diameter lateral anchoring cable : 350 mm

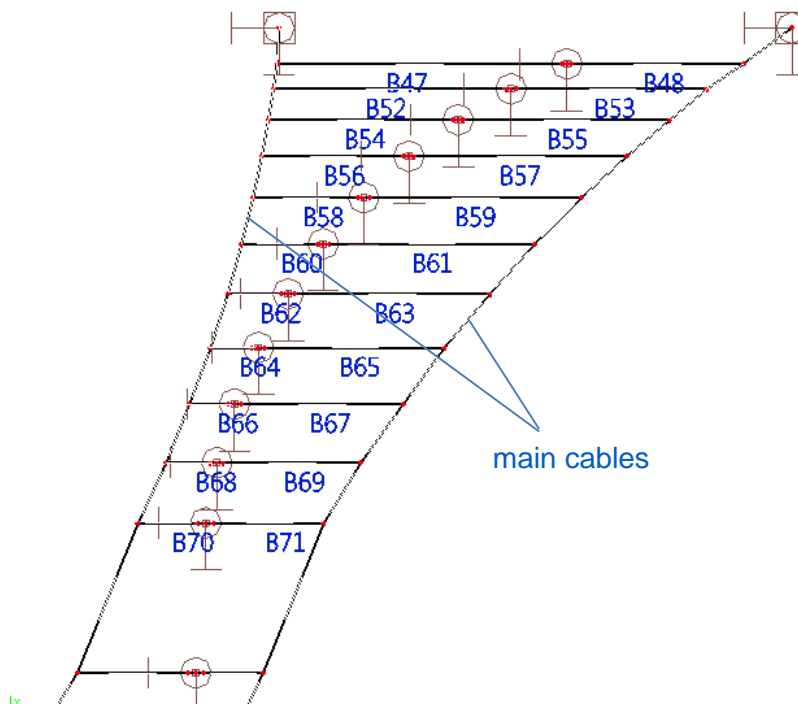


FIGURE 6-7 CABLE NUMBERING

TABLE 6-1 CABLE LENGTHS

Anchoring cable	Length (m)
main	4465
B47	932
B48	561
B52	758
B53	623
B54	602
B55	675
B56	462
B57	695
B58	344
B59	694
B60	249
B61	674
B62	175
B63	639
B64	134
B65	588
B66	126
B67	531
B68	143
B69	450
B70	194
B71	361

Cable Lengths

The cable lengths are given in Table 6-1. The numbering of the cable members is specified in Figure 6-7.

Prestressing in the Anchoring Cables

The anchoring cables are prestressed by their own self-weight. To facilitate the erection, additional pretensioning in anchoring cables is avoided. This leads to the internal forces in the cables. The maximum tension forces in the cables are shown in Table 6-2.

TABLE 6-2 TENSION FORCE IN CABLES

	Internal tension force due to self-weight (kN)
main cable	829,9 · 10 ³
lateral cable	57,5 · 10 ³

6.4 Pontoon Properties

6.4.1 General Properties

The concrete pontoons are cylindrical shaped, containing ballast, as shown in Figure 6-8. The pontoon length and radius varies for every pontoon. These values are shown in Table 6-3. The pontoon numbering is shown in Figure 6-9.

The following properties are estimated to be equal for every pontoon:

Thickness top	: 1,0 meter
Thickness sides	: 1,5 meters
Density concrete	: 2500 kg/m ³
Density ballast	: 2000 kg/m ³

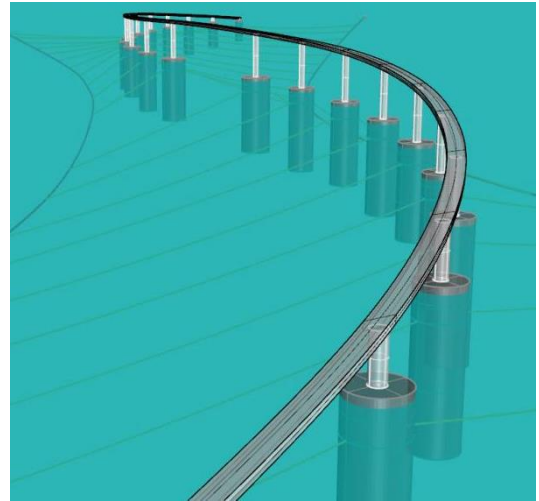


FIGURE 6-8 CYLINDRICAL SHAPED PONTOONS

TABLE 6-3 PONTOON DIMENSIONS

Pontoon number	Length (m)	Radius (m)
1	77	15
2	93	18
3	104	18
4	115	18
5	124	18
6	134	18
7	114	21
8	127	21
9	125	21
10	138	21
11	136	26

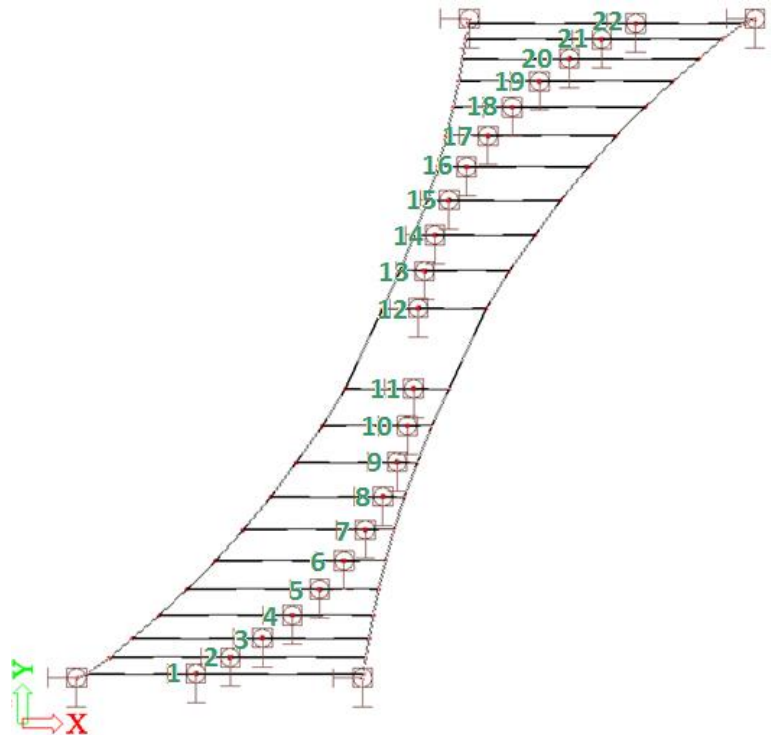


FIGURE 6-9 PONTOON NUMBERING

The top of the pontoons should be located above water level. In case the top gets submerged, the pontoons will sink to the bottom of the fjord. Therefore, as margin, each pontoon has a freeboard varying from 4,3 to 4,9 meters when loaded by the total self-weight of the bridge. The freeboard and draught of the pontoon in this state is shown in Figure 6-10.

In Figure 6-11 and Figure 6-12, respectively the pontoon radii and lengths are shown in graphs.

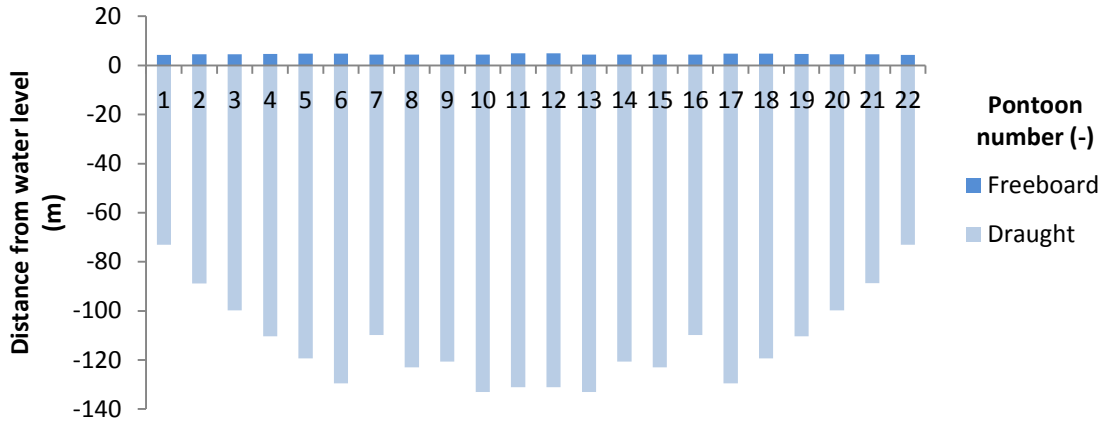


FIGURE 6-10 PONTOON FREEBOARD AND DRAUGHT

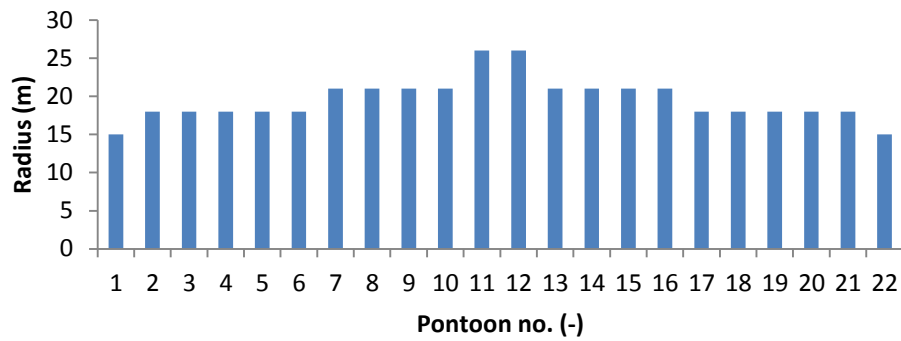


FIGURE 6-11 PONTOON RADIUS

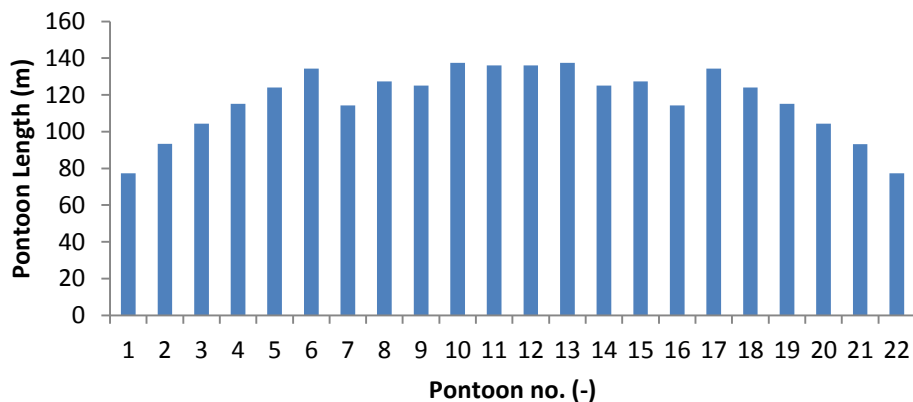


FIGURE 6-12 PONTOON LENGTH

6.4.2 Eccentric Ballasting in x-z Plane

Eccentric ballasting in the x-z plane is applied to all pontoons to compensate the asymmetric anchoring cable weights acting on the pontoons. It is assumed that ballast will be applied in such a way in the x-z plane, that the rotations of the pontoons are equal to approximately zero when the structure is loaded only by the self-weight.

6.4.3 Eccentric Ballasting in y-z Plane

In the direction along the bridge girder (approximately y-z plane), the ballast is applied symmetrically for all pontoons, except for the pontoons at the main span. The main span is larger than the side spans (respectively 465 meters versus 200 meters), causing the pontoons adjacent to the main span to rotate (in the y-z plane). Therefore, it is assumed that for the pontoons at the main span, eccentric ballasting can be applied in the y-z plane as well to compensate the rotation in this plane. In ANNEX T: Rotational Stiffness along Bridge Girder, a sub study shows that there is sufficient ballast present to compensate the larger superstructure self-weight of the main span. This eccentric ballasting at the main span is however not yet incorporated in the pontoon design. This detailed pontoon design is to be done in further design stages. It is possible that the sizes of the pontoons at the main span will increase. For this preliminary study however, it is considered sufficient to know the order of magnitude of the pontoons and whether the buoyancy bridge concept is feasible. More detailed and accurate calculations can then be done in further design stages.

It should be remarked, that the properties are approximately based on the superstructure from previous studies. Since a new superstructure for the buoyancy bridge will be designed, it is possible that the final (required) pontoon properties, which will belong to the final proposed superstructure, will be different.

6.4.4 Recommendation: Investigate Option to Use Water as Ballast

It is assumed that the ballast has a density of 2000 kg/m^3 . This is the density of certain types of gravel, sand, earth or the like. However, water could also be used as ballast, since sufficient water is available at the site. A disadvantage is that the density of water is lower than 2000 kg/m^3 . This will probably lead to larger pontoon sizes. This option can be further investigated.

6.5 Load Capacity

The proposed anchoring system is designed to be able to resist the following loads:

- self-weight anchoring system
- self-weight pontoons
- self-weight superstructure
- vertical traffic load
- horizontal wind load
- wave and current load

The total values for these loads are given in Table 6-4. In ANNEX U: Load Cases, the load cases are shown.

The unity checks for the maximum stresses that occur in the main cables and the transversal cables in the serviceability limit state (SLS) and ultimate limit state (ULS) are presented in Table 6-5. According to the Eurocode [25], the ULS stress limit is 1240 N/mm^2 and the SLS stress limit is 837 N/mm^2 for Y1860 (see section J.3.3 for the calculation). As can be seen in the table, all unity checks are satisfied.

TABLE 6-4 TOTAL LOADS THE SUBSTRUCTURE CAN RESIST

Loads that the substructure is able to resist	Total load	Proportion per direction
Self-weight anchoring system	$0,81 \cdot 10^6$ kN	2,6 %
Self-weight pontoons	$28,60 \cdot 10^6$ kN	92,1 %
Self-weight superstructure	$1,61 \cdot 10^6$ kN	5,2 %
Vertical traffic load	$0,02 \cdot 10^6$ kN	0,1 %
Total vertical loads	$31,04 \cdot 10^6$ kN	100 %
Horizontal wind load	$62,3 \cdot 10^6$ kN	65 %
Wave and current load	$30,2 \cdot 10^6$ kN	35 %
Total horizontal loads	$84,4 \cdot 10^6$ kN	100 %

TABLE 6-5 UNITY CHECKS CABLES IN SLS AND ULS

	SLS	ULS
Maximum stress in main cable (N/mm ²)	778,8	908,7
Maximum stress in lateral cable (N/mm ²)	607,3	701,5
Stress limit unity check	$\frac{778,8}{837} = 0,83$	$\frac{908,7}{1240} = 0,73$

6.6 Displacements and Rotations

6.6.1 Coordinate System

The coordinate system is as shown in Figure 6-13.

The x-axis is in the same direction as the bridge deck width.
 The y-axis is in the same direction as the fjord span.
 The z-axis is orthogonal to the bridge deck.

The x-y plane is also referred to as the horizontal plane.
 The x-z plane is also referred to as the cross-sectional plane.
 The y-z plane is also referred to as the vertical plane.

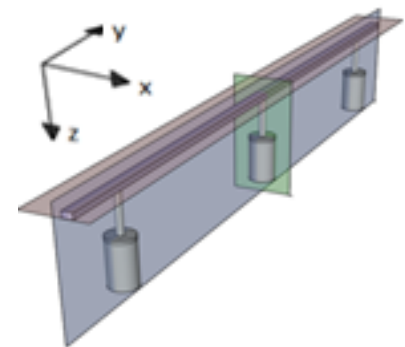


FIGURE 6-13 COORDINATE SYSTEM

6.6.2 Displacements in x-direction are Small

The maximum wind, wave and current loads occur in the same direction as the fjord. Due to these horizontal loads, the pontoons displace. This displacement along the fjord direction (x-direction) is

resisted by the anchoring system. The displacements are shown in Figure 6-14. The y-direction coincided with the direction of the fjord span.

It can be seen that the maximum displacement of 5,6 meters occurs at the middle of the fjord. This displacement is considered to be small compared to the span of the fjord (3507 meters).

6.6.3 Displacements in y-direction to be Resisted by Bridge Girder

As can be seen in the top view of the anchoring system in Figure 6-1, the anchoring system includes 44 transversal anchoring cables which are approximately placed in the same direction as the fjord (x-direction). Therefore, the anchoring system barely provides resistance against displacements perpendicular to the cable direction, the z-direction. The displacements will have to be restrained by the bridge girder.

6.6.4 Displacements in z-direction to be Resisted by Bridge Girder

Vertical wind uplift forces, horizontal environmental (wind, wave and current) loads and traffic load can cause displacements in z-direction. For now, it is assumed that the self-weight of the bridge would be sufficient large to neglect the effects of vertical wind lift forces.

The displacements of the pontoons in z-direction caused by the horizontal loads and the traffic load are shown in Figure 6-15. The maximum displacement is 8 meters for pontoons 6 and 17. This should be taken into account when designing the superstructure.

6.6.5 Rotations around y-axis within Limits

The horizontal loads cause the pontoons to rotate. In Figure 6-16, the rotation around the y-axis caused by horizontal wind load and asymmetrical water load are shown. It can be seen that the maximum rotation at the pontoon adjacent to the main span is 44 mrad, equal to the maximum allowed rotation of the bridge deck.

6.6.6 Rotations around z-axis Very Small

The rotations around the z-axis of the pontoons are very small. The maximum rotation is 3,1 mrad.

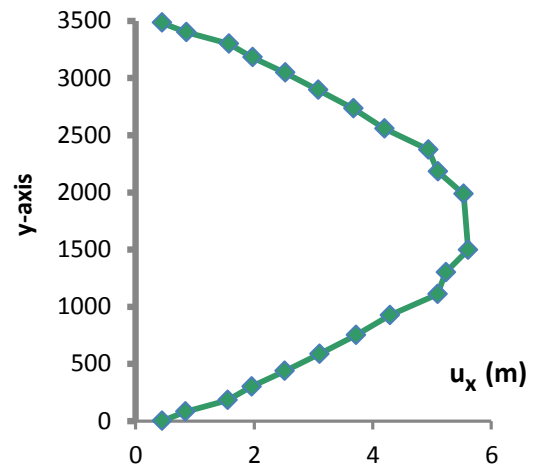


FIGURE 6-14 DISPLACEMENTS IN X-DIRECTION

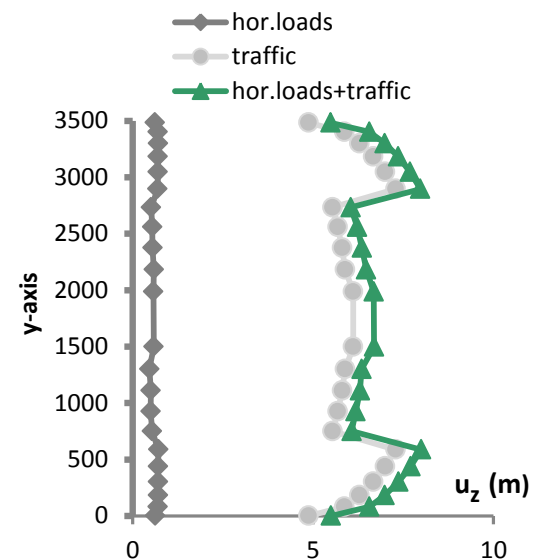


FIGURE 6-15 DISPLACEMENTS IN Z-DIRECTION

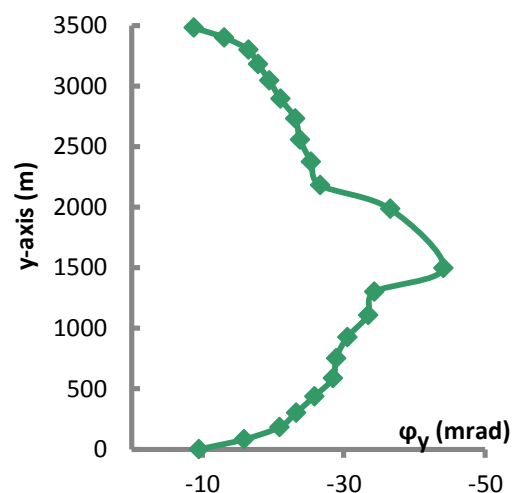


FIGURE 6-16 ROTATIONS AROUND Y-AXIS

7. STARTING POINT SUPERSTRUCTURE: DESIGN PHILOSOPHY AND BOUNDARY CONDITIONS

In the previous chapter an anchoring system for the buoyancy bridge was proposed. This anchoring system demonstrates a certain behavior which gives rise to certain requirements for the superstructure of the buoyancy bridge. In this chapter, the requirements and other boundary conditions for the design of the superstructure will be discussed.

7.1 Coordinate System

The coordinate system is as shown in Figure 7-1.

The x-axis is in the same direction as the bridge deck width.

The y-axis is in the same direction as the bridge girder.

The z-axis is orthogonal to the bridge deck.

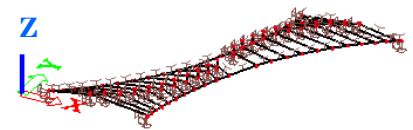


FIGURE 7-1 COORDINATE SYSTEM

7.2 Design Philosophy: Flexible and Light Superstructure

In general, the superstructure of a separate pontoon floating bridge must be of sufficient strength and stiffness to resist horizontal and vertical forces and to maintain the relative position of the separated pontoons. However, for this bridge concept, this relative position of the separate pontoons is already maintained by the anchoring system.

Also, in section 2.5.1, it was mentioned that, since the dimensions of the superstructure are very small compared to the substructure (mainly pontoons), the superstructure will not have sufficient strength and stiffness to restrain the displacements and rotations.

Therefore, for the design of the superstructure, the objective is to design a flexible superstructure, which is able to follow the displacements and rotations due to the loads acting on the whole structure.

Since a flexible superstructure is not stiff, it won't require much material to create stiffness. This complies with another objective, which is to design a light superstructure. Light superstructures are preferred for buoyancy bridges.

7.3 Hinged Bridge Girder Parts for Flexibility

As discussed in the previous section above, the objective is to design a flexible superstructure which is able to follow all movements due to the loads, and not to design a superstructure which restrains all displacements and rotations. Since no high structural stiffness is required to restrain displacements and rotations, it is also favorable that less material will be needed so that the self-weight of the superstructure will be smaller.

To create a flexible superstructure, the bridge girder parts between the pontoons will be connected to each other by hinged connections. The connection will be flexible in the x-y plane and in the y-z plane. In these two planes, the bridge girder will be hinged. This way, pontoon movements will induce less effect on the bridge girder and a flexible and slender superstructure is desired.

7.4 Material: Steel Grade S460 for Efficiency

For a buoyancy bridge, efficiency is of great importance. Therefore, it is chosen to mainly use a higher strength material for the main structure, which will allow size reduction of structural sections, and consequently allowing realization of lighter buildings with equal strength capacity.

In comparison to steel grade S355, the weight reduction for using S460 is generally between 10 to 30 percent. For trusses, weight saving is on average usually more than 20 percent, sometimes even up to 35 percent [20]. Therefore, steel grade S460 will be used for this study.

After this study, more studies can be done to optimize the design. One of them could be a study about using higher strength steels such as S690.

7.5 Aesthetics: Singular, Dynamic Clean Line

The superstructure concept will be developed together with the architecture firm Zwarts & Jansma Architects. The architects take mainly the aesthetics of the bridge into consideration. The design guidelines of the architects for a *“Concept of Rhythm, Elegance and Fluidity”* are given in ANNEX V: Aesthetical Design Guidelines from the Architects.

The most important aesthetical requirement that follows from the guidelines is that the superstructure will be a singular, clean line for viewers on land or water. In other words, no bridge parts should stand out. The options of designing a suspension bridge, cable bridge, arched bridge, and etcetera are ruled out.

This also means that for the large span of approximately 465 meters at the middle of the fjord, a suitable solution will have to be found which will not result in a sudden change of superstructure at the middle of the fjord.

As for the bridge piers/pylons, the piers and pontoons will be combined into an unibody geometry. This means, that there will be a smooth transition from the pontoons to the piers. Apart from the pontoons, the dimensions of the piers must also correspond to the bridge girder geometry.

7.6 Assumption Pontoon Dimensions for Design Superstructure

Because a smooth transition from the pontoon to the pier is desired, the dimensions of the pontoons will influence the geometry of the piers.

As discussed in section 3.2 about pontoon design, the pontoon dimensions depend greatly on the metacentric height of the pontoons. In this feasibility study, only the static loads are taken into account, leading to a range of possible metacentric heights and consequently also to different possible shapes of the pontoons. Short, “fat” pontoons and also long, “skinny” pontoons are possible. From this point on, a conventional radius-draught ratio of existing offshore spar structures is used for the design of the pontoons and piers. This ratio is approximately 0,2 [18, p. 552], smaller than the previous assumed ratio 0,4. The effect of the slightly more slender pontoons is neglected and a concept for the superstructure will be developed, based on the loads and displacements which were presented previously in chapter 6. In case the concept is feasible, then more accurate and detailed calculations can be done. For instance, the dynamic effects should be checked as well.

The new pontoon dimensions with a conventional radius-draught ratio of approximately 0,2 are presented Table 7-1 for all pontoons (pontoon numbering is shown in Figure 7-2).

TABLE 7-1 NEW PONTOON DIMENSIONS

Pontoon number	Length (m)	Radius (m)
1	115	12
2	143	14
3	158	14
4	154	15
5	166	15
6	161	16
7	172	16
8	176	17
9	172	17
10	191	17
11	202	20

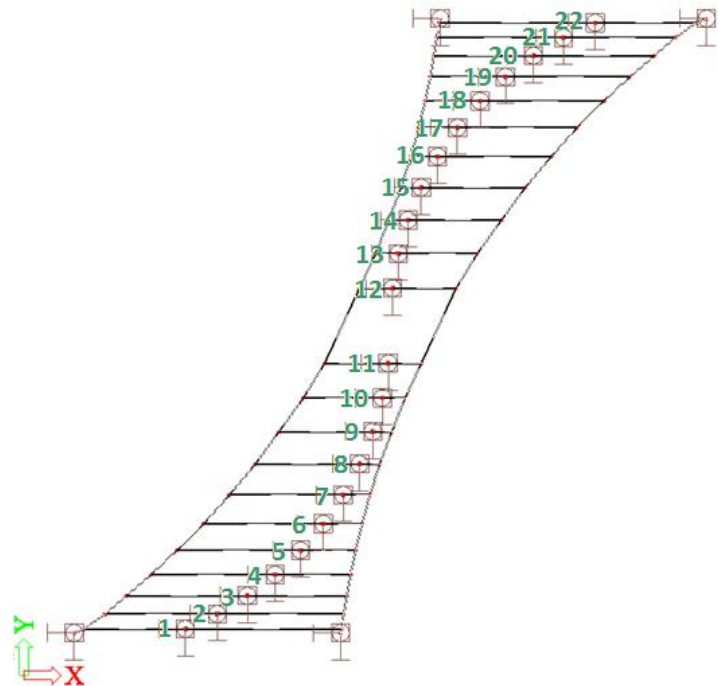


FIGURE 7-2 PONTOON NUMBERING

7.7 Straight Bridge Girders and Minimum Bridge Deck Width

The dimensions of the bottom of the pier will be decided by the pontoon dimensions and the top of the piers will have to correspond to the bridge girder geometry.

To avoid additional torsional stresses and other complications, the bridge girders between the piers will be straight. The road for vehicles on the bridge deck will however be slightly curved. The required radii and angles were given in Table 2-7. To accommodate the curved roads, a certain bridge deck width is required. The calculation of this width is shown in ANNEX W: Required Bridge Deck Width. In this Annex, it can be seen that the required bridge deck width for the main span ($L = 465$ meters) is 23,2 meters, and the required width for all other spans ($L = 200$ meters) is 18,7 meters.

7.8 Piers: Form Finding Study

In the previous sections (7.5 to 7.7), it was explained that the pier design depends on the pontoon properties and bridge girder geometries. These properties however, especially the pontoon dimensions, have to be optimized and adjustments will be made before deciding on the final properties. Therefore, the piers, only a form finding study will be done and no strength or stability checks will be done in this study. The form of the piers should satisfy the guidelines below (for more design guidelines, see ANNEX V: Aesthetical Design Guidelines from the Architects).

- The pier should have sense of robustness, transparency and lightness.
- The pier and pontoon floating devices can be combined into a unibody geometry.
- The geometry corresponds to the girder geometry.
- Geometry avoids growth of marine life and ice deposition (preferably).
- Pier and girders meeting point at a hinge must be well thought of and resolved.

7.9 Internal Forces Acting on the Bridge Part at Main Span

As explained in section 7.3, the bridge superstructure will consist of bridge parts, which will be simply supported on the piers. The most challenging will be the bridge part at the main span of approximately 465 meters. Therefore, in this study, only this bridge part at the main span will be designed under the assumption that, if the bridge part for the main span can be designed, then the bridge parts for the other smaller spans are also feasible.

To design the bridge part at the main span, there must be a good insight present into the forces and rotations acting on the bridge part. Due to wind load, wave load, current load, traffic load and self-weight (SW) on the global system, axial forces, shear forces, bending moments and torsion will act on the bridge part. The maximum values for these effects are given in Table 7-2. For torsion, the angle is shown between two pontoons.

The calculations and modeling of these effects can be found in ANNEX X: Internal Forces and Rotations of Superstructure. The load cases are shown in ANNEX U: Load Cases.

TABLE 7-2 MAXIMUM VALUES INTERNAL FORCES AND ROTATIONS AT MAIN SPAN*

Axial force	Tension	900 kN	LC7 (extreme torsion)
	Compression	- 422 kN	LC8 (temperature)
Shear force	V_x	3 162 kN	LC2, LC3 (wind)
	V_z	81 375 kN	LC2, LC3, LC5, LC6a (SW+traffic)
Bending moment	M_z	$368 \cdot 10^3$ kNm	LC2, LC3 (wind)
	M_x	$9 460 \cdot 10^3$ kNm	LC2, LC3, LC5, LC6a (SW+traffic)
Angle for torsion	ϕ_{xy}	5,26°	LC7 (extreme torsion)

*the coordinate system indicated in section 7.1 is used.

8. TO DESIGN THE SUPERSTRUCTURE: PROCESS AND METHODS

In the previous chapter, the boundary conditions for the design of the superstructure were given. In this chapter, the process developing the new proposed concept for the superstructure is described.

8.1 Collaboration with Architects to Find a Functional and Aesthetic Superstructure

Close cooperation with the architecture firm Zwarts & Jansma lead to a structurally and aesthetically competitive bridge concept.

To develop a competitive bridge concept, there was a continual exchange of information and ideas with the architects. The guidelines of the architects for an aesthetically pleasing design are given in ANNEX V: Aesthetical Design Guidelines from the Architects.

The most important aesthetical requirements that follow from the guidelines are discussed previously in sections 7.5 and 7.6.

8.2 Estimation Superstructure Height for Architects

The choice for the bridge superstructure type influences the bridge height and layout. Different bridge types are suspension bridge, cable stayed bridge, lattice girder bridge, arch bridge, etc. The architects attempt to find an aesthetically attractive layout for the bridge. To give them a sense of what consequences the choice for the bridge type will have, the required bridge height for several bridge types are estimated. The height estimations of the bridge at the largest span (465 meters) are given in Table 8-1. The 'Netkous' bridge is based on the existing tram viaduct in The Hague, in the Netherlands, see Figure 8-1. Sketches are shown in ANNEX Y: Sketches with Height Estimation of Different Superstructure Types.

From the table and sketches it can be seen, that the 'Netkous' type of bridge would require an extremely large bridge height. A box girder or lattice girder type of bridge is more favorable.

In ANNEX Z: For Architects - Feasibility Bridge Girder Height of 12 meters, a document for the architects is given. This document was drafted on request of the architects. As can be seen in the document, the bridge girder height of 12 meters was not recommended.

TABLE 8-1 BRIDGE HEIGHT ESTIMATION FOR DIFFERENT BRIDGE TYPES

Bridge type	Estimated bridge height (m)
Arch bridge	66
Box girder bridge	16
Lattice girder bridge	31
'Netkous' bridge	103



FIGURE 8-1 NETKOUS VIADUCT IN THE HAGUE [34]

8.3 Bridge Type: Lattice Girder Bridge

8.3.1 Lattice Girder Bridge like the Echinghen Viaduct

In section 7.5, it was explained that resulting from these guidelines, the superstructure was to be a singular, clean line for viewers on land or water. In other words, no bridge parts should stand out. The options of designing a suspension bridge, cable stayed bridge, arch bridge, etcetera are ruled out. Therefore, it is decided to design a lattice superstructure.

The lattice Echinghen Viaduct in France was source of inspiration. The viaduct can be seen in Figure 8-2, Figure 8-3 and Figure 8-4. As can be seen in the figures, the Echinghen Viaduct is a composite lattice girder bridge with concrete top and bottom flanges, and with steel lattice structures at the sides.



FIGURE 8-2 ECHINGHEN VIADUCT IN FRANCE [35]



FIGURE 8-3 SECTION OF ECHINGHEN VIADUCT [36]

8.3.2 Composite Girder vs. Steel Girder

The architects desire a composite lattice girder bridge, comparable to the Echinghen Viaduct, with concrete flanges and steel lattice sides. Concrete flanges will lead to a smooth and simple surface, which coincides with the aesthetical design guidelines, set up by the architects. However, rough calculations show that using concrete for the flanges will result in a large total self-weight of the bridge superstructure, much more than was assumed. These calculations are given in ANNEX AA: For Architects - Feasibility Composite Box Girder. It is concluded that also using steel instead of concrete would be more suitable for a buoyancy bridge.



FIGURE 8-4 INSIDE THE ECHINGHEN VIADUCT [37]

For this study, mainly steel will be used for the superstructure concept. In case a feasible concept is found, a variation study can be done with Ultra High Strength Concrete (UHSC) flanges. Alternatively, a flat steel box girder, which serves as the bottom flange, can also give a smooth appearance from the outside, see Figure 8-5.

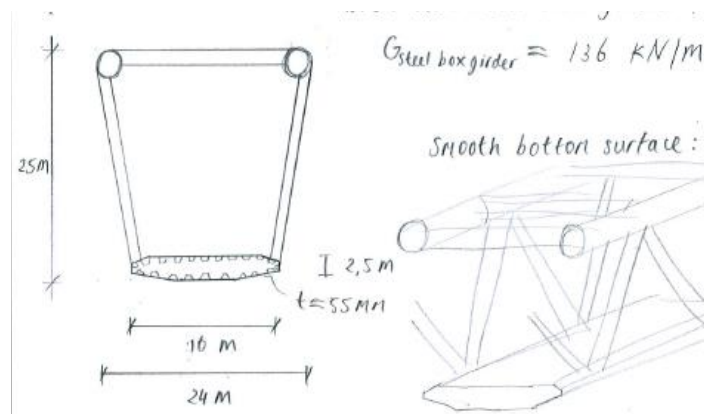


FIGURE 8-5 STEEL BOX GIRDER AS BOTTOM FLANGE

8.3.3 Sketches of Possible Lattice Girder Bridges

Many lattice girder bridges were considered. In Figure 8-6 to Figure 8-9 some sketches of lattice girder bridges are shown, which were proposed to the architects. More sketches can be found in ANNEX BB: Sketches of Possible Superstructures.

As can be seen in the figures, every proposed bridge concept consists of lattice girder bridge parts on pontoons. The concepts in Figure 8-6 and Figure 8-8 have varying torsional rigidity along the bridge length.

The bridge piers/pylons are shaped in such a way that the transition from the pontoon to the piers is smooth. The supports at the piers are further discussed in section 8.4.

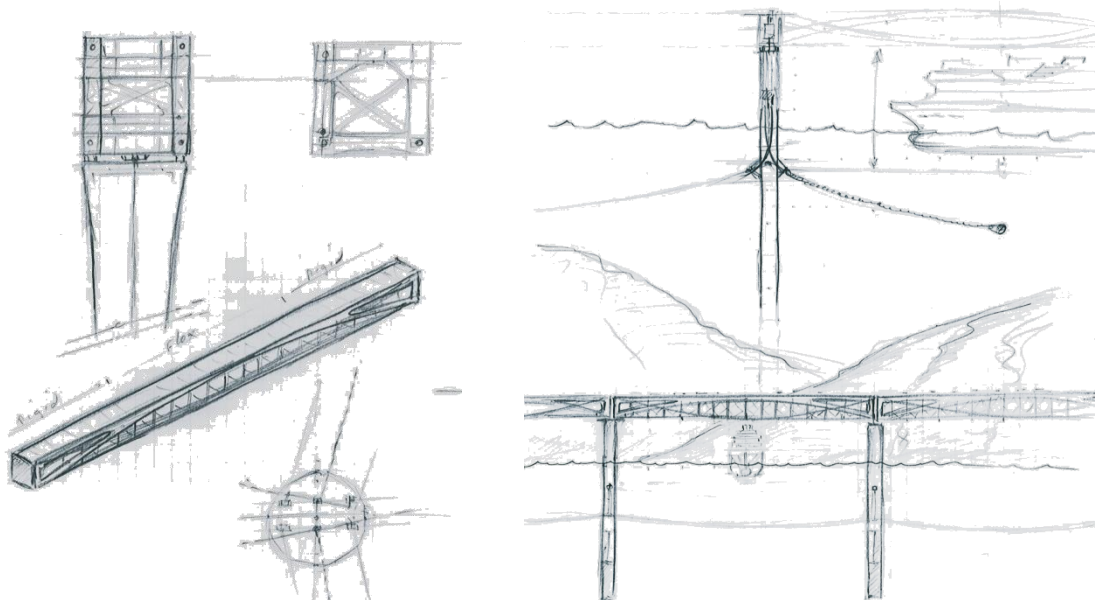


FIGURE 8-6 SUGGESTED LATTICE GIRDER BRIDGE WITH TWO HIDDEN ARCHES

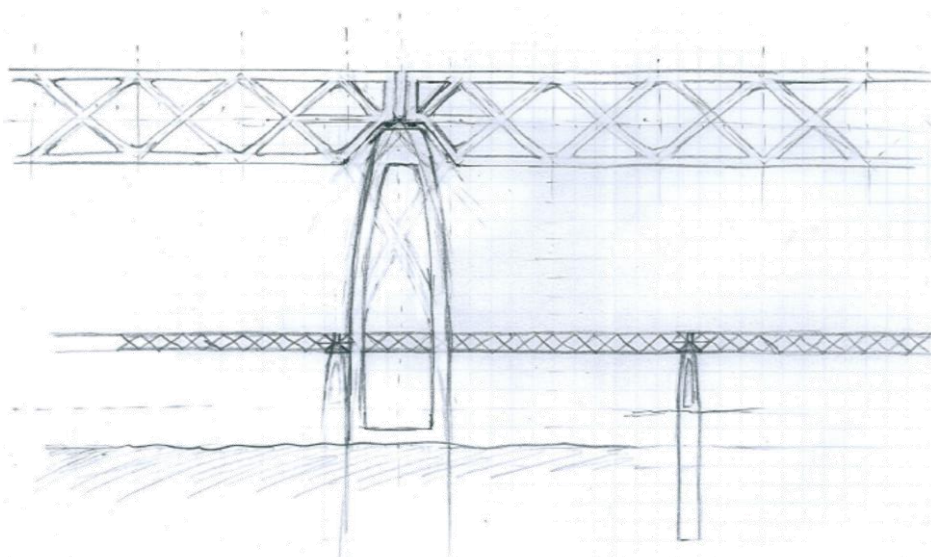


FIGURE 8-7 SUGGESTED LATTICE GIRDER BRIDGE WHICH IS SUPPORTED AT THE GIRDER AXIS

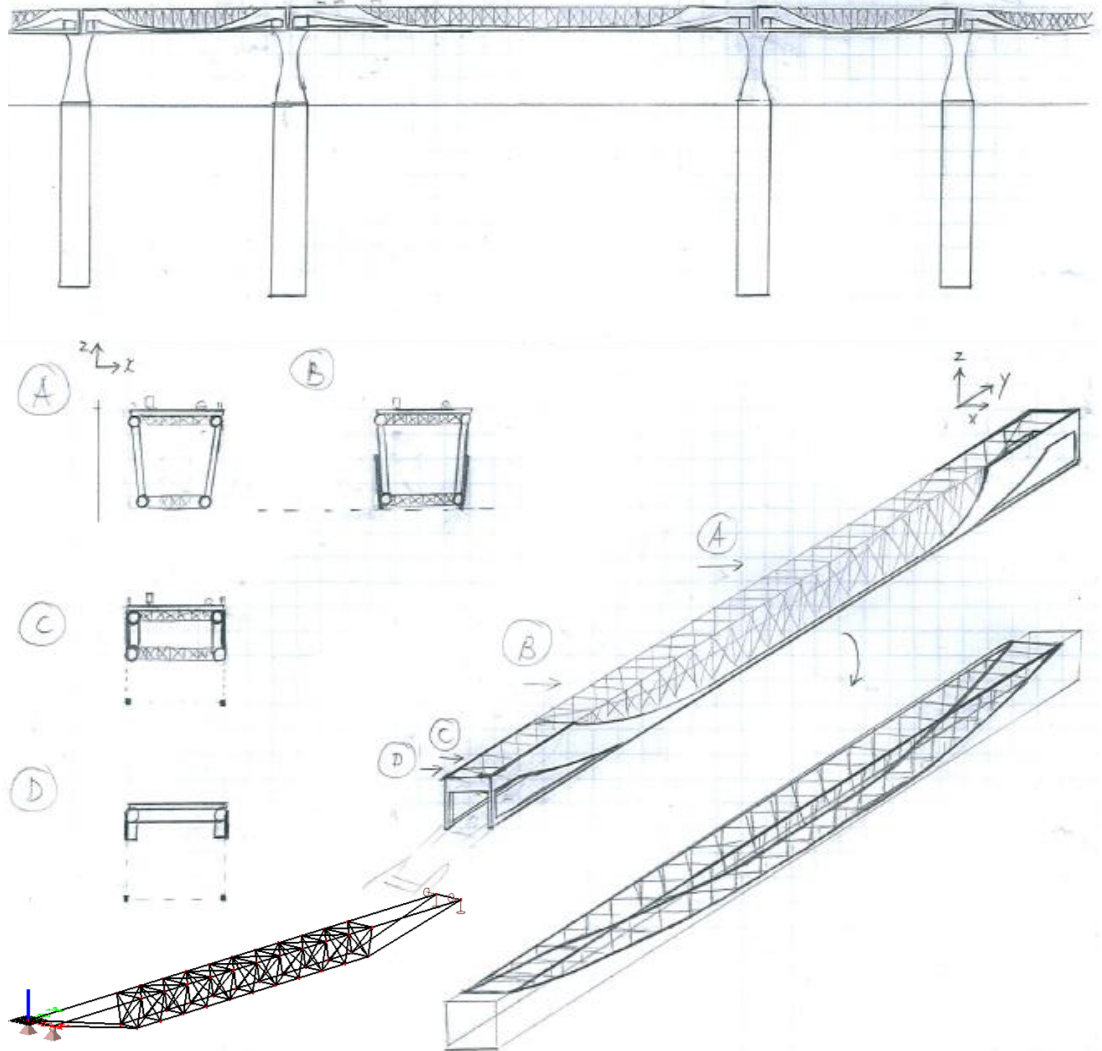


FIGURE 8-8 SUGGESTED LATTICE GIRDER BRIDGE WITH VARIING TORSIONAL RIGIDITY ALONG THE BRIDGE LENGTH

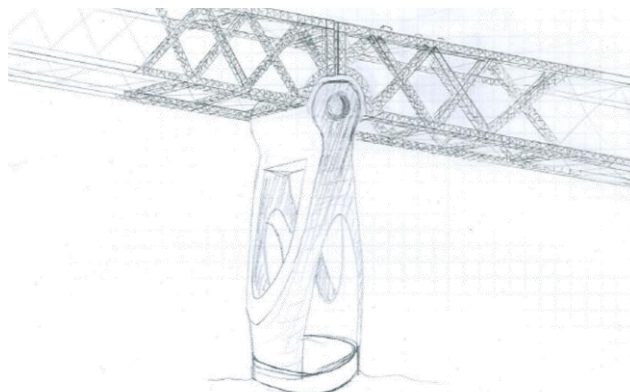


FIGURE 8-9 SUGGESTED BRIDGE CONCEPT WITH LATTICE STRUCTURES

8.4 Supports at Bridge Piers/Pylons

8.4.1 Support Layout

It is of great importance to gain insight into the supports between the bridge piers and the bridge girders. To develop a good bridge concept, there should be a good notion about the displacements and rotations at the supports. These give a good indication of the movements of the bridge and the resulting required clearances to allow these movements.

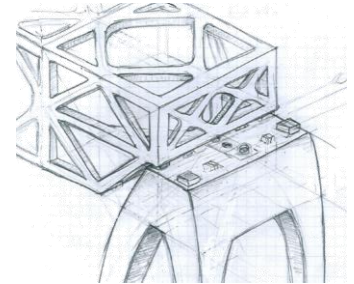


FIGURE 8-10 RECOMMENDED SUPPORTS

The first estimation of the dimension and displacements of the supports, which were also provided to the architects, are shown in ANNEX CC: Supports at Bridge Piers/Pylons – Dimensions and Displacements (First Estimation).

A more refined recommendation about the supports is given in ANNEX DD: For Architects – Recommendation Supports (Location and Dimensions). The recommended support is presented in Figure 8-10 and Figure 8-11.

At the middle of a bridge girder end, there will be a pin which resists the horizontal forces and which allows rotations in the horizontal plane (φ_z), see Figure 8-11. At the corners of the bridge girder ends, the bridge girder will be supported on deformable bearing blocks. These blocks transfer the vertical forces between the bridge girders and the piers/pylons. Due to the flexibility of the deformable bearing blocks, the blocks will allow rotation in the y-z plane (φ_x).

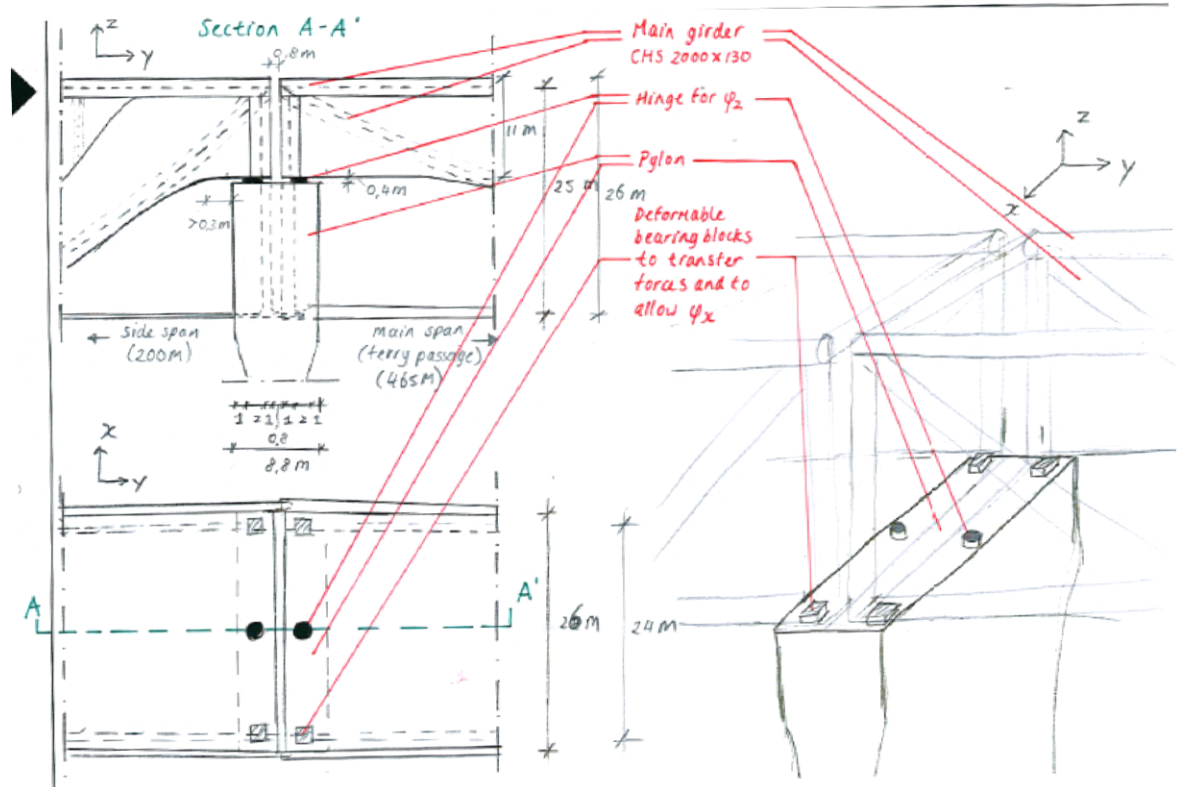


FIGURE 8-11 PROPERTIES OF RECOMMENDED SUPPORTS

Comments

Note that these are rough assumptions for the function of the supports. The detailed design of the support elements is not included in this study. For instance, it is assumed that a flexible deformable block of 2 x 2 x 1 meters (length x width x height) will provide enough capacity to resist the vertical forces and enough rotation capacity. The design of this block is not done yet. Moreover, different elements may be used instead of a block, as long as the element is capable to resist all vertical forces and rotations.

8.4.2 Deformations

In Figure 8-12, the required clearance (indicated by “movement range of the expansion joint” in the figure) is shown to be 350 mm. Because the lattice bridge girder segments are not aligned in a straight line due to the global S-shape of the bridge, cantilevered bridge deck parts are added to the lattice girder bridge segments. These cantilevered parts are fixed.

Due to possible movements of the bridge, the distance a and b in between the cantilevered bridge parts may vary. In the most extreme situation, the distance at a and b can be respectively 573 mm and 118 mm. In other words, with this concept, there is still a margin of 118 mm before the bridge segments collide in the most extreme situation that is considered. The considered load cases to determine the required spacings at the support are shown in Figure 8-13 to Figure 8-16. In ANNEX DD: For Architects – Recommendation Supports (Location and Dimensions), the determination of these displacements are shown more in detail.

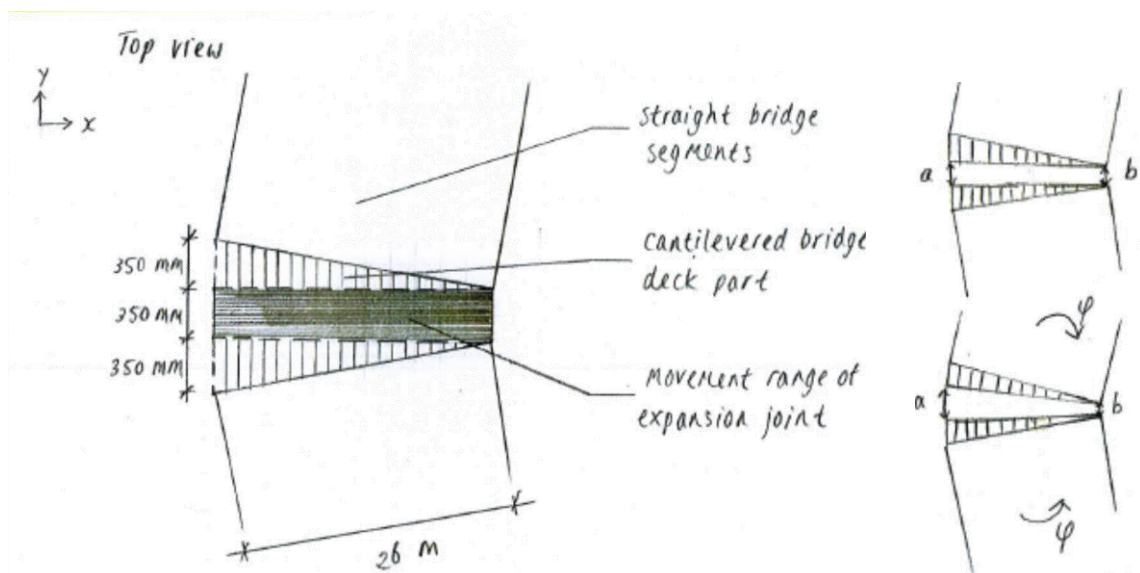


FIGURE 8-12 DIMENSIONS AND DEFORMATION AT THE SUPPORT

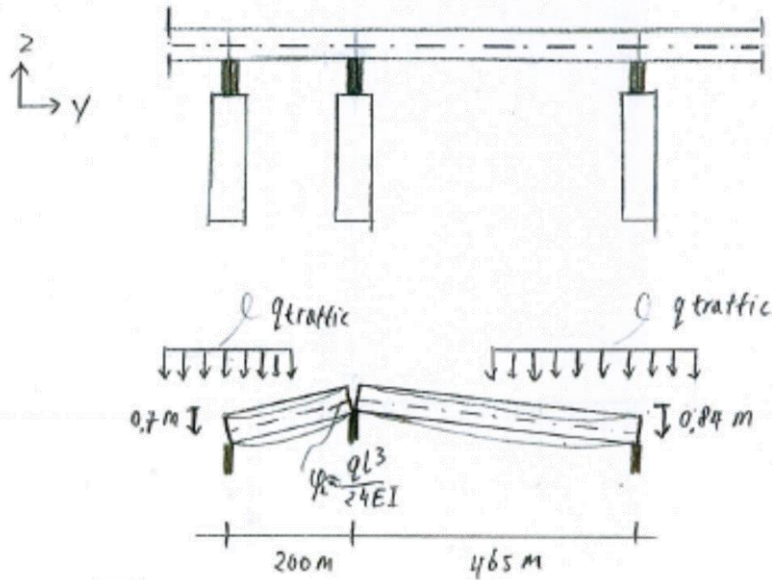


FIGURE 8-13 LOAD CASE WITH FULL TRAFFIC LOAD AT THE PONTOONS AT THE SIDES

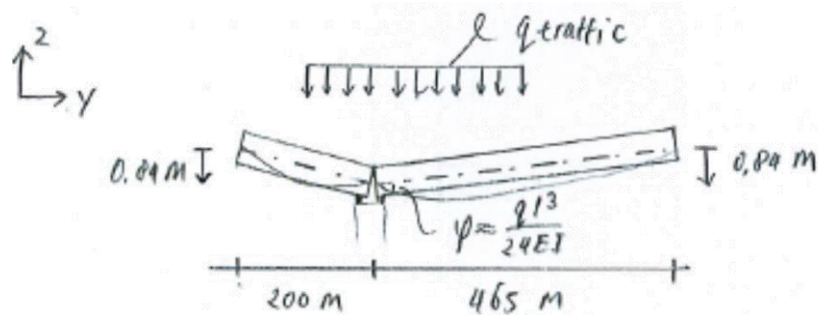


FIGURE 8-14 LOAD CASE WITH FULL TRAFFIC LOAD AT THE PONTOON IN THE MIDDLE

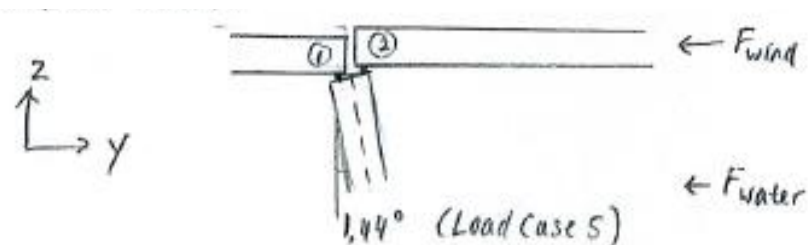


FIGURE 8-15 LOAD CASE WITH WIND AND WATER LOAD IN THE DIRECTION ALONG THE BRIDGE GIRDER

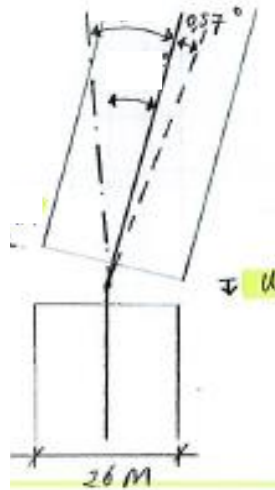


FIGURE 8-16 ROTATIONS AND DISPLACEMENTS OF THE BRIDGE GIRDER PARTS DUE TO LOADING THE GLOBAL SYSTEM

The rotation shown in Figure 8-16 is obtained from the model of the global system (whole bridge structure, also including the substructure) in Scia Engineer. This maximum rotation occurs in the load case representing an extreme situation, in which a hurricane occurs; see load case 7 in ANNEX U: Load Cases.

Comments

The displacements at the supports caused by this load case are considered the largest. However, in this design stage, no detailed calculations are done yet for the erection phase.

In this study, it is assumed that all bridge girder segments are placed simultaneously on the pontoons. Results show, that the displacements at the supports during the erection are not governing in this case. However, in reality the bridge girder segments will most likely not be installed at the same time. When only one bridge girder segment is placed on top of the pontoon and no other bridge girder segments is placed at the opposite side to balance the pontoon, large rotations might occur, which require larger spacing's at the supports. A solution would be to use temporary structures to limit the movements of the pontoons during the erection. The spacing's at the supports should be checked again when the erection method is known.

8.5 Form Study Piers/Pylons

As explained in section 7.8, for the bridge piers/pylons, a form finding study is done. The full exchange of ideas with the architects about the piers is shown in ANNEX EE: Idea Exchange with Architects - Superstructure. According to the design guidelines in ANNEX V: Aesthetical Design Guidelines from the Architects, the piers should have a sense of robustness, transparency and lightness, the transition between the piers and the pontoons should be smooth, and the geometry at the top of the pier should correspond to the geometry of the bridge girder. Several pier forms which were considered during the process are shown in Figure 8-17 to Figure 8-19.

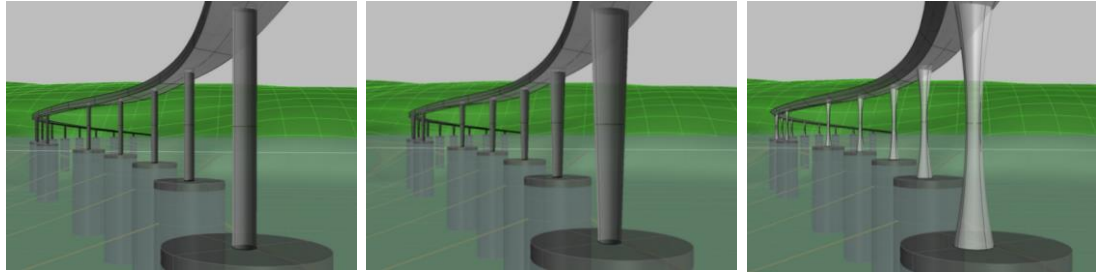


FIGURE 8-17 SUGGESTED PIER FORMS IN THE PRELIMINARY PHASE [38]

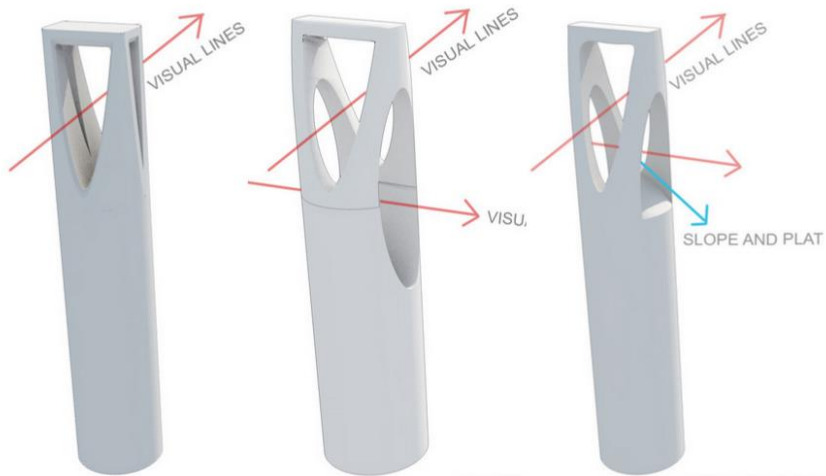


FIGURE 8-18 SUGGESTED PIER FORMS (1) [38]

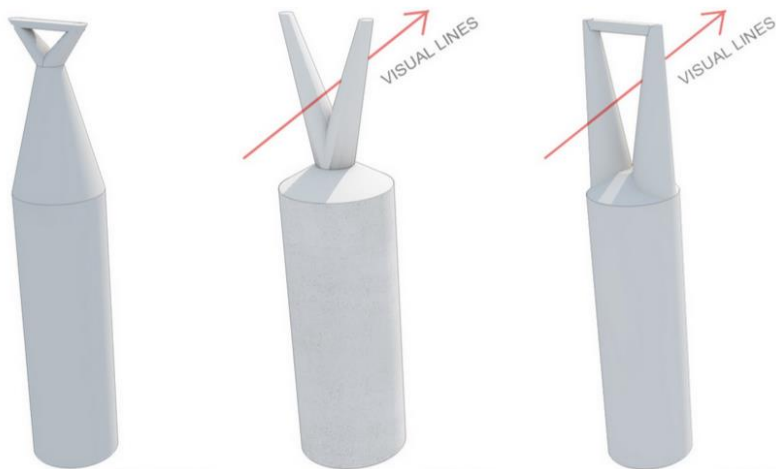


FIGURE 8-19 SUGGESTED PIER FORMS (2) [38]

9. PROPOSED SUPERSTRUCTURE

In chapter 7 and 8, respectively the boundary conditions and the design process were described. This resulted into a superstructure concept, which consists of separate lattice girder segments which are supported on top of the bridge piers. The governing segment for the largest span is modeled in Scia Engineer and tested, see ANNEX GG: Modeling the Final Superstructure in Scia Engineer. In this chapter, the most important properties of the superstructure concept are summarized and presented.

9.1 Superstructure Overview

The superstructure consists of 23 lattice girder bridge segments which are supported on top of 22 piers. The bridge height varies along the length of the bridge. In the middle of the fjord, where also the largest span of 465 meters is present, the bridge height at its largest. Near the shores, the bridge height is smaller. Besides the height, also the bridge width varies along its length, see Figure 9-1. At the main span in the middle of the fjord, the bridge deck width is 24 meters. Near the shore, the bridge deck is 19 meters (see ANNEX W: Required Bridge Deck Width). The bridge piers on top of the pontoons will have varying lengths as well. The length of the first pier near the shore will be 4 meters (see ANNEX S: Calculation File Pontoon Properties and Loads for Model 5). Then, the length of the piers will increase until the pier length of the piers at the middle of the fjord will be 80 meters to provide a fairway clearance. This elevation of the bridge deck can be seen in Figure 9-2. The road will be located at the top of the girder. More sketches of the superstructure can be found in ANNEX FF: Sketches Final Proposed Superstructure.

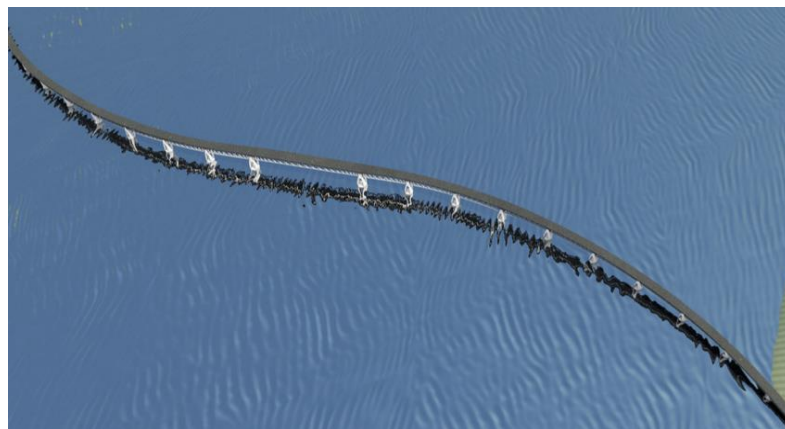


FIGURE 9-1 TOP VIEW: VARYING BRIDGE DECK WIDTH ALONG THE BRIDGE LENGTH [38]



FIGURE 9-2 BRIDGE DECK ELEVATION OF THE PROPOSED CONCEPT [38]

9.2 Bridge Piers/Pylons



FIGURE 9-3 BRIDGE PIER AND PONTOON SHAPE (WITH RANDOM BRIDGE GIRDER LAYOUT) [38]

As discussed in the previous section, the bridge piers lengths varies. The length of the first pier near the shore will be 4 meters. Then, the length of the piers will increase as they are situated further away from the shores. In the middle of the fjord, the length of the piers will be 80 meters (see page 2 of ANNEX S: Calculation File Pontoon Properties and Loads for Model 5).

The form of the piers can be seen in Figure 9-3. It can be seen that the most important requirements in the design guidelines are met (ANNEX V: Aesthetical Design Guidelines from the Architects). The form creates an unibody of the pier and pontoons; there is a smooth transition from the pontoon part to the pier part. Due to the large outer diameter of the pier, more material is used for the pier, when compared to the case shown in Figure 8-17. This final form of the piers is much more robust. Although the robust look, the piers also give a sense of transparency and lightness due to the openings in the piers, which provide visual lines through the piers in different directions.

Comments

As was explained before in chapter 7.8, only a form finding study for the pier is done and no calculations were made for the piers. When the final dimensions of the bridge girder and pontoons are known, the dimensions of the piers can be adjusted accordingly and checks may be done for the piers. Moreover, after the piers are designed, the final self-weight of the piers should be compared to the assumed self-weight, which the pontoon design was based on. If the final weight of the piers proves to be larger than the assumed self-weight, the pontoon design should be adjusted as well.

9.3 Lattice Bridge Girders

9.3.1 Lattice Structure

The superstructure consists of 23 lattice girder segments on top of 22 piers. The lattice girder is shown in Figure 9-4. In Figure 9-5, the top is removed and the lattice structure can be seen.



FIGURE 9-4 LATTICE BRIDGE GIRDERS [38]

The vertical diagonals of the lattice structure are not all equally divided along the girder. As can be seen in Figure 9-6, the diagonals near the supports are denser when compared to the diagonals at the middle of the girder. This does not only create a flow in the aesthetics, but it is also beneficial to resist the global shear forces on the girder, which are larger near the supports.

More detailed figures of the lattice bridge girder segment at the main span are shown in Figure 9-7.



FIGURE 9-5 LATTICE BRIDGE GIRDERS WITHOUT THE TOP [38]



FIGURE 9-6 THE VERTICAL DIAGONALS ARE DENSER NEAR THE SUPPORTS [38]

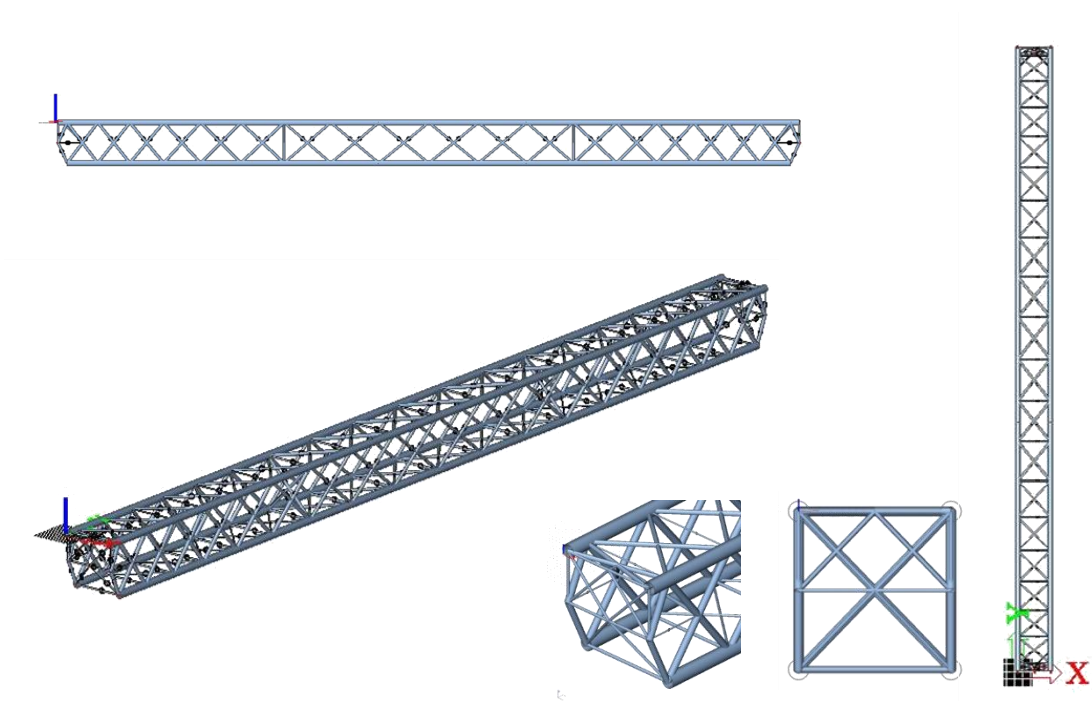


FIGURE 9-7 DIFFERENT VIEWS OF THE LATTICE BRIDGE GIRDER SEGMENT AT THE MAIN SPAN

9.3.2 Varying Torsional Rigidity along the Girder

The torsional rigidity of the girder is not constant. As can be seen in Figure 9-8, the girder parts near the supports are torsional flexible and in the middle, the girder is torsional rigid. This is due to the omitting the bottom horizontal diagonals at the ends of the girder. This can be seen in Figure 9-9, where the main girders and vertical diagonals are hidden to show the horizontal diagonals more clearly. By leaving out the horizontal diagonals at the ends of the girder, the girder section will become an open section with small torsional rigidity, in contrast to closed sections.

This girder is proposed instead of a conventional lattice girder with constant torsional rigidity along its length, because the purpose was to develop a flexible and lightweight bridge structure, which is able to follow the movements due to external loads. A rigid structure would lead to a large, robust and heavy structure, which is not desired for the buoyancy bridge.

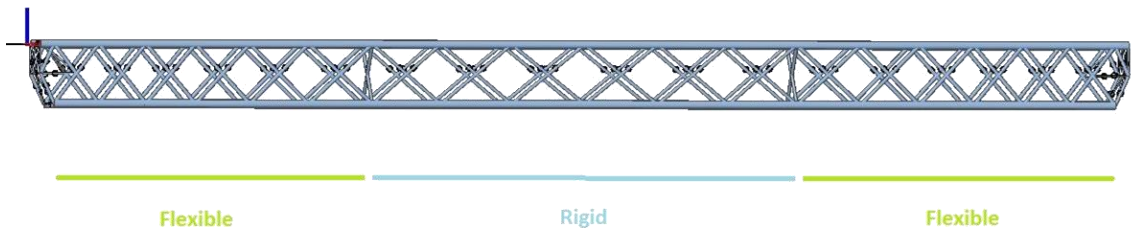


FIGURE 9-8 VARYING TORSIONAL RIGIDITY IN THE GIRDER

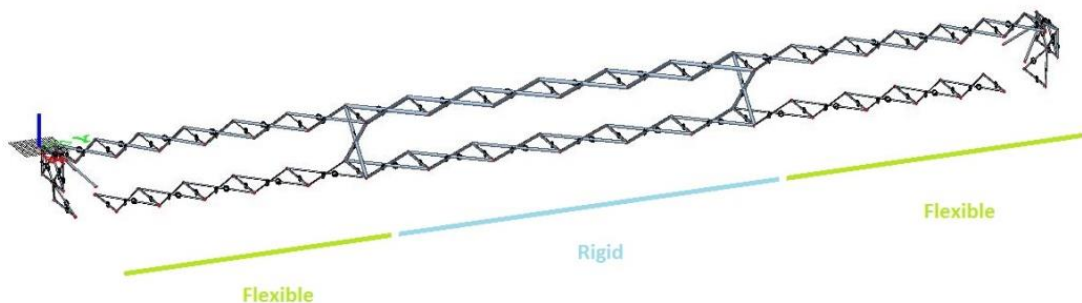


FIGURE 9-9 BOTTOM HORIZONTAL DIAGONALS AT THE ENDS ARE OMITTED TO CREATE MORE TORSIONAL FLEXIBILITY

Comments

Although omitting the horizontal diagonals at the ends provides advantages, the effects should be researched carefully in further design stages. For example, the bottom part at the ends without the horizontal diagonals may largely deform due to loads. It should be checked whether this deformation is allowable. Since the freeway is not located at the bottom of the girder but at the top, large deformation due to external horizontal loads (wind) at the bottom end of the girder will not hinder the traffic. Another effect of omitting the diagonals is the occurrence of warping.

9.3.3 Circular Hollow Section Members

For the lattice girder, circular hollow sections are used. Circular hollow sections are advantageous to resist the wind load and connections can be made easier when compared to rectangular hollow sections.

The four main girders are the largest. The diameter of the four main girders is 3300 mm and the thickness is 80 mm. Hereafter, the vertical diagonals near the supports are the second largest members, the diameter is 1600 mm and the thickness is 32 mm. For the dimensions of the other members, see ANNEX GG: Modeling the Final Superstructure in Scia Engineer.

Comments

For this study, no checks are done for the connections. Only the strength and stability of the members in the lattice structure are checked, see section 9.4. It is possible however, that these dimensions of the members are not favorable for the connections. Larger diameters and smaller thickness might be more favorable for the diagonals. However, when the thickness becomes very small, the member will be more susceptible to local buckling. Using extra stiffeners might be a solution for local buckling. This should be further investigated.

Moreover, second order effects and fatigue are also not considered in this study. Therefore, after it is determined that this concept is feasible, more detailed calculations of the members and the connections should be done in further design stages.

9.3.4 High Strength Steel S460

High Strength Steel S460 is used for all members in the lattice structure. Grade S460 is chosen instead of the more regular S235 grade steel to obtain a more favorable strength-self-weight ratio for the superstructure of the buoyancy bridge.

For further studies, the use of even higher strength steel grades can be investigated, for example steel grade S690.

9.3.5 Supports

The bridge girder will be supported on two deformable blocks and one pin at each end, as shown in Figure 9-10.

At the middle of a bridge girder end, there will be a pin which resists the horizontal forces and which allows rotations in the horizontal plane (φ_z), see Figure 9-11. At the corners of the bridge girder ends, the bridge girder will be supported on deformable bearing blocks. These blocks transfer the vertical forces between the bridge girders and the piers/pylons. Due to the flexibility of the deformable bearing blocks, the blocks will allow rotation in the y-z plane (φ_x).

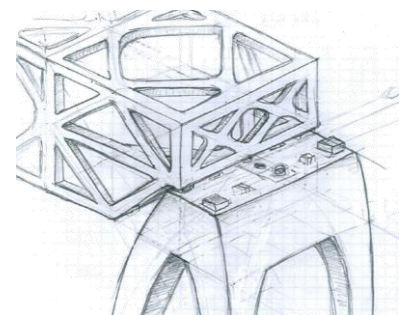


FIGURE 9-10 SUPPORTS

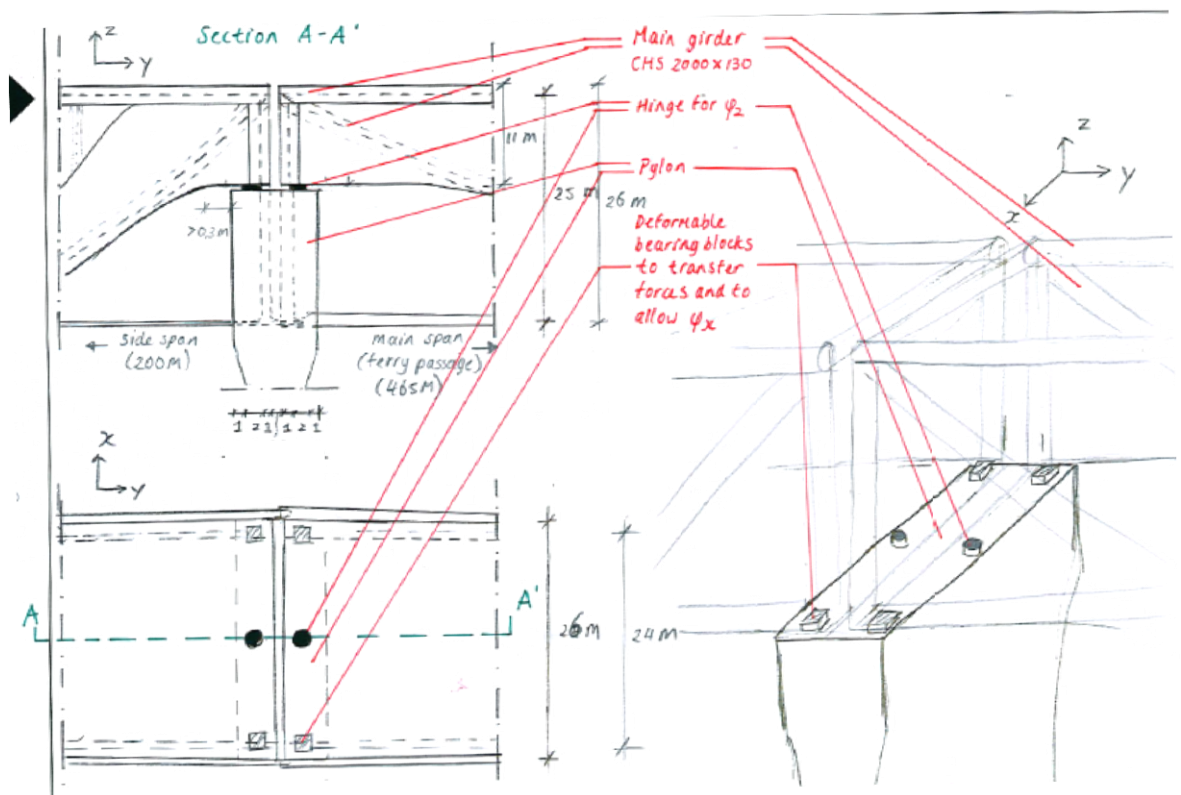


FIGURE 9-11 PROPERTIES OF THE SUPPORTS

Comments

Note that these are rough assumptions for the function of the supports. The detailed design of the support elements is not included in this study. For instance, it is assumed that a flexible deformable block of 2 x 2 x 1 meters (length x width x height) will provide enough capacity to resist the vertical forces and enough rotation capacity. The design of this block is not done yet. Moreover, different elements may be used instead of a block, as long as the element is capable to resist all vertical forces and rotations.

In Figure 8-12, the required clearance (indicated by “movement range of the expansion joint” in the figure) is shown to be 350 mm. Because the lattice bridge girder segments are not aligned in a straight line due to the global S-shape of the bridge, cantilevered bridge deck parts are added to the lattice girder bridge segments. These cantilevered parts are fixed.

Due to possible movements of the bridge, the distance a and b in between the cantilevered bridge parts may vary. In the most extreme situation, the distance a and b can be respectively 573 mm and 118 mm. The considered load cases to determine the required spacing at the support are shown in Figure 8-13 to Figure 8-16 of the previous chapter. In ANNEX DD: For Architects – Recommendation Supports (Location and Dimensions), the determination of these displacements are shown more in detail.

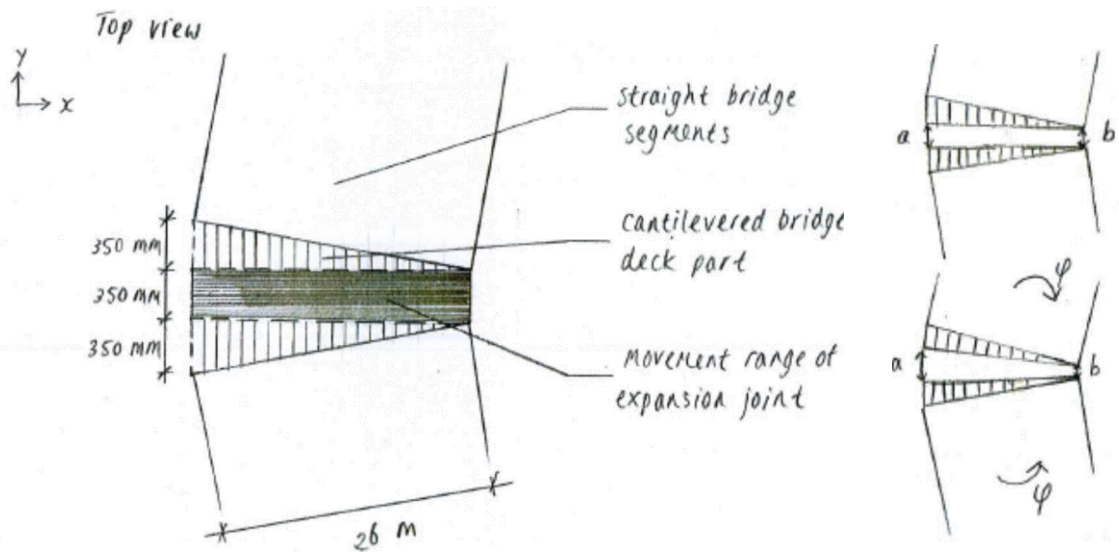


FIGURE 9-12 DIMENSIONS AND DEFORMATION AT THE SUPPORT

9.4 Unity Checks

For the unity checks, only the bridge girder at the main span (465 meters) is checked. It is assumed, that in case the unity checks suffice for a span of 465 meters, then solutions will also be possible for all the others spans of 200 meters.

Strength

The unity checks for strength are shown in Table 9-1. For these checks, load factor 1,2 is used for permanent loads and load factor 1,5 is used for variable loads. To see which loads are included in each load case, see ANNEX U: Load Cases.

As can be seen in the table, the largest unity check occurs for the load case with the hurricane. At this extreme situation, the unity check is 0,91. Hereafter, load case 3 is the largest with an unity check of 0,86. In all load cases, the bottom main girder is governing.

TABLE 9-1 STRENGTH UNITY CHECKS

Load case	UC (-)	Member	Stress (N/mm ²)
1 : Self-weight only	0,74	bottom main girder	287
2 : Maximum displacements in x-direction	0,85	bottom main girder	369
3 : Asymmetric water load	0,86	bottom main girder	370
5 : Maximum displacements in y-direction	0,82	bottom main girder	319
6 : Self-weight and traffic load	0,82	bottom main girder	319
7 : Hurricane	0,91	bottom main girder	363
8 : Self-weight, traffic load and temperature load	0,83	bottom main girder	322

Stability

The unity checks for stability are shown in Table 9-2. For these checks, also load factor 1,2 is used for permanent loads and load factor 1,5 is used for variable loads. The load cases are explained in ANNEX U: Load Cases.

As can be seen in the table, the largest unity check occurs again for the load case with the hurricane. At this extreme situation, the unity check is 0,91. Hereafter, load case 3 and 4 are the largest with unity check of 0,90.

TABLE 9-2 STABILITY UNITY CHECKS

Load case	UC (-)	Member
1 : Self-weight only	0,69	bottom lateral girder at main span
2 : Maximum displacements in x-direction	0,90	top main girder
3 : Asymmetric water load	0,90	top main girder
5 : Maximum displacements in y-direction	0,79	vertical diagonal near midspan
6 : Self-weight and traffic load	0,77	bottom lateral girder at main span
7 : Hurricane	0,91	top horizontal diagonal near midspan
8 : Self-weight, traffic load and temperature load	0,77	bottom lateral girder at main span

Comments

The unity checks for strength and stability are both the largest for the extreme load case, in which a hurricane occurs. The unity check is then 0,91.

However, it should be noted that very favorable load factors are used ($\gamma_G = 1,2$ and $\gamma_Q = 1,5$). According to the Eurocode, bridges belong to consequence class 3. The load factors should then even be multiplied with 1,1. Therefore, the unity checks will be larger in case the correct load factors are used.

When regarding the strength capacity, in every load case, the capacity of the bottom main girder is governing. In further studies, higher strength steel can be considered for the bottom main girder. Then, the unity checks for the strength capacities will be lower.

When regarding the stability, the second largest unity check after load case 7 with the hurricane is for load cases 2 and 3. In both cases, the top main girder is governing. In reality, this unity check may be lower. In this model, the bridge deck is not modeled. However, the bridge deck can have a beneficent effect on the stability of the top main girders, if these are connected to the bridge deck. This can be taken into account in further stages, when more detailed and accurate modeling will be done.

In case in future, more accurate modeling, the unity checks for strength appear to be larger than the unity checks for stability, then the use of high strength steel can be considered for the whole structure. (This is only applicable in case the displacements are not governing.) The use of high strength steel will require less material for the structure, i.e. smaller self-weight, which in turn results in smaller required strength capacity of the structure to carry its own self-weight. Then a lighter and more efficient superstructure will be possible.

These checks should also be done again in later design phases when the self-weight of the bridge deck, finishing and connections are known. For now, 20 kN/m is assumed. In case the self-weight proves to be larger, then the strength and stability should be checked again.

It is also important to note that only first order checks are done in this feasibility study. For further design stages second order effects, eccentricity, etc. should be checked as well. Also, the strength and stability checks are only done for the members in the lattice structure. The connections between the members are not checked.

9.5 Displacements and Rotations

Vertical Deflection

The lattice girder will be precambered by 2617 mm (the vertical displacement due to self-weight, see Figure GG-9).

Then, due to external loads (load case 3 from ANNEX U:), the vertical deflection at midspan will become **778 mm**.

The limit for vertical deflection is $L/350 = 1329 \text{ mm}$ (see Table 2-7). This means that the requirement for vertical deflection is met.

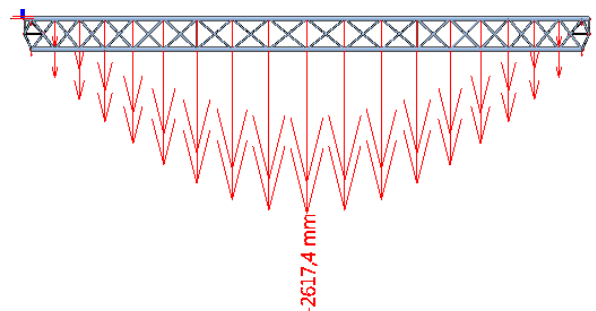


FIGURE 9-13 VERTICAL DISPLACEMENTS DUE TO SELF-WEIGHT

Comments

No calculations or checks are done in this study for the precambering. This should be done in later design phases, as precambering might influence the stresses in the members.

Horizontal Deflection

Horizontally, there are almost no displacements due to self-weight. Therefore, no horizontal precambering is needed.

The largest deformation at the bridge deck level is **712 mm** at midspan (load case 2 from ANNEX U:). This is smaller than the deflection limit (1329 mm).

The largest horizontal displacement, however, occurs for load case 3 at the bottom main members, near the ends of the lattice girder, instead of at midspan (which is more common). The exaggerated deformed structure can be seen in Figure 9-14. This deformed shape is due to omitting the bottom horizontal diagonals near the support. Near the supports, the displacement is 1749 mm. The displacements at bridge deck level are however much smaller. Therefore, the deflection of the bottom girder will not hinder the serviceability at the bridge deck level.

Comment

Even though the deflection at the bottom girders does not hinder the serviceability at bridge deck level, the capacity of the connections at the bottom girders should be checked thoroughly.

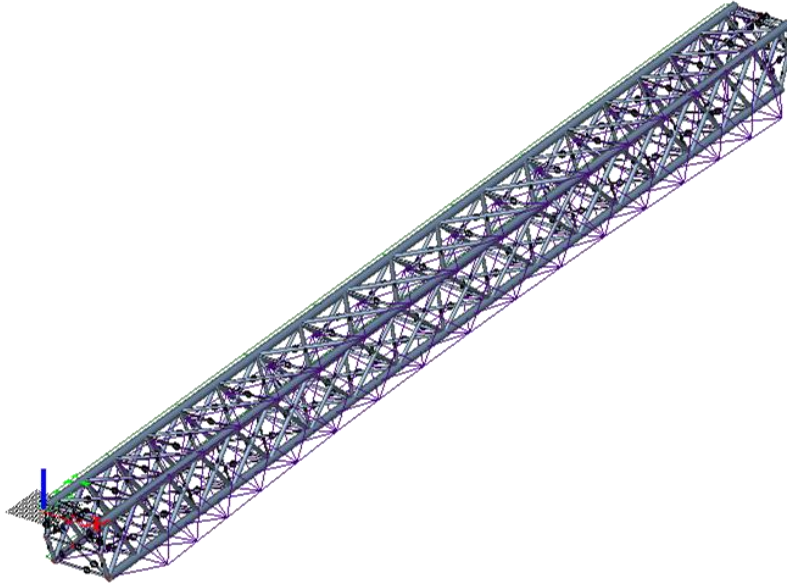


FIGURE 9-14 DEFORMED STRUCTURE DUE TO LOAD CASE 3

Rotations

Rotation in the bridge girder mainly occurs due to rotation of the pontoons. The maximum rotation that occur during the considered load cases are applied in the model. The purpose was to apply the rotations and to design a superstructure, which has to capacity to follow these rotations. The applied rotations are within the serviceability limits. (This is logical, since the substructure was designed in such a way that the rotations would be within the limits).

9.6 Total Self-Weight of Bridge Girder

The total self-weight of all the members in the lattice structure is 158 565 kN. This is approximately 341 kN/m. The self-weight of the bridge deck, finishing and connections in the lattice structure are assumed to be 20 kN/m. In total, the self-weight of the proposed superstructure is 361 kN/m.

However, the total self-weight was assumed to be 265 kN/m during the design of the pontoons. In chapter 10.4, the consequences of this underestimation will be discussed.

Comments

When the final design for the bridge deck and connections are known, it should be checked whether the assumed self-weight is sufficient.

10. CONCLUSION FEASIBILITY STUDY: THE POSSIBILITIES AND LIMITATIONS

10.1 The Buoyancy Bridge Concept for Sognefjord is Feasible

The purpose of this Master thesis is to find a feasible concept for a circa 4500 m long buoyancy bridge, which is located at the Sognefjord in Norway. The bridge concept should be structurally and aesthetically competitive.

The buoyancy bridge consists of 20 spans of 200 m and a large central main span of 465 m. Furthermore, the bridge deck elevates up to 80 m above water level. This span and elevation is required at the 1000 m deep Sognefjord to create a large fairway clearance under the bridge. A buoyancy bridge with these properties is unprecedented.

This study provides the first steps to the design of this buoyancy bridge. Although much more investigation is needed before the proposed concept can be deemed reliable, results of this study show that a buoyancy bridge for the Sognefjord is feasible and it is recommended to conduct further investigations on this promising buoyancy bridge concept.

10.2 Substructure: pontoons and Anchoring System

For the substructure of the buoyancy bridge concept in this study, 22 long, slim cylindrical shaped pontoons are used, which provide upward buoyancy forces and restoring moments to limit the rotations of the structure. The slim shape of the pontoons leads to smaller water loads. The radii and lengths of the pontoons vary respectively from 12 to 20 m and from 115 to 202 m.

For common buoyancy bridges, the relative position of pontoons is maintained by the superstructure. However in this case, the dimensions of the cylindrical pontoons are so large, that a superstructure with plausible dimensions will not be able to restrain the movements of the massive pontoons. Therefore, an anchoring system, consisting of 2 main cables with diameters of 1200 mm and 44 cables of 350 mm, has been designed to maintain the relative positions of the pontoons as much as possible.

From the top view, the anchoring system looks like two mirrored horizontal suspension systems, which restrain the displacements in the direction parallel to the fjord. The displacement due to the maximum combined wind and water load is approximately 6 m for the circa 4500 m long bridge.

With this, a substructure is designed, which is capable of restraining the rotations and displacements of the bridge in such a way, that these movements are within the serviceability limits.

10.3 Superstructure: Lattice Bridge Girders

Because the substructure is able to sufficiently restrain the movements of the bridge, the possibility arises for a slender and light-weight superstructure.

Separate lattice bridge girders with a width and height of respectively 24 and 25 m are designed, which will be supported on the piers by hinged like supports. Only in the plane transversal to the superstructure, the rotation of the bridge girder around its longitudinal axis is coupled to the rotation of the pontoons, and therefore limited by the restoring moments of the pontoons. Furthermore, the torsional rigidity of the lattice girder varies along its length. This way, a light-weight and flexible bridge girder is possible.

Preliminary checks show that the lattice bridge girder can be designed in such a way that all members of the lattice structure have sufficient capacity regarding strength and stability. These results should be interpreted as an encouragement for further investigation and development of the concept. This is due

to the fact that also the connections and more effects should be investigated before this structure can be deemed reliable.

For the bridge piers, a form study has been done. The recommended shape of the piers has a large outer diameter, which gives a sense of robustness. Openings in the piers provides visual lines, which results in a light and transparent appearance. This way, an aesthetic pier has been achieved.

10.4 Underestimation of Superstructure Weight in this Study can be Easily Adjusted

The proposed concept for the buoyancy bridge was designed from the 'bottom' to the 'top'. First, the substructure, i.e. the anchoring system and the pontoons, was designed by assuming the properties of the superstructure. Hereafter, a concept for the superstructure has been developed. Results show that one of the assumptions for the superstructure was underestimated: the self-weight of the superstructure is 36% larger than the initially assumed value for the design of the substructure.

Despite this increased weight of the superstructure, the buoyancy bridge concept is still feasible. This is due to the fact that the self-weight of the superstructure is just a small portion (5%) of the total self-weight of the whole bridge structure. To provide extra buoyancy force for the heavier superstructure, the pontoons must be elongated by approximately 4 m (the pontoon lengths are approximately 200 m). In this study, the relation between the pontoon sizes and water load has been investigated. It is found, that an increase of 2% of the pontoon sizes will lead to a smaller increase of the water load (< 2%). Therefore, the underestimation of the self-weight of the superstructure has little consequences and the proposed concept is still feasible.

10.5 Limitations

There are several limitations for the validity of the proposed substructure and superstructure. These are summarized below.

Limitations for the substructure design:

- The results of this study are only valid when the recommended erection method is used. The recommended erection method involves no mechanical pretensioning. The prestress in the anchoring cables is obtained as result of its own self-weight and the buoyancy of the pontoons. Different erection methods will induce different forces into the structure. This could result into larger deflections and insufficient capacity. Therefore, the structural design and the erection design should be defined together.
- In the proposed design, it is assumed that the bridge superstructure will be flexibly connected to the shore, i.e. the landing place of the bridge is flexible. If the design would be changed and the bridge becomes rigidly connected to the shores, then the axial loads and displacements of the buoyancy bridge will be different. The capacity and displacements of the structure should then be checked again, and if necessary, adjustments in the substructure design should then be made.

Limitations for the superstructure design:

- It is assumed that the lattice bridge girder at the main span is precambered by approximately 2 meters. With this, there will be no deflection due to self-weight. Precambering can also be applied at the side spans.
- An erection method is used, which induces almost no axial forces into the lattice bridge girders when the structure is loaded only by its self-weight. If it is decided on another erection method in the future, then the resistance of the lattice girder should be checked again.

10.6 Not Considered Factors: To be Further Investigated

This preliminary study shows the possibilities of the proposed buoyancy bridge concept. However, many factors should be (further) investigated, before the concept can be deemed reliable. These are summarized in the following for both the substructure and the superstructure.

Not considered factors in the substructure design:

- Effects on the substructure due to impacts.
- Dynamic effects.
- Detailed pontoon design.
- Effects due to ice.
- Effects due to marine growth.
- Detailed calculations for the erection.
- Connections in the anchoring system.
- The final properties of the superstructure. When the final design of the superstructure is known, then the total self-weight can accurately be determined for the design of the pontoons. Also the wind load can then be determined more accurately to design the anchoring system by taking into account the final form of the superstructure (superstructure height, member sizes, member shapes, which determines the wind drag coefficient, etc.).

Not considered factors in the superstructure design:

- Second order effects.
- Effects due to eccentricity.
- Design of the connections.
- Fatigue design.
- Dynamic effects.
- To check whether the assumed self-weight of the bridge deck, finishing and connections is sufficient.
- New unity checks by using the correct load factors according to the Norwegian codes.
- Effects on the members due to a precambering of 2617 mm
- More accurate determination of the wind load by using correct drag coefficients once the final design of the superstructure is known. The bridge girder must have sufficient capacity to resist the wind load.
- The detailed design of the piers.
- The detailed design of the supports.
- Effects due to temperature change.
- The design of the lattice bridge girders at other spans. The height and the width of the lattice bridge girder vary for all side spans.
- The design of a flexible connection between the bridge and the shores.
- Detailed calculations for the erection of the bridge superstructure.
- Effects at the last bays of the lattice bridge girder, where horizontal diagonals are omitted to create a more flexible bridge girder. For example: Do the connections also have sufficient deformation capacity?

10.7 Recommendations

In this study, a buoyancy bridge concept is proposed. However, this is just the product of a preliminary study. There are many possibilities to optimize the design. These are summarized in the following for both the substructure and the superstructure.

Topics for further investigation to optimize the substructure design:

- The use of water as ballast in the pontoons. By replacing the sand by water, the pontoon sizes will increase, since the density of water is smaller. However, using water can still be economically beneficial since there is an abundance of water available at the site.
- The use of steel for the pontoons instead of concrete.
- The diameter of the pontoons can be varied to a certain extent. There is room to either design fat, short pontoons or to design slim, long pontoons, as long as the metacentric height is positive and as long as it does not lead to unfavorable dynamic effects. This freedom is advantageous for the aesthetics of the bridge, since the diameters of the pontoons also influences the design of the bridge piers.
- Solving eccentricity by eccentric ballasting.
- Further detailed calculations and planning for the erection method. The recommended erection method requires no mechanical pretensioning. All stresses in the cables are obtained by the self-weight of the anchoring cables and the buoyancy of the pontoons.
- If an erection method will be used, which requires mechanical pretensioning, the use of materials with smaller weights can be considered for the anchoring cables. This will reduce the pontoon sizes. For example, fiber-reinforced polymer composite wires can be considered.
- The pontoons which are the nearest to the shores can be replaced by fixed supports, the water depth is not deep near the shore.

Topics for further investigation to optimize the superstructure design:

- Take into account the contribution of the bridge deck against buckling. This was not done in this study. However, the bridge deck can increase the buckling resistance of the members at the top in the lattice structure.
- Consider the use of high strength steel. The displacements are not governing for the design. Furthermore, by also taking into account the contribution of the bridge deck, the resistance against buckling will increase and the stability will also not be governing for the design. In this case, when the strength is governing for the design, using higher strength steel can be a good option to make the lattice girder lighter and more efficient.
- Whole different types of supports can be considered. For instance, supports with hydraulic drive systems that compensate rotations of the bridge girder hydraulically. Variation studies for designs, in which the bridge girders are supported in the axis of the pontoons, will also be favorable.
- For the aesthetics, different illumination can be used for the vertical diagonals. By making the dense diagonals near the support dark and the more scattered diagonals near the midspan light, the girder will look more transparent at midspan.

11. REFERENCES

- [1] O. Ellevset, „Project Overview Coastal Highway Route E39,” Statens vesvesen, 2012.
- [2] W.-F. Chen en L. Duan, Bridge Engineering Handbook 2nd Edition, Fundamentals, CRC Press, 2014.
- [3] R. Hermans, „Buoyancy aided Crossing for Bridging Extreme Widths,” TU Delft, 2014.
- [4] „News Source,” [Online]. Available: <http://newsourcegy.com/NEWS/APNU-MOVES-TO-NATIONAL-ASSEMBLY-TO-REDUCE-BERBICE-BRIDGE-FEES/>. [Geopend 25 11 2015].
- [5] „Panoramio,” [Online]. Available: <http://www.panoramio.com/photo/72390131>. [Geopend 25 11 2014].
- [6] „Demerara Harbour Bridge,” [Online]. Available: <http://www.harbourbridge.gov.gy>. [Geopend 25 11 2014].
- [7] „Open Buildings,” [Online]. Available: <http://openbuildings.com/buildings/nordhordland-bridge-profile-2319/media?group=image>. [Geopend 25 11 2014].
- [8] T. Maruyama, „Construction of a Floating Swing Bridge - Yumemai Bridge,” Osaka, 2000.
- [9] „Floating Object Database,” [Online]. Available: <http://db.flexibilni-architektura.cz/o/35?tag=Bridge>. [Geopend 25 11 2014].
- [10] „Environmental Conditions and Environmental Loads from Recommended Practice DNV-RP-C205,” Det Norske Veritas, Norway, 2007.
- [11] „NEN-EN-1991-1-4,” NEN, 2005.
- [12] „Mulighetsstudie for Kryssing Av Sognefjorden Opedal-Lavik,” SINTEF, 2011.
- [13] Reinertsen en O. Olsen, Feasibility study for corssing Sognefjorden: Submerged Floating Tunnel., Leikanger: Norway: Statens Vegvesen Region West, 2012.
- [14] „NEN-EN 1991-2 Traffic Load on Bridges,” NEN, 2003.
- [15] O. Gudmestad en J. Comuny Emesum, Design basis for strait crossings, Bergen: NPRA, 2013.

- [16] M. Karimirad, Offshore Energie Structures, Switzerland: Springer International Publishing, 2014.
- [17] W. Molenaar, J. Vrijling, S. van Baars, K. Bezuyen, W. Colenbrander, H. Kuijper en C. Spaargaren, Hydraulic Structures, Delft: TU Delft, 2009.
- [18] „Anchor Manual,” Vryhof Anchors, 2010.
- [19] „NEN-EN 1993-1-11,” NEN, 2007.
- [20] „High strength thermomechanical steels S460,” Arcelor Mittal, [Online]. Available: http://www.constructalia.com/english/products/structures/steel_sections_and_merchant_bars/structural_steel_grades/high_strength_thermomechanical_steels_s460#.VZ_Gf_ntlHw. [Geopend 10 7 2015].
- [21] S. Chakrabarti, Handbook of Offshore Engineering, Volumes 1-2, Elsevier, 2005.
- [22] „Road Viaducts & Bridges in Norway,” 24 11 2014. [Online]. Available: <http://www.lotsberg.net/data/norway/bru.html>.
- [23] „Demerara Harbour Floating Bridge,” 24 11 2014. [Online]. Available: http://www.thos-storey.co.uk/demerara_bridge.php.
- [24] A. Saleh, „Mega Floating Concrete Bridges,” TU Delft, Delft, 2010.
- [25] „Basic Reference Guide,” Nemetschek Scia, 2010.1.
- [26] A. Simone, An Introduction to the Analysis of Slender Structures, Delft, 2011.
- [27] „BS 5896:2010,” Technical Committee ISE/104 , 2010.
- [28] „NEN-EN 1991-1-3 Norwegian Annex,” 2011.
- [29] „Ferjefri E39,” NPRA, [Online]. Available: <http://www.vegvesen.no/Vegprosjekter/ferjefriE39>. [Geopend 5 11 2014].
- [30] [Online]. Available: <http://nortus.pinger.pl/m/437511>. [Geopend 19 3 2015].
- [31] O. Ellevset, „Ferjefri E39 Summary English,” 2012.

- [32] „NEN-EN 1990 A1,” NEN, 2011.
- [33] S. E. Jakobsen, *Concept Development of a Sognefjord Floating Bridge Crossing*, 2013.
- [34] „Spoor Pro,” [Online]. Available: <http://www.spoorpro.nl/spoorbouw/2014/08/26/haagse-netkous-in-top-twaalf-mooiste-stations/>. [Geopend 17 07 2015].
- [35] „Flickriver,” 1 7 2015. [Online]. Available: <http://www.flickriver.com/places/France/Nord-Pas-de-Calais/Echinghen/>.
- [36] „Structurae 2,” [Online]. Available: <http://structurae.net/photos/4441-viaducs-du-boulonnais-a16-viaduc-dechinghen>. [Geopend 1 7 2015].
- [37] „Structurae 1,” [Online]. Available: <http://structurae.net/photos/4439-viaducs-du-boulonnais-a16-viaduc-dechinghen>. [Geopend 1 7 2015].
- [38] Z. & J. Architects.

ANNEX A: STATE OF THE ART BUOYANCY BRIDGES

In this sections, the state of the art of buoyancy bridges will be shown to illustrate the challenge to find a structurally and aesthetically competitive concept for the buoyancy bridge at Sognefjord.

A.1 Current Buoyancy Bridges

Where the water crossing is wide and deep, buoyancy bridges become a very cost-effective bridge type. For a site where the water is 2 – 5 km wide, 30 – 60 meters deep and a soft bottom extending another 30 – 60 meters, a floating bridge is estimated to cost 3 – 5 times less than a long span fixed bridge [2]. However, extra attention should be paid to wind, waves and currents.

The concept of a floating bridge takes advantage of the natural law of buoyancy of water to support the dead and live loads. There is no need for conventional piers or foundations. However, an anchoring or structural system is needed to maintain transverse and longitudinal alignments of the bridge.

TABLE A-1 FLOATING BRIDGES WHICH ARE CURRENTLY IN USE BY PUBLIC VEHICULAR TRAFFIC

Floating Bridge	Country	Type
Berbice Bridge	Guyana	SPFB
Bergøysund Floating Bridge	Norway	SPFB
Brookfield Floating Bridge	USA	CPF
Demerara Harbour Bridge	Guyana	SPFB
Governor Albert D. Rosellini Bridge	USA	CPF
Homer M. Hadley Memorial Bridge	USA	CPF
Hood Canal Bridge	USA	CPF
Lacey V. Murrow Memorial Bridge	USA	CPF
Nordhordland Bridge	Norway	SPFB
William R. Bennet	Canada	CPF
Yumenai Bridge	Japan	SPFB
New SR520 Bridge (being built)	USA	CPF

Floating bridges have been built since time immemorial. Ancient bridges were generally built for military operations. In the present, there are around 12 floating bridges in use for public vehicular traffic. These are listed in Table 1-1. Floating bridges can be classified into two types, namely the continuous pontoon floating bridge (CPF) and the separate pontoon floating bridge (SPFB). A continuous pontoon floating bridge consists of individual pontoons joined together to form a continuous structure. This leads to large horizontal wave and wind actions and large horizontal movements on the bridge, which needs to be restraint. A separate pontoon floating bridge consists of individual pontoons, acting as supports at a certain interval. Examples for both types of floating bridges are shown in Figure 1-2.



FIGURE A-1 CONTINUOUS PONTOON FLOATING BRIDGE (LEFT) AND SEPARATE PONTOON FLOATING BRIDGE (RIGHT) [25]

In Table 1-1 it can be seen, that all floating bridges in the USA have continuous pontoons. These bridges all cross modest water depths of 60-100 meters, which allows easy anchoring for the large horizontal forces on the continuous pontoons. Achieving horizontal anchoring at the Sognefjord is more complex, since the fjord is more than 1 km deep. An advantage of the continuous pontoon bridge is the omission of a superstructure. However, due to the required elevation of 70 meters and span of more than 400 meters of the bridge girder near the middle of the fjord, a superstructure is required anyway. Previous study show, that a separate pontoon floating bridge is in general cheaper than continuous pontoon floating bridges [3]. More factors and characteristics of both floating bridge types were taken into account and it was concluded that the separate pontoon floating bridge is more suitable for the bridge concept of Sognefjord. More explanation can be found in "*Buoyancy aided crossing for bridging extreme widths*", Annex A, by R.T.H. Hermans.

The bridge concept developed by a previous study is a separate pontoon floating bridge, this concept will be presented in chapter B.1. In general, the superstructure of a separate pontoon floating bridge must be of sufficient strength and stiffness to resist horizontal and vertical forces and to maintain the relative position of the separated pontoons. The superstructure of separate pontoon floating bridges is often made from steel. The truss is most popular, but a box is used as well. Of the bridges listed in Table 1-1, five of them are of the separate pontoon type. These bridges will be analyzed, since the bridge concept for this feasibility study is also a separate pontoon floating bridge.

A.2 Modern Separate Pontoon Bridges

The characteristics of the five separate pontoon bridges from Table 1-1 will be shown below.

Berbice Bridge

Country	: Guyana
Year of completion	: 2008
Length	: 1550 m
Number of spans	: 40
Anchoring system	: Sideways anchored
Superstructure type	: Steel truss
Elevation above water	: 5 m
Costs nowadays value	: 32 million euro
Number of traffic lanes	: 2
Fairway clearance	: 40 x 12 m (width x height)
Fairway solution	: Elevated bridge deck on high pontoons and retractable part



FIGURE A-2 BERBICE BRIDGE [4]

Comparison with the bridge concept for Sognefjord:

As can be seen in Figure A-2, the spanning distances between the pontoons of the Berbice Bridge is much smaller than the spans of the bridge concept for Sognefjord. The longest span in the middle of the Sognefjord is over 400 meters wide and the side spans are 200 meters, while the maximum span of the Berbice Bridge is well below 30 meters.

For the Berbice Bridge, a fairway clearance is achieved by a movable bridge part. In case of passing vessels, the traffic on the bridge will put on a halt and a bridge part will be retracted to make place for the passing of the vessel. Since the purpose of replacing the ferry connections at the Coastal Highway E39 with fixed links was to improve the flow of traffic, the application of a movable bridge part, which would impede the traffic again, is considered to be an ineffective solution.

Moreover, the required clearance height at the mid-fjord span of Sognefjord is 70 meters. The maximum elevation of the Berbice Bridge is 12 meters. This leads to the need of developing a whole new concept of a floating bridge for the Sognefjord. The same conclusion can be reached after the comparisons of the other separate pontoon floating bridges showed in the following.

Bergøysund Floating Bridge

Country	: Norway
Year of completion	: 1992
Length	: 931 m
Longest span	: 106 m [20]
Number of spans	: 13
Superstructure type	: Circular hollow section truss
Elevation above water	: 6 meters
Water depth	: 320 meters
Costs nowadays value	: 48,8 million euro
Pontoon material	: LWA concrete
Pontoon layout	: Rectangular with circular fronts
Pontoon size	: 34 x 20 x 6 m (length x width x height)
Anchoring system	: None, catenary/arch effect
Fairway solution	: Between pontoons
Fairway clearance	: 106 x 6 m (width x height)
Traffic intensity	: low
Ship crossing intensity	: low
Design wind speed	: 27,1 m/s
Tidal Swing	: 4 m
Current	: 1,3 m/s
Wave height	: 1,4 m
Wave period	: 4,5 seconds
Water type	: salt



FIGURE A-3 BERGØYSUND FLOATING BRIDGE [5]

Comparison with the bridge concept for Sognefjord:

Although longer than the Berbice Bridge in Guyana, the spanning distances between the pontoons of the Bergøysund Floating Bridge are smaller (106 meters) than the spans of the bridge concept for Sognefjord (mid-fjord span of over 400 meters wide and side spans of 200 meters).

Moreover, the bridge elevation of the Bergøysund Floating Bridge is quite low (6 meters above water) compared to the required elevation at the mid-fjord span of Sognefjord (70 meters above water). This leads to higher bridge pylons and a whole different bridge design than the Bergøysund Floating Bridge.

Demerara Harbour Bridge

Country	: Guyana
Year of completion	: 1978
Length	: 2010 m
Number of spans	: 61
Superstructure type	: Steel truss



FIGURE A-4 DEMERARA HARBOUR BRIDGE [6]

Elevation above water	: 5 m
Costs nowadays value	: 48,8 million euro
Pontoon material	: Steel
Pontoon size	: 20 x 5 x 2 meters (length x width x height)
Anchoring system	: Sideways anchoring
Fairway solution	: Retractable section at midspan
Fairway clearance	: 77,4 m (width, no height limit)
Fairway small vessels	: 32 x 7,9 m (width x height) (elevated part)
Traffic intensity	: high (24000 vehicles/day) [21]
Number of lanes	: 2
Ship crossing intensity	: low

Comparison with the bridge concept for Sognefjord:

As can be seen in Figure A-4, the spanning distances between the pontoons of the Demerara Harbour Bridge are very small. Since a retractable bridge part, which would impede the vehicular traffic, is considered not an effective solution for the bridge at Sognefjord, a whole different bridge concept with more extreme spanning distances (up to more than 400 meters) and elevation height (more than 70 meters) will need to be developed.

Nordhordland Bridge

Country	: Norway
Year of completion	: 1994
Length	: 1 610 m
Longest pontoon span	: 113 m
Number of spans	: 19
Superstructure type	: Box girder spanning
Elevation above water	: 5,5 m
Water depth	: 500 m
Costs nowadays value	: 102 million euro
Pontoon material	: LWA concrete
Pontoon size	: 42 x 12,5 x 6,8 m (length x width x height) [22]
Anchoring system	: None, catenary/arch effect (R=1700 m)
Fairway solution	: Elevated part by cable-stayed bridge section with one tower near shore
Fairway clearance	: 172 x 32 m (width x height)
Ship crossing intensity	: low
Number of traffic lanes	: 2
Design wind speed	: 27,1 m/s
Tidal Swing	: 3 m
Wave height	: 1,7 m
Wave period	: 5,1 seconds
Water type	: salt



FIGURE A-5 NORDHORDLAND BRIDGE [7]

Comparison with the bridge concept for Sognefjord:

As was the case for the Bergøysund Floating Bridge, the spanning distances between the pontoons of the Nordhordland Bridge are smaller (113 meters) than the spans of the bridge concept for Sognefjord (mid-fjord span of over 400 meters wide and side spans of 200 meters).

A fairway clearance at the Nordhordland Bridge is achieved by realizing an elevated part by a cable-stayed bridge section with one tower near the shore. For the new bridge concept, it is desired to locate the fairway clearance for large vessels at the middle of the Sognefjord to increase the safety for fairway vessels. If a large bridge superstructure, e.g. a large pylon with a cable-stayed system, is to be realized at the middle of the fjord to make the large clearance span possible, this superstructure will then be supported on floating pontoons in the water. At the Nordhordland Bridge, the large pylon of the cable-stayed system is constructed on shore at the side of the river. The design of a large superstructure on pontoons leads to new challenges for the bridge concept of Sognefjord.

Yumemai Bridge

Country	: Japan
Year of completion	: 2001
Length	: 410 m
Longest pontoon span	: 280 m
Superstructure type	: Steel arch bridge
Elevation above water	: 26 m
Water depth	: 12 m
Ground condition	: poor (reclaimed land)
Pontoon material	: Steel
Pontoon size	: 58 x 58 x 8 m (length x width x height)
Anchoring system	: None, uses mooring piles for horizontal restraints
Total weight floating part	: 33 000 tons
Weight superstructure	: 18 200 tons
Weight pontoons	: 6 600 tons
Weight mooring	: 8 200 tons
Fairway solution	: Bridge can be swung around pivot axis near one end of the girder when passage way for very large vessel is the channel is needed during emergency
Fairway clearance	: 200+ m (width, no limit in height)
Fairway small vessels	: 135 x 26 m (width x height) [20]
Number of traffic lanes	: 6
Design wind speed	: 20 m/s
Tidal Swing	: 5,32 m
Wave height	: 1,4 m



FIGURE A-6 YUMEMAI BRIDGE [8]



FIGURE A-7 YUMEMAI BRIDGE SWUNG OPEN [9]

Comparison with the bridge concept for Sognefjord:

In terms of spanning length, the Yumemai Bridge comes the closest to the bridge concept for Sognefjord, although still much smaller (280 meters compared to more than 400 meters). The elevation of the bridge deck of the Yumemai Bridge is also the highest of all current separate pontoon bridges in the world, although it is again much smaller than the expected elevation of the new bridge concept at Sognefjord: 26 meters compared to 70 meters.

The main reason for the majority of the bridges to realize floating bridge types is the large water depths. The choice for a floating bridge in Osaka was primarily due to the poor ground conditions. The bridge connects two reclaimed islands in the port. In case large vessels need to pass the channel, the bridge can be swung around the pivot axis near one end of the girder. This is, however, expected to be seldom needed.

As it is expected that large vessels will pass the bridge at Sognefjord more often, such a movable bridge solution which will impede the vehicular traffic, is considered inefficient. Moreover, mooring piles are used to restraint the horizontal loads on the Yumemai Bridge, where the water depth is 12 meters. This solution for horizontal restraints is less feasible at Sognefjord, where the fjord reaches a depth of more than 1000 meters.

The buoyancy of the Yumemai Bridge can still be studied, since a large superstructure of 33 000 tons is vertically supported on pontoons. The pontoon shape is however very different from the shape of the bridge concept for Sognefjord. The pontoons of the Yumemai bridge are flat (58 x 58 x 8 meters), while the pontoons of the bridge concept for Sognefjord are long cylinders (radius of approximately 15 meters and heights of around 100 meters).

A.3 No Buoyancy Bridge with this Span and Elevation exists

As seen and described in the previous sections, none of the existing floating bridges can be compared to the required characteristics for the buoyancy bridge at Sognefjord.

Three of the separate pontoon floating bridges shown above, facilitate the passing of larger vessels by using retractable parts. During the passing of large vessels, the vehicular traffic on the bridge will be halted and certain bridge parts will be retracted, so large vessels will be able to pass the bridge. Since the purpose of the Norwegian Ministry of Transport and Communication to commission the Coastal Highway E39 project was to reduce the travel time by improving the flow of the traffic, replacing the ferry connection with a movable bridge is not considered to be the most effective solution. Therefore, implementing movable bridge parts, like the Berbice Bridge, Demerara Bridge and Yumemai Bridge, to provide the required fairway clearance, is not an option for the bridge concept at Sognefjord.

The exclusion of the option to install movable bridge parts results in a very high elevated height of 70 meters of the bridge girder at the mid-fjord span. The bridge deck elevation of 26 meters of the Yumemai Bridge is the highest existing bridge deck elevation of a floating bridge. This height is still far smaller than the requirement for the new bridge concept at Sognefjord.

All maximum span widths of the existing buoyancy bridges are much smaller than the required span width of 400 meters for the mid-fjord span at Sognefjord. Currently, the Yumemai Bridge has the largest span between pontoons in the world: a main span of 280 meters.

These facts show that new technological alternatives and concepts must be sought for the extreme bridging at Sognefjord.

ANNEX B: BUOYANCY BRIDGE CONCEPT FROM PREVIOUS STUDY

B.1 Buoyancy Bridge Concept from Previous Study

The buoyancy bridge concept from the research of Hermans (2014) is shown in Figure B-2. A description and explanation about the choices for the structure will be given in section B.2. The full study is reported in *"Buoyancy aided crossing for bridging extreme widths"*, 2014, by R.T.H. Hermans. This concept for the bridge, however, does not comply with the requirements. It was concluded that this concept was not suitable. The complications of the concept are described in section B.3. In chapter 2.3, the comparison between this concept and a new proposed concept is shown.

B.2 Characteristics of Bridge Concept by Hermans (2014)

B.2.1 Desire for Flexible and Slender Bridge Design

A flexible link is desired, as a fully stiff link is considered inefficient. By creating a flexible construction, large deflections and rotations will be allowed, provided that the deflections and rotations happen slowly. This is an elegant way of constructing, which will not require massive amounts of material to fully prevent movement of the large structure.

A slender bridge design is desired for aesthetic appearance and also for structural reasons. Through research it is proven that the bridge concept is majorly influenced by wind induced deformations rather than wave and current [3]. The wind load is the primary cause for large horizontal movement and forces. To resist these effects, the anchorage system and pontoons should be designed accordingly. Therefore, it is of utmost importance to design a slender bridge girder. This way, the wind load will be smaller and consequently, also the overturning moment will decrease. In Figure B-1, it is shown how the load from the environment will cause an overturning moment on the cross-section of the bridge.

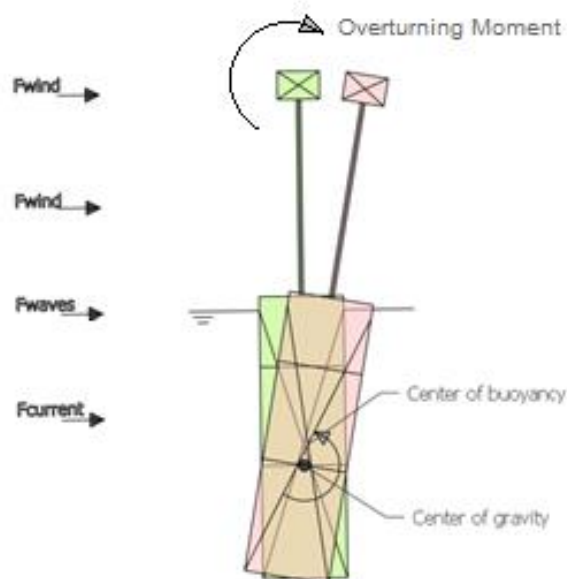


FIGURE B-1 PONTOON ROTATION AND OVERTURNING MOMENT [3]



FIGURE B-2 BUOYANCY BRIDGE CONCEPT FROM PREVIOUS STUDY [3]

B.2.2 Bridge S-Shaped in Top View

In a previous research [3], it was decided together with Zwarts & Jansma Architects to create an S-shape in the top view of the bridge concept. The dimensions and characteristics of the shape are shown below in Table B-1 and Figure B-3.

TABLE B-1 DIMENSIONS AND CHARACTERISTICS OF S-SHAPE

Characteristic	Sign	Unit	Value
Strait length	x_{tot}	[m]	3507,40
Half strait length	x_1	[m]	1753,70
Radius	R	[m]	1866,25
Lateral distance of curve ashore	y_1	[m]	638,29
Lateral distance of curve offshore	y_2	[m]	1227,96
Horizontal angle at shore	α	[rad]	$\pi/9$
Strait length bridge axis	$2*k$	[m]	4281,75
Half-length along bridge deck	$\frac{1}{2} s$	[m]	2280,06
Total length bridge along deck	s	[m]	4560,11

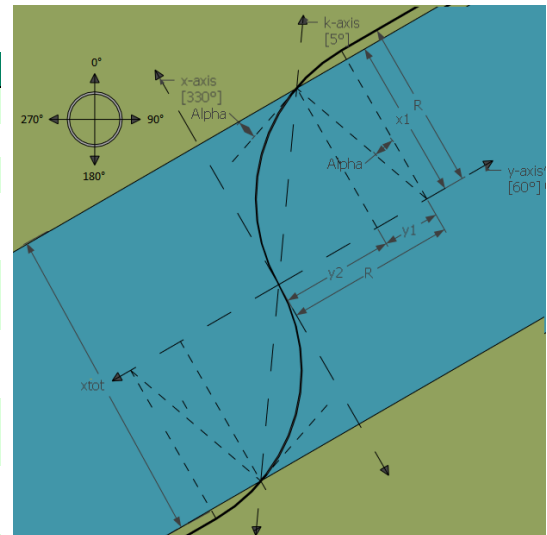


FIGURE B-3 CHARACTERISTICS S-SHAPE [3]

Besides being aesthetically pleasing, another advantage of this shape is that it creates a good connection to the existing road, as can be seen in Figure B-4. The required modifications to the existing road to create a fluent link to the bridge is kept to a minimum, e.g. if the fixed link would be straight from shore to shore, the highway would have to be redirected to the existing road with a certain radius. This could conflict with the surrounding landscape and village, situated near the shore. As the surrounding landscapes contain steep slopes and mountains, the construction of the new roads could be expensive. An S-shaped bridge prevents this.

Moreover, such a shape of the floating bridge can have an advantage in terms of longitudinal expansion of the bridge. If the bridge was straight from shore to shore over a length of almost 4 km, the longitudinal expansion, which is to be absorbed by the structure, would be very large. With an S-shape, the expansion will be absorbed by the shape of the bridge; due to the expansion, the arches will become even more curved. This is illustrated in Figure B-5. Naturally, this behavior should be kept in mind for the design of the bridge.



FIGURE B-4 BRIDGE CONCEPT SOGNEFJORD

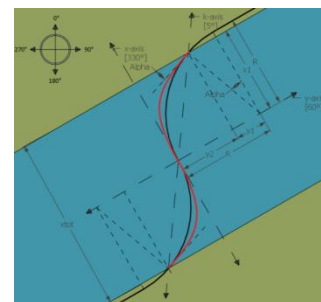


FIGURE B-5 DEFORMATION DUE TO EXPANSION

B.2.3 Pontoon Distance of 200 meters in Side Spans

In terms of aesthetics, a slender bridge with large span distance is preferred, although smaller spanning distances in combination with the use of more columns leads to more slender columns. Structurally, larger pontoons show better results for the static loads, and better results are also expected in the dynamic analysis [3, p. 59]. Therefore, after careful considerations, a trade-off was made between required structural properties and aesthetics. Besides the large main span at the middle of the fjord of 400 meters, which is required for the fairway clearance, pontoon distances of 200 meters were chosen for all side spans.

B.2.4 Continuous Box-Tendon Girder Design in the Superstructure

A simple box design appeared to be insufficient in terms of required stiffness for the longest span at the middle of the fjord, the mid-fjord span. For this reason, the simple box girder was replaced by a continuous box-tendon girder design with incorporation of suspension action, as shown in Figure B-6. In the box-tendon girder design, the tension flange of the simple box girder is replaced by a tendon system, which has a higher steel grade. As result, the stiffness greatly increases, while the total weight and the surface area for the horizontal wind force are reduced. Since the deflections still exceed the requirements, suspension action is introduced by prestressing the tendon. It is assumed that the box-tendon girder design with suspension contribution would be sufficient. The section is not checked further, so no suitable solution is found yet for the mid-fjord span.

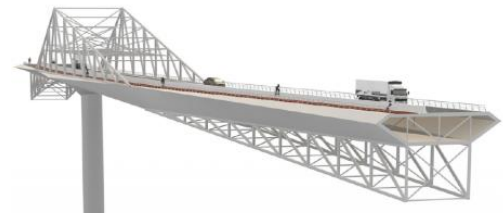


FIGURE B-6 BOX-TENDON GIRDER
IMAGE PROVIDED BY ZWARTS & JANSMA ARCHITECTS

For the side spans, a slender continuous box girder with a span to girder height ratio of 35 and with a small preset positive deflection (precambering) would suffice, but nevertheless, the continuous box-tendon girder design with a span to girder height ratio of 90 was applied to the whole bridge, this is shown in Figure B-7. This slender design was considered the most elegant.

A structural system with simply supported bridge parts responds favorable to pontoon movement: movements hardly affect the bending moments in simply supported beams. Furthermore, a simply supported system is easier to construct. However, a system with simply supported bridge parts gives rise to large initial deflections and rotations. Through research [3] it was proven that both the deflections and rotations in the vertical plane do not meet the limits. For this reason, a fully continuous girder was applied to the whole bridge length to increase the stiffness.

Although the occurring sagging bending moments proved to be smaller by replacing the simply supported system with a continuous system, unfavorable characteristics in pontoon movement response and construction are big liabilities. When pontoon settlement is regarded, the bending moment capacity for the side spans does not suffice. The bending moment capacity for the mid-fjord span was not checked. Furthermore, a bridge deck joint configuration for the continuous system might prove to be challenging.

B.2.5 Torsional Supports at Pontoons

The torsional resistance of the box girder with dimensions shown in Figure B-7, is not sufficient to resist the loads; the rotations at mid span of the mid-fjord span exceed the limits severely. Therefore, torsional supports are applied to each pontoon in this concept to resist the effects from eccentric traffic loading.

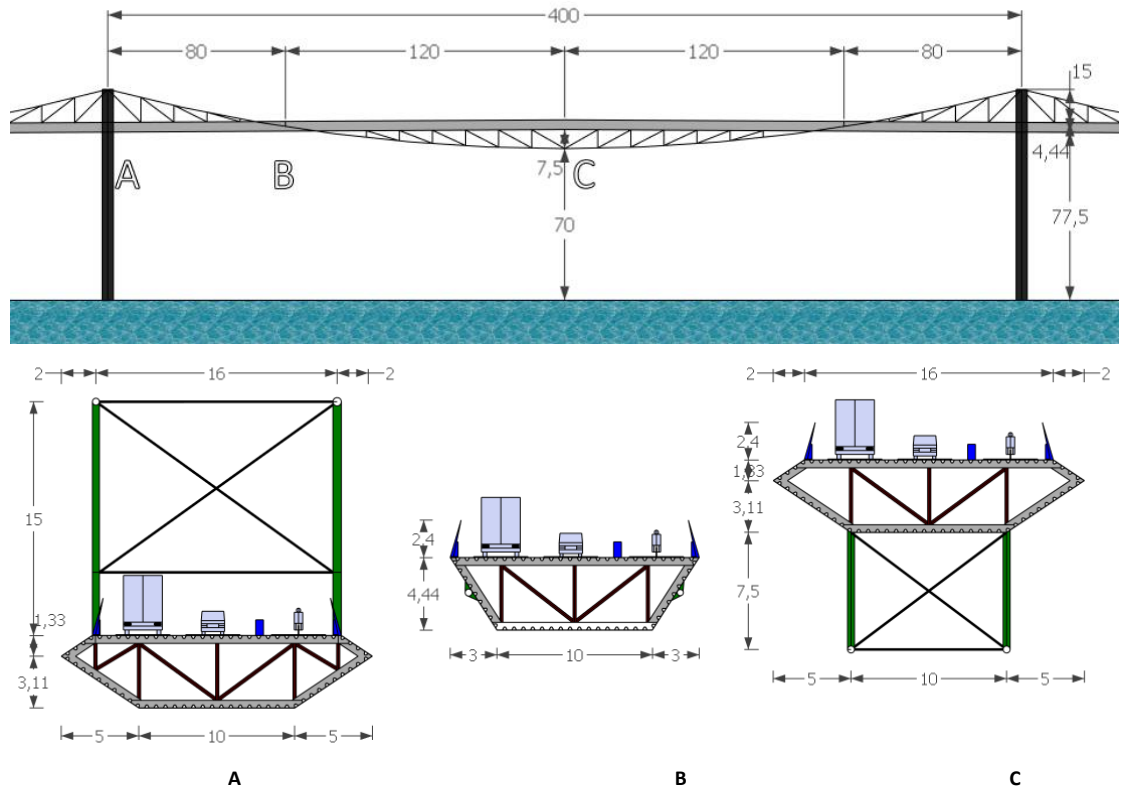


FIGURE B-7 CROSS SECTIONS OF BRIDGE GIRDER ALONG SPANNING LENGTH
 RETRIEVED FROM "BUOYANCY AIDED CROSSING FOR BRIDGING EXTREME WIDTHS", 2014, BY R.T.H. HERMANS

B.2.6 Side Anchoring System with Four Anchored pontoons and Arch Action

End anchored arches have properties favorable to the ones of a side anchored structure. Lot of this has to do with the rotation center being in the bridge girder for end anchored arches, which results in the fact that the governing wind force will have no contribution to the overturning moment equilibrium [3]. However, a satisfying end anchored concept could not be obtained and it was decided to create a combination of a side and end anchored concept, in which five end anchored parts are supported by four side anchored pontoons, as shown in Figure B-8.

In this anchoring concept, the bridge girder needs to transfer the loads from the non-anchored pontoons to the anchored ones. This raises issues on the laterally unsupported bridge length and lateral arch stability of the bridge girder. After investigation, it appeared that the transfer of the lateral forces from the non-anchored pontoons to the anchored ones leads to complications

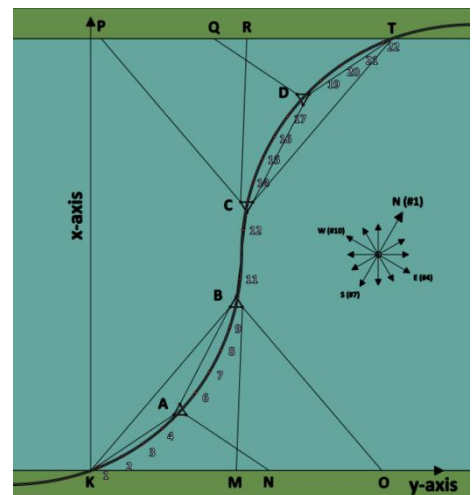


FIGURE B-8 ANCHORING SYSTEM WITH FOUR ANCHORED PONTOONS [3]

regarding instability and unacceptable lateral deformations. For this reason, arch/chain action of the bridge part is introduced to stiffen the bridge parts laterally.

In order to incorporate this arch affect, the bridge parts are longitudinally fixed at the anchored pontoons by the use of the anchoring tendons to create a tie, as can be seen in Figure B-8. These tendons are then stressed, introducing also stresses in the arched bridge girder, increasing the lateral stiffness of the girder. Implementing arch/chain action however, subjects the arch to normal forces caused by pontoon movement. In this system, overturning moments of the non-anchored pontoon element are compensated for by the pontoon's buoyancy restoring moment. However, some rotation will still occur. Since the bridge deck is fixed to the pontoon, those rotations will be imposed on the bridge deck. Simultaneously, the torsion of the pontoon imposes a vertical displacement on the bridge girder. The combination of the above effects and its implications on the lateral arch stability creates a complex system, which will be further discussed in chapter B.3. In the research of R.T.H. Hermans (2014) these effects and implications are not further assessed in analytical models.

B.2.7 Prestressed Anchoring Tendons

The anchoring tendons are prestressed by their submerged self-weight, causing them to comply with a parabolic shape. Prestressing the tendons limits the deflections, as the spring stiffness in the usable length range is increased. The tendon stiffness is chosen to have a drap ratio of $L/16$.

Results have shown that when the bridge girder is not considered to contribute to keeping the pontoon in place, the lateral deflections exceed the limits excessively. In case the bridge deck contribution to the pontoon movement is taken into account, the displacements have decreased greatly compared to the concept without bridge girder contribution, although it still exceeds the limits. Stiffer tendons in combination with a contributing bridge girder is recommended but not verified.

B.2.8 Cylindrical Pontoon Elements with Ballast

Two mechanisms can make a restoring overturning moment to occur: the stiffness of the bridge girder and the buoyancy of the pontoon. Through studies it was proven that with this bridge concept, the buoyancy restoring moment stiffness is the only significant variable which can limit the rotations to meet the requirements. The stiffness of the bridge deck has limited contribution to compensate the overturning moment. This emphasizes the importance of the buoyance property of the pontoons.

For the pontoon shape, it was decided on a simple cylindrical shape as shown in Figure B-9, which is also often used for spar structure in the offshore industry. Ballast weight in the lower parts of the pontoons leads to a low center of gravity. Consequently, the buoyance force lever arm increases, leading to a larger buoyancy restoring moment. Another advantage of the cylindrical shape is the small dynamic wave response.

A tripod pontoon shape with larger submerged area was also investigated, but these were considered aesthetically not suitable, although it performed more material efficient. Another drawback for the tripod is the large decrease in passage way, since a distance of 100 meters would be required between the pontoons in the tripod.

For the cylindrical pontoons, a radius of 15 meters was chosen over large radii. Smaller pontoon radii proved to be more material efficient, to have better dynamic behavior and are considered aesthetically more pleasing.

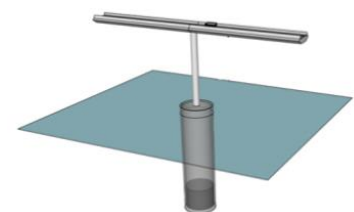


FIGURE B-9 CYLINDRICAL PONTOON ELEMENT [3]

B.3 Complications Encountered for the Extreme Buoyancy Bridge Concept

B.3.1 Slenderness and Flexibility leads to excessive Displacements

Since this is a project of such magnitude and complexity, a lot of complications arose during previous studies and researches. The buoyancy bridge concept, which is developed in a previous research, is shown in Figure B-2. This design, however, comes with quite some remarks and questionable feasibility and actually no suitable concept was found for a flexible and slender bridge design, which shows an acceptable behavior at bridge deck level.

A slender bridge design is desired for aesthetic appearance and also for structural reasons. Through research it is proven that the bridge concept is majorly influenced by wind induced deformations rather than wave and current [3]. The wind load is the primary cause for large horizontal movement and forces. To resist these effects, the anchorage system and pontoons should be designed accordingly. Therefore, it is of utmost importance to design a slender bridge girder. This way, the wind load will be smaller and consequently, also the overturning moment will decrease.

However, the slenderness of the bridge concept shown in Figure B-2 has led to complications for deflections, rotations and also for torsional loads due to eccentric traffic load and arch stability. Even the capacity in terms of strength appeared to be insufficient (e.g. in load configurations with settled pontoons). These shortcomings and other factors, for which the concept has failed to meet the requirements, will be described in the next sections. Because of these complications, no adequate design is found yet for the buoyancy bridge.

B.3.2 Required Clearance at Mid-Fjord Span not Achieved

A shortcoming of the bridge concept shown in Figure B-2 is the fact that it does not comply with the required fairway clearance. In the middle of the fjord, at the mid-fjord span, a fairway clearance should be present for vessels, like large cruise ships as shown in Figure B-10. The required clearance must have a passage width of at least 400 meters, a passage height of 70 meters and a draught of 20 meters. In this concept however, the pylons at this span were designed with a center to center distance of 400 meters. As a result, the clearance width is smaller than the required 400 meters.



FIGURE B-10 FAIRWAY CLEARANCE FOR LARGE VESSELS [26]

B.3.3 Design Mid-Fjord Span Insufficient: Extensive Vertical Deflections and Difficult Detailing

The deflections and rotations of the box-tendon girder with variable tendon drape over the length exceed the requirements severely. To compensate this, suspension action was incorporated by prestressing the tendon of the bridge girder. The feasibility of this system was however not investigated yet. It was assumed that the box-tendon girder design with suspension contribution would be sufficient. The section is not checked further, so no suitable solution is found yet for the mid-fjord span.

The implementation of suspension action requires longitudinal shear connections between tendon and truss. These connections are subjected to fatigue load and no special detailing for them is investigated yet.

B.3.4 Continuous System: Low Robustness and Difficult Construction

A fully continuous girder was applied to the whole bridge length to increase the stiffness. Although the occurring bending moments prove to be smaller than for a system with simply supported bridge parts, unfavorable characteristics in pontoon movement response and construction are a big liability. When pontoon settlement is regarded, the bending moment capacity for the side spans does not suffice. Therefore, the concept design in Figure B-2 leads to a system with a low robustness; unforeseen load configurations may lead to failure or plasticity.

Furthermore, the design of a bridge deck joint configuration with such large deformation capacity and the construction of the continuous system will prove to be challenging.

B.3.5 Anchoring System: Lateral Displacements exceed Limits and Unfavorable for Bridge Girder

The floating bridge is horizontally loaded by wind, wave and current loads. Due to these loads, rotation and horizontal translations occur. In such a situation, a superstructure with sufficient strength and stiffness may contribute to maintaining the relative position of the pontoons. This contribution depends on the ratio between the stiffness of the superstructure and the stiffness of the anchoring system. In order to allow a slender bridge girder design, it is desirable that the position of the pontoons is maintained primarily by the anchoring system.

The translation of the floating bridge due to environmental loads was addressed in case of with and without the bridge deck contribution to pontoon movement. Obtained translations and rotations for the case without bridge deck contribution exceed the limits by ten times. With bridge contribution taken into account, the translations and rotations still exceed the limits, although being much smaller. For these reasons, stiffer tendons in the anchoring system in combination with a contributing bridge girder is recommended, but not verified in the previous study. A suitable solution must be found.

To solve the excessive lateral translations, the stiffness of the anchoring tendons and the contribution of the bridge girder need to be increased. The contribution of the bridge girder to the lateral restraining system is determined by the ratio of anchoring tendon stiffness and bridge part's upper longitudinal stiffness. The latter consists of the stiffness of the longitudinal flexibility due to pontoon rotation, the longitudinal stiffness of the arch and the longitudinal stiffness of the connection arch to pylon. As all stiffness values are non-linear, this is complicated and it is doubtful whether a reliable design can be obtained. The stiffness of the anchoring system needs to be increased, but it is not verified whether feasible anchor cable diameters can be obtained to limit the translations.

B.3.6 Prestressing the Horizontal Arch has no Structural Contribution, only Complications

Through previous studies and research it was concluded that the S-shape of bridge in the top view, as can be seen in Figure B-2, has no structural contribution. In order to incorporate the arch action, the bridge parts are longitudinally fixed at the anchored pontoons by using the anchoring tendons to create a tie, as could be seen before in Figure B-8. Implementing arch/chain action however, subjects the arch to normal forces caused by pontoon movement.

Furthermore, due to possible pontoon motion and rotation, the supports might be longitudinally flexible, which leads to a reduced arch effect. When making use of a part of the arch, the drupe is too small to contribute to the stiffness. When using the whole arch, the structure becomes prone to instability [3].

Moreover, the arch/chain action due to prestressing leads to an undesired effect: it induces torsional loads. In this system, overturning moments of the non-anchored pontoon element are compensated for by the pontoon's buoyancy restoring moment. However, some rotation will still occur. Since the bridge deck is fixed to the pontoon, those rotations will be imposed on the bridge deck. What's more, the torsion of the pontoon imposes a vertical displacement on the bridge girder.

The prestressing of the horizontal arches also burdens the anchoring system for both the longitudinal and lateral anchoring tendons. Because a certain ratio between the stiffness of the bridge girder and the stiffness of the anchoring system is needed to achieve a specific contribution of the bridge girder, large forces are required in the anchoring tendons. For example, if the bridge girder is fully flexible compared to the anchoring system, the contribution of the bridge girder would be negligible. If the bridge girder was fully fixed, the girder would be fully contributing. However, this would require a robust girder with sufficient capacity. It is desired to have a small bridge girder contribution, so a slender girder can be realized, while the contribution is big enough for the arch action of the bridge girder to contribute. This demands a large anchoring stiffness and consequently, also large forces in the anchoring tendons.

The combination of the above effects and its implications on the lateral arch stability creates a complex system and it is not further assessed in analytical models in the research of R.T.H. Hermans (2014). Because of the complexities and disadvantages it induces on the structure without an effective contribution to the lateral stiffness, it is worth considering omitting the arch/chain action.

B.3.7 Anchoring System: Anchoring Four pontoons leads to Unfavorable Effects


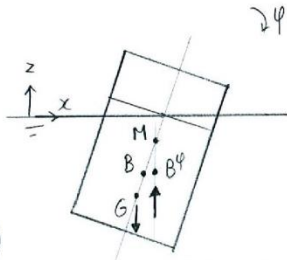
The transfer of lateral forces from non-anchored pontoons to anchored pontoons leads to instability and large deflections of non-anchored bridge parts. According to results from previous studies [3], stability issues arise for the bridge girder due to rotation and vertical movement from non-anchored pontoons, which does not fulfill the requirements.

B.3.8 No Satisfying Joint Design Obtained Yet

Another important result from previous research [3], is that the longitudinal forces exceed the lateral forces induced by lateral loading by a factor up to four, while the study of Hermans (2014) was conducted under the assumption that the longitudinal and lateral forces were equal (which led to cylindrical shaped pontoons with equal stiffness's in every direction). The components that were taken into account for the longitudinal forces are the spalling forces from arch action and the longitudinal forces due to the lateral retaining system. If the situation, for which one bridge part is in compression while the adjacent one is in tension, would be incorporated, the longitudinal loads would increase even further. This leads to significant problems for the transfer of these forces from bridge deck level to the anchor tendon, since the forces in longitudinal direction due to lateral pontoon movements are large. Moreover, this also leads to the requirement that the buoyant rotational stiffness for transferring the longitudinal loads must be very large. This could result in complicated joint design.

For the bridge concept of Hermans (2014), no satisfying joint designs are obtained for the joints between the pontoons and anchoring system and the joints between the bridge girders and pylons. It is still uncertain what kind of expansion or hinged joints should be used that allows longitudinal pontoon translation while inducing limited forces in the bridge girder. It is also uncertain which degrees of freedom of the joint should be restrained.

ANNEX C: VERIFICATION CALCULATION METHOD ROTATIONAL STIFFNESS PONTOONS

Project	: Buoyancy Bridge Sognefjord	
Part	: Verification rotational stiffness of pontoons	
<p><u>Introduction</u></p> <p>In the Maple calculation file in Annex L of Extreme Buoyancy Bridge Sognefjord by T. Yip (2015), the rotational stiffness of each pontoon is determined by using bending moment equilibrium and the following expressions:</p> $MG = MB + GB = \frac{I_{yy}}{V_s} + GB \quad (\text{metacentric height})$ <p>with</p> <ul style="list-style-type: none"> I_{yy} = area moment of inertia of the plane intersected by the waterline V_s = volume of the immersed part of the pontoon $M_{\text{restoring}} = G_{\text{tot}} \cdot MG \cdot \sin \varphi \quad (\text{restoring moment})$ <p>with</p> <ul style="list-style-type: none"> G_{tot} = total self-weight of the structure $k_{r_{Bu}} = \frac{M_{\text{restoring}}}{\varphi} \quad (\text{rotational stiffness})$		
<div style="display: flex; justify-content: space-between;"> <div style="width: 60%;"> <p>Fig 1 Floating Pontoon</p> <ul style="list-style-type: none"> G = Center of Gravity B = Center of Buoyancy M = Metacenter B^φ = center of Buoyancy in tilted position </div> <div style="width: 35%; text-align: center;">  </div> </div>		
<p>To verify whether these expressions are correct, the rotational spring stiffness of a rectangular pontoon is calculated analytically, with the use of AutoCAD and by using the expressions, which are shown above. Hereafter, the three obtained rotational stiffness values can be compared to check the validity.</p> <p>The expressions are based on principles of hydrostatics. An explanation of the expression can be found in 'Multi-span Suspension Bridge with floating towers', chapter 2.1 by Krijan Brunstad, 2013.</p>		
Name:	Christine Yip	Date: 21-4-2015
Page:	1/8	Rev:

Project : Buoyancy Bridge Sognefjord

Part : (Analytical) verification restoring moment



Analytical Pontoon II properties (source: Maple calculation file, see Annex).

$$\left. \begin{aligned} y_{COG} &= -28,02 \\ y_{COB} &= -26,12 \end{aligned} \right\} GB = 1,9 \text{ m}$$

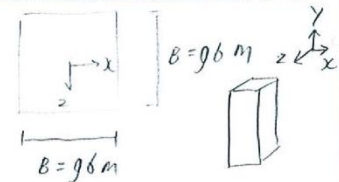
$$L_{\text{pontoon}} = 55,85 \text{ m}$$

$$\frac{1}{2} \cdot B = 48 \text{ m}$$

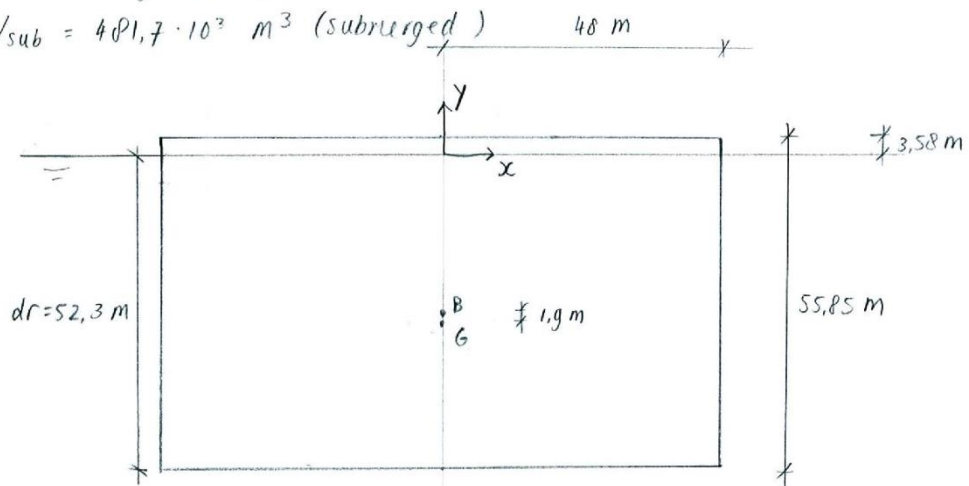
$$t_{SL} = 3,58 \text{ m}$$

$G_{\text{tot}} = 3706 \cdot 10^3 \text{ kN}$ (Total self-weight of pontoon, ballast, pylons and bridge deck)

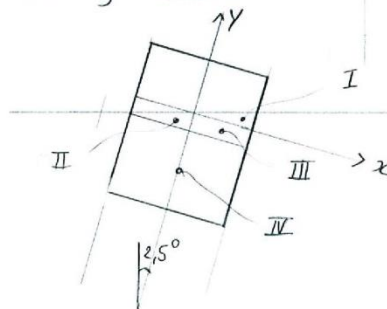
$$V_{\text{sub}} = 481,7 \cdot 10^3 \text{ m}^3 \text{ (submerged)}$$



Assume rectangular pontoon shapes



In the following calculations:



Name: Christine Yip

Date: 21-4-2015 Page: 2/8

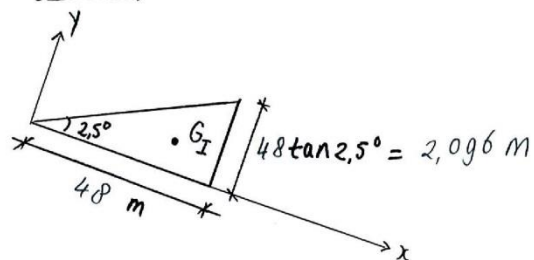
Rev:

Project : Buoyancy Bridge Sognefjord

Part : Verification rotational stiffness (analytical part)



Pontoon 11, **part I**:

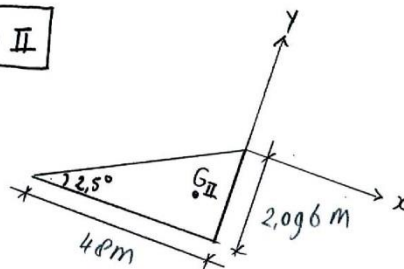


$$G_I : x_{G_I} = \frac{2}{3} \cdot 48 = 32 \text{ m}$$

$$y_{G_I} = \frac{1}{3} \cdot 2,096 = 0,699 \text{ m}$$

$$A_{G_I} = \frac{1}{2} \cdot 48 \cdot 2,096 = 50,30 \text{ m}^2$$

Part II

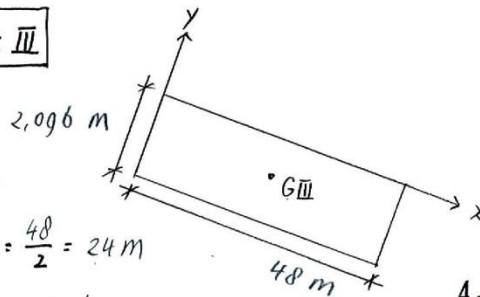


$$G_{II} : x_{G_{II}} = -\frac{1}{3} \cdot 48 = -16 \text{ m}$$

$$y_{G_{II}} = -\frac{2}{3} \cdot 2,096 = -1,397 \text{ m}$$

$$A_{G_{II}} = \frac{1}{2} \cdot 48 \cdot 2,096 = 50,30 \text{ m}^2$$

Part III



$G_{III} :$

$$x_{G_{III}} = \frac{48}{2} = 24 \text{ m}$$

$$y_{G_{III}} = \frac{-2,096}{2} = -1,048$$

$$A_{G_{III}} = 2,096 \cdot 48 = 100,61 \text{ m}^2$$

Name: Christine Yip

Date: 21-4-2015 Page: 3/8

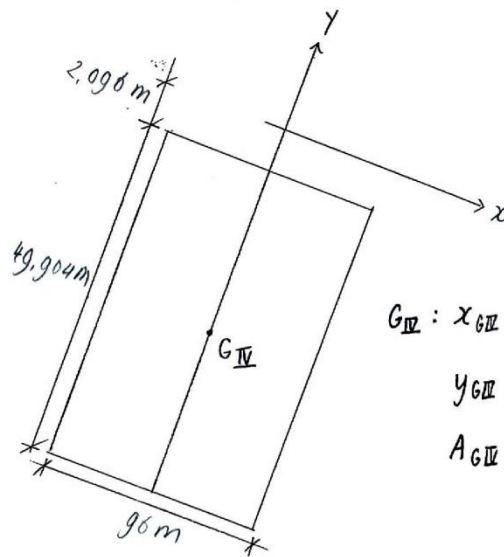
Rev:

Project : Buoyancy Bridge Sognefjord

Part : Verification rotational stiffness



Pontoon 11. Part IV



$$G_{IV} : x_{G_{IV}} = 0 \text{ m}$$

$$y_{G_{IV}} = -\left(2.096 + \frac{49.904}{2}\right) = -27.05 \text{ m}$$

$$A_{G_{IV}} = 49.904 \cdot 96 = 4790,8 \text{ m}^2$$

New center of buoyancy:

$$x_{COG,N} = \frac{\overbrace{50,3 \cdot 32}^{\text{Part I}} + \overbrace{50,3 \cdot -16}^{\text{Part II}} + \overbrace{100,61 \cdot 24}^{\text{Part III}} + \overbrace{4790,8 \cdot 0}^{\text{Part IV}}}{50,3 + 50,3 + 100,61 + 4790,8} = 0,645 \text{ m}$$

$$y_{COG,N} = \frac{50,3 \cdot 0,699 + 50,3 \cdot -1,397 + 100,61 \cdot -1,048 + 4790,8 \cdot -27}{50,3 + 50,3 + 100,61 + 4790,8} = -25,99 \text{ m}$$

Name: Christine Yip

Date: 21-4-2015

Page: 4/8

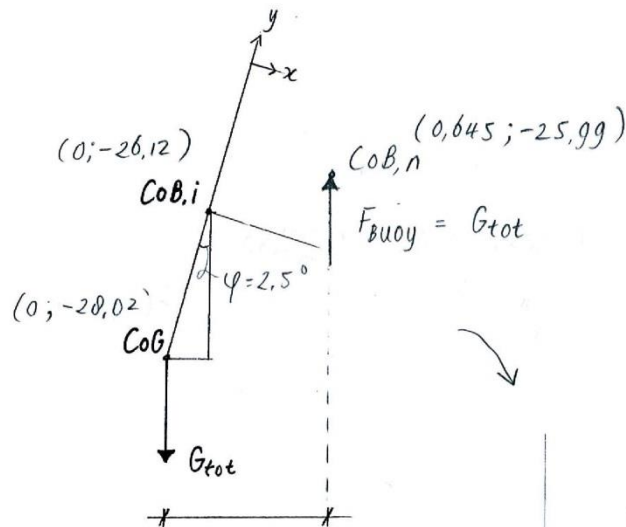
Rev:

Project : Buoyancy Bridge Sognefjord

Part : Verification rotational stiffness



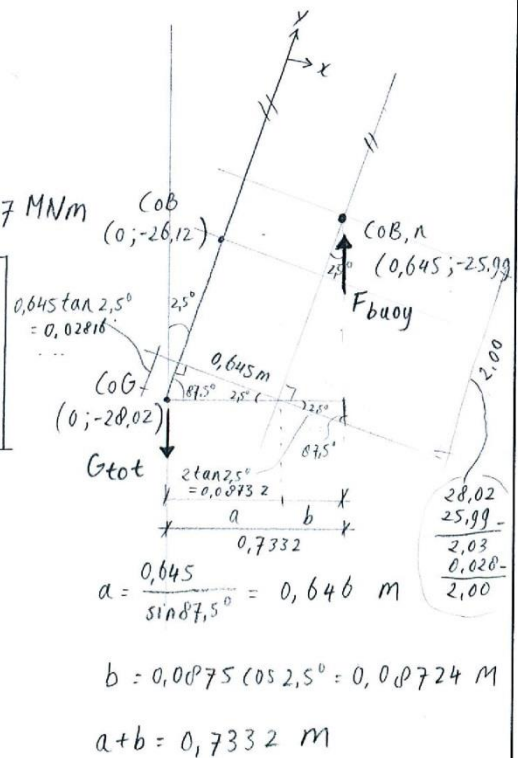
Restoring moment couple:



$$M_{restor} = G_{tot} \cdot 0,7332 = 2717 \text{ MNm}$$

$$K_{rot} = \frac{M_{restor}}{\varphi} = 62278 \text{ MNm/rad}$$

Analytical



Name: Christine Yip

Date: 21-4-2015 Page: 5/8

Rev:

Project : Buoyancy Bridge Sognefjord

Part : Verification restoring moment (by using AutoCAD)



AutoCAD

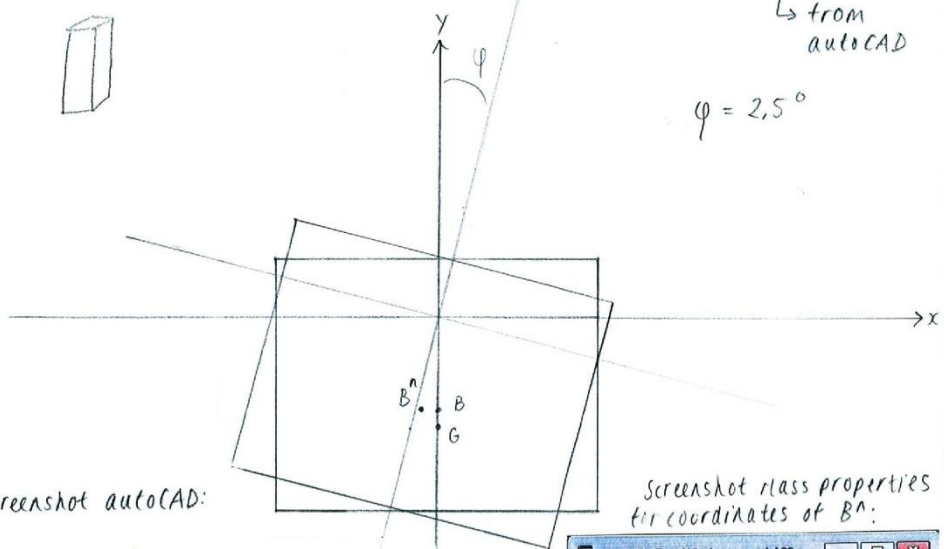
Assume rectangular pontoon shapes:



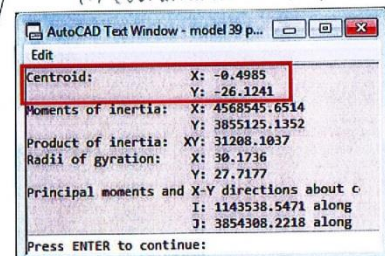
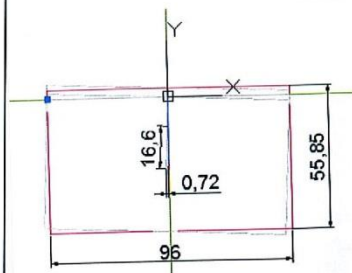
coordinates $\left\{ \begin{array}{l} G = (0 ; -28.02) \\ B = (0 ; -26.135) \\ B^A = (-0.4985 ; -26.1241) \end{array} \right.$

↳ from autoCAD

$$\varphi = 2.5^\circ$$



screenshot autoCAD:



screenshot class properties for coordinates of B^A:

$$B^A G = 0.72 \text{ m (see page 2)}$$

$$M_{\text{restoring}} = G_{\text{tot}} \cdot B^A G = 3706 \cdot 10^3 \cdot 0.72 = 2668 \text{ MNm}$$

Same as analytical ✓

$$K_{\text{Bu}} = \frac{M_{\text{restoring}}}{\varphi} = 61153 \text{ MNm/rad}$$

AutoCAD

Name: Christine Yip

Date: 21-4-2015 Page: 6/8

Rev:

Project : Buoyancy Bridge Sognefjord

Part : Verification Restoring Moment (by equations/expressions)



Expressions

Assume rectangular pontoons

$$MG = \frac{I_0}{V_s} + GB \text{ (metacentric height)}$$

$$= \frac{\frac{1}{12} \cdot 96 \cdot 96^3}{96^2 \cdot (55,85 - 3,58)} + 1,9$$

$$= 16,6 \text{ m} \quad \leftarrow \text{AutoCAD} \rightarrow 16,6 \text{ m (see page 6)}$$

(see page 2)



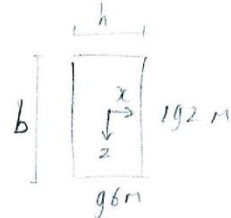
$$K_\theta = \frac{M}{\varphi} = \frac{G_{tot} \cdot MG \cdot \sin \varphi}{\varphi} = 61\,500 \text{ MNm/rad}$$

Expressions

Assume another section:

$$MG = \frac{\frac{1}{12} \cdot 192 \cdot 96^3}{96 \cdot 192 \cdot 52,27} + 1,9$$

$$= 16,6 \text{ m}$$



$$\left(MG = \frac{\frac{1}{12} b h^3}{b h l_{dr}} + GB = \frac{h^2}{12 l_{dr}} + GB \right) \rightarrow \text{metacentric height is not influenced by } b$$

Name: Christine Yip

Date: 21-4-2015

Page: 7/8

Rev:

Project : Buoyancy Bridge Sognefjord

Part : Verification rotational stiffness



Summary Results

	Analytical	AutoCAD	Expressions
rotational stiffness K_{Bu} (MNm/rad) rectangular pontoon	62 278	61 153	61 500

Rotational stiffness K_{Bu} determined by pontoon properties

Conclusion

Since the rotational stiffness values of a pontoon, which are determined analytically, by the use of AutoCAD and by the use of the expressions from the introduction, are all almost the same, it can be concluded that it is reliable to use these expressions in the Maple calculation file to calculate the rotational stiffness of the pontoons.

Name:


Date:

Page:

8/8

Rev:

ANNEX D: VERIFICATION RESTORING MOMENT CALCULATION

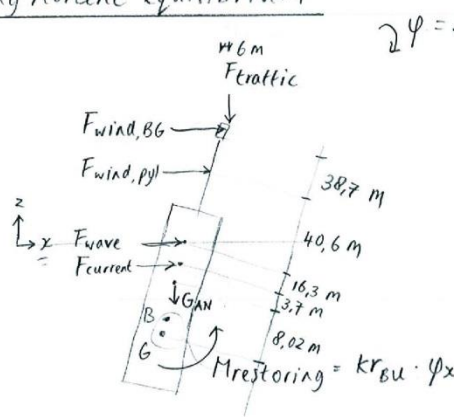
Project	: Buoyancy Bridge Sognefjord									
Part	: Verification Restoring Moment calculation									
<p><u>Introduction</u></p> <p>The pontoon properties determine the rotational stiffness of the pontoon. Therefore, when the required rotational stiffness is known, the required pontoon properties can also be</p> <div style="display: flex; justify-content: space-around; align-items: center; margin: 20px 0;"> <table border="1" style="border-collapse: collapse; width: 45%;"> <tr><td style="text-align: center;">Resistance</td></tr> <tr><td style="padding: 5px;">Rotational spring stiffness determined by pontoon properties.</td></tr> <tr><td style="padding: 5px;">Calculated either by:</td></tr> <tr><td style="padding: 5px;"> <ul style="list-style-type: none"> • analytical calculations or • autoCAD or • expressions </td></tr> </table> <div style="font-size: 2em; margin: 0 10px;">≥</div> <table border="1" style="border-collapse: collapse; width: 45%;"> <tr><td style="text-align: center;">Effect of the action</td></tr> <tr><td style="padding: 5px;">Required rotational spring stiffness determined by external loads.</td></tr> <tr><td style="padding: 5px;">Calculated by</td></tr> <tr><td style="padding: 5px;"> <ul style="list-style-type: none"> • Bending moment equilibrium </td></tr> </table> </div> <p style="text-align: center;">Fig. 2 Overview rotational spring stiffness calculations</p> <p>calculated. To determine the required rotational stiffness, the pontoon is loaded by the maximum loads and bending moment equilibrium can be used. This is done in the Maple calculation file in Annex and also done in page 2 for pontoon 11 (values for the final design may differ). To check the validity of the calculation codes in maple, both outcomes will be compared.</p> <p>With the required rotational stiffness known, the pontoon properties can be calculated by using different methods, see Fig. 1 for an overview. These methods are validated in 'Verification rotational stiffness of pontoons'.</p>			Resistance	Rotational spring stiffness determined by pontoon properties.	Calculated either by:	<ul style="list-style-type: none"> • analytical calculations or • autoCAD or • expressions 	Effect of the action	Required rotational spring stiffness determined by external loads.	Calculated by	<ul style="list-style-type: none"> • Bending moment equilibrium
Resistance										
Rotational spring stiffness determined by pontoon properties.										
Calculated either by:										
<ul style="list-style-type: none"> • analytical calculations or • autoCAD or • expressions 										
Effect of the action										
Required rotational spring stiffness determined by external loads.										
Calculated by										
<ul style="list-style-type: none"> • Bending moment equilibrium 										
Name:	Christine Yip	Date: 4-5-2015								
		Page: 1/3								
		Rev:								

Project : Buoyancy Bridge Sognefjord

Part : Verification Restoring Moment Calculation



Bending moment equilibrium



$\varphi = 2,5^\circ$

- $F_{wind,BG} = 5801,64 \text{ kN}$
- $F_{wind,pyl} = 1000,26 \text{ kN}$
- $F_{wave} = 66,33 \text{ kN}$
- $F_{current} = 2375,12 \text{ kN}$
- $F_{traffic} = 6125 \text{ kN}$
- $G_{AN} = 41618 \text{ kN}$

Pontoon shape : cylinder

$M_{\text{around } G} \rightarrow -F_{wind,BG} \cdot a_{w,BG} - F_{wind,pyl} \cdot a_{w,pyl} - F_{wave} \cdot a_{wave} - F_{current} \cdot a_{cur} - G_{AN} \cdot a_{AN} - F_{traffic} \cdot a_{traffic} + \underbrace{kr_{BU} \cdot \varphi}_{M_{restoring}} = 0$ equilibrium

$\rightarrow kr_{BU} = \frac{(F_{wind,BG} \cdot a_{w,BG} + F_{wind,pyl} \cdot a_{w,pyl}) + F_{wave} \cdot a_{wave} + F_{current} \cdot a_{cur} + G_{AN} \cdot a_{AN} + F_{traffic} \cdot a_{traffic}}{\varphi}$

$= \frac{\left\{ 5801,64 \cdot (8,02 + 3,7 + 16,3 + 40,6 + 38,7) + 1000,26 \cdot (8,02 + 3,7 + 16,3) + 66,33 \cdot (8,02 + 3,7 + 16,3) + 2375,12 \cdot (8,02 + 3,7) + 6125 \cdot ((8,02 + 3,7 + 16,3 + 40,6 + 38,7) \tan\left(\frac{2,5\pi}{180}\right) + 6) + 41618 \cdot 8,02 \tan\left(\frac{2,5}{360} \cdot 2\pi\right) \right\}}{\left(\frac{2,5\pi}{180}\right)}$

$= \frac{\left\{ 5801,64 \cdot 107,2 + 1000,26 \cdot 68,4 + 66,33 \cdot 28,03 + 2375,12 \cdot 11,68 + 6125 \cdot 10,674 + 41618 \cdot 0,35 \right\}}{\left(\frac{2,5}{180} \cdot \pi\right)}$

$= 18332 \text{ MNm/rad}$

$kr_{BU} \text{ from Maple: } 18326 \text{ MNm/rad}$ } approximately equal ✓

Name: Christine Yip

Date: 4-5-2015 Page: 2/3

Rev:

Project : Buoyancy Bridge Sognefjord

Part : Verification Restoring Moment Calculation



Conclusion

The hand calculated bending moment equilibrium coincides with the results of the bending moment equilibrium in the Maple calculation file. It can be concluded that this calculation was done correctly in Maple.

Name: Christine Yrp

Date: 4-5-2015

Page:

3/3

Rev:

ANNEX E: PONTOON PROPERTIES AND LOADS CALCULATION FILE

Pontoon Properties and Loads Calculation File

Table of Contents

- 1 Introduction
- 2 Input Pontoon and Bridge Deck Position
 - 2.1 S-Curve Characteristics
 - 2.2 Pontoon positions
 - 2.3 Elevation Bridge Deck
 - 2.4 Plot S-Curve
 - 2.5 Pontoon Coordinates
- 3 Input Parameters
 - 3.1 Parameters Superstructure
 - 3.2 Parameters pontoons
 - 3.3 Parameters Vertical Loads
 - 3.4 Other Input Parameters
- 4 Determination External Loads
 - 4.1 Definition Angles
 - 4.2 Input for Determination Wind Load

4.3	Input for Determination Wave Load
4.4	Input for Determination Current Load
4.5	Calculation Projected Girder Length at Different Angles
4.6	Calculation Concentrated Wind Load
4.7	Calculation Concentrated Wave and Current Load
4.8	Calculation Total Horizontal Loads
5	Required Buoyancy Determines Pontoon Lengths
5.1	Determination Required Buoyancy Force
5.2	Determination Pontoon Dimensions (Length, Draught, Freeboard and Center of Gravity)
6	Calculation Rotational Stiffness and Ballast Height of pontoons
6.1	Provided Rotational Stiffness by pontoons
6.2	Required Rotational Stiffness due to Loads
6.3	Stability Check
7	Overview Results
7.1	Pontoon Properties
7.2	Vertical Loads
7.3	Horizontal Loads

1 Introduction

In this file, the calculations done with Maple are shown. The pontoon properties and external loads are obtained as shown in the following. The explanations and descriptions of the calculation are stated in black. The inputted variables and equations for the calculations are shown in green. Results from the calculation codes are shown in blue. In orange, the expressions for the properties of pontoon 11 are shown.

If not otherwise stated, all lengths are expressed in meters (m) and all forces are expressed in kilonewtons (kN) and kilonewtons per meter (kN/m).

```
restart; unprotect( $\gamma$ ); with(plots) : with(plots) : color1 := "DarkRed" : color2 := "DarkMagenta" : color6
:= "SkyBlue" : color7 := "DarkSlateGrey" : color8 := "DarkKhaki" : color9 := "DarkCyan" : color10
:= "DarkGoldenrod" : color11 := "SandyBrown" : color12 := "YellowGreen" : colorVec := [color1, color2, color3,
color4, color5, color6, color7, color8] : interface( rtablesize = 30 ) :
```

2 Input Pontoon and Bridge Deck Position

In this section, the properties of the target S-shape of the bridge from the top view is inputted. In this calculation file, it is assumed that this is the final shape of the bridge. However, in reality, due to the self-weight of the anchoring system, the S-shape will deform a bit; the curves will be fainter. Since this effect is considered to be small, it will be assumed that the bridge stays in this perfect S-shape for the calculations of the loads and pontoon properties. These calculations are similar to the ones by Hermans (2014), p.39.

The span at the middle of the fjord is decided by the required clearance. The required clearance is 70 x 400 x 20 meters (height x width x draught). To accommodate this clearance, the radius of the pylons and pontoons should be taken into account. Moreover, the displacements due to the self-weight and external loads should also be taken into account; the clearance should be sufficient in every load configuration.

2.1 S-Curve Characteristics

Length side span $l_{g,n}$:= 200 :

Length main span (= span at the middle of the fjord) $l_{g, mid} := 465$:

Half of the shore-to-shore-distance $x_{hs} := 1753.7$:

Half of the length along the bridge girder $s_{hs} := 2280.05$:

Longitudinal distance of one curve in the direction along the fjord $Y_{hs} := 1228$:

Lateral distance of curve ashore $Y_1 := \sin(\alpha_a) \cdot R_{ha}$:

Lateral distance of curve offshore $Y_2 := R_{ho} - Y_1$:

Horizontal angle ashore $\alpha_a := \left(\frac{\pi}{9} \right)$:

Radius of curves $R_{ha} := 1866.25$:

Comment: This radius is inputted in Scia Engineer. However, due to the self-weight of the anchoring cables, the pontoon move in such a way that the radius of curves becomes larger. This is however not incorporated in the calculations yet. In further design phases, more accurate positions of the pontoons should be used in the calculations.

2.2 Pontoon Positions

Number of side spans in a half bridge $n_{nspans, hs} := \text{floor} \left(\frac{(s_{hs} - 0.5 \cdot l_{g, mid})}{l_{g, n}} \right)$;
10

Resulting remaining bridge deck length near shore $l_{gl} := s_{hs} - 0.5 \cdot l_{g, mid} - n_{nspans, hs} \cdot l_{g, n}$;
47.55

Number of pontoons in a half bridge $n_{spans, hs} := n_{nspans, hs} + 1$;

Number of spans in the whole bridge $n_{spans} := 2 \cdot n_{spans, hs} + 1$;

(2)

$$\beta_1 := \frac{l_{gl}}{R_{ha}} : \beta_n := \frac{l_{g,mid}}{R_{ha}} :$$

$n_{spans,hs}$

11

```

for  $j$  from 1 to  $n_{spans,hs}$  do  $\beta_{p,j} := (\alpha_o + \beta_1 + (j-1) \cdot \beta_n) : dx_{p,j} := evalf(x_{hs} - \cos(\alpha_o + \beta_1 + (j-1) \cdot \beta_n) \cdot R_n) : b_{p,j}$ 
:=  $dx_{p,j} \cdot \alpha_{p,j} := 2 \cdot x_{hs} - b_{p,j} : \text{enddo}$ 
for  $j$  from  $n_{spans,hs} + 1$  to  $2 \cdot n_{spans,hs}$  do  $\beta_{p,j} := \beta_{p,(n_{spans,hs} - (j-1 - n_{spans,hs}))} : dx_{p,j} := \sin(\beta_m + (j - (n_{spans,hs} + 1))$ 
 $\cdot \beta_n) \cdot R_{ha} + x_{hs} : b_{p,j} := dx_{p,j} : \alpha_{p,j} := 2 \cdot x_{hs} - b_{p,j} : \text{enddo}$ 
for  $j$  from 1 to  $n_{spans,hs}$  do  $d_{p,j} := evalf(\sin(\alpha_o + \beta_1 + (j-1) \cdot \beta_n) \cdot R_{ha} - y_1) : c_{p,j} := evalf(2 \cdot y_2 - d_{p,j}) : \text{enddo}$ 
for  $j$  from  $n_{spans,hs} + 1$  to  $2 \cdot n_{spans,hs}$  do  $d_{p,j} := evalf(y_2 + (y_2 - d_{p,(n_{spans,hs} - (j - (n_{spans,hs} + 1)))))) : c_{p,j} := evalf(2 \cdot y_2$ 
 $- d_{p,j}) : \text{enddo}$ 

```

2.3 Elevation Bridge Deck

The freeboard height of the pontoons must always be positive in any situation, so the pontoons do not sink to the bottom of the fjord. To create some margin, the freeboard of the pontoon when the structure is loaded by the maximum vertical loads should be $fr_{p,mn} := 3$:

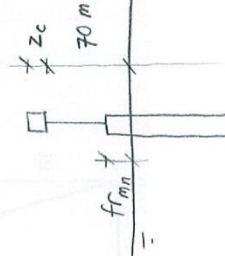
Estimation required pylon height $z_b := 70 + z_c - fr_{p,mn}$:

Estimation half of the bridge girder height $z_c := \frac{15}{2}$:

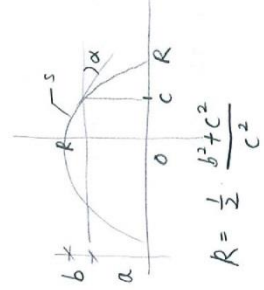
Radius of the vertical arc (elevation of bridge deck) $R_{va} := \frac{0.5 \cdot ((z_b)^2 + s_{hs}^2)}{(z_b)} : R_{va}$

34927.37082

Plot of the elevation of the bridge deck $fz := sa \rightarrow \text{sqrt}(R_{va}^2 - (sa - s_{hs})^2) - (R_{va} - z_b) : \text{plot}(fz, 0..2 \cdot s_{hs})$



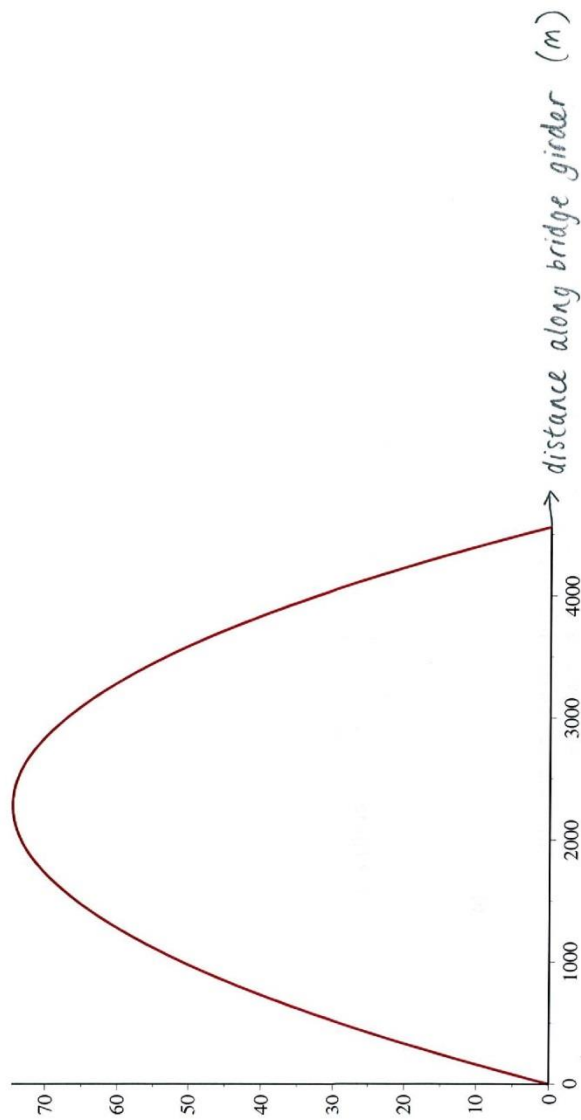
(4)



(5)

$$R = \frac{1}{2} \cdot \frac{\beta^2 + c^2}{c^2}$$

$$s = R^2 (2 \cdot \alpha)$$



Height of the bridge deck at the first pontoon near the shore $eval(fz(sa), sa = 30.05)$
 1.95283

(6)

2.4 Plot S-Curve

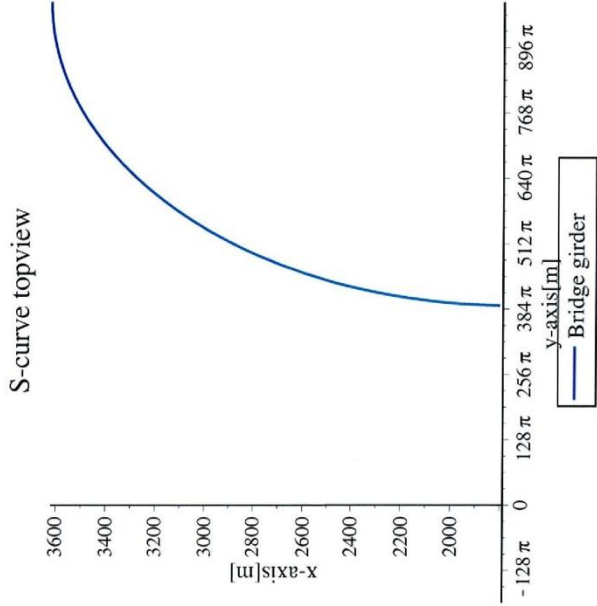
$dy := R_{ha} + Y_2$

```

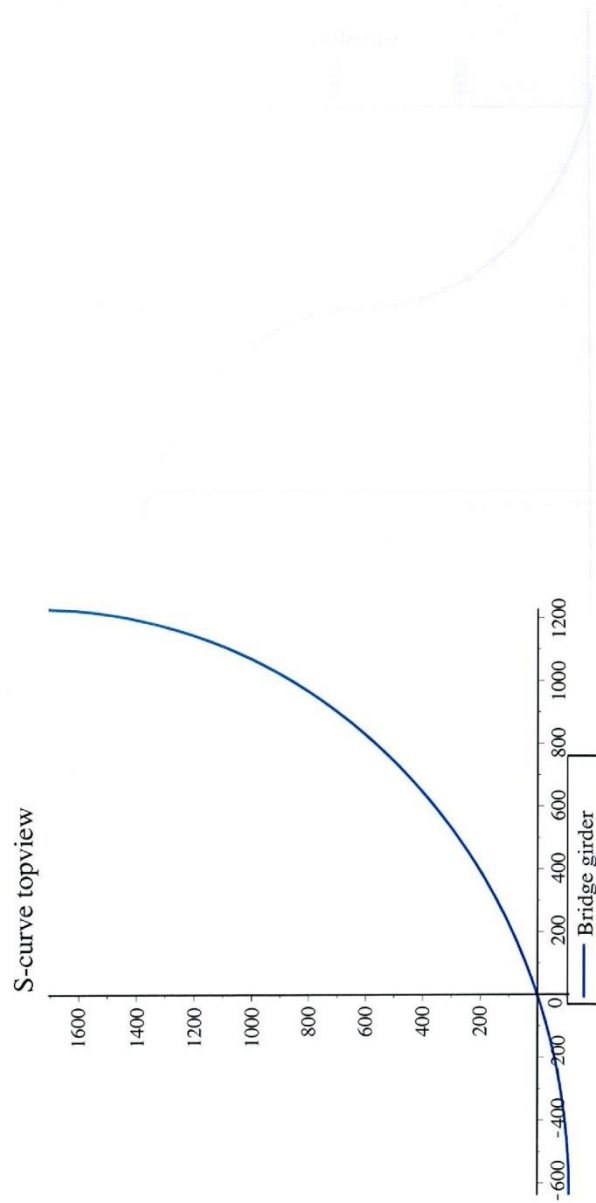
dx := xhs :
ta := sqrt(Rho2 - (ya - dy)2) + dx :
Plot of the top half of the S-curve
with (plots) : Pta := plot(ta, ya = -600 .. Rho + y2, color = blue, title = typeset("S-curve topview"), titlefont = ["calibri",
14], legend = "Bridge girder", labels = ["y-axis[m]", "x-axis[m]"], labelfont = ["calibri", 12], labeldirections
= ["horizontal", "vertical"]) : display([Pta]);

```





Plot of the bottom half of the S-curve $P_{ba} := \text{reflect}(\text{reflect}(P_{ta}, [[0, x_{hs}], [5000, x_{hs}]]), [[y_2, 0], [y_2, 5000]])$:



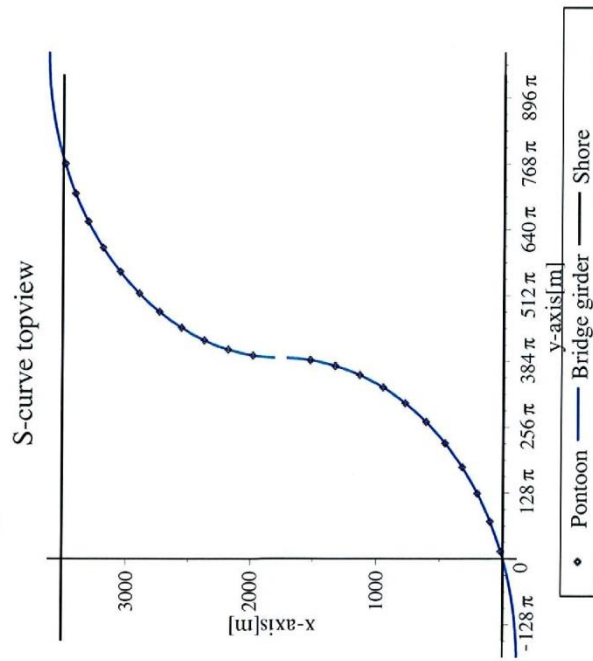
Plot of the S-curve with also the locations of the pontoons

```

PP := pointplot(((d_p,1',d_p,2',d_p,3',d_p,4',d_p,5',d_p,6',d_p,7',d_p,8',d_p,9',d_p,10',d_p,11',d_p,12',d_p,13',d_p,14',d_p,15',d_p,16',d_p,17',d_p,18',d_p,19',
d_p,20',d_p,21',d_p,22')|(b_p,1',b_p,2',b_p,3',b_p,4',b_p,5',b_p,6',b_p,7',b_p,8',b_p,9',b_p,10',b_p,11',b_p,12',b_p,13',b_p,14',b_p,15',b_p,16',b_p,17',b_p,18',
b_p,19',b_p,20',b_p,21',b_p,22')), legend = "Pontoon") :
Psn := pointplot((( -500, 2 * y_2 + 500)|(2 * x_1 - 2 * x_2)), style = line, color = black, legend = "Shore") :

```

```
Pss := pointplot((( -500, 2·y2 + 500)|(0, 0)), style = line, color = black) :
display([Pta, Pba, PP, Psn, Pss])
```



2.5 Pontoon Coordinates

```
lg,1 := lgl: Sp,1 := lg,1 :
for i from 2 to 11 do
lg,i := lg,n :
```

```

enddo:
   $l_{g,12} := l_{g,mid}$ ;
for  $i$  from 13 to 22 do
   $l_{g,i} := l_{g,n}$ ;
enddo:
   $l_{g,23} := l_{g,i}$ ;
for  $i$  from 2 to 22 do
   $s_{p,i} := s_{p,i-1} + l_{g,i}$ ;
   $z_{bv_{p,i}} := fz(s_{p,i})$ ;
enddo:
   $z_{bv_{p,5}}$ 

45.11159000

for  $i$  from 1 to 22 do
   $x_{p,i} := b_{p,i}$ ;
   $y_{p,i} := d_{p,i}$ ;
   $z_{p,i} := eval(fz(sa), sa = s_{p,i}) + fr_{p,nc,i}$ ;
   $lc_{p,i} := \langle x_{p,i} | y_{p,i} | z_{p,i} \rangle : sa := 'sa'$ ;
enddo:

for  $i$  from 1 to 22 do
   $x_{p,i} := b_{p,i}$ ;
   $y_{p,i} := d_{p,i}$ ;
   $z_{p,i} := eval(fz(sa), sa = s_{p,i}) + fr_{p,nc,i}$ ;
   $lc_{p,i} := \langle x_{p,i} | y_{p,i} | z_{p,i} \rangle : sa := 'sa'$ ;
enddo:

   $x_{g,23} := x_{g,1}$ ;
for  $i$  from 2 to 22 do

```



```

a_mvm,i := evalf ( zbv_p,i - cos ( 2.5 * pi / 180 ) * zbv_p,i ) ;
b_mvm,i := evalf ( sin ( 2.5 * pi / 180 ) * zbv_p,i ) ;
enddo;

```

Coordinates of the bridge deck on top of the 22 pontoons. The y-direction is along the fjord. The x-direction is across the fjord. The z-direction indicates the elevation.

```

( ("#P", 1, 2, 3, 4, 5, 6, 7, 8, 9, 10, 11, 12, 13, 14, 15, 16, 17, 18, 19, 20, 21, 22) | ("v_p", d_p,1', d_p,2', d_p,3', d_p,4', d_p,5', d_p,6', d_p,7', d_p,8',
d_p,9', d_p,10', d_p,11', d_p,12', d_p,13', d_p,14', d_p,15', d_p,16', d_p,17', d_p,18', d_p,19', d_p,20', d_p,21', d_p,22) | ("x_p", b_p,1', b_p,2', b_p,3', b_p,4', b_p,5',
b_p,6', b_p,7', b_p,8', b_p,9', b_p,10', b_p,11', b_p,12', b_p,13', b_p,14', b_p,15', b_p,16', b_p,17', b_p,18', b_p,19', b_p,20', b_p,21', b_p,22) | ("z", 4.19456, zbv_p,2',
zbv_p,3', zbv_p,4', zbv_p,5', zbv_p,6', zbv_p,7', zbv_p,8', zbv_p,9', zbv_p,10', zbv_p,11', zbv_p,12', zbv_p,13', zbv_p,14', zbv_p,15', zbv_p,16', zbv_p,17',
zbv_p,18', zbv_p,19', zbv_p,20', zbv_p,21', zbv_p,22) )

```

"#p"	"y_p"	"x_p"	"z"
1	44.4703786	16.829143	4.19456
2	226.3322191	99.823138	15.31204000
3	398.2735586	201.793271	26.39488000
4	558.3215876	321.569564	36.32774000
5	704.6399596	457.777737	45.11159000
6	835.5498556	608.854974	52.74730000
7	949.5492516	773.0678540	59.23562000
8	1045.330148	948.5322438	64.57720000
9	1121.793581	1133.234912	68.77255000
10	1178.062231	1325.056630	71.82211000
11	1213.490485	1521.796487	73.72615000
12	1242.419330	1985.599046	73.72615000
13	1277.847584	2182.338988	71.82211000
14	1334.116234	2374.160842	68.77255000
15	1410.579667	2558.863694	64.57720000
16	1506.360563	2734.328315	59.23562000
17	1620.359959	2898.541470	52.74730000
18	1751.269855	3049.619023	45.11159000
19	1897.588227	3185.827549	36.32774000
20	2057.636256	3305.604228	26.39488000
21	2229.577596	3407.574776	15.31204000
22	2411.439436	3490.569210	3.07811000

(8)

3 Input Parameters

3.1 Parameters Superstructure

Width bridge box girder $b_g := 10$:

Width bridge deck $b_{deck} := 16$:

Radius pylons $R_{pylon} := 2.5$:

Thickness pylon shell $t_{pylon} := \frac{R_{pylon}}{15}$:

More properties superstructure (these are assumed to be the same as the superstructure of Hermans (2014))

$h_{ws} := 2.4$:

$t_{girder} := 0.022514$; $\alpha_g := 90$; $d_{tn} := 0.4531$:

$a_{truss} := 15$; $h_{truss} := 3.5$; $d_{truss} := 1$; $l_{trussdia} := \text{sqrt}(h_{truss}^2 + a_{truss}^2)$; $d_{trussdia} := 0.5$:

3.2 Parameters pontoons

All pontoons are cylindrical shaped.

Distance between water surface and anchoring connection point on pontoon $z_o := 20$:

Thickness pontoon at the top $t_{p,top} := 1$:

Thickness pontoon at bottom $t_{p,bot} := 1 + \frac{l_p}{50}$:

The pontoon have different sizes:

Radius pontoon no. 1 = 15 m

Radius pontoon no. 2 to 6 = 18 m

Radius pontoon no. 7 to 10 = 21 m

Radius pontoon no. 11 = 26 m

The buoyancy bridge is rotationally symmetric. Therefore, the properties of pontoons no. 12 to 22 are the same to respectively pontoons no. 11 to 1. Below, the pontoons radiuses, pontoon thicknesses at the sides and the area moment of inertia of the plane intersected by the water off all pontoons are specified.

for i from 1 to 1 do

$R_{\text{pontoon},i} := 15 :$

$t_{p,side,i} := 0.5 + \frac{R_{\text{pontoon},i}}{15} :$

$INER_i := \frac{\pi}{4} \cdot (R_{\text{pontoon},i}^4 - (R_{\text{pontoon},i} - t_{p,side,i})^4) :$

enddo:

for i from 2 to 6 do

$R_{\text{pontoon},i} := 18 :$

$t_{p,side,i} := 0.5 + \frac{R_{\text{pontoon},i}}{15} :$

$INER_i := \frac{\pi}{4} \cdot (R_{\text{pontoon},i}^4 - (R_{\text{pontoon},i} - t_{p,side,i})^4) :$

enddo:

for i from 7 to 10 do

$R_{\text{pontoon},i} := 21 :$

$$t_{p,side,i} := 0.5 + \frac{R_{pontoon,i}}{15} :$$

$$INER_i := \frac{\pi}{4} \cdot (R_{pontoon,i}^4 - (R_{pontoon,i} - t_{p,side,i})^4) :$$

enddo:

for i from 11 to 12 do

$$R_{pontoon,i} := 26 :$$

$$t_{p,side,i} := 0.5 + \frac{R_{pontoon,i}}{15} :$$

$$INER_i := \frac{\pi}{4} \cdot (R_{pontoon,i}^4 - (R_{pontoon,i} - t_{p,side,i})^4) :$$

enddo:

for i from 13 to 16 do

$$R_{pontoon,i} := 21 :$$

$$t_{p,side,i} := 0.5 + \frac{R_{pontoon,i}}{15} :$$

$$INER_i := \frac{\pi}{4} \cdot (R_{pontoon,i}^4 - (R_{pontoon,i} - t_{p,side,i})^4) :$$

enddo:

for i from 17 to 21 do

$$R_{pontoon,i} := 18 :$$

$$t_{p,side,i} := 0.5 + \frac{R_{pontoon,i}}{15};$$

$$INER_i := \frac{\pi}{4} \cdot (R_{pontoon,i}^4 - (R_{pontoon,i} - t_{p,side,i})^4);$$

enddo;

for i from 22 to 22 do

$$R_{pontoon,i} := 15;$$

$$t_{p,side,i} := 0.5 + \frac{R_{pontoon,i}}{15};$$

$$INER_i := \frac{\pi}{4} \cdot (R_{pontoon,i}^4 - (R_{pontoon,i} - t_{p,side,i})^4);$$

enddo;

Example radius pontoon 11 $R_{pontoon,11}$

26

(9)

Example thickness of the side of pontoon 11 $t_{p,side,11}$

2.2333333333

(10)

(11)

Length of the pontoons are defined

for i from 1 to 22 do

$$l_{p,i} := dr_{p,i,ULS} + fr_{p,mm};$$

enddo;

As can be seen, the pontoon lengths are still unknown, since it depends on the draught (submerged height) of the pontoons in SLS ($dr_{p,i,SLS}$)

Example length pontoon 11 $l_{p,11}$

$$dr_{p,11,ULS} + 3 \quad (12)$$

Definition freeboard of the pontoon in different situations. The freeboard also depends on the draught of the pontoon.

for i from 1 to 22 do

$$fr_{p,i,SLS} := l_{p,i} - dr_{p,i,SLS};$$

$$fr_{p,i,nt,SLS} := l_{p,i} - dr_{p,i,nt,SLS};$$

$$:= dr_{p,i,ULS} + fr_{p,mn};$$

enddo;

Example freeboard of pontoon 11 in SLS with no traffic taken into account: $fr_{p,11,nt,SLS}$

$$dr_{p,11,ULS} + 3 - dr_{p,11,nt,SLS} \quad (13)$$

3.3 Parameters Vertical Loads

Distributed traffic load $q_{traffic}$:= 35 :

$$\text{Concentrated traffic load on pontoon } F_{traffic,hfb,SLS} := \frac{1}{2} \cdot q_{traffic} \cdot l_g \cdot F_{traffic,hfb,ULS} := \frac{1}{2} \cdot q_{traffic} \cdot l_g :$$

Eccentric traffic load leverarm $a_{traffic,hfb}$:= 6 :

$$\text{Self-weight pylons } G_{pylon,SLS} := \frac{fz(sa)}{z_b} \cdot 28410 \cdot G_{pylon,ULS} := \gamma_g \cdot G_{pylon,SLS} \cdot f_{y,pylon} := 460 \cdot 10^3 :$$

Scia Engineer.

(15

$G_{AN,1} := 6328 : G_{AN,2} := 7335 : G_{AN,3} := 6467 : G_{AN,4} := 8205 : G_{AN,5} := 10029 : G_{AN,6} := 13565 : G_{AN,7} := 17665 :$
 $G_{AN,8} := 34933 : G_{AN,9} := 25363 : G_{AN,10} := 45137 : G_{AN,11} := 41618 : G_{AN,12} := G_{AN,11} : G_{AN,13} := G_{AN,10} :$
 $G_{AN,14} := G_{AN,9} : G_{AN,15} := G_{AN,8} : G_{AN,16} := G_{AN,7} : G_{AN,17} := G_{AN,6} : G_{AN,18} := G_{AN,5} : G_{AN,19} := G_{AN,4} : G_{AN,20}$
 $:= G_{AN,3} : G_{AN,21} := G_{AN,2} : G_{AN,22} := G_{AN,1} :$

3.4 Other Input Parameters

Load safety factor for dead loads $\gamma_g := 1.2 :$

Load safety factor for live loads $\gamma_q := 1.5 :$

Modulus of Elasticity of steel $E_s := 210 \cdot 10^6 : E_m := 195 \cdot 10^6 :$

Shear modulus of steel $G_s := 79.3 \cdot 10^6 :$

Density steel $\rho_s := 7850 :$

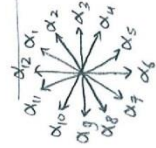
Density concrete $\rho_c := 2500 :$

Density ballast $\rho_b := 2000 :$

Density water $\rho_w := 1004.85 :$

Density air (from NEN-EN 1991-1-4, p. 24) $\rho_o := 1.25 :$

4 Determination External Loads



4.1 Definition Angles
 External loads like the wind load can act in different directions. 12 directions are considered in this calculation. The 12 directions are defined as shown below.

$$\alpha_1 := \frac{0 \cdot \pi}{180} : \alpha_2 := \frac{30 \cdot \pi}{180} : \alpha_3 := \frac{60 \cdot \pi}{180} : \alpha_4 := \frac{90 \cdot \pi}{180} : \alpha_5 := \frac{120 \cdot \pi}{180} : \alpha_6 := \frac{150 \cdot \pi}{180} : \alpha_7 := \frac{180 \cdot \pi}{180} : \alpha_8 := \frac{210 \cdot \pi}{180} : \alpha_9 := \frac{240 \cdot \pi}{180} : \alpha_{10} := \frac{270 \cdot \pi}{180} : \alpha_{11} := \frac{300 \cdot \pi}{180} : \alpha_{12} := \frac{330 \cdot \pi}{180} :$$

4.2 Input for Determination Wind Load

Input coefficients:

$$C_{d, gw} := \text{piecewise} \left(1 \leq \beta_{BG} < 2, 1.1 - (\beta_{BG} - 1) \cdot (1.1 - 0.6), 2 \leq \beta_{BG} < 4, 0.6 - (\beta_{BG} - 2) \cdot 0.5 \cdot (0.6 - 0.35), \beta_{BG} \geq 4, 0.35 \right) :$$

$$\beta_{BG} := \frac{20}{h_g + h_{ws}} :$$

$$C_{d, pww} := 1.1 : C_{d, tn} := 1.1 : C_{d, traffic} := 1.05 : C_{d, truss} := 1.1 : C_{d, pc} := 1.5 :$$

Wind load according to NEN-EN 1991-1-4:

$$q_{p, g, SLS} := ze \rightarrow \left(1 + \frac{7 \cdot k_f}{c_0 \cdot \ln \left(\frac{ze}{z_0} \right)} \right) \cdot \left(\frac{1}{2} \right) \cdot \frac{\left[p_o \cdot \left(\frac{z_0}{z_{0, II}} \cdot \ln \left(\frac{ze}{z_0} \right) \cdot c_0 \cdot v_b, SLS \right) \right]^2}{1000} :$$

$$\begin{aligned}
 q_{p,p,sLS} &:= ze \rightarrow \left(1 + \frac{7 \cdot k_f}{c_0 \cdot \ln\left(\frac{0.5 \cdot ze}{z_0}\right)} \right) \cdot \left(\frac{1}{2} \right) \cdot \frac{\left[\rho_\sigma \cdot 0.19 \cdot \left(\frac{z_0}{z_{0,fl}} \cdot \ln\left(\frac{0.5 \cdot ze}{z_0}\right) \cdot c_0 \cdot v_{b,sLS} \right)^2 \right]}{1000} : \\
 q_{p,g,ULS} &:= ze \rightarrow \left(1 + \frac{7 \cdot k_f}{c_0 \cdot \ln\left(\frac{ze}{z_0}\right)} \right) \cdot \left(\frac{1}{2} \right) \cdot \frac{\left[\rho_\sigma \cdot 0.19 \cdot \left(\frac{z_0}{z_{0,fl}} \cdot \ln\left(\frac{ze}{z_0}\right) \cdot c_0 \cdot v_{b,ULS} \right)^2 \right]}{1000} : \\
 q_{p,p,ULS} &:= ze \rightarrow \left(1 + \frac{7 \cdot k_f}{c_0 \cdot \ln\left(\frac{0.5 \cdot ze}{z_0}\right)} \right) \cdot \left(\frac{1}{2} \right) \cdot \frac{\left[\rho_\sigma \cdot 0.19 \cdot \left(\frac{z_0}{z_{0,fl}} \cdot \ln\left(\frac{0.5 \cdot ze}{z_0}\right) \cdot c_0 \cdot v_{b,ULS} \right)^2 \right]}{1000} : \\
 z_0 &:= 0.05 : z_{0,fl} := 0.05 : c_0 := 1.0 : k_f := 1.0 : \\
 n_{prob} &:= 0.1 : K_{prob} := 0.2 : p_{prob} := 0.99 : c_{prob} := \text{evalf}\left(\left(\frac{(1 - K_{prob} \cdot \ln(-\ln(1 - p_{prob})))^n}{1 - K_{prob} \cdot \ln(-\ln(0.99))}\right)^{\frac{1}{n_{prob}}}\right) \\
 &0.9033175203
 \end{aligned}$$

(16)

Extreme values of wind speed per direction (Hermans, 2014, Figure 4-3):

$$\begin{aligned}
 V_{b,\alpha,1,ULS} &:= 21 : V_{b,\alpha,2,ULS} := 26 : V_{b,\alpha,3,ULS} := 26 : V_{b,\alpha,4,ULS} := 23 : V_{b,\alpha,5,ULS} := 24 : V_{b,\alpha,6,ULS} := 28 : V_{b,\alpha,7,ULS} \\
 &:= 35 : V_{b,\alpha,8,ULS} := 35 : V_{b,\alpha,9,ULS} := 35 : V_{b,\alpha,10,ULS} := 33 : V_{b,\alpha,11,ULS} := 33 : V_{b,\alpha,12,ULS} := 23 :
 \end{aligned}$$

4.3 Input for Determination Wave Load

Extreme values of wind wave height per direction (Hermans, 2014, Figure 4-5):

$$\begin{aligned}
 H_{s,ww,\alpha,1,ULS} &::= 1.01 : H_{s,ww,\alpha,2,ULS} ::= 1.62 : H_{s,ww,\alpha,3,ULS} ::= 1.81 : H_{s,ww,\alpha,4,ULS} ::= 1.49 : H_{s,ww,\alpha,5,ULS} ::= 1.4 : \\
 H_{s,ww,\alpha,6,ULS} &::= 1.57 : H_{s,ww,\alpha,7,ULS} ::= 2.22 : H_{s,ww,\alpha,8,ULS} ::= 2.24 : H_{s,ww,\alpha,9,ULS} ::= 2.34 : H_{s,ww,\alpha,10,ULS} ::= 2.13 : \\
 H_{s,ww,\alpha,11,ULS} &::= 1.83 : H_{s,ww,\alpha,12,ULS} ::= 1.00 :
 \end{aligned}$$

Significant wave height (Hermans, 2014, Figure 4-6):

$$\begin{aligned}
 H_{s,sw,\alpha,1,ULS} &::= 0.01 : H_{s,sw,\alpha,2,ULS} ::= 0.01 : H_{s,sw,\alpha,3,ULS} ::= 0.01 : H_{s,sw,\alpha,4,ULS} ::= 0.01 : H_{s,sw,\alpha,5,ULS} ::= 0.01 : \\
 H_{s,sw,\alpha,6,ULS} &::= 0.01 : H_{s,sw,\alpha,7,ULS} ::= 0.01 : H_{s,sw,\alpha,8,ULS} ::= 0.01 : H_{s,sw,\alpha,9,ULS} ::= 0.01 : H_{s,sw,\alpha,10,ULS} ::= 0.01 : \\
 H_{s,sw,\alpha,11,ULS} &::= 0.01 : H_{s,sw,\alpha,12,ULS} ::= 0.01 :
 \end{aligned}$$

4.4 Input for Determination Current Load

Currents - three scenarios.

- 1 - constant current over full width of the fjord.
- 2 - constant current in the mid half of the fjord
- 3 - constant current asymmetrical about fjord's mid axis

$$\begin{aligned}
 u_{c1,\alpha,1} &::= 1.27 : u_{c1,\alpha,2} ::= 1.27 : u_{c1,\alpha,3} ::= 1.27 : u_{c1,\alpha,4} ::= 1.27 : u_{c1,\alpha,5} ::= 1.27 : u_{c1,\alpha,6} ::= 1.27 : u_{c1,\alpha,7} ::= 1.27 : \\
 u_{c1,\alpha,8} &::= 1.27 : u_{c1,\alpha,9} ::= 1.27 : u_{c1,\alpha,10} ::= 1.27 : u_{c1,\alpha,11} ::= 1.27 : u_{c1,\alpha,12} ::= 1.27 :
 \end{aligned} \tag{17}$$

$$\begin{aligned}
 u_{c2,\alpha,1} &::= 0.875 : u_{c2,\alpha,2} ::= 0.875 : u_{c2,\alpha,3} ::= 0.875 : u_{c2,\alpha,4} ::= 0.875 : u_{c2,\alpha,5} ::= 0.875 : u_{c2,\alpha,6} ::= 0.875 : u_{c2,\alpha,7} \\
 &::= 0.875 : u_{c2,\alpha,8} ::= 0.875 : u_{c2,\alpha,9} ::= 0.875 : u_{c2,\alpha,10} ::= 0.875 : u_{c2,\alpha,11} ::= 0.875 : u_{c2,\alpha,12} ::= 0.875 :
 \end{aligned}$$

```

u_{c3,\alpha,1} := 0.48 : u_{c3,\alpha,2} := 0.48 : u_{c3,\alpha,3} := 0.48 : u_{c3,\alpha,4} := 0.48 : u_{c3,\alpha,5} := 0.48 : u_{c3,\alpha,6} := 0.48 : u_{c3,\alpha,7} := 0.48 :
u_{c3,\alpha,8} := 0.48 : u_{c3,\alpha,9} := 0.48 : u_{c3,\alpha,10} := 0.48 : u_{c3,\alpha,11} := 0.48 : u_{c3,\alpha,12} := 0.48 :

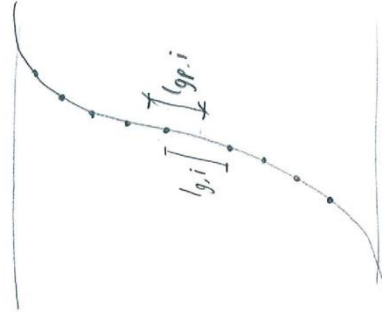
```

(18)

4.5 Calculation Effective and Projected Girder Length at Different Angles

The effective length is $l_{gp,i}$ and the pontoon span is $l_{p,i}$.

$l_{g,i}$ and $l_{gp,i}$:



```

l_{gp,i} := (l_{g,i} + l_{p,i}) / 2 :

```

```

l_g := l_{gp,i} :
sa := s_{p,i} :

```

```

\alpha_{b,i} := arctan( (y_{p,i} - y_{p,i(i-1)}) / (x_{p,i} - x_{p,i(i-1)}) ) :

```

```

ss_{b,i} := sqrt( (x_{p,i} - x_{p,i(i-1)})^2 + (y_{p,i} - y_{p,i(i-1)})^2 ) :

```

```

\alpha_{d,i,n} := abs( evalf( ( \alpha_n - \alpha_{b,i} + \frac{\pi}{6} ) ) ) :

```

```

if \alpha_{d,i,n} > evalf( \frac{\pi}{2} ) then \alpha_{d,i,n} := ( \alpha_n - \alpha_{b,i} - \frac{\pi}{2} + \frac{\pi}{6} ) ; l_{g,i,\alpha,n} := abs( evalf( ss_{b,i} * cos( \alpha_{d,i,n} ) ) ) ; else \alpha_{d,i,n} := ( \alpha_n

```

```

- \alpha_{b,i} + \frac{\pi}{6} ) ; l_{g,i,\alpha,n} := abs( evalf( ss_{b,i} * sin( \alpha_{d,i,n} ) ) ) ; end if :

```

```

end do :

```

```

l_{g,i,\alpha,7} := l_{g,i,\alpha,1} :

```

```

l_{g,i,\alpha,8} := l_{g,i,\alpha,2} :

```

```

l_{g,i,\alpha,9} := l_{g,i,\alpha,3} :
l_{g,i,\alpha,10} := l_{g,i,\alpha,4} :
l_{g,i,\alpha,11} := l_{g,i,\alpha,5} :
l_{g,i,\alpha,12} := l_{g,i,\alpha,6} :
l := l' : sa := 'sa' :
g
enddo:

```

Example span between pontoon 10 and 11 $evalf_4(l_{g,11})$ 200.

Example span between pontoon 11 and 12 $evalf_4(l_{g,12})$ 465.

Example: effective girder length pontoon 11 $evalf_4(l_{gp,11})$ 332.5

Example: length of girder where the external loads acts on from direction 3, for which pontoon 11 has to resist the loads $l_{g,11,\alpha,3}$

196.7398570

```

for n from 1 to 12 do
l_{g,23,\alpha,n} := l_{g,1,\alpha,n} :
enddo:

```

Repeat definition of the freeboard of the pontoon in different situations. (Length and draught of the pontoons still unknown.)

```

for i from 1 to 22 do
fr_{p,i,SLS} := l_{p,i} - dr_{p,i,SLS} :
fr_{p,i,nt,SLS} := l_{p,i} - dr_{p,i,nt,SLS} : l_{p,i}
:= dr_{p,i,ULS} + fr_{p,mn} :

```

(19)

(20)

(21)

(22)

end do;

Example freeboard of pontoon 11 in SLS with no traffic taken into account: $fr_{p,11,nt,SLS}$

$$dr_{p,11,ULS} + 3 - dr_{p,11,nt,SLS} \quad (23)$$

4.6 Calculation Concentrated Wind Load

for n from 1 to 12 do
for i from 1 to 22 do

$V_{b,SLS} := C_{prob} \cdot V_{b,\alpha,n,ULS}$; $V_{b,ULS} := V_{b,\alpha,n,ULS}$;

$SA := S_{p,i} \cdot l_{gp,i} := \frac{(l_{g,i,\alpha,n} + l_{g,(i+1),\alpha,n})}{2}$; $l_g := l_{gp,i}$;

$h_{gp,i} := \frac{l_{gp,i}}{90}$; $h_g := h_{gp,i} \cdot z_{BG,i} := fz(s_{p,i}) + \frac{h_g}{2} + fr_{p,i,nt,SLS}$;

$F_{wind,BG,\alpha,SLS} := q_{p,g,SLS}(z_{BG,i}) \cdot l_{gp,i,\alpha,n} \cdot (h_g + h_{ws}) \cdot C_{d,gw}$; $F_{wind,BG,\alpha,ULS} := q_{p,g,ULS}(z_{BG,i}) \cdot l_{gp,i,\alpha,n} \cdot (h_g + h_{ws}) \cdot C_{d,gw}$;

$F_{wind,truss,\alpha,SLS} := \frac{2 \cdot q_{p,g,SLS}(z_{BG,i}) \cdot l_{gp,i,\alpha,n}}{a_{truss}} \cdot (d_{truss} \cdot h_{truss} + d_{trussdia} \cdot l_{trussdia}) \cdot C_{d,truss}$;

$F_{wind,truss,\alpha,ULS} := \frac{2 \cdot q_{p,g,ULS}(z_{BG,i}) \cdot l_{gp,i,\alpha,n}}{a_{truss}} \cdot (d_{truss} \cdot h_{truss} + d_{trussdia} \cdot l_{trussdia}) \cdot C_{d,truss}$;

$F_{wind,traffic,\alpha,SLS} := q_{p,g,SLS}(z_{BG,i}) \cdot \max(4 - h_{ws}, 0) \cdot 0.5 \cdot l_{gp,i,\alpha,n} \cdot C_{d,traffic}$;

$F_{wind,tn,\alpha,SLS} := q_{p,g,SLS}(z_{BG,i}) \cdot d_{tn,gp,i,\alpha,n} \cdot C_{d,tn}$;

$F_{wind,tn,\alpha,ULS} := q_{p,g,ULS}(z_{BG,i}) \cdot d_{tn,gp,i,\alpha,n} \cdot C_{d,tn}$;

$F_{wind,gi,\alpha,SLS} := F_{wind,BG,\alpha,SLS} + F_{wind,tn,\alpha,SLS} + F_{wind,truss,\alpha,SLS} + F_{wind,traffic,\alpha,SLS}$; $q_{wind,gi,\alpha,SLS} := \frac{F_{wind,gi,\alpha,SLS}}{l_{gp,i,\alpha,n}}$;

$$F_{wind, g, i, \alpha, n, ULS} := \gamma_q \cdot \left(F_{wind, BG, \alpha, ULS} + F_{wind, tr, \alpha, ULS} + F_{wind, truss, \alpha, ULS} \right) : q_{wind, g, i, \alpha, n, ULS} := \frac{F_{wind, g, i, \alpha, ULS}}{l_{gp, i, \alpha, n}}$$

$$F_{wind, py, i, \alpha, n, SLS} := q_{p, p, SLS}(z_{BG, i}) \cdot fz(s_{p, i}) \cdot 2 \cdot R_{pylon} \cdot C_{d, pyw} :$$

$$F_{wind, py, i, \alpha, n, ULS} := \gamma_q \cdot q_{p, p, ULS}(z_{BG, i}) \cdot fz(s_{p, i}) \cdot 2 \cdot R_{pylon} \cdot C_{d, pyw} :$$

sa := 'sa';
 enddo;
 enddo;

Example concentrated wind load in SLS on pylon on top of pontoon 11 by wind from direction 9: $F_{wind, g, 11, \alpha, 9, SLS}$

$$84.34156749 \left(\frac{1}{2} + \frac{3.500000000}{\ln(1571.467444 + 20.00000000 dr_{p, 11, ULS} - 20.00000000 dr_{p, 11, mt, SLS})} \right) \ln(1571.467444 + 20.00000000 dr_{p, 11, ULS} - 20.00000000 dr_{p, 11, mt, SLS})^2 \quad (25)$$

4.7 Calculation Concentrated Current and Wave Load

Calculation of the current load, wave load and the position where the concentrated current load is acting (z_FC,i,alpha, n,eq)(this is the distance measured from the water level).

for n from 1 to 12 do
 for i from 1 to 22 do

$$H_{s, ww} := H_{s, ww, \alpha, 1, ULS} ;$$

$$H_{s, sw} := H_{s, sw, \alpha, 1, ULS} ;$$

$$u_{c1, ULS} := u_{c1, \alpha, n} ;$$

$$u_{c2, ULS} := u_{c2, \alpha, n} ;$$

$$u_{c3, ULS} := u_{c3, \alpha, n} ;$$

$$\begin{aligned}
 U_{c1,SLS} &:= C_{prob} \cdot U_{c1,\alpha,n} ; \\
 U_{c2,SLS} &:= C_{prob} \cdot U_{c2,\alpha,n} ; \\
 U_{c3,SLS} &:= C_{prob} \cdot U_{c3,\alpha,n} ; \\
 dr_p &:= dr_{p,i,SLS} ; \\
 l_g &:= l_{gp,i} ; \\
 h_g &:= \frac{l_{gp,i}}{90} ; \\
 F_{current1,SLS} &:= \frac{1}{2} \cdot \frac{\rho_w \cdot U_{c1,SLS}^2 \cdot C_{d,pc} \cdot 2 \cdot R_{pontoon,i} \cdot 10}{1000} ; \\
 F_{current2,SLS} &:= \frac{1}{2} \cdot \frac{\rho_w \cdot U_{c2,SLS}^2 \cdot C_{d,pc} \cdot 2 \cdot R_{pontoon,i} \cdot \min(dr_{p,i,SLS} - 10, 20)}{1000} ; \\
 F_{current3,SLS} &:= \frac{1}{2} \cdot \frac{\rho_w \cdot U_{c3,SLS}^2 \cdot C_{d,pc} \cdot 2 \cdot R_{pontoon,i} \cdot \max(dr_{p,i,SLS} - 30, 0)}{1000} ; \\
 F_{current1,ULS} &:= \frac{1}{2} \cdot \gamma_q \cdot \frac{\rho_w \cdot U_{c1,ULS}^2 \cdot C_{d,pc} \cdot 2 \cdot R_{pontoon,i} \cdot 10}{1000} ; \\
 F_{current2,ULS} &:= \frac{1}{2} \cdot \gamma_q \cdot \frac{\rho_w \cdot U_{c2,ULS}^2 \cdot C_{d,pc} \cdot 2 \cdot R_{pontoon,i} \cdot \min(dr_{p,i,ULS} - 10, 20)}{1000} ; \\
 F_{current3,ULS} &:= \frac{1}{2} \cdot \gamma_q \cdot \frac{\rho_w \cdot U_{c3,ULS}^2 \cdot C_{d,pc} \cdot 2 \cdot R_{pontoon,i} \cdot \max(dr_{p,i,ULS} - 30, 0)}{1000} ; \\
 F_{FC,eq,i,\alpha,n,SLS} &:= (F_{current1,SLS} + F_{current2,SLS} + F_{current3,SLS}) ; \\
 F_{FC,eq,i,\alpha,n,ULS} &:= (F_{current1,ULS} + F_{current2,ULS} + F_{current3,ULS}) ; \\
 z_{FC1} &:= 5 ; \\
 z_{FC2} &:= 10 + \min(dr_{p,i,SLS} - 10, 10) ; \\
 z_{FC3} &:= 30 + \frac{(dr_{p,i,SLS} - 30)}{2} ;
 \end{aligned}$$

```

ZFC,i,α,n,eq := ( Fcurrent1,SLS·ZFC1 + Fcurrent2,SLS·ZFC2 + Fcurrent3,SLS·ZFC3 ) / ( Fcurrent1,SLS + Fcurrent2,SLS + Fcurrent3,SLS );
Fww,i,α,n,SLS := 1 / ( 16·1000 · ρw · 9.81 · Hs,ww · 2 · Rpontoon,i );
Fww,i,α,n,ULS := γg · Fww,i,α,n,SLS;
Fsw,i,α,n,SLS := 1 / ( 16·1000 · ρw · 9.81 · Hs,sw · 2 · Rpontoon,i );
Fsw,i,α,n,ULS := γg · Fsw,i,α,n,SLS;
Fwa,i,α,n,SLS := Fww,i,α,n,SLS + Fsw,i,α,n,SLS;
Fwa,i,α,n,ULS := Fww,i,α,n,ULS + Fsw,i,α,n,ULS;
hg := hg;
lg := lg;
drp := drp;
end do;
end do;

```

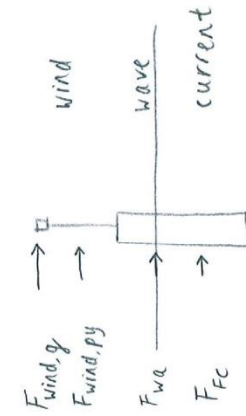
Example concentrated wave load in ULS from direction 9 on pontoon 11 $F_{wa,11,\alpha,9,ULS}$ 49.01680909 (26)

Example concentrated current load in SLS from direction 9 on pontoon 11 $F_{FC,eq,11,\alpha,9,SLS}$ 515.7677143 + 24.48289767 min(20, dr_{p,11,SLS} - 10) + 7.367653379 max(0, dr_{p,11,SLS} - 30) (27)

As can be seen, the current load is dependent on the submerged part of the pontoon. Since the pontoon lengths are still unknown, the exact value of the concentrated wave load is also unknown.

4.8 Calculation Total Horizontal Loads

The total horizontal load is the sum of the wind load, wave load and current load.



```

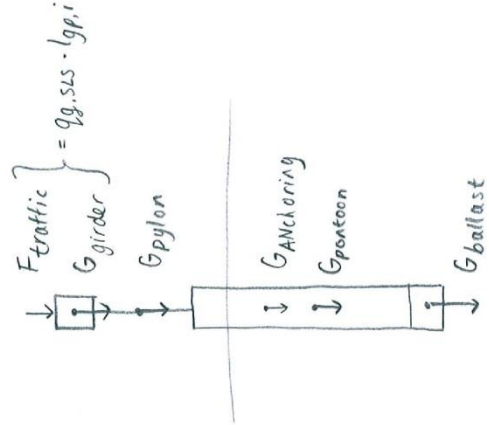
for n from 1 to 12 do
for i from 1 to 22 do
F_Htop,i,α,n,SLS := F_wa,i,α,n,SLS + F_FC,eq,i,α,n,SLS + F_wind,py,i,α,n,SLS + F_wind,g,i,α,n,SLS
F_Htop,i,α,n,ULS := F_wa,i,α,n,ULS + F_FC,eq,i,α,n,ULS + F_wind,py,i,α,n,ULS + F_wind,g,i,α,n,ULS
enddo:
enddo:

```

5 Required Buoyancy Determines Pontoon Length

5.1 Determination Required Buoyancy Force

The pontoon length is determined by the required upward buoyancy force. Since there is equilibrium of vertical forces, the upward buoyancy force is equal to the total downward vertical force, caused by the total self-weight of the structure and the traffic load. Below, the total downward vertical force is determined. All downward forces are known, except the self-weight of the ballast. The required ballast height (h_b) to obtain sufficient rotational stiffness of the pontoon will be determined further on in 6.2.



```

for i from 1 to 22 do
sa := s_p,i : l := l_gp,i : dr_p,ULS := dr_p,i,ULS : l := l_p,i :
G_pylon,i,SLS := G_pylon,SLS : G_pylon,i,ULS := G_pylon,ULS :
F_pontoon,i,SLS := q_g,SLS * l_gp,i + G_pylon,SLS + G_AN,i : F_pontoon,i,ULS := q_g,ULS * l_gp,i + G_pylon,ULS + G_AN,i :
G_ballast,i,SLS := (p_b * h_b * π * (R_pontoon,i - t_p,side,i)^2 * 9.81) / 1000 :
G_ballast,i,ULS := G_ballast,i,SLS :
G_p,i,SLS := (p_c * (l_p,i * π * R_pontoon,i^2 - (l_p,i - t_p,bot - t_p,top) * π * (R_pontoon,i - t_p,side,i)^2) * 9.81) / 1000 :

```

```

Gp,i,ULS := Gp,i,SLS;
Gtot,i,SLS := Gballast,i,SLS + Gp,i,SLS + Gpylon,SLS + (qg,SLS) · lgp,i + GAN,i;
Gtot,i,ULS := Gballast,i,ULS + Gp,i,ULS + Gpylon,ULS + (qg,ULS) · lgp,i + GAN,i;
lp := lp;
enddo;

```

The total vertical forces acting on pontoon 11 and 12 at the middle of the fjord are larger, since the span at the middle of the fjord is also larger. So the calculation code is adjusted for pontoon 11 and 12:

```

for i from 11 to 11 do
sa := sp,i · lg := lgp,i; drp,i,ULS := drp,i,ULS · lp := lp,i;
Gpylon,i,SLS := Gpylon,SLS; Gpylon,i,ULS := Gpylon,ULS;
Fpontoon,i,SLS :=  $\frac{q_{g,SLS} \cdot l_{g,i+1}}{2} + \frac{q_{g,SLS} \cdot l_{g,i}}{2} + G_{pylon,SLS} + G_{AN,i}$ ; Fpontoon,i,ULS :=  $\frac{q_{g,ULS} \cdot l_{g,i+1}}{2} + \frac{q_{g,ULS} \cdot l_{g,i}}{2} + G_{pylon,ULS} + 1.2 \cdot G_{AN,i}$ ;
Gballast,i,SLS :=  $\frac{\rho_b \cdot h_b \cdot \pi \cdot (R_{ponton,i} - t_{p,side,i})^2 \cdot 9.81}{1000}$ ;
Gballast,i,ULS := Gballast,i,SLS;
Gp,i,SLS :=  $\frac{\rho_c \cdot (l_{p,i} \cdot \pi \cdot R_{ponton,i}^2 - (l_{p,i} - t_{p,bot} - t_{p,top}) \cdot \pi \cdot (R_{ponton,i} - t_{p,side,i})^2) \cdot 9.81}{1000}$ ;
Gp,i,ULS := Gp,i,SLS;
Gtot,i,SLS := Gballast,i,SLS + Gp,i,SLS + Gpylon,SLS + (qg,SLS) · lgp,i + GAN,i;
Gtot,i,ULS := Gballast,i,ULS + Gp,i,ULS + Gpylon,ULS + (qg,ULS) · lgp,i + 1.2 · GAN,i;
lp := lp;
enddo;

```

```

for i from 12 to 12 do

```

```

sa := sp,i · lg := lgp,i; drp,i,ULS := drp,i,ULS · lp := lp,i;

```

$$\begin{aligned}
 G_{\text{pylon},i,\text{SLS}} &::= G_{\text{pylon},\text{SLS}} \cdot G_{\text{pylon},i,\text{ULS}} \quad ; G_{\text{pylon},\text{ULS}} \\
 F_{\text{ponton},i,\text{SLS}} &::= \frac{q_{g,\text{SLS},\text{mid}} \cdot l_{g,i}}{2} + \frac{q_{g,\text{SLS}} \cdot l_{g,i+1}}{2} + G_{\text{pylon},\text{SLS}} + G_{\text{AN},i} \quad ; F_{\text{ponton},i,\text{ULS}} \\
 &+ G_{\text{pylon},\text{ULS}} + 1.2 \cdot G_{\text{AN},i} \\
 G_{\text{ballast},i,\text{SLS}} &::= \frac{p_b \cdot h_b \cdot \pi \cdot (R_{\text{ponton},i} - t_{p,\text{side},i})^2 \cdot 9.81}{1000} \\
 G_{\text{ballast},i,\text{ULS}} &::= G_{\text{ballast},i,\text{SLS}} \\
 G_{p,i,\text{SLS}} &::= \frac{p_c \cdot (l_{p,i} \cdot \pi \cdot R_{\text{ponton},i}^2 - (l_{p,i} - t_{p,\text{bot}} - t_{p,\text{top}}) \cdot \pi \cdot (R_{\text{ponton},i} - t_{p,\text{side},i})^2) \cdot 9.81}{1000} \\
 G_{p,i,\text{ULS}} &::= G_{p,i,\text{SLS}} \\
 G_{\text{tot},i,\text{SLS}} &::= G_{\text{ballast},i,\text{SLS}} + G_{p,i,\text{SLS}} + G_{\text{pylon},\text{SLS}} + (q_{g,\text{SLS}}) \cdot l_{gp,i} + G_{\text{AN},i} \\
 G_{\text{tot},i,\text{ULS}} &::= G_{\text{ballast},i,\text{ULS}} + G_{p,i,\text{ULS}} + G_{\text{pylon},\text{ULS}} + (q_{g,\text{ULS}}) \cdot l_{gp,i} + 1.2 \cdot G_{\text{AN},i} \\
 l_p &:= l_p \\
 \text{enddo} &
 \end{aligned}$$

Example total downward vertical force (is equal to upward buoyancy force) of pontoon 11 in ULS

$$\begin{aligned}
 &G_{\text{tot},11,\text{ULS}} \\
 &11082.44420 h_{p,11} \pi + 16578.90000 (dr_{p,11,\text{ULS}} + 3) \pi - 13853.05526 \left(\frac{49}{50} dr_{p,11,\text{ULS}} + \frac{47}{50} \right) \pi \\
 &+ 2.068707300 10^5 \quad (28)
 \end{aligned}$$

Table with total self-weight (SW) of each pontoon and its ballast. Note that the height of the ballast is not determined yet. The height of the ballast will be determined by the required rotational stiffness of the pontoon.

$$\begin{aligned}
 \text{SWPB} &::= \{ \langle \langle \text{"Pontoon no."}, [\text{"m"}], \text{seq}(i,i=1..11) \rangle \} \{ \langle \text{"SW pontoon + ballast"}, [\text{"kN"}], \text{seq}(\text{eval}f_4(G_{p,i,\text{SLS}} + G_{\text{ballast},i,\text{SLS}}), i \\
 &= 1..11) \rangle \} \\
 &\text{SWPB}
 \end{aligned}$$

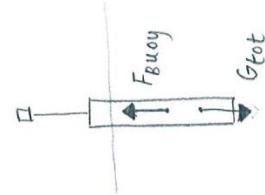
"Pontoon no." "[m]"	"SW pontoon+ballast" "[kN]"
1	$11240 \cdot h_{b,1} + 3580 \cdot dr_{p,1} \cdot ULS + 38810$
2	$16380 \cdot h_{b,2} + 4910 \cdot dr_{p,2} \cdot ULS + 55660$
3	$16380 \cdot h_{b,3} + 4910 \cdot dr_{p,3} \cdot ULS + 55660$
4	$16380 \cdot h_{b,4} + 4910 \cdot dr_{p,4} \cdot ULS + 55660$
5	$16380 \cdot h_{b,5} + 4910 \cdot dr_{p,5} \cdot ULS + 55660$
6	$16380 \cdot h_{b,6} + 4910 \cdot dr_{p,6} \cdot ULS + 55660$
7	$22490 \cdot h_{b,7} + 6450 \cdot dr_{p,7} \cdot ULS + 75580$
8	$22490 \cdot h_{b,8} + 6450 \cdot dr_{p,8} \cdot ULS + 75580$
9	$22490 \cdot h_{b,9} + 6450 \cdot dr_{p,9} \cdot ULS + 75580$
10	$22490 \cdot h_{b,10} + 6450 \cdot dr_{p,10} \cdot ULS + 75580$
11	$34810 \cdot h_{b,11} + 9450 \cdot dr_{p,11} \cdot ULS + 1.154 \cdot 10^5$

5.2 Determination Pontoon Dimensions (Length, Draught, Freeboard and Center of Gravity)

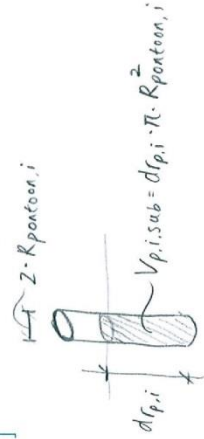
The required upward buoyancy force is determined in the previous section. The buoyancy force is provided by the amount of displaced water. Therefore, the submerged volume and consequently also the draught (submerged length) c the pontoon can be calculated. The pontoon length is then the sum of the submerged length and the freeboard length. This expression was already inputted at the end of section 3.2, while the draught was still unknown. Now, the draught, pontoon length and freeboards can be calculated.

for / from 1 to 22 do

$l_p := l_{p,i}$



$$\begin{aligned} \Sigma F_{vertical} &= 0 \\ F_{buoy} - G_{tot} &= 0 \\ F_{buoy} &= G_{tot} \\ V_{p,i,sub} \cdot \rho_{water} \cdot g &= G_{tot} \\ \downarrow \text{so} \\ V_{p,i,sub} &= \frac{G_{tot}}{\rho_{water} \cdot g} \end{aligned}$$



```

V_{p,i,sub,SLS} := (F_{ponton,i,SLS} + G_{p,i,SLS} + G_{ballast,i,SLS}) / (rho_w * 9.81) ;
V_{p,i,sub,nt,SLS} := (F_{ponton,i,SLS} - q_{traffic} * l_{p,i} + G_{p,i,SLS} + G_{ballast,i,SLS}) / (rho_w * 9.81) ;
V_{p,i,sub,ULS} := (F_{ponton,i,ULS} + G_{p,i,ULS} + G_{ballast,i,ULS}) / (rho_w * 9.81) ;
dr_{p,i,ULS} := solve(dr_{p,i,ULS} = (V_{p,i,sub,ULS} / (pi * R_{ponton,i}^2)), dr_{p,i,ULS}) ;
dr_{p,i,SLS} := evalf((V_{p,i,sub,SLS} / (pi * R_{ponton,i}^2))) ;
dr_{p,i,nt,SLS} := evalf((V_{p,i,sub,nt,SLS} / (pi * R_{ponton,i}^2))) ;
l_p := l_p ;
enddo ;

(("Pontoon no.", " [m]", seq(i, i = 1..11)) | ("Pontoon Length", " [m]", seq(evalf_5(l_{p,i}), i = 1..11)) | ("Draught SLS", " [m]", seq(evalf_5(dr_{p,i,SLS}), i = 1..11)) | ("Draught SLS (no traffic)", " [m]", seq(evalf_5(dr_{p,i,nt,SLS}), i = 1..11)) | ("Freeboard SLS", " [m]", seq(evalf_4(fr_{p,i,SLS}), i = 1..11)))

```

"Pontoon no."	"Pontoon Length"	"Draught SLS"	"Draught SLS (no traffic)"	"Freeboard SLS"
"[m]"	"[m]"	"[m]"	"[m]"	"[m]"
1	$3.3105 h_{b,1} + 30.231$	$3.3105 h_{b,1} + 25.945$	$25.323 + 3.3105 h_{b,1}$	4.28
2	$3.1912 h_{b,2} + 31.078$	$3.1912 h_{b,2} + 26.557$	$25.859 + 3.1912 h_{b,2}$	4.52
3	$3.1912 h_{b,3} + 31.897$	$3.1912 h_{b,3} + 27.291$	$26.594 + 3.1912 h_{b,3}$	4.61
4	$3.1912 h_{b,4} + 33.122$	$3.1912 h_{b,4} + 28.440$	$27.743 + 3.1912 h_{b,4}$	4.68
5	$3.1912 h_{b,5} + 34.260$	$3.1912 h_{b,5} + 29.512$	$28.815 + 3.1912 h_{b,5}$	4.75
6	$3.1912 h_{b,6} + 35.630$	$3.1912 h_{b,6} + 30.824$	$30.127 + 3.1912 h_{b,6}$	4.81
7	$3.1124 h_{b,7} + 29.906$	$3.1124 h_{b,7} + 25.542$	$25.030 + 3.1124 h_{b,7}$	4.37
8	$3.1124 h_{b,8} + 32.634$	$3.1124 h_{b,8} + 28.241$	$27.728 + 3.1124 h_{b,8}$	4.39
9	$3.1124 h_{b,9} + 31.575$	$3.1124 h_{b,9} + 27.159$	$26.646 + 3.1124 h_{b,9}$	4.42
10	$3.1124 h_{b,10} + 34.505$	$3.1124 h_{b,10} + 30.072$	$29.559 + 3.1124 h_{b,10}$	4.44
11	$32.230 + 3.0273 h_{b,11}$	$27.333 + 3.0273 h_{b,11}$	$26.777 + 3.0273 h_{b,11}$	4.90

(30)

The expression for the center of gravity can be inserted. However, since the required ballast weight and height are not yet known, the exact distance between the center of gravity and the top of the pontoon is not yet known.

for i from 1 to 22 do

$$l_p := l_{p,i} \cdot z_{G,i,SLS} := \text{evalf} \left(\frac{1}{G_{\text{tot},i,SLS}} \left(\frac{(q_{g,SLS}) \cdot l_{gp,i} \cdot h_{gp,i}}{2} + G_{p/lon,i,SLS} \left(\frac{fz(s_{p,i})}{2} + h_{gp,i} \right) + G_{p,i,SLS} \left(\frac{l_{p,i}}{2} + fz(s_{p,i}) + h_{gp,i} \right) + G_{\text{ballast},i,SLS} \left(l_{p,i} + fz(s_{p,i}) + h_{gp,i} - t_{p,bot} - \frac{h_{b,i}}{2} \right) - h_{gp,i} - fz(s_{p,i}) \right) \right) :$$

$$z_{G,i,ULS} := \text{evalf} \left(\frac{1}{G_{\text{tot},i,ULS}} \left(\frac{(q_{g,ULS}) \cdot l_{gp,i} \cdot h_{gp,i}}{2} + G_{\text{pylon},i,ULS} \cdot \left(\frac{fz(s_{p,i})}{2} + h_{gp,i} \right) + G_{p,i,ULS} \cdot \left(\frac{l_{p,i}}{2} + fz(s_{p,i}) + h_{gp,i} \right) \right) + G_{\text{ballast},i,ULS} \cdot \left(l_{p,i} + fz(s_{p,i}) + h_{gp,i} - t_{p,\text{bot}} - \frac{h_{b,i}}{2} \right) - h_{gp,i} - fz(s_{p,i}) \right) :$$

$l_p := l_p$;

$t_{p,\text{bot}} := t_{p,\text{bot}}$;

enddo:

for i from 1 to 22 do

$l_p := l_{p,i}$;

$t_{p,\text{bot},i} := t_{p,\text{bot}}$;

$l_p := l_p$;

enddo:

Example position center of gravity of pontoon 11 (SLS) $z_{G,11,SLS}$

$$\frac{1}{63375.92629 h_{b,11} + 5.60575328 \cdot 10^5} \left(1.324531020 \cdot 10^6 + (3.91092428 \cdot 10^5 \right. \tag{31}$$

$$+ 28559.4010 h_{b,11}) (93.53539804 + 1.513657131 h_{b,11}) + 34816.52529 h_{b,11} (108.0056095$$

$$+ 2.466767977 h_{b,11}) - 77.42059444$$

(32)

6 Calculation Rotational Stiffness and Ballast Height of pontoons

The ballast height is one of the factors which decide the rotational stiffness. In the cylinder shaped pontoons, the center of buoyancy is located above the center of gravity. The more ballast weight there is at the bottom of the pontoon, the lower the center of gravity will be located, which will consequently lead to a higher rotational stiffness of the pontoon.

6.1 Provided Rotational Stiffness by pontoons

For small rotations ($\phi < 10$ degrees), the relationship between moment and rotation can be assumed to be linear. This relationship is given by the equation below. As can be seen in the example below the equation, all pontoon properties are already known, except the ballast height.

for i from 1 to 22 do

$$k_{r_{x, BU, i}} := \left(\left(\frac{p_w \cdot 9.81}{1000} \cdot \pi \cdot R_{pontoon, i}^2 \cdot dr_{p, i, SLS} \right) \cdot \left(\frac{INER_i}{\pi \cdot R_{pontoon, i}^2 \cdot dr_{p, i, SLS}} - \left((fr_{p, i, SLS} + 0.5 \cdot dr_{p, i, SLS}) - Z_{G, i, SLS} \right) \right) \right) ;$$

end do;

(33)

Example rotational stiffness of pontoon 11 $k_{r_{x, BU, 11}}$

$$6663.723066 \pi (27.33262163 + 3.027314259 h_{b, 11}) \left(\frac{51.00423683}{27.33262163 + 3.027314259 h_{b, 11}} - 95.98389082 \right) \quad (34)$$

$$- 1.513657133 h_{b, 11} + \frac{1}{63375.92629 h_{b, 11} + 5.60573328 \cdot 10^5} (1.324531020 \cdot 10^6 + (3.91092428 \cdot 10^5$$

$$+ 28559.4010 h_{b, 11}) (93.53539804 + 1.513657131 h_{b, 11}) + 34816.52529 h_{b, 11} (108.0056095$$

$$+ 2.466767977 h_{b, 11})))$$

6.2 Required Rotational Stiffness due to Loads

The pontoon is required to have a certain rotational stiffness, so no instability occurs when the bridge is subjected to loads. The bending moment equilibrium of the structure in a rotated position is used to obtain the required rotational stiffness. For the rotated position, the maximum allowed rotation is used.

Counter-clockwise is considered to be the positive direction. The bending moment equilibrium is checked at the center of gravity of the pontoon. Larger external loads (120% wind load and 110% wave and current loads) than calculated before are taken into account to create some margin for the design. The required rotational stiffness and the consequently required ballast height are shown in the table below the calculation.

$$\phi_x := -\frac{2.5}{360} \cdot 2 \cdot \pi :$$

$$h_b := 'h_b' :$$

for i from 1 to 22 do

gvdR := piecewise(i ≤ 5, 11, 5 < i ≤ 10, 10, 10 < i ≤ 12, 9, 12 < i ≤ 17, 10, 17 < i ≤ 22, 11) :

l_g := l_gp,i : sa := s_p,i : l_p := l_p,i :

aa := $\frac{h_{gp,i}}{2}$: bb := fz(s_p,i) : cc := fr_p,i,SLS : dd := z_d'ee := z_{FC,i,\alpha(gvdR),eq} : ff := z_{G,i,SLS} :

$$eq6 := -1.2 \cdot F_{wind,g,i,\alpha(gvdR),SLS} \cdot (aa + bb + ff) - 1.2 \cdot F_{wind,py,i,\alpha(gvdR),SLS} \cdot \left(\frac{bb}{2} + ff\right) - 1.1 \cdot F_{wa,i,\alpha(gvdR),SLS} \cdot (ff - cc)$$

$$- 1.1 \cdot F_{FC,eq,i,\alpha(gvdR),SLS} \cdot (ff - cc - ee) - F_{traffic,hfb,SLS} \cdot ((aa + bb + ff) \cdot \tan(-1 \cdot \phi_x) + a_{traffic,hfb}) - (G_{AN,i} \cdot ((ff$$

$$- cc - dd) \cdot \tan(-1 \cdot \phi_x)) - kr_{x,BU,i} \cdot \phi_x = 0 :$$

func := {eq6} :

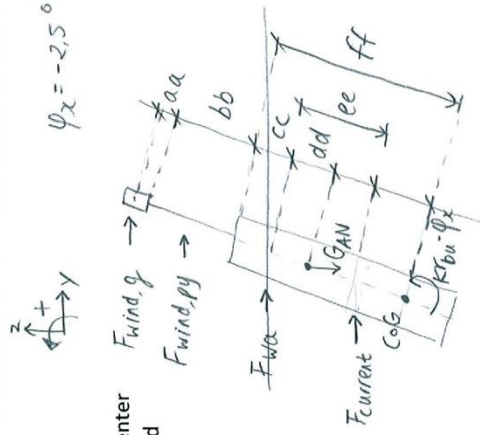
TEMP := (fsolve(func, {h_b, i = 0..infinity})) :

h_b,req,scap,i := subs(TEMP, h_b,i) :

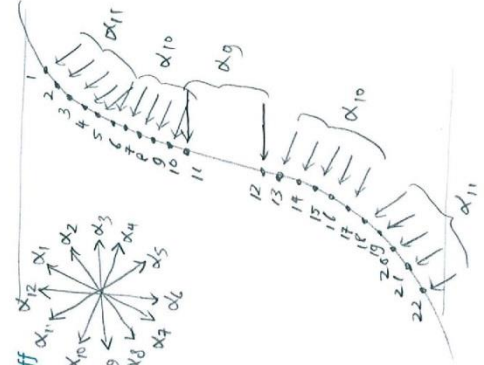
$$GM_i := \frac{INER_i}{\pi \cdot R_{pontoon,i}^2 \cdot dr_{p,i,SLS}} - ((fr_{p,i,SLS} + 0.5 \cdot dr_{p,i,SLS}) - z_{G,i,SLS}) :$$

$$z_{BC,i,SLS} := fr_{p,i,SLS} + 0.5 \cdot dr_{p,i,SLS} :$$

$$l_p := 'l_p' :$$



Load directions:



```

enddo;
for i from 1 to 22 do
   $h_{b,i} := h_{b,req,scaa,i}$ ;
end do;
 $\phi_x := \phi_x^t$ ;
<<"Pontoon no.", "[-]", seq(i, i = 1 .. 11)>>{"Rotational stiffness", "[MNm/rad]", seq(kr_x_BU, i = 1 .. 11)}
|>{"Ballast height", "[m]", seq(h_b_req_scaa, i = 1 .. 11)}>>

```

"Pontoon no."	"Rotational stiffness"	"Ballast height"
"[-]"	"[MNm/rad]"	"[m]"
1	$5.698889348 \cdot 10^5 \pi$	14.243885711
2	$1.446002971 \cdot 10^6 \pi$	19.49064593
3	$1.923911567 \cdot 10^6 \pi$	22.72030758
4	$2.404830444 \cdot 10^6 \pi$	25.68919708
5	$2.827856969 \cdot 10^6 \pi$	28.14926184
6	$3.393406570 \cdot 10^6 \pi$	30.92643567
7	$3.379001763 \cdot 10^6 \pi$	27.07192943
8	$4.094257325 \cdot 10^6 \pi$	30.44979428
9	$4.028948462 \cdot 10^6 \pi$	30.01375696
10	$4.683088807 \cdot 10^6 \pi$	33.10699468
11	$8.739609754 \cdot 10^6 \pi$	34.29079906

(35)

For example, the loads and leverarm in the bending moment equilibrium of pontoon 11 are given below.

Leverarm concentrated wind load on bridge girder $arm_{wind,BG,11} := \frac{h_{gp,11}}{2} + (fz(s_{p,11})) + z_{G,11,SLS}$
 155.6530501 (36)

Leverarm concentrated wind load on pylon $arm_{wind,py,11} := \frac{(fz(s_{p,11}))}{2} + z_{G,11,SLS}$
 116.9427529 (37)

Leverarm concentrated wave load $arm_{wave,11} := z_{G,11,SLS} - fr_{p,11,SLS}$
 75.18269216 (38)

Leverarm concentrated current load $arm_{cur,11} := z_{G,11,SLS} - fr_{p,11,SLS} - z_{FG,11,\alpha,9,eq}$
 33.81893363 (39)

Leverarm concentrated traffic load $arm_{traffic,11} := evalf_5 \left(\left(\frac{h_{gp,11}}{2} + (fz(s_{p,11})) + z_{G,11,SLS} \right) \cdot \tan \left(\frac{2.5}{360} \cdot 2 \cdot \pi \right) + 6 \right)$
 12.786

Leverarm self-weight anchoring system $arm_{AN,11} := evalf_5 \left((z_{G,11,SLS} - fr_{p,11,SLS} - z_o) \cdot \tan \left(\frac{2.5}{360} \cdot 2 \cdot \pi \right) \right)$
 2.4092 (42)

Height bridge girder $evalf_4(h_{gp,11})$
 3.694 (43)

Height pylon $(fz(s_{p,11}))$
 73.72615000 (44)

Height freeboard of pontoon in SLS $fr_{p,11,SLS}$
 4.8969857 (46)

Distance between water surface and anchoring connection point on pontoon z_o
 20 (47)

Distance between water surface and line of action of the concentrated current load $z_{FC, 11, \alpha, 9, eq}$	(48)
Distance between top of the pontoon and the center of gravity of the pontoon $z_{G, 11, SLS}$	(49)
Concentrated wind load on bridge girder with margin (120%) $1.2 \cdot F_{wind, g, 11, \alpha, 9, SLS}$	(50)
Concentrated wind load on pylon with margin (120%) $1.2 \cdot F_{wind, py, 11, \alpha, 9, SLS}$	(51)
Concentrated wave load with margin (110%) $1.1 \cdot F_{wo, 11, \alpha, 9, SLS}$	
Concentrated current load with margin (110%) $1.1 \cdot F_{FC, eq, 11, \alpha, 9, SLS}$	
Concentrated traffic load $F_{traffic, hfb, SLS}$	(53)
Self-weight anchoring system resisted by pontoon $G_{AN, 11}$	41618

6.3 Stability Check

In the cylindrical pontoons, the center of buoyancy should be located above the center of gravity. In the table below, the z-coordinates of the center of gravity and the center of buoyancy are measured downwards from the top of the pontoon.

In the second column the metacentric height, the distance between the metacenter and the center of gravity, is given. The pontoons are statically stable when the metacentric heights are positive. For the dynamic stability, the natural oscillation period of the pontoons should be much larger than the period of the water movements. The natural oscillation period of the pontoons depend on the metacentric height. However, for this feasibility study only the static calculations are done. A conventional radius/draught ratio of existing spar structures is used for the design of the pontoons as well, which is approximately 0,19 (Handbook of offshore engineering volume 1, by C. Subatta, 2005, Table 7.11).

In later design phases, of course the dynamic effects should be checked as well.

```

<<"Pontoon no.", "[m]", seq(i, i = 1 ..22)>> <<"Radius", "[m]", seq(R_pontoon, i = 1 ..22)>> <<"Length", "[m]", seq( evalf_4(L_p, i), i
= 1 ..22)>> <<"draught", "[m]", seq( evalf_5(dr_p, i, sLS), i = 1 ..22)>> <<"radius/draught", "[m]", seq( evalf_4( R_pontoon /
dr_p, i, sLS), i =
..22)>> <<"z_CoG", "[m]", seq( evalf_4(z_G, i, sLS), i = 1 ..22)>> <<"z_CoB", "[m]", seq( evalf_4(z_BC, i, sLS), i = 1 ..22)>> <<"GM",
"[m]", seq( evalf_4(GM), i = 1 ..22)>>

```

"Pontoon no."	"Radius"	"Length"	"draught"	"radius/draught"	"z_CoG"	"z_CoB"	"GM"
"[-]"	"[m]"	"[m]"	"[m]"	"[m]"	"[m]"	"[m]"	"[m]"
1	15	77.38	73.100	0.2052	44.04	40.83	3.47
2	18	93.27	88.757	0.2028	53.71	48.91	5.10
3	18	104.4	99.795	0.1804	60.32	54.51	6.08
4	18	115.1	110.42	0.1630	66.55	59.90	6.89
5	18	124.1	119.34	0.1509	71.57	64.43	7.3
6	18	134.3	129.52	0.1390	77.53	69.58	8.1
7	21	114.2	109.80	0.1913	65.94	59.25	7.0
8	21	127.4	123.01	0.1707	73.30	65.89	7.7
9	21	125.0	120.58	0.1741	72.01	64.70	7.6
10	21	137.5	133.11	0.1578	78.76	70.99	8.0
11	26	136.0	131.14	0.1983	80.08	70.48	10.0
12	26	136.0	131.14	0.1983	80.08	70.48	10.0
13	21	137.5	133.11	0.1578	78.76	70.99	8.0
14	21	125.0	120.58	0.1741	72.01	64.70	7.6
15	21	127.4	123.01	0.1707	73.30	65.89	7.7
16	21	114.2	109.80	0.1913	65.94	59.25	7.0
17	18	134.3	129.52	0.1390	77.53	69.58	8.1
18	18	124.1	119.34	0.1509	71.57	64.43	7.3
19	18	115.1	110.42	0.1630	66.55	59.90	6.89
20	18	104.4	99.795	0.1804	60.32	54.51	6.08
21	18	93.27	88.757	0.2028	53.71	48.91	5.10
22	15	77.38	73.100	0.2052	44.04	40.83	3.47

7 Overview Results

To give an overview, the results are summarized in tables. Below, the equations and codes can be seen, which are used to gather all results of the calculations and to assemble tables.

```

for i from 1 to 22 do
  lg := lgp,i ;
  Mtraffic,i,SLS := Ftraffic,hfb,SLS · atraffic,hfb ;
  Mtraffic,i,ULS := Ftraffic,hfb,ULS · atraffic,hfb ;
  lg := lg ;
  tp,side,i := tp,req side,i ;
enddo;

for i from 1 to 22 do
  gvdr := piecewise ( i ≤ 5, 11, 5 < i ≤ 10, 10, 10 < i ≤ 12, 9, 12 < i ≤ 17, 10, 17 < i ≤ 22, 11 ) ;
  lg := lgp,i ; sa := sp,i ; hb,i := hb,req,scaa,i ;
  drp,i,scaa,SLS := evalf( drp,i,SLS ) : drp,i,scaa,ULS := evalf( drp,i,ULS ) : drp,i,scaa,nt,SLS := drp,i,nt,SLS : krx,BU,i,scaa
  := evalf( krx,BU,i ) ;
  lp,i,scaa := evalf( lp,i ) : frp,i,scaa,SLS := evalf( frp,i,SLS ) : frp,i,scaa,nt,SLS := evalf( frp,i,nt,SLS ) : frp,i,scaa,ULS
  := evalf( frp,mm ) ;
  fz,i := fz( sp,i ) ;
for n from 1 to 12 do
  Fwind,g,scaa,i,α,n,SLS := Fwind,g,i,α,n,SLS · windg,scaa,i,α,n,SLS : Fwind,g,i,α,n,ULS := Fwind,g,i,α,n,ULS ;
  Fwind,py,scaa,i,α,n,SLS := Fwind,py,i,α,n,SLS · windpy,scaa,i,α,n,ULS : Fwind,py,i,α,n,ULS := Fwind,py,i,α,n,ULS ;
  Fwa,scaa,i,α,n,SLS := Fwa,i,α,n,SLS · wascaa,i,α,n,ULS := Fwa,i,α,n,ULS ;

```

```

FFC,eq,scaa,i,α,n,SLS := FFC,eq,i,α,n,SLS · FFC,eq,scaa,i,α,n,ULS := FFC,eq,i,α,n,ULS
FHtotp,scaa,i,α,n,SLS := Fwa,scaa,i,α,n,SLS + FFC,eq,scaa,i,α,n,SLS + Fwind,py,scaa,i,α,n,SLS + Fwind,g,scaa,i,α,n,SLS
FHtotp,scaa,i,α,n,ULS := Fwa,scaa,i,α,n,ULS + FFC,eq,scaa,i,α,n,ULS + Fwind,py,scaa,i,α,n,ULS + Fwind,g,scaa,i,α,n,ULS
Fpontoon,scaa,i,α,n,SLS := Fpontoon,i,SLS · Fpontoon,scaa,i,ULS := Fpontoon,i,ULS
enddo

lp := lp,i,scaa · hb := hb,req,scaa,i · Vc,scaa,i :=  $\frac{(\rho_c \cdot (l_p \cdot \pi \cdot R_{pontoon}^2 - (l_p - t_{p,bot} - t_{p,top}) \cdot \pi \cdot (R_{pontoon} - t_{p,side})^2) \cdot 9.81)}{1000}$ 
Vb,scaa,i :=  $\frac{(\rho_b \cdot (h_b) \cdot \pi \cdot (R_{pontoon} - t_{p,side})^2 \cdot 9.81)}{1000}$ 
sa := 'sa': lg := 'l': CRWp,i,scaa := (evalf4(lp,i,scaa) | evalf4(Rpontoon,i) | evalf3(hb,req,scaa,i) | evalf4(drp,i,scaa,SLS) | evalf5(frp,i,scaa,SLS) | evalf3(frp,i,scaa,SLS) | evalf8( $\frac{kr_{x,BU,i,scaa}}{1000}$ ) | evalf3(tp,bot,i) | unassign('hb,i') :
FRWp,i,scaa,SLS := (evalf5(Fwind,g,scaa,i,α,(gvar),SLS) | evalf5(Fwind,py,scaa,i,α,(gvar),SLS) | evalf3(Fwa,scaa,i,α,(gvar),SLS) | evalf5(FFC,eq,scaa,i,α,(gvar),SLS) | evalf5(FHtotp,scaa,i,α,(gvar),SLS) :
FRWp,i,scaa,ULS := (evalf5(Fwind,g,scaa,i,α,(gvar),ULS) | evalf5(Fwind,py,scaa,i,α,(gvar),ULS) | evalf5(Fwa,scaa,i,α,(gvar),ULS) | evalf5(FFC,eq,scaa,i,α,(gvar),ULS) | evalf5(FHtotp,scaa,i,α,(gvar),ULS)) : l := 'l': hb := 'hb':
LULSp,i := (evalf4(Fwind,g,scaa,i,α,(gvar),ULS + Fwind,py,scaa,i,α,(gvar),ULS) | evalf4(Fwa,scaa,i,α,(gvar),ULS + FFC,eq,scaa,i,α,(gvar),ULS)) :
LULSp,i,mult := < | evalf4(1.2 · Fwind,g,scaa,i,α,(gvar),ULS + 1.2 · Fwind,py,scaa,i,α,(gvar),ULS + 1.1 · Fwa,scaa,i,α,(gvar),ULS

```

```

+ 1.1 · FFC,eq,scaa,i,α(gvdr),ULS |evalf5(1.2 · Fwind,g,scaa,i,α(gvdr),ULS + 1.2 · Fwind,py,scaa,i,α(gvdr),ULS + 1.1
· Fwa,scaa,i,α(gvdr),ULS + 1.1 · FFC,eq,scaa,i,α(gvdr),ULS) >:

LSLSp,i := < |evalf4(Fwind,g,scaa,i,α(gvdr),SLS + Fwind,py,scaa,i,α(gvdr),SLS) |evalf4(Fwa,scaa,i,α(gvdr),SLS
+ FFC,eq,scaa,i,α(gvdr),SLS) >:
+ 1.1 · FFC,eq,scaa,i,α(gvdr),SLS |evalf4(1.2 · Fwind,g,scaa,i,α(gvdr),SLS + 1.2 · Fwind,py,scaa,i,α(gvdr),SLS) |evalf4(1.1 · Fwa,scaa,i,α(gvdr),SLS
+ 1.1 · FFC,eq,scaa,i,α(gvdr),SLS) |evalf5(1.2 · Fwind,g,scaa,i,α(gvdr),SLS + 1.2 · Fwind,py,scaa,i,α(gvdr),SLS + 1.1
· Fwa,scaa,i,α(gvdr),SLS + 1.1 · FFC,eq,scaa,i,α(gvdr),SLS) >:

enddo:
for ifrom 1 to 22 do
hb,j := hb,req,scaa,i :
enddo:
for ifrom 1 to 22 do
MTRAFp,i := ( |evalf5(Mtraffic,i,SLS) |evalf5(Mtraffic,i,ULS) )
enddo:
MTR := ("NR|M_traffic,SLS|M_traffic,ULS") :
for ifrom 1 to 22 do
gvdr := piecewise(i ≤ 5, 11, 5 < i ≤ 10, 10 < i ≤ 12, 9, 12 < i ≤ 17, 10, 17 < i ≤ 22, 11) :
Fxwaves,i := Fwa,scaa,i,α(gvdr),SLS :
Fxcurr,i := FFC,eq,scaa,i,α(gvdr),SLS · Fxwind,i := Fwind,g,scaa,i,α(gvdr),SLS + Fwind,py,scaa,i,α(gvdr),SLS :
enddo:

```

```

CRWT := <"NR"|"L_p"|"R_p"|"H_b"|"DR_p_SLS"|"FR_SLS"|"FR_NT_SLS"|"kr_BU"|"t_bot" >;
CRWTU := <"L"|"R"|"H_b"|"DR_p_SLS"|"FR_SLS"|"FR_NT_SLS"|"kr_BU"|"t_bot" >;
FRWTSLS := <"NR"|"F_wind,BG"|"F_wind,pyl"|"F_WA"|"F_FC"|"F_H,tot" >;
FRWTULS := <"NR"|"F_wind,BG"|"F_wind,pyl"|"F_WA"|"F_FC"|"F_H,tot" >;
LULSN := <"NR"|"F_wind,tot,ULS"|"F_water,tot,ULS" >;
LSLSN := <"NR"|"F_wind,tot,SLS"|"F_water,tot,SLS" >;
LULSMN := <"NR"|"F_wind,m,ULS"|"F_water,m,ULS"|"Total Fx,m" >;
LSLSMN := <"NR"|"F_wind,m,SLS"|"F_water,m,SLS"|"Total Fx,m" >;

```

7.1 Pontoon Properties

L_p = pontoon length ;

H_b = height ballast ;

DR_p_SLS = draught of pontoon in SLS ;

FR_SLS = freeboard of pontoon in SLS ;

FR_NT_SLS = freeboard of pontoon without traffic in SLS ;

kr_BU = rotational spring stiffness of pontoon (small angles) ;

t_bot = thickness of the bottom of the pontoon ;

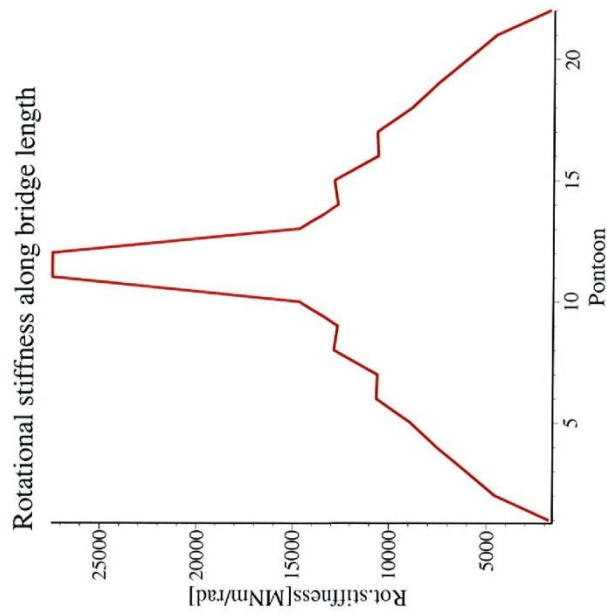
$\langle CRWT, CRWTU, seq(CRW_{p,i,scaod}, i = 1 \dots 22) \rangle$

(56)

"NR"	"L_p"	"R_p"	"H_b"	"DR_p_SLS"	"FR_SLS"	"FR_NT,SLS"	"kr_BU"	"t_bot"
"[-]"	"[m]"	"[m]"	"[m]"	"[m]"	"[m]"	"[m]"	"[MNm/rad]"	"[m]"
1	77.39	15.	14.2	73.10	4.29	4.91	1790.3589	2.54
2	93.28	18.	19.5	88.76	4.52	5.22	4542.7523	2.86
3	104.4	18.	22.7	99.80	4.61	5.30	6044.1464	3.09
4	115.1	18.	25.7	110.4	4.68	5.38	7554.9977	3.30
5	124.1	18.	28.1	119.3	4.75	5.45	8883.9747	3.48
6	134.3	18.	30.9	129.5	4.81	5.50	10660.701	3.68
7	114.2	21.	27.1	109.8	4.36	4.88	10615.447	3.29
8	127.4	21.	30.4	123.0	4.39	4.91	12862.489	3.54
9	125.0	21.	30.0	120.6	4.42	4.93	12657.315	3.50
10	137.5	21.	33.1	133.1	4.43	4.95	14712.357	3.75
11	136.0	26.	34.3	131.1	4.90	5.45	27456.294	3.72
12	136.0	26.	34.3	131.1	4.90	5.45	27456.297	3.72
13	137.5	21.	33.1	133.1	4.43	4.95	14712.362	3.75
14	125.0	21.	30.0	120.6	4.42	4.93	12657.321	3.50
15	127.4	21.	30.4	123.0	4.39	4.91	12862.497	3.54
16	114.2	21.	27.1	109.8	4.36	4.88	10615.456	3.29
17	134.3	18.	30.9	129.5	4.81	5.50	10660.712	3.68
18	124.1	18.	28.1	119.3	4.75	5.45	8883.9807	3.48
19	115.1	18.	25.7	110.4	4.68	5.38	7555.0032	3.30
20	104.4	18.	22.7	99.80	4.61	5.30	6044.1514	3.09
21	93.28	18.	19.5	88.76	4.52	5.22	4542.7562	2.86
22	77.39	15.	14.2	73.10	4.29	4.91	1790.3599	2.54

```
PKRBU := pointplot(
  << 1, 2, 3, 4, 5, 6, 7, 8, 9, 10, 11, 12, 13, 14, 15, 16, 17, 18, 19, 20, 21, 22 >>
  seq(
     $\frac{k_{r, BU, i, scaa}}{1000}$ , i = 1
    ..22
  ), style = line, title = "Rotational stiffness along bridge length", titlefont = ["calibri", 14], color = red, labels
  = ["Pontoon", "Rot.stiffness[MNm/rad]"], labelfont = ["calibri", 12], labeldirections = ["horizontal", "vertical"]):
display([PKRBU])
```





Distance between node where the wind load is acting on the bridge girder and the anchoring point:

```
for i from 1 to 22 do
```

$$a1 := \frac{h_{gp,i}}{2} + \frac{fz(s_{p,i})}{2}; a2 := \frac{fz(s_{p,i})}{2} + fr_{p,i,mt,slg} \cdot a3 := z_d;$$

```

arm_krbu,i := (a1 + a2 + a3) :
arm_krbu,i := evalf5(arm_krbu,i) :
enddo:

```

Distance between node where wind load is acting on the pylons and anchoring point:

```

for i from 1 to 22 do

```

$$a1 := \frac{h_{gp,i}}{2} + \frac{fz(s_{p,i})}{2}; a2 := \frac{fz(s_{p,i})}{2} + fr_{p,i,nt,sls}; a3 := z_a;$$

```

arm_pyl,i := evalf5(a2 + a3) :
enddo:

```

Distance between node where wave load is acting on and anchoring point is 20 meters for every pontoon.

Distance between node where current load is acting on and anchoring point:

```

for i from 1 to 22 do

```

```

gvdri := piecewise(i ≤ 5, 11, 5 < i ≤ 10, 10, 10 < i ≤ 12, 9, 12 < i ≤ 17, 10, 17 < i ≤ 22, 11) :
arm_kr,i := -1 * evalf5(z_{FC,i,α,(gvdri)} - z_a) :
enddo:

```

Distance between anchoring point and center of gravity:

```

for i from 1 to 22 do

```

```

armAG_i := z_{G,i,sls} - fr_{p,i,nt,sls} - z_a :
armAG_i := evalf5(armAG_i) :
enddo:

```

(57)

Table with all distances shown between the line of action of the forces and the anchoring point. The origin is at the anchoring point, upwards is considered positive here and downwards is negative.

```

{{"#P", " ", 1, 2, 3, 4, 5, 6, 7, 8, 9, 10, 11, 12, 13, 14, 15, 16, 17, 18, 19, 20, 21, 22} | {"z_wind BG-anch", "[m]", arm_krbu, 1'
arm_krbu, 2' arm_krbu, 3' arm_krbu, 4' arm_krbu, 5' arm_krbu, 6' arm_krbu, 7' arm_krbu, 8' arm_krbu, 9' arm_krbu, 10' arm_krbu, 11' arm_krbu, 12'
arm_krbu, 13' arm_krbu, 14' arm_krbu, 15' arm_krbu, 16' arm_krbu, 17' arm_krbu, 18' arm_krbu, 19' arm_krbu, 20' arm_krbu, 21' arm_krbu, 22}
| {"z_wind PY-anch", "[m]", arm_pyl, 1' arm_pyl, 2' arm_pyl, 3' arm_pyl, 4' arm_pyl, 5' arm_pyl, 6' arm_pyl, 7' arm_pyl, 8' arm_pyl, 9' arm_pyl, 10'

```



```

arm pyl, 11' arm pyl, 12' arm pyl, 13' arm pyl, 14' arm pyl, 15' arm pyl, 16' arm pyl, 17' arm pyl, 18' arm pyl, 19' arm pyl, 20' arm pyl, 21' arm pyl, 22'
| ("z_current-anch", "[m]", arm_kr, 1' arm_kr, 2' arm_kr, 3' arm_kr, 4' arm_kr, 5' arm_kr, 6' arm_kr, 7' arm_kr, 8' arm_kr, 9' arm_kr, 10'
arm_kr, 11' arm_kr, 12' arm_kr, 13' arm_kr, 14' arm_kr, 15' arm_kr, 16' arm_kr, 17' arm_kr, 18' arm_kr, 19' arm_kr, 20' arm_kr, 21' arm_kr, 22'
| ("z_anch-CoG", "[m]", seq(armAG, i = 1..22)))

```

"#P"	"z_wind BG-anch"	"z_wind PY-anch"	"z_current-anch"	"z_anch-CoG"
" "	"[m]"	"[m]"	"[m]"	"[m]"
1	28.673	26.447	-1.725	19.178
2	41.642	32.875	-6.473	28.482
3	52.810	38.501	-10.101	34.971
4	62.818	43.543	-13.775	41.091
5	71.668	48.002	-16.979	46.171
6	79.362	51.877	-20.752	52.060
7	85.223	54.494	-13.556	41.150
8	90.594	57.194	-18.325	48.367
9	94.813	59.315	-17.433	47.172
10	97.879	60.857	-22.108	53.876
11	101.03	62.316	-21.363	54.627
12	101.03	62.316	-21.363	54.627
13	97.879	60.857	-22.108	53.876
14	94.813	59.315	-17.433	47.172
15	90.594	57.194	-18.325	48.367
16	85.223	54.494	-13.556	41.150
17	79.362	51.877	-20.752	52.060
18	71.668	48.002	-16.979	46.171
19	62.818	43.543	-13.775	41.091
20	52.810	38.501	-10.101	34.971
21	41.642	32.875	-6.473	28.482
22	28.673	26.447	-1.725	19.178

7.2 Vertical Loads

The total selfweight of the pontoons is (in kN) $evalf_5(add(G_{p,i,SLS} \ i = 1..22)) + evalf_5(add(G_{ballast,i,SLS} \ i = 1..22))$ (59)

The total length of all pontoons is (in m) $evalf_5(add(l_{p,i} \ i = 1..22))$ (60)

The total vertical forces acting on the pontoons (self-weight bridge girder, pylons, traffic and self-weight anchoring system) is (in kN) $evalf_5(add(F_{ponton,i,SLS} \ i = 1..22))$ (61)

2.2047 10⁶

for *i* **from** 1 **to** 22 **do**

*l*_{tijdelijk} := *l*_{gp,i} ;

*F*_{traffic,i,SLS} := *q*_{traffic} · *l*_{tijdelijk} ;

unassign(*l*_{tijdelijk}) ;

enddo;

for *i* **from** 1 **to** 10 **do**

*G*_{BG,i} := (*q*_{g,SLS} - 35) · *l*_{gp,i} ;

enddo;

*G*_{BG,11} := $\frac{(q_{g,SLS,mid} - 35) \cdot l_{g,12}}{2} + \frac{(q_{g,SLS} - 35) \cdot l_{g,11}}{2}$;

for *i* **from** 1 **to** 11 **do**

*s*_{p,i} := *l*_{gp,i} ; *d*_{r,p,U,S} := *d*_{r,p,i,U,S} ; *l*_p := *l*_{p,i} ;

*G*_{pyl,i} := *G*_{pylon,SLS} ;

*l*_p := *l*_p ;

enddo;

Table with all vertical loads:

- F_traffic = vertical load due to traffic ;
- SW_BG = self-weight of bridge girder ;
- SW_PYL = self-weight of pylon ;
- SW_pontoon+ballast = self-weight of pontoon and ballast ;
- SW_AN = part of self-weight of anchoring system resisted by pontoon ;
- Fz total = total vertical load on pontoon ;

$$\begin{aligned}
 & \langle \langle \text{"pontoon"}, [-], \text{seq}(i, i = 1..11) \rangle \rangle \langle \langle \text{"F_traffic"}, [\text{[kN]}], \text{evalf}_5(\text{seq}(F_{\text{traffic}, i, SLS}, i = 1..11)) \rangle \rangle \langle \langle \text{"SW BG"}, [\text{[kN]}], \\
 & \text{seq}(\text{evalf}_5(G_{BG, i}, i = 1..11)) \rangle \rangle \langle \langle \text{"SW PYL"}, [\text{[kN]}], \text{seq}(\text{evalf}_5(G_{pyl, i}, i = 1..11)) \rangle \rangle \langle \langle \text{"SW sup"}, [\text{[kN]}], \text{seq}(\text{evalf}_5(G_{BG, i} \\
 & + G_{pyl, i}, i = 1..11)) \rangle \rangle \langle \langle \text{"SW pont+ball"}, [\text{[kN]}], \text{seq}(\text{evalf}_5(G_{p, i, SLS} + G_{ballast, i, SLS}, i = 1..11)) \rangle \rangle \langle \langle \text{"SW AN"}, [\text{[kN]}], \\
 & \text{seq}(\text{evalf}_6(G_{AN, i}, i = 1..11)) \rangle \rangle \langle \langle \text{"Fz total"}, [\text{[kN]}], \text{seq}(\text{evalf}_5(G_{\text{tot}, i, SLS}, i = 1..11)) \rangle \rangle
 \end{aligned}$$

[-]	"F_traffic"	"SW BG"	"SW PYL"	"SW sup"	"SW pont+ball"	"SW AN"	"Fz total"
"[kN]"	"[kN]"	"[kN]"	"[kN]"	"[kN]"	"[kN]"	"[kN]"	"[kN]"
1	4332.1	32800.	1173.8	33974.	4.6471 10 ⁵	6328.	5.0934 10 ⁵
2	7000.	53000.	5839.1	58839.	8.1741 10 ⁵	7335.	8.9058 10 ⁵
3	7000.	53000.	10065.	63065.	9.2482 10 ⁵	6467.	1.0014 10 ⁶
4	7000.	53000.	13853.	66853.	1.0259 10 ⁶	8205.	1.1080 10 ⁶
5	7000.	53000.	17203.	70203.	1.1102 10 ⁶	10029.	1.1974 10 ⁶
6	7000.	53000.	20115.	73115.	1.2059 10 ⁶	13565.	1.2996 10 ⁶
7	7000.	53000.	22589.	75589.	1.3995 10 ⁶	17665.	1.4998 10 ⁶
8	7000.	53000.	24626.	77626.	1.5609 10 ⁶	34933.	1.6805 10 ⁶
9	7000.	53000.	26226.	79226.	1.5354 10 ⁶	25363.	1.6470 10 ⁶
10	7000.	53000.	27389.	80389.	1.6854 10 ⁶	45137.	1.8179 10 ⁶
11	11638.	99738.	28115.	1.2785 10 ⁵	2.5642 10 ⁶	41618.	2.7337 10 ⁶

(62)

"NR"	"F_wind,BG"	"F_wind,pyl"	"F_WA"	"F_FC"	"F_H,tot"
"[-]"	"[kN]"	"[kN]"	"[kN]"	"[kN]"	"[kN]"
1	664.81	17.364	18.9	763.25	1464.3
2	1459.1	112.38	22.6	995.76	2589.9
3	1606.7	215.72	22.6	1052.1	2897.2
4	1684.0	317.00	22.6	1106.3	3129.9
5	1711.7	411.70	22.6	1151.8	3297.8
6	1817.5	497.24	22.6	1203.7	3541.0
7	1870.6	570.62	26.4	1287.0	3754.6
8	1896.9	633.37	26.4	1365.6	3922.3
9	1892.9	683.40	26.4	1351.1	3953.8
10	1859.6	720.15	26.4	1425.7	4031.8
11	4485.0	838.94	32.7	1750.6	7107.2

(66)

To simplify the modeling in Scia Engineer, both the wind load on the bridge girders and pylons are concentrated at the bridge girder (conservative) and the wave and current load are concentrated at the point where the wave load is acting on.

```
L1LSNU := { "[-]" | "[kN]" | "[kN]" } :
{ L1LSN, L1LSNU, seq( L1LS_{p,r}, i = 1..11 ) }
```

"I-]"	"F_wind,tot,SLS" [kN]"	"F_water,tot,SLS" [kN]"
1	682.2	782.2
2	1571.	1018.
3	1823.	1075.
4	2001.	1129.
5	2124.	1175.
6	2314.	1227.
7	2442.	1313.
8	2530.	1392.
9	2576.	1377.
10	2580.	1452.
11	5324.	1784.

(67

To create some margin for the design of the superstructure, the wind load will be multiplied by a factor 1,2 and the load due to the water is multiplied by 1,1.

$(L_{LSMN,seq}(L_{LS}_{p,i,mult}^{i=1..11}))$

"NR"	"F_wind,m,SLS"	"F_water,m,SLS"	"Total Fx,m"
1	818.6	860.3	1678.9
2	1886.	1120.	3006.0
3	2187.	1182.	3369.1
4	2401.	1242.	3643.0
5	2548.	1292.	3839.9
6	2777.	1349.	4126.7
7	2930.	1445.	4374.1
8	3036.	1532.	4567.5
9	3092.	1515.	4606.8
10	3096.	1598.	4693.0
11	6389.	1962.	8350.3

(68)

The horizontal loads (ULS) acting on the buoyancy bridge are shown in the table below.

(FRWTULS, FRW_{p,1,scaa,ULS}, FRW_{p,2,scaa,ULS}, FRW_{p,3,scaa,ULS}, FRW_{p,4,scaa,ULS}, FRW_{p,5,scaa,ULS}, FRW_{p,6,scaa,ULS}, FRW_{p,7,scaa,ULS}, FRW_{p,8,scaa,ULS}, FRW_{p,9,scaa,ULS}, FRW_{p,10,scaa,ULS}, FRW_{p,11,scaa,ULS})

"NR"	"F_wind,BG"	"F_wind,pyl"	"F_WA"	"F_FC"	"F_H,tot"
1	983.52	31.920	28.279	1413.1	2456.8
2	2192.3	206.58	33.935	1844.7	4277.6
3	2414.1	396.55	33.935	1949.1	4793.7
4	2530.2	582.74	33.935	2049.4	5196.3
5	2571.9	756.82	33.935	2133.7	5496.3
6	2730.8	914.06	33.935	2229.6	5908.4
7	2810.6	1049.0	39.590	2380.7	6279.9
8	2850.2	1164.3	39.590	2525.5	6579.6
9	2844.2	1256.3	39.590	2499.1	6639.2
10	2794.1	1323.8	39.590	2636.5	6794.0
11	7021.4	1542.2	49.017	3243.8	11856.

(69)

$$\text{Total wind load with margin (in kN)} \quad \text{evalf}_6(1.2 \cdot (\text{add}(F_{xwind, i=1..22})))$$

62320.2

(70)

$$\text{Total wave and current load with margin (in kN)} \\ \text{evalf}_6(1.1 \cdot (\text{add}(F_{xwaves, i=1..22})) + \text{evalf}_5(\text{add}(F_{xcurr, i=1..22})))$$

27502.5

(71)

$$\text{Total horizontal loads with margin (in kN)} \\ \text{evalf}_8(1.2 \cdot (\text{add}(F_{xwind, i=1..22})) + (1.1 \cdot (\text{add}(F_{xwaves, i=1..22})) + \text{evalf}_5(\text{add}(F_{xcurr, i=1..22}))))$$

89822.823

(72)

The loads (ULS) caused by wind and water are concentrated to simplify the modeling.
 $\langle LULSN_{seq}(LULS_{i=1..11}) \rangle$

"NR"	"F_wind,tot,ULS"	"F_water,tot,ULS"
1	1015.	1441.
2	2399.	1879.
3	2810.	1983.
4	3113.	2083.
5	3329.	2168.
6	3645.	2264.
7	3860.	2421.
8	4014.	2566.
9	4100.	2539.
10	4118.	2676.
11	8563.	3293.

(73)

The loads (ULS) with margin taken into account (120% for wind and 110% for water) are shown in the table below.

$\langle LULSMN, seq(LULS_{p,i,mult}, i = 1..11) \rangle$

"NR"	"F_wind,m,ULS"	"F_water,m,ULS"	"Total Fx,m"
1	1218.	1585.	2804.0
2	2878.	2067.	4945.2
3	3373.	2181.	5554.1
4	3735.	2291.	6027.1
5	3994.	2384.	6378.9
6	4374.	2490.	6863.8
7	4632.	2663.	7293.8
8	4817.	2823.	7638.9
9	4920.	2793.	7713.1
10	4942.	2944.	7885.2
11	10280.	3622.	13898.

(74)

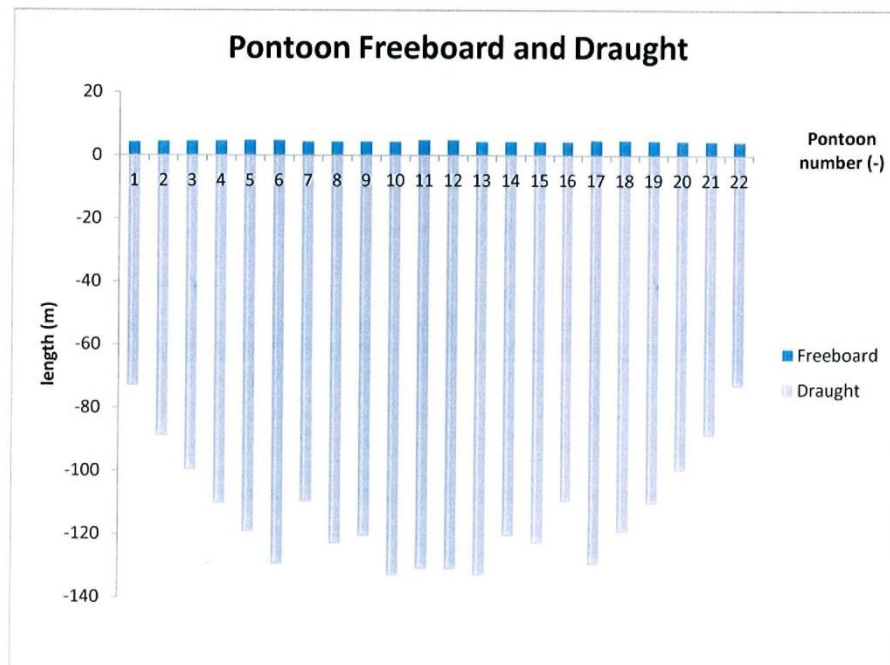
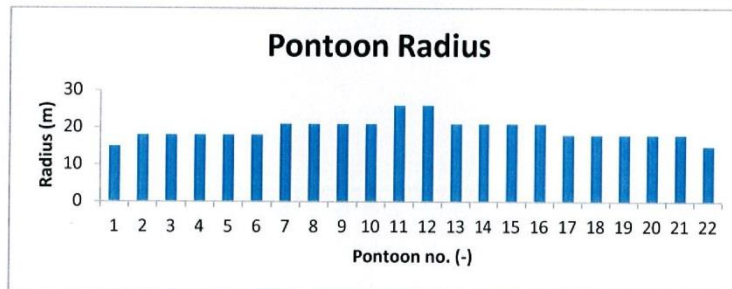
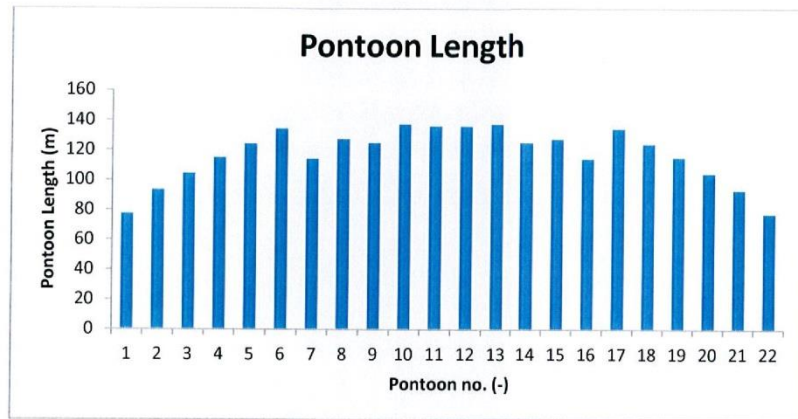
The bending moment caused by traffic is shown below.

$$MTRU := \langle \{[-]^{111}[kNm]^{111}[kNm]^{11}\} \rangle$$

$$\langle MTR, MTRU, seq(MTRAF_{p,i} \ i = 1..11) \rangle$$

"NR"	"M_traffic,SLS"	"M_traffic,ULS"
"[-]"	"[kNm]"	"[kNm]"
1	12996.	19495.
2	21000.	31500.
3	21000.	31500.
4	21000.	31500.
5	21000.	31500.
6	21000.	31500.
7	21000.	31500.
8	21000.	31500.
9	21000.	31500.
10	21000.	31500.
11	34912.	52369.

(75



ANNEX F:INTRODUCTION MODELING CABLES IN SCIA ENGINEER

In this section, a simple explanation is given about the modeling of slack cables in SCIA Engineer.

F.1 SCIA Engineer Settings

To model slack cable elements in Scia Engineer, the proper settings must be made in the project setup dialogue, functionality tab: options initial stress, nonlinearity and 2nd order calculation must be selected. In the solver setup of the nonlinear calculation the initial stress and initial stress as input must both be set ON.

For slack cables, several parameters should be inputted. The cable is subjected to self-weight load and a pre-stressing force. These parameters determine the slack of the cable. All calculations of Scia Engineer are carried out on the deformed structure. That means that the final deformation of a cable is calculated from this “slack” shape and not from the ideal straight shape of 1D member [23, p. 405].

F.2 Structure Input and Computational Results

A simply supported member is modeled in Scia Engineer, see Figure F-1. The member is modeled as a slack cable. The properties of the structure are shown below. Results are shown in Table F-1.

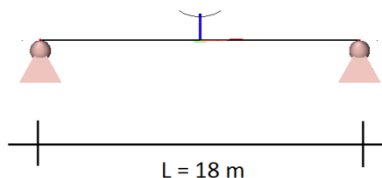


FIGURE F-1 STRUCTURE WITH CABLE IN SCIA ENGINEER

Span	: 18 m
Load	: self-weight
Cable diameter	: 20 mm
Cable section area	: 314,16 mm ²
Elasticity modulus cable	: 210 000 N/mm ²
Density cable	: 7850 kg/m ³
Prestressing Force in cable	: 1,0 kN and 10 kN

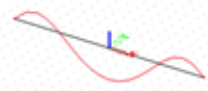
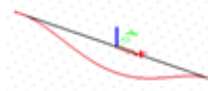
Settings in SCIA Engineer to model cable elements:

Beam nonlinearity	: cable
Initial mesh	: calculated
Normal force	: 1,0 kN and 10 kN
Self-weight	: yes

Nonlinear calculation settings for cables in SCIA Engineer:

Maximum iteraton	: 50
Geometrical nonlinearity (II, III order)	: Newton Raphson
Number of increments	: 5
Solver precision ratio	: 1

TABLE F-1 COMPUTATIONAL RESULTS SIMPLE CABLE IN SCIA ENGINEER

			H=1 kN	H=10 kN	
Deformed structure	Shape				
	Global deformation	Uz/uz (mm)	midspan	-981,1	-98
			at x=	-625,3	-
			at x=	-625,3	-
		Ux/ux (mm)	at x=	-27,1	-0,7
			at x=	27,1	-1,4
			at x=	-1,5	-0,00015
	Initial	Uz/uz (mm)	midspan	1,2	0
			at x=	1,2	0
			at x=	1,2	0
		Ux/ux (mm)	at x=	0,1	0
			at x=	-0,1	0
at x=			-0,1	0	
Support reactions	Rx (kN)		1	10	
	Rz (kN)		0,22	0,22	
internal forces on beam	N (kN)		1,03	10	
relative deformation	uz	at x=	1,2	0	
		midspan	-1,5	0	
member stress	normal (MPa=N/mm ²)		3,2	31,8	
Computational results match the analytical results			yes: $z(\text{midspan}) = \frac{q \cdot x^2}{2 \cdot H} = 979 \text{ mm}$	yes $z(\text{midspan}) = \frac{q \cdot x^2}{2 \cdot H} = 98 \text{ mm}$	

F.3 Analytical Results Matching the Computational Results

The computational results in the previous chapter match the analytical results, which can be calculated with the equations shown below:

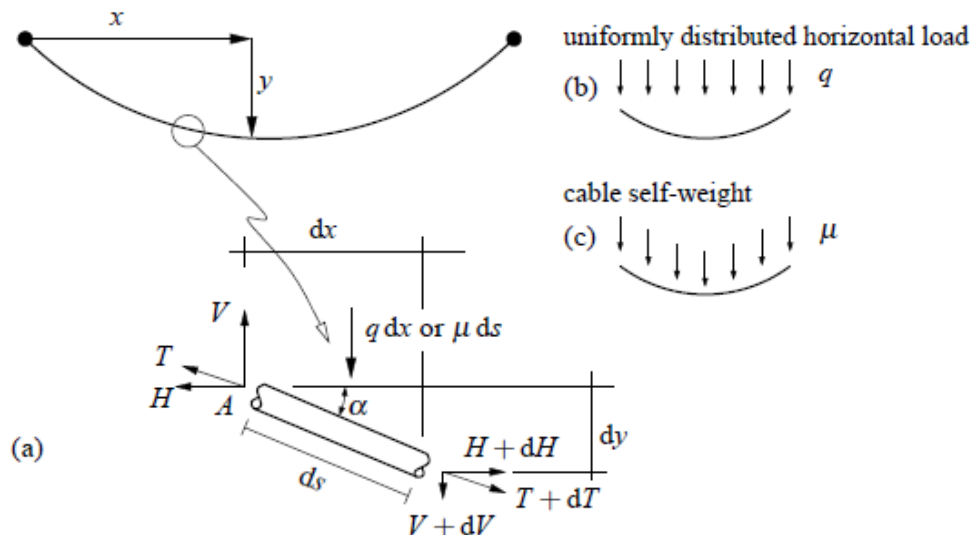


FIGURE F-2 MECHANICAL MODEL OF SAGGING CABLE [20]

Kinematic relation: $\tan \alpha = \frac{dy}{dx}$ (Eq. B.1)

Constitutive relation: $\tan \alpha = \frac{V}{H}$ (Eq. B.2)

Equilibrium relations: $\sum F_x = 0 \rightarrow -H + H + dH = 0 \rightarrow dH = 0$ (Eq. B.3)

$$\sum F_y = 0 \rightarrow -V + V + dV + q dx = 0 \rightarrow \frac{dV}{dx} = -q$$
 (Eq. B.4)

Combine (Eq. B.1) and (Eq. B.2): $\frac{dy}{dx} = \frac{V}{H} \rightarrow V = H \frac{dy}{dx}$ (Eq. B.5)

Combine (Eq. B.4) and (Eq. B.5): $-H \frac{d^2y}{dx^2} = q$ (Eq. B.6)

Successive integrations of (Eq. B.6) yields: $y = -\frac{q}{2H}x^2 + C_1x + C_2$ (Eq. B.7)

The integration constants can be determined by considering $y(0)=0$ and $y(l)=0$, where l is the cable span ($C_2=0$, $C_1=q_0l/2H$). Hence: $y = \frac{q_0}{2H}x(l-x)$ (Eq. B.8)

In this case, the deflection at the midspan of the cable is the cable sag f and it is equal to:

$$f = \frac{ql^2}{8H}$$
 (Eq. B.9)

In case of a catenary cable deformed under the influence of gravity, not q , an uniformly distributed horizontal load, must be used, but μ , the weight per unit length of the cable:

$$qdx = \mu ds \quad (\text{Eq. B.10})$$

The infinitesimal length ds of the cable is then equal to: $ds = \sqrt{dy^2 + dx^2}$ (Eq. B.11)

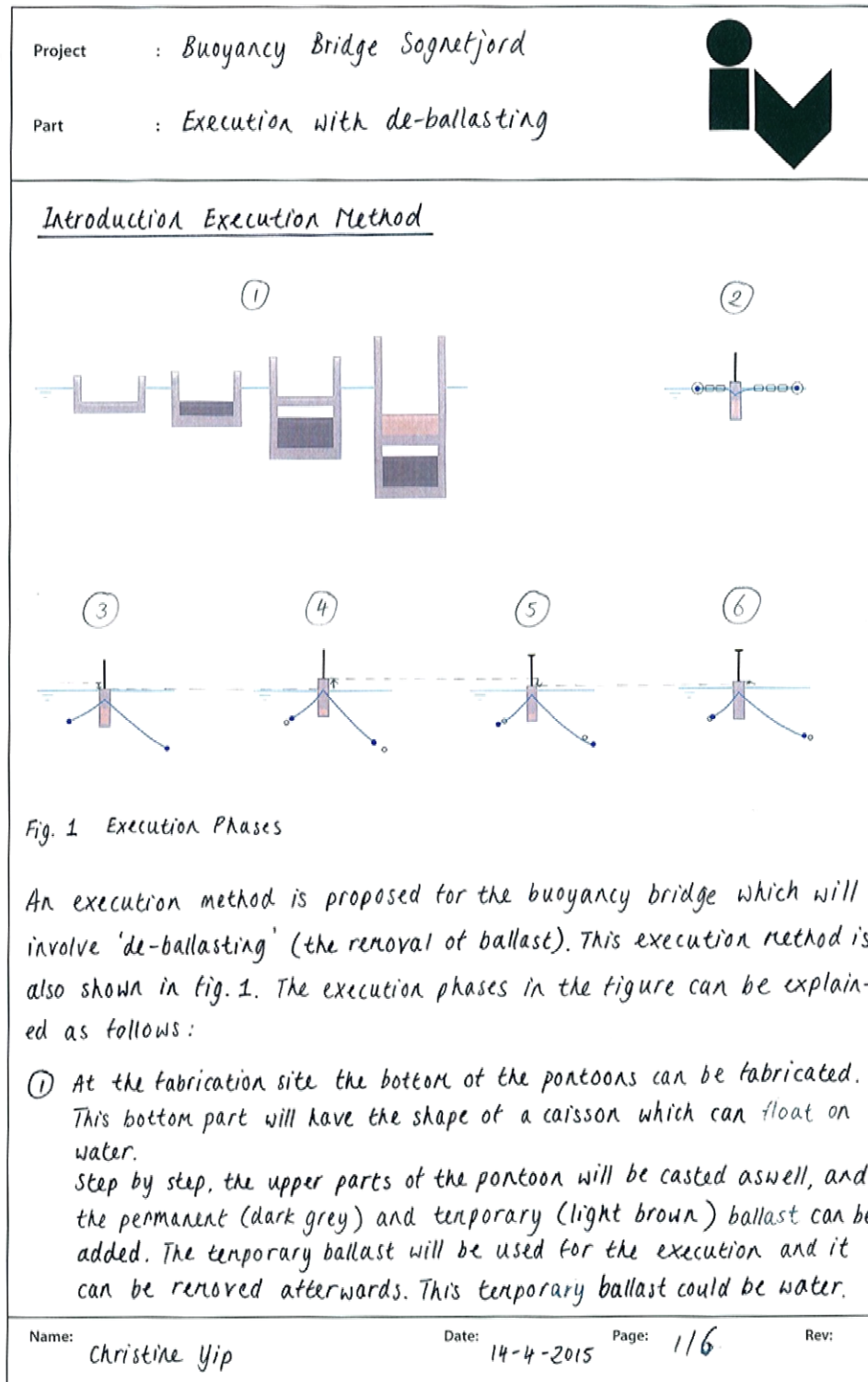
After simple derivations, the deflection of the catenary cable at midspan yields:

$$y = \frac{\mu x^2}{2H} \quad (\text{Eq. B.12})$$

This expression matches the computational results in Table F-1.

Side note: the parabolic assumption for flat profile cables is accurate enough even with ratios sag to span up to 1:5 [24, p. 47].

ANNEX G: ERECTION METHOD INVOLVING DE-BALLASTING



Project : Buoyancy Bridge Sognefjord

Part : Execution with de-ballasting



- ② The completed pontoons can be transported to the site (over water). On site also the anchoring cables will be put in place on the water surface by using temporary buoyancy elements. The anchoring cables will be connected to the pontoons. However, due to the temporary buoyancy elements which are connected to the cables, the pontoons will not sink due to the weight of the cables.
- ③ The temporary buoyancy elements are removed from the anchoring cables and all cables sink into position due to their self-weight. The pontoon also sinks a bit due to the self-weight of the cables.
- ④ A part of the temporary ballast (T.Ball.1) is removed from the pontoon. Due to this removal, the pontoon rises a bit from the water. As the pontoon rises, the cables will also be pulled upward.
- ⑤ The superstructure (bridge deck, girders, pylons, etc.) will be installed on top of the pontoons. Due to the weight of the superstructure, the position of the pontoons are lowered again.
- ⑥ In the final phase (a part of) the remaining temporary ballast (T.Ball.2) will be removed so the attachment points between the pontoons and anchoring cables will be positioned at 20 meters below water level. This is done to comply with the clearance requirement.

During the whole execution phase, the pontoons must be stable and the top of the pontoons may not be submerged.

Modeling in Scia Engineer

To analyse the tension in the anchoring cables, the execution method which is explained before, is also taken into account in the model of Scia Engineer. The execution phases which were shown in Fig. 1, are modeled as shown in Fig. 2 on the next page.

Name: Christine Yip

Date: 14-4-2015

Page: 216

Rev:

Project : Buoyancy Bridge Sognefjord

Part : Execution with de-ballasting

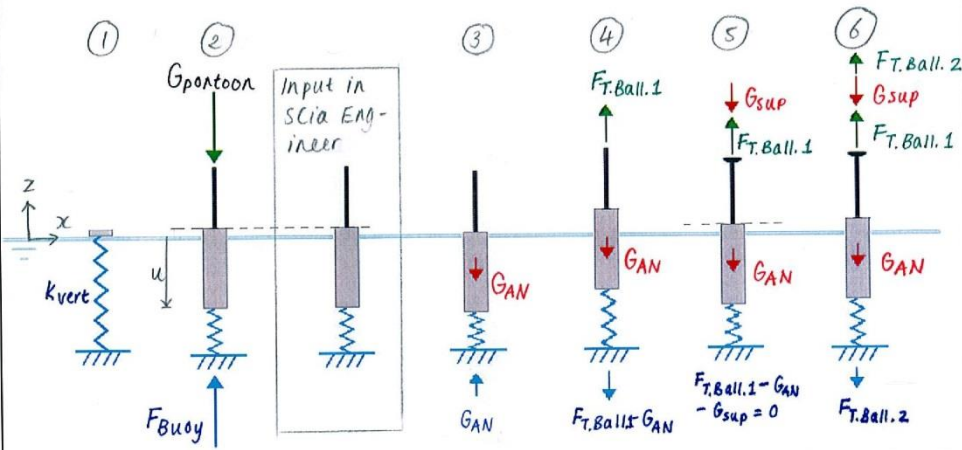


Fig.2 Modeling the execution phases in Scia Engineer

k_{vert} = spring stiffness which represents the buoyancy of the pontoon.
 $= \rho_{water} \cdot g \cdot \pi \cdot r_{pontoon}^2$

$G_{pontoon}$ = Self-weight of the pontoon, including the permanent and temporary (T.Ball.1 and T.Ball.2) ballasts.

F_{Buoy} = buoyancy of the pontoon
 $= k_{vert} \cdot u$

G_{AN} = self-weight of the anchoring cables

$F_{T.Ball.1}$ = self-weight of a part of the temporary ballast which will be removed in execution phase 4. $F_{T.Ball.1}$ is chosen to be equal to $G_{AN} + G_{sup}$

G_{sup} = self-weight of the superstructure

$F_{T.Ball.2}$ = self-weight of a part of the temporary ballast which will be removed in execution phase 6. To test the effect, $F_{T.Ball.2}$ is chosen in such a way that the structure will be 20 meters higher than the input position. In reality, the structure will not rise to this position; this is only done in the modeling to investigate the effect.

Name: Christine Yip Date: 14/4-2015 Page: 3/6 Rev:

Project : Buoyancy Bridge Sognefjord

Part : Execution with de-ballasting

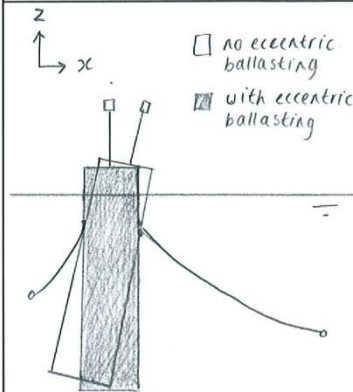


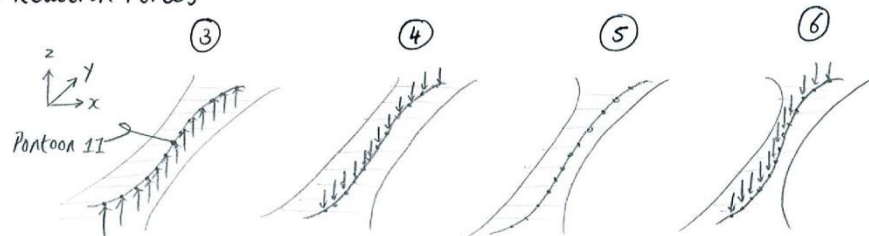
Fig. 3 Rotation due to asymmetric anchoring

Rotation due to asymmetric anchoring compensated by asymmetric ballasting

The anchoring cables which are attached to the pontoons have different lengths. This causes a rotation of the pontoons. To compensate this rotation, it is assumed that eccentric permanent ballast is present in the pontoon, in such a way that the rotation in execution phase ③ is equal to zero. The eccentric ballast is modeled as bending moments ($M_{x, ecc}$ and $M_{y, ecc}$). See fig. 3 for the rotation.

Modeling Results from SCia Engineer

• Reaction Forces



The reaction forces act in the same direction as predicted in Fig. 2. The resultant of the reaction forces of execution phase ③ equals the self-weight of the anchoring system: $806 \cdot 10^3$ kN. This is in the same scale of magnitude as the anchoring system from Annex J ($772 \cdot 10^3$ kN).

• Vertical displacements

The vertical displacement of pontoon 11 in different execution phases are:

$$\begin{array}{cccc}
 \textcircled{3} & \Delta u_z = +2,7 \text{ m} & \textcircled{4} & \Delta u_z = -1,78 \text{ m} & \textcircled{5} & \Delta u_z = +19,96 \text{ m} & \textcircled{6} \\
 u_z \text{ (m)} & -0,94 \text{ m} & \rightarrow & 1,76 \text{ m} & \rightarrow & -0,02 \text{ m} & \rightarrow & 19,94 \text{ m}
 \end{array}$$

Name: Christine Yip

Date: 14-4-2015 Page: 4/6

Rev:

Project : Buoyancy Bridge Sognefjord

Part : Execution with de-ballasting



$u_{z,③}$ can be easily checked:

$$G_{AN} = 41\,618 \text{ kN}$$

$$K_{vert} = \rho_w \cdot g \cdot \pi \cdot r^2 = 99\% \cdot 1015 - 9,81 \cdot \pi \cdot 38^2 = 44\,719 \text{ kN/m}$$

$$u_z = \frac{G_{AN}}{K_{vert}} = \frac{41\,618}{44\,719} = 0,93 \text{ m} \approx 0,94 u_{z,③}$$

$u_{z,④}$ can also be checked:

$$G_{sup} = 76\,625 \text{ kN}$$

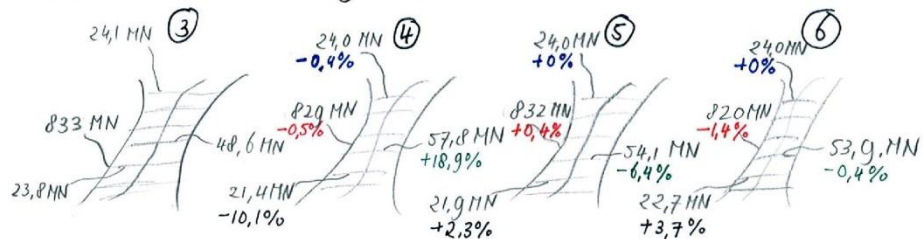
$$F_{r,ball.1} = G_{AN} + G_{sup} \text{ (this was chosen)}$$

$$= 41\,618 + 76\,625 = 118\,243 \text{ kN}$$

$$\Delta u_z = \frac{G_{AN} + G_{sup}}{K_{vert}} = \frac{118\,243}{44\,719} = 2,6 \text{ m}$$

$$u_{z,④, \text{check}} = u_{z,③} + \Delta u_z = -0,94 + 2,6 = 1,70 \text{ m} \approx u_{z,④}$$

• Tension in the anchoring cables



The maximum tension force in the main and lateral anchoring cables in the different erection phases are shown above.

It can be seen that the tension in the main cable increases when the pontoons sink (phase ③ and ⑤) and it decreases when the pontoons rise (phase ④ and ⑥).

For the lateral anchoring cables the relation between the cable tension and the vertical pontoon displacement is not so

Name: Christine Yip

Date: 14-4-2015 Page: 5/6

Rev:

Project : Buoyancy Bridge Sognefjord

Part : Execution with de-ballasting



straightforward. Each lateral anchoring cable reacts differently (increase/decrease of the tension) when the pontoon displaces.

Conclusion

The execution method involving de-ballasting is not effective.

Name: Christine Yip


Date: 14-4-2015 Page: 6/6

Rev:

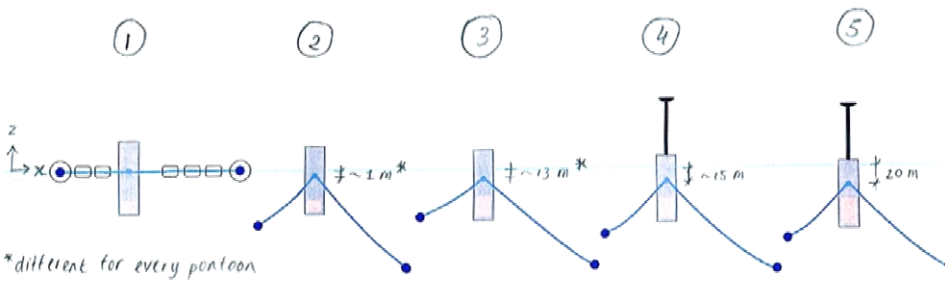
ANNEX H: ERECTION METHOD WITH ANCHORING CABLES AT WATER LEVEL AT START

Project : Buoyancy Bridge Sognefjord

Part : Erection method starting with cables at water level



Introduction Erection Method



*different for every pontoon

Fig. 1 Erection phases and Fig. 3

The erection method shown in Fig. 1 is proposed for the buoyancy bridge of Sognefjord. The phases can be explained as follows:

① In the first phase, the anchoring cables will be placed at water surface in a certain configuration with the help of temporary buoyancy elements. The configuration, whether the cables are straight or curved at water surface, depends on the cable lengths, see Fig. 2.

At the middle of the fjord the cables will sag into the water to create a clearance of 400 meters width and 20 meters deep for passing vessels. However, to simplify the modeling, it will be assumed that all anchoring cables are located at water level in phase ①.

As can be seen in Fig. 1, the pontoon contains exactly a certain amount of ballast, so the anchoring attachment points on the

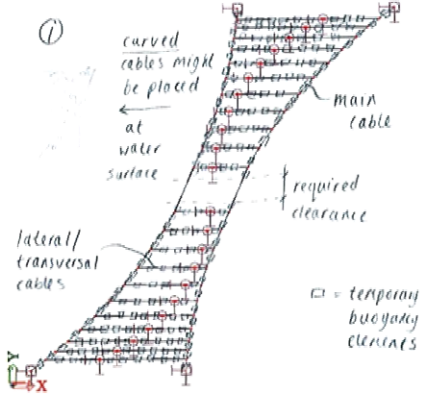


Fig. 2 Top view of anchoring system in execution phase ①

Name: Christine Yip

Date: 20-4-2015

Page: 1/8

Rev:

Project : Buoyancy Bridge Sognefjord

Part : Execution method starting with cables at water level



pontoons will also be located at water level. The anchoring cables will be connected to the pontoons in this phase.

- ② Hereafter, the temporary buoyancy elements are removed, causing the anchoring system to sink into the water. Due to the self-weight of the anchoring cables, the pontoons will also sink. The vertical displacement will be around 1 meter, but this value is different for every pontoon.
- ③ At the end of phase ④, the anchoring attachment points^{of all pontoons} should be at approximately 15 meters below water level (the reason for this will be explained in the description of phase ⑤). Since the self-weight of the superstructure will cause the pontoon to sink approximately 2 meters, extra ballast ($G_{BALL,1}$) will be added to the pontoon in this phase to realise this. This required ballast ($G_{BALL,1}$) should be determined for every pontoon.
- ④ The superstructure of the bridge will be installed on top of the pontoons. After the installation, it is expected that the pontoons will have sunk again, and the anchoring attachment points will be located at approximately -15 meters.
- ⑤ In practice, the anchoring points will seldomly end up at exactly at 15 meters at the end of phase ④. Therefore, ballast is used at this last execution phase to regulate the pontoon heights. For example, in case at the end of phase ④, the anchoring points are located at 14 meters below water level, some more ballast will be added. In case the anchoring points are located at 16 meters below water level, less ballast will be added to those pontoons. At the end of the execution, all anchoring

Name: Christine Yip

Date: 20-4-2015

Page: 2/8

Rev:

Project : Buoyancy Bridge Sognefjord

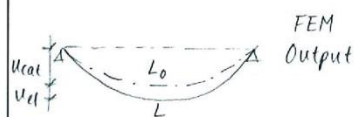
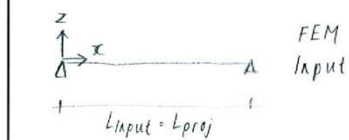
Part : Erection method starting with cables at water level



points should be located at 20 meters below water level

Modeling in Scia Engineer

Before modeling in Scia Engineer, special attention should be paid to principles of cable analyses.



$$L = L_0 + L_{elastic}$$

with

$$L_0 > L_{proj}$$

$$L_{elastic} = L_0 \epsilon = L_0 \frac{N}{EA}$$

Flexible ends:

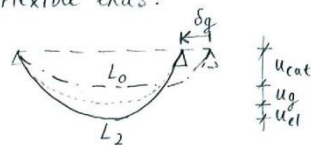


Fig 3 Principle cable analysis

As can be seen in Fig.3, to model cables in FEM software, a certain L_{input} of the cables should be inputted in the software. Note that this length is not the actual cable length, but it is the cable span! Due to the self-weight of the cable, there will be a certain cable shape in the FEM Output with the cable length L . L is the sum of L_0 (length of catenary cable) and $L_{elastic}$ (elastic deformation). In case $EA = \infty$, then $L = L_0$ (no elastic deformation occurs). L_0 is the initial length of the cable, which is larger than the cable span L_{proj} .


In the anchoring system of the buoyancy bridge, especially the transversal/lateral anchoring cables do not have fixed ends. At one end the transversal cable is connected to the floating pontoons, which can displace, and at the other end the transversal cables are connected to the main cable, which displaces significantly from the input position due to self-weight of the anchoring system. In this situation, cable sag is not only caused by self-weight and elastic elongation, but also by geometric change (displacements of cable ends) of the anchoring

Name: Christine Yip

Date: 4-5-2015

Page: 3/8

Rev:

Project	:		
Part	:		
<p>system configuration.</p> <p>Therefore, what will actually be done in Scia Engineer, can be explained as follows. First, an anchoring system with (random) cable spans (L_{input}) is inputted in Scia Engineer. This cable system configuration is also shown in Fig.2 (configuration with straight cables). Hereafter, in the Scia Engineer output, the final anchoring system configuration can be obtained and the final cable lengths can be calculated (L_2 of Fig.3). To find out the initial lengths of the cables in the anchoring system, the displacements due to elastic deformation and geometric change of the system should be 'subtracted' from the final configuration of the cable.</p> <p>Because insight had already been gained in previous studies and modelings, it is known that the chosen input configuration will lead to sufficient tension in the cables.</p> <p>In this study, the initial lengths of the cables will not be calculated. However, this should be done in later design phases as it is of importance for the erection. If it turns out that the initial lengths of the cables are to be shorter than the cable span, then mechanical tension regulation will be needed during the erection. In case the required initial cable lengths are equal or longer than the cable spans, then the anchoring system can be erected by using the buoyancy of the pontoons alone and no mechanical tension regulation will be needed.</p>			
Name:	Christine Yip	Date:	4-5-2015
Page:	4/8	Rev:	

Project : Buoyancy Bridge Sognefjord

Part : Execution method starting with cables at water level

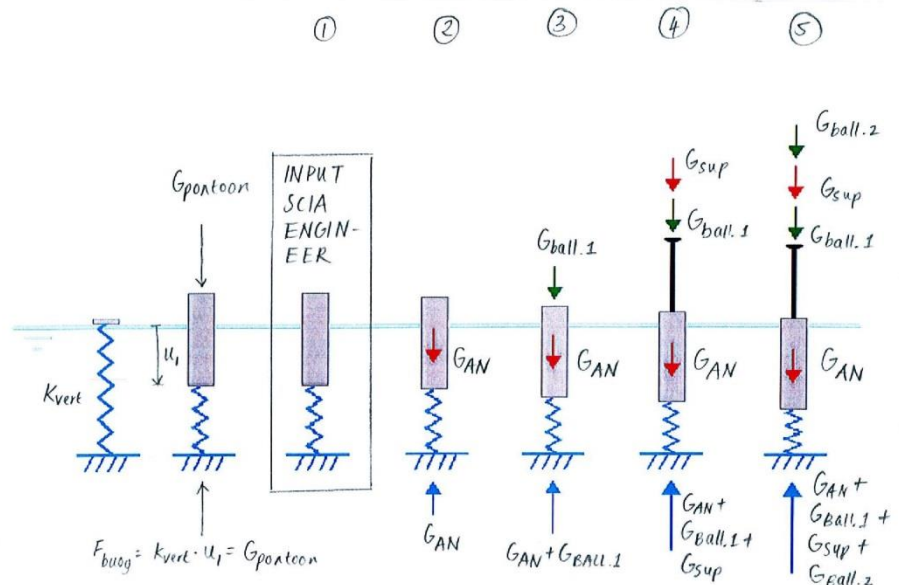


Fig. 3 Modeling steps in Scia Engineer

K_{vert} = spring stiffness which represents the buoyancy of the pontoon
 $= \rho_{water} \cdot g \cdot \pi \cdot r_{pontoon}^2$

$G_{pontoon}$ = self-weight of the pontoon including a part of the final ballast. Due to the selfweight, the pontoon sinks into the water for a certain height. This is taken into account in the model by modeling the pontoon at that certain height.


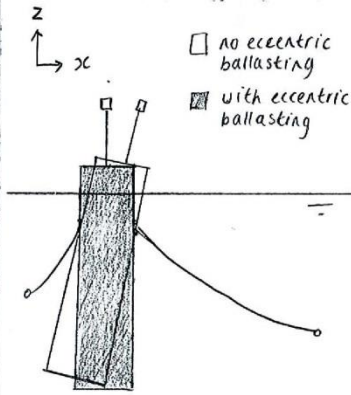
G_{AN} = self-weight of anchoring system

$G_{BALL.1}$ = self-weight of the ballast which will be added in execution phase ③. $G_{BALL.1}$ is determined for each pontoon, so that the anchoring attachment points will be at 15 meters below water level in phase ④.

Name: Christine Yip

Date: 26-4-2015 Page: 5/8

Rev:

<p>Project : Buoyancy Bridge Sognefjord</p> <p>Part : Execution method starting with cables at water level</p>	
<p>G_{sup} = self-weight of bridge superstructure. (pylons + deck)</p> <p>$G_{BALL,2}$ = self-weight of the ballast which will be added in the last execution phase (5). The purpose of applying this ballast is to regulate the (vertical) position of the pontoon. The anchoring attachment point of the pontoon should be at 20 meters below water level for every pontoon. In case the anchoring attachment point already appears to be in the right position during the execution, then $G_{BALL,2} = 0$.</p>	
<div style="display: flex; align-items: flex-start;"> <div style="margin-right: 20px;"> <p>z</p> <p>→ x</p>  </div> <div> <p>□ no eccentric ballasting</p> <p>■ with eccentric ballasting</p> </div> </div> <p>Fig. 4 Rotation due to asymmetric anchoring</p>	<p>Rotation due to asymmetric anchoring compensated by asymmetric ballasting:</p> <p>The anchoring cables which are attached to the pontoons have different lengths. This causes a rotation of the pontoons. To compensate this rotation, it is assumed that eccentric permanent ballast is present in the pontoon, in such a way that the rotation in execution phase (3) is equal to zero. The eccentric ballast is modeled as bending moments ($M_{x,ecc}$ and $M_{y,ecc}$). See fig. 3 for the rotation.</p>
<p>Note: For simplicity of this substudy, the rotational spring stiffness for every execution phase is considered to be equal. This is not the case in reality, since the ballast in the pontoon is different for every stage in the execution. This should be taken into account in further design stages. Also, the pontoons should be stable in all phases.</p>	
<p>Name: Christine Yip</p>	<p>Date: 20-4-2015 Page: 6/8 Rev:</p>

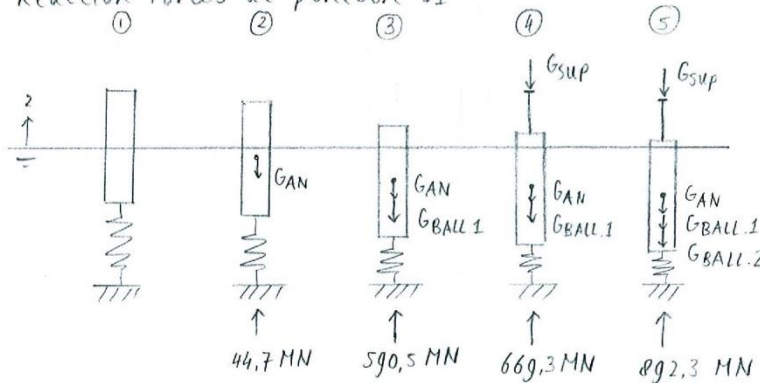
Project : Buoyancy Bridge Sognefjord

Part : Execution method starting with cables at water level



Modeling Results from Scia Engineer

- Reaction Forces at pontoon 11 :



As predicted according to Fig.3, the reaction forces increase for every load step/execution phase.

The resultant of reactions in z-direction of phase (2) equals the self-weight of the anchoring system; 806 MN (see substudy 'Execution

- Vertical displacements : [with debalasting' and Annex J)

Pontoon 11

$$k_{vert,11} = \rho \cdot g \cdot \pi \cdot r_{11}^2 = 99\% \cdot 1015 \text{ kg/m}^3 \cdot 9.81 \text{ m/s}^2 \cdot \pi \cdot 38^2 = 44719 \text{ kN/m}$$

$$r_{11} = 38 \text{ m (radius might change in the final design)}$$

	(2)	(3)	(4)	(5)
$u_z \text{ (m)}$	-1,0 m	-13,2 m	-15,0 m	-20,0 m
		$\Delta u_z = -12,2 \text{ m}$	$\Delta u_z = -1,8 \text{ m}$	$\Delta u_z = -5,0 \text{ m}$

Pontoon 10

$$r_{10} = 18 \text{ m (radius might change in the final design)}$$

$$k_{vert} = \rho \cdot g \cdot \pi \cdot r_{10}^2 = 10034 \text{ kN/m}$$

	(2)	(3)	(4)	(5)
$u_z \text{ (m)}$	-3,9 m	-10,9 m	-15,0 m	-20,0 m
		$\Delta u_z = -7 \text{ m}$	$\Delta u_z = -4,1 \text{ m}$	$\Delta u_z = -5,0 \text{ m}$


Name: Christine Yip

Date: 20-4-2015 Page: 7/8

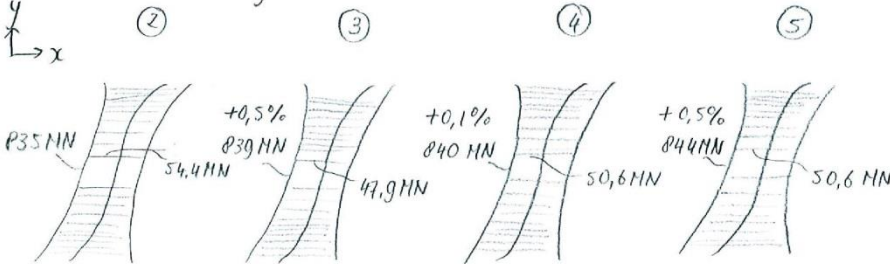
Rev:

Project : Buoyancy Bridge Sognefjord

Part : Execution method starting with cables at water level



• Tension in anchoring cables:



It can be seen that as the vertical displacement of the pontoons increase, the tension in the main cables also increases. The tension increase over a vertical displacement of 16,1-19,5 meters (phase ② to ⑤) is however small: +1,1%. It is expected that larger vertical displacements will lead to larger tension forces in the main cables.

This is however probably not needed, since the displacements of a previously modeled anchoring system with 687 MN in the main cables were already sufficient. (see Annex J.2.2. in *Extreme Bridge for Sognefjord* by T. Yip, 2015).

Conclusion

The execution method where anchoring cables are placed at water surface at the start, is an effective method.

Name: Christine Yip Date: 20-4-2015 Page: 8/8 Rev:

ANNEX I: CABLE LENGTH CHECK FOR AVOIDING MECHANICAL PRETENSIONING

For the erection of the buoyancy bridge, it is preferred not to use mechanical pretensioning for the anchoring cables, but to induce tension in the cables by using the self-weight of the cables, the self-weight of the pontoons and the buoyancy of the pontoons alone. This way, good use is made of the buoyancy property of the pontoons during the erection phase, besides the use phase. See chapter 3.4.2 for more about the erection method.

No mechanical pretensioning is required during the erection if the initial cable lengths are larger than the cable spans. If the initial cable length is smaller than the span, then it is needed to mechanically pretension the cable. This check for the proposed substructure in chapter 6 is given below.

The final length of the cables in deformed state (L_1) is equal to the sum of the initial length (L_0) and the elastic deformation (ΔL_{EL}) of the cables. Therefore, the initial length can be obtained by:

$$L_0 = L_1 - \Delta L_{EL} = L_1 - \frac{NL}{EA}$$

Mechanical pretensioning can be avoided when:

$$L_0 - L_{span} \geq 0$$

In Table I-1, the cable lengths and cable spans are shown and compared. The cable numbering is shown in Figure I-1. Other cable properties are:

Modulus of Elasticity	: 195 000 N/mm ²
Diameter main anchoring cable	: 1200 mm
Diameter lateral anchoring cable	: 350 mm

In the table it can be seen, that mechanical pretensioning can be avoided for the most part of the cables. Only in the transversal cables B64, B66, B68 and B70, the cable span between the pontoon and main cable is smaller than the cable length. However, since the main cable is more than 9 meters longer than the span, it is assumed that this "remaining" length of the main cable can be used to shift the main cable in such a way, that the cable spans at B64, B66, B68 and B70 can be made smaller. It is assumed that the cable span of these transversal cables can decrease sufficiently so no mechanical pretensioning is needed for these cables as well.

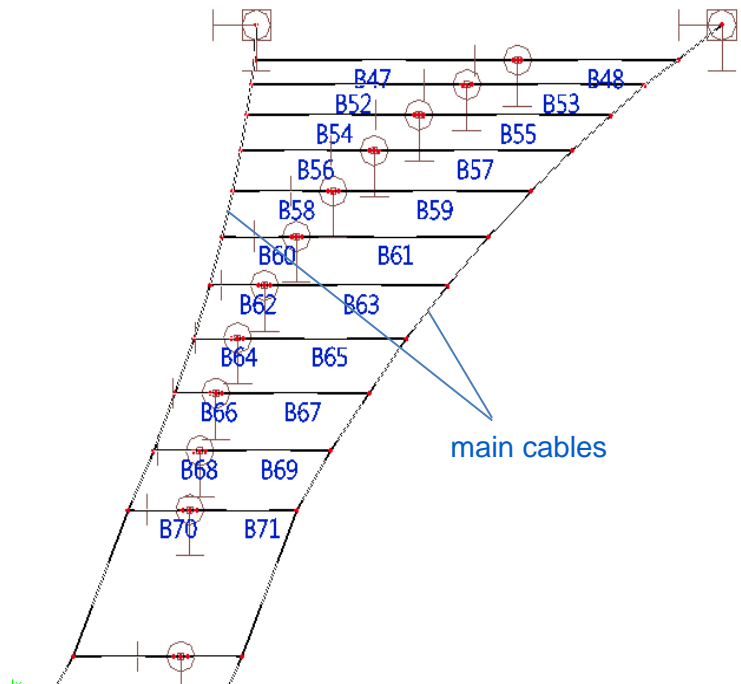


FIGURE I-1 ANCHORING CABLE NUMBERINGS

TABLE I-1 INITIAL CABLE LENGTH (L_0) CHECK

Anchoring cable	L_1 (m)	N (kN)	ΔL_{EL} (m)	L_0 (m)	$L_0 - L_{span}$ (m)
main	4468,76	829864	4,20	4465	9,31
B47	932,48	26086	0,32	932	0,96
B48	561,37	25998	0,19	561	0,58
B52	758,45	29429	0,30	758	0,89
B53	623,27	29489	0,24	623	0,72
B54	602,20	17431	0,14	602	0,41
B55	674,75	17581	0,16	675	0,44
B56	462,26	22524	0,14	462	0,41
B57	694,89	22757	0,21	695	0,58
B58	343,81	23927	0,11	344	0,32
B59	694,25	24156	0,22	694	0,59
B60	248,98	26914	0,09	249	0,23
B61	674,02	26914	0,24	674	0,62
B62	175,39	27266	0,06	175	0,07
B63	639,01	26494	0,23	639	0,54
B64	134,24	44182	0,08	134	-0,15
B65	588,52	40336	0,32	588	0,80
B66	125,66	24954	0,04	126	-0,58
B67	530,69	21630	0,15	531	0,23
B68	143,53	57544	0,11	143	-0,54
B69	450,02	50696	0,30	450	0,66
B70	193,78	48363	0,12	194	-0,35
B71	361,00	45384	0,22	361	0,29

ANNEX J: COMPUTATIONAL MODEL SUBSTRUCTURE EXAMPLE 1 (FIXED SUPPORTS)

To investigate the horizontal suspension anchoring system, the system is modeled into SCIA Engineering. First, a rough model will be inputted in Scia Engineer. In case the behavior of the system is correct and realistic, the model will be refined step by step.

The purpose is to obtain a suitable anchoring system after stepwise refining of the computational models. By only modeling and loading the final anchoring system without the superstructure of the bridge, the movements of the pontoons resulting from the anchoring system alone will then be visible and it can be investigated what effects the bridge girder will be required to resist.

J.1 Assumptions Model 1

To start, the following assumptions were made for a preliminary rough model:

- All degrees of freedom of the supports for the main anchoring cables are fixed
- All degrees of freedom of the supports at the pontoons are fixed, except the displacements in x-direction to investigate how much the S-shape of the pontoon locations will be retained
- All anchoring cables have the same cross sectional area ($d=500$ mm)
- The input prestressing force for the main anchoring cables is 10 000 kN (arbitrary)
- The input prestressing force for all lateral side anchoring cables is 1000 kN (arbitrary)
- The anchoring system is modeled as if it is constructed over ground; the reduced weight of the cables in water is not taken into account
- No bridge girder is modeled, only the anchoring system

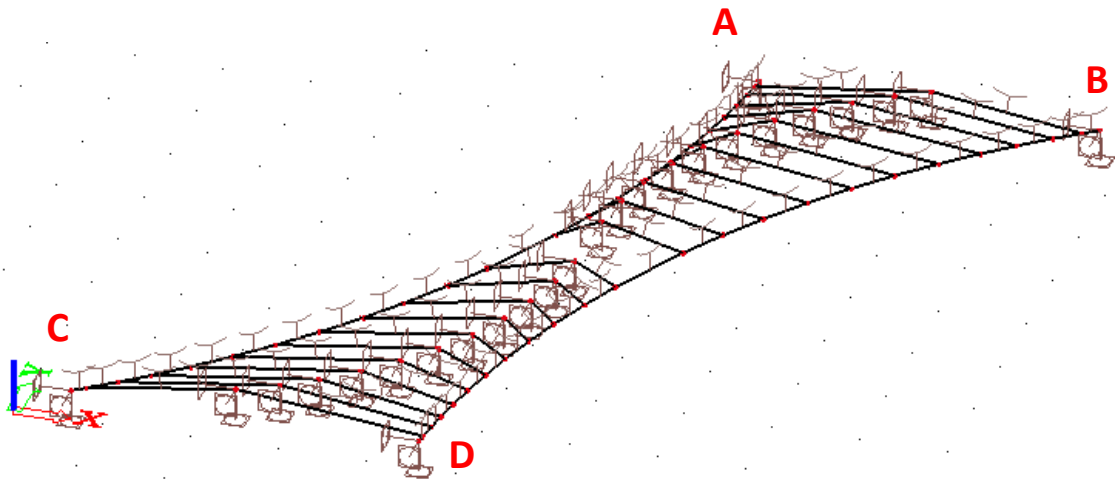


FIGURE J-1 ANCHORING MODEL 1 IN SCIA ENGINEER

J.2 Input

J.2.1 Coordinates Anchoring System

The rough model of the anchoring system is shown in Figure J-1. The two main cables are fixed from shore (AB) to shore (CD), one main cable is fixed from A to C and the other is fixed from B to D. The lateral anchoring cables are attached to these two main cables and the pontoons, which are placed in an S-shape from the top view.

The node numbering and node coordinates are shown respectively in Figure J-2 and Table J-1. These coordinates were inputted in SCIA Engineer graphically.

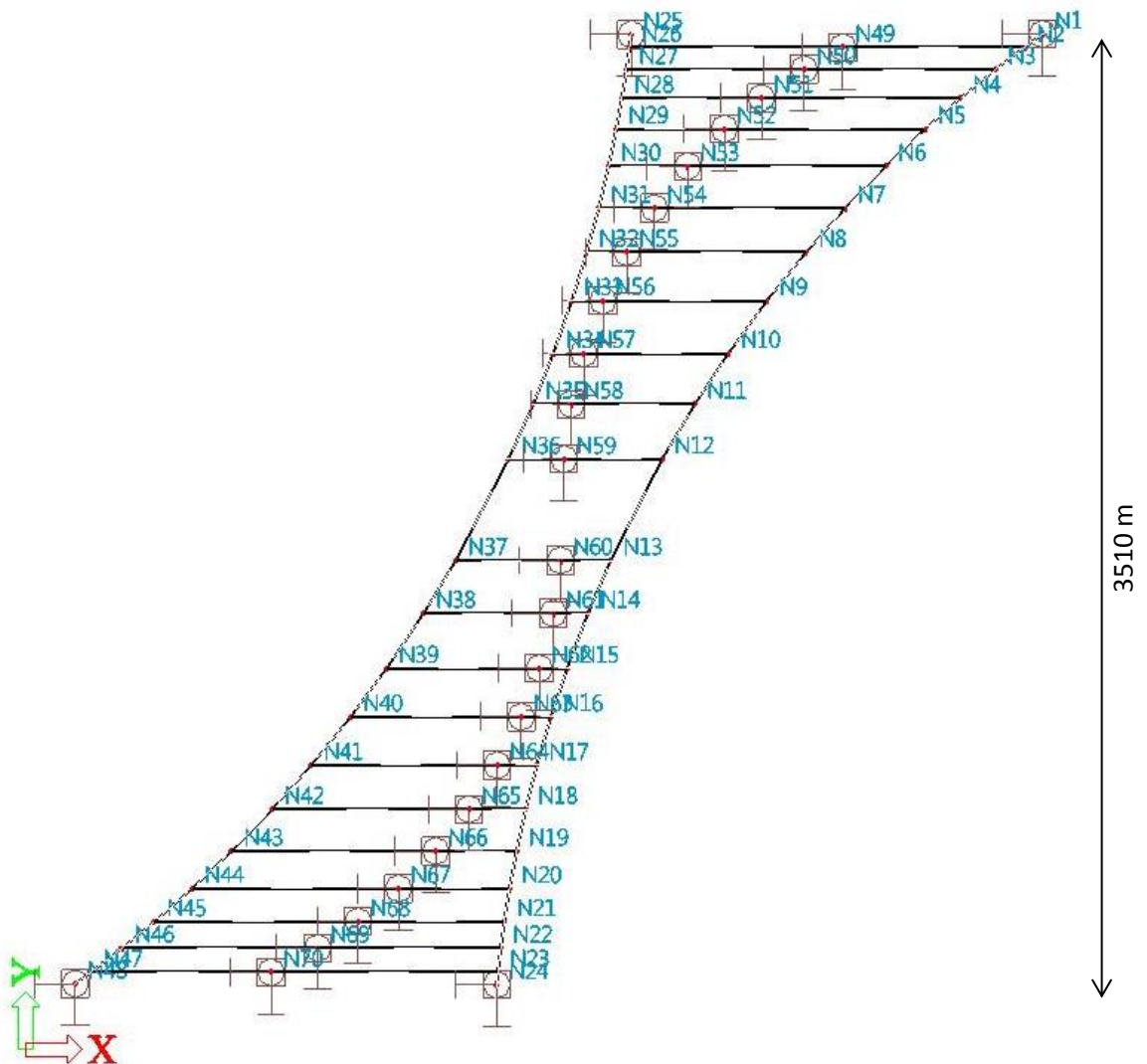


FIGURE J-2 ANCHORING SYSTEM WITH NODE NUMBERINGS

TABLE J-1 COORDINATES NODES ANCHORING SYSTEM

Node Number	x (m)	y (m)	z (m)	Node Number	x (m)	y (m)	z (m)
N1	3814	3750	0	N36	1812	2181	0
N2	3746	3702	0	N37	1613	1807	0
N3	3638	3620	0	N38	1493	1612	0
N4	3506	3515	0	N39	1354	1408	0
N5	3374	3401	0	N40	1219	1229	0
N6	3226	3262	0	N41	1071	1050	0
N7	3074	3108	0	N42	924	888	0
N8	2927	2945	0	N43	772	733	0
N9	2780	2766	0	N44	624	595	0
N10	2635	2571	0	N45	483	473	0
N11	2510	2384	0	N46	363	375	0
N12	2387	2181	0	N47	245	286	0
N13	2194	1807	0	N48	186	243	0
N14	2109	1612	0	N49	3065	3702	100
N15	2031	1408	0	N50	2919	3620	100
N16	1970	1229	0	N51	2760	3515	100
N17	1917	1050	0	N52	2620	3401	100
N18	1875	888	0	N53	2483	3262	100
N19	1841	733	0	N54	2359	3108	100
N20	1815	595	0	N55	2254	2945	100
N21	1795	473	0	N56	2165	2766	100
N22	1782	375	0	N57	2093	2571	100
N23	1771	286	0	N58	2047	2384	100
N24	1766	240	0	N59	2019	2181	100
N25	2271	3749	0	N60	2006	1807	100
N26	2265	3702	0	N61	1979	1612	100
N27	2253	3620	0	N62	1926	1408	100
N28	2236	3515	0	N63	1859	1229	100
N29	2215	3401	0	N64	1768	1050	100
N30	2186	3262	0	N65	1663	888	100
N31	2149	3108	0	N66	1538	733	100
N32	2104	2945	0	N67	1399	595	100
N33	2048	2766	0	N68	1247	473	100
N34	1979	2571	0	N69	1096	375	100
N35	1904	2384	0	N70	920	286	100

J.2.2 Material Properties

Steel Y1860 anchoring cables are used with material properties shown below.

Y1860

Tensile strength : 1860 N/mm²

Modulus of Elasticity: 195 000 N/mm²

Unit mass : 7850 kg/m³

All cables are modeled to have circular cross-sections with diameters of 500 mm.

J.2.3 SCIA Engineer Input Options

Supports

The supports of the main cables to the shore (at nodes N1, N24, N25 and N48) are fixed for all degrees of freedom:

$$u_x = \textit{fixed} \qquad \varphi_x = \textit{fixed}$$

$$u_y = \textit{fixed} \qquad \varphi_y = \textit{fixed}$$

$$u_z = \textit{fixed} \qquad \varphi_z = \textit{fixed}$$

The supports at the location of the pontoons (nodes N49 to N70) are all also fixed, except the displacements in x-direction:

$$u_x = \textit{free} \qquad \varphi_x = \textit{fixed}$$

$$u_y = \textit{fixed} \qquad \varphi_y = \textit{fixed}$$

$$u_z = \textit{fixed} \qquad \varphi_z = \textit{fixed}$$

Cables

All cables are modeled as slack cables with self-weight checked ON.

The inputted pretension in the main anchoring cables is 10 000 kN.

The inputted pretension in the lateral anchoring cables is 1000 kN.

Note that this is not the real normal force in the cables, this is just an initial input value for the model in Scia Engineer.

Loads

The structure will be subjected to its self-weight. The reduced weight of the steel cables under water is neglected in this preliminary model. No safety factors are used.

Mesh

Average size of cables in the mesh setup is 100 meters.

J.3 Results and Evaluation

J.3.1 Deformed Structure

The deformed structure is shown in Figure J-3, Figure J-4, Figure J-5 and below in green.

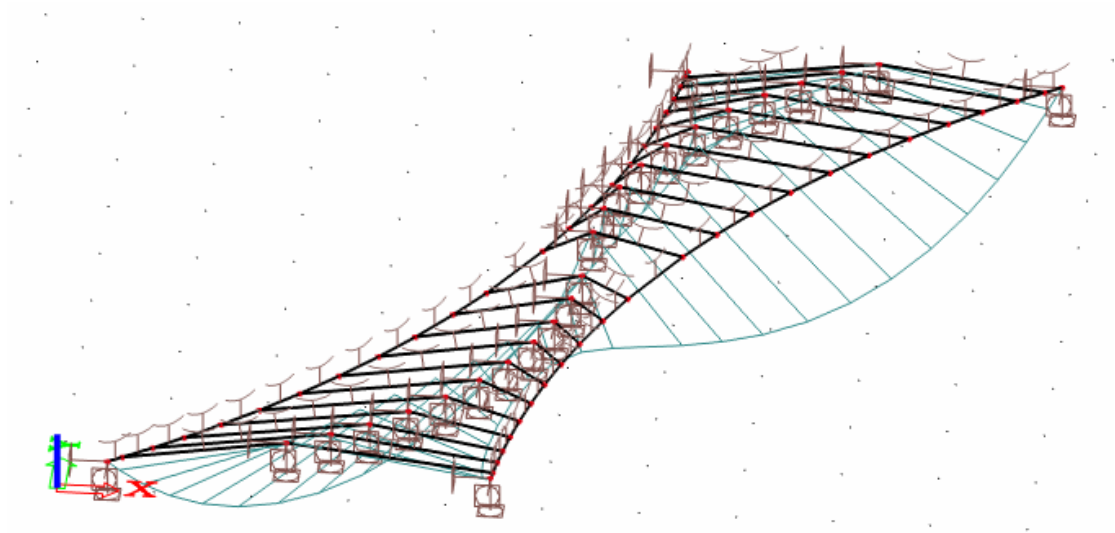


FIGURE J-3 DEFORMED STRUCTURE 3D VIEW

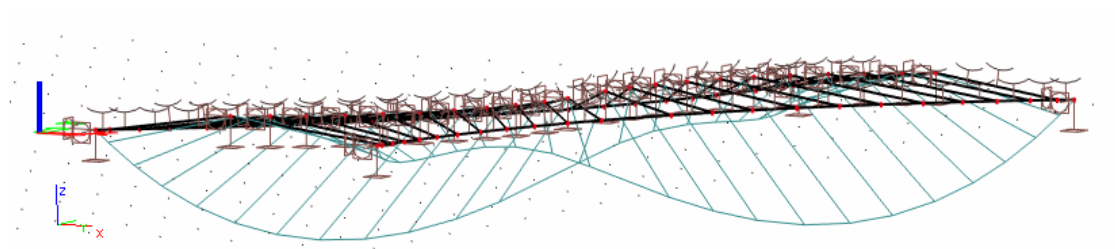


FIGURE J-4 DEFORMED STRUCTURE 3D VIEW (2)

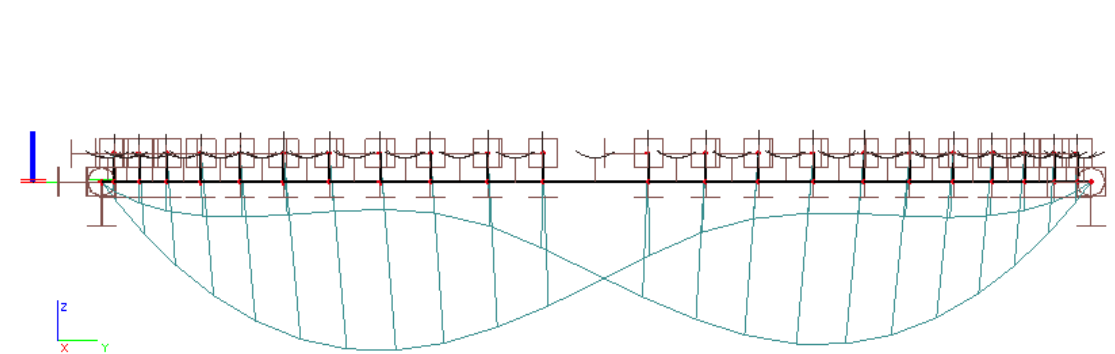


FIGURE J-5 DEFORMED STRUCTURE IN Y-Z PLANE

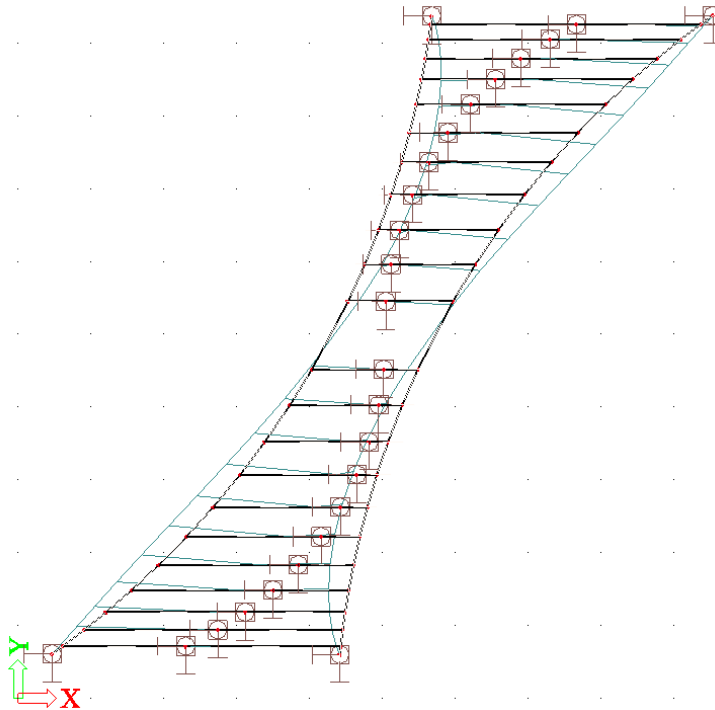


FIGURE J-6 DEFORMED STRUCTURE TOP VIEW/ X-Y PLANE

J.3.2 Reaction Forces

The total reaction force of the whole structure is $515,2 \cdot 10^3$ kN. This is the total weight of all the anchoring cables.

For this model however, the anchoring system is modeled as if it is located over ground. For a more refined model, the reduced weight of the cables in water can also be taken into account. Then, the total weight of the anchoring system will be reduced and the deformation of the structure resulting from the self-weight of the cables will also be smaller.

In Figure J-7, the reaction forces in y-direction can be seen. This implies that in case the restraints in y-direction are set free, the bridge superstructure parts will want to move to the middle of the bridge (at the center of fjord). Then, the bridge girder at the main span in the center of the fjord will be loaded under compression.

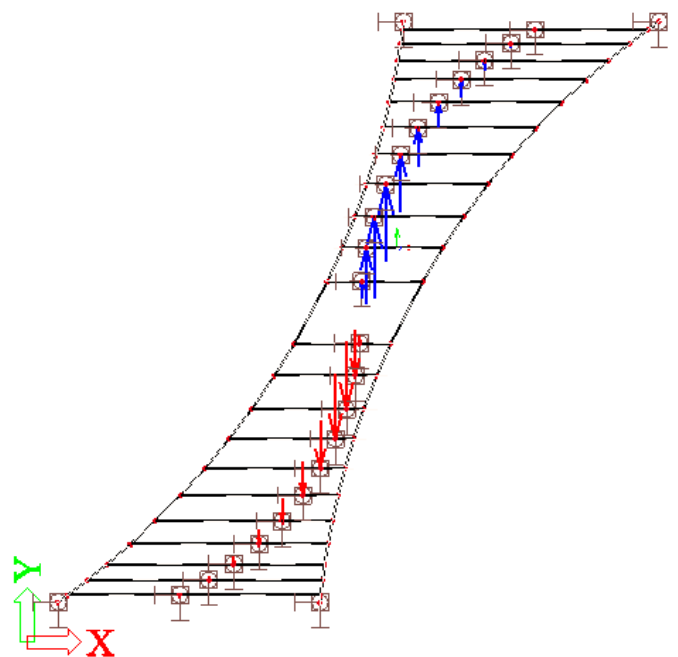


FIGURE J-7 REACTION FORCES IN Y-DIRECTION

J.3.3 Forces and Stresses: Lateral cables not loaded to Full Capacity

As can be seen in Figure J-9 and Figure J-8, the internal forces and stresses of the main anchoring cables are much larger than the forces and stresses in the lateral anchoring cables. The maximum normal force in the main cable is $F_{E,k} = 181,5 \cdot 10^3$ kN and the maximum stress in the cable is 924,6 N/mm². The resistance of the cables can be checked in the ultimate limit state (ULS) and the serviceability limit state (SLS) according to NEN-EN 1993-1-11.

ULS: Approximation Tension Resistance F_{Rd}

$$F_{Rd} = \min \left\{ \frac{F_{uk}}{1,5\gamma_R}; \frac{F_k}{\gamma_R} \right\} \quad [25, \text{p. 18}]$$

With the following assumptions:

$$F_{uk} = A \cdot f_{uk}$$

$$F_k = 89\% \cdot F_{uk} \quad [26]$$

$$\gamma_R = 1,0$$

Thus:

$$F_{Rd} = \frac{A \cdot f_{uk}}{1,5 \cdot 1,0} = \frac{\pi \cdot 250^2 \cdot 1860}{1,5} = 243,5 \cdot 10^3 \text{ kN}$$

$$f_{Rd} = \frac{F_{Rd}}{A} = \frac{243,5 \cdot 10^6}{\pi \cdot 250^2} = 1240 \text{ N/mm}^2$$

SLS: Stress Limit

Besides a stress limit for the ultimate limit state, there is also a stress limit for the serviceability limit state [25]:

$$f_{SLS} = 0,45 \cdot f_{uk} = 0,45 \cdot 1860 = 837 \text{ N/mm}^2 \quad ([25, \text{p. 24}])$$

Stress limit f_{SLS} may be increased to $0,50 \cdot f_{uk}$ in case detailing measures are applied.

$$\frac{\sigma_k}{f_{SLS}} = \frac{924,6}{837,0} = 1,1$$

The results for the loads without safety factors show that the stress limit of the serviceability limit state is exceeded. Therefore, larger size cables are required for the main cables. On the contrary, only a very small part of the capacity of the lateral anchoring cables is used. This indicates that cables of smaller size might be sufficient for the lateral anchoring cables.

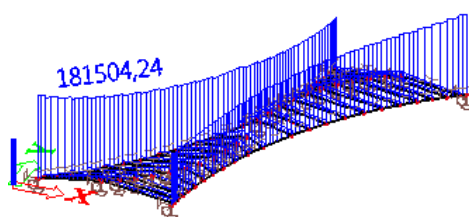


FIGURE J-9 INTERNAL FORCE IN CABLES IN [KN]

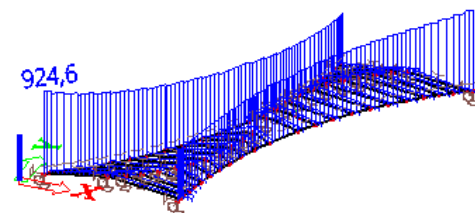


FIGURE J-8 STRESSES IN CABLES IN [N/MM2]

J.3.4 Displacement of Nodes

The nodes at the location of the pontoons can only displace in x-direction. These displacements resulting from the self-weight of the structure are shown in Figure J-10. It can be seen that the pontoons move out the S-shape as result of its self-weight and the predefined prestressing in the cables. The maximum displacement is approximately 66 meters.

For this model, the pretensioning in the lateral anchoring cables is all chosen to be 1000 kN. The pretensioning in each lateral anchoring cable can be adjusted to obtain an anchoring system, which retains the S-shape of the pontoons as much as possible. As shown in the previous section J.3.3, the anchoring cables, especially the lateral anchoring cables, can resist much larger loads. This adjustment can be made for the next more refined modeling of the anchoring system.

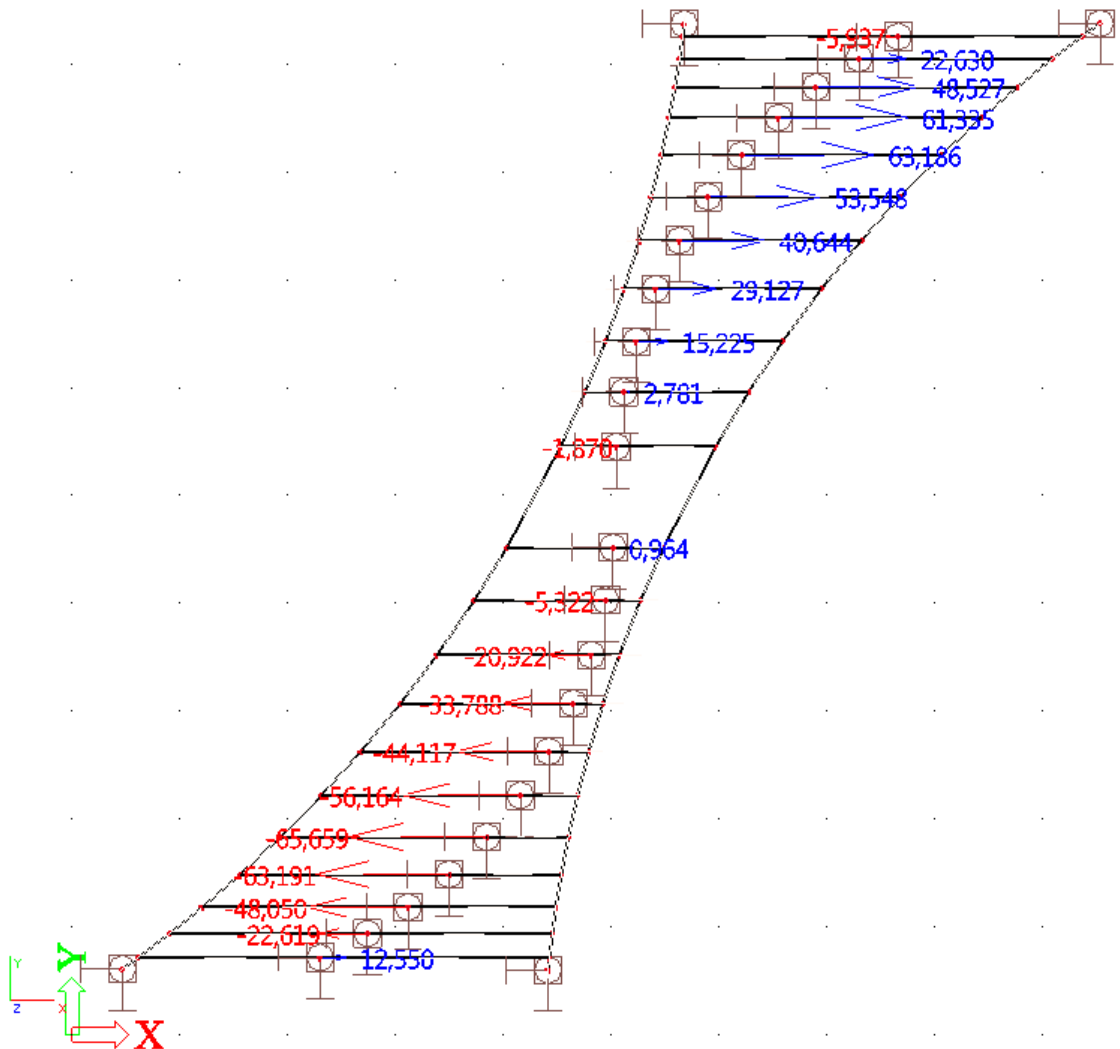


FIGURE J-10 DISPLACEMENT OF PONTOONS IN [M]

J.3.5 Equilibrium Check

Only normal force N is present in the cables. The shear force and bending moment of the cables are equal to zero. In Figure J-11, the normal force in two lateral anchoring cables, which are attached to each other at the location of the pontoon (red dot), is shown. As can be seen, the two internal forces are not equal. The forces at the pontoon can be drawn as shown in Figure J-12.

From the results in Scia Engineer, the angles are calculated:

$$\alpha = 51^\circ$$

$$\beta = 45^\circ$$

Then, the horizontal components are:

$$H_1 = 14095 \cos 51^\circ = 8870 \text{ kN}$$

$$H_2 = 11537 \cos 45^\circ = 8161 \text{ kN}$$

Since there must be equilibrium, the two horizontal components should be equal.

$$H_1 = 8870 \text{ kN} \approx H_2 = 8161 \text{ kN}$$

There is a small deviation. This can be explained by the fact, that the angles are calculated by using u_z at a certain chosen length. However, to obtain accurate values for the angles, u_z should be measured for an infinitesimal small element dx . It is assumed that the equilibrium check is sufficient.

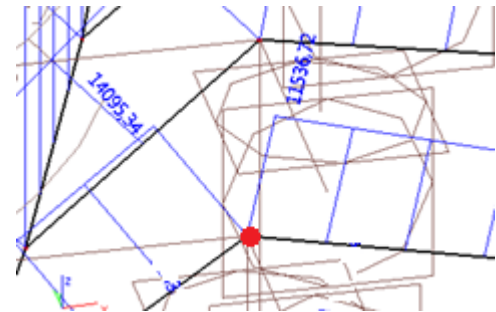


FIGURE J-11 NORMAL FORCE IN CABLE IN [KN]

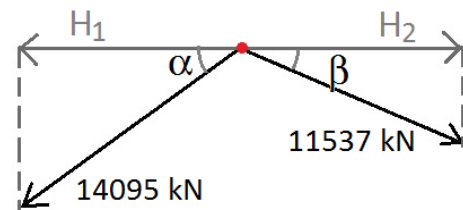


FIGURE J-12 FORCES FROM THE CABLES ON PONTOON

J.4 Conclusion

For this preliminary model the same arbitrary prestressing force was chosen for all lateral cables. This resulted in a certain displacement of the nodes at the pontoons. These nodes move out of the S-shape, as could be seen in Figure J-10. For the next model, the prestressing force in the lateral cables can be adjusted, so the S-shape will be retained as much as possible. The increase of the prestressing is possible since according to the results, only a small part of the total capacity of the lateral cables is loaded.

Furthermore, the displacements due to the self-weight of the anchoring system can also be reduced in the next refined model by using the smaller submerged weight for the steel anchoring cables instead of the regular weight.

In reality, the pontoon elements are floating in the fjord. Here, only the displacements in x-direction were free. The rest of the degrees of freedom were fixed. In the next refined model the displacements in y-direction can also be set free. Considering the reaction forces in y-directions from the results, it can be expected that the nodes at the location of the pontoons will move towards the center of the fjord if the restraints in y-direction will be set free. This indicates that the bridge girder will be loaded under compression at this location.

Remark: The results of this modeling are not rotationally symmetric. This can be explained by the fact that the inputted structure is actually also not exactly rotationally symmetric; the structure was inputted graphically.

ANNEX K: COMPUTATIONAL MODEL SUBSTRUCTURE EXAMPLE 2 (ADJUSTED PRESTRESSING)

To investigate the horizontal suspension anchoring system, the system is modeled into SCIA Engineering. First, a rough model was inputted in Scia Engineer, see ANNEX J: Computational Model Substructure Example 1 (Fixed Supports). Results showed that refinements of this model were possible.

K.1 Assumptions Model 2

In this section, the model from ANNEX J: Computational Model Substructure Example 1 (Fixed Supports) is refined by the following adjustments:

- Reduced weight of steel cables submerged in water
- Adjusted pretensioning in lateral anchoring cables
- All degrees of freedom of the supports at the pontoons are fixed, except the displacement in x-direction and y-direction

The remaining assumptions of the previous model, also given in section J.1, remain the same:

- All degrees of freedom of the supports for the main anchoring cables are fixed
- All anchoring cables have the same cross sectional area ($d=500$ mm)
- The input prestressing force for the main anchoring cables is 10.000 kN (arbitrary)
- No bridge girder is modeled, only the anchoring system

K.2 Input

All properties of the model remains the same as the previous model, except the few properties mentioned below (supports, reduced cable weight and pretensioning of lateral anchoring cables). The coordinates of the nodes and the material properties can be found in respectively sections J.2.1 and J.2.2.

K.2.1 Supports

The supports of the main cables to the shore (at nodes N1, N24, N25 and N48 in Figure J-2) are fixed for all degrees of freedom:

$$u_x = \textit{fixed} \qquad \varphi_x = \textit{fixed}$$

$$u_y = \textit{fixed} \qquad \varphi_y = \textit{fixed}$$

$$u_z = \textit{fixed} \qquad \varphi_z = \textit{fixed}$$

The supports at the location of the pontoons (nodes N49 to N70 in Figure J-2) are all also fixed, except the displacements in x- and y-directions:

$$u_x = \textit{free} \qquad \varphi_x = \textit{fixed}$$

$$u_y = \textit{free} \qquad \varphi_y = \textit{fixed}$$

$$u_z = \textit{fixed} \qquad \varphi_z = \textit{fixed}$$

K.2.2 Reduced Submerged Cable Weight

In the previous preliminary model, the steel anchoring cables were modeled as if the anchoring system is located over ground. In reality, the anchoring system is submerged under water, causing the cables to have a reduced submerged weight.

In chapter 2.5.6, it was stated that the mean seawater density at the Sognefjord is 1.015 kg/m^3 . To account for salinity, a general 1,0% variation in the seawater density is applied. The specific weight is then $9.858 - 10.055 \text{ N/m}^3$ [3]. The submerged weight of the steel cables can then be calculated.

$$\text{Unit mass/density steel} : 7850 \text{ kg/m}^3 = 7850 \text{ kg/m}^3 \cdot 9,81 \text{ m/s}^2 = 77\,009 \text{ N/m}^3$$

$$\text{Submerged unit mass steel} : 77009 - 9858 = 67\,151 \text{ N/m}^3$$

$$\text{Submerged self-weight cable} : 67151 \cdot \pi \cdot 0,25^2 = \mathbf{13,18 \text{ kN/m}}$$

This new submerged self-weight of the cable should be inputted in Scia Engineer at the cable/beam nonlinearity properties (uncheck self-weight and input 13,18 kN/m at Pn).

K.2.3 Adjustment Pretensioning Lateral Anchoring Cables

In section J.3.4, it could be seen that the pontoons move maximum 66 meters from the S-shape due to self-weight when the same prestressing (1000 kN) is inputted for all lateral anchoring cables. The results from the previous model also showed, that a large part of the capacity of the lateral anchoring cables is not used (section J.3.3). Therefore, the prestressing of the lateral anchoring cables will be increased in such a way, so the S-shape will be more retained.

The displacements of the pontoon nodes of the previous model (also shown in section J.3.4) and the adjusted input data for the pretensioning are given in Table K-1. The member and node numbering is shown in Figure K-1. Note that the input data for the pretensioning is not the real internal force in the cables. These are just input data which will influence the deformed slack shape of the cables and the consequent internal force in the cable. More information about modeling cables in Scia Engineer can be found in ANNEX F: Introduction Modeling Cables in SCIA Engineer.

TABLE K-1 DISPLACEMENTS OF PREVIOUS MODEL AND NEW PRESTRESS INPUT DATA

Pontoon Number	Node Number	Original Prestress (kN)	u_x (m)	New Prestress (kN)	New Prestress in Member Number
1	N49	1000	-5,94	1000	B48
2	N50	1000	22,63	2730	B52
3	N51	1000	48,53	7397	B54
4	N52	1000	61,34	11940	B56
5	N53	1000	63,19	16410	B58
6	N54	1000	53,55	18742	B60
7	N55	1000	40,64	18327	B62
8	N56	1000	29,13	15415	B64
9	N57	1000	15,23	8150	B66
10	N58	1000	2,78	1297	B68
11	N59	1000	-1,87	1000	B71
12	N60	1000	0,96	1000	B72
13	N61	1000	-5,32	2635	B75
14	N62	1000	-20,92	11764	B77
15	N63	1000	-33,79	18341	B79
16	N64	1000	-44,12	20000	B81
17	N65	1000	-56,16	19450	B83
18	N66	1000	-65,66	16706	B85
19	N67	1000	-63,19	11996	B87
20	N68	1000	-48,05	7003	B89
21	N69	1000	-22,62	2653	B91
22	N70	1000	12,55	1193	B92

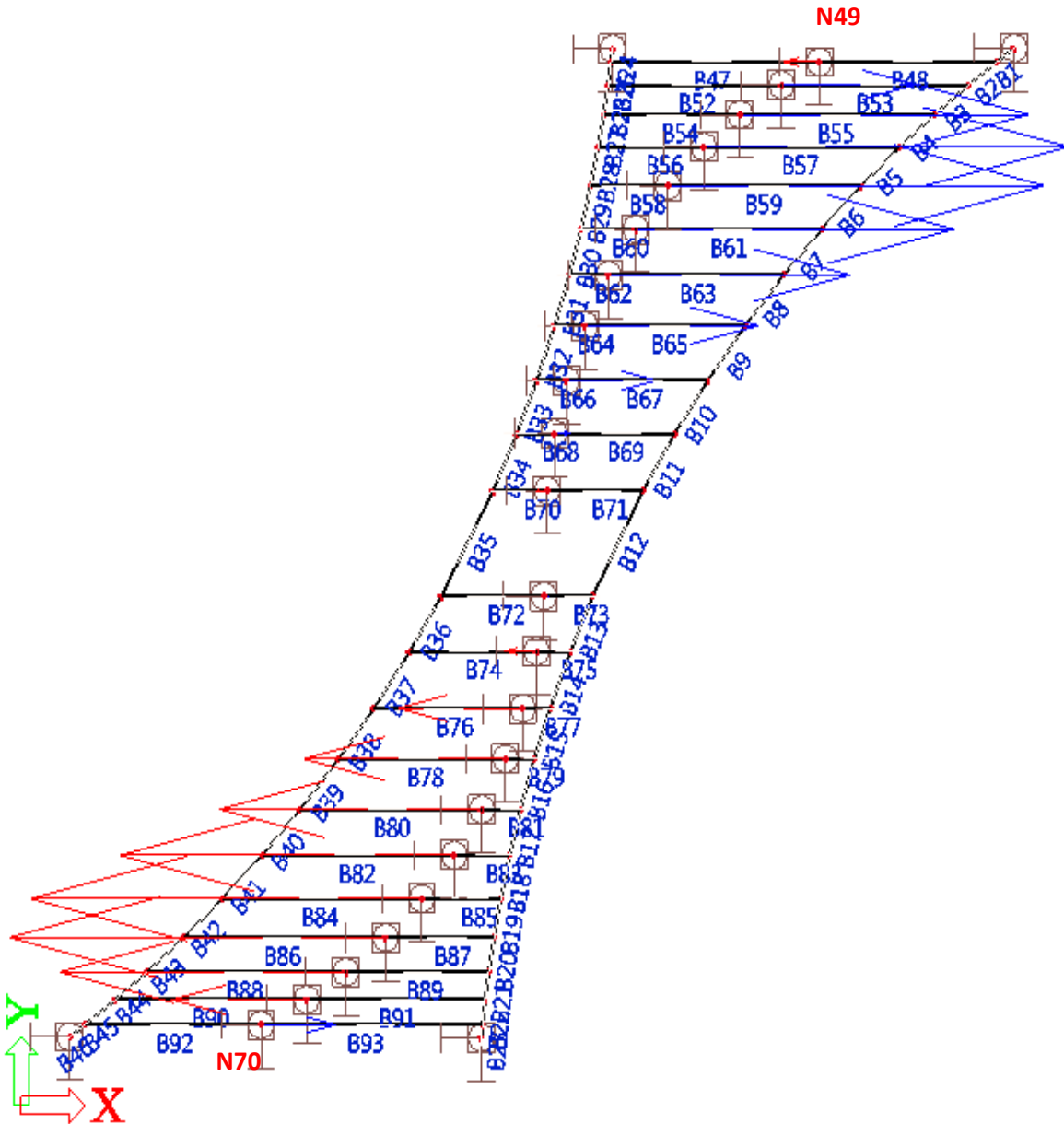


FIGURE K-1 DISPLACEMENTS OF PREVIOUS MODEL (ARROWS) WITH MEMBER AND NODE NUMBERING

K.3 Results and Evaluation

K.3.1 Deformed Structure

The deformed structure is shown from different angles in Figure K-2, Figure K-3, Figure K-4 and Figure K-5.

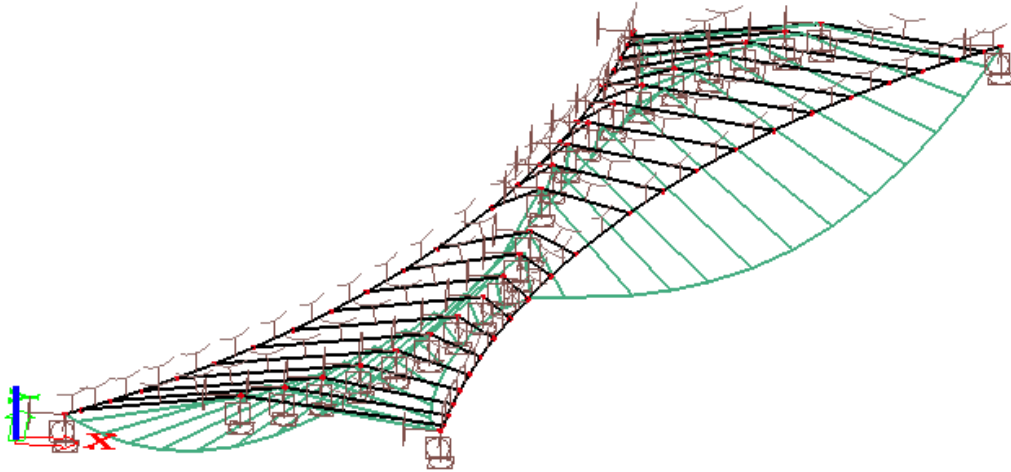


FIGURE K-2 DEFORMED STRUCTURE IN 3D VIEW

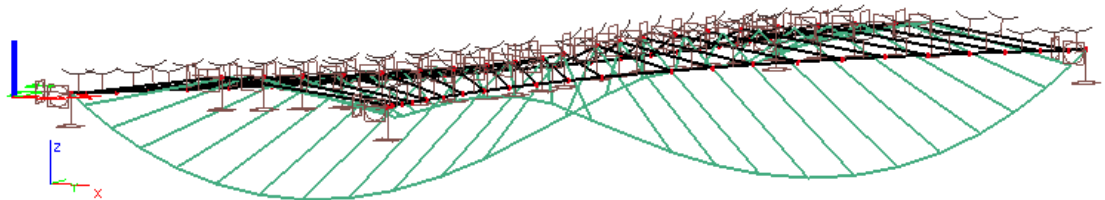


FIGURE K-3 DEFORMED STRUCTURE IN 3D VIEW (2)

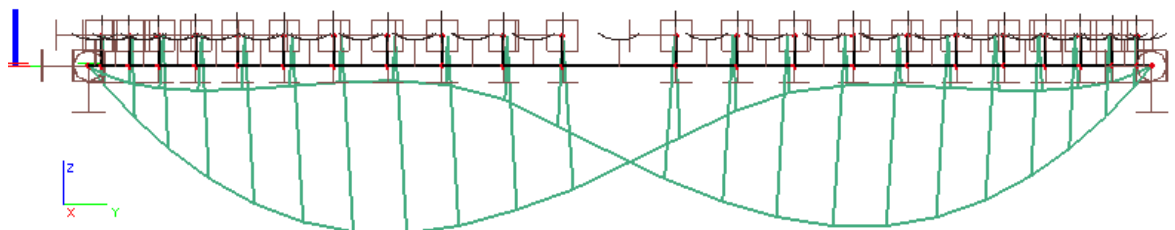


FIGURE K-4 DEFORMED STRUCTURE IN Y-Z PLANE

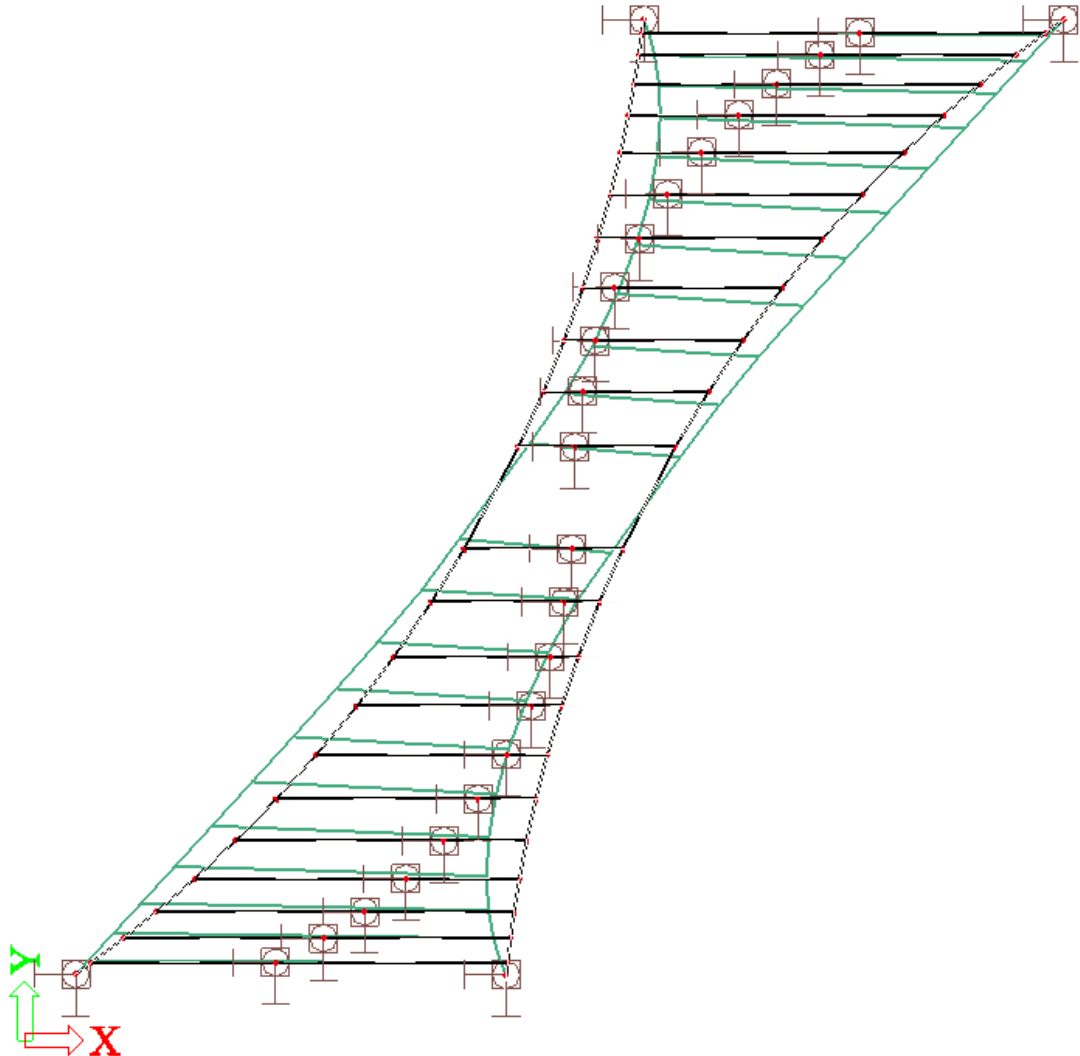


FIGURE K-5 DEFORMED STRUCTURE TOP VIEW/ X-Y PLANE

K.3.2 Total Vertical Resultant Force Reduced

The total vertical reaction force of the previous model was $515,2 \cdot 10^3$ kN (see section J.3.2). For this refined model the total vertical reaction force is reduced to $507,0 \cdot 10^3$ kN. This is due to the use of the reduced submerged weight for the anchoring cables. Since in reality the cables are submerged, this value is more realistic.

K.3.3 Displacement of Nodes

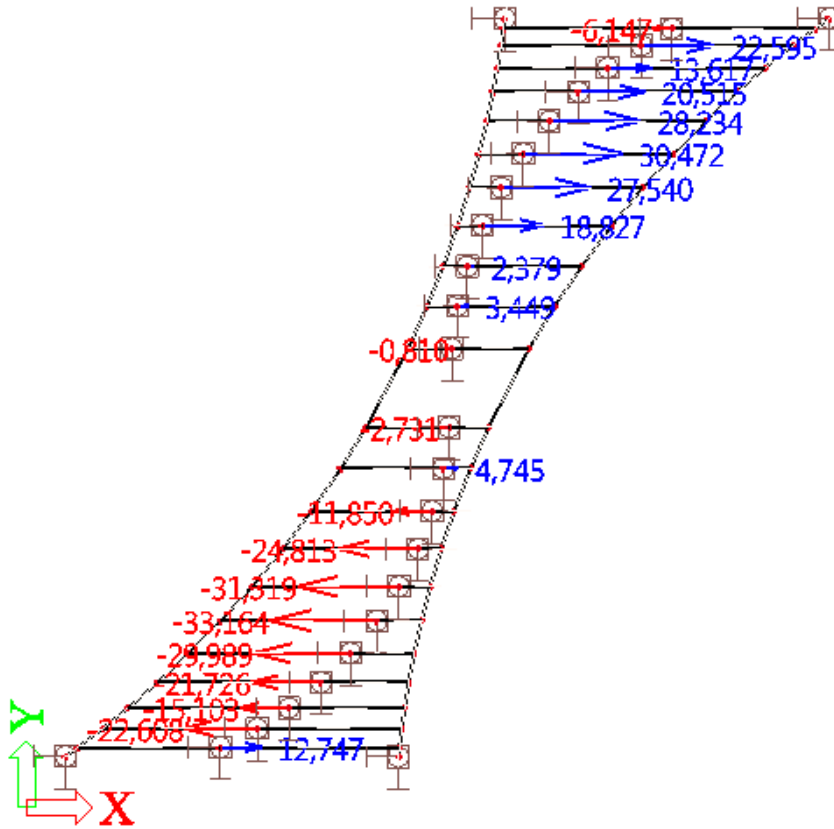


FIGURE K-6 DISPLACEMENT OF PONTOONS IN X-DIRECTION IN [M]

The displacement of the nodes in x-direction at the location of the pontoons is shown in Figure K-6. In Table K-2, the displacements of the previous model and this model can be compared. It can be seen that the maximum displacement in x-direction is reduced by $65,7 - 35,5 = 30,2$ meters. This is more favorable, since the S-shape of the pontoon locations is then retained more.

In Figure K-7, the displacements of the pontoons in y-direction are shown graphically and the values are given in Table K-2. The displacements in y-direction are smaller, the maximum displacement in this direction is 10 meters. In Figure K-7, it can be seen that the upper part of the bridge superstructure will want to move downwards in negative y-direction and the lower part of the bridge superstructure will want to move upwards in positive y-direction. This indicates that the bridge girder at the center of the fjord will be loaded under compression.

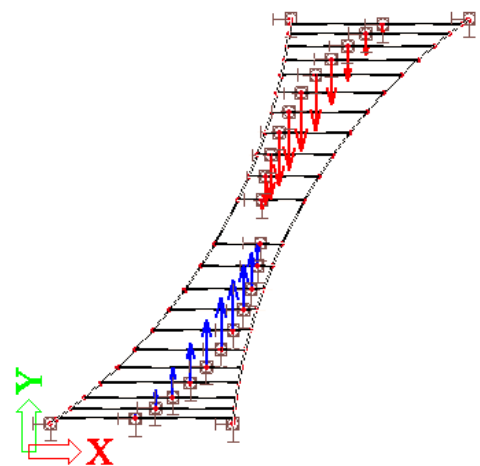


FIGURE K-7 DISPLACEMENT IN Y-DIRECTION

TABLE K-2 DISPLACEMENTS MODEL 1 AND MODEL 2

Pontoon Number	Prestress input model 1 (kN)	$U_{x, \text{model 1}}$ (m)	Prestress input model 2 (kN)	$U_{x, \text{model 2}}$ (m)	$U_{y, \text{model 2}}$ (m)
1	1000	-5,9	1000	-6,1	-1,2
2	1000	22,6	2730	22,6	-3,5
3	1000	48,5	7397	13,6	-5,6
4	1000	61,3	11940	20,5	-7,4
5	1000	63,2	16410	28,2	-8,8
6	1000	53,5	18742	30,5	-9,5
7	1000	40,6	18327	27,5	-9,3
8	1000	29,1	15415	18,8	-8,5
9	1000	15,2	8150	2,4	-7,0
10	1000	2,8	1297	3,5	-4,5
11	1000	-1,9	1000	-0,8	-1,3
12	1000	1,0	1000	-2,7	-0,1
13	1000	-5,3	2635	4,8	3,4
14	1000	-20,9	11764	-11,9	5,9
15	1000	-33,8	18341	-24,8	7,3
16	1000	-44,1	20000	-31,3	8,1
17	1000	-56,2	19450	-33,2	8,2
18	1000	-65,7	16706	-30,0	7,7
19	1000	-63,2	11996	-21,7	6,4
20	1000	-48,1	7003	-15,1	4,6
21	1000	-22,6	2653	-22,6	2,9
22	1000	12,6	1193	12,7	0,8

K.3.4 Forces and Stresses

The graphs of the internal forces and stresses are shown in Figure K-8. In section J.3.3, it was calculated that the stress limit in serviceability limit state of the steel anchoring cables is 837 N/mm^2 .

As can be seen in Figure K-8, the maximum normal force in the cables is $194,0 \cdot 10^3 \text{ kN}$ and the maximum stress is 988 N/mm^2 . The maximum stress in the main cable exceeds the stress limit in serviceability limit state. Therefore, larger size cables are required for the main cables. On the contrary, only a very small part of the capacity of the lateral anchoring cables is used. This indicates that cables of smaller size might be sufficient for the lateral anchoring cables.

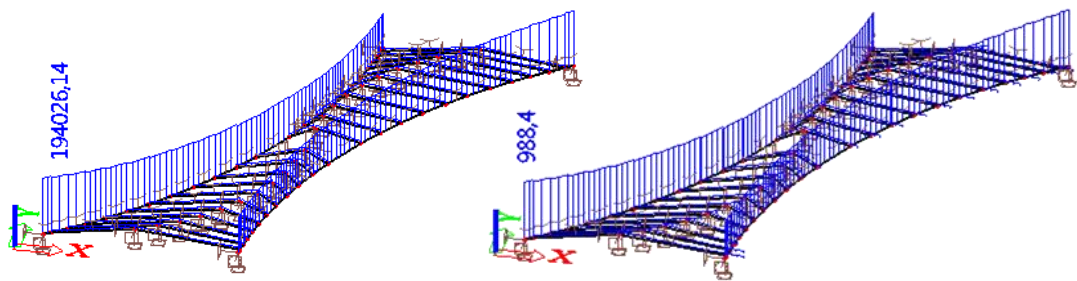


FIGURE K-8 INTERNAL FORCES IN [KN] (LEFT) AND STRESSES IN [N/MM2] (RIGHT)


K.4 Conclusions

The application of variable prestressing force in the lateral anchoring cables leads to smaller displacements of the nodes at the location of the pontoons. Therefore, the S-shape is retained more in this model than in the previous model (ANNEX J: Computational Model Substructure Example 1 (Fixed Supports)). This prestressing proportion will be kept.

In this model, the displacements in y-direction of the nodes at the location of the pontoons are set free. As result, these nodes displace also in y-direction now, although the displacements in y-direction are smaller than the displacements in x-direction. The maximum displacements in x- and y- direction are respectively 33 meters and 10 meters. In Figure K-7, it could be seen that the upper half of the pontoons want to displace downwards in negative y-direction and the lower half of the pontoons want to displace upwards in positive y-direction. This indicates that the bridge girder at the center of the fjord will be loaded under compression.

Now the displacements of the anchoring system due to self-weight are considered, the next step is to apply external loads on the system and to investigate its behavior. For this, the external loads will first have to be investigated.

ANNEX L: Verification Restoring Moment Calculation

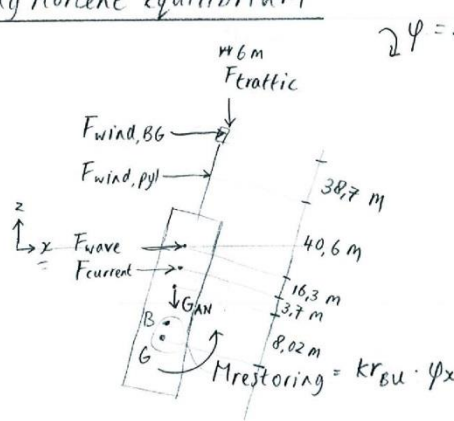
Project	: Buoyancy Bridge Sognefjord											
Part	: Verification Restoring Moment calculation											
<p><u>Introduction</u></p> <p>The pontoon properties determine the rotational stiffness of the pontoon. Therefore, when the required rotational stiffness is known, the required pontoon properties can also be</p> <div style="display: flex; justify-content: space-around; align-items: center; margin: 20px 0;"> <table border="1" style="border-collapse: collapse; width: 30%;"> <tr><td style="text-align: center;">Resistance</td></tr> <tr><td style="padding: 5px;">Rotational spring stiffness determined by pontoon properties.</td></tr> <tr><td style="padding: 5px;">Calculated either by:</td></tr> <tr><td style="padding: 5px;">• analytical calculations or</td></tr> <tr><td style="padding: 5px;">• autoCAD or</td></tr> <tr><td style="padding: 5px;">• expressions</td></tr> </table> <div style="font-size: 2em; margin: 0 10px;">≥</div> <table border="1" style="border-collapse: collapse; width: 30%;"> <tr><td style="text-align: center;">Effect of the action</td></tr> <tr><td style="padding: 5px;">Required rotational spring stiffness determined by external loads.</td></tr> <tr><td style="padding: 5px;">Calculated by</td></tr> <tr><td style="padding: 5px;">• Bending moment equilibrium</td></tr> </table> </div> <p>Fig. 2 Overview rotational spring stiffness calculations</p> <p>calculated. To determine the required rotational stiffness, the pontoon is loaded by the maximum loads and bending moment equilibrium can be used. This is done in the Maple calculation file in Annex and also done in page 2 for pontoon 11 (values for the final design may differ). To check the validity of the calculation codes in maple, both outcomes will be compared.</p> <p>With the required rotational stiffness known, the pontoon properties can be calculated by using different methods, see Fig. 1 for an overview. These methods are validated in 'Verification rotational stiffness of pontoons'.</p>			Resistance	Rotational spring stiffness determined by pontoon properties.	Calculated either by:	• analytical calculations or	• autoCAD or	• expressions	Effect of the action	Required rotational spring stiffness determined by external loads.	Calculated by	• Bending moment equilibrium
Resistance												
Rotational spring stiffness determined by pontoon properties.												
Calculated either by:												
• analytical calculations or												
• autoCAD or												
• expressions												
Effect of the action												
Required rotational spring stiffness determined by external loads.												
Calculated by												
• Bending moment equilibrium												
Name:	Christine Yip	Date: 4-5-2015										
Page:	1/3	Rev:										

Project : Buoyancy Bridge Sognefjord

Part : Verification Restoring Moment Calculation



Bending moment equilibrium



$\varphi = 2,5^\circ$

$F_{wind,BG} = 5801,64 \text{ kN}$
 $F_{wind,pyl} = 1000,26 \text{ kN}$
 $F_{wave} = 66,33 \text{ kN}$
 $F_{current} = 2375,12 \text{ kN}$
 $F_{traffic} = 6125 \text{ kN}$
 $G_{AN} = 41618 \text{ kN}$

Pontoon shape : cylinder

$\sum M_{around G} \rightarrow -F_{wind,BG} \cdot a_{w,BG} - F_{wind,pyl} \cdot a_{w,pyl} - F_{wave} \cdot a_{wave} - F_{current} \cdot a_{cur} - G_{AN} \cdot a_{AN} - F_{traffic} \cdot a_{traffic} + \underbrace{k_{rBU} \cdot \varphi}_{M_{restoring}} = 0$ (equilibrium)

$$\rightarrow k_{rBU} = \frac{(F_{wind,BG} \cdot a_{w,BG} + F_{wind,pyl} \cdot a_{w,pyl}) + F_{wave} \cdot a_{wave} + F_{current} \cdot a_{cur} + G_{AN} \cdot a_{AN} + F_{traffic} \cdot a_{traffic}}{\varphi}$$

$$= \left\{ 5801,64 \cdot (8,02 + 3,7 + 16,3 + 40,6 + 38,7) + 1000,26 \cdot (8,02 + 3,7 + 16,3 + 40,6) + 66,33 \cdot (8,02 + 3,7 + 16,3) + 2375,12 \cdot (8,02 + 3,7) + 6125 \cdot ((8,02 + 3,7 + 16,3 + 40,6 + 38,7) \tan\left(\frac{2,5\pi}{180}\right) + 6) + 41618 \cdot 8,02 \tan\left(\frac{2,5}{360} \cdot 2\pi\right) \right\} // \left(\frac{2,5\pi}{180}\right)$$

$$= \left\{ 5801,64 \cdot 107,2 + 1000,26 \cdot 68,4 + 66,33 \cdot 28,03 + 2375,12 \cdot 11,68 + 6125 \cdot 10,674 + 41618 \cdot 0,35 \right\} // \left(\frac{2,5}{180} \cdot \pi\right)$$

$$= 18332 \text{ MNm/rad}$$

k_{rBU} from Maple : 18326 MNm/rad } approximately equal ✓

Name: Christine Yip

Date: 4-5-2015 Page: 2/3

Rev:

Project : Buoyancy Bridge Sognefjord

Part : Verification Restoring Moment Calculation



Conclusion

The hand calculated bending moment equilibrium coincides with the results of the bending moment equilibrium in the Maple calculation file. It can be concluded that this calculation was done correctly in Maple.

Name: Christine Yrp

Date: 4-5-2015

Page:

3/3

Rev:

ANNEX M: PONTOON PROPERTIES AND LOADS CALCULATION FILE

Pontoon Properties and Loads Calculation File

Table of Contents

- 1 Introduction
- 2 Input Pontoon and Bridge Deck Position
 - 2.1 S-Curve Characteristics
 - 2.2 Pontoon positions
 - 2.3 Elevation Bridge Deck
 - 2.4 Plot S-Curve
 - 2.5 Pontoon Coordinates
- 3 Input Parameters
 - 3.1 Parameters Superstructure
 - 3.2 Parameters pontoons
 - 3.3 Parameters Vertical Loads
 - 3.4 Other Input Parameters
- 4 Determination External Loads
 - 4.1 Definition Angles
 - 4.2 Input for Determination Wind Load

4.3	Input for Determination Wave Load
4.4	Input for Determination Current Load
4.5	Calculation Projected Girder Length at Different Angles
4.6	Calculation Concentrated Wind Load
4.7	Calculation Concentrated Wave and Current Load
4.8	Calculation Total Horizontal Loads
5	Required Buoyancy Determines Pontoon Lengths
5.1	Determination Required Buoyancy Force
5.2	Determination Pontoon Dimensions (Length, Draught, Freeboard and Center of Gravity)
6	Calculation Rotational Stiffness and Ballast Height of pontoons
6.1	Provided Rotational Stiffness by pontoons
6.2	Required Rotational Stiffness due to loads
6.3	Stability Check
7	Overview Results
7.1	Pontoon Properties
7.2	Vertical Loads
7.3	Horizontal Loads

1 Introduction

In this file, the calculations done with Maple are shown. The pontoon properties and external loads are obtained as shown in the following. The explanations and descriptions of the calculation are stated in black. The inputted variables and equations for the calculations are shown in green. Results from the calculation codes are shown in blue. In orange, the expressions for the properties of pontoon 11 are shown.

If not otherwise stated, all lengths are expressed in meters (m) and all forces are expressed in kilonewtons (kN) and kilonewtons per meter (kN/m).

```
restart; unprotect( $\gamma$ ); with(plots) : with(plottools) : color1 := "DarkRed" : color2 := "DarkMagenta" : color6
:= "SkyBlue" : color7 := "DarkSlateGrey" : color8 := "DarkKhaki" : color9 := "DarkCyan" : color10
:= "DarkGoldenrod" : color11 := "SandyBrown" : color12 := "YellowGreen" : colorVec := [color1, color2, color3,
color4, color5, color6, color7, color8] : interface( rtablesize = 30 ) :
```

2 Input Pontoon and Bridge Deck Position

In this section, the properties of the target S-shape of the bridge from the top view is inputted. In this calculation file, it is assumed that this is the final shape of the bridge. However, in reality, due to the self-weight of the anchoring system, the S-shape will deform a bit; the curves will be fainter. Since this effect is considered to be small, it will be assumed that the bridge stays in this perfect S-shape for the calculations of the loads and pontoon properties. These calculations are similar to the ones by Hermans (2014), p.39.

The span at the middle of the fjord is decided by the required clearance. The required clearance is 70 x 400 x 20 meters (height x width x draught). To accommodate this clearance, the radius of the pylons and pontoons should be taken into account. Moreover, the displacements due to the self-weight and external loads should also be taken into account; the clearance should be sufficient in every load configuration.

2.1 S-Curve Characteristics

Length side span $l_{g,n}$:= 200 :

Length main span (= span at the middle of the fjord) $l_{g, mid} := 465$:

Half of the shore-to-shore-distance $x_{hs} := 1753.7$:

Half of the length along the bridge girder $s_{hs} := 2280.05$:

Longitudinal distance of one curve in the direction along the fjord $Y_{hs} := 1228$:

Lateral distance of curve ashore $Y_1 := \sin(\alpha_a) \cdot R_{ha}$:

Lateral distance of curve offshore $Y_2 := R_{ho} - Y_1$:

Horizontal angle ashore $\alpha_a := \left(\frac{\pi}{9} \right)$:

Radius of curves $R_{ha} := 1866.25$:

Comment: This radius is inputted in Scia Engineer. However, due to the self-weight of the anchoring cables, the pontoon move in such a way that the radius of curves becomes larger. This is however not incorporated in the calculations yet. In further design phases, more accurate positions of the pontoons should be used in the calculations.

2.2 Pontoon Positions

Number of side spans in a half bridge $n_{nspans, hs} := \text{floor} \left(\frac{(s_{hs} - 0.5 \cdot l_{g, mid})}{l_{g, n}} \right)$;
10

Resulting remaining bridge deck length near shore $l_{gl} := s_{hs} - 0.5 \cdot l_{g, mid} - n_{nspans, hs} \cdot l_{g, n}$;
47.55

Number of pontoons in a half bridge $n_{spans, hs} := n_{nspans, hs} + 1$:

Number of spans in the whole bridge $n_{spans} := 2 \cdot n_{spans, hs} + 1$:

(2)

$$\beta_1 := \frac{l_{gl}}{R_{ha}} : \beta_n := \frac{l_{g,mid}}{R_{ha}} :$$

$n_{spans,hs}$

11

```

for  $j$  from 1 to  $n_{spans,hs}$  do  $\beta_{p,j} := (\alpha_o + \beta_1 + (j-1) \cdot \beta_n) : dx_{p,j} := evalf(x_{hs} - \cos(\alpha_o + \beta_1 + (j-1) \cdot \beta_n) \cdot R_n) : b_{p,j}$ 
:=  $dx_{p,j} \cdot \alpha_{p,j} := 2 \cdot x_{hs} - b_{p,j} : \mathbf{enddo}$ 
for  $j$  from  $n_{spans,hs} + 1$  to  $2 \cdot n_{spans,hs}$  do  $\beta_{p,j} := \beta_{p,(n_{spans,hs} - (j-1 - n_{spans,hs}))} : dx_{p,j} := \sin(\beta_m + (j - (n_{spans,hs} + 1))$ 
 $\cdot \beta_n) \cdot R_{ha} + x_{hs} : b_{p,j} := dx_{p,j} : \alpha_{p,j} := 2 \cdot x_{hs} - b_{p,j} : \mathbf{enddo}$ 
for  $j$  from 1 to  $n_{spans,hs}$  do  $d_{p,j} := evalf(\sin(\alpha_o + \beta_1 + (j-1) \cdot \beta_n) \cdot R_{ha} - y_1) : c_{p,j} := evalf(2 \cdot y_2 - d_{p,j}) : \mathbf{enddo}$ 
for  $j$  from  $n_{spans,hs} + 1$  to  $2 \cdot n_{spans,hs}$  do  $d_{p,j} := evalf(y_2 + (y_2 - d_{p,(n_{spans,hs} - (j - (n_{spans,hs} + 1)))))) : c_{p,j} := evalf(2 \cdot y_2$ 
 $- d_{p,j}) : \mathbf{enddo}$ 

```

2.3 Elevation Bridge Deck

The freeboard height of the pontoons must always be positive in any situation, so the pontoons do not sink to the bottom of the fjord. To create some margin, the freeboard of the pontoon when the structure is loaded by the maximum vertical loads should be $fr_{p,mn} := 3$:

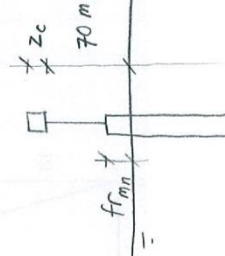
Estimation required pylon height $z_b := 70 + z_c - fr_{p,mn}$:

Estimation half of the bridge girder height $z_c := \frac{15}{2}$:

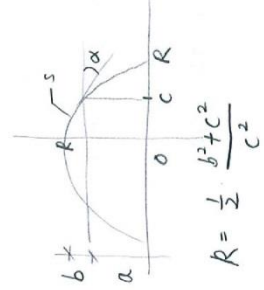
Radius of the vertical arc (elevation of bridge deck) $R_{va} := \frac{0.5 \cdot ((z_b)^2 + s_{hs}^2)}{(z_b)} : R_{va}$

34927.37082

Plot of the elevation of the bridge deck $fz := sa \rightarrow \text{sqrt}(R_{va}^2 - (sa - s_{hs})^2) - (R_{va} - z_b) : \text{plot}(fz, 0..2 \cdot s_{hs})$



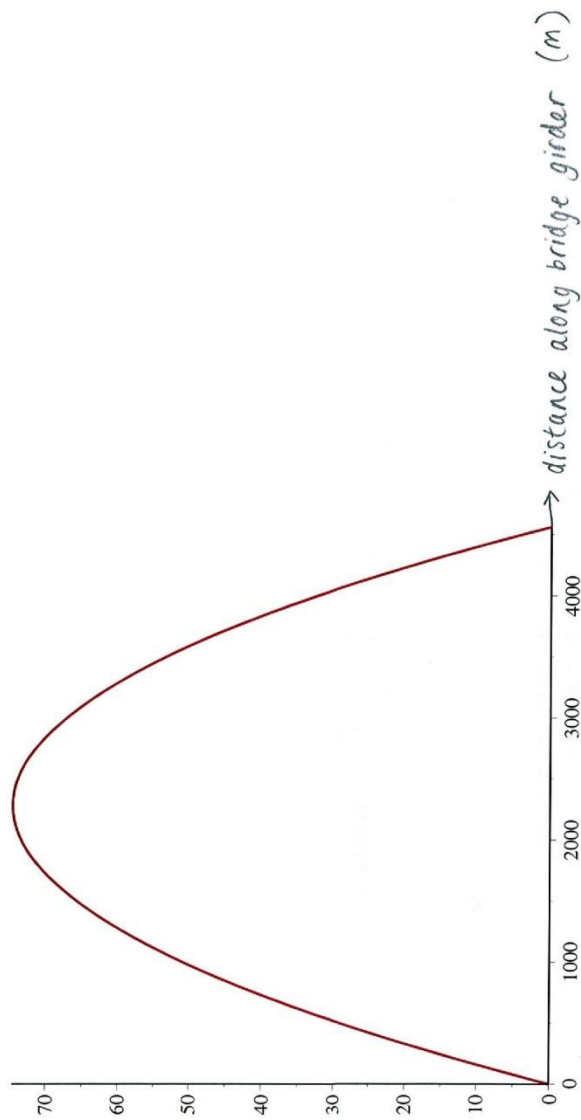
(4)



(5)

$$R = \frac{1}{2} \cdot \frac{\beta^2 + C^2}{C^2}$$

$$S = R^2 \cdot (2 \cdot \alpha)$$



Height of the bridge deck at the first pontoon near the shore $eval(fz(sa), sa = 30.05)$
 1.95283

(6)

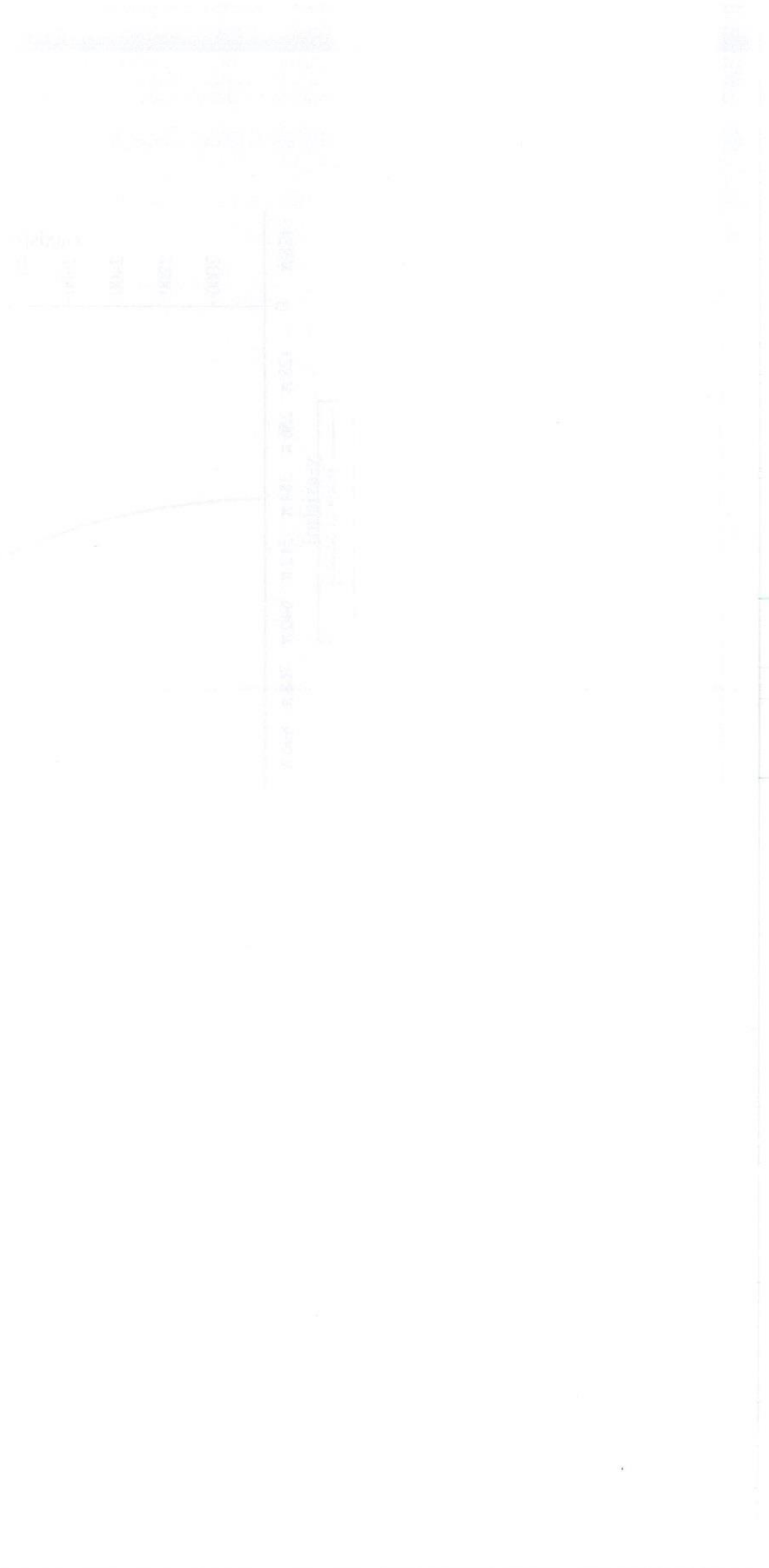
2.4 Plot S-Curve

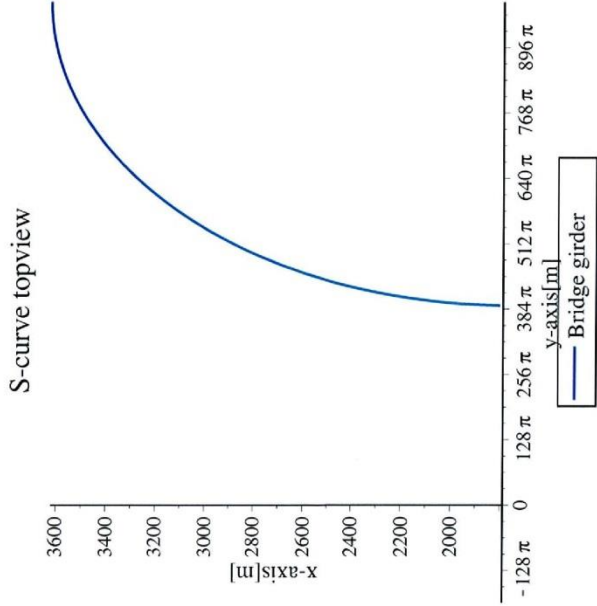
$dy := R_{na} + Y_2$

```

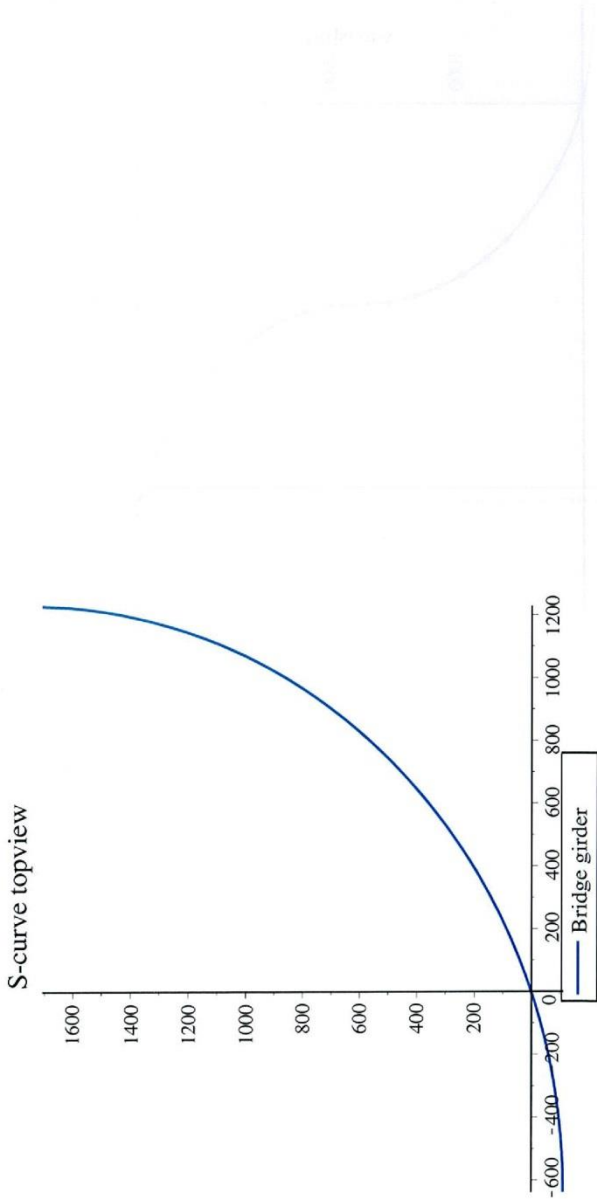
dx := xhs :
ta := sqrt(Rho2 - (ya - dy)2) + dx :
Plot of the top half of the S-curve
with (plots) : Pta := plot(ta, ya = -600 .. Rho + y2, color = blue, title = typeset("S-curve topview"), titlefont = ["calibri",
14], legend = "Bridge girder", labels = ["y-axis[m]", "x-axis[m]"], labelfont = ["calibri", 12], labeldirections
= ["horizontal", "vertical"]) : display([Pta]);

```





Plot of the bottom half of the S-curve $P_{ba} := \text{reflect}(\text{reflect}(P_{ta}, [[0, x_{hs}], [5000, x_{hs}]]) , [[y_2, 0], [y_2, 5000]])$:



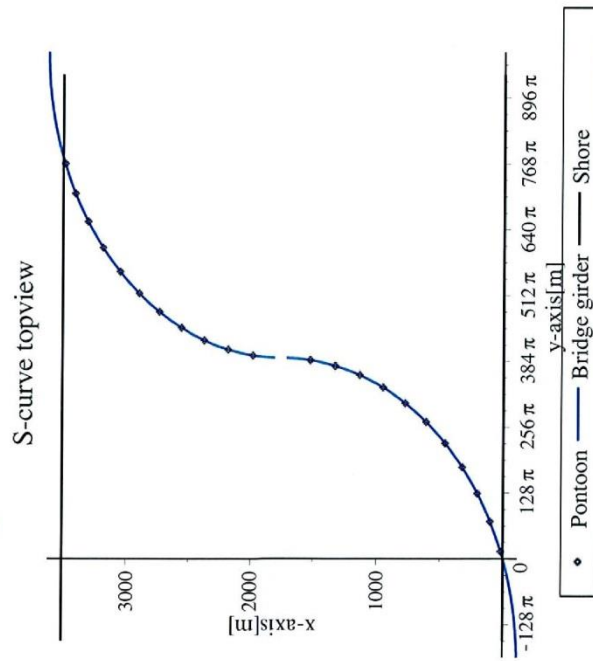
Plot of the S-curve with also the locations of the pontoons

```

PP := pointplot(((d_p,1',d_p,2',d_p,3',d_p,4',d_p,5',d_p,6',d_p,7',d_p,8',d_p,9',d_p,10',d_p,11',d_p,12',d_p,13',d_p,14',d_p,15',d_p,16',d_p,17',d_p,18',d_p,19',
d_p,20',d_p,21',d_p,22))|(b_p,1',b_p,2',b_p,3',b_p,4',b_p,5',b_p,6',b_p,7',b_p,8',b_p,9',b_p,10',b_p,11',b_p,12',b_p,13',b_p,14',b_p,15',b_p,16',b_p,17',b_p,18',
b_p,19',b_p,20',b_p,21',b_p,22)),legend = "Pontoon") :
Psn := pointplot((( -500, 2·y_2 + 500)|(2·x_hs, 2·x_hs)),style = line,color = black,legend = "Shore") :

```

```
Pss := pointplot((( -500, 2·y2 + 500)|(0, 0)), style = line, color = black) :
display([Pta, Pba, PP, Psn, Pss])
```



2.5 Pontoon Coordinates

```
lg,1 := lgl: Sp,1 := lg,1 :
for i from 2 to 11 do
lg,i := lg,n :
```



```

enddo:
   $l_{g,12} := l_{g,mid}$ ;
for  $i$  from 13 to 22 do
   $l_{g,i} := l_{g,n}$ ;
enddo:
   $l_{g,23} := l_{g,i}$ ;
for  $i$  from 2 to 22 do
   $s_{p,i} := s_{p,i-1} + l_{g,i}$ ;
   $z_{bv_{p,i}} := fz(s_{p,i})$ ;
enddo:
   $z_{bv_{p,5}}$ 

45.11159000

for  $i$  from 1 to 22 do
   $x_{p,i} := b_{p,i}$ ;
   $y_{p,i} := d_{p,i}$ ;
   $z_{p,i} := eval(fz(sa), sa = s_{p,i}) + fr_{p,nc,i}$ ;
   $lc_{p,i} := \langle x_{p,i} | y_{p,i} | z_{p,i} \rangle : sa := 'sa'$ ;
enddo:

for  $i$  from 1 to 22 do
   $x_{p,i} := b_{p,i}$ ;
   $y_{p,i} := d_{p,i}$ ;
   $z_{p,i} := eval(fz(sa), sa = s_{p,i}) + fr_{p,nc,i}$ ;
   $lc_{p,i} := \langle x_{p,i} | y_{p,i} | z_{p,i} \rangle : sa := 'sa'$ ;
enddo:

   $x_{g,23} := x_{g,1}$ ;
for  $i$  from 2 to 22 do

```

```

a_mvm,i := evalf ( zbv_p,i - cos ( 2.5 * pi / 180 ) * zbv_p,i ) :
b_mvm,i := evalf ( sin ( 2.5 * pi / 180 ) * zbv_p,i ) :
enddo:

```

Coordinates of the bridge deck on top of the 22 pontoons. The y-direction is along the fjord. The x-direction is across the fjord. The z-direction indicates the elevation.

```

( ("#P", 1, 2, 3, 4, 5, 6, 7, 8, 9, 10, 11, 12, 13, 14, 15, 16, 17, 18, 19, 20, 21, 22) | ("v_p", d_p,1', d_p,2', d_p,3', d_p,4', d_p,5', d_p,6', d_p,7', d_p,8',
d_p,9', d_p,10', d_p,11', d_p,12', d_p,13', d_p,14', d_p,15', d_p,16', d_p,17', d_p,18', d_p,19', d_p,20', d_p,21', d_p,22) | ("x_p", b_p,1', b_p,2', b_p,3', b_p,4', b_p,5',
b_p,6', b_p,7', b_p,8', b_p,9', b_p,10', b_p,11', b_p,12', b_p,13', b_p,14', b_p,15', b_p,16', b_p,17', b_p,18', b_p,19', b_p,20', b_p,21', b_p,22) | ("z", 4.19456, zbv_p,2',
zbv_p,3', zbv_p,4', zbv_p,5', zbv_p,6', zbv_p,7', zbv_p,8', zbv_p,9', zbv_p,10', zbv_p,11', zbv_p,12', zbv_p,13', zbv_p,14', zbv_p,15', zbv_p,16', zbv_p,17',
zbv_p,18', zbv_p,19', zbv_p,20', zbv_p,21', zbv_p,22) )

```

"#p"	"y_p"	"x_p"	"z"
1	44.4703786	16.829143	4.19456
2	226.3322191	99.823138	15.31204000
3	398.2735586	201.793271	26.39488000
4	558.3215876	321.569564	36.32774000
5	704.6399596	457.777737	45.11159000
6	835.5498556	608.854974	52.74730000
7	949.5492516	773.0678540	59.23562000
8	1045.330148	948.5322438	64.57720000
9	1121.793581	1133.234912	68.77255000
10	1178.062231	1325.056630	71.82211000
11	1213.490485	1521.796487	73.72615000
12	1242.419330	1985.599046	73.72615000
13	1277.847584	2182.338988	71.82211000
14	1334.116234	2374.160842	68.77255000
15	1410.579667	2558.863694	64.57720000
16	1506.360563	2734.328315	59.23562000
17	1620.359959	2898.541470	52.74730000
18	1751.269855	3049.619023	45.11159000
19	1897.588227	3185.827549	36.32774000
20	2057.636256	3305.604228	26.39488000
21	2229.577596	3407.574776	15.31204000
22	2411.439436	3490.569210	3.07811000

(8)

3 Input Parameters

3.1 Parameters Superstructure

Width bridge box girder $b_g := 10$:

Width bridge deck $b_{deck} := 16$:

Radius pylons $R_{pylon} := 2.5$:

Thickness pylon shell $t_{pylon} := \frac{R_{pylon}}{15}$:

More properties superstructure (these are assumed to be the same as the superstructure of Hermans (2014))

$h_{ws} := 2.4$:

$t_{girder} := 0.022514$; $\alpha_g := 90$; $d_{tn} := 0.4531$:

$a_{truss} := 15$; $h_{truss} := 3.5$; $d_{truss} := 1$; $l_{trussdia} := \text{sqrt}(h_{truss}^2 + a_{truss}^2)$; $d_{trussdia} := 0.5$:

3.2 Parameters pontoons

All pontoons are cylindrical shaped.

Distance between water surface and anchoring connection point on pontoon $z_o := 20$:

Thickness pontoon at the top $t_{p,top} := 1$:

Thickness pontoon at bottom $t_{p,bot} := 1 + \frac{l_p}{50}$:

The pontoon have different sizes:

Radius pontoon no. 1 = 15 m

Radius pontoon no. 2 to 6 = 18 m

Radius pontoon no. 7 to 10 = 21 m

Radius pontoon no. 11 = 26 m

The buoyancy bridge is rotationally symmetric. Therefore, the properties of pontoons no. 12 to 22 are the same to respectively pontoons no. 11 to 1. Below, the pontoons radiuses, pontoon thicknesses at the sides and the area moment of inertia of the plane intersected by the water off all pontoons are specified.

for i from 1 to 1 do

$R_{\text{pontoon},i} := 15 :$

$t_{p,side,i} := 0.5 + \frac{R_{\text{pontoon},i}}{15} :$

$INER_i := \frac{\pi}{4} \cdot (R_{\text{pontoon},i}^4 - (R_{\text{pontoon},i} - t_{p,side,i})^4) :$

enddo:

for i from 2 to 6 do

$R_{\text{pontoon},i} := 18 :$

$t_{p,side,i} := 0.5 + \frac{R_{\text{pontoon},i}}{15} :$

$INER_i := \frac{\pi}{4} \cdot (R_{\text{pontoon},i}^4 - (R_{\text{pontoon},i} - t_{p,side,i})^4) :$

enddo:

for i from 7 to 10 do

$R_{\text{pontoon},i} := 21 :$

$$t_{p,side,i} := 0.5 + \frac{R_{pontoon,i}}{15} :$$

$$INER_i := \frac{\pi}{4} \cdot (R_{pontoon,i}^4 - (R_{pontoon,i} - t_{p,side,i})^4) :$$

enddo:

for i from 11 to 12 do

$$R_{pontoon,i} := 26 :$$

$$t_{p,side,i} := 0.5 + \frac{R_{pontoon,i}}{15} :$$

$$INER_i := \frac{\pi}{4} \cdot (R_{pontoon,i}^4 - (R_{pontoon,i} - t_{p,side,i})^4) :$$

enddo:

for i from 13 to 16 do

$$R_{pontoon,i} := 21 :$$

$$t_{p,side,i} := 0.5 + \frac{R_{pontoon,i}}{15} :$$

$$INER_i := \frac{\pi}{4} \cdot (R_{pontoon,i}^4 - (R_{pontoon,i} - t_{p,side,i})^4) :$$

enddo:

for i from 17 to 21 do

$$R_{pontoon,i} := 18 :$$

$$t_{p,side,i} := 0.5 + \frac{R_{pontoon,i}}{15};$$

$$INER_i := \frac{\pi}{4} \cdot (R_{pontoon,i}^4 - (R_{pontoon,i} - t_{p,side,i})^4);$$

enddo;

for i from 22 to 22 do

$$R_{pontoon,i} := 15;$$

$$t_{p,side,i} := 0.5 + \frac{R_{pontoon,i}}{15};$$

$$INER_i := \frac{\pi}{4} \cdot (R_{pontoon,i}^4 - (R_{pontoon,i} - t_{p,side,i})^4);$$

enddo;

Example radius pontoon 11 $R_{pontoon,11}$

26

(9)

Example thickness of the side of pontoon 11 $t_{p,side,11}$

2.2333333333

(10)

(11)

Length of the pontoons are defined

for i from 1 to 22 do

$$l_{p,i} := dr_{p,i,ULS} + fr_{p,mm};$$

enddo;

As can be seen, the pontoon lengths are still unknown, since it depends on the draught (submerged height) of the pontoons in SLS ($dr_{p,i,SLS}$)

Example length pontoon 11 $l_{p,11}$

$$dr_{p,11,ULS} + 3 \quad (12)$$

Definition freeboard of the pontoon in different situations. The freeboard also depends on the draught of the pontoon.

for i from 1 to 22 do

$$fr_{p,i,SLS} := l_{p,i} - dr_{p,i,SLS};$$

$$fr_{p,i,nt,SLS} := l_{p,i} - dr_{p,i,nt,SLS};$$

$$:= dr_{p,i,ULS} + fr_{p,mn};$$

enddo;

Example freeboard of pontoon 11 in SLS with no traffic taken into account: $fr_{p,11,nt,SLS}$

$$dr_{p,11,ULS} + 3 - dr_{p,11,nt,SLS} \quad (13)$$

3.3 Parameters Vertical Loads

Distributed traffic load $q_{traffic}$:= 35 :

$$\text{Concentrated traffic load on pontoon } F_{traffic,hfb,SLS} := \frac{1}{2} \cdot q_{traffic} \cdot l_g \cdot F_{traffic,hfb,ULS} := \frac{1}{2} \cdot q_{traffic} \cdot l_g :$$

Eccentric traffic load leverarm $a_{traffic,hfb}$:= 6 :

$$\text{Self-weight pylons } G_{pylon,SLS} := \frac{fz(sa)}{z_b} \cdot 28410 \cdot G_{pylon,ULS} := l_g \cdot G_{pylon,SLS} \cdot f_{y,pylon} := 460 \cdot 10^3 :$$

Sum of self-weight superstructure (pylons excluded) and traffic load in SLS and ULS for both the side spans and the main span (at the middle of the fjord).

Self-weight of the side span bridge girders (span=200m) according to Hermans (2014) = 114,3959 kN/m.

Self-weight of the main span bridge girder (span=400m) according to Hermans (2014) = 118,5179 kN/m.

Since the strength and stability of the bridge of Hermans (2014) were insufficient, the required superstructure is assumed to be larger and heavier.

Estimation extra self-weight of bridge girder at side span (span=200m) = 150,6041 kN/m.

Estimation extra self-weight of bridge girder at main span (span=450m) = 196,4821 kN/m.

$$\begin{aligned}
 q_{g,SLS} &::= 300 && \text{dead load} \\
 q_{g,ULS} &::= 370.5 && \text{live load} \\
 q_{g,SLS,mid} &::= 350 && \\
 q_{g,ULS,mid} &::= 430.5 && \\
 \end{aligned}$$

} traffic load included

$$\begin{aligned}
 q_{g,SLS} &= 1,0 \cdot q_G + 1,0 \cdot q_Q \\
 q_{g,ULS} &= 1,2 \cdot q_G + 1,5 \cdot q_Q
 \end{aligned}$$

$q_{g,SLS} = q_{traffic} + q_{bridge\ girder\ (200m)}$;

$q_{g,ULS} = 1,5 * q_{traffic} + 1,2 * q_{bridge\ girder\ (200m)}$;

$q_{g,SLS, mid} = q_{traffic} + q_{bridge\ girder\ (450m)}$;

$q_{g,ULS, mid} = 1,5 * q_{traffic} + 1,2 * q_{bridge\ girder\ (450m)}$;

Example contrated traffic load $F_{traffic, hfb, SLS}$

$$\frac{35}{2} l_g \quad (14)$$

Self-weight anchoring system resisted by the pontoons. These values are retrieved from the anchoring system model in

Scia Engineer.

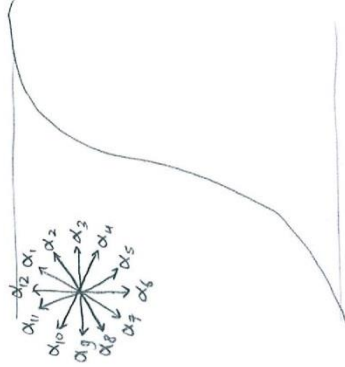
(15

$G_{AN,1} := 6328 : G_{AN,2} := 7335 : G_{AN,3} := 6467 : G_{AN,4} := 8205 : G_{AN,5} := 10029 : G_{AN,6} := 13565 : G_{AN,7} := 17665 :$
 $G_{AN,8} := 34933 : G_{AN,9} := 25363 : G_{AN,10} := 45137 : G_{AN,11} := 41618 : G_{AN,12} := G_{AN,11} : G_{AN,13} := G_{AN,10} :$
 $G_{AN,14} := G_{AN,9} : G_{AN,15} := G_{AN,8} : G_{AN,16} := G_{AN,7} : G_{AN,17} := G_{AN,6} : G_{AN,18} := G_{AN,5} : G_{AN,19} := G_{AN,4} : G_{AN,20}$
 $:= G_{AN,3} : G_{AN,21} := G_{AN,2} : G_{AN,22} := G_{AN,1} :$

3.4 Other Input Parameters

Load safety factor for dead loads $\gamma_g := 1.2 :$
 Load safety factor for live loads $\gamma_q := 1.5 :$
 Modulus of Elasticity of steel $E_s := 210 \cdot 10^6 : E_m := 195 \cdot 10^6 :$
 Shear modulus of steel $G_s := 79.3 \cdot 10^6 :$
 Density steel $\rho_s := 7850 :$
 Density concrete $\rho_c := 2500 :$
 Density ballast $\rho_b := 2000 :$
 Density water $\rho_w := 1004.85 :$
 Density air (from NEN-EN 1991-1-4, p. 24) $\rho_o := 1.25 :$

4 Determination External Loads



4.1 Definition Angles
 External loads like the wind load can act in different directions. 12 directions are considered in this calculation. The 12 directions are defined as shown below.

$$\alpha_1 := \frac{0 \cdot \pi}{180} : \alpha_2 := \frac{30 \cdot \pi}{180} : \alpha_3 := \frac{60 \cdot \pi}{180} : \alpha_4 := \frac{90 \cdot \pi}{180} : \alpha_5 := \frac{120 \cdot \pi}{180} : \alpha_6 := \frac{150 \cdot \pi}{180} : \alpha_7 := \frac{180 \cdot \pi}{180} : \alpha_8 := \frac{210 \cdot \pi}{180} : \alpha_9 := \frac{240 \cdot \pi}{180} : \alpha_{10} := \frac{270 \cdot \pi}{180} : \alpha_{11} := \frac{300 \cdot \pi}{180} : \alpha_{12} := \frac{330 \cdot \pi}{180} :$$

4.2 Input for Determination Wind Load

Input coefficients:

$$C_{d, gw} := \text{piecewise} \left(1 \leq \beta_{BG} < 2, 1.1 - (\beta_{BG} - 1) \cdot (1.1 - 0.6), 2 \leq \beta_{BG} < 4, 0.6 - (\beta_{BG} - 2) \cdot 0.5 \cdot (0.6 - 0.35), \beta_{BG} \geq 4, 0.35 \right) :$$

$$\beta_{BG} := \frac{20}{h_g + h_{ws}} :$$

$$C_{d, pww} := 1.1 : C_{d, tn} := 1.1 : C_{d, traffic} := 1.05 : C_{d, truss} := 1.1 : C_{d, pc} := 1.5 :$$

$$\alpha_1 = 0^\circ$$

$$\alpha_2 = 30^\circ$$

$$\alpha_3 = 60^\circ$$

$$\vdots$$

$$\alpha_{12} = 330^\circ$$

Wind load according to NEN-EN 1991-1-4:

$$q_{p, g, SLS} := ze \rightarrow \left(1 + \frac{7 \cdot k_f}{c_0 \cdot \ln \left(\frac{ze}{z_0} \right)} \right) \cdot \left(\frac{1}{2} \right) \cdot \frac{\left[p_o \cdot \left(\frac{z_0}{z_{0, II}} \cdot \ln \left(\frac{ze}{z_0} \right) \cdot c_0 \cdot v_b, SLS \right) \right]^2}{1000} :$$

$$\begin{aligned}
 q_{p,p,sLS} &:= ze \rightarrow \left(1 + \frac{7 \cdot k_f}{c_0 \cdot \ln\left(\frac{0.5 \cdot ze}{z_0}\right)} \right) \cdot \left(\frac{1}{2} \right) \cdot \frac{\left[\rho_\sigma \cdot 0.19 \cdot \left(\frac{z_0}{z_{0,fl}} \cdot \ln\left(\frac{0.5 \cdot ze}{z_0}\right) \cdot c_0 \cdot v_{b,sLS} \right)^2 \right]}{1000} : \\
 q_{p,g,ULS} &:= ze \rightarrow \left(1 + \frac{7 \cdot k_f}{c_0 \cdot \ln\left(\frac{ze}{z_0}\right)} \right) \cdot \left(\frac{1}{2} \right) \cdot \frac{\left[\rho_\sigma \cdot 0.19 \cdot \left(\frac{z_0}{z_{0,fl}} \cdot \ln\left(\frac{ze}{z_0}\right) \cdot c_0 \cdot v_{b,ULS} \right)^2 \right]}{1000} : \\
 q_{p,p,ULS} &:= ze \rightarrow \left(1 + \frac{7 \cdot k_f}{c_0 \cdot \ln\left(\frac{0.5 \cdot ze}{z_0}\right)} \right) \cdot \left(\frac{1}{2} \right) \cdot \frac{\left[\rho_\sigma \cdot 0.19 \cdot \left(\frac{z_0}{z_{0,fl}} \cdot \ln\left(\frac{0.5 \cdot ze}{z_0}\right) \cdot c_0 \cdot v_{b,ULS} \right)^2 \right]}{1000} : \\
 z_0 &:= 0.05 : z_{0,fl} := 0.05 : c_0 := 1.0 : k_f := 1.0 : \\
 n_{prob} &:= 0.1 : K_{prob} := 0.2 : p_{prob} := 0.99 : c_{prob} := \text{evalf}\left(\left(\frac{(1 - K_{prob} \cdot \ln(-\ln(1 - p_{prob})))^n}{1 - K_{prob} \cdot \ln(-\ln(0.99))}\right)^{\frac{1}{n_{prob}}}\right) \\
 &0.9033175203
 \end{aligned}$$

(16)

Extreme values of wind speed per direction (Hermans, 2014, Figure 4-3):

$$\begin{aligned}
 V_{b,\alpha,1,ULS} &:= 21 : V_{b,\alpha,2,ULS} := 26 : V_{b,\alpha,3,ULS} := 26 : V_{b,\alpha,4,ULS} := 23 : V_{b,\alpha,5,ULS} := 24 : V_{b,\alpha,6,ULS} := 28 : V_{b,\alpha,7,ULS} \\
 &:= 35 : V_{b,\alpha,8,ULS} := 35 : V_{b,\alpha,9,ULS} := 35 : V_{b,\alpha,10,ULS} := 33 : V_{b,\alpha,11,ULS} := 33 : V_{b,\alpha,12,ULS} := 23 :
 \end{aligned}$$

4.3 Input for Determination Wave Load

Extreme values of wind wave height per direction (Hermans, 2014, Figure 4-5):

$$\begin{aligned}
 H_{s,ww,\alpha,1,ULS} &::= 1.01 : H_{s,ww,\alpha,2,ULS} ::= 1.62 : H_{s,ww,\alpha,3,ULS} ::= 1.81 : H_{s,ww,\alpha,4,ULS} ::= 1.49 : H_{s,ww,\alpha,5,ULS} ::= 1.4 : \\
 H_{s,ww,\alpha,6,ULS} &::= 1.57 : H_{s,ww,\alpha,7,ULS} ::= 2.22 : H_{s,ww,\alpha,8,ULS} ::= 2.24 : H_{s,ww,\alpha,9,ULS} ::= 2.34 : H_{s,ww,\alpha,10,ULS} ::= 2.13 : \\
 H_{s,ww,\alpha,11,ULS} &::= 1.83 : H_{s,ww,\alpha,12,ULS} ::= 1.00 :
 \end{aligned}$$

Significant wave height (Hermans, 2014, Figure 4-6):

$$\begin{aligned}
 H_{s,sw,\alpha,1,ULS} &::= 0.01 : H_{s,sw,\alpha,2,ULS} ::= 0.01 : H_{s,sw,\alpha,3,ULS} ::= 0.01 : H_{s,sw,\alpha,4,ULS} ::= 0.01 : H_{s,sw,\alpha,5,ULS} ::= 0.01 : \\
 H_{s,sw,\alpha,6,ULS} &::= 0.01 : H_{s,sw,\alpha,7,ULS} ::= 0.01 : H_{s,sw,\alpha,8,ULS} ::= 0.01 : H_{s,sw,\alpha,9,ULS} ::= 0.01 : H_{s,sw,\alpha,10,ULS} ::= 0.01 : \\
 H_{s,sw,\alpha,11,ULS} &::= 0.01 : H_{s,sw,\alpha,12,ULS} ::= 0.01 :
 \end{aligned}$$

4.4 Input for Determination Current Load

Currents - three scenarios.

- 1 - constant current over full width of the fjord.
- 2 - constant current in the mid half of the fjord
- 3 - constant current asymmetrical about fjord's mid axis

$$\begin{aligned}
 u_{c1,\alpha,1} &::= 1.27 : u_{c1,\alpha,2} ::= 1.27 : u_{c1,\alpha,3} ::= 1.27 : u_{c1,\alpha,4} ::= 1.27 : u_{c1,\alpha,5} ::= 1.27 : u_{c1,\alpha,6} ::= 1.27 : u_{c1,\alpha,7} ::= 1.27 : \\
 u_{c1,\alpha,8} &::= 1.27 : u_{c1,\alpha,9} ::= 1.27 : u_{c1,\alpha,10} ::= 1.27 : u_{c1,\alpha,11} ::= 1.27 : u_{c1,\alpha,12} ::= 1.27 :
 \end{aligned} \tag{17}$$

$$\begin{aligned}
 u_{c2,\alpha,1} &::= 0.875 : u_{c2,\alpha,2} ::= 0.875 : u_{c2,\alpha,3} ::= 0.875 : u_{c2,\alpha,4} ::= 0.875 : u_{c2,\alpha,5} ::= 0.875 : u_{c2,\alpha,6} ::= 0.875 : u_{c2,\alpha,7} \\
 &::= 0.875 : u_{c2,\alpha,8} ::= 0.875 : u_{c2,\alpha,9} ::= 0.875 : u_{c2,\alpha,10} ::= 0.875 : u_{c2,\alpha,11} ::= 0.875 : u_{c2,\alpha,12} ::= 0.875 :
 \end{aligned}$$

```

u_{c3,\alpha_1} := 0.48 : u_{c3,\alpha_2} := 0.48 : u_{c3,\alpha_3} := 0.48 : u_{c3,\alpha_4} := 0.48 : u_{c3,\alpha_5} := 0.48 : u_{c3,\alpha_6} := 0.48 : u_{c3,\alpha_7} := 0.48 :
u_{c3,\alpha_8} := 0.48 : u_{c3,\alpha_9} := 0.48 : u_{c3,\alpha_{10}} := 0.48 : u_{c3,\alpha_{11}} := 0.48 : u_{c3,\alpha_{12}} := 0.48 :

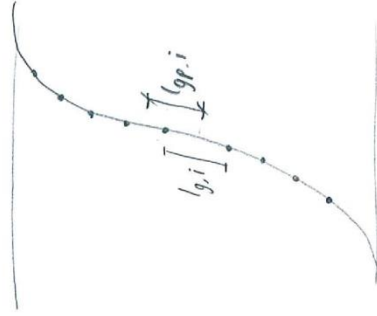
```

(18)

4.5 Calculation Effective and Projected Girder Length at Different Angles

The effective length is $l_{gp,i}$ and the pontoon span is $l_{p,i}$.

$l_{g,i}$ and $l_{gp,i}$:



```

l_{gp,i} := (l_{g,i} + l_{p,i}) / 2 :

```

```

l_g := l_{gp,i} :
s_{p,i} := s_{p,i} :

```

```

\alpha_{b,i} := arctan( (y_{p,i} - y_{p,i(i-1)}) / (x_{p,i} - x_{p,i(i-1)}) ) :

```

```

ss_{b,i} := sqrt( (x_{p,i} - x_{p,i(i-1)})^2 + (y_{p,i} - y_{p,i(i-1)})^2 ) :

```

```

\alpha_{d,i,n} := abs( evalf( ( \alpha_n - \alpha_{b,i} + \frac{\pi}{6} ) ) ) :

```

```

if \alpha_{d,i,n} > evalf( \frac{\pi}{2} ) then \alpha_{d,i,n} := ( \alpha_n - \alpha_{b,i} - \frac{\pi}{2} + \frac{\pi}{6} ) ; l_{g,i,\alpha_n} := abs( evalf( ss_{b,i} * cos( \alpha_{d,i,n} ) ) ) ; else \alpha_{d,i,n} := ( \alpha_n - \alpha_{b,i} + \frac{\pi}{6} ) ; l_{g,i,\alpha_n} := abs( evalf( ss_{b,i} * sin( \alpha_{d,i,n} ) ) ) ; end if :

```

```

end do :

```

```

l_{g,i,\alpha_7} := l_{g,i,\alpha_1} :

```

```

l_{g,i,\alpha_8} := l_{g,i,\alpha_2} :

```

```

l_{g,i,\alpha_9} := l_{g,i,\alpha_3} :
l_{g,i,\alpha_{10}} := l_{g,i,\alpha_4} :
l_{g,i,\alpha_{11}} := l_{g,i,\alpha_5} :
l_{g,i,\alpha_{12}} := l_{g,i,\alpha_6} :
l_g := l_g : sa := 'sa' :
enddo:

```

Example span between pontoon 10 and 11 $evalf_4(l_{g,11})$ 200.

Example span between pontoon 11 and 12 $evalf_4(l_{g,12})$ 465.

Example: effective girder length pontoon 11 $evalf_4(l_{gp,11})$ 332.5

Example: length of girder where the external loads acts on from direction 3, for which pontoon 11 has to resist the loads $l_{g,11,\alpha_3}$

196.7398570

```

for n from 1 to 12 do
l_{g,23,\alpha_n} := l_{g,1,\alpha_n} :
enddo:

```

Repeat definition of the freeboard of the pontoon in different situations. (Length and draught of the pontoons still unknown.)

```

for i from 1 to 22 do
fr_{p,i,SLS} := l_{p,i} - dr_{p,i,SLS} :
fr_{p,i,nt,SLS} := l_{p,i} - dr_{p,i,nt,SLS} : l_{p,i}
:= dr_{p,i,ULS} + fr_{p,mn} :

```

end do;

Example freeboard of pontoon 11 in SLS with no traffic taken into account: $fr_{p,11,nt,SLS}$

$$dr_{p,11,ULS} + 3 - dr_{p,11,nt,SLS} \quad (23)$$

4.6 Calculation Concentrated Wind Load

for n from 1 to 12 do
for i from 1 to 22 do

$V_{b,SLS} := C_{prob} \cdot V_{b,\alpha,n,ULS}$; $V_{b,ULS} := V_{b,\alpha,n,ULS}$;

$sa := s_{p,i} / l_{gp,i}$; $l_g := l_{gp,i}$;

$h_{gp,i} := \frac{l_{gp,i}}{90} \cdot h_g := h_{gp,i} \cdot z_{BG,i} := fz(s_{p,i}) + \frac{h_g}{2} + fr_{p,i,nt,SLS}$;

$F_{wind,BG,\alpha,SLS} := q_{p,g,SLS}(z_{BG,i}) \cdot l_{gp,i,\alpha,n} \cdot (h_g + h_{ws}) \cdot C_{d,gw}$;

$F_{wind,BG,\alpha,ULS} := q_{p,g,ULS}(z_{BG,i}) \cdot l_{gp,i,\alpha,n} \cdot (h_g + h_{ws}) \cdot C_{d,gw}$;

$F_{wind,truss,\alpha,SLS} := \frac{2 \cdot q_{p,g,SLS}(z_{BG,i}) \cdot l_{gp,i,\alpha,n}}{a_{truss}} \cdot (d_{truss} \cdot h_{truss} + d_{trussdia} \cdot l_{trussdia}) \cdot C_{d,truss}$;

$F_{wind,truss,\alpha,ULS} := \frac{2 \cdot q_{p,g,ULS}(z_{BG,i}) \cdot l_{gp,i,\alpha,n}}{a_{truss}} \cdot (d_{truss} \cdot h_{truss} + d_{trussdia} \cdot l_{trussdia}) \cdot C_{d,truss}$;

$F_{wind,traffic,\alpha,SLS} := q_{p,g,SLS}(z_{BG,i}) \cdot \max(4 - h_{ws}, 0) \cdot 0.5 \cdot l_{gp,i,\alpha,n} \cdot C_{d,traffic}$;

$F_{wind,tn,\alpha,SLS} := q_{p,g,SLS}(z_{BG,i}) \cdot d_{tn,gp,i,\alpha,n} \cdot C_{d,tn}$;

$F_{wind,tn,\alpha,ULS} := q_{p,g,ULS}(z_{BG,i}) \cdot d_{tn,gp,i,\alpha,n} \cdot C_{d,tn}$;

$F_{wind,gi,\alpha,n,SLS} := F_{wind,BG,\alpha,SLS} + F_{wind,tn,\alpha,SLS} + F_{wind,truss,\alpha,SLS} + F_{wind,traffic,\alpha,SLS}$; $q_{wind,gi,\alpha,n,SLS} := \frac{F_{wind,gi,\alpha,n,SLS}}{l_{gp,i,\alpha,n}}$;


```

Fwind,gi,α,n,ULS := γq · ( Fwind,BG,α,ULS + Fwind,tn,α,ULS + Fwind,truss,α,ULS ) : qwind,gi,α,n,ULS :=  $\frac{F_{wind,gi,\alpha,ULS}}{l_{gp,i,\alpha,n}}$  ;
Fwind,py,i,α,n,SLS := qp,p,SLS(zBG,i) · fz(sp,i) · 2 · Rpylon · Cd,pyw ;
Fwind,py,i,α,n,ULS := γq · qp,p,ULS(zBG,i) · fz(sp,i) · 2 · Rpylon · Cd,pyw ;
sa := 'sa' ;
enddo ;
enddo ;

```

Example concentrated wind load in SLS on pylon on top of pontoon 11 by wind from direction 9: $F_{wind,g,11,\alpha,9,SLS}$

$$84.34156749 \left(\frac{1}{2} + \frac{3.500000000}{\ln(1571.467444 + 20.00000000 dr_{p,11,ULS} - 20.00000000 dr_{p,11,mt,SLS})} \right) \ln(1571.467444 + 20.00000000 dr_{p,11,ULS} - 20.00000000 dr_{p,11,mt,SLS})^2 \quad (25)$$

4.7 Calculation Concentrated Current and Wave Load

Calculation of the current load, wave load and the position where the concentrated current load is acting (z_{FC,i,alpha}, n,eq)(this is the distance measured from the water level).

```

for n from 1 to 12 do
for i from 1 to 22 do

```

```

Hs,ww := Hs,ww,α,1,ULS ;
Hs,sw := Hs,sw,α,1,ULS ;
uc1,ULS := uc1,α,n ;
uc2,ULS := uc2,α,n ;
uc3,ULS := uc3,α,n ;

```

$$\begin{aligned}
 U_{c1,SLS} &:= C_{prob} \cdot U_{c1,\alpha,n} ; \\
 U_{c2,SLS} &:= C_{prob} \cdot U_{c2,\alpha,n} ; \\
 U_{c3,SLS} &:= C_{prob} \cdot U_{c3,\alpha,n} ; \\
 dr_p &:= dr_{p,i,SLS} ; \\
 l_g &:= l_{gp,i} ; \\
 h_g &:= \frac{l_{gp,i}}{90} ; \\
 F_{current1,SLS} &:= \frac{1}{2} \cdot \frac{\rho_w \cdot U_{c1,SLS}^2 \cdot C_{d,pc} \cdot 2 \cdot R_{pontoon,i} \cdot 10}{1000} ; \\
 F_{current2,SLS} &:= \frac{1}{2} \cdot \frac{\rho_w \cdot U_{c2,SLS}^2 \cdot C_{d,pc} \cdot 2 \cdot R_{pontoon,i} \cdot \min(dr_{p,i,SLS} - 10, 20)}{1000} ; \\
 F_{current3,SLS} &:= \frac{1}{2} \cdot \frac{\rho_w \cdot U_{c3,SLS}^2 \cdot C_{d,pc} \cdot 2 \cdot R_{pontoon,i} \cdot \max(dr_{p,i,SLS} - 30, 0)}{1000} ; \\
 F_{current1,ULS} &:= \frac{1}{2} \cdot \gamma_q \cdot \frac{\rho_w \cdot U_{c1,ULS}^2 \cdot C_{d,pc} \cdot 2 \cdot R_{pontoon,i} \cdot 10}{1000} ; \\
 F_{current2,ULS} &:= \frac{1}{2} \cdot \gamma_q \cdot \frac{\rho_w \cdot U_{c2,ULS}^2 \cdot C_{d,pc} \cdot 2 \cdot R_{pontoon,i} \cdot \min(dr_{p,i,ULS} - 10, 20)}{1000} ; \\
 F_{current3,ULS} &:= \frac{1}{2} \cdot \gamma_q \cdot \frac{\rho_w \cdot U_{c3,ULS}^2 \cdot C_{d,pc} \cdot 2 \cdot R_{pontoon,i} \cdot \max(dr_{p,i,ULS} - 30, 0)}{1000} ; \\
 F_{FC,eq,i,\alpha,n,SLS} &:= (F_{current1,SLS} + F_{current2,SLS} + F_{current3,SLS}) ; \\
 F_{FC,eq,i,\alpha,n,ULS} &:= (F_{current1,ULS} + F_{current2,ULS} + F_{current3,ULS}) ; \\
 z_{FC1} &:= 5 ; \\
 z_{FC2} &:= 10 + \min(dr_{p,i,SLS} - 10, 10) ; \\
 z_{FC3} &:= 30 + \frac{(dr_{p,i,SLS} - 30)}{2} ;
 \end{aligned}$$

```

ZFC,i,α,n,eq := ( Fcurrent1,SLS·ZFC1 + Fcurrent2,SLS·ZFC2 + Fcurrent3,SLS·ZFC3 ) / ( Fcurrent1,SLS + Fcurrent2,SLS + Fcurrent3,SLS );
Fww,i,α,n,SLS := 1 / ( 16·1000 ) · ρw · 9.81 · Hs,ww · 2 · Rpontoon,i;
Fww,i,α,n,ULS := γq · Fww,i,α,n,SLS;
Fsw,i,α,n,SLS := 1 / ( 16·1000 ) · ρw · 9.81 · Hs,sw · 2 · Rpontoon,i;
Fsw,i,α,n,ULS := γq · Fsw,i,α,n,SLS;
Fwa,i,α,n,SLS := Fww,i,α,n,SLS + Fsw,i,α,n,SLS;
Fwa,i,α,n,ULS := Fww,i,α,n,ULS + Fsw,i,α,n,ULS;
hg := hg;
lg := lg;
drp := drp;
end do;
end do;

```

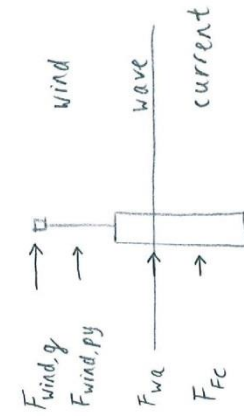
Example concentrated wave load in ULS from direction 9 on pontoon 11 $F_{wa,11,\alpha,9,ULS}$ 49.01680909 (26)

Example concentrated current load in SLS from direction 9 on pontoon 11 $F_{FC,eq,11,\alpha,9,SLS}$ 515.7677143 + 24.48289767 min(20, dr_{p,11,SLS} - 10) + 7.367653379 max(0, dr_{p,11,SLS} - 30) (27)

As can be seen, the current load is dependent on the submerged part of the pontoon. Since the pontoon lengths are still unknown, the exact value of the concentrated wave load is also unknown.

4.8 Calculation Total Horizontal Loads

The total horizontal load is the sum of the wind load, wave load and current load.



```

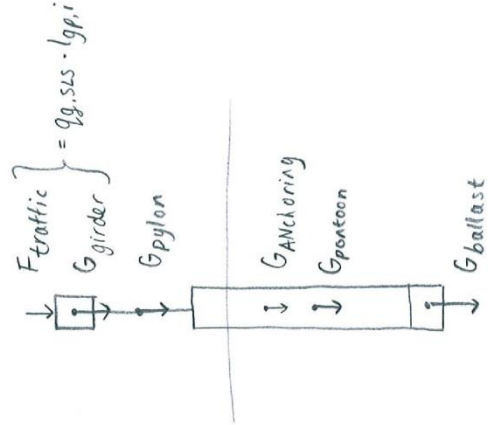
for n from 1 to 12 do
for i from 1 to 22 do
F_Htop,i,α,n,SLS := F_wa,i,α,n,SLS + F_FC,eq,i,α,n,SLS + F_wind,py,i,α,n,SLS + F_wind,g,i,α,n,SLS
F_Htop,i,α,n,ULS := F_wa,i,α,n,ULS + F_FC,eq,i,α,n,ULS + F_wind,py,i,α,n,ULS + F_wind,g,i,α,n,ULS
enddo:
enddo:

```

5 Required Buoyancy Determines Pontoon Length

5.1 Determination Required Buoyancy Force

The pontoon length is determined by the required upward buoyancy force. Since there is equilibrium of vertical forces, the upward buoyancy force is equal to the total downward vertical force, caused by the total self-weight of the structure and the traffic load. Below, the total downward vertical force is determined. All downward forces are known, except the self-weight of the ballast. The required ballast height (h_b) to obtain sufficient rotational stiffness of the pontoon will be determined further on in 6.2.



```

for i from 1 to 22 do
sa := s_p,i : l := l_gp,i : dr_p,ULS := dr_p,i,ULS : l := l_p,i :
G_pylon,i,SLS := G_pylon,SLS : G_pylon,i,ULS := G_pylon,ULS :
F_pontoon,i,SLS := q_g,SLS * l_gp,i + G_pylon,SLS + G_AN,i : F_pontoon,i,ULS := q_g,ULS * l_gp,i + G_pylon,ULS + G_AN,i :
G_ballast,i,SLS := (p_b * h_b * π * (R_pontoon,i - t_p,side,i)^2 * 9.81) / 1000 :
G_ballast,i,ULS := G_ballast,i,SLS :
G_p,i,SLS := (p_c * (l_p,i * π * R_pontoon,i^2 - (l_p,i - t_p,bot - t_p,top) * π * (R_pontoon,i - t_p,side,i)^2) * 9.81) / 1000 :

```

```

Gp,i,ULS := Gp,i,SLS;
Gtot,i,SLS := Gballast,i,SLS + Gp,i,SLS + Gpylon,SLS + (qg,SLS) · lgp,i + GAN,i;
Gtot,i,ULS := Gballast,i,ULS + Gp,i,ULS + Gpylon,ULS + (qg,ULS) · lgp,i + GAN,i;
lp := lp;
enddo;

```

The total vertical forces acting on pontoons 11 and 12 at the middle of the fjord are larger, since the span at the middle of the fjord is also larger. So the calculation code is adjusted for pontoon 11 and 12:

```

for i from 11 to 11 do
sa := sp,i · lg := lgp,i; drp,i,ULS := drp,i,ULS · lp := lp,i;
Gpylon,i,SLS := Gpylon,SLS; Gpylon,i,ULS := Gpylon,ULS;
Fpontoon,i,SLS :=  $\frac{q_{g,SLS} \cdot l_{g,i+1}}{2} + \frac{q_{g,SLS} \cdot l_{g,i}}{2} + G_{pylon,SLS} + G_{AN,i}$ ; Fpontoon,i,ULS :=  $\frac{q_{g,ULS} \cdot l_{g,i+1}}{2} + \frac{q_{g,ULS} \cdot l_{g,i}}{2} + G_{pylon,ULS} + 1.2 \cdot G_{AN,i}$ ;
Gballast,i,SLS :=  $\frac{\rho_b \cdot h_b \cdot \pi \cdot (R_{ponton,i} - t_{p,side,i})^2 \cdot 9.81}{1000}$ ;
Gballast,i,ULS := Gballast,i,SLS;
Gp,i,SLS :=  $\frac{\rho_c \cdot (l_{p,i} \cdot \pi \cdot R_{ponton,i}^2 - (l_{p,i} - t_{p,bot} - t_{p,top}) \cdot \pi \cdot (R_{ponton,i} - t_{p,side,i})^2) \cdot 9.81}{1000}$ ;
Gp,i,ULS := Gp,i,SLS;
Gtot,i,SLS := Gballast,i,SLS + Gp,i,SLS + Gpylon,SLS + (qg,SLS) · lgp,i + GAN,i;
Gtot,i,ULS := Gballast,i,ULS + Gp,i,ULS + Gpylon,ULS + (qg,ULS) · lgp,i + 1.2 · GAN,i;
lp := lp;
enddo;

```

```

for i from 12 to 12 do

```

```

sa := sp,i · lg := lgp,i; drp,i,ULS := drp,i,ULS · lp := lp,i;

```

$$\begin{aligned}
 G_{pylon, i, SLS} &::= G_{pylon, SLS} \cdot G_{pylon, i, ULS} \quad G_{pylon, ULS} := G_{pylon, ULS} \\
 F_{ponton, i, SLS} &::= \frac{q_{g, SLS, mid, i}}{2} + \frac{q_{g, SLS, i+1}}{2} + G_{pylon, SLS} + G_{AN, i} \quad F_{ponton, i, ULS} := \frac{q_{g, ULS, mid, i}}{2} + \frac{q_{g, ULS, i+1}}{2} \\
 &+ G_{pylon, ULS} + 1.2 \cdot G_{AN, i} \\
 G_{ballast, i, SLS} &::= \frac{p_b \cdot h_b \cdot \pi \cdot (R_{ponton, i} - t_{p, side, i})^2 \cdot 9.81}{1000} \\
 G_{ballast, i, ULS} &::= G_{ballast, i, SLS} \\
 G_{p, i, SLS} &::= \frac{p_c \cdot (l_p \cdot \pi \cdot R_{ponton, i}^2 - (l_p - t_{p, bot} - t_{p, top}) \cdot \pi \cdot (R_{ponton, i} - t_{p, side, i})^2) \cdot 9.81}{1000} \\
 G_{p, i, ULS} &::= G_{p, i, SLS} \\
 G_{tot, i, SLS} &::= G_{ballast, i, SLS} + G_{p, i, SLS} + G_{pylon, SLS} + (q_{g, SLS})_{gp, i} \cdot l_{gp, i} + G_{AN, i} \\
 G_{tot, i, ULS} &::= G_{ballast, i, ULS} + G_{p, i, ULS} + G_{pylon, ULS} + (q_{g, ULS})_{gp, i} \cdot l_{gp, i} + 1.2 \cdot G_{AN, i} \\
 l_p &:= l_p \\
 p &:= p \\
 \text{enddo:} &
 \end{aligned}$$

Example total downward vertical force (is equal to upward buoyancy force) of pontoon 11 in ULS

$$\begin{aligned}
 &G_{tot, 11, ULS} \\
 &11082.44420 h_{p, 11} \pi + 16578.90000 (dr_{p, 11, ULS} + 3) \pi - 13853.05526 \left(\frac{49}{50} dr_{p, 11, ULS} + \frac{47}{50} \right) \pi \\
 &+ 2.068707300 10^5 \quad (28)
 \end{aligned}$$

Table with total self-weight (SW) of each pontoon and its ballast. Note that the height of the ballast is not determined yet. The height of the ballast will be determined by the required rotational stiffness of the pontoon.

$$\begin{aligned}
 SWPB &:= \{ \langle \langle \text{"Pontoon no."}, [m], seq(i, i=1..11) \rangle \rangle | \langle \text{"SW pontoon + ballast"}, [kN] \rangle, seq(evalf_4(G_{p, i, SLS} + G_{ballast, i, SLS}), i \\
 &= 1..11) \rangle \} \\
 &SWPB
 \end{aligned}$$

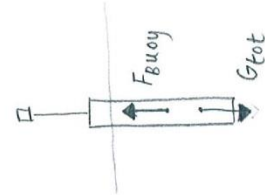
"Pontoon no." "[m]"	"SW pontoon+ballast" "[kN]"
1	$11240 \cdot h_{b,1} + 3580 \cdot dr_{p,1} \cdot ULS + 38810$
2	$16380 \cdot h_{b,2} + 4910 \cdot dr_{p,2} \cdot ULS + 55660$
3	$16380 \cdot h_{b,3} + 4910 \cdot dr_{p,3} \cdot ULS + 55660$
4	$16380 \cdot h_{b,4} + 4910 \cdot dr_{p,4} \cdot ULS + 55660$
5	$16380 \cdot h_{b,5} + 4910 \cdot dr_{p,5} \cdot ULS + 55660$
6	$16380 \cdot h_{b,6} + 4910 \cdot dr_{p,6} \cdot ULS + 55660$
7	$22490 \cdot h_{b,7} + 6450 \cdot dr_{p,7} \cdot ULS + 75580$
8	$22490 \cdot h_{b,8} + 6450 \cdot dr_{p,8} \cdot ULS + 75580$
9	$22490 \cdot h_{b,9} + 6450 \cdot dr_{p,9} \cdot ULS + 75580$
10	$22490 \cdot h_{b,10} + 6450 \cdot dr_{p,10} \cdot ULS + 75580$
11	$34810 \cdot h_{b,11} + 9450 \cdot dr_{p,11} \cdot ULS + 1.154 \cdot 10^5$

5.2 Determination Pontoon Dimensions (Length, Draught, Freeboard and Center of Gravity)

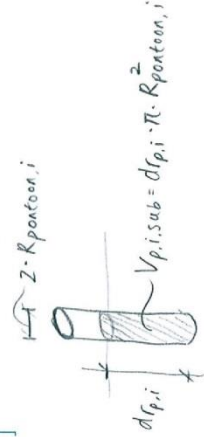
The required upward buoyancy force is determined in the previous section. The buoyancy force is provided by the amount of displaced water. Therefore, the submerged volume and consequently also the draught (submerged length) c the pontoon can be calculated. The pontoon length is then the sum of the submerged length and the freeboard length. This expression was already inputted at the end of section 3.2, while the draught was still unknown. Now, the draught, pontoon length and freeboards can be calculated.

for / from 1 to 22 do

$l_p := l_{p,i}$



$$\begin{aligned} \Sigma F_{vertical} &= 0 \\ F_{buoy} - G_{tot} &= 0 \\ F_{buoy} &= G_{tot} \\ V_{p,i,sub} \cdot \rho_{water} \cdot g &= G_{tot} \\ \downarrow \text{so} \\ V_{p,i,sub} &= \frac{G_{tot}}{\rho_{water} \cdot g} \end{aligned}$$



```

V_{p,i,sub,SLS} := (F_{ponton,i,SLS} + G_{p,i,SLS} + G_{ballast,i,SLS}) / (rho_w * 9.81) ;
V_{p,i,sub,nt,SLS} := (F_{ponton,i,SLS} - q_{traffic} * l_{p,i} + G_{p,i,SLS} + G_{ballast,i,SLS}) / (rho_w * 9.81) ;
V_{p,i,sub,ULS} := (F_{ponton,i,ULS} + G_{p,i,ULS} + G_{ballast,i,ULS}) / (rho_w * 9.81) ;
dr_{p,i,ULS} := solve(dr_{p,i,ULS} = V_{p,i,sub,ULS} / (pi * R_{ponton,i}^2), dr_{p,i,ULS}) ;
dr_{p,i,SLS} := evalf(V_{p,i,sub,SLS} / (pi * R_{ponton,i}^2)) ;
dr_{p,i,nt,SLS} := evalf(V_{p,i,sub,nt,SLS} / (pi * R_{ponton,i}^2)) ;
l_p := l_p ;
enddo:

(("Pontoon no.", " [m]", seq(i, i = 1..11)) | ("Pontoon Length", " [m]", seq(evalf_5(l_{p,i}), i = 1..11)) | ("Draught SLS", " [m]", seq(evalf_5(dr_{p,i,SLS}), i = 1..11)) | ("Draught SLS (no traffic)", " [m]", seq(evalf_5(dr_{p,i,nt,SLS}), i = 1..11)) | ("Freeboard SLS", " [m]", seq(evalf_4(fr_{p,i,SLS}), i = 1..11)))

```


"Pontoon no."	"Pontoon Length"	"Draught SLS"	"Draught SLS (no traffic)"	"Freeboard SLS"
"[m]"	"[m]"	"[m]"	"[m]"	"[m]"
1	$3.3105 h_{b,1} + 30.231$	$3.3105 h_{b,1} + 25.945$	$25.323 + 3.3105 h_{b,1}$	4.28
2	$3.1912 h_{b,2} + 31.078$	$3.1912 h_{b,2} + 26.557$	$25.859 + 3.1912 h_{b,2}$	4.52
3	$3.1912 h_{b,3} + 31.897$	$3.1912 h_{b,3} + 27.291$	$26.594 + 3.1912 h_{b,3}$	4.61
4	$3.1912 h_{b,4} + 33.122$	$3.1912 h_{b,4} + 28.440$	$27.743 + 3.1912 h_{b,4}$	4.68
5	$3.1912 h_{b,5} + 34.260$	$3.1912 h_{b,5} + 29.512$	$28.815 + 3.1912 h_{b,5}$	4.75
6	$3.1912 h_{b,6} + 35.630$	$3.1912 h_{b,6} + 30.824$	$30.127 + 3.1912 h_{b,6}$	4.81
7	$3.1124 h_{b,7} + 29.906$	$3.1124 h_{b,7} + 25.542$	$25.030 + 3.1124 h_{b,7}$	4.37
8	$3.1124 h_{b,8} + 32.634$	$3.1124 h_{b,8} + 28.241$	$27.728 + 3.1124 h_{b,8}$	4.39
9	$3.1124 h_{b,9} + 31.575$	$3.1124 h_{b,9} + 27.159$	$26.646 + 3.1124 h_{b,9}$	4.42
10	$3.1124 h_{b,10} + 34.505$	$3.1124 h_{b,10} + 30.072$	$29.559 + 3.1124 h_{b,10}$	4.44
11	$32.230 + 3.0273 h_{b,11}$	$27.333 + 3.0273 h_{b,11}$	$26.777 + 3.0273 h_{b,11}$	4.90

(30)

The expression for the center of gravity can be inserted. However, since the required ballast weight and height are not yet known, the exact distance between the center of gravity and the top of the pontoon is not yet known.

for i from 1 to 22 do

$$l_p := l_{p,i} \cdot z_{G,i,SLS} := \text{evalf} \left(\frac{1}{G_{\text{tot},i,SLS}} \left(\frac{(q_{g,SLS}) \cdot l_{gp,i} \cdot h_{gp,i}}{2} + G_{p/lon,i,SLS} \left(\frac{fz(s_{p,i})}{2} + h_{gp,i} \right) + G_{p,i,SLS} \left(\frac{l_{p,i}}{2} + fz(s_{p,i}) + h_{gp,i} \right) + G_{\text{ballast},i,SLS} \left(l_{p,i} + fz(s_{p,i}) + h_{gp,i} - t_{p,bot} - \frac{h_{b,i}}{2} \right) - h_{gp,i} - fz(s_{p,i}) \right) \right) :$$

$$z_{G,i,ULS} := \text{evalf} \left(\frac{1}{G_{\text{tot},i,ULS}} \left(\frac{(q_{g,ULS}) \cdot l_{gp,i} \cdot h_{gp,i}}{2} + G_{\text{pylon},i,ULS} \cdot \left(\frac{fz(s_{p,i})}{2} + h_{gp,i} \right) + G_{p,i,ULS} \cdot \left(\frac{l_{p,i}}{2} + fz(s_{p,i}) + h_{gp,i} \right) + G_{\text{ballast},i,ULS} \cdot \left(l_{p,i} + fz(s_{p,i}) + h_{gp,i} - t_{p,\text{bot}} - \frac{h_{b,i}}{2} \right) - h_{gp,i} - fz(s_{p,i}) \right) \right);$$

$l_p := l_p$;

$t_{p,\text{bot}} := t_{p,\text{bot}}$;

enddo;

for i from 1 to 22 do

$l_p := l_{p,i}$;

$t_{p,\text{bot},i} := t_{p,\text{bot}}$;

$l_p := l_p$;

enddo;

Example position center of gravity of pontoon 11 (SLS) $z_{G,11,SLS}$

$$\frac{1}{63375.92629 h_{b,11} + 5.60575328 \cdot 10^5} \left(1.324531020 \cdot 10^6 + (3.91092428 \cdot 10^5 \right. \tag{31}$$

$$+ 28559.4010 h_{b,11}) (93.53539804 + 1.513657131 h_{b,11}) + 34816.52529 h_{b,11} (108.0056095$$

$$+ 2.466767977 h_{b,11}) - 77.42059444$$

(32)

6 Calculation Rotational Stiffness and Ballast Height of pontoons

The ballast height is one of the factors which decide the rotational stiffness. In the cylinder shaped pontoons, the center of buoyancy is located above the center of gravity. The more ballast weight there is at the bottom of the pontoon, the lower the center of gravity will be located, which will consequently lead to a higher rotational stiffness of the pontoon.

6.1 Provided Rotational Stiffness by pontoons

For small rotations ($\phi < 10$ degrees), the relationship between moment and rotation can be assumed to be linear. This relationship is given by the equation below. As can be seen in the example below the equation, all pontoon properties are already known, except the ballast height.

for i from 1 to 22 do

$$k_{r_{x, BU, i}} := \left(\left(\frac{p_w \cdot 9.81}{1000} \cdot \pi \cdot R_{\text{pontoon}, i}^2 \cdot dr_{p, i, SLS} \right) \cdot \left(\frac{INER_i}{\pi \cdot R_{\text{pontoon}, i}^2 \cdot dr_{p, i, SLS}} - \left((fr_{p, i, SLS} + 0.5 \cdot dr_{p, i, SLS}) - z_{G, i, SLS} \right) \right) \right) ;$$

end do;

(33)

Example rotational stiffness of pontoon 11 $k_{r_{x, BU, 11}}$

$$6663.723066 \pi (27.33262163 + 3.027314259 h_{b, 11}) \left(\frac{51.00423683}{27.33262163 + 3.027314259 h_{b, 11}} - 95.98389082 \right) \quad (34)$$

$$- 1.513657133 h_{b, 11} + \frac{1}{63375.92629 h_{b, 11} + 5.60573328 \cdot 10^5} (1.324531020 \cdot 10^6 + (3.91092428 \cdot 10^5$$

$$+ 28559.4010 h_{b, 11}) (93.53539804 + 1.513657131 h_{b, 11}) + 34816.52529 h_{b, 11} (108.0056095$$

$$+ 2.466767977 h_{b, 11})))$$

6.2 Required Rotational Stiffness due to Loads

The pontoon is required to have a certain rotational stiffness, so no instability occurs when the bridge is subjected to loads. The bending moment equilibrium of the structure in a rotated position is used to obtain the required rotational stiffness. For the rotated position, the maximum allowed rotation is used.

Counter-clockwise is considered to be the positive direction. The bending moment equilibrium is checked at the center of gravity of the pontoon. Larger external loads (120% wind load and 110% wave and current loads) than calculated before are taken into account to create some margin for the design. The required rotational stiffness and the consequently required ballast height are shown in the table below the calculation.

$$\phi_x := -\frac{2.5}{360} \cdot 2 \cdot \pi :$$

$$h_b := 'h_b' :$$

for ifrom 1 to 22 do

gvdR := piecewise($i \leq 5, 11, 5 < i \leq 10, 10 < i \leq 12, 9, 12 < i \leq 17, 10, 17 < i \leq 22, 11$) :

$l_g := l_{gp,i} ; sa := s_{p,i} ; l_p := l_{p,i} :$

$aa := \frac{h_{gp,i}}{2} ; bb := fz(s_{p,i}) ; cc := fr_{p,i,SLS} ; dd := z_d'ee := z_{FC,i,\alpha(gvdR),eq} ; ff := z_{G,i,SLS} :$

$$eq6 := -1.2 \cdot F_{wind,g,i,\alpha(gvdR),SLS} \cdot (aa + bb + ff) - 1.2 \cdot F_{wind,py,i,\alpha(gvdR),SLS} \cdot \left(\frac{bb}{2} + ff \right) - 1.1 \cdot F_{wa,i,\alpha(gvdR),SLS} \cdot (ff - cc)$$

$$- 1.1 \cdot F_{FC,eq,i,\alpha(gvdR),SLS} \cdot (ff - cc - ee) - F_{traffic,hfb,SLS} \cdot ((aa + bb + ff) \cdot \tan(-1 \cdot \phi_x) + a_{traffic,hfb}) - (G_{AN,i} \cdot ((ff$$

$$- cc - dd) \cdot \tan(-1 \cdot \phi_x)) - kr_{x,BU,i} \cdot \phi_x = 0 :$$

func := {eq6} :

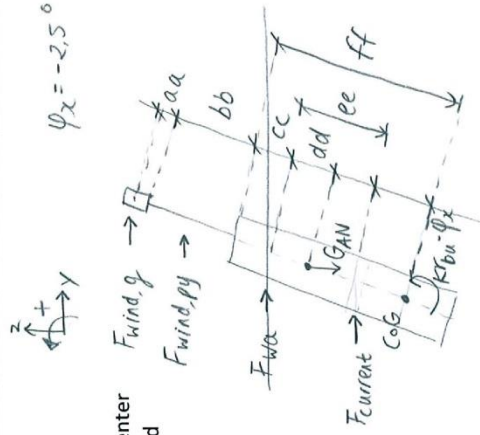
TEMP := (fsolve(func, {h_b, i = 0..infinity})) :

$h_{b,req,scap,i} := subs(TEMP, h_{b,i}) :$

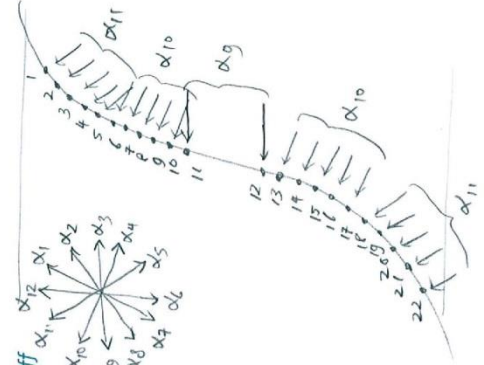
$$GM_i := \frac{INER_i}{\pi \cdot R_{pontoon,i}^2 \cdot dr_{p,i,SLS}} - \left((fr_{p,i,SLS} + 0.5 \cdot dr_{p,i,SLS}) \cdot z_{G,i,SLS} \right) :$$

$$z_{BC,i,SLS} := fr_{p,i,SLS} + 0.5 \cdot dr_{p,i,SLS} :$$

$$l_p := 'l_p' :$$



Load directions:



```

enddo;
for i from 1 to 22 do
   $h_{b,i} := h_{b,req,scaa,i}$ ;
end do;
 $\phi_x := \phi_x^t$ ;
<<"Pontoon no.", "[-]", seq(i, i = 1 ..11)>>{"Rotational stiffness", "[MNm/rad]", seq(kr_x_BUL, i = 1 ..11)}
|>{"Ballast height", "[m]", seq(h_b_req_scaa, i = 1 ..11)}

```

"Pontoon no."	"Rotational stiffness"	"Ballast height"
"[-]"	"[MNm/rad]"	"[m]"
1	$5.698889348 \cdot 10^5 \pi$	14.243885711
2	$1.446002971 \cdot 10^6 \pi$	19.49064593
3	$1.923911567 \cdot 10^6 \pi$	22.72030758
4	$2.404830444 \cdot 10^6 \pi$	25.68919708
5	$2.827856969 \cdot 10^6 \pi$	28.14926184
6	$3.393406570 \cdot 10^6 \pi$	30.92643567
7	$3.379001763 \cdot 10^6 \pi$	27.07192943
8	$4.094257325 \cdot 10^6 \pi$	30.44979428
9	$4.028948462 \cdot 10^6 \pi$	30.01375696
10	$4.683088807 \cdot 10^6 \pi$	33.10699468
11	$8.739609754 \cdot 10^6 \pi$	34.29079906

(35)

For example, the loads and leverarm in the bending moment equilibrium of pontoon 11 are given below.

Leverarm concentrated wind load on bridge girder $arm_{wind, BG, 11} := \frac{h_{gp, 11}}{2} + (fz(s_{p, 11})) + z_{G, 11, SLS}$
 155.6530501 (36)

Leverarm concentrated wind load on pylon $arm_{wind, py, 11} := \frac{(fz(s_{p, 11}))}{2} + z_{G, 11, SLS}$
 116.9427529 (37)

Leverarm concentrated wave load $arm_{wave, 11} := z_{G, 11, SLS} - fr_{p, 11, SLS}$
 75.18269216 (38)

Leverarm concentrated current load $arm_{cur, 11} := z_{G, 11, SLS} - fr_{p, 11, SLS} - z_{FG, 11, \alpha, 9, eq}$
 33.81893363 (39)

Leverarm concentrated traffic load $arm_{traffic, 11} := evalf_5 \left(\left(\frac{h_{gp, 11}}{2} + (fz(s_{p, 11})) + z_{G, 11, SLS} \right) \cdot \tan \left(\frac{2.5}{360} \cdot 2 \cdot \pi \right) + 6 \right)$
 12.786

Leverarm self-weight anchoring system $arm_{AN, 11} := evalf_5 \left((z_{G, 11, SLS} - fr_{p, 11, SLS} - z_o) \cdot \tan \left(\frac{2.5}{360} \cdot 2 \cdot \pi \right) \right)$
 2.4092 (42)

Height bridge girder $evalf_4(h_{gp, 11})$
 3.694 (43)

Height pylon $(fz(s_{p, 11}))$
 (44)

Height freeboard of pontoon in SLS $fr_{p, 11, SLS}$
 73.72615000

Distance between water surface and anchoring connection point on pontoon z_o
 4.8969857 (46)

20 (47)

Distance between water surface and line of action of the concentrated current load $Z_{FC, 11, \alpha, 9, eq}$	(48)
Distance between top of the pontoon and the center of gravity of the pontoon $Z_{G, 11, SLS}$	(49)
Concentrated wind load on bridge girder with margin (120%) $1.2 \cdot F_{wind, g, 11, \alpha, 9, SLS}$	(50)
Concentrated wind load on pylon with margin (120%) $1.2 \cdot F_{wind, py, 11, \alpha, 9, SLS}$	
Concentrated wave load with margin (110%) $1.1 \cdot F_{wo, 11, \alpha, 9, SLS}$	
Concentrated current load with margin (110%) $1.1 \cdot F_{FC, eq, 11, \alpha, 9, SLS}$	(51)
Concentrated traffic load $F_{traffic, hfb, SLS}$	
Self-weight anchoring system resisted by pontoon $G_{AN, 11}$	(53)
	41618

6.3 Stability Check

In the cylindrical pontoons, the center of buoyancy should be located above the center of gravity. In the table below, the z-coordinates of the center of gravity and the center of buoyancy are measured downwards from the top of the pontoon.

In the second column the metacentric height, the distance between the metacenter and the center of gravity, is given. The pontoons are statically stable when the metacentric heights are positive. For the dynamic stability, the natural oscillation period of the pontoons should be much larger than the period of the water movements. The natural oscillation period of the pontoons depend on the metacentric height. However, for this feasibility study only the static calculations are done. A conventional radius/draught ratio of existing spar structures is used for the design of the pontoons as well, which is approximately 0,19 (Handbook of offshore engineering volume 1, by C. Subatra, 2005, Table 7.11).

In later design phases, of course the dynamic effects should be checked as well.

```

<<"Pontoon no.", "[m]", seq(i, i = 1 .. 22)>> <<"Radius", "[m]", seq(R_pontoon, i = 1 .. 22)>> <<"Length", "[m]", seq(evalf_4(L_p, i), i
= 1 .. 22)>> <<"draught", "[m]", seq(evalf_5(dr_p, i, sLS), i = 1 .. 22)>> <<"radius/draught", "[m]", seq(evalf_4(R_pontoon, i
dr_p, i, sLS))>>, i =
..22)>> <<"z_CoG", "[m]", seq(evalf_4(z_G, i, sLS), i = 1 .. 22)>> <<"z_CoB", "[m]", seq(evalf_4(z_BC, i, sLS), i = 1 .. 22)>> <<"GM",
"[m]", seq(evalf_4(GM), i = 1 .. 22)>>

```


"Pontoon no."	"[-]"	"Radius"	"Length"	"draught"	"radius/draught"	"z_CoG"	"z_CoB"	"GM"
	"[m]"	"[m]"	"[m]"	"[m]"	"[m]"	"[m]"	"[m]"	"[m]"
1	15	77.38	73.100	0.2052	44.04	40.83	3.47	
2	18	93.27	88.757	0.2028	53.71	48.91	5.10	
3	18	104.4	99.795	0.1804	60.32	54.51	6.08	
4	18	115.1	110.42	0.1630	66.55	59.90	6.89	
5	18	124.1	119.34	0.1509	71.57	64.43	7.3	
6	18	134.3	129.52	0.1390	77.53	69.58	8.1	
7	21	114.2	109.80	0.1913	65.94	59.25	7.0	
8	21	127.4	123.01	0.1707	73.30	65.89	7.7	
9	21	125.0	120.58	0.1741	72.01	64.70	7.6	
10	21	137.5	133.11	0.1578	78.76	70.99	8.0	
11	26	136.0	131.14	0.1983	80.08	70.48	10.0	
12	26	136.0	131.14	0.1983	80.08	70.48	10.0	
13	21	137.5	133.11	0.1578	78.76	70.99	8.0	
14	21	125.0	120.58	0.1741	72.01	64.70	7.6	
15	21	127.4	123.01	0.1707	73.30	65.89	7.7	
16	21	114.2	109.80	0.1913	65.94	59.25	7.0	
17	18	134.3	129.52	0.1390	77.53	69.58	8.1	
18	18	124.1	119.34	0.1509	71.57	64.43	7.3	
19	18	115.1	110.42	0.1630	66.55	59.90	6.89	
20	18	104.4	99.795	0.1804	60.32	54.51	6.08	
21	18	93.27	88.757	0.2028	53.71	48.91	5.10	
22	15	77.38	73.100	0.2052	44.04	40.83	3.47	

7 Overview Results

To give an overview, the results are summarized in tables. Below, the equations and codes can be seen, which are used to gather all results of the calculations and to assemble tables.

```

for i from 1 to 22 do
  lg := lgp,i ;
  Mtraffic,i,SLS := Ftraffic,hfb,SLS · atraffic,hfb ;
  Mtraffic,i,ULS := Ftraffic,hfb,ULS · atraffic,hfb ;
  lg := lg ;
  tp,side,i := tp,req side,i ;
enddo;

for i from 1 to 22 do
  gvdr := piecewise ( i ≤ 5, 11, 5 < i ≤ 10, 10, 10 < i ≤ 12, 9, 12 < i ≤ 17, 10, 17 < i ≤ 22, 11 ) ;
  lg := lgp,i ; sa := sp,i ; hb,i := hb,req,scaa,i ;
  drp,i,scaa,SLS := evalf( drp,i,SLS ) ; drp,i,scaa,ULS := evalf( drp,i,ULS ) ; drp,i,scaa,nt,SLS := drp,i,nt,SLS ; krx,BU,i,scaa
  := evalf( krx,BU,i ) ;
  lp,i,scaa := evalf( lp,i ) ; frp,i,scaa,SLS := evalf( frp,i,SLS ) ; frp,i,scaa,nt,SLS := evalf( frp,i,nt,SLS ) ; frp,i,scaa,ULS
  := evalf( frp,mn ) ;
  fz,i := fz( sp,i ) ;
for n from 1 to 12 do
  Fwind,g,scaa,i,α,n,SLS := Fwind,g,i,α,n,SLS · windg,scaa,i,α,n,SLS ; Fwind,g,i,α,n,ULS := Fwind,g,i,α,n,ULS ;
  Fwind,py,scaa,i,α,n,SLS := Fwind,py,i,α,n,SLS · windpy,scaa,i,α,n,ULS ; Fwind,py,i,α,n,ULS := Fwind,py,i,α,n,ULS ;
  Fwa,scaa,i,α,n,SLS := Fwa,i,α,n,SLS · wascaa,i,α,n,ULS ; Fwa,i,α,n,ULS := Fwa,i,α,n,ULS ;

```

```

FFC,eq,scaa,i,α,n,SLS := FFC,eq,i,α,n,SLS · FFC,eq,scaa,i,α,n,ULS := FFC,eq,i,α,n,ULS
FHtotp,scaa,i,α,n,SLS := Fwa,scaa,i,α,n,SLS + FFC,eq,scaa,i,α,n,SLS + Fwind,py,scaa,i,α,n,SLS + Fwind,g,scaa,i,α,n,SLS
FHtotp,scaa,i,α,n,ULS := Fwa,scaa,i,α,n,ULS + FFC,eq,scaa,i,α,n,ULS + Fwind,py,scaa,i,α,n,ULS + Fwind,g,scaa,i,α,n,ULS
Fpontoon,scaa,i,α,n,SLS := Fpontoon,i,SLS · Fpontoon,scaa,i,ULS := Fpontoon,i,ULS
enddo

lp := lp,i,scaa · hb := hb,req,scaa,i · Vc,scaa,i :=  $\frac{(\rho_c \cdot l_p \cdot \pi \cdot R_{pontoon}^2 - (l_p - t_{p,bot} - t_{p,top}) \cdot \pi \cdot (R_{pontoon} - t_{p,side})^2) \cdot 9.81}{1000}$ 
Vb,scaa,i :=  $\frac{(\rho_b \cdot (h_b) \cdot \pi \cdot (R_{pontoon} - t_{p,side})^2 \cdot 9.81)}{1000}$ 
sa := 'sa': lg := 'l': CRWp,i,scaa := (evalf4(lp,i,scaa) | evalf4(Rpontoon,i) | evalf3(hb,req,scaa,i) | evalf4(drp,i,scaa,SLS) | evalf5(frp,i,scaa,SLS) | evalf3(frp,i,scaa,SLS) | evalf8( $\frac{kr_{x,BU,i,scaa}}{1000}$ ) | evalf3(tp,bot,i) | unassign('hb,i') :
FRWp,i,scaa,SLS := (evalf5(Fwind,g,scaa,i,α,(gvar),SLS) | evalf5(Fwind,py,scaa,i,α,(gvar),SLS) | evalf3(Fwa,scaa,i,α,(gvar),SLS) | evalf5(FFC,eq,scaa,i,α,(gvar),SLS) | evalf5(FHtotp,scaa,i,α,(gvar),SLS) :
FRWp,i,scaa,ULS := (evalf5(Fwind,g,scaa,i,α,(gvar),ULS) | evalf5(Fwind,py,scaa,i,α,(gvar),ULS) | evalf5(Fwa,scaa,i,α,(gvar),ULS) | evalf5(FFC,eq,scaa,i,α,(gvar),ULS) | evalf5(FHtotp,scaa,i,α,(gvar),ULS)) : l := 'l': hb := 'hb':
LULSp,i := (evalf4(Fwind,g,scaa,i,α,(gvar),ULS + Fwind,py,scaa,i,α,(gvar),ULS) | evalf4(Fwa,scaa,i,α,(gvar),ULS + FFC,eq,scaa,i,α,(gvar),ULS)) :
LULSp,i,mult := < | evalf4(1.2 · Fwind,g,scaa,i,α,(gvar),ULS + 1.2 · Fwind,py,scaa,i,α,(gvar),ULS + 1.1 · Fwa,scaa,i,α,(gvar),ULS | evalf4(1.1 · Fwa,scaa,i,α,(gvar),ULS

```

```

+ 1.1 · FFC,eq,scaa,i,α(gvdr),ULS |evalf5(1.2 · Fwind,g,scaa,i,α(gvdr),ULS + 1.2 · Fwind,py,scaa,i,α(gvdr),ULS + 1.1
· Fwa,scaa,i,α(gvdr),ULS + 1.1 · FFC,eq,scaa,i,α(gvdr),ULS) >:

LSLSp,i := < |evalf4(Fwind,g,scaa,i,α(gvdr),SLS + Fwind,py,scaa,i,α(gvdr),SLS) |evalf4(Fwa,scaa,i,α(gvdr),SLS
+ FFC,eq,scaa,i,α(gvdr),SLS) >:
+ 1.1 · FFC,eq,scaa,i,α(gvdr),SLS |evalf4(1.2 · Fwind,g,scaa,i,α(gvdr),SLS + 1.2 · Fwind,py,scaa,i,α(gvdr),SLS) |evalf4(1.1 · Fwa,scaa,i,α(gvdr),SLS
+ 1.1 · FFC,eq,scaa,i,α(gvdr),SLS) |evalf5(1.2 · Fwind,g,scaa,i,α(gvdr),SLS + 1.2 · Fwind,py,scaa,i,α(gvdr),SLS + 1.1
· Fwa,scaa,i,α(gvdr),SLS + 1.1 · FFC,eq,scaa,i,α(gvdr),SLS) >:

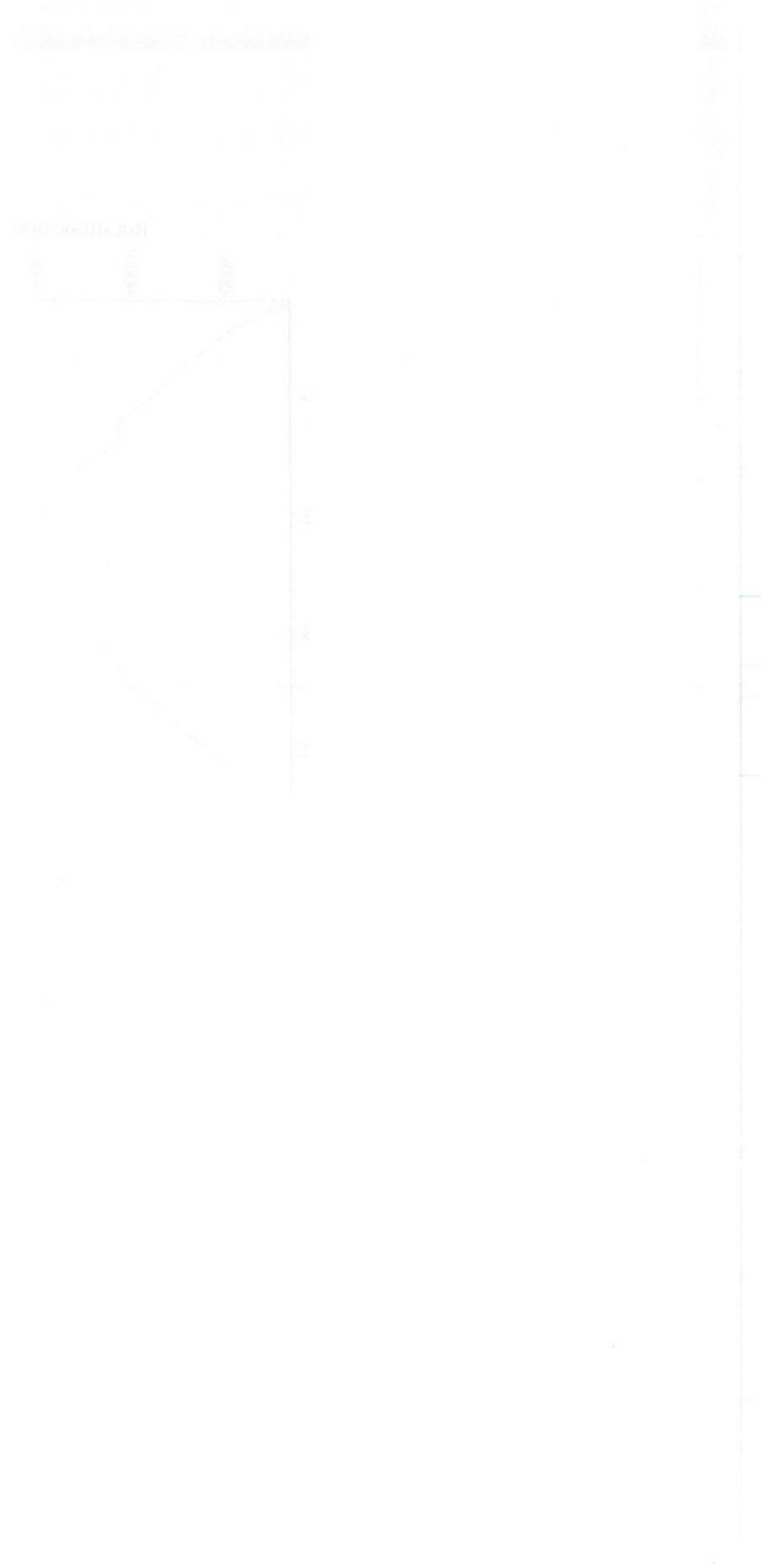
enddo:
for ifrom 1 to 22 do
hb,j := hb,req,scaa,i :
enddo:
for ifrom 1 to 22 do
MTRAFp,i := ( |evalf5(Mtraffic,i,SLS) |evalf5(Mtraffic,i,ULS) )
enddo:
MTR := ("NR|M_traffic,SLS|M_traffic,ULS") :
for ifrom 1 to 22 do
gvdr := piecewise(i ≤ 5, 11, 5 < i ≤ 10, 10 < i ≤ 12, 9, 12 < i ≤ 17, 10, 17 < i ≤ 22, 11) :
Fxwaves,i := Fwa,scaa,i,α(gvdr),SLS :
Fxcurr,i := FFC,eq,scaa,i,α(gvdr),SLS · Fxwind,i := Fwind,g,scaa,i,α(gvdr),SLS + Fwind,py,scaa,i,α(gvdr),SLS :
enddo:

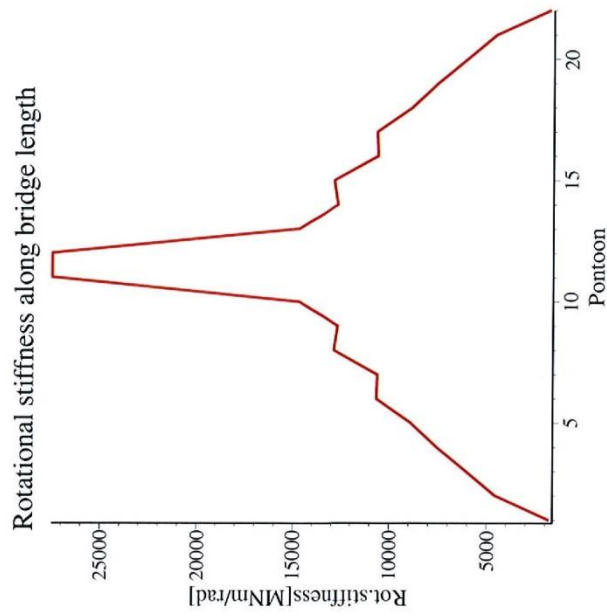
```


(56)

"NR"	"L_p"	"R_p"	"H_b"	"DR_p_SLS"	"FR_SLS"	"FR_NT,SLS"	"kr_BU"	"t_bot"
"[-]"	"[m]"	"[m]"	"[m]"	"[m]"	"[m]"	"[m]"	"[MNm/rad]"	"[m]"
1	77.39	15.	14.2	73.10	4.29	4.91	1790.3589	2.54
2	93.28	18.	19.5	88.76	4.52	5.22	4542.7523	2.86
3	104.4	18.	22.7	99.80	4.61	5.30	6044.1464	3.09
4	115.1	18.	25.7	110.4	4.68	5.38	7554.9977	3.30
5	124.1	18.	28.1	119.3	4.75	5.45	8883.9747	3.48
6	134.3	18.	30.9	129.5	4.81	5.50	10660.701	3.68
7	114.2	21.	27.1	109.8	4.36	4.88	10615.447	3.29
8	127.4	21.	30.4	123.0	4.39	4.91	12862.489	3.54
9	125.0	21.	30.0	120.6	4.42	4.93	12657.315	3.50
10	137.5	21.	33.1	133.1	4.43	4.95	14712.357	3.75
11	136.0	26.	34.3	131.1	4.90	5.45	27456.294	3.72
12	136.0	26.	34.3	131.1	4.90	5.45	27456.297	3.72
13	137.5	21.	33.1	133.1	4.43	4.95	14712.362	3.75
14	125.0	21.	30.0	120.6	4.42	4.93	12657.321	3.50
15	127.4	21.	30.4	123.0	4.39	4.91	12862.497	3.54
16	114.2	21.	27.1	109.8	4.36	4.88	10615.456	3.29
17	134.3	18.	30.9	129.5	4.81	5.50	10660.712	3.68
18	124.1	18.	28.1	119.3	4.75	5.45	8883.9807	3.48
19	115.1	18.	25.7	110.4	4.68	5.38	7555.0032	3.30
20	104.4	18.	22.7	99.80	4.61	5.30	6044.1514	3.09
21	93.28	18.	19.5	88.76	4.52	5.22	4542.7562	2.86
22	77.39	15.	14.2	73.10	4.29	4.91	1790.3599	2.54

```
PKRBU := pointplot(
  << 1, 2, 3, 4, 5, 6, 7, 8, 9, 10, 11, 12, 13, 14, 15, 16, 17, 18, 19, 20, 21, 22 >>
  seq(
     $\frac{k_{r, BU, i, scaa}}{1000}$ , i = 1
    ..22
  ),
  style = line,
  title = "Rotational stiffness along bridge length",
  titlefont = ["calibri", 14],
  color = red,
  labels
= ["Pontoon", "Rot.stiffness[MNm/rad]"],
  labelfont = ["calibri", 12],
  labeldirections = ["horizontal", "vertical"]
):
display([PKRBU])
```





Distance between node where the wind load is acting on the bridge girder and the anchoring point:

```
for i from 1 to 22 do
```

$$a1 := \frac{h_{gp,i}}{2} + \frac{fz(s_{p,i})}{2}; a2 := \frac{fz(s_{p,i})}{2} + fr_{p,i,mt,sl,g} \cdot a3 := z_d;$$


```

arm_krbu,i := (a1 + a2 + a3) :
arm_krbu,i := evalf5(arm_krbu,i) :
enddo:

```

Distance between node where wind load is acting on the pylons and anchoring point:

```

for i from 1 to 22 do

```

$$a1 := \frac{h_{gp,i}}{2} + \frac{fz(s_{p,i})}{2}; a2 := \frac{fz(s_{p,i})}{2} + fr_{p,i,nt,sls}; a3 := z_a;$$

```

arm_pyl,i := evalf5(a2 + a3) :
enddo:

```

Distance between node where wave load is acting on and anchoring point is 20 meters for every pontoon.

Distance between node where current load is acting on and anchoring point:

```

for i from 1 to 22 do

```

$$gvd := \text{piecewise}(i \leq 5, 11, 5 < i \leq 10, 10 < i \leq 12, 9, 12 < i \leq 17, 10, 17 < i \leq 22, 11) :$$

$$arm_{kr,i} := -1 \cdot \text{evalf}_5(z_{FC,i,\alpha,(gvd)}, eq - z_a) :$$

```

enddo:

```

Distance between anchoring point and center of gravity:

```

for i from 1 to 22 do

```

$$armAG_i := z_{G,i,sls} - fr_{p,i,nt,sls} - z_a :$$

$$armAG_i := \text{evalf}_5(armAG_i) :$$

```

enddo:

```

(57)

Table with all distances shown between the line of action of the forces and the anchoring point. The origin is at the anchoring point, upwards is considered positive here and downwards is negative.

```

(("#P", " ", 1, 2, 3, 4, 5, 6, 7, 8, 9, 10, 11, 12, 13, 14, 15, 16, 17, 18, 19, 20, 21, 22) | ("z_wind BG-anch", "[m]", arm_krbu, 1'
arm_krbu, 2' arm_krbu, 3' arm_krbu, 4' arm_krbu, 5' arm_krbu, 6' arm_krbu, 7' arm_krbu, 8' arm_krbu, 9' arm_krbu, 10' arm_krbu, 11' arm_krbu, 12'
arm_krbu, 13' arm_krbu, 14' arm_krbu, 15' arm_krbu, 16' arm_krbu, 17' arm_krbu, 18' arm_krbu, 19' arm_krbu, 20' arm_krbu, 21' arm_krbu, 22)
| ("z_wind PY-anch", "[m]", arm_pyl, 1' arm_pyl, 2' arm_pyl, 3' arm_pyl, 4' arm_pyl, 5' arm_pyl, 6' arm_pyl, 7' arm_pyl, 8' arm_pyl, 9' arm_pyl, 10'

```

```

arm pyl, 11' arm pyl, 12' arm pyl, 13' arm pyl, 14' arm pyl, 15' arm pyl, 16' arm pyl, 17' arm pyl, 18' arm pyl, 19' arm pyl, 20' arm pyl, 21' arm pyl, 22'
| ("z_current-anch", "[m]", arm_kr, 1' arm_kr, 2' arm_kr, 3' arm_kr, 4' arm_kr, 5' arm_kr, 6' arm_kr, 7' arm_kr, 8' arm_kr, 9' arm_kr, 10'
arm_kr, 11' arm_kr, 12' arm_kr, 13' arm_kr, 14' arm_kr, 15' arm_kr, 16' arm_kr, 17' arm_kr, 18' arm_kr, 19' arm_kr, 20' arm_kr, 21' arm_kr, 22'
| ("z_anch-CoG", "[m]", seq(armAG, i = 1..22)))

```

"#P"	"z_wind BG-anch"	"z_wind PY-anch"	"z_current-anch"	"z_anch-CoG"
" "	"[m]"	"[m]"	"[m]"	"[m]"
1	28.673	26.447	-1.725	19.178
2	41.642	32.875	-6.473	28.482
3	52.810	38.501	-10.101	34.971
4	62.818	43.543	-13.775	41.091
5	71.668	48.002	-16.979	46.171
6	79.362	51.877	-20.752	52.060
7	85.223	54.494	-13.556	41.150
8	90.594	57.194	-18.325	48.367
9	94.813	59.315	-17.433	47.172
10	97.879	60.857	-22.108	53.876
11	101.03	62.316	-21.363	54.627
12	101.03	62.316	-21.363	54.627
13	97.879	60.857	-22.108	53.876
14	94.813	59.315	-17.433	47.172
15	90.594	57.194	-18.325	48.367
16	85.223	54.494	-13.556	41.150
17	79.362	51.877	-20.752	52.060
18	71.668	48.002	-16.979	46.171
19	62.818	43.543	-13.775	41.091
20	52.810	38.501	-10.101	34.971
21	41.642	32.875	-6.473	28.482
22	28.673	26.447	-1.725	19.178

7.2 Vertical Loads

The total selfweight of the pontoons is (in kN) $evalf_5(add(G_{p,i,SLS} \ i = 1..22)) + evalf_5(add(G_{ballast,i,SLS} \ i = 1..22))$ (59)

The total length of all pontoons is (in m) $evalf_5(add(l_{p,i} \ i = 1..22))$ (60)

The total vertical forces acting on the pontoons (self-weight bridge girder, pylons, traffic and self-weight anchoring system) is (in kN) $evalf_5(add(F_{ponton,i,SLS} \ i = 1..22))$ (61)

2.2047 10⁶

for *i* **from** 1 **to** 22 **do**

*l*_{tijdelijk} := *l*_{gp,i} ;

*F*_{traffic,i,SLS} := *q*_{traffic} · *l*_{tijdelijk} ;

unassign(*l*_{tijdelijk}) ;

enddo;

for *i* **from** 1 **to** 10 **do**

*G*_{BG,i} := (*q*_{g,SLS} - 35) · *l*_{gp,i} ;

enddo;

*G*_{BG,11} := $\frac{(q_{g,SLS,mid} - 35) \cdot l_{g,12}}{2} + \frac{(q_{g,SLS} - 35) \cdot l_{g,11}}{2}$;

for *i* **from** 1 **to** 11 **do**

*s*_{p,i} := *l*_{gp,i} ; *dr*_{p,U,S} := *dr*_{p,i,U,S} ; *l*_p := *l*_{p,i} ;

*G*_{pyl,i} := *G*_{pylon,SLS} ;

*l*_p := *l*_p ;

enddo;

Table with all vertical loads:

- F_traffic = vertical load due to traffic ;
- SW_BG = self-weight of bridge girder ;
- SW_PYL = self-weight of pylon ;
- SW_pontoon+ballast = self-weight of pontoon and ballast ;
- SW_AN = part of self-weight of anchoring system resisted by pontoon ;
- Fz total = total vertical load on pontoon ;

```

(<<"pontoon", "[-]", seq(i, i = 1..11)) << "F_traffic", "[kN]", evalf5(seq(F_traffic, i, SLS, i = 1..11)) << "SW_BG", "[kN]",
seq(evalf5(G_BG, i, i = 1..11)) << "SW_PYL", "[kN]", seq(evalf5(G_PYL, i, i = 1..11)) << "SW sup", "[kN]", seq(evalf5(G_BG, i
+ G_PYL, i, i = 1..11)) << "SW pont+ball", "[kN]", seq(evalf5(G_P, i, SLS + G_ballast, i, SLS), i = 1..11)) << "SW AN", "[kN]",
seq(evalf5(G_AN, i, i = 1..11)) << "Fz total", "[kN]", seq(evalf5(G_tot, i, SLS), i = 1..11))

```

"[-]"	"F_traffic"	"SW_BG"	"SW_PYL"	"SW sup"	"SW pont+ball"	"SW AN"	"Fz total"
"[kN]"	"[kN]"	"[kN]"	"[kN]"	"[kN]"	"[kN]"	"[kN]"	"[kN]"
1	4332.1	32800.	1173.8	33974.	4.6471 10 ⁵	6328.	5.0934 10 ⁵
2	7000.	53000.	5839.1	58839.	8.1741 10 ⁵	7335.	8.9058 10 ⁵
3	7000.	53000.	10065.	63065.	9.2482 10 ⁵	6467.	1.0014 10 ⁶
4	7000.	53000.	13853.	66853.	1.0259 10 ⁶	8205.	1.1080 10 ⁶
5	7000.	53000.	17203.	70203.	1.1102 10 ⁶	10029.	1.1974 10 ⁶
6	7000.	53000.	20115.	73115.	1.2059 10 ⁶	13565.	1.2996 10 ⁶
7	7000.	53000.	22589.	75589.	1.3995 10 ⁶	17665.	1.4998 10 ⁶
8	7000.	53000.	24626.	77626.	1.5609 10 ⁶	34933.	1.6805 10 ⁶
9	7000.	53000.	26226.	79226.	1.5354 10 ⁶	25363.	1.6470 10 ⁶
10	7000.	53000.	27389.	80389.	1.6854 10 ⁶	45137.	1.8179 10 ⁶
11	11638.	99738.	28115.	1.2785 10 ⁵	2.5642 10 ⁶	41618.	2.7337 10 ⁶

(62)

"NR"	"F_wind,BG"	"F_wind,pyl"	"F_WA"	"F_FC"	"F_H,tot"
"[-]"	"[kN]"	"[kN]"	"[kN]"	"[kN]"	"[kN]"
1	664.81	17.364	18.9	763.25	1464.3
2	1459.1	112.38	22.6	995.76	2589.9
3	1606.7	215.72	22.6	1052.1	2897.2
4	1684.0	317.00	22.6	1106.3	3129.9
5	1711.7	411.70	22.6	1151.8	3297.8
6	1817.5	497.24	22.6	1203.7	3541.0
7	1870.6	570.62	26.4	1287.0	3754.6
8	1896.9	633.37	26.4	1365.6	3922.3
9	1892.9	683.40	26.4	1351.1	3953.8
10	1859.6	720.15	26.4	1425.7	4031.8
11	4485.0	838.94	32.7	1750.6	7107.2

(66)

To simplify the modeling in Scia Engineer, both the wind load on the bridge girders and pylons are concentrated at the bridge girder (conservative) and the wave and current load are concentrated at the point where the wave load is acting on.

```

L1LSNU := { "[-]" | "[kN]" | "[kN]" } :
(L1LSN, L1LSNU, seq(L1LS, i=1..11))

```

"I-]"	"F_wind,tot,SLS" [kN]	"F_water,tot,SLS" [kN]
1	682.2	782.2
2	1571.	1018.
3	1823.	1075.
4	2001.	1129.
5	2124.	1175.
6	2314.	1227.
7	2442.	1313.
8	2530.	1392.
9	2576.	1377.
10	2580.	1452.
11	5324.	1784.

(67)

To create some margin for the design of the superstructure, the wind load will be multiplied by a factor 1,2 and the load due to the water is multiplied by 1,1.

$(L_{LSMN, seq} (L_{LS, mult}^{i=1 \dots 11}))$

"NR"	"F_wind,m,SLS"	"F_water,m,SLS"	"Total Fx,m"
1	818.6	860.3	1678.9
2	1886.	1120.	3006.0
3	2187.	1182.	3369.1
4	2401.	1242.	3643.0
5	2548.	1292.	3839.9
6	2777.	1349.	4126.7
7	2930.	1445.	4374.1
8	3036.	1532.	4567.5
9	3092.	1515.	4606.8
10	3096.	1598.	4693.0
11	6389.	1962.	8350.3

(68)

The horizontal loads (ULS) acting on the buoyancy bridge are shown in the table below.

(FRWTULS, FRW_{p,1,scaa,ULS}, FRW_{p,2,scaa,ULS}, FRW_{p,3,scaa,ULS}, FRW_{p,4,scaa,ULS}, FRW_{p,5,scaa,ULS}, FRW_{p,6,scaa,ULS}, FRW_{p,7,scaa,ULS}, FRW_{p,8,scaa,ULS}, FRW_{p,9,scaa,ULS}, FRW_{p,10,scaa,ULS}, FRW_{p,11,scaa,ULS})

"NR"	"F_wind,BG"	"F_wind,pyl"	"F_WA"	"F_FC"	"F_H,tot"
1	983.52	31.920	28.279	1413.1	2456.8
2	2192.3	206.58	33.935	1844.7	4277.6
3	2414.1	396.55	33.935	1949.1	4793.7
4	2530.2	582.74	33.935	2049.4	5196.3
5	2571.9	756.82	33.935	2133.7	5496.3
6	2730.8	914.06	33.935	2229.6	5908.4
7	2810.6	1049.0	39.590	2380.7	6279.9
8	2850.2	1164.3	39.590	2525.5	6579.6
9	2844.2	1256.3	39.590	2499.1	6639.2
10	2794.1	1323.8	39.590	2636.5	6794.0
11	7021.4	1542.2	49.017	3243.8	11856.

(69)

$$\text{Total wind load with margin (in kN)} \quad \text{evalf}_6(1.2 \cdot (\text{add}(F_{xwind, i=1..22})))$$

62320.2

(70)

$$\text{Total wave and current load with margin (in kN)} \\ \text{evalf}_6(1.1 \cdot (\text{add}(F_{xwaves, i=1..22})) + \text{evalf}_5(\text{add}(F_{xcurr, i=1..22})))$$

27502.5

(71)

$$\text{Total horizontal loads with margin (in kN)} \\ \text{evalf}_8(1.2 \cdot (\text{add}(F_{xwind, i=1..22})) + (1.1 \cdot (\text{add}(F_{xwaves, i=1..22})) + \text{evalf}_5(\text{add}(F_{xcurr, i=1..22}))))$$

89822.823

(72)

The loads (ULS) caused by wind and water are concentrated to simplify the modeling.
 $\langle LULSN_{seq}(LULS_{i=1..11}) \rangle$

"NR"	"F_wind,tot,ULS"	"F_water,tot,ULS"
1	1015.	1441.
2	2399.	1879.
3	2810.	1983.
4	3113.	2083.
5	3329.	2168.
6	3645.	2264.
7	3860.	2421.
8	4014.	2566.
9	4100.	2539.
10	4118.	2676.
11	8563.	3293.

(73)

The loads (ULS) with margin taken into account (120% for wind and 110% for water) are shown in the table below.

$\langle LULSMN, seq(LULS_{p,i,mult}, i = 1..11) \rangle$

"NR"	"F_wind,m,ULS"	"F_water,m,ULS"	"Total Fx,m"
1	1218.	1585.	2804.0
2	2878.	2067.	4945.2
3	3373.	2181.	5554.1
4	3735.	2291.	6027.1
5	3994.	2384.	6378.9
6	4374.	2490.	6863.8
7	4632.	2663.	7293.8
8	4817.	2823.	7638.9
9	4920.	2793.	7713.1
10	4942.	2944.	7885.2
11	10280.	3622.	13898.

(74

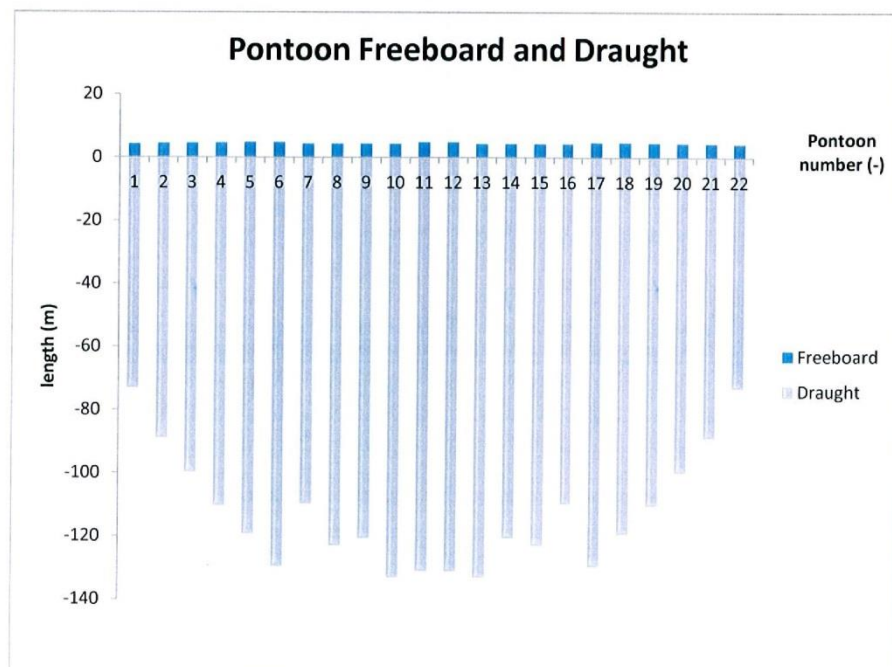
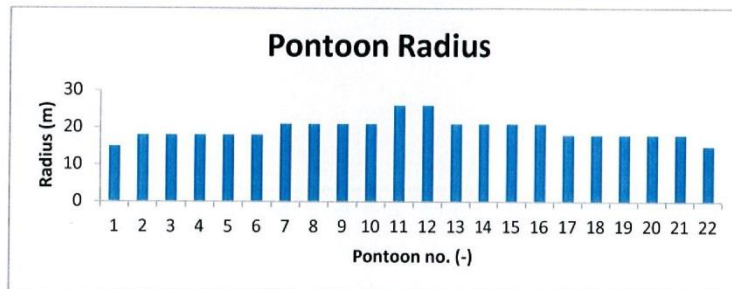
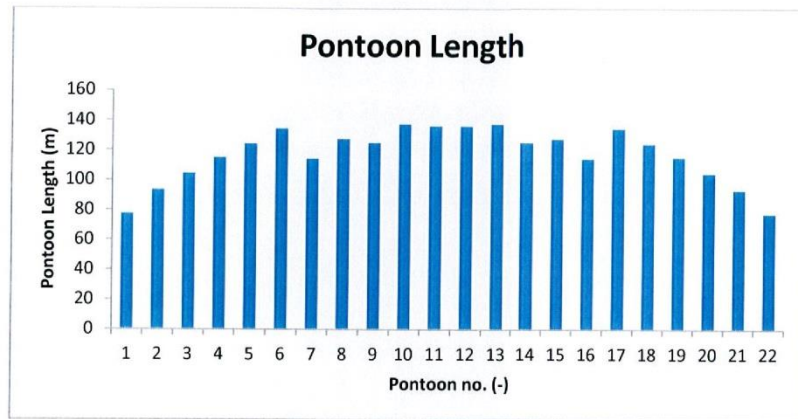
The bending moment caused by traffic is shown below.

$$MTRU := \langle \{[-]^{111} [kNm]^{111} [kNm]^{11} \rangle :$$

$$\langle MTR, MTRU, seq(MTRAF_{p,i}, i = 1..11) \rangle$$

"NR"	"M_traffic,SLS"	"M_traffic,ULS"
"[-]"	"[kNm]"	"[kNm]"
1	12996.	19495.
2	21000.	31500.
3	21000.	31500.
4	21000.	31500.
5	21000.	31500.
6	21000.	31500.
7	21000.	31500.
8	21000.	31500.
9	21000.	31500.
10	21000.	31500.
11	34912.	52369.

(75



ANNEX N: ESTIMATING EXTERNAL LOADS: CALCULATION FILE

In this section, an estimation will be made of the external loads. This is still an estimation, since the dimensions and other properties of the final structure are still unknown (wind load, wave load and current load all depend on the dimensions of the structure). However, such an estimation is sufficient, since the purpose is to gain insight into the effects on the anchoring system without the contribution of the bridge girder. This way, awareness of the required resistance of the superstructure can be obtained.

Wind Load

Wind load can be divided into a slowly varying (static) mean wind component and a rapidly fluctuating (dynamic) component, called turbulence or wind gusts. The mean wind velocity is the basis of calculation for both [3]. For the estimation of the loads, the wind load will be taken into account as a static load. Aerodynamic effects, such as galloping, divergence, flutter and resonance are not taken into account, since the properties of the whole bridge structure are still unknown.

Furthermore, the purpose of this thesis research is to first investigate whether a suitable design can be obtained for an aesthetic floating bridge loaded by static loads. If a suitable design is found, then a continuation of this research could be to investigate the resistance of the structure to dynamic effects.

The wind load is determined according to the Eurocode (EC) NEN-EN 1991-1-4 Wind Actions. The used method for calculating the wind load is shown in Table N-1.

Wave Load

The same calculation for the wave load is used, as was done in the previous study [3]. The mean wave drift force is obtained by using the wave in the spectrum. The mean wave drift force is then expressed in terms of the significant wave height, as can be seen in . This calculation gives a time averaged value of the load from a wave on a vertical wall given by Massie & Journee. However, such a fully reflected wave is a very conservative assumption. In reality, the pontoon has a round face where the wave hits. As result, the reflection will not cause a standing wave as assumed. As a first approximation this calculation is assumed to be reasonable.

Current Load

The same calculation for the current load is used, as was done in the previous study [3]. An object in a uniform flow field, as current is often considered, is subjected to forces both in the direction of the flow (drag force) and perpendicular to the flow (lift force). Both fluctuate in time. The resultant force on an object in the flow is reasonably proportional to the velocity head times the density of the fluid. The empirical formulas are given in Table N-1. Both formulas contain static coefficients (C_D and C_L) and dynamic ones (C'_D and C'_L).

The estimated loads are shown in Table N-2. The calculations were done in Maple. The calculation files are also given in the next pages.

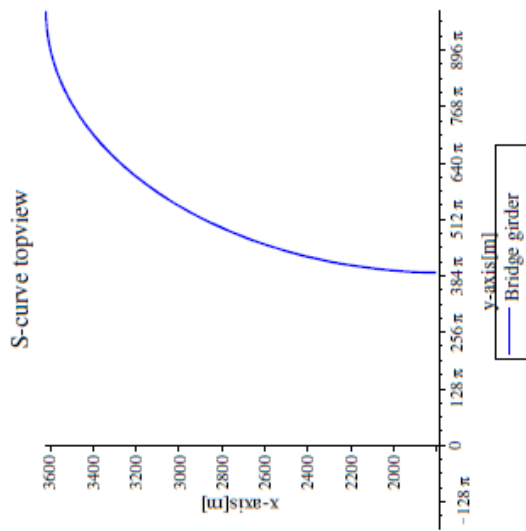
TABLE N-1 USED METHODS AND EQUATIONS FOR ESTIMATING THE LOADS

Load Type	Formula	Eq. in EC.
Wind Load	Peak velocity pressure $q_p(z) = [1 + 7 \cdot I_v(z)] \cdot \frac{1}{2} \cdot \rho \cdot v_m^2(z)$	(4.8)
	Wind force $F_w = c_s c_d \cdot \sum_{elements} c_p \cdot q_p(z_e) \cdot A_{ref}$	(5.4)
	With: $z_D, z_{0,II} =$ Height factors, both 0,05. [m] $c_D =$ Direction factor, 1,0. [-]	
Wave Load	Mean wave drift force $F = -\frac{1}{16} \cdot \rho \cdot g \cdot H_s^2$	
	with $\rho =$ Water density [kg/m ³] $H_s =$ Significant wave height [m]	
Current Load	Drag force $F_D = \frac{1}{2} \cdot \rho \cdot u^2 \cdot (C_D + C'_D) \cdot A$	
	Lift force $F_L = \frac{1}{2} \cdot \rho \cdot u^2 \cdot (C_L + C'_L) \cdot A$	
	with $\rho =$ Water density [kg/m ³]	
	$u =$ Undisturbed flow velocity [m/s]	
	$A =$ Area facing the flow [m ²]	
	$C_D, C_L =$ Static drag and lift coefficients [-]	
	$C'_D, C'_L =$ Dynamic drag and lift coefficients [-]	

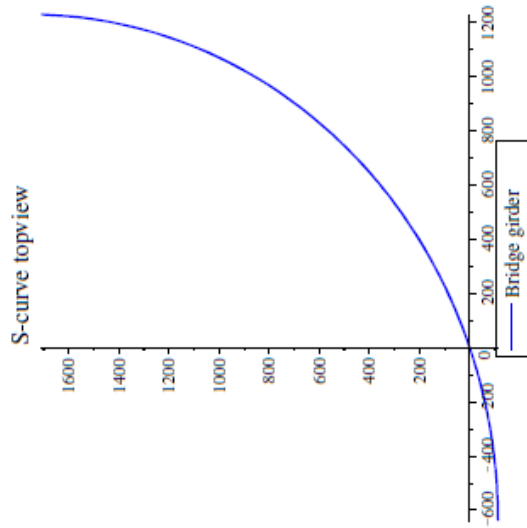
TABLE N-2 LOADS IN X-DIRECTION

Pontoon number	SLS				ULS			
	F _{wind} (kN)	F _{wave} (kN)	F _{current} (kN)	Total F _x (kN)	F _{wind} (kN)	F _{wave} (kN)	F _{current} (kN)	Total F _x (kN)
1	834	19	601	1454	1250	29	1111	2389
2	1620	19	696	2335	2477	29	1290	3796
3	1857	19	736	2613	2868	29	1365	4262
4	2026	19	769	2814	3156	29	1426	4610
5	2140	19	795	2954	3359	29	1474	4862
6	2341	19	821	3181	3688	29	1524	5241
7	2466	19	841	3326	3901	29	1561	5490
8	2548	19	857	3423	4044	29	1589	5662
9	2586	19	867	3473	4119	29	1609	5757
10	2583	19	873	3475	4124	29	1620	5774
11	4961	19	1012	5722	7514	29	1880	9422


```
= "Bridge girder", labels = ["y-axis[m]", "x-axis[m]"], labelfont = ["calibri",
12], labeldirections = ["horizontal", "vertical"] : display([Pta]);
```



```
Pba := reflect(reflect(Pta, [[0, x_hs], [5000, x_hs]]), [[y_2', 0], [y_2', 5000]]);
```




```

xp,i := bp,i;
yp,i := dp,i;
zp,i := eval(fz(sa), sa = sp,i) + frp,mi,i;
lcp,i := ⟨xp,i | yp,i | zp,i⟩; sa := sa;
end do;
xg,23 := xg,1;
bg := 10;
bdeck := 16;
Rpylon := 2.5;
Rpontoon := 15;
za := 20;

tp,top := 1; tp,bot := 1 +  $\frac{l}{50}$ ; tp,side := 0.5 +  $\frac{R_{pontoon}}{15}$ ; tpylon :=  $\frac{R_{pylon}}{15}$ ;

for i from 1 to 22 do
lp,i := drp,i,ULS + frp,mi;
end do;

hws := 2.4;

tgirder := 0.022514; αR := 90; dm := 0.4531;

dtruss := 15 · btruss := 3.5 · dtruss := 1 · ltruss := sqrt(ltruss2 + dtruss2) · dtruss;
:= ULS;

```

Vertical forces input

Vertical forces

q_{traffic} := 35;

$$F_{traffic,hfb,SLS} := \frac{1}{2} \cdot q_{traffic} \cdot l \cdot F_{traffic,hfb,ULS} := \frac{1}{2} \cdot q_{traffic,hfb,ULS} \cdot l \cdot F_{traffic,hfb} := 6;$$

$$G_{pylon,SLS} := \frac{f_z(sa)}{z_b} \cdot 28410; G_{pylon,ULS} := \gamma \cdot G_{pylon,SLS}; f_y,pylon := 460 \cdot 10^3;$$

```

qg,SLS := 149.3959;
qg,ULS := 189.7752;
qg,SLS,mid := 153.5179;
qg,ULS,mid := 194.7215;

```

General Input

γ_{pos} := 0.9;

γ_g := 1.2;

γ_q := 1.5;

E_s := 210 · 10⁶; G_s := 79.3 · 10⁶; E_m := 195 · 10⁶;

p_w := 1025; p_s := 7850; p_c := 2500; p_b := 2000; p_a := 1.25;

Horizontal Force Expressions per Direction

Input

C_{d,gw} := piecewise(1 ≤ β_{BG} < 2, 1, 1 - (β_{BG} - 1) · (1.1 - 0.6), 2 ≤ β_{BG} < 4, 0.6 - (β_{BG} - 2) · 0.5 · (0.6 - 0.35), β_{BG} ≥ 4, 0.35);

β := 20;

Wind load according to NEN-EN 1991-1-4:

$$q_{p,g,SLS} := z_e \rightarrow \left[1 + \frac{7 \cdot k_1}{c_0 \cdot \ln\left(\frac{z_e}{z_0}\right)} \right] \cdot \left(\frac{1}{2}\right)$$

$$\left[p_d \cdot \left(0.19 \cdot \left(\frac{z_0}{z_{0,H}} \right) \cdot \ln\left(\frac{z_e}{z_0}\right) \cdot c_{0,y_b,SLS} \right)^2 \right] \cdot \frac{1}{1000};$$

$$q_{p,p,SLS} := ze \rightarrow \left(1 + \frac{7 \cdot k_I}{c_0 \cdot \ln\left(\frac{0.5 \cdot ze}{z_0}\right)} \right) \cdot \left(\frac{1}{2}\right)$$

$$q_{p,p,ULS} := ze \rightarrow \left(1 + \frac{7 \cdot k_I}{c_0 \cdot \ln\left(\frac{ze}{z_0}\right)} \right) \cdot \left(\frac{1}{2}\right)$$

$$q_{p,p,ULS} := ze \rightarrow \left(\frac{p_a \cdot \left(0.19 \cdot \left(\frac{z_0}{z_{0,H}} \cdot \ln\left(\frac{ze}{z_0}\right) \cdot c_0 \cdot v_{b,ULS} \right) \right)^2}{1000} \right) \cdot \left(\frac{1}{2}\right)$$

$$q_{p,p,ULS} := ze \rightarrow \left(1 + \frac{7 \cdot k_I}{c_0 \cdot \ln\left(\frac{0.5 \cdot ze}{z_0}\right)} \right) \cdot \left(\frac{1}{2}\right)$$

$$z_0 := 0.05; z_{0,H} := 0.05; c_0 := 1.0; k_I := 1.0;$$

$$:= evalif\left(\left(\frac{(1 - K_{prob}) \cdot \ln(-\ln(1 - P_{prob}))}{1 - K_{prob} \cdot \ln(-\ln(0.99))}\right)^{n_{prob}}\right)$$

0.9033175203

$$v_{b,\alpha,1,ULS} := 21; v_{b,\alpha,2,ULS} := 26; v_{b,\alpha,3,ULS} := 26; v_{b,\alpha,4,ULS} := 23;$$

$$v_{b,\alpha,5,ULS} := 24; v_{b,\alpha,6,ULS} := 28; v_{b,\alpha,7,ULS} := 35; v_{b,\alpha,8,ULS} := 35;$$

$$v_{b,\alpha,9,ULS} := 35; v_{b,\alpha,10,ULS} := 33; v_{b,\alpha,11,ULS} := 33; v_{b,\alpha,12,ULS} := 23;$$

Extreme values of wind wave height per direction (Hermans, 2014, Figure 4-5):

$$H_{s,wpw,\alpha,1,ULS} := 1.01; H_{s,wpw,\alpha,2,ULS} := 1.62; H_{s,wpw,\alpha,3,ULS} := 1.81;$$

$$H_{s,wpw,\alpha,4,ULS} := 1.49; H_{s,wpw,\alpha,5,ULS} := 1.4; H_{s,wpw,\alpha,6,ULS} := 1.57;$$

$$H_{s,wpw,\alpha,7,ULS} := 2.22; H_{s,wpw,\alpha,8,ULS} := 2.24; H_{s,wpw,\alpha,9,ULS} := 2.34;$$

$$H_{s,wpw,\alpha,10,ULS} := 2.13; H_{s,wpw,\alpha,11,ULS} := 1.83; H_{s,wpw,\alpha,12,ULS} := 1.00;$$

Significant wave height (Hermans, 2014, Figure 4-6):

$$H_{s,sw,\alpha,1,ULS} := 0.01; H_{s,sw,\alpha,2,ULS} := 0.01; H_{s,sw,\alpha,3,ULS} := 0.01;$$

$$H_{s,sw,\alpha,4,ULS} := 0.01; H_{s,sw,\alpha,5,ULS} := 0.01; H_{s,sw,\alpha,6,ULS} := 0.01;$$

2 - constant current in the mid part of the fjord
 3 - constant current asymmetrical about fjord's mid axis

$$u_{cl,\alpha,1} := 1.27; u_{cl,\alpha,2} := 1.27; u_{cl,\alpha,3} := 1.27; u_{cl,\alpha,4} := 1.27; u_{cl,\alpha,5} := 1.27;$$

$$u_{cl,\alpha,6} := 1.27; u_{cl,\alpha,7} := 1.27; u_{cl,\alpha,8} := 1.27; u_{cl,\alpha,9} := 1.27;$$

$$u_{cl,\alpha,10} := 1.27; u_{cl,\alpha,11} := 1.27; u_{cl,\alpha,12} := 1.27;$$

```

u_{c2,\alpha,1} := 0.875 : u_{c2,\alpha,2} := 0.875 : u_{c2,\alpha,3} := 0.875 : u_{c2,\alpha,4} := 0.875 : u_{c2,\alpha,5}
:= 0.875 : u_{c2,\alpha,6} := 0.875 : u_{c2,\alpha,7} := 0.875 : u_{c2,\alpha,8} := 0.875 : u_{c2,\alpha,9}

```

```

l_{g,i,\alpha,8} := l_{g,i,\alpha,2}
l_{g,i,\alpha,9} := l_{g,i,\alpha,3}
l_{g,i,\alpha,10} := l_{g,i,\alpha,4}

```

```

end do;

```

Length Expressions and Forces

```

y_{p,0} := 0;
x_{p,0} := 0;
for i from 1 to 22 do
for n from 1 to 6 do
l_{gp,i} := \frac{(l_{g,i} + l_{g,(i+1)})}{2};
l_{g} := l_{gp,i};
sa := s_{p,i};
\alpha_{b,i} := \arctan\left(\frac{(y_{p,i} - y_{p,(i-1)})}{(x_{p,i} - x_{p,(i-1)})}\right);
ss_{b,i} := \sqrt{(x_{p,i} - x_{p,(i-1)})^2 + (y_{p,i} - y_{p,(i-1)})^2};
\alpha_{d,i,n} := \text{abs}\left(\text{evalf}\left(\left(\alpha_n - \alpha_{b,i} + \frac{\pi}{6}\right)\right)\right);
if \alpha_{d,i,n} > \text{evalf}\left(\frac{\pi}{2}\right) then \alpha_{d,i,n} := \left(\alpha_n - \alpha_{b,i} - \frac{\pi}{2} + \frac{\pi}{6}\right); l_{g,i,\alpha,n}
:= \text{abs}\left(\text{evalf}\left(ss_{b,i} \cdot \cos(\alpha_{d,i,n})\right)\right); else \alpha_{d,i,n} := \left(\alpha_n - \alpha_{b,i} + \frac{\pi}{6}\right); l_{g,i,\alpha,n}
:= \text{abs}\left(\text{evalf}\left(ss_{b,i} \cdot \sin(\alpha_{d,i,n})\right)\right); end if;
end do;
l_{g,i,\alpha,7} := l_{g,i,\alpha,1};

```

```

for n from 1 to 12 do
l_{g,23,\alpha,n} := l_{g,1,\alpha,n};
end do;

```

Force Expressions

```

for i from 1 to 22 do
fr_{p,i,SLS} := l_{p,i} - dr_{p,i,SLS};
fr_{p,i,nt,SLS} := l_{p,i} - dr_{p,i,nt,SLS}; l_{p,i}
:= dr_{p,i,ULS} + fr_{p,nt};
end do;
for n from 1 to 12 do
for i from 1 to 22 do
v_{b,SLS} := c_{prob}^{v_{b,\alpha,n,ULS}} \cdot v_{b,ULS}^{v_{b,\alpha,n,ULS}} := v_{b,\alpha,n,ULS};
sa := s_{p,i}; l_{gp,i,\alpha,n} := \frac{(l_{g,i,\alpha,n} + l_{g,(i+1),\alpha,n})}{2}; l_{g} := l_{gp,i};
l_{gp,i} := \frac{h_{gp,i}}{90}; h := h_{gp,i}; z_{BG,i} := fz(s_{p,i}) + \frac{h}{2} + fr_{p,i,nt,SLS};
F_{wind,BG,\alpha,SLS} := q_{p,g,SLS}(z_{BG,i}) \cdot l_{gp,i,\alpha,n} \cdot (h_g + h_{ws}) \cdot C_{d,gw};
F_{wind,BG,\alpha,ULS} := q_{p,g,ULS}(z_{BG,i}) \cdot l_{gp,i,\alpha,n} \cdot (h_g + h_{ws}) \cdot C_{d,gw};
F_{wind,irass,\alpha,SLS} := \frac{2 \cdot q_{p,g,SLS}(z_{BG,i}) \cdot l_{gp,i,\alpha,n} \cdot (d_{irass} \cdot h_{irass} + d_{irass,d,irass})}{a_{irass}} \cdot C_{d,irass};

```

$$F_{wind, truss, \alpha, ULS} := \frac{2 \cdot q_{p, g, ULS}(z_{BG, i}) \cdot l_{gp, i, \alpha, n}}{a_{truss}} \cdot (d_{truss} \cdot h_{truss} + d_{truss, dia, truss, dia}) \cdot C_{d, truss}$$

$$l_g := l_{gp, i}$$

$$h_g := \frac{l_{gp, i}}{90}$$

```

wind, traffic, \alpha, SLS := wind, g, i, \alpha, n, SLS
F_{wind, g, i, \alpha, n, ULS} := \gamma \cdot (F_{wind, BG, \alpha, ULS} + F_{wind, m, \alpha, ULS} + F_{wind, truss, \alpha, ULS})
q_{wind, g, i, \alpha, n, ULS} := \frac{l_{gp, i, \alpha, n}}{l_{wind, g, i, \alpha, ULS}}
F_{wind, py, i, \alpha, n, SLS} := q_{p, p, SLS}(z_{BG, i}) \cdot f_z(s_{p, i}) \cdot 2 \cdot R_{pylon, d, pyw} \cdot C_{d, pyw}
F_{wind, py, i, \alpha, n, ULS} := \gamma \cdot q_{p, p, ULS}(z_{BG, i}) \cdot f_z(s_{p, i}) \cdot 2 \cdot R_{pylon, d, pyw} \cdot C_{d, pyw}
sa := 'sa'
end do;
end do;

for n from 1 to 12 do
for i from 1 to 22 do
H_{s, ww} := H_{s, ww, \alpha, 1, ULS}
H_{s, sw} := H_{s, sw, \alpha, 1, ULS}
u_{c1, ULS} := u_{c1, \alpha, n}
u_{c2, ULS} := u_{c2, \alpha, n}
u_{c3, ULS} := u_{c3, \alpha, n}
u_{c1, SLS} := c_{prob, c1, \alpha, n}
u_{c2, SLS} := c_{prob, c2, \alpha, n}
u_{c3, SLS} := c_{prob, c3, \alpha, n}
dr_p := dr_{p, i, SLS}
F_{current1, ULS} := \frac{1}{2} \cdot \gamma \cdot \frac{\rho \cdot u_{c1, ULS}^2 \cdot C_{d, pc} \cdot 2 \cdot R_{pontoon} \cdot 10}{1000}
F_{current2, ULS} := \frac{1}{2} \cdot \gamma \cdot \frac{\rho \cdot u_{c2, ULS}^2 \cdot C_{d, pc} \cdot 2 \cdot R_{pontoon} \cdot \min(dr_{p, i, ULS} - 10, 20)}{1000}
F_{current3, ULS} := \frac{1}{2} \cdot \gamma \cdot \frac{\rho \cdot u_{c3, ULS}^2 \cdot C_{d, pc} \cdot 2 \cdot R_{pontoon} \cdot \max(dr_{p, i, ULS} - 30, 0)}{1000}
F_{FC, eq, i, \alpha, n, SLS} := (F_{current, SLS} + F_{current2, SLS} + F_{current3, SLS})
F_{FC, eq, i, \alpha, n, ULS} := (F_{current1, ULS} + F_{current2, ULS} + F_{current3, ULS})
z_{FC1} := 5;
z_{FC2} := 10 + \min(dr_{p, i, SLS} - 10, 10);
z_{FC3} := 30 + \frac{(dr_{p, i, SLS} - 30)}{2};
z_{FC, i, \alpha, n, eq} := \frac{(F_{current1, SLS} \cdot z_{FC1} + F_{current2, SLS} \cdot z_{FC2} + F_{current3, SLS} \cdot z_{FC3})}{F_{current1, SLS} + F_{current2, SLS} + F_{current3, SLS}}
F_{sw, i, \alpha, n, SLS} := \frac{1}{16 \cdot 1000} \cdot \rho \cdot 9.81 \cdot H_{s, ww}^2 \cdot R_{pontoon}
F_{sw, i, \alpha, n, ULS} := \gamma \cdot F_{sw, i, \alpha, n, SLS}
F_{sw, i, \alpha, n, SLS} := \frac{1}{16 \cdot 1000} \cdot \rho \cdot 9.81 \cdot H_{s, sw}^2 \cdot R_{pontoon}
F_{sw, i, \alpha, n, ULS} := \gamma \cdot F_{sw, i, \alpha, n, SLS}
F_{wa, i, \alpha, n, SLS} := F_{sw, i, \alpha, n, SLS} + F_{wa, i, \alpha, n, SLS}
F_{wa, i, \alpha, n, ULS} := F_{sw, i, \alpha, n, ULS} + F_{wa, i, \alpha, n, ULS}
h_g := h_g

```



```

l_g := l';
dr_p := dr';
end do;
end do;

```

```

G_tot,i, ULS := G_ballast,i, ULS + G_p,i, ULS + G_pylon, ULS + (q_g, ULS) * l_gp,i';
l := l';
end do;

```

```

end do;

```



```

F_Htop,i, alpha_n, ULS := F_wa,i, alpha_n, ULS + F_FC, eq, i, alpha_n, ULS + F_wind, ps, i, alpha_n, ULS
+ F_wind, g, i, alpha_n, ULS';
end do;
end do;

```

```

+ h_gp,i) + G_p,i, SLS * ( (l_p,i) / 2 + fz(s_p,i) + h_gp,i) + G_ballast,i, SLS * ( l_p,i + fz(s_p,i)
+ h_gp,i - t_p,bot - (h_b,i) / 2 ) - h_gp,i - fz(s_p,i) );

```

Calculation Ballast Height; Simple Cylindrical, All

Anchored

Vertical forces subpart;

```

for i from 1 to 22 do

```

```

s := s_p,i; l := l_gp,i; dr_p, ULS := dr_p, ULS_p_p; l := l';

```

```

G_pylon,i, SLS := G_pylon, SLS; G_pylon,i, ULS := G_pylon, ULS';

```

```

F_pontoon,i, SLS := q_g, SLS * l + G_pylon, SLS; F_pontoon,i, ULS := q_g, ULS * l
+ G_pylon, ULS';

```

```

G_ballast,i, SLS := (p_b * h_b * pi * (R_pontoon - t_p,side) ^ 2) * 9.81
/ 1000;

```

```

G_ballast,i, ULS := G_ballast,i, SLS';

```

```

G_p,i, SLS

```

```

:= 1 / 1000 * (rho_c * (l_p,i * pi * R_pontoon ^ 2 * (l_p,i - t_p,bot - t_p,top) * pi * (R_pontoon
- t_p,side) ^ 2) * 9.81)';

```

```

G_p,i, ULS := G_p,i, SLS';

```

```

G_tot,i, SLS := G_ballast,i, SLS + G_p,i, SLS + G_pylon, SLS + (q_g, SLS) * l_gp,i';

```

```

G_tot,i, ULS := G_ballast,i, ULS + G_p,i, ULS + G_pylon, ULS + (q_g, ULS) * l_gp,i';

```

```

dr_p,i, ULS := solve dr_p,i, ULS = (V_p,i,sub, ULS) / (pi * R_pontoon ^ 2), dr_p,i, ULS';

```

```

end do;

```

```

G_tot,i, SLS :=

```

```

+ h_gp,i) + G_p,i, SLS * ( (l_p,i) / 2 + fz(s_p,i) + h_gp,i) + G_ballast,i, SLS * ( l_p,i + fz(s_p,i)
+ h_gp,i - t_p,bot - (h_b,i) / 2 ) - h_gp,i - fz(s_p,i) );

```

```

z_G,i, ULS := evalf ( G_tot,i, ULS * ( (q_g, ULS) * l_gp,i / 2 + G_pylon,i, ULS * (fz(s_p,i)
+ h_gp,i) + G_p,i, ULS * ( (l_p,i) / 2 + fz(s_p,i) + h_gp,i) + G_ballast,i, ULS * ( l_p,i + fz(s_p,i)
+ h_gp,i - t_p,bot - (h_b,i) / 2 ) - h_gp,i - fz(s_p,i) ) );

```

```

+ h_gp,i) + G_p,i, ULS * ( (l_p,i) / 2 + fz(s_p,i) + h_gp,i) + G_ballast,i, ULS * ( l_p,i + fz(s_p,i)
+ h_gp,i - t_p,bot - (h_b,i) / 2 ) - h_gp,i - fz(s_p,i) );

```

```

V_p,i, sub, SLS := (F_pontoon,i, SLS + G_p,i, SLS + G_ballast,i, SLS) /
(9.81 * 1000);

```

```

V_p,i, sub, mt, SLS := (F_pontoon,i, SLS - q_traffic_gp,i * l + G_p,i, SLS + G_ballast,i, SLS) /
(9.81 * 1000);

```

```

V_p,i, sub, ULS := (F_pontoon,i, ULS + G_p,i, ULS + G_ballast,i, ULS) /
(9.81 * 1000);

```

```

dr_p,i, ULS := solve dr_p,i, ULS = (V_p,i,sub, ULS) / (pi * R_pontoon ^ 2), dr_p,i, ULS';

```

```

dr_{p,i,SLS} := evalf  $\left( \frac{V_{p,i,sub,SLS}}{\pi \cdot R_{pontoon}^2} \right)$ ;
dr := evalf  $\left( \frac{V_{p,i,sub,nt,SLS}}{\pi \cdot R_{pontoon}^2} \right)$ ;

for i from 1 to 22 do
l := l_{gp,i};
sa := s_{p,i};
h_g := h_{gp,i};
y_p := sqrt(R_{pontoon}^2 - x_p^2);
A_{inmm} :=  $\frac{1}{2} \cdot y_p \cdot \tan(\phi_x) \cdot y_p$ ;
A_{em} :=  $\frac{1}{2} \cdot y_p \cdot \tan(\phi_x) \cdot y_p$ ;
ac_{inmm} :=  $\cos\left(\frac{2}{3} \cdot \phi_x\right) \cdot \sqrt{\left(y_p \cdot \frac{\tan(\phi_x)}{3}\right)^2 + \left(\frac{2}{3} \cdot y_p\right)^2}$ ;
ac_{em} :=  $\cos\left(\frac{2}{3} \cdot \phi_x\right) \cdot \sqrt{\left(y_p \cdot \frac{\tan(\phi_x)}{3}\right)^2 + \left(\frac{2}{3} \cdot y_p\right)^2}$ ;
C_{inmm} := -A_{inmm} \cdot (ac_{inmm});
C_{em} := +A_{em} \cdot (ac_{em});
y_{bf,i} := evalf  $\left( \frac{C_{inmm} + C_{em}}{dr_{p,i,SLS} \cdot y_p} \right)$ ;
x_p := 0;
y_{bmx} := y_{bf,i};
x_p := x_p;
y_{b,i} := 0.4 \cdot y_{bmx};
BGd_i :=  $\left( \frac{dr_{p,i,SLS}}{2} - z_{G,i,SLS} \right)$ ;

```

```

y_{BG,i} := evalf  $\left( -\sin(\phi_x) \cdot \left( \frac{dr_{p,i,SLS}}{2} - z_{G,i,SLS} \right) \right)$ ;
a_{B,i} := (y_{b,i} - y_{BG,i});
M_{x,BU,i} := evalf(G_{tot,i,SLS} \cdot a_{B,i});

```

end do;

```

kr_{x,BU,1}
-  $\frac{1}{\phi_x} \left( (22599.35738 h_{k,1} + 1.302214818 \cdot 10^5) \left( \frac{2.000000000 \tan(\phi_x) \cos(0.6666666667 \phi_x) \sqrt{225 \tan(\phi_x)^2 + 900}}{3.179587830 h_{k,1} + 18.32134568} \right. \right.$ 
 $\left. \left. + 1. \sin(\phi_x) \left( 1.589793915 h_{k,1} + 15.86100617 \right. \right. \right.$ 
 $\left. \left. - \frac{1}{22599.35734 h_{k,1} + 1.302214816 \cdot 10^5} \left( 1. (29418.14486 + (11365.82312 h_{k,1} \right. \right. \right.$ 
 $\left. \left. + 1.073405107 \cdot 10^5) (1.589793916 h_{k,1} + 17.78635662) + 11233.53422 h_{k,1} (2.615996075 h_{k,1} \right. \right.$ 
 $\left. \left. + 27.42893898) \right) \right) \right)$ 

```

Overtuning Angle Anchored Pontoons

```

k_{AN} := 1237.8556; k_{BG} := 0; kr_{BG} := 0; \phi_x := \phi_x;

```

for i from 1 to 22 do

```

gvd_r := piecewise(i ≤ 5, 11, 5 < i ≤ 10, 10 < i ≤ 12, 9, 12 < i ≤ 17, 10, 17 < i ≤ 22, 11);

```

```

l := l_{gp,i}; sa := s_{p,i}; dr_{p,i,SLS} := dr_{p,i,SLS};

```

```

aa :=  $\frac{h_{gp,i}}{2} + \frac{fz(s_{p,i})}{2}$ ; bb :=  $\frac{fz(s_{p,i})}{2} + fr_{p,i,SLS}$ ; cc := z_a; dd

```

```

:= z_{FC,i,\alpha,(gvd_r),eq} - z_a;

```

```

eq1 := M_{BG} = kr_{BG} \cdot \phi_x;

```

```

eq2 := M_{BU} = kr_{BU} \cdot \phi_x;

```

(8)

$$V_{b, scaa, i} := \frac{\left(\rho_b \cdot (h_b) \cdot \pi \cdot (R_{pontonoon} - t_{p, side})^2 \cdot 9.81 \right)}{1000};$$

```

FRW_{p, i, scaa, ULS} := ( |F_{wind, g, scaa, i, \alpha} (gvdtr), ULS| |F_{wind, py, scaa, i, \alpha} (gvdtr), ULS|
|F_{wa, scaa, i, \alpha} (gvdtr), ULS| |F_{FC, eq, scaa, i, \alpha} (gvdtr), ULS| |F_{Htop, scaa, i, \alpha} (gvdtr), ULS| ) : 1 :=
\gamma_p \cdot h_b := H_b;
end do;

```

```

CRWT := ( "NR"|"L_p"|"Hb"|"DR_p_SLS"|"FR_SLS"|"FR_NT_SLS"|"kr_BU" );
FRWTSLS := ( "NR"|"Fwind_g"|"Fwind_py"|"F_WA"|"F_FC"|"F_Htop" );
FRWTULS := ( "NR"|"Fwind_g"|"Fwind_py"|"F_WA"|"F_FC"|"F_Htop" );

```

```

( CRWT, CRW_{p, 1, scaa}, CRW_{p, 2, scaa}, CRW_{p, 3, scaa}, CRW_{p, 4, scaa}, CRW_{p, 5, scaa},
CRW_{p, 6, scaa}, CRW_{p, 7, scaa}, CRW_{p, 8, scaa}, CRW_{p, 9, scaa}, CRW_{p, 10, scaa},
CRW_{p, 11, scaa} )

```

"NR"	"L_p"	"Hb"	"DR_p_SLS"	"FR_SLS"	"FR_NT_SLS"	"kr_BU"
1	35.927	4.326007323	32.07626592	3.85070091	4.54022329	1.014834534 10 ⁶
8	95.949	19.73824102	91.11211322	4.83732025	5.82217634	5.179197235 10 ⁶
9	98.412	20.34947250	93.53183620	4.88034019	5.86519628	5.414494565 10 ⁶
10	99.797	20.66823813	94.88553457	4.91106601	5.89592210	5.515691379 10 ⁶
11	132.38	29.15690926	126.8834536	5.4976114	6.9748956	1.039189078 10 ⁷

```

( FRWTSLS, FRW_{p, 1, scaa, SLS}, FRW_{p, 2, scaa, SLS}, FRW_{p, 3, scaa, SLS}, FRW_{p, 4, scaa, SLS},
FRW_{p, 5, scaa, SLS}, FRW_{p, 6, scaa, SLS}, FRW_{p, 7, scaa, SLS}, FRW_{p, 8, scaa, SLS},
FRW_{p, 9, scaa, SLS}, FRW_{p, 10, scaa, SLS}, FRW_{p, 11, scaa, SLS} );

```

"NR"	"Fwind_g"	"Fwind_py"	"F_WA"	"F_FC"	"F_Htop"
1	803.6661554	307.3494492	19.23066563	600.6872134	1454.318979
2	1490.709299	129.1085005	19.23066563	695.9253196	2334.973785
3	1624.397702	232.6515586	19.23066563	736.3489768	2612.628903
4	1692.694375	333.1698232	19.23066563	768.9228570	2814.017721
5	1713.400099	426.5822260	19.23066563	794.9939475	2954.206938
6	1830.110938	510.5130720	19.23066563	821.4259848	3181.280660
7	1882.227112	583.4152585	19.23066563	841.4505893	3326.323625
8	1903.341408	644.2235293	19.23066563	856.6551255	3423.450728
9	1894.292375	692.1890413	19.23066563	867.1465721	3472.858654
10	1856.069670	726.7900611	19.23066563	873.0159440	3475.106541
11	3845.809308	844.7561069	19.23066563	1011.752676	5721.548757

(10)

```

( FRWTULS, FRW_{p, 1, scaa, ULS}, FRW_{p, 2, scaa, ULS}, FRW_{p, 3, scaa, ULS},
FRW_{p, 4, scaa, ULS}, FRW_{p, 5, scaa, ULS}, FRW_{p, 6, scaa, ULS}, FRW_{p, 7, scaa, ULS},
FRW_{p, 8, scaa, ULS}, FRW_{p, 9, scaa, ULS}, FRW_{p, 10, scaa, ULS}, FRW_{p, 11, scaa, ULS} );

```

(11)

"NR"	"Fwind_g"	"Fwind_py"	"F_WA"	"F_FC"	"F_Htop"
1	1193.110535	56.49926923	28.84599845	1111.008487	2389.464289
2	2239.823096	237.3368798	28.84599845	1289.828314	3795.834288
3	2440.692823	427.6774563	28.84599845	1365.069982	4262.286259
4	2543.310057	612.4576305	28.84599845	1425.783265	4610.396951
5	2574.420857	784.1752799	28.84599845	1474.444380	4861.886515
6	2749.781428	938.4632245	28.84599845	1523.670827	5240.761478
7	2828.087112	1072.477464	28.84599845	1561.020530	5490.431104
8	2859.811800	1184.259765	28.84599845	1589.411556	5662.329119
9	2846.215431	1272.433549	28.84599845	1609.040602	5756.535580
10	2788.784986	1336.039724	28.84599845	1620.075016	5773.745724
11	5960.610563	1552.893714	28.84599845	1879.786232	9422.136507

ANNEX O: COMPUTATIONAL MODEL SUBSTRUCTURE EXAMPLE 3 (WITH LOADS)

In the previous sections, the anchoring system was modeled to investigate its behavior when loaded under self-weight (see ANNEX J: Computational Model Substructure Example 1 (Fixed Supports) and ANNEX K: Computational Model Substructure Example 2 (Adjusted Prestressing)). In this section, external loads, which are calculated in ANNEX N: Estimating External Loads, will be applied to the system and the new behavior will be investigated.

O.1 Assumptions Model 3

In this section, the model from ANNEX K: Computational Model Substructure Example 2 (Adjusted Prestressing) is refined by the following adjustments:

- In addition to the self-weight, the anchoring system will also be loaded by horizontal external loads

The remaining assumptions of the previous model, also given in section J.1 and K.1, remain the same:

- All degrees of freedom of the supports for the main anchoring cables are fixed
- All degrees of freedom of the supports at the pontoons are fixed, except the displacement in x-and y-direction
- All anchoring cables have the same cross sectional area ($d=500$ mm)
- The input prestressing force for the main anchoring cables is 10 000 kN (arbitrary)
- No bridge girder is modeled, only the anchoring system
- Reduced weight of steel cables submerged in water
- Adjusted pretensioning in lateral anchoring cables

O.2 Input

All properties of the model remain the same as the previous model, except the few properties mentioned below (supports of pontoons and additional horizontal external loads). The coordinates of the nodes, the material properties, submerged cable weight and the prestressing input can be found in respectively sections J.2.1, J.2.2, K.2.1 and K.2.3.

Horizontal External Loads

The horizontal loads were calculated in ANNEX N: Estimating External Loads. Since the purpose of this modeling is to investigate the displacements, the characteristic loads will be inputted to study the behavior of the anchoring system in serviceability limit state (SLS). These characteristic loads are shown in . In the table only the loads on 11 pontoons are shown, because the anchoring system is rotationally symmetric. The total $F_{k,x}$ will be applied to the nodes N49 to N70, see Figure O-1. Since the wind and wave loads are maximal in 240 degrees relative to the north, see respectively Figure 2-6 and Figure 2-8, the loads are also applied in this direction. 240 degrees relative to the north is parallel to the fjord, in outward direction.

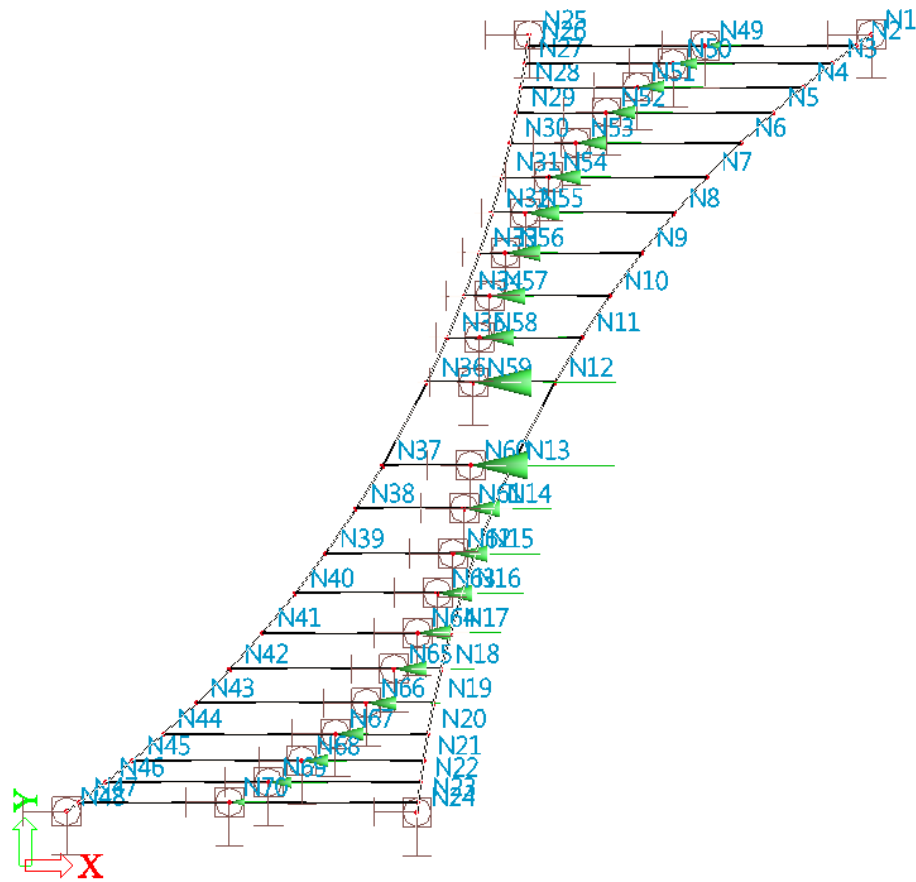


FIGURE O-1 APPLICATION HORIZONTAL LOADS ON ANCHORING SYSTEM

TABLE O-1 SLS LOAD INPUT

Pontoon number	$F_{k,wind, girder}$ (kN)	$F_{k,wind, pylon}$ (kN)	$F_{k,wind, total}$ (kN)	$F_{k,wave}$ (kN)	$F_{k,current}$ (kN)	$F_{k,current and wave}$ (kN)	Total $F_{k,x}$ (kN)
1	804	31	835	19	601	620	1455
2	1491	129	1620	19	696	715	2335
3	1624	233	1857	19	736	755	2612
4	1693	333	2026	19	769	788	2814
5	1713	427	2140	19	795	814	2954
6	1830	511	2341	19	821	840	3181
7	1882	583	2461	19	841	860	3325
8	1900	644	2544	19	857	876	3420
9	1894	692	2586	19	867	886	3472
10	1856	728	2584	19	873	892	3476
11	3846	845	4691	19	1012	1031	5722

O.3 Results and Evaluation

O.3.1 Deformed Structure

The deformed structure is shown below from different angles in Figure O-2, Figure O-3, Figure O-4 and Figure O-5.

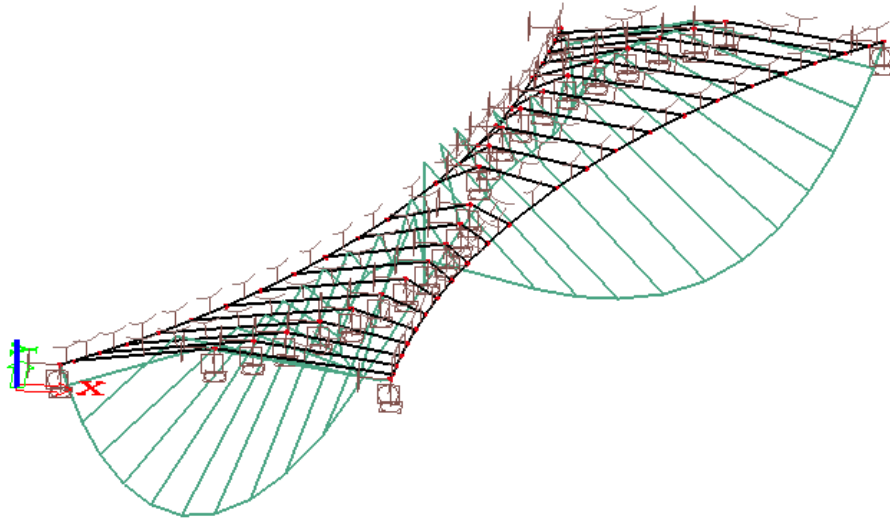


FIGURE O-2 DEFORMED STRUCTURE 3D VIEW

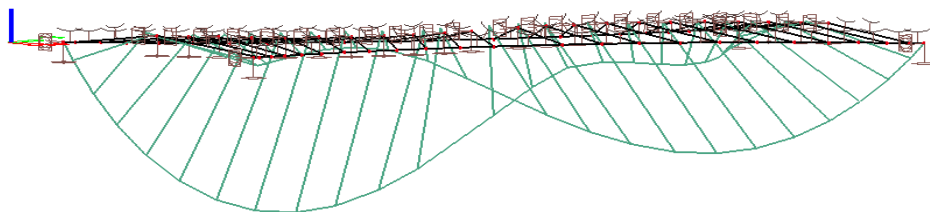


FIGURE O-3 DEFORMED STRUCTURE 3D VIEW (2)

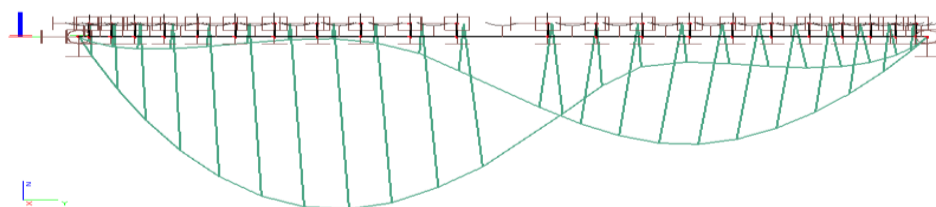


FIGURE O-4 DEFORMED STRUCTURE IN Y-Z PLANE

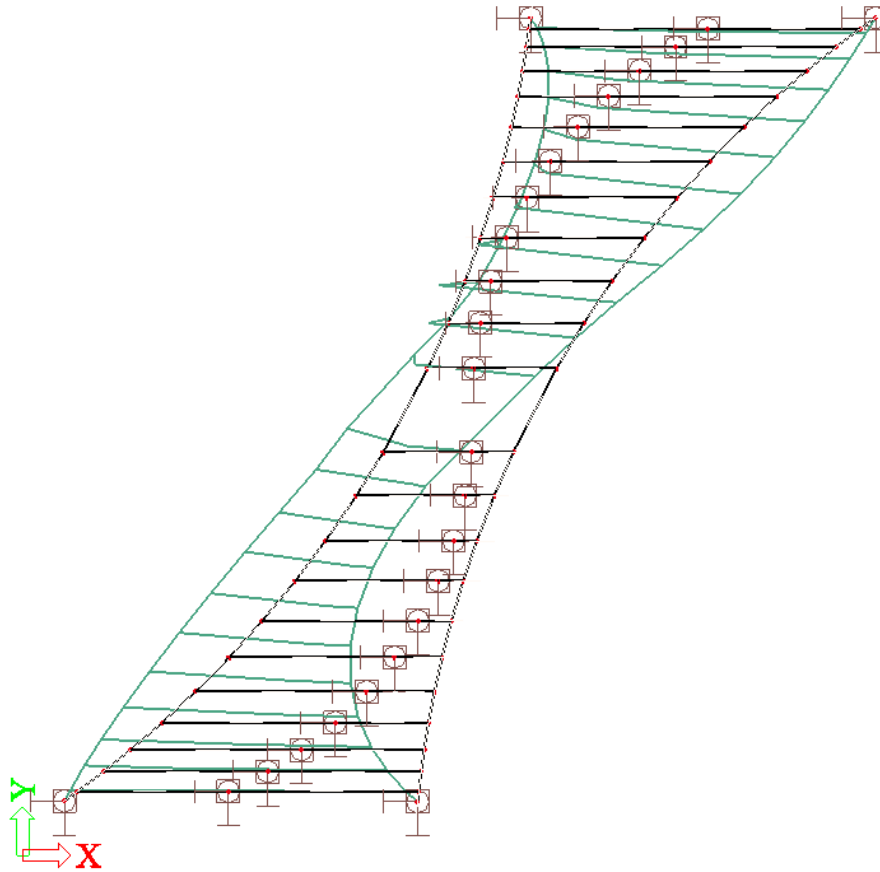


FIGURE O-5 DEFORMED STRUCTURE IN TOP VIEW/ X-Y PLANE

O.3.2 Displacement of Nodes

The nodes at the location of the pontoons can displace in x- and y-directions. The displacement of the nodes due to self-weight and horizontal loads in x- and y-direction is shown respectively in Figure O-6 and Figure O-7.

It can be seen that in x-direction, all nodes at the pontoons displace in the same direction as the one of the applied horizontal load. In Table O-2, the displacements due to solely the self-weight and the displacements due to the self-weight and the additional horizontal loads are compared. It can be seen that when the structure is also subjected to external horizontal loads, a maximum increase of the displacements in x-direction of 41,7 meters occurs. This is equal to a ratio of $L/89$ with $L=3702$ meters.

The displacements in y-direction are also given in Table O-2 and shown in Figure O-7. Similar to the case where the anchoring system is only loaded by its self-weight, the nodes of the pontoons tend to move to the center of the structure. However, if the displacement due to only the self-weight is compared to the displacement due to self-weight and external load, it can be seen that the system behaves differently. The bridge parts in the center will tend to move in positive y-direction (upwards) and the bridge parts at the sides near the shores will tend to move in negative y-direction (downwards). Overall, the displacements in y-direction are much smaller than the displacements in x-direction. The maximum increase of the displacements in y-direction is 4,3 meters.

TABLE O-2 COMPARISON PREVIOUS MODEL 2 (ANNEX D) AND CURRENT MODEL 3

Pontoon Number	Model 2 (only SW)		Model 3 (SW+Fx)		Δu_x (m)	Δu_y (m)
	u_x (m)	u_y (m)	u_x (m)	u_y (m)		
1	-6,1	-1,2	-26,5	-1,6	-20,4	-0,4
2	22,6	-3,5	-13,7	-4,4	-36,3	-0,9
3	13,6	-5,6	-14,5	-6,7	-28,1	-1,1
4	20,5	-7,4	-6,9	-8,3	-27,4	-0,9
5	28,2	-8,8	-0,7	-9,0	-28,9	-0,2
6	30,5	-9,5	-2,0	-8,4	-32,5	1,1
7	27,5	-9,3	-8,9	-6,8	-36,4	2,5
8	18,8	-8,5	-20,2	-4,8	-39,0	3,7
9	2,4	-7	-36,2	-2,8	-38,6	4,2
10	3,5	-4,5	-36,2	-0,2	-39,7	4,3
11	-0,8	-1,3	-41,2	2,7	-40,4	4,0
12	-2,7	-0,1	-44,4	4,1	-41,7	4,2
13	4,8	3,4	-35,2	7,7	-40,0	4,3
14	-11,9	5,9	-50,7	9,6	-38,8	3,7
15	-24,8	7,3	-60,8	10,5	-36,0	3,2
16	-31,3	8,1	-62,8	10,3	-31,5	2,2
17	-33,2	8,2	-59,8	9,3	-26,6	1,1
18	-30	7,7	-52,4	7,6	-22,4	-0,1
19	-21,7	6,4	-41,8	5,6	-20,1	-0,8
20	-15,1	4,6	-37,3	3,7	-22,2	-0,9
21	-22,6	2,9	-57,6	2,1	-35,0	-0,8
22	12,7	0,8	-8,7	0,5	-21,4	-0,3

*maximum values are indicated by the red color

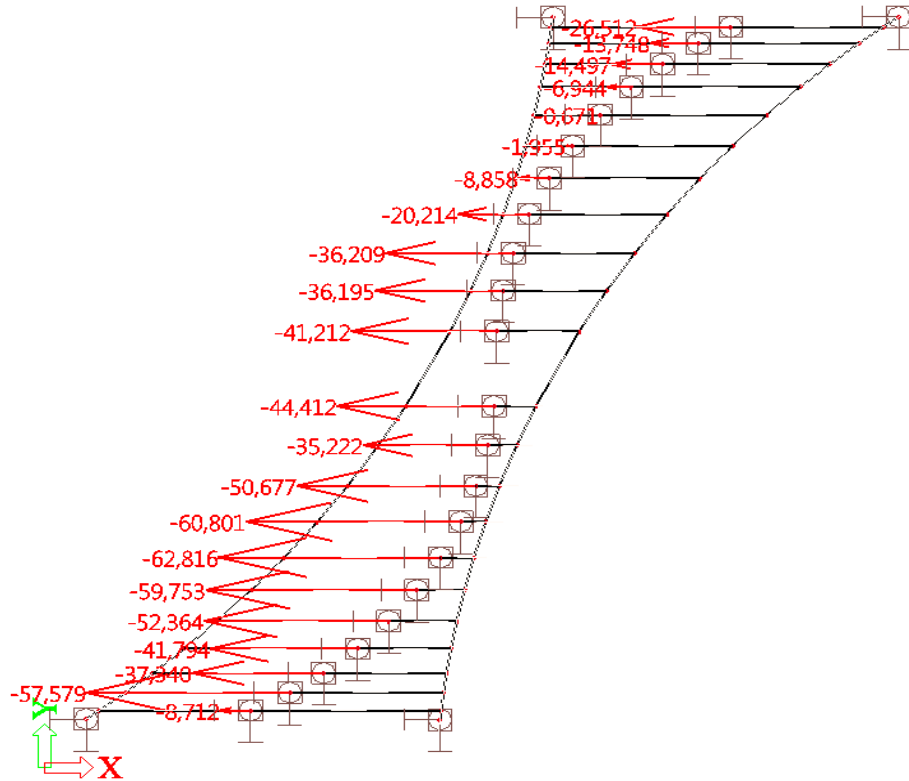


FIGURE O-6 DISPLACEMENT OF PONTOONS IN X-DIRECTION [M]

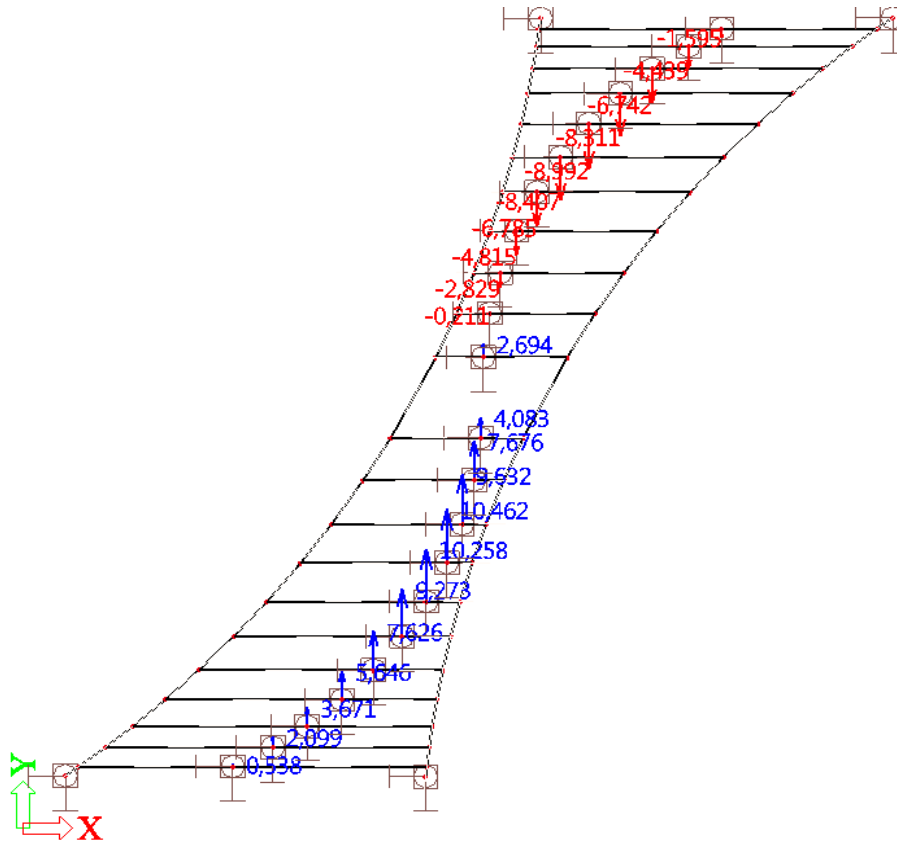


FIGURE O-7 DISPLACEMENTS OF PONTOONS IN Y-DIRECTION

O.3.3 Total Vertical Resultant Force Check

The total vertical reaction force is $507,0 \cdot 10^3$ kN. This is equal to the total vertical reaction force of the previous model. This is correct, since no extra vertical load is applied.

O.3.4 Forces and Stresses

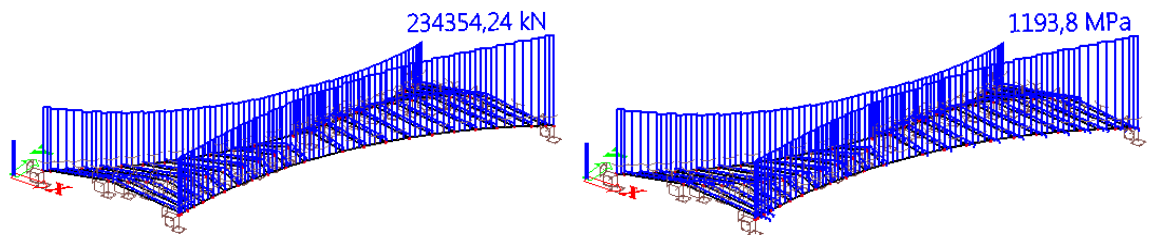


FIGURE O-8 INTERNAL FORCES (LEFT) AND STRESSES (RIGHT)

In Figure O-8, the internal forces and stresses are shown. It can be seen that the maximum internal force and stress is respectively $234,5 \cdot 10^3$ kN and $1193,8$ N/mm². These are larger than the internal forces and stresses when the anchoring system is loaded by only the self-weight, see Figure K-8.

In section J.3.3, it was calculated that the stress limit in serviceability limit state is 837 N/mm². The internal stresses of the main anchoring cable exceed this limit. On the contrary, the maximum internal stress in the lateral anchoring cables is $82,3$ N/mm².

These results indicate that larger size cables are required for the main anchoring cables. For the lateral anchoring cables, however, smaller cables may be used.

O.4 Conclusions

When the results of the anchoring system loaded by only the self-weight and the results of the system loaded by both the self-weight and the external horizontal loads in x-direction are compared, it can be seen that the largest displacements also occur in x-direction. The maximum difference between the displacements in x-direction of both cases is 41,7 meters. This is equal to $L/89$ with $L=3702$ meters.

The pontoons also move in y-direction, but the displacements are comparably small. The difference between the displacements of both cases is 4,3 meters.

Results show that larger dimensions of the main anchoring cable are required. On the contrary, smaller cables may be used for the lateral anchoring cables.

ANNEX P: COMPUTATIONAL MODELING: MORE VARIATIONS ANCHORING CABLES

In the previous sections, the setup of the computational model for the anchoring system was shown. The first discussed model in ANNEX J: Computational Model Substructure Example 1 (Fixed Supports) was the simplest model. This annex was followed by sections, each with a more refined model, where a few changes were applied each time. Results had shown that the initially chosen cables sizes were not optimal. Moreover, the prestressing force in the cables can be adjusted to limit more the displacements.

These suggested changes are applied in Scia Engineer and the results, namely concerning the displacements, are shown in Table P-1 to Table P-5. The results for previously discussed computational anchoring models 1, 2 and 3 are also included in this overview.

As can be seen in the overview, the roughest model of ANNEX J: Computational Model Substructure Example 1 (Fixed Supports), indicated as *Report model 1* and *Scia model 1* in the tables, give the largest displacements. After fine tuning the dimensions and prestressing of the anchoring cables, *Scia model 12* in the tables give the smallest displacements (especially when the system loaded by self-weight and horizontal loads, see Table P-5). For the further development of the anchoring system, the properties of *Scia model 12* will be used.

Hereafter, an adjusted *Scia model 12* was also tested, where the width of the anchoring system was increased. The main cables were placed further from each other and longer intermediate lateral anchoring cables were used. Results showed that the displacements did not differ greatly with the original *Scia model 12*, while the self-weight of the anchoring system did increase significantly. This has many consequences for the system, since the anchoring cables are actually ‘hanging’ on the pontoons. Increase of self-weight would lead to larger required pontoon sizes and increased loads. Since the wider anchoring system did not prove to be more effective, this idea was omitted.

Explanation: How to read the figures

d_main	= diameter main anchoring cables
d_lat	= diameter lateral anchoring cables
P_main	= input prestressing force in the main anchoring cables in Scia Engineer. Note that this is only an input value for Scia Engineer, this is not the real resulting internal force in the cables.
P_lat	= input prestressing force in the lateral anchoring cables in Scia Engineer. Note that this is only an input value for Scia Engineer, this is not the real resulting internal force in the cables.
density	= the weight of the anchoring cables
restraint u_x	= the restraint for the displacements of the pontoons in x-direction
restraint u_y	= the restraint for the displacements of the pontoons in y-direction
max stress main	= the resulting maximum internal stresses in the main anchoring cables
max stress lat	= the resulting maximum internal stresses in the lateral anchoring cables

In case the input prestressing force in Scia Engineer for the lateral anchoring cables is adjusted for a model, the new input prestressing force values for all the lateral anchoring cables (P_lat) connected to the pontoons are listed. The input changes for each model with respect of the previous model are shown in green.

TABLE P-2 DISPLACEMENTS DUE TO SELF-WEIGHT (2)

Input	Scia model 9			Scia model 10			Scia model 11			Scia model 12		
Pontoon	P_lat3 (both side input) (kN)	u_x (m)	u_y (m)	P_lat4 (both side input) (kN)	u_x (m)	u_y (m)	P_lat5 (both side input) (kN)	u_x (m)	u_y (m)	P_lat5 (both side input) (kN)	u_x (m)	u_y (m)
1	10.000	5,4	-3,1	10.000	5,2	-3,2	15.000	5,5	-3,1	15.000	5,5	-3,3
2	10.000	13,1	-6,6	10.000	12,8	-6,9	15.000	12,9	-6,8	15.000	12,2	-7,3
3	14.794	21,2	-9,2	14.794	20,6	-9,5	15.000	19,6	-9,6	15.000	18,0	-10,1
4	23.880	29,1	-10,5	23.880	28,2	-10,9	15.000	24,9	-11,2	15.000	22,9	-11,5
5	32.820	36,3	-11,3	32.820	35,2	-11,6	15.000	29,6	-11,8	15.000	27,9	-11,9
6	37.484	40,7	-11,5	37.484	39,2	-11,8	15.000	33,1	-11,7	15.000	31,7	-11,8
7	36.654	41,9	-11,1	36.654	39,9	-11,4	15.000	34,5	-11,3	15.000	33,3	-11,4
8	30.830	39,5	-10,2	30.830	36,8	-10,4	15.000	33,0	-10,6	15.000	31,9	-10,7
9	16.300	30,5	-8,4	16.300	27,8	-8,9	15.000	27,3	-9,6	15.000	26,5	-9,7
10	2.594	-7,4	-0,9	10.000	16,3	-6,8	15.000	18,8	-7,9	15.000	18,3	-8,0
11	2.000	-13,8	1,5	10.000	7,4	-3,8	15.000	8,3	-4,3	15.000	8,1	-4,3
12	2.000	10,4	-2,2	10.000	-8,9	3,4	15.000	-10,5	4,3	15.000	-10,3	4,4
13	5.270	-7,9	2,9	10.000	-17,4	5,8	15.000	-20,6	7,2	15.000	-20,0	7,5
14	23.528	-35,9	7,8	23.528	-31,5	8,1	15.000	-29,4	8,7	15.000	-28,5	9,0
15	36.682	-42,2	9,2	36.682	-38,5	9,4	15.000	-33,9	9,6	15.000	-32,7	9,8
16	40.000	-43,5	10,2	40.000	-40,7	10,4	15.000	-34,6	10,4	15.000	-33,3	10,5
17	38.900	-41,6	10,7	38.900	-39,5	10,9	15.000	-32,8	10,9	15.000	-31,2	11,1
18	33.412	-36,7	10,6	33.412	-35,1	10,9	15.000	-29,1	11,1	15.000	-27,2	11,3
19	23.992	-29,3	9,9	23.992	-28,1	10,3	15.000	-24,4	10,6	15.000	-22,3	11,0
20	14.006	-20,7	8,7	14.006	-19,9	9,0	15.000	-19,0	9,1	15.000	-17,3	9,6
21	10.000	-13,3	6,4	10.000	-12,9	6,7	15.000	-13,0	6,6	15.000	-12,2	7,1
22	10.000	-4,7	2,6	10.000	-4,6	2,7	15.000	-4,9	2,6	15.000	-5,0	2,9

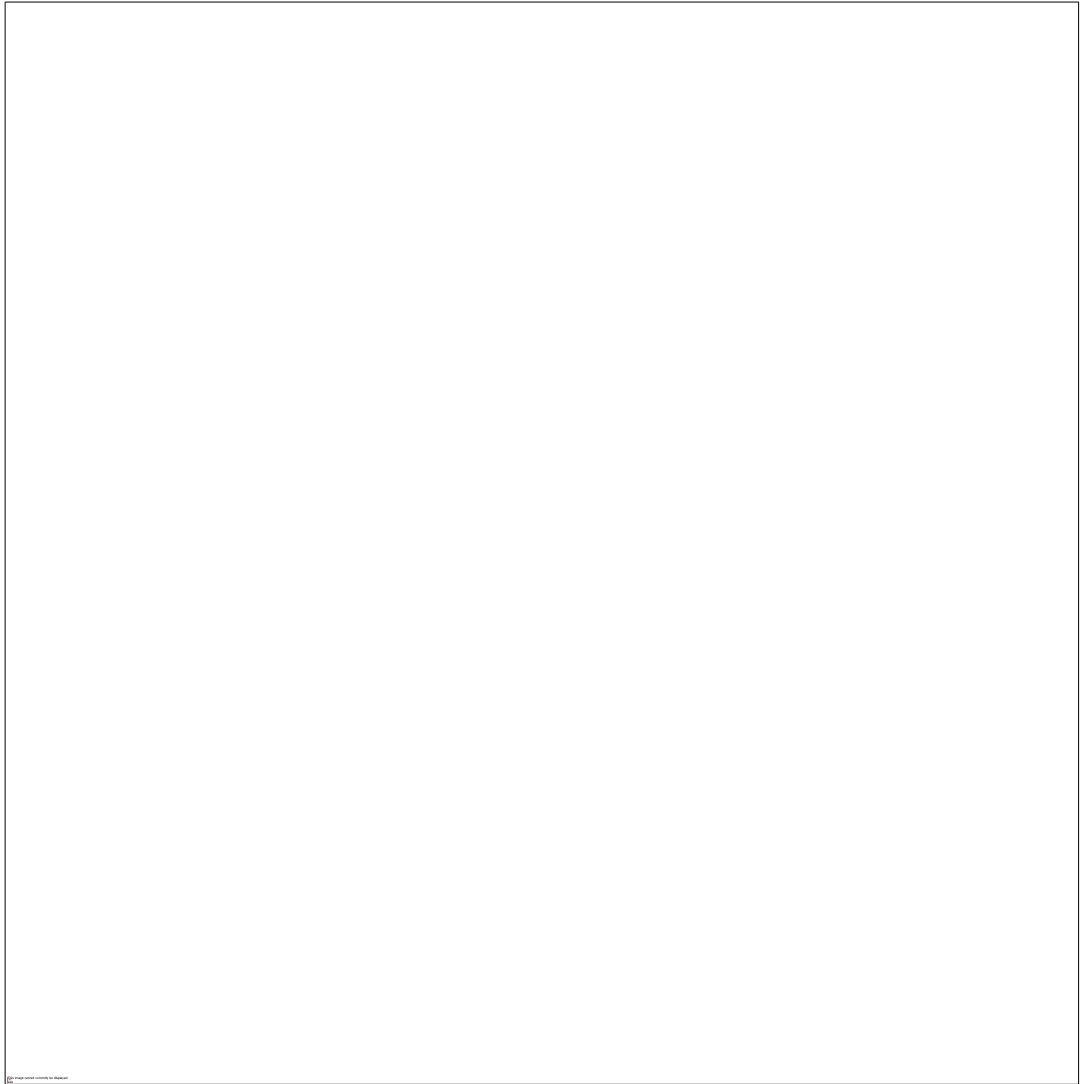
TABLE P-3 DISPLACEMENTS DUE TO SELF-WEIGHT AND HORIZONTAL LOADS (FX) IN SLS (1)

Input	Report model 2				Report model 3				SCIA model 5a				SCIA model 6				SCIA model 7			
	SW	u _x (m)	u _y (m)	du	SW	u _x (m)	u _y (m)	du	SW	u _x (m)	u _y (m)	du	SW	u _x (m)	u _y (m)	du	SW	u _x (m)	u _y (m)	du
d _{main} (mm)	500				1.000				1.000				1.200				1.200			
d _{lat} (mm)	500				500				500				450				450			
P _{main} (kN)	10.000				500.000				500.000				100.000				100.000			Real: 815.000 kN
P _{lat} (kN)	Var 1				Var 2				Var 2				Var 2				Var 2			
density (kg/m ³)	reduced				reduced				reduced				reduced				reduced			
restraint ux	free				free				free				free				free			
restraint uy	free				free				free				free				free			
max stress main (N/mm ²)																				
max stress lat (N/mm ²)																				
Pontoon																				
1	-6,1	-1,2	-26,5	-1,6	20,4	0,4			-8,1	-3,1	-27,0	-3,3	18,9	0,2			-7,9	-3,1	-30,7	-3,4
2	22,6	-3,5	-13,7	-4,4	36,3	0,9			12,7	-6,7	7,9	-7,1	4,9	0,5			12,9	-6,8	7,3	-7,3
3	13,6	-5,6	-14,5	-6,7	28,1	1,1			21,0	-9,1	18,7	-9,7	2,3	0,5			20,9	-9,3	18,5	-9,8
4	20,5	-7,4	-6,9	-8,3	27,5	0,9			28,8	-10,4	26,8	-10,7	2,0	0,3			28,8	-10,5	26,8	-10,8
5	28,2	-8,8	-0,7	-9,0	28,9	0,2			35,7	-10,9	33,3	-11,1	2,4	0,2			36,0	-11,3	33,5	-11,4
6	30,5	-9,5	-2,0	-8,4	32,4	-1,1			40,1	-10,6	37,0	-10,7	3,0	0,1			40,4	-11,4	37,2	-11,4
7	27,5	-9,3	-8,9	-6,8	36,4	-2,5			41,6	-9,6	37,9	-9,5	3,7	-0,1			41,6	-11,0	37,8	-10,8
8	18,8	-8,5	-20,2	-4,8	39,0	-3,7			39,4	-8,0	35,1	-7,7	4,3	-0,3			39,2	-10,0	34,8	-9,6
9	2,4	-7,0	-36,2	-2,8	38,6	-4,2			30,5	-5,7	25,7	-5,1	4,8	-0,6			30,3	-8,1	25,3	-7,5
10	3,5	-4,5	-36,2	-0,2	39,6	-4,3			-2,1	1,1	-11,4	-2,3	9,3	3,4			-7,1	-0,7	-16,8	-3,7
11	-0,8	-1,3	-41,2	2,7	40,4	-4,0			-10,5	2,6	-19,4	-0,6	8,9	3,1			-13,7	1,6	-22,0	0,7
12	-2,7	-0,1	-44,4	4,1	41,7	-4,2			7,9	-3,6	-1,0	-6,4	8,9	2,8			10,3	-2,3	1,2	-4,5
13	4,8	3,4	-35,2	7,7	40,0	-4,3			-8,6	0,1	-14,7	0,9	6,1	-0,8			-7,9	2,7	-14,1	3,5
14	-11,9	5,9	-50,7	9,6	38,8	-3,7			-35,3	5,1	-40,2	5,6	4,9	-0,6			-35,7	7,6	-40,7	8,1
15	-24,8	7,3	-60,8	10,5	36,0	-3,2			-42,0	7,1	-46,5	7,4	4,5	-0,3			-42,0	9,1	-46,6	9,4
16	-31,3	8,1	-62,8	10,3	31,5	-2,2			-43,0	8,8	-46,8	8,9	3,8	-0,1			-43,2	10,1	-47,1	10,3
17	-33,2	8,2	-59,8	9,3	26,6	-1,1			-40,9	9,9	-44,0	9,8	3,1	0,1			-41,3	10,7	-44,5	10,7
18	-30,0	7,7	-52,4	7,6	22,4	0,1			-36,1	10,3	-38,6	10,1	2,5	0,2			-36,4	10,6	-39,0	10,5
19	-21,7	6,4	-41,8	5,6	20,1	0,8			-28,8	9,9	-30,9	9,6	2,0	0,3			-28,8	10,1	-30,9	9,8
20	-15,1	4,6	-37,3	3,7	22,2	0,9			-22,2	8,8	-22,6	8,3	2,4	0,5			-20,1	8,9	-22,6	8,3
21	-22,6	2,9	-57,6	2,1	35,0	0,8			-12,6	6,7	-36,2	5,9	23,5	0,8			-12,8	6,7	-40,6	5,8
22	12,7	0,8	-8,7	0,5	21,5	0,3			14,6	2,7	-5,6	2,6	20,2	0,2			14,4	2,8	-10,5	2,5

TABLE P-4 DISPLACEMENTS TO SELF-WEIGHT AND HORIZONTAL LOADS (FX) IN SLS (2)

Input	SCIA model 7				SCIA model 8				SCIA model 9				SCIA model 10				
	SW	u _x (m)	u _y (m)	du (m)	SW	u _x (m)	u _y (m)	du (m)	SW	u _x (m)	u _y (m)	du (m)	SW	u _x (m)	u _y (m)	du (m)	
d _{main} (mm)	1,200				1,200				1,200				1,200				
d _{lat} (mm)	450				450				450				450				
P _{main} (kN)	200,000			Real: 799,000 kN	50,000				50,000				50,000				
P _{lat} (kN)	Var 2			Var 2	Var 3				Var 3				Var 4				
density (kg/m ³)	reduced			reduced	reduced				reduced				reduced				
restraint ux	free			free	free				free				free				
restraint uy	free			free	free				free				free				
max stress main (N/mm ²)	SW				SW				SW				SW				
max stress lat (N/mm ²)																	
Pontoon	u _x (m)	u _y (m)	du (m)	du (m)	u _x (m)	u _y (m)	du (m)	du (m)	u _x (m)	u _y (m)	du (m)	du (m)	u _x (m)	u _y (m)	du (m)	du (m)	
1	-8,0	-3,2	-7,9	-3,1	-30,7	-3,4	22,8	0,3	5,4	-3,1	1,4	-3,2	3,9	0,1	5,2	-3,2	3,9
2	12,7	-6,8	13,0	-6,7	7,4	-7,3	5,6	0,6	13,1	-6,6	7,4	-7,2	5,7	0,6	12,8	-6,9	7,2
3	20,6	-9,3	21,1	-9,2	18,7	-9,7	2,4	0,5	21,2	-9,2	18,8	-9,7	2,4	0,5	20,6	-9,5	18,3
4	28,4	-10,6	29,1	-10,5	27,0	-10,7	2,1	0,3	29,1	-10,5	27,0	-10,7	2,1	0,3	28,2	-10,9	26,4
5	35,5	-11,3	36,3	-11,3	33,7	-11,4	2,6	0,1	36,3	-11,3	33,7	-11,4	2,6	0,1	35,2	-11,6	32,9
6	40,0	-11,3	40,7	-11,5	37,4	-11,4	3,3	0,0	40,7	-11,5	37,4	-11,4	3,3	0,0	39,2	-11,8	36,3
7	41,3	-10,8	41,9	-11,1	37,9	-10,9	4,0	-0,2	41,9	-11,1	37,9	-10,9	4,0	-0,2	39,9	-11,4	36,5
8	39,0	-9,6	39,4	-10,2	34,8	-9,8	4,6	-0,4	39,5	-10,2	34,8	-9,8	4,6	-0,4	36,8	-10,4	32,8
9	30,1	-7,7	30,4	-8,4	25,2	-7,8	5,2	-0,6	30,5	-8,4	25,3	-7,8	5,2	-0,6	27,8	-8,9	23,3
21	-12,6	6,8	-12,9	6,7	40,8	5,7	27,9	0,9	-13,3	6,4	-19,2	5,9	5,9	0,5	-12,9	6,7	-18,6
22	14,5	2,8	14,4	2,7	-10,5	2,5	24,9	0,2	-4,7	2,6	-9,3	2,5	4,6	0,1	-4,6	2,7	-9,2

TABLE P-5 DISPLACEMENTS DUE TO SELF-WEIGHT AND HORIZONTAL LOADS (FX) IN SLS (3)



ANNEX Q: COMPUTATIONAL MODEL SUBSTRUCTURE EXAMPLE 4 (WITH SPRINGS)

In the previous sections, simple and rough models of the anchoring system were modeled in Scia Engineer. Through this process, the dimensions and prestressing of the anchoring cables are decided.

The anchoring system was inputted graphically. Consequently, the node coordinates were not very accurate. In this section, the coordinates are adjusted. All side spans are now exactly 200 meters and the main span is 430 meters. The anchoring system is now also rotational symmetric.

Furthermore, to model the anchoring system more realistic, springs have replaced the restraints at the supports at the location of the pontoons. Except for the restraints at the pontoons, where the rotations around the z-axis are still fixed, all other properties of the anchoring system are modeled realistically.

Q.1 Input in Scia Engineer

Q.1.1 Modeling the Anchoring System

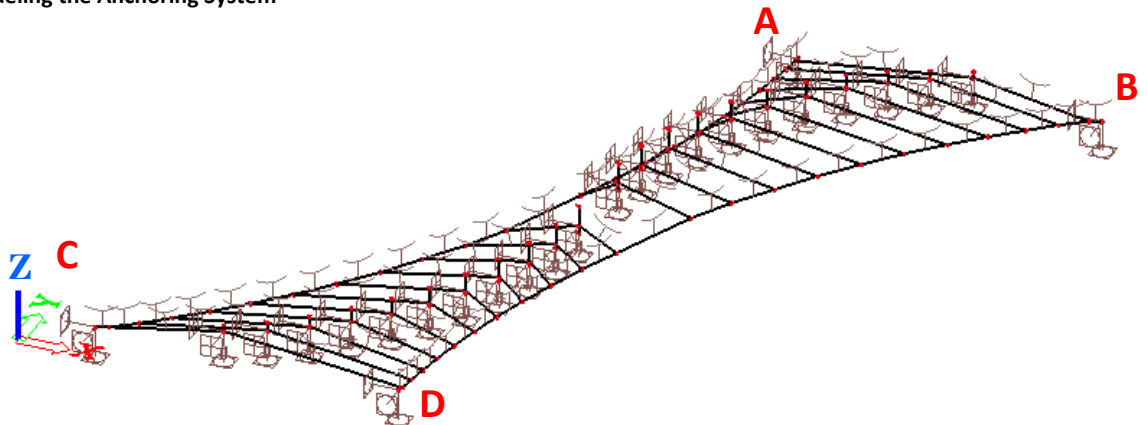


FIGURE Q-1 ANCHORING SYSTEM MODELED IN SCIA ENGINEER

The model of the anchoring system is shown in Figure Q-1. The two main cables are fixed from shore (AB) to shore (CD), one main cable is fixed from A to C and the other is fixed from B to D. The lateral anchoring cables are attached to these two main cables and the pontoons, which are placed in an S-shape from the top view. The anchoring system is rotational symmetric.

The pontoon elements themselves are not modeled. The lateral anchoring cables are attached to nodes, which represent the rotation center (RC) of the pontoons. On top of these nodes, members are placed, which represent the lever arm between the rotation center and the node, on which the wind load is modeled, see Figure Q-2. The bridge superstructure should be placed on top of these members, but in this model, the superstructure is left out. By leaving out the superstructure and thus also leaving also out the stiffness contribution of the superstructure, the effects of the loads can be investigated, when only the properties of the anchoring system is taken into account.

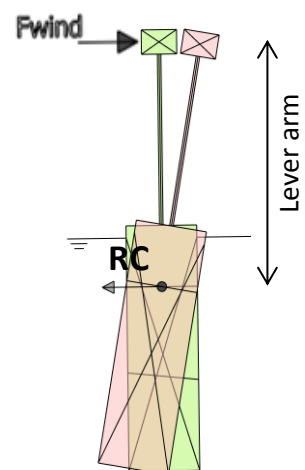


FIGURE Q-2 LEVERARM BETWEEN ROTATION CENTER (RC) AND THE LOCATION OF THE WIND LOAD

Q.1.2 **Coordinates**

The node numbering and node coordinates are shown respectively in Figure Q-3 and Table Q-1. The lateral anchoring cables are connected to 22 pontoon elements. These are also shown in the figure.

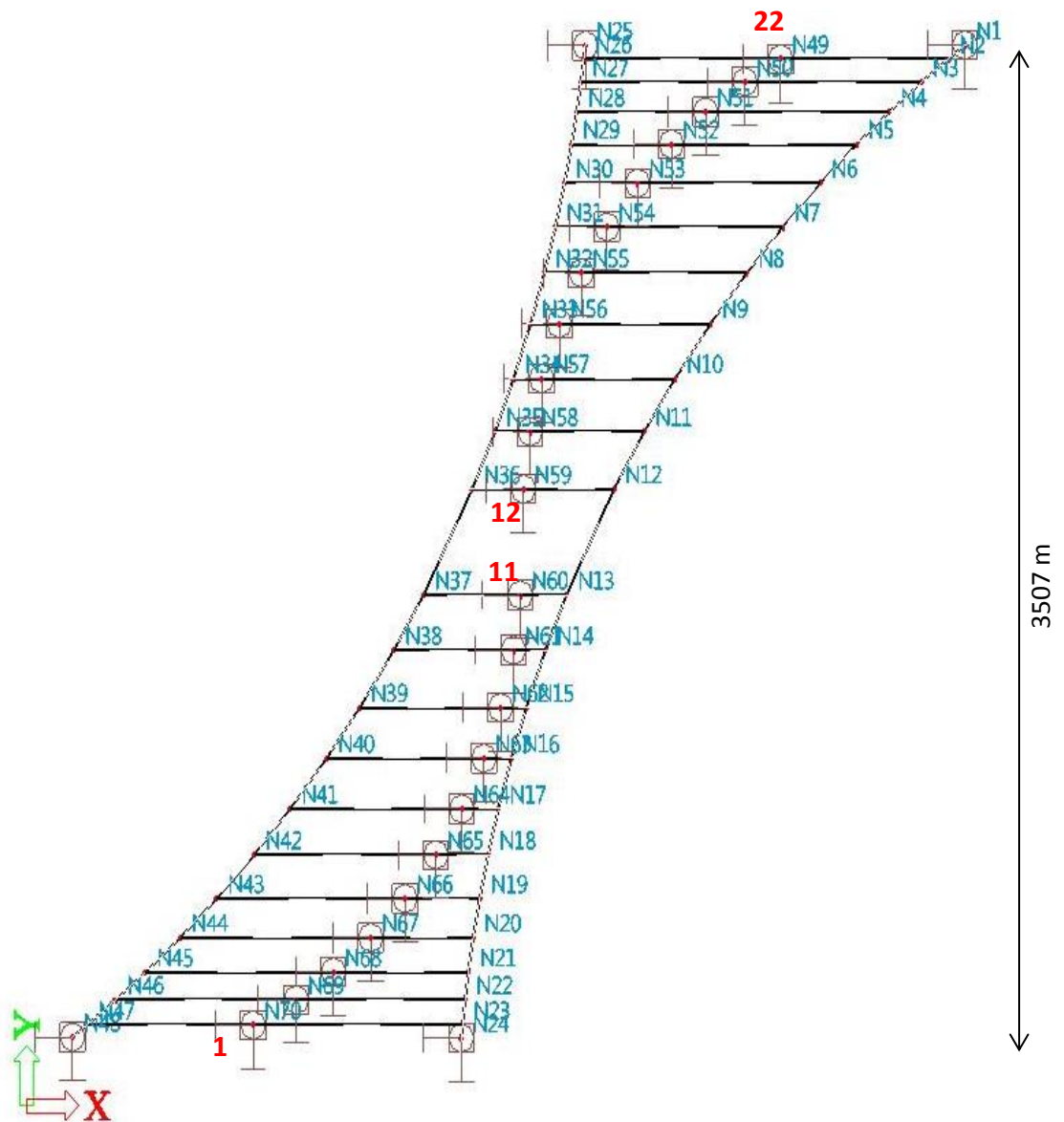


FIGURE Q-3 ANCHORING SYSTEM WITH NODE (BLUE) AND PONTOON (RED) NUMBERINGS

TABLE Q-1 COORDINATES NODES ANCHORING SYSTEM

Node Number	x (m)	y (m)	z (m)	Node Number	x (m)	y (m)	z (m)
N1	3889	3749	0	N36	1912	2210	0
N2	3831	3726	0	N37	1713	1781	0
N3	3713	3641	0	N38	1593	1584	0
N4	3592	3538	0	N39	1454	1392	0
N5	3451	3416	0	N40	1319	1206	0
N6	3303	3279	0	N41	1171	1030	0
N7	3151	3127	0	N42	1024	865	0
N8	3004	2961	0	N43	872	713	0
N9	2856	2785	0	N44	724	575	0
N10	2722	2600	0	N45	583	454	0
N11	2583	2407	0	N46	463	350	0
N12	2462	2210	0	N47	345	265	0
N13	2264	1781	0	N48	286	242	0
N14	2172	1584	0	N49	3255	3726	100
N15	2097	1392	0	N50	3074	3641	100
N16	2027	1206	0	N51	2903	3538	100
N17	1971	1030	0	N52	2744	3416	100
N18	1926	865	0	N53	2599	3279	100
N19	1889	713	0	N54	2470	3127	100
N20	1860	575	0	N55	2357	2961	100
N21	1839	454	0	N56	2263	2785	100
N22	1822	350	0	N57	2188	2600	100
N23	1811	265	0	N58	2134	2407	100
N24	1805	242	0	N59	2100	2210	100
N25	2371	3749	0	N60	2075	1781	100
N26	2365	3726	0	N61	2042	1584	100
N27	2353	3641	0	N62	1987	1392	100
N28	2336	3538	0	N63	1913	1206	100
N29	2315	3416	0	N64	1819	1030	100
N30	2286	3279	0	N65	1706	865	100
N31	2249	3127	0	N66	1577	713	100
N32	2204	2961	0	N67	1432	575	100
N33	2148	2785	0	N68	1273	454	100
N34	2079	2600	0	N69	1102	350	100
N35	2004	2407	0	N70	921	265	100

Q.1.3 Anchoring Cables and Pylon Properties

Steel Y1860 anchoring cables are used with material properties shown below.

Y1860

Tensile strength	: 1860 N/mm ²
Modulus of Elasticity	: 195 000 N/mm ²
Reduced unit mass in water	: 7850 kg/m ³ – 1015 kg/m ³ = 6835 kg/m ³
Diameter main anchoring cable	: 1200 mm
Diameter lateral anchoring cable	: 350 mm

The lever arm members are modeled to have the same dimension and stiffness as the pylons of the bridge.

Modulus of Elasticity	: 210 000 N/mm ²
Section	: circular hollow section
Outer diameter	: 5 meters
Thickness	: 167 mm

Q.1.4 Supports

The supports of the main cables to the shore (at nodes N1, N24, N25 and N48) are fixed for all degrees of freedom:

$$\begin{aligned} u_x &= \textit{fixed} & \varphi_x &= \textit{fixed} \\ u_y &= \textit{fixed} & \varphi_y &= \textit{fixed} \\ u_z &= \textit{fixed} & \varphi_z &= \textit{fixed} \end{aligned}$$

Supports are also placed at the nodes, which represent the rotation center of the pontoons (nodes N49 to N70):

$$\begin{aligned} u_x &= \textit{free} & \varphi_x &= \textit{flexible} \\ u_y &= \textit{free} & \varphi_y &= \textit{flexible} \\ u_z &= \textit{flexible} & \varphi_z &= \textit{fixed} \end{aligned}$$

u_x and u_y - The pontoon elements are floating on the water. They can float freely in x- and y-direction.

u_z - The pontoon elements are floating on the water. The (vertical) displacements in z-direction are not restrained by fixed restraints, but by springs. The stiffness of the spring can be calculated by $k_{vert} = A_{pontoon} \cdot \rho_{water} \cdot g$.

The governing seawater weight is 9,858 kN/m³ (see chapter 2.5.6). Since all pontoons have the same radius (15 meters), then $A_{pontoon}$ and therefore also k_{vert} are equal for all pontoon supports:

$$k_{vert} = A_{pontoon} \cdot g_{water} = \pi \cdot 15^2 \cdot 9,858 = 6968,21 \text{ kN/m}$$

φ_x and φ_y - The pontoon elements are floating freely on the water and they are able to rotate around the x- and y-axes. The buoyancy of the pontoons provides a restoring moment in case the pontoon elements rotate. The buoyancy restoring moment depends on the pontoon dimensions and the ballast heights.

These are variable for every pontoon. These rotational stiffness's are modeled as rotational springs. In ANNEX S: Calculation File Pontoon Properties and Loads, the calculation files can be found. Since the pontoon are cylindrical shaped, the rotational springs for φ_x and φ_y are equal. The anchoring system is rotational symmetric, so the values of the spring elements for half of the supports at the pontoon elements are shown in Table Q-2.

TABLE Q-2 ROTATIONAL SPRING STIFFNESS

Pontoon number	kr_{BU} (MNm/rad)
1	734
2	1988
3	2686
4	3348
5	3926
6	4645
7	5222
8	5717
9	5939
10	6261
11	12682

Q.1.5 Loads

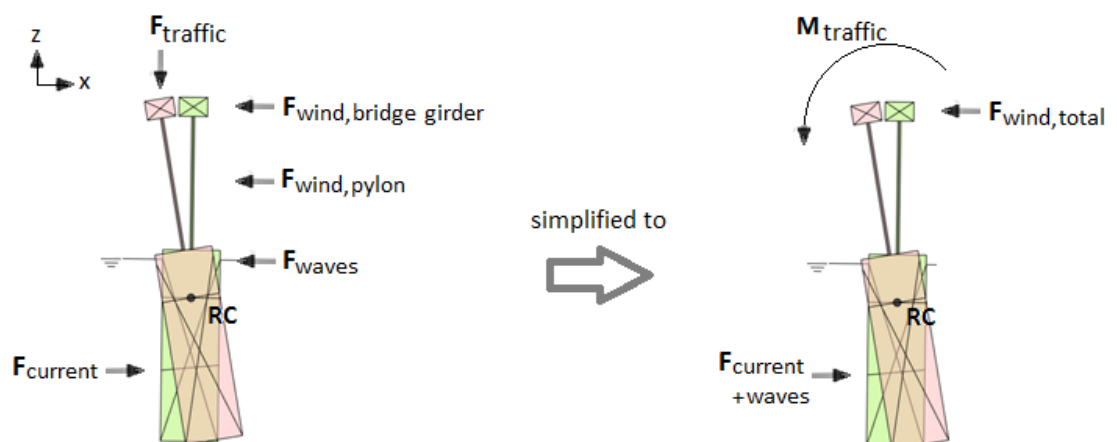
Load case 1: initial shape due to self-weight (SLS)

In the first load case, the anchoring system is only loaded by its submerged self-weight. This will yield the initial shape of the system due to self-weight.

Load case 2: maximum rotation at bridge deck level (SLS)

In the second load case, the system is loaded in such a way that the rotation around the y-axis is maximal. The loads contributing to this rotation are shown in Figure Q-4. Since parameters might change due to the fact that it is not decided yet on the bridge superstructure, (conservative) simplifications of the loads are made and inserted into Scia Engineer.

The wind, current and traffic load varies between the pontoons. Since the pontoon lengths also vary, the lever arms are also different for every pontoon. The loads and leverarms are shown in Figure Q-4. The calculation of these values are given in ANNEX S: Calculation File Pontoon Properties and Loads.



Load case 3: maximum displacements in x-direction (SLS)

FIGURE Q-4 : LOAD CASE 2: CAUSES MAXIMUM ROTATION (LEFT) AND LOAD CASE SIMPLIFICATION (RIGHT)

In load case 3, the loads are configured in such a way, that the displacements in x-direction will be the largest. Again, for the modeling in Scia Engineer, the load input is simplified as shown in Figure Q-5.

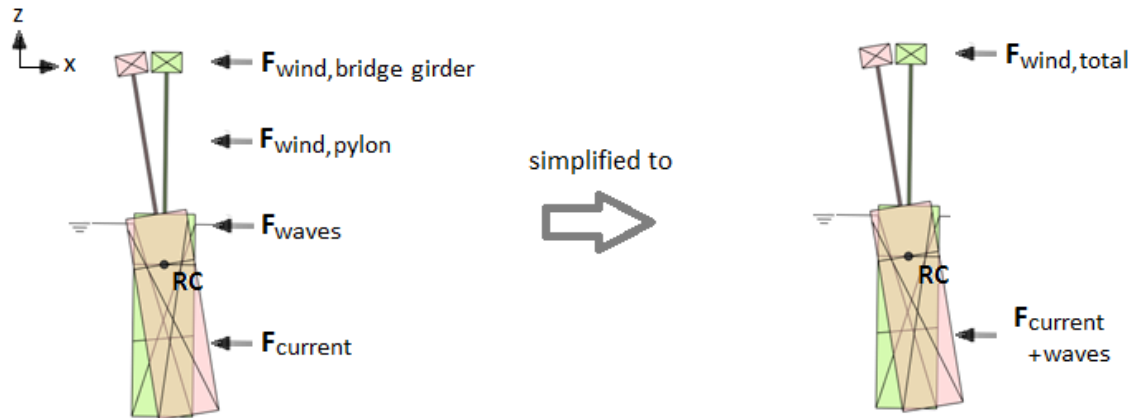


FIGURE Q-5 LOAD CASE 3: CAUSES MAXIMUM DISPLACEMENTS IN X-DIRECTION (LEFT) AND LOAD CASE SIMPLIFICATION (RIGHT)

For all load cases the self-weight of the anchoring system (consisting of the anchoring cables) is taken into account. Since the (vertical) support in z-direction at the pontoons is modelled as a spring (see section Q.1.4), horizontal upward loads are applied. These values are the vertical reaction forces at the pontoons in case the displacements in z-direction are fixed. This way, any additional displacements in z-direction will be due to additional loads. The load values are shown in Table Q-3. The calculation files are given in ANNEX S: Calculation File Pontoon Properties and Loads.

TABLE Q-3 SLS LOAD INPUT

Pontoon number	$M_{k,traffic}$ (kNm)	$F_{k,wind, total}$ (kN)	Lever arm wind (m)	$F_{k,current and wave}$ (kN)	Lever arm Current +wave (m)	Total $F_{k,x}$ (kN)	$F_{k,SW ANCH}$ (kN)
1	13915	909	29	716	0	1625	22602
2	21000	1918	42	824	0	2761	16704
3	21000	2210	53	886	-2,2	3097	10985
4	21000	2418	63	938	-5,5	3356	13955
5	21000	2560	72	981	-8,4	3541	16834
6	21000	2796	80	1029	-11,9	3825	22297
7	21000	2949	86	1067	-14,7	4016	26208
8	21000	3052	91	1121	-18,7	4173	38330
9	21000	3102	95	1097	-16,9	4199	24250
10	21000	3102	98	1186	-24,1	4288	52478
11	33075	5987	101	1367	-38,9	7354	51744

TABLE Q-4 DEFORMED STRUCTURE IN 3D FOR ALL LOAD CASES

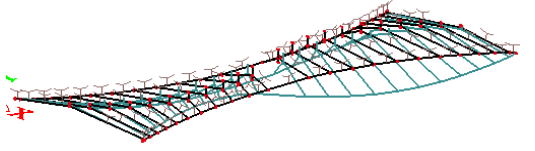
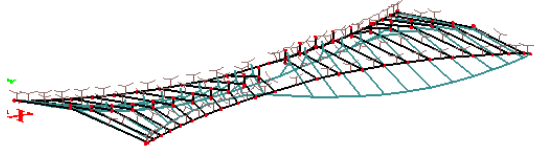
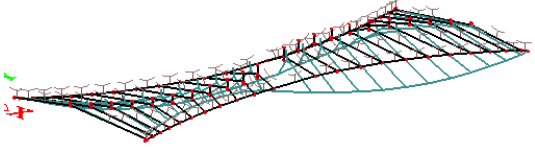
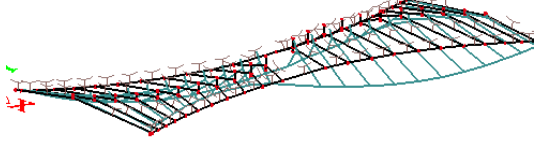
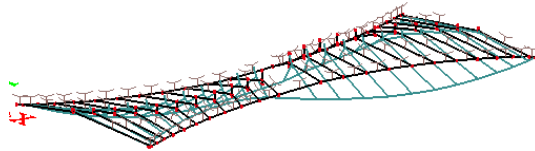
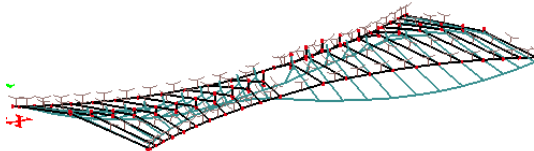
Load case 1: self-weight (SLS)	Load case 2: maximum φ_y (SLS)
	
Load case 3: maximum u_x (SLS)	Load case 4: maximum φ_y 1 (ULS)
	
Load case 5: maximum φ_y 2 (ULS)	Load case 6: maximum u_x (ULS)
	

TABLE Q-5 DEFORMED STRUCTURE IN Y-Z PLANE FOR ALL LOAD CASES

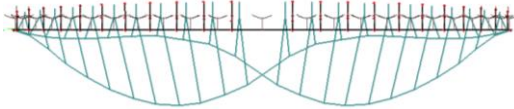
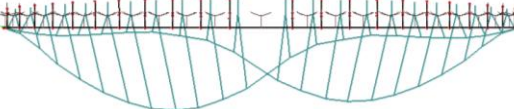
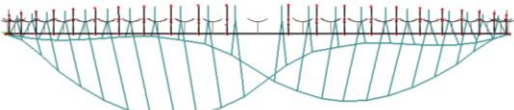
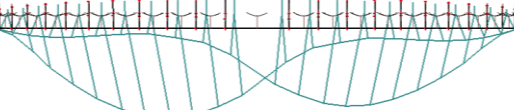
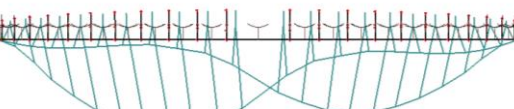
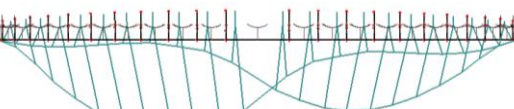
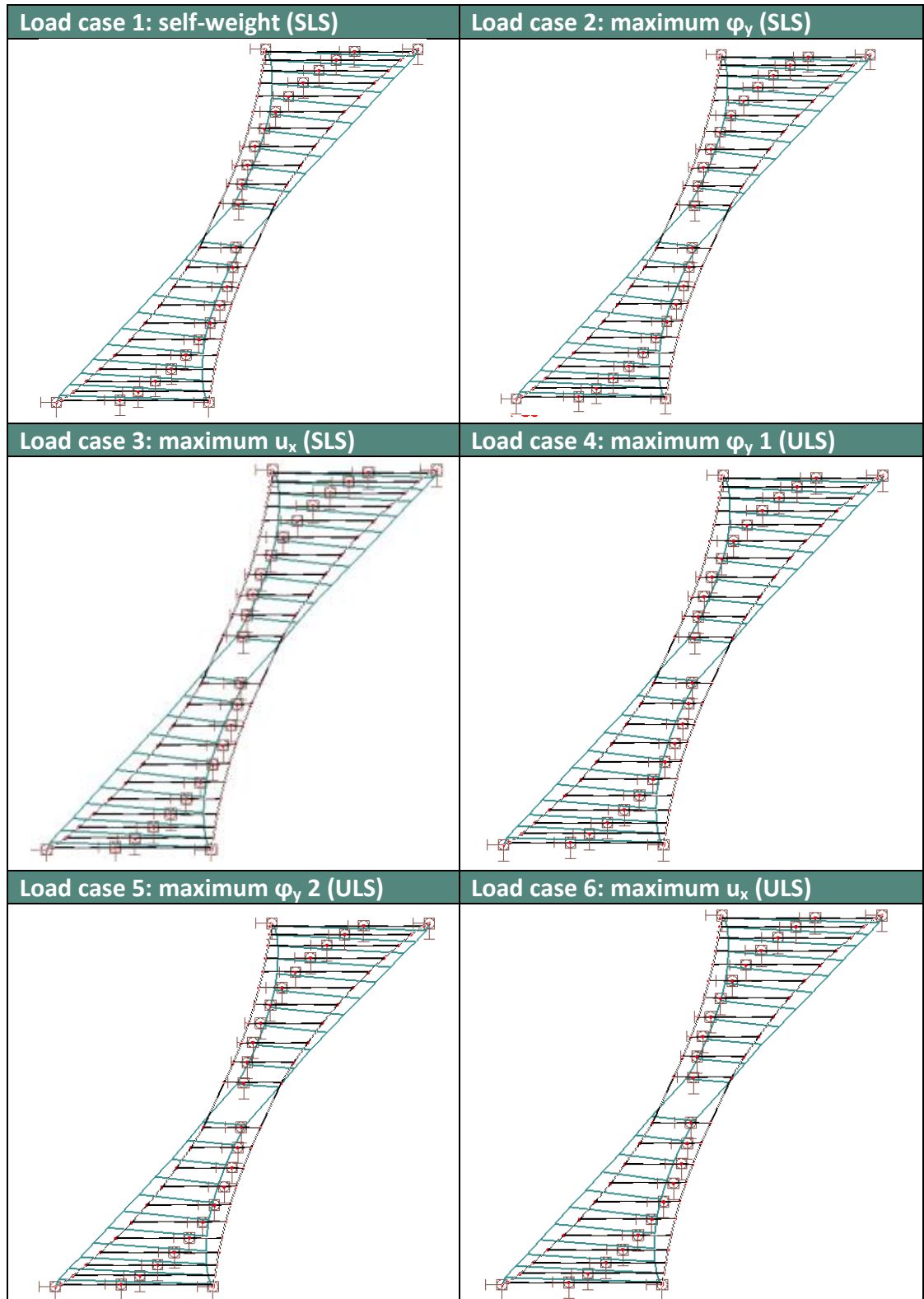
Load case 1: self-weight (SLS)	Load case 2: maximum φ_y (SLS)
	
Load case 3: maximum u_x (SLS)	Load case 4: maximum φ_y 1 (ULS)
	
Load case 5: maximum φ_y 2 (ULS)	Load case 6: maximum u_x (ULS)
	

TABLE Q-6 DEFORMED STRUCTURE IN X-Y PLANE FOR ALL LOAD CASES



Q.2.2 Displacements

The displacements as result of the load cases in serviceability limit state (SLS), which are load case 1, 2 and 3, are shown in Table Q-7. In load case 1, the anchoring system is only subjected to its self-weight. The displacements of the other load cases will be compared to this initial displacement. This is also shown in the table. It can be seen, that with respect to the initial displacement, the largest displacements after applying the loads are located at pontoon 11 and 12 at the main span.

In Table Q-8, the displacements in y-direction and the rotation around the y-axis are shown. Just as was the case for the displacements in x-direction, the displacements in y-direction are the largest at pontoon 11 and 12. The rotations around the y-axis for load case 1 are zero, since that load case only includes the self-weight and no loads are applied, which can contribute to the rotation. The rotations due to the other load cases are given in the table.

The displacements in z-direction, the rotation around the x-axis and the rotation around the z-axis are all equal to zero. The displacements shown in the tables are at the displacements at bridge deck level.

TABLE Q-7 DISPLACEMENTS IN X-DIRECTION FOR THE SLS LOAD CASES

Pontoon number	$u_{x,LC1}$ (m)	$u_{x,LC2}$ (m)	$du_{x,LC2}$ (m)	$u_{x,LC3}$ (m)	$du_{x,LC3}$ (m)
1	9,28	8,25	-1,03	8,18	-1,10
2	19,59	17,67	-1,92	17,30	-2,29
3	27,12	24,09	-3,03	23,26	-3,86
4	34,46	30,41	-4,05	29,37	-5,10
5	40,70	35,59	-5,11	34,19	-6,51
6	45,21	39,07	-6,14	37,36	-7,86
7	45,31	38,00	-7,30	35,91	-9,39
8	44,29	36,03	-8,26	33,70	-10,59
9	38,28	29,00	-9,28	26,15	-12,13
10	32,01	22,36	-9,65	19,94	-12,07
11	22,47	11,64	-10,83	9,15	-13,32
12	-22,53	-33,39	-10,86	-35,96	-13,43
13	-32,06	-41,76	-9,70	-44,32	-12,26
14	-38,33	-47,69	-9,35	-50,77	-12,44
15	-44,34	-52,64	-8,30	-55,11	-10,76
16	-45,35	-52,67	-7,32	-54,84	-9,49
17	-45,24	-51,38	-6,14	-53,13	-7,89
18	-40,40	-45,51	-5,11	-46,92	-6,52
19	-34,46	-38,49	-4,03	-39,52	-5,06
20	-27,12	-30,13	-3,01	-30,94	-3,81
21	-19,60	-21,51	-1,91	-21,86	-2,26
22	-9,28	-10,30	-1,02	-10,37	-1,09

TABLE Q-8 DISPLACEMENTS IN Y-DIRECTION AND ROTATION AROUND THE Y-AXIS FOR THE SLS LOAD CASES

Pontoon number	$u_{y,LC1}$ (m)	$u_{y,LC2}$ (m)	$du_{y,LC2}$ (m)	$u_{y,LC3}$ (m)	$du_{y,LC3}$ (m)	$\varphi_{y,LC2}$ (mrad)	$\varphi_{y,LC3}$ (mrad)
1	-8,90	-8,98	-0,08	-9,10	-0,20	-36,10	-36,10
2	-12,39	-12,65	-0,26	-12,91	-0,51	-41,60	-41,60
3	-12,48	-12,95	-0,47	-13,46	-0,98	-46,20	-44,90
4	-13,56	-13,97	-0,41	-14,39	-0,83	-50,20	-46,90
5	-13,83	-14,14	-0,31	-14,47	-0,64	-53,10	-49,20
6	-13,61	-13,76	-0,15	-13,93	-0,32	-55,70	-50,40
7	-12,02	-12,01	0,02	-12,04	-0,01	-58,50	-52,40
8	-11,12	-10,87	0,26	-10,73	0,40	-60,30	-52,90
9	-10,25	-9,99	0,27	-9,90	0,35	-61,70	-55,40
10	-9,60	-9,04	0,57	-8,76	0,84	-62,60	-53,50
11	-8,20	-7,60	0,60	-7,28	0,92	-71,40	-63,00
12	8,22	8,82	0,60	9,14	0,91	-71,40	-63,00
13	9,63	10,19	0,57	10,47	0,85	-62,60	-53,50
14	10,27	10,53	0,26	10,62	0,34	-61,70	-55,40
15	11,15	11,40	0,25	11,55	0,40	-60,30	-52,90
16	12,04	12,08	0,03	12,08	0,04	-58,60	-52,40
17	13,63	13,50	-0,13	13,38	-0,24	-55,70	-50,40
18	13,66	13,38	-0,29	13,10	-0,56	-53,10	-49,20
19	13,58	13,20	-0,38	12,83	-0,74	-50,20	-46,90
20	12,49	12,05	-0,44	11,58	-0,91	-46,20	-44,90
21	12,40	12,15	-0,25	11,91	-0,49	-41,60	-41,60
22	8,90	8,82	-0,08	8,71	-0,19	-36,10	-36,10

Q.2.3 Internal Forces and Stresses

The internal forces and stresses due to each load case is different, an example is given in Figure Q-7. The maximum internal forces and stresses for each load case is given in

Table Q-9.

According to the Eurocode [25], the ULS stress limit is 1240 N/mm^2 and the SLS stress limit is 837 N/mm^2 for Y1860 (see section J.3.3 for the calculation). As can be seen in the table, all unity checks are satisfied.

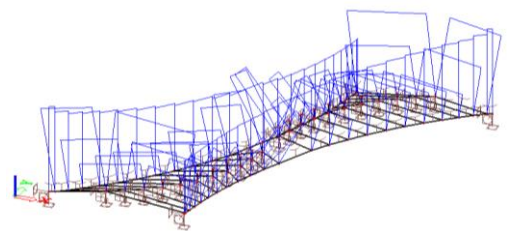


FIGURE Q-7 EXAMPLE STRESS DISTRIBUTION

TABLE Q-9 MAXIMUM INTERNAL FORCES AND STRESSES FOR EACH LOAD CASE

	LC1 (SLS)	LC2 (SLS)	LC3 (SLS)	LC4 (ULS)	LC5 (ULS)	LC6 (ULS)
Maximum force in main cable (kN)	$737,4 \cdot 10^3$	$762,7 \cdot 10^3$	$791,4 \cdot 10^3$	$887,2 \cdot 10^3$	$912,0 \cdot 10^3$	$931,1 \cdot 10^3$
Maximum force in lateral cable (kN)	$61,2 \cdot 10^3$	$61,4 \cdot 10^3$	$61,9 \cdot 10^3$	$67,2 \cdot 10^3$	$67,6 \cdot 10^3$	$68,2 \cdot 10^3$
Maximum stress in main cable (N/mm ²)	652,1	674,5	699,9	784,6	806,6	823,4
Maximum stress in lateral cable (N/mm ²)	636,1	637,8	643,2	698,4	702,7	708,6
Stress limit unity check	$\frac{651}{837} = 0,78$	$\frac{675}{837} = 0,81$	$\frac{700}{837} = 0,84$	$\frac{785}{1240} = 0,63$	$\frac{807}{1240} = 0,65$	$\frac{823}{1240} = 0,66$

Q.3 Evaluation/Verification of the Model

Q.3.1 Reaction forces in x-direction

The reaction forces in x-direction should equal the sum of the loads applied in x-direction. In Table Q-10, the horizontal reaction forces from Scia Engineer of each load case are shown. These will be compared to the inputted loads.

Load case 1 (LC1): The anchoring system is only subject to its own self-weight, no horizontal loads are applied. Therefore, the reaction force in x-direction should be equal to zero. As can be seen in the table, this is indeed the case.

Load case 2 (LC2): The anchoring system is subject to its self-weight, an outward (in negative x-direction) wind load and an inward (in positive x-direction) load in the water. The loads can be found in Table Q-3.

$$F_{wind,tot} - F_{water,tot} = 62,0 \cdot 10^3 - 22,4 \cdot 10^3 = 40,2 \cdot 10^3 \text{ kN}$$

This corresponds to the $39,6 \cdot 10^3$ kN in Table Q-10.

Load case 3 (LC3): The anchoring system is subject to its self-weight and both wind and water load in an outward direction.

$$F_{wind,tot} + F_{water,tot} = 62,0 \cdot 10^3 + 22,4 \cdot 10^3 = 84,4 \cdot 10^3 \text{ kN}$$

This is equal to the $84,4 \cdot 10^3$ kN in Table Q-10.

TABLE Q-10 REACTION FORCES IN X-DIRECTION FOR EACH LOAD CASE

	LC1 (SLS)	LC2 (SLS)	LC3 (SLS)	LC4 (ULS)	LC5 (ULS)	LC6 (ULS)
Reaction forces in x-direction (kN)	0	$39,6 \cdot 10^3$	$84,4 \cdot 10^3$	$59,4 \cdot 10^3$	$93,0 \cdot 10^3$	$126,6 \cdot 10^3$

Load case 4 (LC4): The anchoring system is subject to its self-weight, an outward (in negative x-direction) wind load and an inward (in positive x-direction) load in the water. Since this load case is in ultimate limit state (ULS), load factors of 1,5 should be applied.

$$1,5 \cdot F_{wind,tot} - 1,5 \cdot F_{water,tot} = 93,0 \cdot 10^3 - 33,6 \cdot 10^3 = 59,4 \cdot 10^3 \text{ kN}$$

This corresponds to the $59,4 \cdot 10^3$ kN in Table Q-10.

Load case 5 (LC5): The anchoring system is subject to its self-weight, an outward wind load and an asymmetrical water load. The resultant force in x-direction caused by the asymmetrical water load is equal to zero. This means, that the total resultant reaction force in x-direction must be equal to the wind load. Since this is an ULS analysis, the load factor of 1,2 should be applied.

$$1,5 \cdot F_{wind,tot} = 1,5 \cdot 62,0 \cdot 10^3 = 93,0 \cdot 10^3$$

This is equal to the $93,0 \cdot 10^3$ kN in Table Q-10.

Load case 6 (LC6): The anchoring system is subject to its self-weight and both wind and water load in an outward direction. Since this is an ULS analysis, load factor 1,5 should be applied.

$$1,5 \cdot F_{wind,tot} + 1,5 \cdot F_{water,tot} = 93,0 \cdot 10^3 + 33,6 \cdot 10^3 = 126,6 \cdot 10^3 \text{ kN}$$

This is equal to the $126,6 \cdot 10^3$ kN in Table Q-10.

Q.3.2 Reaction forces in z-direction

In this model, only the self-weight of the anchoring system is taken into account. The anchoring system consists of 2 main cables and 44 lateral anchoring cables. The total length of the main cable is 8.410 meters and the total length of the lateral anchoring cables is 20.598 meters.

Analytically, the total reaction force in z-direction should then be:

$$\begin{aligned} \sum F_z &= \rho \cdot g (\pi \cdot r_{main}^2 \cdot L_{main} + \pi \cdot r_{lateral}^2 \cdot L_{lateral}) \\ &= (7850 - 1015) \cdot 9,81 \cdot (\pi \cdot 0,6^2 \cdot 8.410 + \pi \cdot 0,175^2 \cdot 20.598) = 771 \cdot 10^3 \text{ kN} \end{aligned}$$

To compare this to the results from Scia Engineer, the model has to be adjusted slightly. In this model, the four supports connecting the main cables to the shores are fixed supports. The supports in z-direction at the location of the pontoons are modeled as springs. In case all springs at the pontoons are changed to fixed constraints in z-direction, the reaction force in z-direction would be larger. This result from Scia Engineer and the other reaction forces in z-direction for each load case are given in Table Q-11.

It can be seen that the above calculated $771 \cdot 10^3$ kN corresponds well to the reaction force according to Scia Engineer ($777 \cdot 10^3$ kN), as can be seen in the second column of the table.

TABLE Q-11 REACTION FORCES IN Z-DIRECTION FOR EACH LOAD CASE

	Model without springs	LC1 (SLS)	LC2 (SLS)	LC3 (SLS)	LC4 (ULS)	LC5 (ULS)	LC6 (ULS)
Reaction forces in z-direction (kN)	$778 \cdot 10^3$	$185 \cdot 10^3$	$185 \cdot 10^3$	$185 \cdot 10^3$	$222 \cdot 10^3$	$222 \cdot 10^3$	$222 \cdot 10^3$

LC1, LC2 and LC3: In these analyses, the pontoons are vertically supported by springs and upward buoyancy forces. The sum of the inputted buoyancy forces is $593 \cdot 10^3$ kN (see Table Q-3, last column). The reaction force in z-direction should then be the difference between the total resultant force in case there were no springs and the sum of the inputted buoyancy force.

$$R_{z,total} - F_{b,total} = 778 \cdot 10^3 - 593 \cdot 10^3 = 185 \cdot 10^3 \text{ kN}$$

This corresponds well to the results from Scia Engineer, as can be seen in Table Q-11.

LC4, LC5 and LC6: These load cases are in ultimate limit state (ULS). Therefore, a load factor of 1,2 should be applied for the buoyancy force, which compensates the self-weight of the anchoring system.

$$1,2 (R_{z,total} - F_{b,total}) = 1,2 (778 \cdot 10^3 - 593 \cdot 10^3) = 222 \cdot 10^3 \text{ kN}$$

This corresponds well to the results from Scia Engineer, as can be seen in Table Q-11.

Q.3.3 Effect of the Rotational Spring

To verify the effect of the rotational spring, results of the system with the rotational springs will be compared to the results of the system without the springs.

In an anchoring system without the rotational spring, the horizontal deformation on an arbitrary chosen pontoon and pylon looks like as shown in Figure Q-9. It can be seen that the deformation on the beam is almost constant over the whole height. This means that the deformation is particularly caused by displacement of the member in x-direction, there is no rotation of the member around the rotation center. In Figure Q-9, the horizontal deformation can be seen of the pontoon and pylon in an anchoring system *with* rotational springs. It can be seen that the pontoon/pylon has rotated.

TABLE Q-12 VARYING THE PRETENSIONING

Q.3.4 Effect of Varying the Prestressing Force

The prestressing force is varied to investigate the behavior of the anchoring system. The original tension force in the cable and the new, decreased value are shown in Table Q-12. By decreasing the internal force in the anchoring cables, it is expected that the stresses in the cables also decrease, the total resultant forces should remain the same, the displacements of the nodes will increase and the rotation should remain the same.

	Original model	Variant model
Tension force in main cable (kN)	$737,4 \cdot 10^3$	$672,5 \cdot 10^3$
Maximum force in lateral cable (kN)	$61,2 \cdot 10^3$	$58,4 \cdot 10^3$

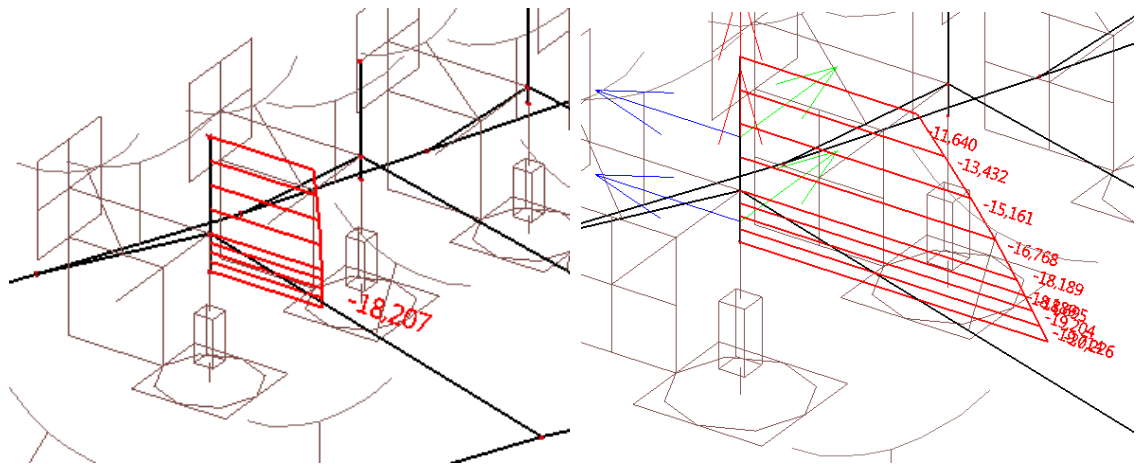


FIGURE Q-9 DISPLACEMENT IN CASE WITHOUT ROTATIONAL SPRING IN [M]

FIGURE Q-9 DISPLACEMENT IN CASE WITH ROTATIONAL SPRING IN [M]

In Table Q-13, the comparisons between the original and variant model can be seen. The internal stresses of the cables have indeed decreased and the total resultant forces have remained the same.

In the displacements in x-direction can be compared in Figure Q-10. These are the displacements as result of load case 3; the anchoring system is subject to its self-weight and external wind and water load in negative x-direction. It can be seen that the displacements of the variant anchoring system with smaller pretensioned cables yield larger displacements.

Results also show that the rotation of the pontoons remains the same for both the anchoring systems, independent of the magnitude of the pretensioning, see Figure Q-11. This was also as expected.

After these validations, it can be assumed that the computational model gives reliable results.

TABLE Q-13 COMPARISON ORIGINAL AND VARIANT MODEL

	Original model	Variant model
Internal stress main cable (N/mm ²)	700	643
Maximum internal stress in lateral cable (N/mm ²)	643	616
Total resultant Fz (kN)	185 · 10 ³	185 · 10 ³

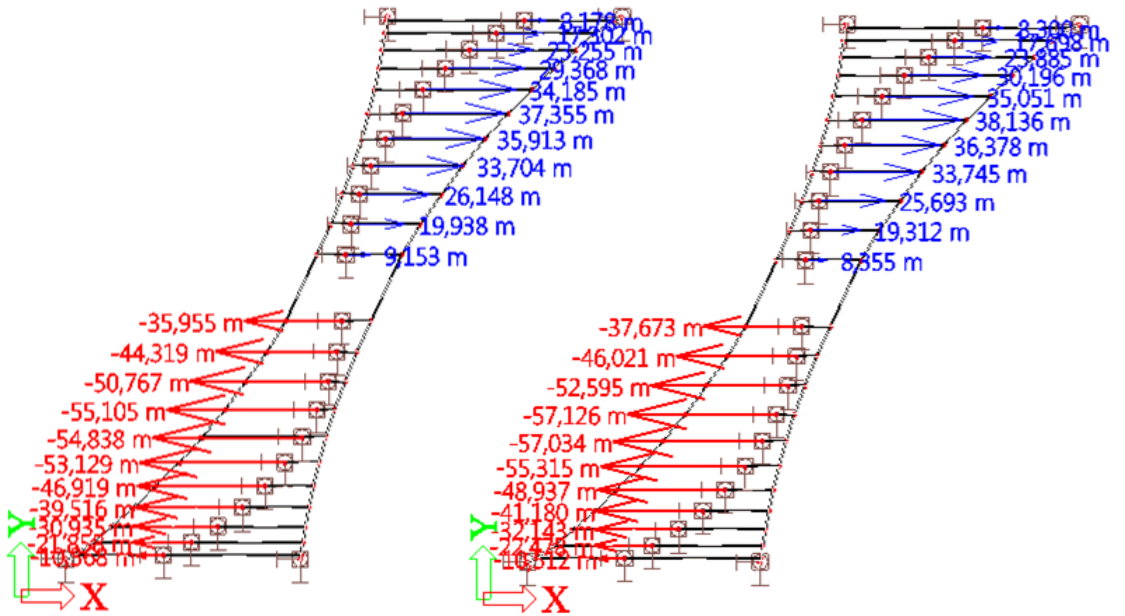


FIGURE Q-10 COMPARISON DISPLACEMENTS ORIGINAL SYSTEM (LEFT) AND VARIANT SYSTEM (RIGHT)

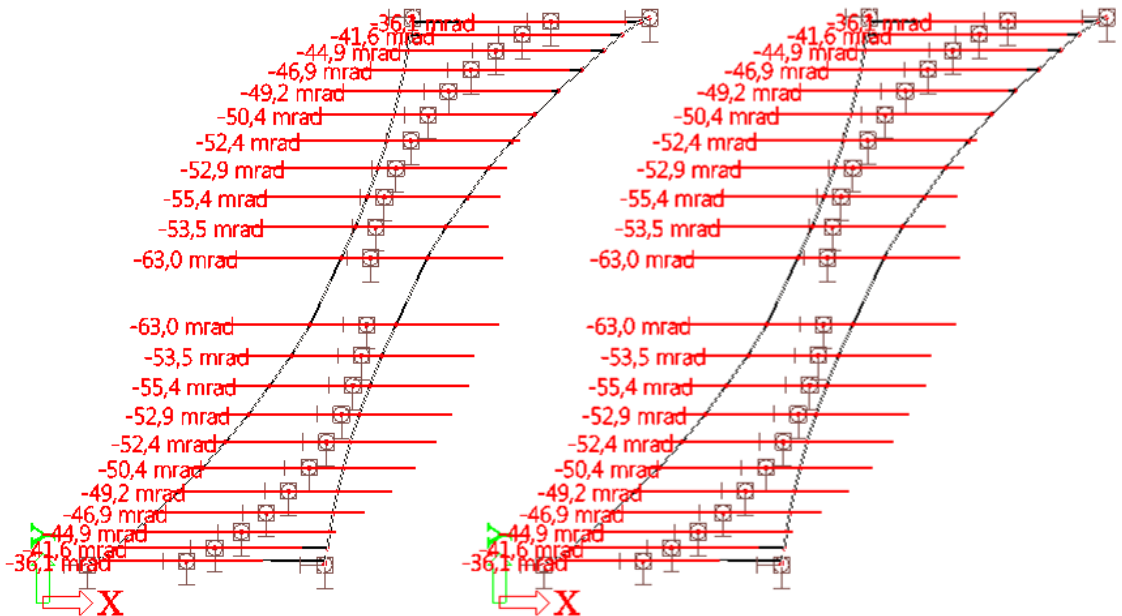


FIGURE Q-11 COMPARISON ROTATIONS AROUND Y-AXIS OF ORIGINAL SYSTEM (LEFT) AND VARIANT SYSTEM (RIGHT)

ANNEX R: COMPUTATIONAL MODEL SUBSTRUCTURE EXAMPLE 5

In the annexes I to N, rough models of the anchoring system were modeled in structural analysis software Scia Engineer. Through this process, the dimensions and prestressing of the anchoring cables are decided. Hereafter, Annex P followed with a computational model with accurate the node coordinates.

In this section, the model the anchoring system will be made even more realistic, by setting free the rotations around the z-axis at the supports at the location of the pontoons. Now all degrees of freedom of the rotation centers at the pontoons are modeled realistically. Furthermore, the lateral anchoring cables in this model are solely prestressed by their own self-weight. No additional pretensioning forces are applied on these cables. This is decided while keeping the ease of the erection in mind. The properties and results of this final anchoring system are shown in this section.

R.1 Input in Scia Engineer

R.1.1 Modeling the Anchoring System

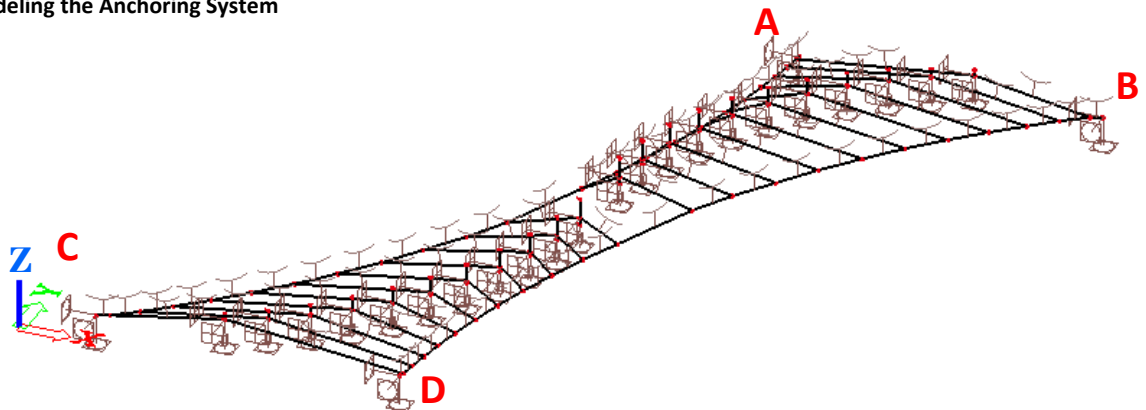


FIGURE R-1 ANCHORING SYSTEM MODELED IN SCIA ENGINEER

The model of the anchoring system is shown in Figure Q-1. The two main cables are fixed from shore (AB) to shore (CD) at 120 meters below water level, one main cable is fixed from A to C and the other is fixed from B to D. The lateral anchoring cables are attached to these two main cables and the pontoons, which are placed in an S-shape from the top view. The anchoring system is rotational symmetric.

The pontoon elements themselves are not modeled, but the rotation center (RC) of the pontoons are. The rotation centers of all pontoons are modeled at 20 meters below water level to comply the clearance requirement. On top and beneath the rotation centers, members are placed, which represent respectively the lever arms between the rotation center and the nodes, on which the wind and current load are modeled, see Figure Q-2.

To make it possible for the pontoon elements to rotate around the z-axis, the anchoring cables are no longer attached to the rotation center (as was the case for anchoring model 4 of ANNEX Q:), but they are now attached to nodes at a distance equal to the radius of the pontoons from the rotation center. Since all pontoons have the same radius, these horizontal members are the same for all pontoons.

The purpose is to design an anchoring system, which maintains the relative position of the pontoons as much as possible. This way, the required strength and stiffness of the superstructure will be smaller. Therefore, only the anchoring system is modeled without the superstructure.

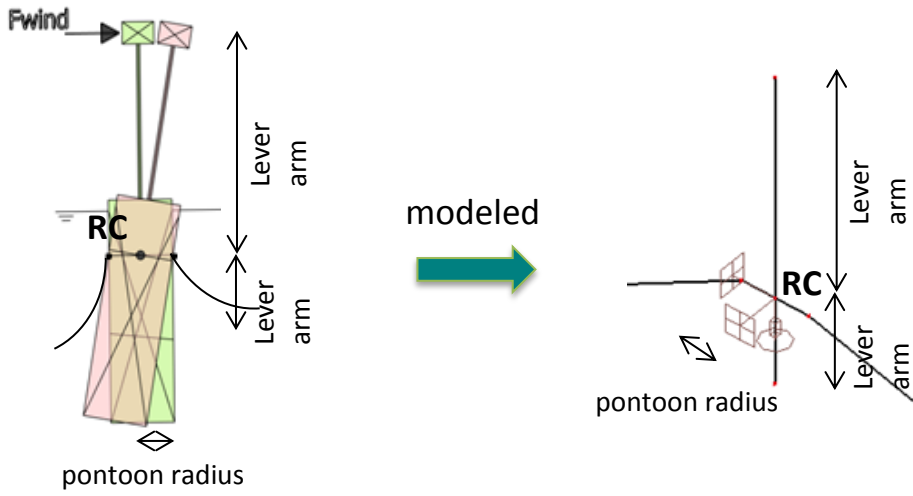


FIGURE R-2 MODELING ROTATION CENTER, LEVER ARMS AND CABLE ATTACHEMENT NODES

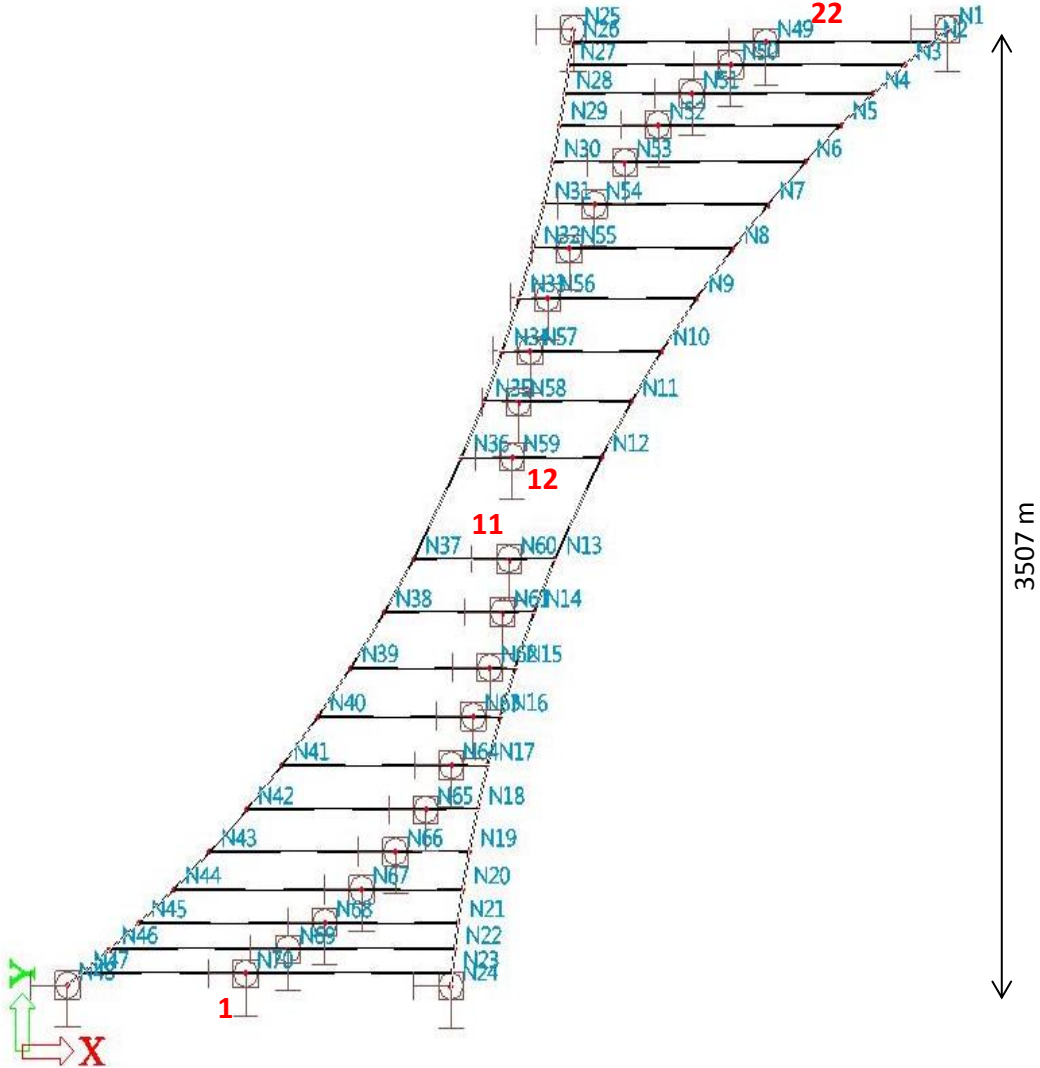


FIGURE R-3 ANCHORING SYSTEM WITH NODE (BLUE) AND PONTOON (RED) NUMBERINGS

R.1.2 Coordinates

The node numbering and node coordinates are shown respectively in Figure Q-3 and Table Q-1. The lateral anchoring cables are connected to 22 pontoon elements. These are also shown in the figure.

TABLE R-1 COORDINATES NODES ANCHORING SYSTEM

Node Number	x (m)	y (m)	z (m)	Node Number	x (m)	y (m)	z (m)
N1	3889	3749	0	N36	1912	2210	0
N2	3831	3726	0	N37	1713	1781	0
N3	3713	3641	0	N38	1593	1584	0
N4	3592	3538	0	N39	1454	1392	0
N5	3451	3416	0	N40	1319	1206	0
N6	3303	3279	0	N41	1171	1030	0
N7	3151	3127	0	N42	1024	865	0
N8	3004	2961	0	N43	872	713	0
N9	2856	2785	0	N44	724	575	0
N10	2722	2600	0	N45	583	454	0
N11	2583	2407	0	N46	463	350	0
N12	2462	2210	0	N47	345	265	0
N13	2264	1781	0	N48	286	242	0
N14	2172	1584	0	N49	3255	3726	100
N15	2097	1392	0	N50	3074	3641	100
N16	2027	1206	0	N51	2903	3538	100
N17	1971	1030	0	N52	2744	3416	100
N18	1926	865	0	N53	2599	3279	100
N19	1889	713	0	N54	2470	3127	100
N20	1860	575	0	N55	2357	2961	100
N21	1839	454	0	N56	2263	2785	100
N22	1822	350	0	N57	2188	2600	100
N23	1811	265	0	N58	2134	2407	100
N24	1805	242	0	N59	2100	2210	100
N25	2371	3749	0	N60	2075	1781	100
N26	2365	3726	0	N61	2042	1584	100
N27	2353	3641	0	N62	1987	1392	100
N28	2336	3538	0	N63	1913	1206	100
N29	2315	3416	0	N64	1819	1030	100
N30	2286	3279	0	N65	1706	865	100
N31	2249	3127	0	N66	1577	713	100
N32	2204	2961	0	N67	1432	575	100
N33	2148	2785	0	N68	1273	454	100
N34	2079	2600	0	N69	1102	350	100
N35	2004	2407	0	N70	921	265	100

R.1.3 Anchoring Cables and Pylon Properties

Steel Y1860 anchoring cables are used with material properties shown below.

Y1860

Tensile strength	: 1860 N/mm ²
Modulus of Elasticity	: 195 000 N/mm ²
Reduced unit mass in water	: 7850 kg/m ³ – 1015 kg/m ³ = 6835 kg/m ³
Diameter main anchoring cable	: 1200 mm
Diameter lateral anchoring cable	: 350 mm

The lever arm members are modeled to have the same dimension and stiffness as the pylons of the bridge.

Modulus of Elasticity	: 210 000 N/mm ²
Unit mass	: 0 kg/m ³
Section	: circular hollow section
Outer diameter	: 5 meters
Thickness	: 167 mm

The members from the rotation center to the attachment points of the anchoring cables:

Modulus of Elasticity	: 210 000 N/mm ²
Unit mass	: 0 kg/m ³
Section	: solid circular section
Outer diameter	: 2 meters

Not that only the self-weight of the anchoring system is taken into account. The self-weight of all other members are modeled as 0 kg/m³. It is assumed that all vertical forces are compensated by buoyancy forces of the pontoons. The pontoons are modelled to have springs, which restrain the vertical displacements. Therefore, as can be seen in section R.1.5, buoyancy forces that compensate the self-weight of the anchoring system are applied in such a way, that the rotation centers of all pontoons are positioned on the same height despite of the vertical springs.

R.1.4 Supports

The supports of the main cables to the shore (at nodes N1, N24, N25 and N48) are fixed for all degrees of freedom:

$$\begin{aligned}
 u_x &= \textit{fixed} & \varphi_x &= \textit{fixed} \\
 u_y &= \textit{fixed} & \varphi_y &= \textit{fixed} \\
 u_z &= \textit{fixed} & \varphi_z &= \textit{fixed}
 \end{aligned}$$

Supports are also placed at the nodes, which represent the rotation center of the pontoons (nodes N49 to N70):

$$\begin{aligned}
 u_x &= \textit{free} & \varphi_x &= \textit{flexible} \\
 u_y &= \textit{free} & \varphi_y &= \textit{flexible} \\
 u_z &= \textit{flexible} & \varphi_z &= \textit{fixed}
 \end{aligned}$$

u_x and u_y - The pontoon elements are floating on the water. They can float freely in x- and y-direction.

u_z - The pontoon elements are floating on the water. The (vertical) displacements in z-direction are not restrained by fixed restraints, but by springs. The stiffness of the spring can be calculated by $k_{vert} = A_{pontoon} \cdot \rho_{water} \cdot g$.

The governing seawater weight is $9,858 \text{ kN/m}^3$ (see chapter 2.5.6). Since all pontoons have the same radius (15 meters), then $A_{pontoon}$ and therefore also k_{vert} are equal for all pontoon supports:

$$k_{vert} = A_{pontoon} \cdot g_{water} = \pi \cdot 15^2 \cdot 9,858 = 6968,21 \text{ kN/m}$$

φ_x and φ_y - The pontoon elements are floating freely on the water and they are able to rotate around the x- and y-axes. The buoyancy of the pontoons provides a restoring moment in case the pontoon elements rotate. The buoyancy restoring moment depends on the pontoon dimensions and the ballast heights.

These are variable for every pontoon. These rotational stiffness's are modeled as rotational springs. In ANNEX S: Calculation File Pontoon Properties and Loads, the calculation files can be found. Since the pontoon are cylindrical shaped, the rotational springs for φ_x and φ_y are equal. The anchoring system is rotational symmetric, so the values of the spring elements for half of the supports at the pontoon elements are shown in Table Q-2.

TABLE R-2 ROTATIONAL SPRING STIFFNESS

Pontoon number	kr_{BU} (MNm/rad)
1	734
2	1988
3	2686
4	3348
5	3926
6	4645
7	5222
8	5717
9	5939
10	6261
11	12682

R.1.5 Loads and Load Cases

Load case 1: initial shape due to self-weight (SLS)

In the first load case, the anchoring system is only loaded by its submerged self-weight. This will yield the initial shape of the system due to self-weight.

Load case 2: maximum rotation at bridge deck level (SLS)

In the second load case, the system is loaded in such a way that the rotation around the y-axis is maximal. The loads contributing to this rotation are shown in Figure Q-4. Since parameters might change due to the fact that it is not decided yet on the bridge superstructure, (conservative) simplifications of the loads are made and inserted into Scia Engineer.

The wind, current and traffic load varies between the pontoons. Since the pontoon lengths also vary, the lever arms are also different for every pontoon. The loads and leverarms are shown in Figure Q-4. The calculation of these values are given in ANNEX S: Calculation File Pontoon Properties and Loads.

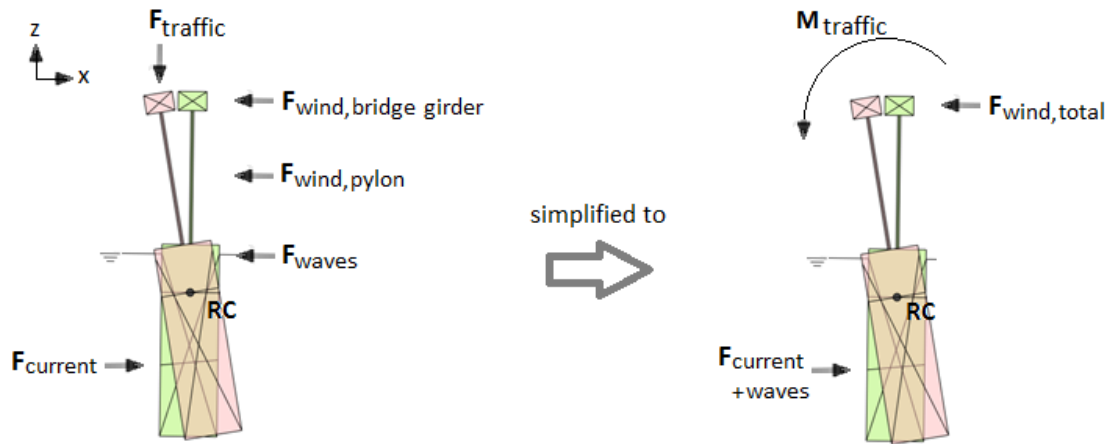


FIGURE R-4 : LOAD CASE 2: CAUSES MAXIMUM ROTATION (LEFT) AND LOAD CASE SIMPLIFICATION (RIGHT)

Load case 3: maximum displacements in x-direction (SLS)

In load case 3, the loads are configured in such a way, that the displacements in x-direction will be the largest. Again, for the modeling in Scia Engineer, the load input is simplified as shown in Figure Q-5.

For all load cases the self-weight of the anchoring system (consisting of the anchoring cables) is taken into account. Since the (vertical) support in z-direction at the pontoons is modelled as a spring (see section Q.1.4), horizontal upward loads are applied. These values are the vertical reaction forces at the pontoons in case the displacements in z-direction are fixed. This way, any additional displacements in z-direction will be due to additional loads. The load values are shown in Table Q-3. The calculation files are given in ANNEX S: Calculation File Pontoon Properties and Loads.

TABLE R-3 SLS LOAD INPUT

Pontoon number	$M_{k,traffic}$ (kNm)	$F_{k,wind, total}$ (kN)	Lever arm wind (m)	$F_{k,current and wave}$ (kN)	Lever arm Current +wave (m)	Total $F_{k,x}$ (kN)	$F_{k,SW ANCH}$ (kN)
1	13915	909	29	716	0	1625	16684
2	21000	1918	42	824	0	2761	15084
3	21000	2210	53	886	-2,2	3097	10645
4	21000	2418	63	938	-5,5	3356	13887
5	21000	2560	72	981	-8,4	3541	16536
6	21000	2796	80	1029	-11,9	3825	22869
7	21000	2949	86	1067	-14,7	4016	26713
8	21000	3052	91	1121	-18,7	4173	37343
9	21000	3102	95	1097	-16,9	4199	24470
10	21000	3102	98	1186	-24,1	4288	51927
11	33075	5987	101	1367	-38,9	7354	53779

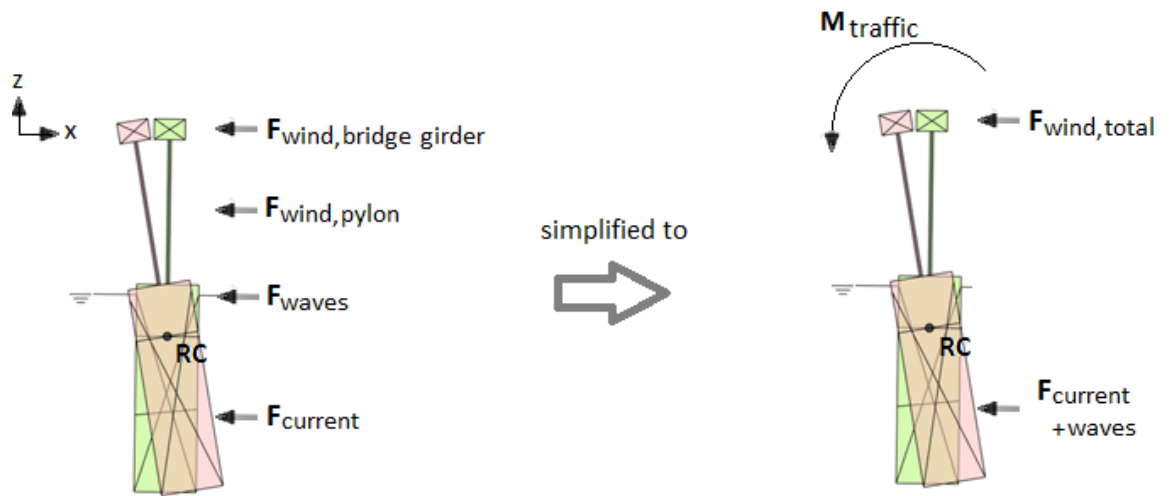


FIGURE R-5 LOAD CASE 3: CAUSES MAXIMUM DISPLACEMENTS IN X-DIRECTION (LEFT) AND LOAD CASE SIMPLIFICATION (RIGHT)

Load case 4: rotation 1 (ULS)

The same load types are applied as load case 2, shown in Figure Q-4, but now ultimate limit state (ULS) loads will be applied. The required torsional stiffness of the superstructure will be obtained.

Load case 5: rotation 2 (ULS)

This load case is almost the same as load case 4: traffic load, an outward (in negative x-direction) wind load and instead of an inward load from the water, an asymmetrical water load will be applied. Moreover, the traffic load is only applied at the bottom half of the pontoons. The asymmetrical load from the water is shown in Figure Q-6. By this kind of loading, a required torsional stiffness of the superstructure will be obtained.

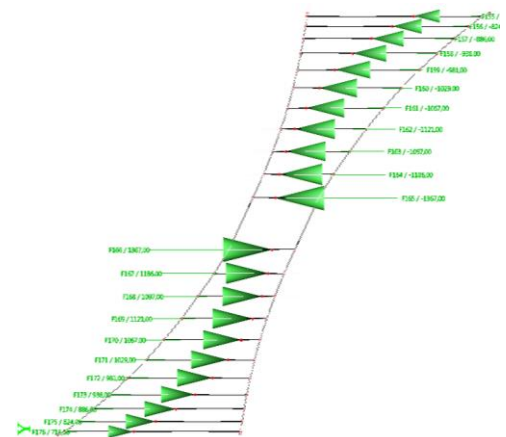


FIGURE R-6 ASYMMETRICAL WATER LOAD

Load case 6: maximum bending moment in horizontal plane (ULS)

The same load types as load case 3 are applied, shown in Figure Q-5, but now ultimate limit state (ULS) loads will be applied. The required horizontal bending stiffness of the bridge superstructure will be obtained from the results.

The ultimate limit state (ULS) loads are multiplied by the load factors $\gamma_G = 1,2$ and $\gamma_Q = 1,5$ for respectively the dead load and the variable loads. The calculation files can be seen in . In the calculations the self-weight is somewhat exaggerated. This is to create some margin for the design of the superstructure.

Load case 7: self-weight only (ULS)

For this load case, only the self-weight is taken into account. Load factor $\gamma_G = 1,35$ is used for the self-weight.

R.1.6 Other Scia Engineer Input Options

Cables

All cables are modeled as slack cables with self-weight checked ON.

The inputted pretension in the main anchoring cables is 200 000 kN.

The inputted pretension in the lateral anchoring cables is 0 kN.

Note that this is not the real normal force in the cables, this is just an initial input value for the model in Scia Engineer.

Mesh

Average size of cables in the mesh setup is 5 meters.

R.2 Results

R.2.1 Deformed Structures of Different Load Cases

The deformed structures from different views are shown in Table Q-4 to Table Q-6 for load case 1 to 6.

TABLE R-4 DEFORMED STRUCTURE IN 3D FOR ALL LOAD CASES

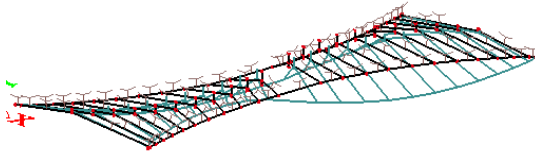
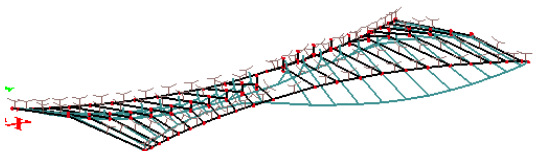
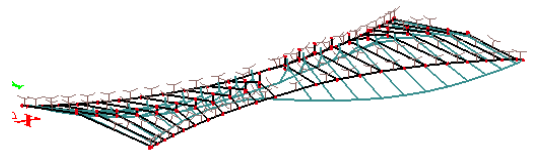
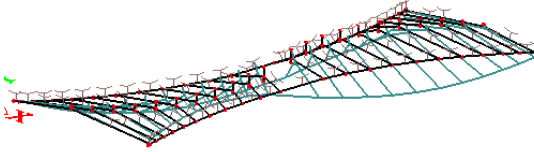
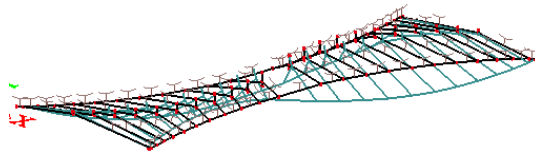
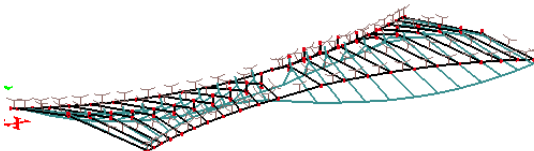
Load case 1: self-weight (SLS)	Load case 2: maximum ϕ_y (SLS)
	
Load case 3: maximum u_x (SLS)	Load case 4: maximum ϕ_y 1 (ULS)
	
Load case 5: maximum ϕ_y 2 (ULS)	Load case 6: maximum u_x (ULS)
	

TABLE R-5 DEFORMED STRUCTURE IN Y-Z PLANE FOR ALL LOAD CASES

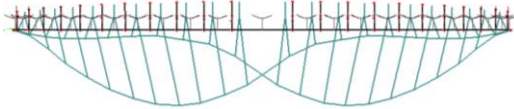
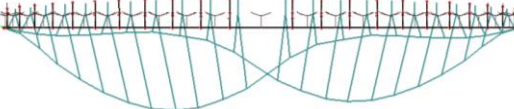
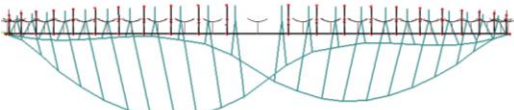
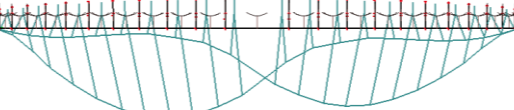
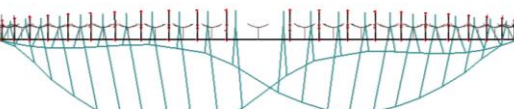
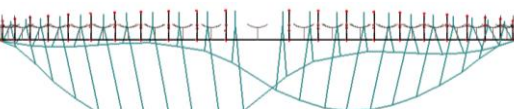
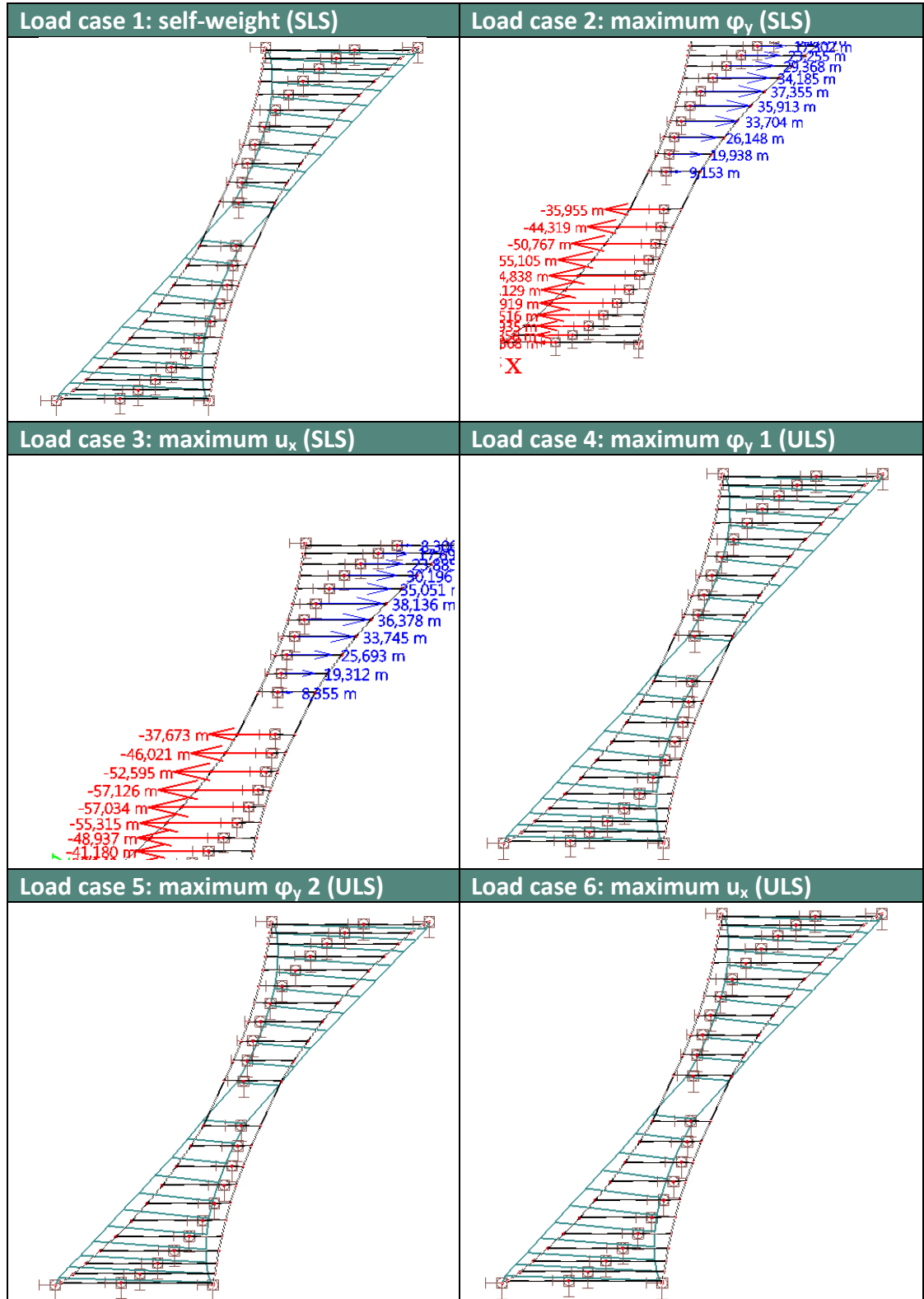
Load case 1: self-weight (SLS)	Load case 2: maximum φ_y (SLS)
	
Load case 3: maximum u_x (SLS)	Load case 4: maximum φ_y 1 (ULS)
	
Load case 5: maximum φ_y 2 (ULS)	Load case 6: maximum u_x (ULS)
	

TABLE R-6 DEFORMED STRUCTURE IN X-Y PLANE FOR ALL LOAD CASES



R.2.2 Displacements

The displacements at the pontoons on bridge deck level as result of the load cases in serviceability limit state (SLS), which are load case (LC) 1, 2 and 3, will be shown in this section.

Global displacements

In load case 1 (LC1) the anchoring system is only subjected to its self-weight. As can be seen in Figure R-7, due to self-weight the S-shape of the location of the pontoons becomes slightly fainter. In Table R-7 **Error! Reference source not found.** it can e seen that the largest displacements in x-direction is around 45 meters from the inputted perfect S-shape.

Displacements in x-direction

The displacements in x-direction of load case 3 (LC3) will be compared to this initial displacement due to self-weight only. This is shown in Table R-7 as du_x . The displacements of load case 3 are viewed, because this load case gives the largest displacements. It can be seen in the table, that with respect to the initial displacement, the largest displacements after applying the loads are located at pontoon 11 and 12 at the main span.

The displacements due to LC2 and LC3 with respect to the initial shape due to self-weight are shown graphically in Figure R-8. As expected, the largest displacements in x-direction occur for LC3, at pontoon 11 and 12, which corresponds to the values in the table.

Displacements in y-direction

The displacements in y-direction for LC2 and LC3 with respect to the initial shape due to self-weight are shown in Figure R-9. As can be seen, the displacements in y-direction are much smaller than the displacements in x-direction. The maximum displacements in y-direction are around 1 meter for LC3 at pontoons 3 and 20.

Displacements in z-direction

The displacements in z-direction are all zero or negligible small. (The largest displacement in z-direction occurs for LC3, being 0,5 meters.)

TABLE R-7 DISPLACEMENTS IN X-DIRECTION FOR LC1 AND LC3

Pontoon number	$u_{x,LC1}$ (m)	$du_{x,LC3}$ (m)
1	9,28	-0,69
2	19,59	-2,08
3	27,12	-3,87
4	34,46	-5,00
5	40,70	-6,38
6	45,21	-7,71
7	45,31	-9,31
8	44,29	-10,64
9	38,28	-12,28
10	32,01	-12,15
11	22,47	-13,39
12	-22,53	-13,54
13	-32,06	-12,44
14	-38,33	-12,67
15	-44,34	-10,90
16	-45,35	-9,45
17	-45,24	-7,75
18	-40,40	-6,39
19	-34,46	-4,95
20	-27,12	-3,81
21	-19,60	-2,05
22	-9,28	-0,67

Displacements due to self-weight

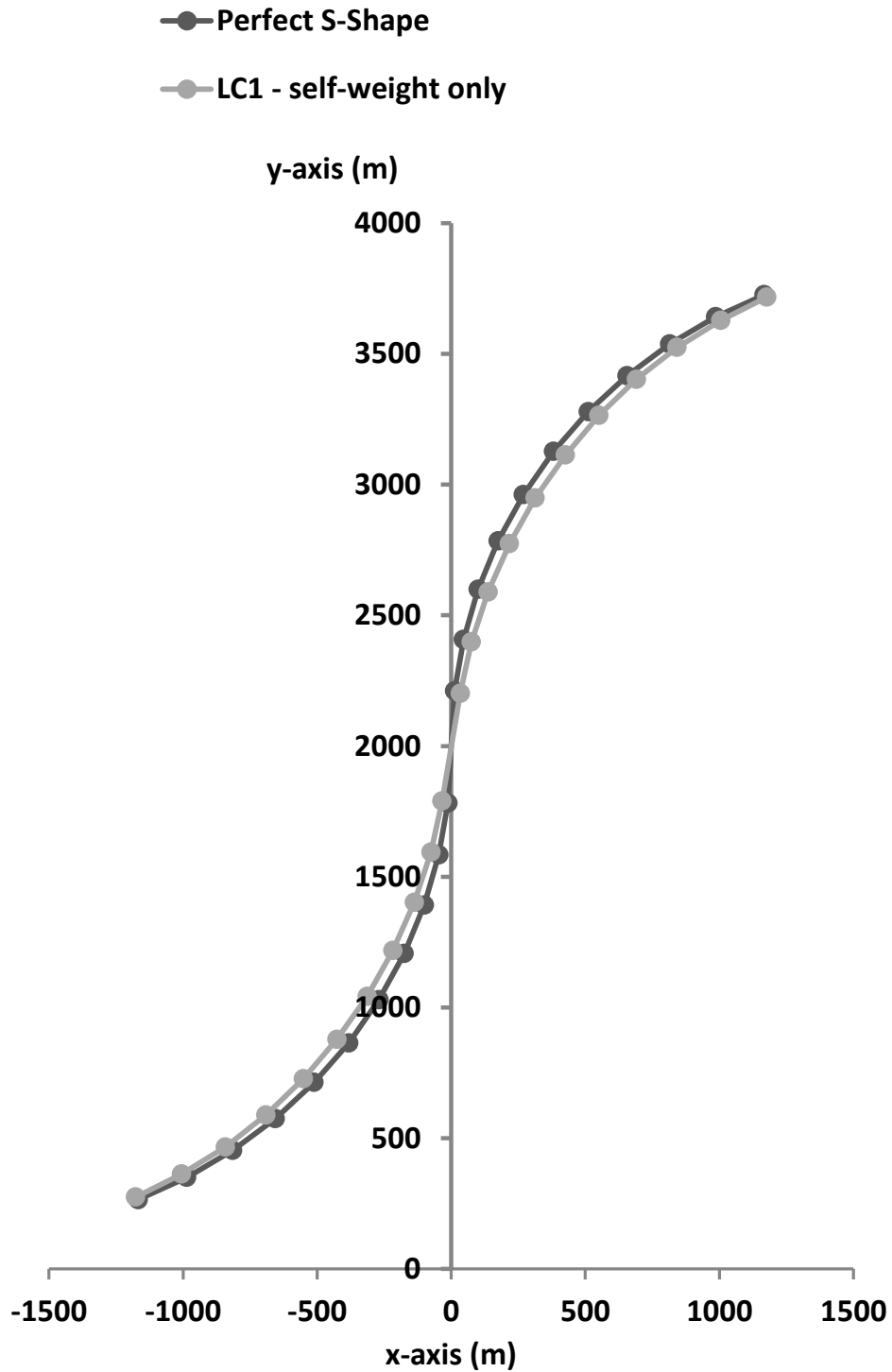


FIGURE R-7 DISPLACEMENTS DUE TO SELF-WEIGHT COMPARED TO THE PERFECT INPUT S-SHAPE

Displacements u_x from initial shape due to self-weight

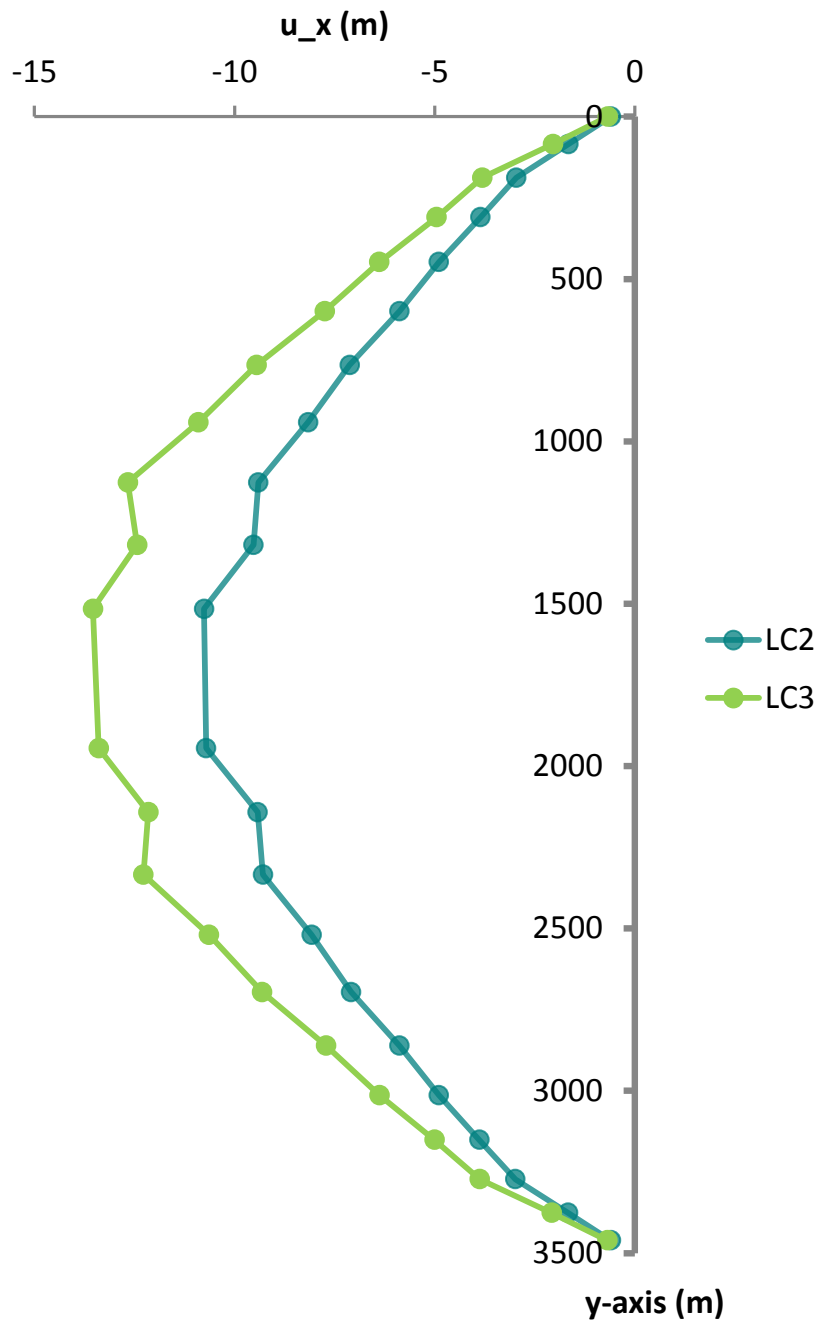


FIGURE R-8 DISPLACEMENTS u_x FROM INITIAL SHAPE DUE TO SELF-WEIGHT

Displacements u_y from initial shape due to self-weight

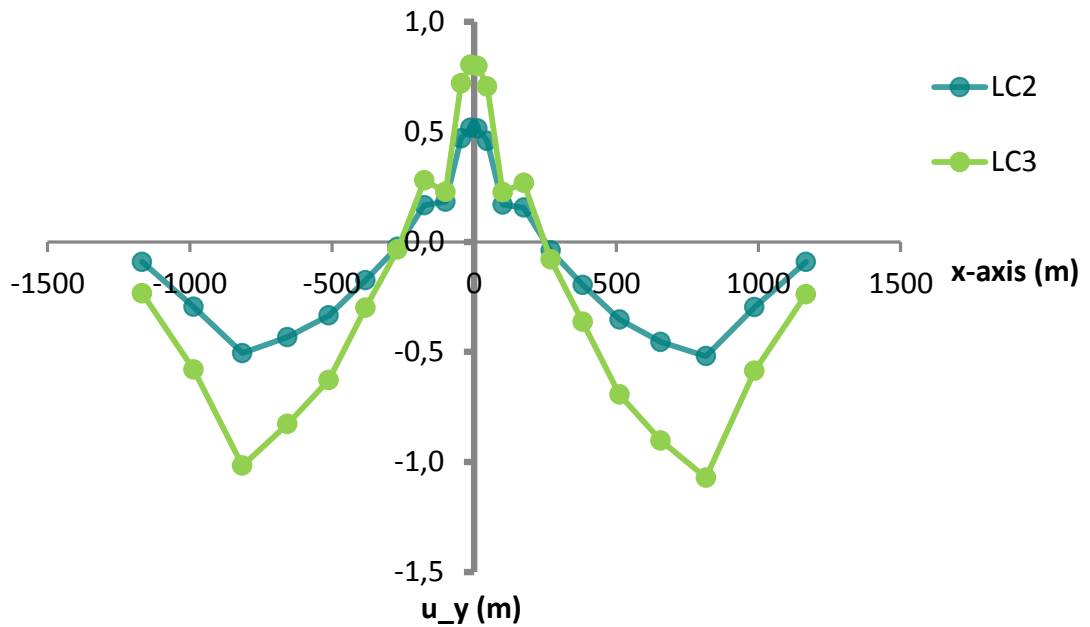


FIGURE R-9 DISPLACEMENTS U_Y FROM INITIAL SHAPE DUE TO SELF-WEIGHT

R.2.3 Rotations

Rotation Around y-axis

The largest rotations occur round the y-axis. Above all, this is due to the fact that only horizontal forces in x-directions are applied, as can be seen in Figure R-10. The rotation at bridge deck level is shown in Figure R-11. In the graph, it can be seen that due to solely the self-weight (LC1), there are already rotations present at bridge deck level. Due to the loading, as shown in (LC2), the maximum rotation becomes -102 mrad.

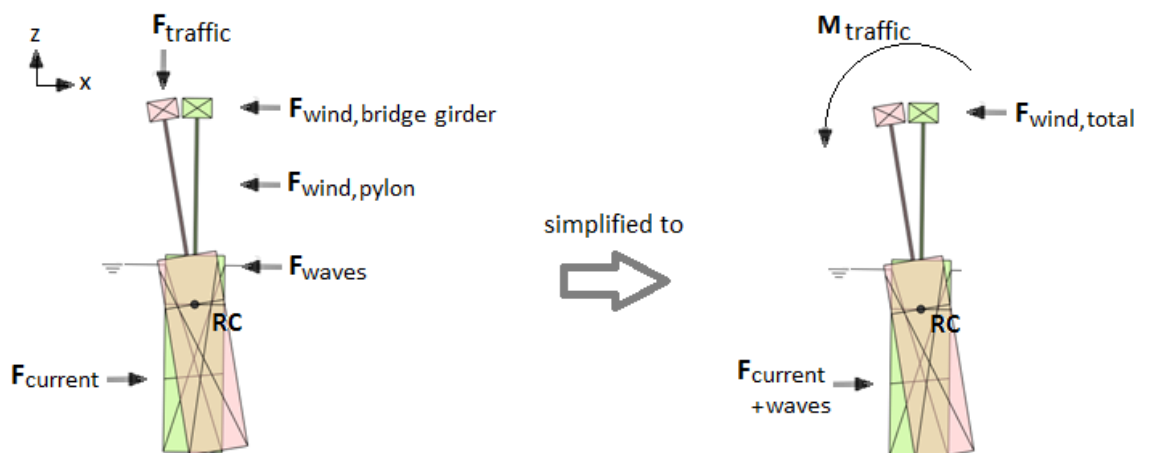


FIGURE R-10 LOAD CASE 2: CAUSING MAXIMUM ROTATION

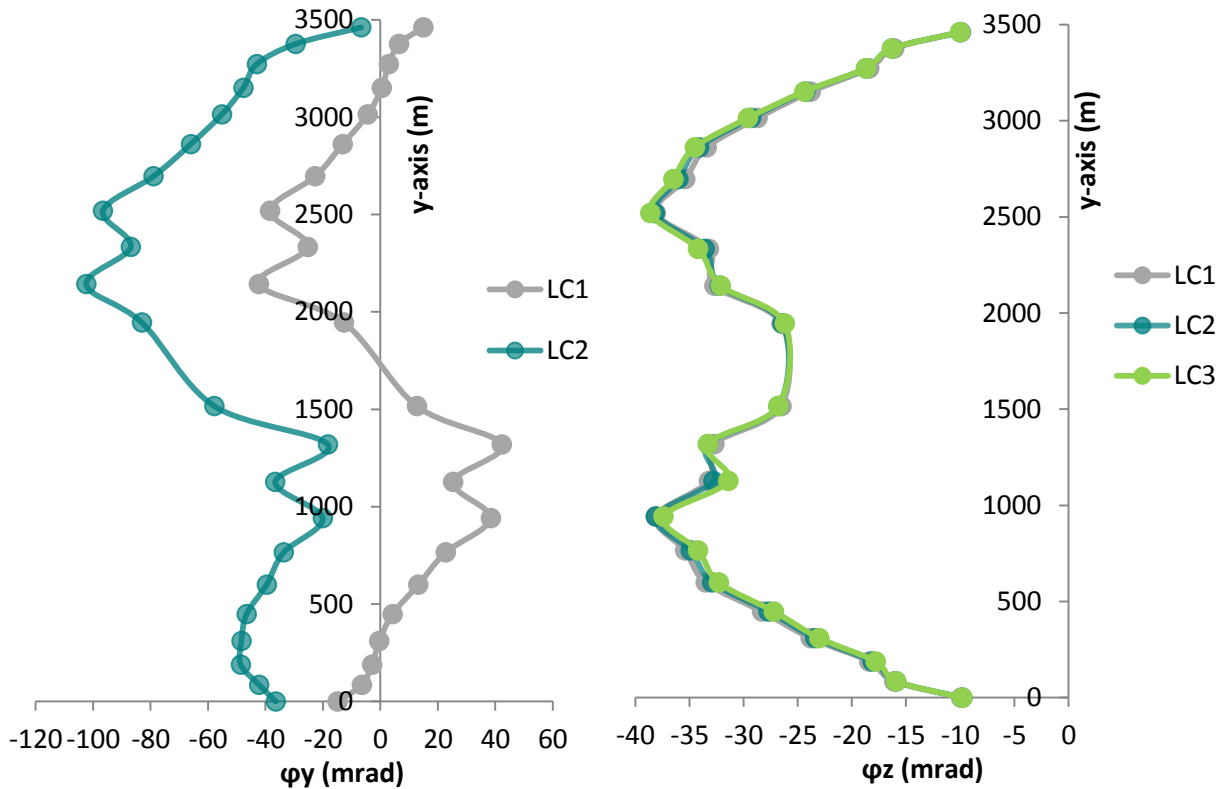


FIGURE R-11 ROTATION AT BRIDGE DECK LEVEL AROUND Y-AXIS (LEFT) AND Z-AXIS (RIGHT)

Rotations Around z-axis

As can be seen in Figure R-11, rotations around the z-axis are present at bridge deck level. However, these rotations are almost the same for all load cases. This indicates, that the horizontal loads do not influence the rotations around z-axis much.

Rotations around x-axis

The rotations around the x-axis are very small. This was expected, since no vertical external load cases are applied and since the displacements in z-direction was zero for all load cases.

R.2.4 Internal Forces and Stresses

The internal forces and stresses due to each load case is different, an example is given in Figure Q-7. The maximum internal forces and stresses for each load case is given in

Table Q-9.

According to the Eurocode [25], the ULS stress limit is 1.270 N/mm^2 and the SLS stress limit is 837 N/mm^2 for Y1860 (see section J.3.3 for the calculation). As can be seen in the table, all unity checks are satisfied.

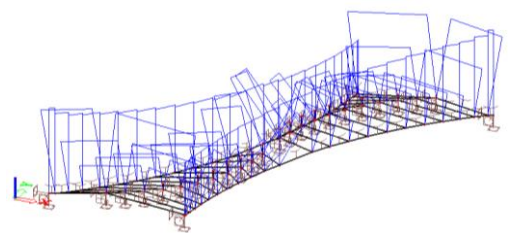


FIGURE R-12 EXAMPLE STRESS DISTRIBUTION

TABLE R-8 MAXIMUM INTERNAL FORCES AND STRESSES FOR EACH LOAD CASE

	LC1 (SLS)	LC2 (SLS)	LC3 (SLS)	LC4 (ULS)	LC5 (ULS)	LC6 (ULS)
Maximum force in main cable (kN)	$687,4 \cdot 10^3$	$713,2 \cdot 10^3$	$742,4 \cdot 10^3$	$833,9 \cdot 10^3$	$857,2 \cdot 10^3$	$879,2 \cdot 10^3$
Maximum force in lateral cable (kN)	$51,8 \cdot 10^3$	$53,9 \cdot 10^3$	$55,1 \cdot 10^3$	$64,0 \cdot 10^3$	$63,8 \cdot 10^3$	$66,0 \cdot 10^3$
Maximum stress in main cable (N/mm ²)	607,9	630,7	656,5	737,5	758,1	777,6
Maximum stress in lateral cable (N/mm ²)	539,0	559,8	573,1	665,5	663,6	686,3
Stress limit unity check	$\frac{608}{837} = 0,73$	$\frac{631}{837} = 0,75$	$\frac{657}{837} = 0,78$	$\frac{738}{1240} = 0,60$	$\frac{758}{1240} = 0,61$	$\frac{778}{1240} = 0,63$

R.3 Evaluation/Verification of the Model

R.3.1 Reaction forces in x-direction

The reaction forces in x-direction should equal the sum of the loads applied in x-direction. In Table Q-10, the horizontal reaction forces from Scia Engineer of each load case are shown. These will be compared to the inputted loads.

Load case 1 (LC1): The anchoring system is only subject to its own self-weight, no horizontal loads are applied. Therefore, the reaction force in x-direction should be equal to zero. As can be seen in the table, this is indeed the case.

Load case 2 (LC2): The anchoring system is subject to its self-weight, an outward (in negative x-direction) wind load and an inward (in positive x-direction) load in the water. The loads can be found in Table Q-3.

$$F_{wind,tot} - F_{water,tot} = 62,0 \cdot 10^3 - 22,4 \cdot 10^3 = 40,2 \cdot 10^3 \text{ kN}$$

This corresponds to the $39,6 \cdot 10^3$ kN in Table Q-10.

Load case 3 (LC3): The anchoring system is subject to its self-weight and both wind and water load in an outward direction.

$$F_{wind,tot} + F_{water,tot} = 62,0 \cdot 10^3 + 22,4 \cdot 10^3 = 84,4 \cdot 10^3 \text{ kN}$$

This is equal to the $84,4 \cdot 10^3$ kN in Table Q-10.

TABLE R-9 REACTION FORCES IN X-DIRECTION FOR EACH LOAD CASE

	LC1 (SLS)	LC2 (SLS)	LC3 (SLS)	LC4 (ULS)	LC5 (ULS)	LC6 (ULS)
Reaction forces in x-direction (kN)	0	$39,6 \cdot 10^3$	$84,4 \cdot 10^3$	$59,4 \cdot 10^3$	$93,0 \cdot 10^3$	$126,6 \cdot 10^3$

Load case 4 (LC4): The anchoring system is subject to its self-weight, an outward (in negative x-direction) wind load and an inward (in positive x-direction) load in the water. Since this load case is in ultimate limit state (ULS), load factors of 1,5 should be applied.

$$1,5 \cdot F_{wind,tot} - 1,5 \cdot F_{water,tot} = 93,0 \cdot 10^3 - 33,6 \cdot 10^3 = 59,4 \cdot 10^3 \text{ kN}$$

This corresponds to the $59,4 \cdot 10^3$ kN in Table Q-10.

Load case 5 (LC5): The anchoring system is subject to its self-weight, an outward wind load and an asymmetrical water load. The resultant force in x-direction caused by the asymmetrical water load is equal to zero. This means, that the total resultant reaction force in x-direction must be equal to the wind load. Since this is an ULS analysis, the load factor of 1,2 should be applied.

$$1,5 \cdot F_{wind,tot} = 1,5 \cdot 62,0 \cdot 10^3 = 93,0 \cdot 10^3$$

This is equal to the $93,0 \cdot 10^3$ kN in Table Q-10.

Load case 6 (LC6): The anchoring system is subject to its self-weight and both wind and water load in an outward direction. Since this is an ULS analysis, load factor 1,5 should be applied.

$$1,5 \cdot F_{wind,tot} + 1,5 \cdot F_{water,tot} = 93,0 \cdot 10^3 + 33,6 \cdot 10^3 = 126,6 \cdot 10^3 \text{ kN}$$

This is equal to the $126,6 \cdot 10^3$ kN in Table Q-10.

R.3.2 Reaction forces in z-direction

In this model, only the self-weight of the anchoring system is taken into account. The anchoring system consists of 2 main cables and 44 lateral anchoring cables. The total length of the main cable is 8410 meters and the total length of the lateral anchoring cables is 20 878 meters.

Analytically, the total reaction force in z-direction should then be:

$$\begin{aligned} \sum F_z &= \rho \cdot g (\pi \cdot r_{main}^2 \cdot L_{main} + \pi \cdot r_{lateral}^2 \cdot L_{lateral}) \\ &= (7850 - 1015) \cdot 9,81 \cdot (\pi \cdot 0,6^2 \cdot 8410 + \pi \cdot 0,175^2 \cdot 20818) = 772 \cdot 10^3 \text{ kN} \end{aligned}$$

To compare this to the results from Scia Engineer, the model has to be adjusted slightly. In this model, the four supports connecting the main cables to the shores are fixed supports. The supports in z-direction at the location of the pontoons are modelled as springs. In case all springs at the pontoons are changed to fixed constraints in z-direction, the reaction force in z-direction would be larger. This result from Scia Engineer and the other reaction forces in z-direction for each load case are given in Table Q-11.

It can be seen that the above calculated $772 \cdot 10^3$ kN corresponds well to the reaction force according to Scia Engineer ($774 \cdot 10^3$ kN), as can be seen in the second column of the table.

TABLE R-10 REACTION FORCES IN Z-DIRECTION FOR EACH LOAD CASE

	Model without springs	LC1 (SLS)	LC2 (SLS)	LC3 (SLS)	LC4 (ULS)	LC5 (ULS)	LC6 (ULS)
Reaction forces in z-direction (kN)	$774 \cdot 10^3$	$194 \cdot 10^3$	$194 \cdot 10^3$	$194 \cdot 10^3$	$233 \cdot 10^3$	$233 \cdot 10^3$	$233 \cdot 10^3$

LC1, LC2 and LC3: In these analyses, the pontoons are vertically supported by springs and upward buoyancy forces. The sum of the inputted buoyancy forces is $580 \cdot 10^3$ kN (see Table Q-3, last column). The reaction force in z-direction should then be the difference between the total resultant forces in case there were no springs and the sum of the inputted buoyancy force.

$$R_{z,total} - F_{b,total} = 774 \cdot 10^3 - 580 \cdot 10^3 = 194 \cdot 10^3 \text{ kN}$$

This corresponds well to the results from Scia Engineer, as can be seen in Table Q-11.

LC4, LC5 and LC6: These load cases are in ultimate limit state (ULS). Therefore, a load factor of 1,2 should be applied for the buoyancy force, which compensates the self-weight of the anchoring system.

$$1,2 (R_{z,total} - F_{b,total}) = 1,2 (774 \cdot 10^3 - 580 \cdot 10^3) = 233 \cdot 10^3 \text{ kN}$$

This corresponds well to the results from Scia Engineer, as can be seen in Table Q-11.

R.3.3 Effect of the Rotational Spring

To verify the effect of the rotational spring, results of the system with the rotational springs will be compared to the results of the system without the springs.

In an anchoring system without the rotational spring, the horizontal deformation on an arbitrary chosen pontoon and pylon looks like as shown in Figure Q-9. It can be seen that the deformation on the beam is almost constant over the whole height. This means that the deformation is particularly caused by displacement of the member in x-direction, there is no rotation of the member around the rotation center. In Figure Q-9, the horizontal deformation can be seen of the pontoon and pylon in an anchoring system *with* rotational springs. It can be seen that the pontoon/pylon has rotated.

R.3.4 Effect of Additional Prestressing Force

The difference between an anchoring system, which is prestressed by solely its own self-weight, and an anchoring system which is prestressed by its self-weight and additional prestressing force is compared to investigate the behavior of the anchoring system.

TABLE R-11 VARYING THE PRETENSIONING

	Model with additional prestress	Model without additional prestress
Tension force in main cable (kN)	$687,4 \cdot 10^3$	$662,8 \cdot 10^3$
Maximum force in lateral cable (kN)	$51,8 \cdot 10^3$	$50,8 \cdot 10^3$

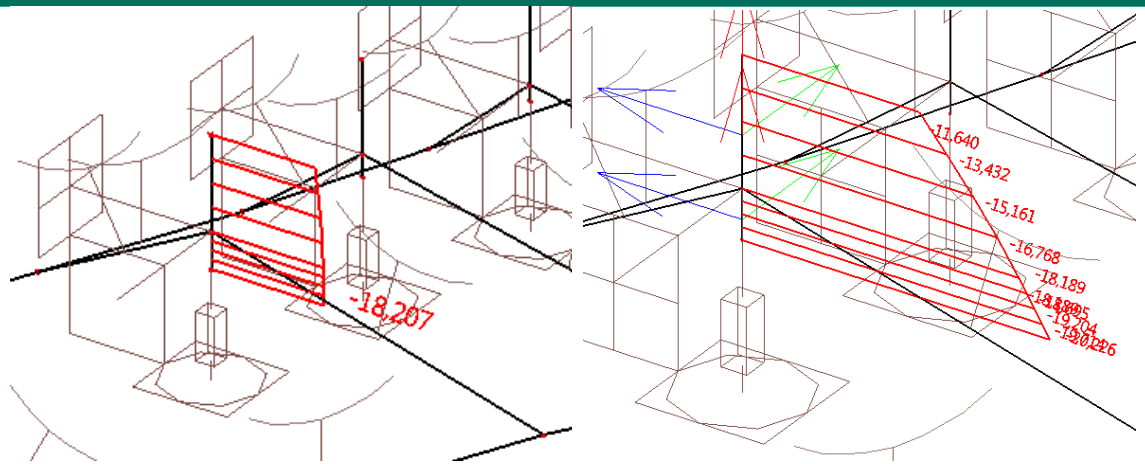


FIGURE R-14 DISPLACEMENT IN CASE WITHOUT ROTATIONAL SPRING IN [M]

FIGURE R-14 DISPLACEMENT IN CASE WITH ROTATIONAL SPRING IN [M]

The tension force in the cable of the model in this section, where additional prestressing is applied, and the tension force in the cable of a model where no additional prestressing is applied, are shown in Table Q-12. It can be seen that $662,8 \cdot 10^3$ kN is due to the self-weight of the cables. This indicates that the additional prestress is actually:

$$687,4 \cdot 10^3 - 662,8 \cdot 10^3 = 24,6 \cdot 10^3 \text{ kN}$$

Since in the model without this additional prestress the internal force is decreased, it is expected that the stresses in the cables also decrease, the total resultant forces remain the same and the displacements of the nodes increase.

In Table Q-13, the comparisons between the original and variant model can be seen. The internal stresses of the cables have indeed decreased and the total resultant forces have remained the same.

TABLE R-12 COMPARISON ORIGINAL AND VARIANT MODEL

	Model with additional prestress	Model without additional prestress
Internal stress main cable (N/mm ²)	607,0	586
Maximum internal stress in lateral cable (N/mm ²)	539,0	528
Total resultant Fz (kN)	$194 \cdot 10^3$	$194 \cdot 10^3$

In the displacements in x-direction as result of load case 3 are compared. The displacements of the variant anchoring system without additional prestress in the cables yield larger displacements.

After these validations, it can be assumed that the computational model gives reliable results.

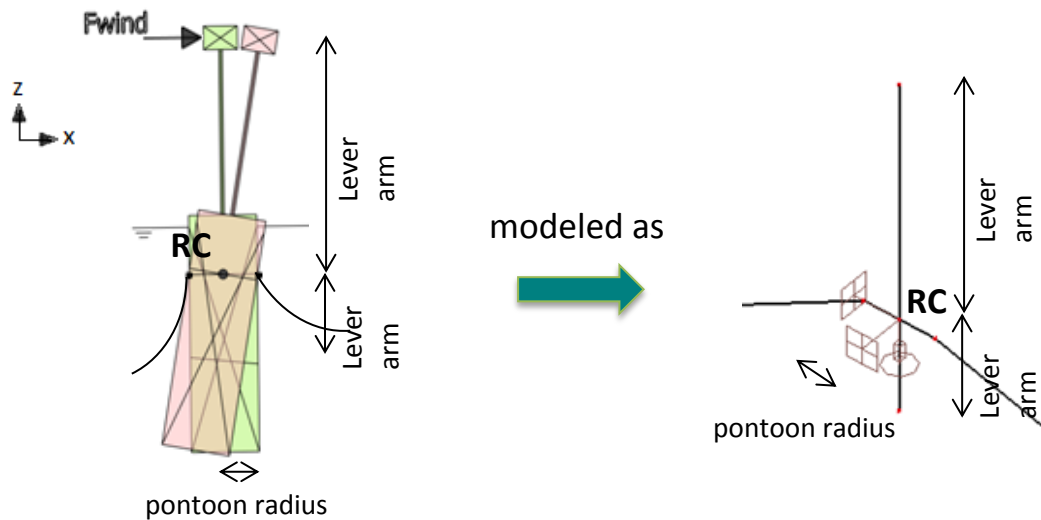


FIGURE R-15 ADDITION MEMBERS BETWEEN ANCHORING CABLE ATTACHMENT NODES AND ROTATION CENTER

R.3.5 Effect of adding members between rotation center and cable attachment nodes

By adding members between the rotation center and cable attachment nodes instead of attaching the cables directly to the rotation center, causes the self-weight of the anchoring cables to contribute to a rotation.

This addition is the only difference between computational model 4 from ANNEX Q: Computational Model Substructure example 4 (with Springs and the proposed anchoring model from this section (computational model 5). In the results of model 4 in section Q.2.2, it could be seen that the rotation around the y-axis is zero when the anchoring system is only loaded by its self-weight. This is logical, since the anchoring cables are attached to the rotation center in this model. Therefore, the self-weight of the cables do not cause a rotation.

In the model from this section however, the self-weight of the anchoring cables and the added leverarm (pontoon radius) causes a bending moment and therefore also causing rotation around the y-axis, see Figure R-11. Subsequently, the maximum rotation when also horizontal loads are applied besides the self-weight (LC2), increases from 76 mrad (see Table Q-8) to 102 mrad (see Figure R-11).

These results also indicate a relation between the pontoon radius, the self-weight of the anchoring system and the rotations around y-axis. The larger the pontoon radius, the larger the lever arm of the cable self-weight and the larger the rotations.

Likewise, the larger the self-weight of the anchoring system, the larger the bending moment due to the self-weight of the cables and the larger the rotations.

To check the rigid connection between the members at the rotation center (RC), can be studied. There it can be seen, that rotation is present in both the vertical and horizontal members. The rotation of the vertical member at the rotation center is -28,4 mrad. Likewise, the rotation of the horizontal member at the rotation center is also -28,4 mrad. It can be concluded that the connection is indeed rigid.

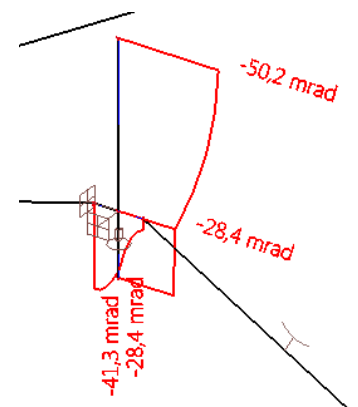


FIGURE R-16 ROTATION OF THE MEMBERS AT RC

R.3.6 Effect of External Forces

To obtain a good understanding about the effect of the external forces on the anchoring system, the increase of the tension force in the cable due to a specific external load type will be compared. The results are given in Table R-13.

TABLE R-13 EFFECT OF EXTERNAL FORCES ON INTERNAL TENSION FORCES IN THE CABLES

Load	Maximum tension force in main cable ($\cdot 10^3$ kN)	Increase tension force in main cable due to self-weight and specific load	Maximum tension force in lateral cable ($\cdot 10^3$ kN)	Increase tension force in main cable due to self-weight and specific load
Self-weight anchoring system	687	0 %	51,8	0 %
Horizontal wind load	727	5,8 %	54,5	5,0 %
Wave and current load	700	1,9 %	52,4	1,2 %

ANNEX S: CALCULATION FILE PONTOON PROPERTIES AND LOADS FOR MODEL 5

Pontoon and Loads Calculation File

In this file, the calculations done with Maple are shown. The pontoon properties and external loads are obtained as shown in the followings.

```
restart, unprotect(γ); with(plots): with(plottools): color_1 := "DarkRed"; color_2
:= "DarkMagenta"; color_6 := "SkyBlue"; color_7 := "DarkSlateGrey"; color_8
:= "DarkKhaki"; color_9 := "DarkCyan"; color_10 := "DarkGoldenrod";
color_11 := "SandyBrown"; color_12 := "YellowGreen"; colorVec := [color_1,
color_2, color_3, color_4, color_5, color_6, color_7, color_8]; interface(riablesize
= 30);
```

Input

S-curve characteristics (RH, p.39)

Main span enlarged from 400 meters to 430 meters, because of the required clearance 70x400x20 (height x width x draught). The pontoons have a radius of 15 meters, so main span must be 430 meters heart to heart.

side span $l_{g,n}$:= 200 : main span $l_{g,mid}$:= 430 :

halve lengte rechtstreeks oever naar oever x_{hs} := 1753.7 : halve lengte in

langsrichting van brugdek s_{hs} := 2280.05 :

lengte van halve S in water in langsrichting van fjord y_{hw} := 1228 :

$y_1 := \sin(\alpha_a) \cdot R_{ha} : y_2 := R_{ha} - y_1 :$

$\alpha_a := \left(\frac{\pi}{9} \right) :$

$R_{ha} := 1866.25 :$

Pontoon locations

aantal hele side spans in halve brug $n_{nspans,hs}$:= floor $\left(\frac{(s_{hs} - 0.5 \cdot l_{g,mid})}{l_{g,n}} \right) ;$

10

(1)

lengte die over is aan oever $l_{gl} := s_{hs} - 0.5 \cdot l_{g,mid} - n_{nspans,hs} \cdot l_{g,n} ;$

aantal pontons in halve brug $n_{nspans,hs}$:= $n_{nspans,hs} + 1 :$

aantal spans in hele brug n_{spans} := $2 \cdot n_{nspans,hs} + 1 :$

$\beta_1 := \frac{l_{gl}}{R_{ha}} : \beta_n := \frac{l_{g,n}}{R_{ha}} : \beta_m := \frac{0.5 \cdot l_{g,mid}}{R_{ha}} ;$

$n_{spans,hs}$

11

(3)

for j from 1 to $n_{spans,hs}$ do $\beta_{p,j} := (\alpha_a + \beta_1 + (j-1) \cdot \beta_n) : dx_{p,j} := evalf(x_{hs} - \cos(\alpha_a + \beta_1 + (j-1) \cdot \beta_n) \cdot R_{ha}) : b_{p,j} := dx_{p,j} : a_{p,j} := 2 \cdot x_{hs} - b_{p,j} : end$

do;

for j from $n_{spans,hs} + 1$ to $2 \cdot n_{spans,hs}$ do $\beta_{p,j} := \beta_{p,(n_{spans,hs} - (j-1 - n_{spans,hs}))} : dx_{p,j} := \sin(\beta_m + (j - (n_{spans,hs} + 1)) \cdot \beta_n) \cdot R_{ha} + x_{hs} : b_{p,j} := dx_{p,j} : a_{p,j} := 2 \cdot x_{hs} - b_{p,j} : end$

do;

for j from 1 to $n_{spans,hs}$ do $d_{p,j} := evalf(\sin(\alpha_a + \beta_1 + (j-1) \cdot \beta_n) \cdot R_{ha} - y_1) : c_{p,j} := evalf(2 \cdot y_2 - d_{p,j}) : end$

do;

for j from $n_{spans,hs} + 1$ to $2 \cdot n_{spans,hs}$ do $d_{p,j} := evalf(y_2 + (y_2 - d_{p,(n_{spans,hs} - (j-1 - n_{spans,hs} + 1))})) : c_{p,j} := evalf(2 \cdot y_2 - d_{p,j}) : end$

(4)

Elevation

$f_{p,mm} := 3 :$

$z_b := 70 + z_c - f_{p,mm} :$

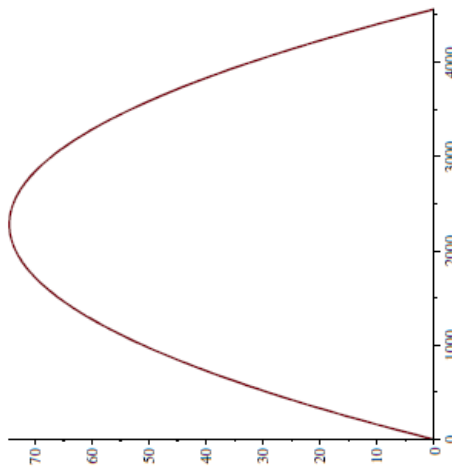
$z_c := \frac{15}{2} :$

$R_{va} := \frac{0.5 \cdot (z_b^2 + s_{hs}^2)}{(z_b)} : R_{va}$

34927.37082

(5)

$$fz := sa \rightarrow \text{sqrt}(R_{va}^2 - (sa - s_{hs})^2) - (R_{va} - z_b) : \text{plot}(fz, 0..2 \cdot s_{hs})$$



$\text{eval}(fz(sa), sa = 65.05)$

4.19456

(6)

Plot

$dy := R_{ha} + y_2 :$

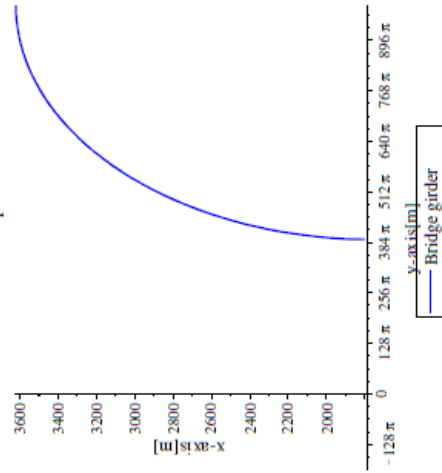
$dx := x_{hs} :$

$ta := \text{sqrt}(R_{ha}^2 - (ya - dy)^2) + dx :$

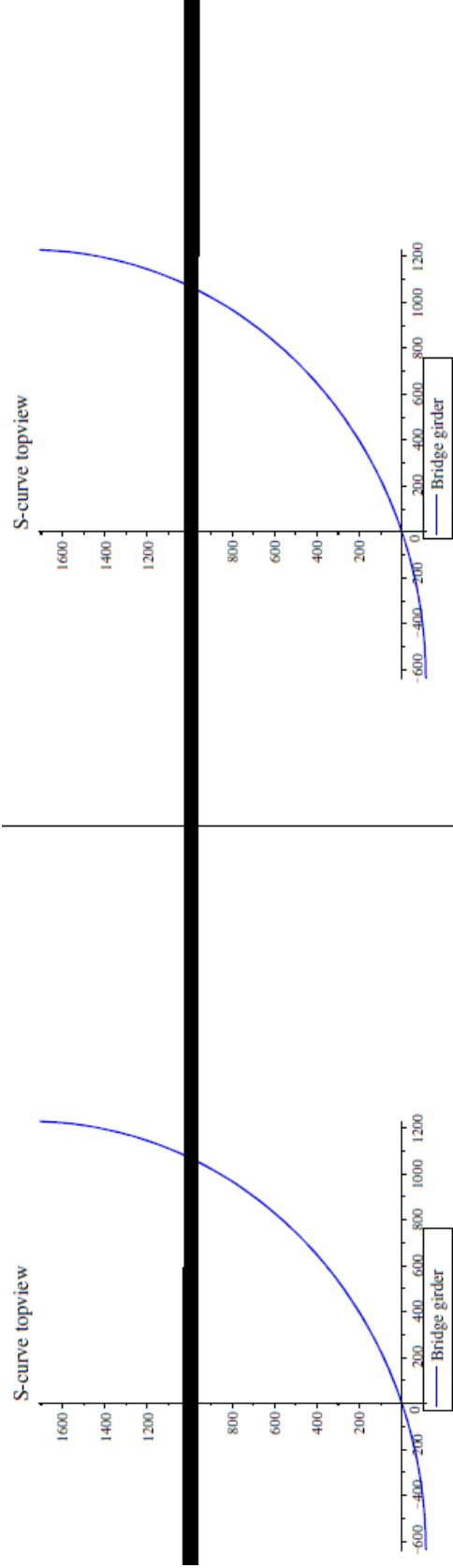
$\text{with}(\text{plots}) : Pta := \text{plot}(ta, ya = -600..R_{ha} + y_2, \text{color} = \text{blue}, \text{title} = \text{typeset}(\text{"S-curve topview"}), \text{titlefont} = [\text{"calibri"}, 14], \text{legend}$

$= \text{"Bridge girder"}, \text{labels} = [\text{"y-axis[m]"}, \text{"x-axis[m]"}], \text{labelfont} = [\text{"calibri"}, 12], \text{labeldirections} = [\text{"horizontal"}, \text{"vertical"}]) : \text{display}([Pta]);$

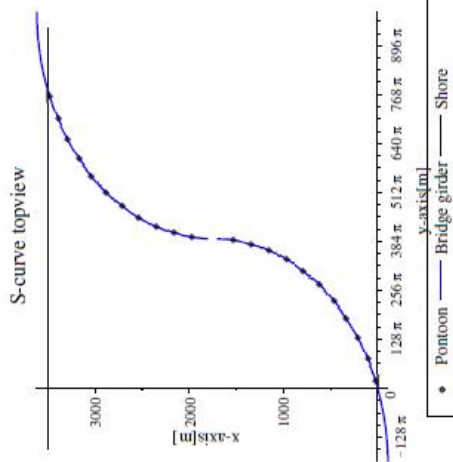
S-curve topview



$Pba := \text{reflect}(\text{reflect}(Pta, [[0, x_{hs}], [5000, x_{hs}]]) \cdot [[y_2, 0], [y_2, 5000]]) :$



sa = s \ | - (R - z \) ; plot(z, 0 ...2 \ s \)
tz = sa -> sort(R - z \)



```

xp,i := bp,i;
yp,i := dp,i;
zp,i := eval(fz(sa), sa = sp,i) + frp,m,i;
lcp,i := (xp,i | yp,i | zp,i) : sa := sa;
end do;
for i from 1 to 22 do
xp,i := bp,i;
yp,i := dp,i;
zp,i := eval(fz(sa), sa = sp,i) + frp,m,i;
lcp,i := < xp,i | yp,i | zp,i > : sa := sa;
end do;
xg,23 := xg,1;
for i from 2 to 22 do
amm,i := evalf ( zbyp,i - cos ( 2.5 · π / 180 ) · zbyp,i );
bmm,i := evalf ( sin ( 2.5 · π / 180 ) · zbyp,i );
end do;

```

```

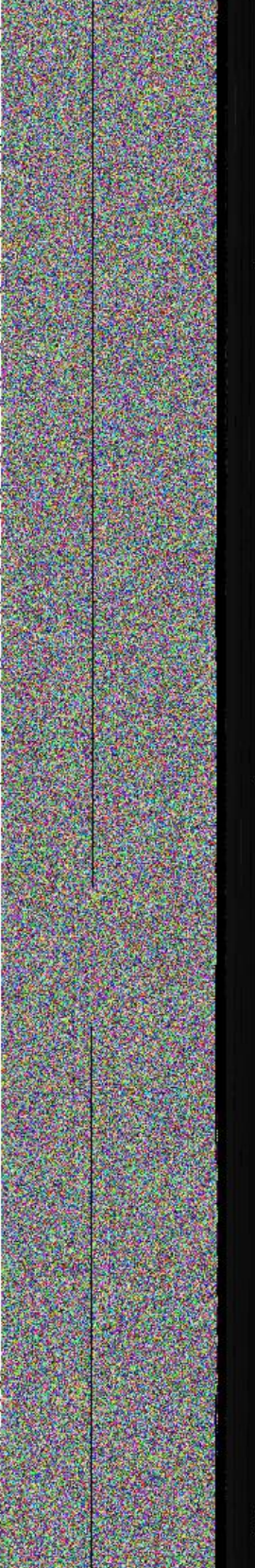
Pontoon coordinates
lg,1 := ls; s := lg,1;
for i from 2 to 11 do
lg,i := lg,n;
end do;
lg,12 := lg,mid;

```

```

(< "#P", 1, 2, 3, 4, 5, 6, 7, 8, 9, 10, 11, 12, 13, 14, 15, 16, 17, 18, 19, 20, 21, 22 >
| ("y_P", dp,1, dp,2, dp,3, dp,4, dp,5, dp,6, dp,7, dp,8, dp,9, dp,10, dp,11, dp,12
dp,13, dp,14, dp,15, dp,16, dp,17, dp,18, dp,19, dp,20, dp,21, dp,22) | ("x_P", bp,1,
bp,2, bp,3, bp,4, bp,5, bp,6, bp,7, bp,8, bp,9, bp,10, bp,11, bp,12, bp,13, bp,14, bp,15, bp,16, bp,17, bp,18, bp,19, bp,20, bp,21, bp,22)

```



7

45.82553000

for i from 1 to 22 do

"#P"	"y_p"	"x_p"	"z"
1	60.7269222	23.307765	4.19456
2	241.8025361	108.003422	16.32772000
3	412.7801466	211.581358	27.30990000
4	571.6980026	332.853149	37.14218000
5	716.7327236	470.427354	45.82553000
6	846.2202196	622.725485	53.36082000
7	958.6747866	788.0001131	59.74878000
8	1052.806150	964.3549220	64.99004000
9	1127.534273	1149.766464	69.08512000
10	1182.001745	1342.107377	72.03443000
11	1215.583621	1539.170793	73.83826000
12	1240.326194	1968.224734	73.83826000
13	1273.908070	2165.288231	72.03443000
14	1328.375542	2357.629276	69.08512000
15	1403.103665	2543.040998	64.99004000
16	1497.235028	2719.396034	59.74878000
17	1609.689595	2884.670933	53.36082000
18	1739.177091	3036.969376	45.82553000
19	1884.211812	3174.543932	37.14218000

(8)

```

R_pylon := 2.5 ;
R_pyloncon := 15 ;
z_a := 20 ;

t_p_top := 1 ; t_p_bot := 1 +  $\frac{p}{50}$  ; t_p_side := 0.5 +  $\frac{R_{pyloncon}}{15}$  ; t_pylon :=  $\frac{R_{pylon}}{15}$  ;

for i from 1 to 22 do
  l_p,i := d r_p,i, ULS + f r_p, mn ;
end do ;
h_ws := 2.4 ;

t_girder := 0.022514 ;  $\alpha_R := 90$  ; d_in := 0.4531 ;

a_truss := 15 ; h_truss := 3.5 ; d_truss := 1 ; l_trussdia := sqrt(h_truss^2 + a_truss^2) ; d_trussdia := 0.5 ;

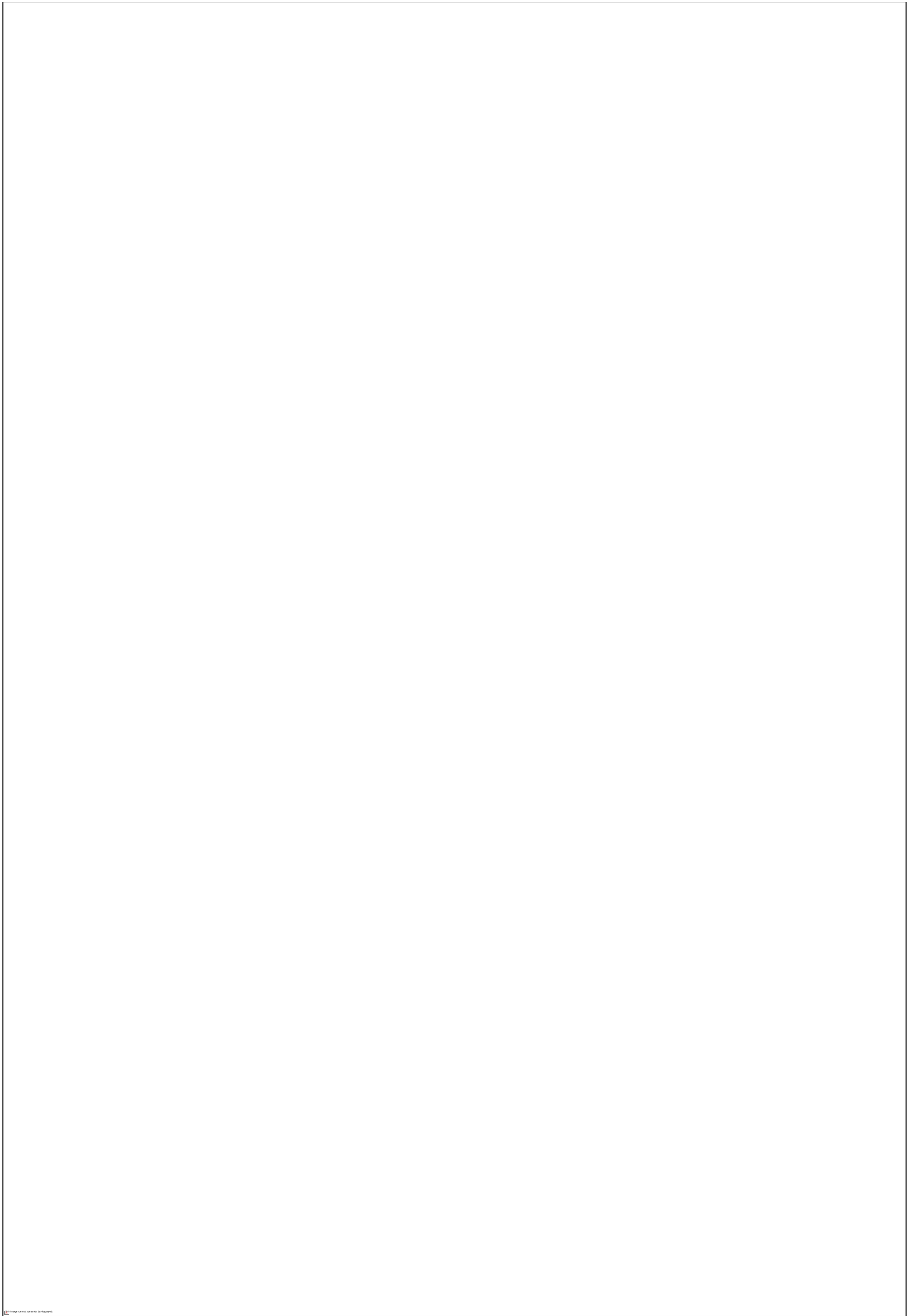
Vertical forces input
Vertical forces
q_traffic := 35 ;

F_g, ULS :=  $\frac{1}{a} \cdot l \cdot F$  ;
F_g, ULS :=  $\frac{1}{a} \cdot l \cdot a$  ;

q_g, SLS, mid := 153.5179 ;
q_g, ULS, mid := 194.7215 ;

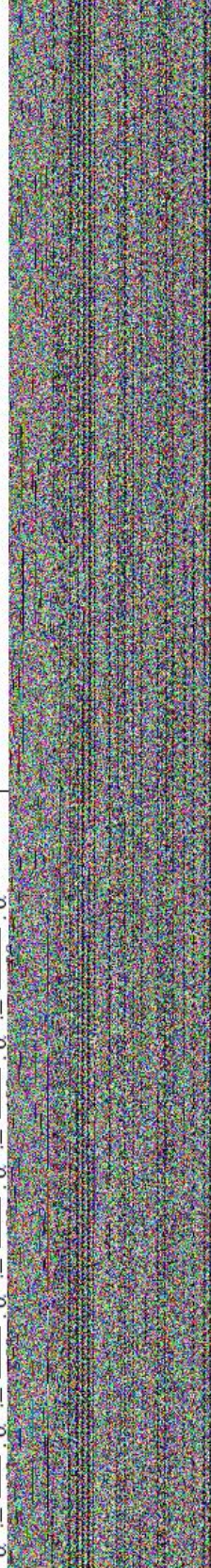
b_g := 10 ;
b_deck := 16 ;

```



Definition angles:

$$\alpha := \frac{0 \cdot \pi}{30 \cdot \pi} ; \alpha := \frac{30 \cdot \pi}{60 \cdot \pi} ; \alpha := \frac{60 \cdot \pi}{90 \cdot \pi} ; \alpha := \frac{90 \cdot \pi}{120 \cdot \pi} ; \alpha$$



$$:= \text{evalf} \left(\left(\frac{(1 - K_{\text{prob}} \cdot \ln(-\ln(1 - P_{\text{prob}})))^{n_{\text{prob}}}}{1 - K_{\text{prob}} \cdot \ln(-\ln(0.99))} \right) \right) \\ 0.9033175203$$

(III)

Extreme values of wind speed per direction (Hermans, 2014, Figure 4-3):

$$V_{b, \alpha, 1, ULS} := 21 ; V_{b, \alpha, 2, ULS} := 26 ; V_{b, \alpha, 3, ULS} := 26 ; V_{b, \alpha, 4, ULS} := 23 ; \\ V_{b, \alpha, 5, ULS} := 24 ; V_{b, \alpha, 6, ULS} := 28 ; V_{b, \alpha, 7, ULS} := 35 ; V_{b, \alpha, 8, ULS} := 35 ; \\ V_{b, \alpha, 9, ULS} := 35 ; V_{b, \alpha, 10, ULS} := 33 ; V_{b, \alpha, 11, ULS} := 33 ; V_{b, \alpha, 12, ULS} := 23 ;$$

Extreme values of wind wave height per direction (Hermans, 2014, Figure 4-5):

$$H_{s, \text{ww}, \alpha, 1, ULS} := 1.01 ; H_{s, \text{ww}, \alpha, 2, ULS} := 1.62 ; H_{s, \text{ww}, \alpha, 3, ULS} := 1.81 ; \\ H_{s, \text{ww}, \alpha, 4, ULS} := 1.49 ; H_{s, \text{ww}, \alpha, 5, ULS} := 1.4 ; H_{s, \text{ww}, \alpha, 6, ULS} := 1.57 ; \\ H_{s, \text{ww}, \alpha, 7, ULS} := 2.22 ; H_{s, \text{ww}, \alpha, 8, ULS} := 2.24 ; H_{s, \text{ww}, \alpha, 9, ULS} := 2.34 ; \\ H_{s, \text{ww}, \alpha, 10, ULS} := 2.13 ; H_{s, \text{ww}, \alpha, 11, ULS} := 1.83 ; H_{s, \text{ww}, \alpha, 12, ULS} := 1.00 ;$$

Significant wave height (Hermans, 2014, Figure 4-6):

$$H_{s, \text{sw}, \alpha, 1, ULS} := 0.01 ; H_{s, \text{sw}, \alpha, 2, ULS} := 0.01 ; H_{s, \text{sw}, \alpha, 3, ULS} := 0.01 ;$$

$$H_{s, \text{sw}, \alpha, 4, ULS} := 0.01 ; H_{s, \text{sw}, \alpha, 5, ULS} := 0.01 ; H_{s, \text{sw}, \alpha, 6, ULS} := 0.01 ; \\ H_{s, \text{sw}, \alpha, 7, ULS} := 0.01 ; H_{s, \text{sw}, \alpha, 8, ULS} := 0.01 ; H_{s, \text{sw}, \alpha, 9, ULS} := 0.01 ; \\ H_{s, \text{sw}, \alpha, 10, ULS} := 0.01 ; H_{s, \text{sw}, \alpha, 11, ULS} := 0.01 ; H_{s, \text{sw}, \alpha, 12, ULS} := 0.01 ;$$

$$u_{cl, \alpha, 1} := 1.27 ; u_{cl, \alpha, 2} := 1.27 ; u_{cl, \alpha, 3} := 1.27 ; u_{cl, \alpha, 4} := 1.27 ; u_{cl, \alpha, 5} \\ := 1.27 ; u_{cl, \alpha, 6} := 1.27 ; u_{cl, \alpha, 7} := 1.27 ; u_{cl, \alpha, 8} := 1.27 ; u_{cl, \alpha, 9} := 1.27 ; \\ u_{cl, \alpha, 10} := 1.27 ; u_{cl, \alpha, 11} := 1.27 ; u_{cl, \alpha, 12} := 1.27 ;$$

$$u_{c2, \alpha, 1} := 0.875 ; u_{c2, \alpha, 2} := 0.875 ; u_{c2, \alpha, 3} := 0.875 ; u_{c2, \alpha, 4} := 0.875 ; u_{c2, \alpha, 5} \\ := 0.875 ; u_{c2, \alpha, 6} := 0.875 ; u_{c2, \alpha, 7} := 0.875 ; u_{c2, \alpha, 8} := 0.875 ; u_{c2, \alpha, 9} \\ := 0.875 ; u_{c2, \alpha, 10} := 0.875 ; u_{c2, \alpha, 11} := 0.875 ; u_{c2, \alpha, 12} := 0.875 ; \\ u_{c3, \alpha, 1} := 0.48 ; u_{c3, \alpha, 2} := 0.48 ; u_{c3, \alpha, 3} := 0.48 ; u_{c3, \alpha, 4} := 0.48 ; u_{c3, \alpha, 5} \\ := 0.48 ; u_{c3, \alpha, 6} := 0.48 ; u_{c3, \alpha, 7} := 0.48 ; u_{c3, \alpha, 8} := 0.48 ; u_{c3, \alpha, 9} := 0.48 ; \\ u_{c3, \alpha, 10} := 0.48 ; u_{c3, \alpha, 11} := 0.48 ; u_{c3, \alpha, 12} := 0.48 ;$$

(14)

Length Expressions and Forces

$$y_{p, 0} := 0 ;$$

$$x_{p, 0} := 0 ;$$

for i from 1 to 22 do
for n from 1 to 6 do

$$l_{gp, i} := \frac{(l_{g, i} + l_{g, (i+1)})}{2} ;$$

$$l_g := l_{gp, i} ;$$

$$s_a := s_{p, i} ;$$


```

αb,i := arctan( ( (yp,i - yp,(i-1)}) / (xp,i - xp,(i-1)}) ) / 2 );
αd,i,n := abs( evalf( ssb,i * cos(αd,i,n) ) ); else αd,i,n := ( αn - αb,i + π / 2 ) / g,i,α,n
end do;
lg,i,α,7 := lg,i,α,1;
lg,i,α,8 := lg,i,α,2;
lg,i,α,9 := lg,i,α,3;
lg,i,α,10 := lg,i,α,4;
lg,i,α,11 := lg,i,α,5;
lg,i,α,12 := lg,i,α,6;
lg := lg; σα := 'sa';
end do;

for n from 1 to 12 do
lg,23,α,n := lg,1,α,n;
end do;

Force Expressions

for i from 1 to 22 do
frp,i,SLS := lp,i - drp,i,SLS;
frn,i,m,SLS := ln,i - drn,i,m,SLS; ln,i
hgp,i := (gp,i / 90) * hg; hgp,i := zBG,i; zBG,i := fz(sp,i) + (g / 2) + frp,i,m,SLS;
Fwind,BG,α,SLS := qp,g,SLS(zBG,i) * lgp,i,α,n * (hg + hws) * Cd,gw;
Fwind,BG,α,ULS := qp,g,ULS(zBG,i) * lgp,i,α,n * (hg + hws) * Cd,gw;
Fwind,truss,α,SLS := (2 * qp,g,SLS(zBG,i) * lgp,i,α,n) / atruss * (dtruss * htruss + dtrussdia * ltrussdia) * Cd,truss;
Fwind,truss,α,ULS := (2 * qp,g,ULS(zBG,i) * lgp,i,α,n) / atruss * (dtruss * htruss + dtrussdia * ltrussdia) * Cd,truss;
Fwind,traffic,α,SLS := qp,g,SLS(zBG,i) * max(4 - hws, 0) * 0.5 * lgp,i,α,n * Cd,traffic;
Fwind,tn,α,SLS := qp,g,SLS(zBG,i) * dtn * lgp,i,α,n * Cd,tn;
Fwind,tn,α,ULS := qp,g,ULS(zBG,i) * dtn * lgp,i,α,n * Cd,tn;
Fwind,g,i,α,n,SLS := Fwind,BG,α,SLS + Fwind,truss,α,SLS + Fwind,traffic,α,SLS; qwind,g,i,α,SLS := (Fwind,g,i,α,SLS) / lgp,i,α,n;
Fwind,g,i,α,n,ULS := γq * (Fwind,BG,α,ULS + Fwind,tn,α,ULS + Fwind,truss,α,ULS);
qwind,g,i,α,n,ULS := (Fwind,g,i,α,ULS) / lgp,i,α,n;
Fwind,py,i,α,n,SLS := qp,p,SLS(zBG,i) * fz(sp,i) * 2 * Rpylon * Cd,pyw;

```

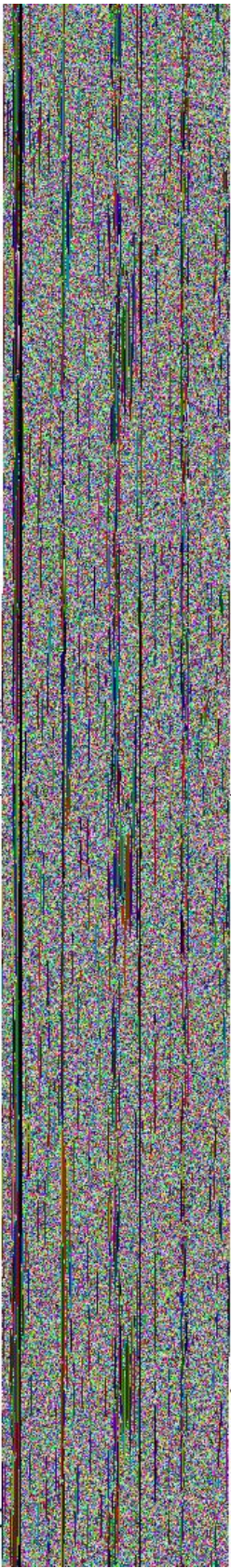
(15)

429.0539409

```

F_wind,py,i,α,n,ULS := γ·qq·pp·ULS(zBG,i)·fz(sp,i)·2·Rpylon·Cd·Cd,pyw;
SA := 'SA';
end do;

```



```

Fc2,ULS := uc2,α,n;
uc3,ULS := uc3,α,n;
ucl,SLS := Cprob·ucl,α,n;
uc2,SLS := Cprob·uc2,α,n;
uc3,SLS := Cprob·uc3,α,n;
drp := drp,i,SLS;
l := lgp,i;
hg :=  $\frac{gp,i}{90}$ ;

```

```

Fww,i,α,n,ULS := γ·Fww,i,α,n,SLS;
Fsw,i,α,n,SLS :=  $\frac{1}{16 \cdot 1000} \cdot \rho \cdot 9.81 \cdot H_w \cdot 2 \cdot R_{pontoon}$ ;
Fsw,i,α,n,ULS := γ·Fsw,i,α,n,SLS;
Fwal,i,α,n,SLS := Fww,i,α,n,SLS + Fsw,i,α,n,SLS;
Fwa,i,α,n,ULS := Fww,i,α,n,ULS + Fsw,i,α,n,ULS;
hg := hg;
l := l;
drp := drp;
end do;
end do;

```

(16)

(17)

```

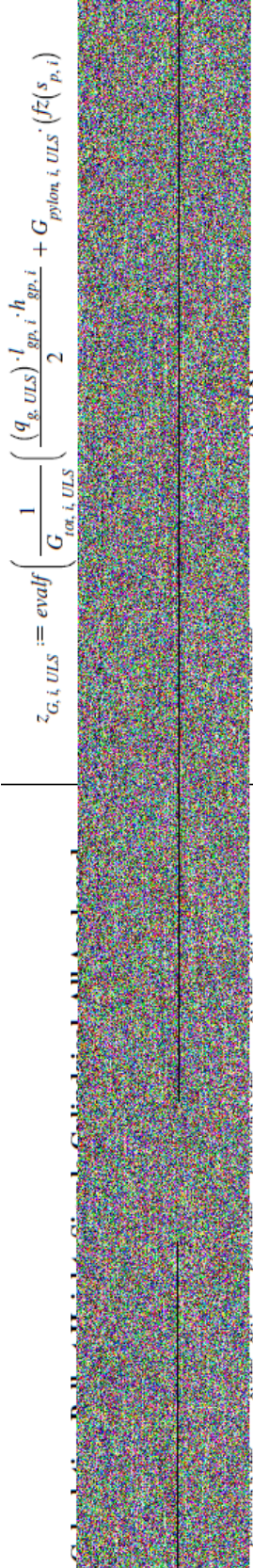
for n from 1 to 12 do
for i from 1 to 22 do
FHtop,i,α,n,SLS := Fwa,i,α,n,SLS + FFC,eq,i,α,n,SLS + Fwind,py,i,α,n,SLS
+ Fwind,g,i,α,n,SLS;
FHtop,i,α,n,ULS := Fwa,i,α,n,ULS + FFC,eq,i,α,n,ULS + Fwind,py,i,α,n,ULS
+ Fwind,g,i,α,n,ULS;
end do;
end do;

```

```

Fcurrent1,SLS :=  $\frac{1}{2} \cdot \frac{\rho \cdot u_{c1,SLS}^2 \cdot C_{d,pc} \cdot 2 \cdot R \cdot 10}{1000}$ ;
Fcurrent2,SLS :=  $\frac{1}{2} \cdot \frac{\rho \cdot u_{c2,SLS}^2 \cdot C_{d,pc} \cdot 2 \cdot R \cdot \min(dr_{p,i,SLS} - 10, 20)}{1000}$ ;
Fcurrent3,SLS :=  $\frac{1}{2} \cdot \frac{\rho \cdot u_{c3,SLS}^2 \cdot C_{d,pc} \cdot 2 \cdot R \cdot \max(dr_{p,i,SLS} - 30, 0)}{1000}$ ;
Fcurrent1,ULS :=  $\frac{1}{2} \cdot \gamma \cdot \frac{\rho \cdot u_{c1,ULS}^2 \cdot C_{d,pc} \cdot 2 \cdot R \cdot 10}{1000}$ ;
Fcurrent2,ULS :=  $\frac{1}{2} \cdot \gamma \cdot \frac{\rho \cdot u_{c2,ULS}^2 \cdot C_{d,pc} \cdot 2 \cdot R \cdot \min(dr_{p,i,ULS} - 10, 20)}{1000}$ ;
Fcurrent3,ULS :=  $\frac{1}{2} \cdot \gamma \cdot \frac{\rho \cdot u_{c3,ULS}^2 \cdot C_{d,pc} \cdot 2 \cdot R \cdot \max(dr_{p,i,ULS} - 30, 0)}{1000}$ ;

```



$$+ G_{pylon, ULS} := \frac{\rho_b \cdot h_b \cdot \pi \cdot (R_{pontoon} - t_{p, side})^2 \cdot 9.81}{1000};$$

$$G_{ballast, i, SLS} := G_{ballast, i, SLS} + G_{pylon, SLS} + (q_{g, SLS}) \cdot l_{gp, i} + G_{AN, i};$$

$$G_{p, i, SLS} := \frac{1}{1000} \left(\rho_c \cdot (l_{p, i} \cdot \pi \cdot R_{pontoon}^2 - (l_{p, i} - t_{p, bot} - t_{p, top}) \cdot \pi \cdot (R_{pontoon} - t_{p, side})^2) \cdot 9.81 \right);$$

$$G_{tot, i, ULS} := G_{ballast, i, SLS} + G_{p, i, SLS} + G_{pylon, SLS} + (q_{g, SLS}) \cdot l_{gp, i} + G_{AN, i};$$

$$G_{tot, i, ULS} := G_{ballast, i, ULS} + G_{p, i, ULS} + G_{pylon, ULS} + (q_{g, ULS}) \cdot l_{gp, i} + G_{AN, i};$$

$$l_p := l_p;$$

$$end\ do;$$

$$z_{G, i, SLS} := evalf \left(\frac{1}{G_{tot, i, SLS}} \left(\frac{(q_{g, SLS}) \cdot l_{gp, i} \cdot h_{gp, i}}{2} + G_{pylon, i, SLS} \cdot f_z(s_{p, i}) \right. \right.$$

$$\left. + h_{gp, i} \right) + G_{p, i, SLS} \cdot \left(\frac{l_{p, i}}{2} + f_z(s_{p, i}) + h_{gp, i} \right) + G_{ballast, i, SLS} \cdot \left(l_{p, i} + f_z(s_{p, i}) \right.$$

$$\left. + h_{gp, i} - t_{p, bot} - \frac{h_{b, i}}{2} \right) - h_{gp, i} \cdot f_z(s_{p, i});$$

$$z_{G, i, ULS} := evalf \left(\frac{1}{G_{tot, i, ULS}} \left(\frac{(q_{g, ULS}) \cdot l_{gp, i} \cdot h_{gp, i}}{2} + G_{pylon, i, ULS} \cdot f_z(s_{p, i}) \right. \right.$$

$$\left. + h_{gp, i} \right) + G_{p, i, ULS} \cdot \left(\frac{l_{p, i}}{2} + f_z(s_{p, i}) + h_{gp, i} \right) + G_{ballast, i, ULS} \cdot \left(l_{p, i} + f_z(s_{p, i}) \right.$$

$$\left. + h_{gp, i} - t_{p, bot} - \frac{h_{b, i}}{2} \right) - h_{gp, i} \cdot f_z(s_{p, i});$$

$$V_{p, i, sub, nt, SLS} := \frac{(F_{pontoon, i, SLS} - q_{traffic, gp, i} \cdot l_{p, i} + G_{p, i, SLS} + G_{ballast, i, SLS})}{\rho_w \cdot 9.81};$$

$$V_{p, i, sub, ULS} := \frac{(F_{pontoon, i, ULS} + G_{p, i, ULS} + G_{ballast, i, ULS})}{\rho_w \cdot 9.81};$$

$$dr_{p, i, ULS} := solve \left(dr_{p, i, ULS} = \frac{V_{p, i, sub, ULS}}{\pi \cdot R_{pontoon}^2}, dr_{p, i, ULS} \right);$$

$$dr_{p, i, SLS} := evalf \left(\frac{V_{p, i, sub, SLS}}{\pi \cdot R_{pontoon}^2} \right);$$

$$dr_{p, i, nt, SLS} := evalf \left(\frac{V_{p, i, sub, nt, SLS}}{\pi \cdot R_{pontoon}^2} \right);$$

$$l_p := l_p;$$

$$end\ do;$$

$$for\ i\ from\ 1\ to\ 22\ do$$

$$l_p := l_p;$$

$$t_{p, bot, i} := t_{p, bot};$$

$$l_p := l_p;$$

$$end\ do;$$

Buoyant Rotational Spring

for i from 1 to 22 do

```

 $l_g := l_{gp,i}$ ;
 $sa := s_{p,i}$ ;
 $h_g := h_{gp,i}$ ;
 $y_p := \sqrt{R_{pontoon}^2 - x_p^2}$ ;
 $A_{imm} := \frac{1}{2} \cdot y_p \cdot \tan(\phi_x) \cdot y_p$ ;

```

```

 $C_{em} := -A_{em} \cdot (ac_{imm})$ ;
 $y_{bf,i} := \text{evalf}\left(\frac{C_{imm} + C_{em}}{dr_{p,i,SLS} \cdot y_p}\right)$ ;

```

$x_p := 0$;

$y_{bmx} := y_{bf,i}$;

$x_p := y_p$;

$y_{b,i} := 0.4 \cdot y_{bmx}$;

```

 $BGd_i := \left(\frac{dr_{p,i,SLS}}{2} - z_{G,i,SLS}\right)$ ;

```

```

 $y_{BG,i} := \text{evalf}\left(-\sin(\phi_x) \cdot \left(\frac{dr_{p,i,SLS}}{2} - z_{G,i,SLS}\right)\right)$ ;

```

$a_{B,i} := (y_{b,i} - y_{BG,i})$;

$M_{x,BU,RI} := \text{evalf}(G_{loc,i,SLS} \cdot a_{B,i})$;

$GM_i := -\text{evalf}\left(\frac{a_{B,i}}{\sin(\phi_x)}\right)$;

```

 $k_{T_x,BU,i} := -\left(\text{evalf}\left(\frac{M_{x,BU,RI}}{\phi_x}\right)\right)$ ;

```

$sa := \text{sd}$;

$l_g := l_g$;

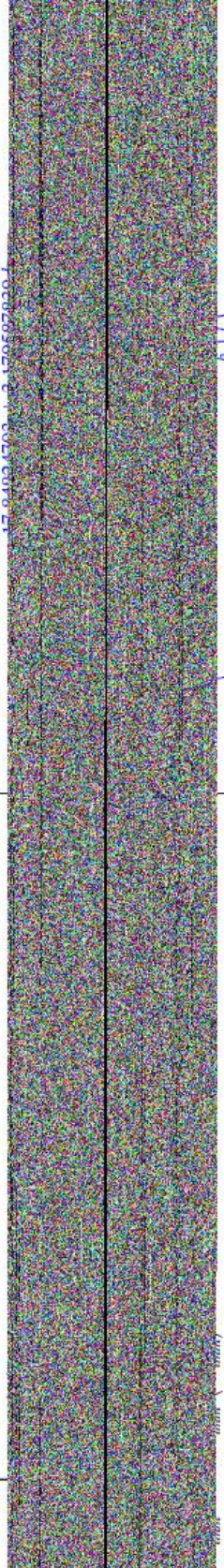
```

 $h_g := h_g$ ;
end do

```

$kr_{x,BU,1}$

$$-\frac{1}{\phi_x} \left((22599.35738 h_{b,1} + 1.644608680 \cdot 10^5) \left(2.000000000 \tan(\phi_x) \cos(0.6666666667 \phi_x) \sqrt{225. \tan(\phi_x)^2 + 900.} \right) \right) \quad (19)$$



$$+ 1.589793916 h_{b,1}) + 11233.53422 h_{b,1} (25.88028338 + 2.615996075 h_{b,1}))$$

Overtuning Angle Anchored pontoons

$k_{AN} := 1237.8556 \cdot k_{BG} := 0$; $\phi_x := \phi_x$;

eq6=evenwicht: som van moment=0

eq7=evenwicht: som van horizontale krachten=0

positieve richting van alle F van externe loads zijn linksgericht, met uitzondering van F_FC

for i from 1 to 22 do

$gvdr := \text{piecewise}(i \leq 5, 11, 5 < i \leq 10, 10, 10 < i \leq 12, 9, 12 < i \leq 17, 10, 17 < i \leq 22, 11)$;

$l_g := l_{gp,i}$; $sa := s_{p,i}$; $dr_{p,i,SLS} := dr_{p,i,SLS}$;

$aa := \frac{h_{gp,i}}{2} + \frac{fz(s_{p,i})}{2}$; $bb := \frac{fz(s_{p,i})}{2} + fr_{p,i,SLS} \cdot cc := z_a$;

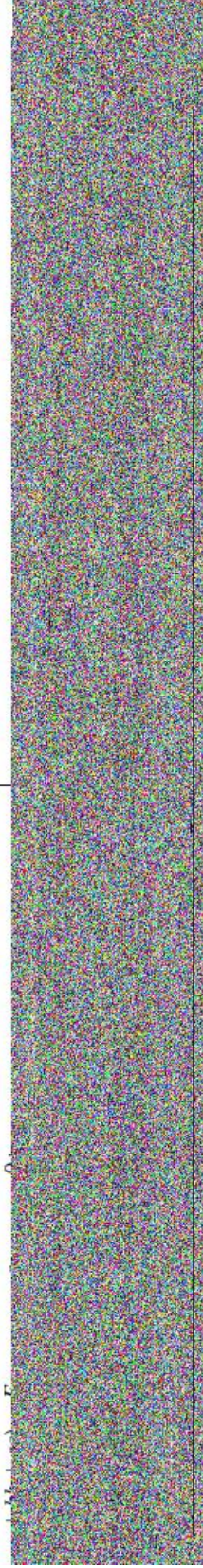
$:= z_{FC,i,\alpha} (gvdr), eq_{-z_a}$;

$eq1 := M_{BG} = kr_{BG} \cdot \phi_x$;

$$\begin{aligned}
 & + \min(10, 7.84824703 + 3.179587830 h_{b,1}) + 4.335804834 \max(0, \\
 & -12.15175297 + 3.179587830 h_{b,1}) (23.92412352 \\
 & + 1.589793915 h_{b,1}) / (303.5251572 + 14.40798862 \min(20, \\
 & 7.84824703 + 3.179587830 h_{b,1}) + 4.335804834 \max(0, -12.15175297 \\
 & + 3.179587830 h_{b,1}))
 \end{aligned}$$

$$\phi_{x,i,SLS} := \phi_x;$$

$$\begin{aligned}
 eq2 & := M_{BU} = k_{BU} \cdot \phi_x; \\
 eq3 & := F_{BG} = k_{BG} \cdot u_{BG}; \\
 eq4 & := F_{AN} = k_{AN} \cdot u_{AN}; \\
 eq5 & := u_{BG} = u_{AN} - \phi_x \cdot (aa + bb + cc); \\
 eq6 & := -F_{wind,g,i,\alpha}(gvdr), SLS \cdot (aa + bb + cc) - F_{wind,py,i,\alpha}(gvdr), SLS \cdot (bb + cc) \\
 & - F_{wa,i,\alpha}(gvdr), SLS \cdot (cc) - F_{FC,eq,i,\alpha}(gvdr), SLS \cdot (dd) - M_{BG} - M_{BU} + F_{BG} \cdot (aa
 \end{aligned}$$



$$\begin{aligned}
 \phi_{x,i,SLS} & := \phi_x \cdot M_{BG,i,SLS} := M_{BG} \cdot M_{BU,i,SLS} := M_{BU} \cdot F_{BG,i,SLS} := F_{AN,i,SLS} \\
 & := F_{AN} \cdot u_{BG,i,SLS} := u_{BG} \cdot u_{AN,i,SLS} := u_{AN}; \\
 M_{BG} & := M_{BG} \cdot M_{BU} := M_{BU} \cdot F_{BG} := F_{AN} \cdot u_{BG} := u_{BG} \cdot u_{AN}; \\
 \phi_x & := \phi_x \cdot sa := sa; l := l; dr := dr; p := p; \\
 \text{end do;}
 \end{aligned}$$

for i from 1 to 22 do

$$\begin{aligned}
 l & := l_{gp,i}; \\
 M_{traffic,i,SLS} & := F_{traffic,hfb,SLS} \cdot a_{traffic,hfb}; \\
 M_{traffic,i,ULS} & := F_{traffic,hfb,ULS} \cdot a_{traffic,hfb}; \\
 l & := l; \\
 \text{end do;}
 \end{aligned}$$

(20)

$$z_{FC,1,\alpha,11,eq}$$

$$(1517.625786 + 14.40798862 \min(20, 7.84824703 + 3.179587830 h_{b,1})) (10) \quad (21)$$

for i from 1 to 22 do

$$\begin{aligned}
 l & := l_{gp,i}; sa := s_{p,i}; \\
 kr_{BU,req,i} & := solve(\phi_{x,i,SLS} = -\phi_x \cdot mx^i, kr_{BU}) : \phi_x := -\phi_x; \\
 h_{b,req,scaa,i} & := (solve(kr_{x,BU,i} = kr_{BU,req,i} h_{b,i} = 0..infinity)) : \\
 kr_{BU} & := kr_{BU} \cdot h_b := h_b; sa := sa;
 \end{aligned}$$

end do;

for i from 1 to 22 do

$$\begin{aligned}
 h_{b,i} & := h_{b,req,scaa,i}; \\
 \text{end do;}
 \end{aligned}$$

for i from 1 to 22 do

$$\begin{aligned}
 gvdr & := piecewise(i \leq 5, 11, 5 < i \leq 10, 10 < i \leq 12, 9, 12 < i \leq 17, 10, 17 \\
 & < i \leq 22, 11); \\
 l & := l_{gp,i}; sa := s_{p,i}; h_b := h_{b,req,scaa,i}; \\
 dr_{p,i,scaa,SLS} & := evalf(dr_{p,i,SLS}) : dr_{p,i,scaa,ULS} := evalf(dr_{p,i,ULS}); \\
 dr_{p,i,scaa,m,SLS} & := dr_{p,i,m,SLS} \cdot kr_{x,BU,i,scaa} := evalf(kr_{x,BU,i}); \\
 l_{p,i,scaa} & := evalf(l_{p,i}) : fr_{p,i,scaa,SLS} := evalf(fr_{p,i,SLS}) : fr_{p,i,scaa,m,SLS}
 \end{aligned}$$

$$\begin{aligned}
& := \text{evalf}(fr_{p,i,nt,SLS}) : fr_{p,i,scaa,ULS} := \text{evalf}(fr_{p,mm}) : \\
& f_{z,i} := f_z^s(p,i) : \\
& \text{for } n \text{ from } 1 \text{ to } 12 \text{ do} \\
& \quad F_{wind,g,scaa,i,\alpha,n,SLS} := F_{wind,g,i,\alpha,n,SLS} : F_{wind,g,scaa,i,\alpha,n,ULS} := F_{wind,g,i,\alpha,n,ULS} : \\
& \quad F_{wind,py,scaa,i,\alpha,n,SLS} := F_{wind,py,i,\alpha,n,SLS} : F_{wind,py,scaa,i,\alpha,n,ULS} := F_{wind,py,i,\alpha,n,ULS} : \\
& \quad F_{wa,scaa,i,\alpha,n,SLS} := F_{wa,i,\alpha,n,SLS} : F_{wa,scaa,i,\alpha,n,ULS} := F_{wa,i,\alpha,n,ULS} : \\
& \quad F_{FC,eq,scaa,i,\alpha,n,SLS} := F_{FC,eq,i,\alpha,n,SLS} : F_{FC,eq,scaa,i,\alpha,n,ULS} := F_{FC,eq,i,\alpha,n,ULS} : \\
& \quad F_{Htop,scaa,i,\alpha,n,SLS} := F_{wa,scaa,i,\alpha,n,SLS} + F_{FC,eq,scaa,i,\alpha,n,SLS} : \\
& \quad + F_{wind,py,scaa,i,\alpha,n,SLS} + F_{wind,g,scaa,i,\alpha,n,SLS} : \\
& \quad F_{Htop,scaa,i,\alpha,n,ULS} := F_{wa,scaa,i,\alpha,n,ULS} + F_{FC,eq,scaa,i,\alpha,n,ULS} : \\
& \quad + F_{wind,py,scaa,i,\alpha,n,ULS} + F_{wind,g,scaa,i,\alpha,n,ULS} : \\
& \quad F_{pontoon,scaa,i,\alpha,n,SLS} := F_{pontoon,i,SLS} : F_{pontoon,scaa,i,ULS} := F_{pontoon,i,ULS} : \\
\text{end do;} \\
& l := l_{p,i,scaa} : h_b := h_{b,req,scaa,i,c,scaa,i} \\
& := \frac{\left(\rho_c \cdot \left(l \cdot \pi \cdot R_{pontoon}^2 - (l - t_{p,bot} - t_{p,py}) \cdot \pi \cdot (R_{pontoon} - t_{p,side})^2 \right) \cdot 9.81 \right)}{1000} : \\
V_{b,scaa,i} & := \frac{(\rho_b \cdot (h_b) \cdot \pi \cdot (R_{pontoon} - t_{p,side})^2) \cdot 9.81}{1000} : \\
sa & := sa : l := l_g : CRW_{p,i,scaa} := (|evalf_3(l_{p,i,scaa})|evalf_3(h_{b,req,scaa,i}) \\
& |evalf_3(dr_{p,i,scaa,SLS})|evalf_2(fr_{p,i,scaa,SLS})|evalf_2(fr_{p,i,scaa,nt,SLS}) \\
& |evalf_5(kr_{x,ru,i,scaa})|evalf_3(t_{p,bot,i})) : unassign(h_{b,i}) : \\
FRW_{p,i,scaa,SLS} & := (|evalf_5(F_{wind,g,scaa,i,\alpha,(gvdR),SLS}) \\
& |evalf_5(F_{wind,py,scaa,i,\alpha,(gvdR),SLS})|evalf_3(F_{wa,scaa,i,\alpha,(gvdR),SLS}) \\
& |evalf_5(F_{FC,eq,scaa,i,\alpha,(gvdR),SLS})|evalf_5(F_{Htop,scaa,i,\alpha,(gvdR),SLS})) : \\
FRW_{p,i,scaa,ULS} & := (|evalf_5(F_{wind,g,scaa,i,\alpha,(gvdR),ULS}) \\
& |evalf_5(F_{wind,py,scaa,i,\alpha,(gvdR),ULS})|evalf_3(F_{wa,scaa,i,\alpha,(gvdR),ULS}) \\
& |evalf_5(F_{FC,eq,scaa,i,\alpha,(gvdR),ULS})|evalf_5(F_{Htop,scaa,i,\alpha,(gvdR),ULS})) : \\
LULS_{p,i} & := (|evalf_4(F_{wind,g,scaa,i,\alpha,(gvdR),ULS}) \\
& + F_{wind,py,scaa,i,\alpha,(gvdR),ULS})|evalf_4(F_{wa,scaa,i,\alpha,(gvdR),ULS}) \\
& + F_{FC,eq,scaa,i,\alpha,(gvdR),ULS}) : \\
LULS_{p,i,mult} & := < |evalf_4(1.2 \cdot F_{wind,g,scaa,i,\alpha,(gvdR),ULS} \\
& \cdot F_{wind,py,scaa,i,\alpha,(gvdR),ULS})|evalf_4(1.1 \cdot F_{wa,scaa,i,\alpha,(gvdR),ULS} \\
& \cdot F_{FC,eq,scaa,i,\alpha,(gvdR),ULS})|evalf_5(1.2 \cdot F_{wind,g,scaa,i,\alpha,(gvdR),ULS} \\
& \cdot F_{wind,py,scaa,i,\alpha,(gvdR),ULS} + 1.1 \cdot F_{wa,scaa,i,\alpha,(gvdR),ULS} \\
& \cdot F_{FC,eq,scaa,i,\alpha,(gvdR),ULS}) > : \\
LSLS_{p,i} & := < |evalf_4(F_{wind,g,scaa,i,\alpha,(gvdR),SLS} + F_{wind,py,scaa,i,\alpha,(gvdR),SLS}) \\
& |evalf_4(F_{wa,scaa,i,\alpha,(gvdR),SLS} + F_{FC,eq,scaa,i,\alpha,(gvdR),SLS}) > : \\
LSLS_{p,i,mult} & := < |evalf_4(1.2 \cdot F_{wind,g,scaa,i,\alpha,(gvdR),SLS} \\
& \cdot F_{wind,py,scaa,i,\alpha,(gvdR),SLS})|evalf_4(1.1 \cdot F_{wa,scaa,i,\alpha,(gvdR),SLS} \\
& \cdot F_{FC,eq,scaa,i,\alpha,(gvdR),SLS})|evalf_5(1.2 \cdot F_{wind,g,scaa,i,\alpha,(gvdR),SLS} \\
& \cdot F_{wind,py,scaa,i,\alpha,(gvdR),SLS} + 1.1 \cdot F_{wa,scaa,i,\alpha,(gvdR),SLS} \\
& \cdot F_{FC,eq,scaa,i,\alpha,(gvdR),SLS}) > : \\
\end{aligned}$$

<pre> end do; for i from 1 to 22 do h_{b,i} := h_{b,req,scat,i}; end do; for i from 1 to 22 do MTRAE_{p,i} := (evalf₅(M_{traffic,SLS})) evalf₅(M_{traffic,r,crs}) end do; MTR := <"NR" "M_traffic,SLS" "M_traffic,ULS">; for i from 1 to 22 do g_{vd} := piecewise(i ≤ 5, 11, 5 < i ≤ 10, 10, 10 < i ≤ 12, 9, 12 < i ≤ 17, 10, 17 < i ≤ 22, 11); F_{xwaves,i} := F_{wa,scat,i,α,(g_{vd}),SLS}; F_{xcurr,i} := F_{FC,eq,scat,i,α,(g_{vd}),SLS}; end do; Total wave and current load: evalf₅(add(F_{xwaves,i} i = 1 ..22)) + evalf₅(add(F_{xcurr,i} i = 1 ..22)) 20423.07 (22) </pre>	<pre> LSLSV := <"NR" "Fwind_tot,SLS" "Fwater_tot,SLS">; LULSMN := <"NR" "Fwind,m,ULS" "Fwater,m,ULS" "Total Fx,m">; LSLSMN := <"NR" "Fwind,m,SLS" "Fwater,m,SLS" "Total Fx,m">; fr_SLS en fr_NT_SLS zijn de hoogtes van de ponton dat boven water uitsteekt, respectievelijk met en zonder variable (verkeersbelasting). (23) </pre>
<pre> FRWT := <"NR" "L_p" "Hb" "DR_p_SLS" "FR_SLS" "FR_NT,SLS" "kr_BU" "t_bot">; [1, 43.0, 6.72, 39.2, 3.8, 4.5, 7.3397 10⁵, 1.86], [2, 70.0, 13.6, 65.7, 4.3, 5.3, 1.9883 10⁶, 2.40], [3, 79.4, 16.1, 75.0, 4.4, 5.4, 2.6857 10⁶, 2.59], [4, 90.3, 19.1, 85.7, 4.5, 5.5, 3.3483 10⁶, 2.80], [5, 99.4, 21.6, 94.8, 4.6, 5.6, 3.9259 10⁶, 2.98], [6, 110., 24.5, 105., 4.7, 5.7, 4.6454 10⁶, 3.19], [7, 118., 26.8, 113., 4.8, 5.8, 5.2220 10⁶, 3.35], [8, 129., 30.2, 124., 4.8, 5.8, 5.7271 10⁶, 3.58], [9, 124., 28.4, 119., 4.9, 5.9, 5.9389 10⁶, 3.48], [10, 143., 34.2, 138., 4.9, 5.9, 6.2613 10⁶, 3.86], [11, 181., 44.3, 176., 5.6, 7.1, 1.2682 10⁷, 4.63] </pre>	<pre> <CRWT, CRW_{p,1,scat}, CRW_{p,2,scat}, CRW_{p,3,scat}, CRW_{p,4,scat}, CRW_{p,5,scat}, CRW_{p,6,scat}, CRW_{p,7,scat}, CRW_{p,8,scat}, CRW_{p,9,scat}, CRW_{p,10,scat}, CRW_{p,11,scat}> (24) </pre>
<pre> CRWT := <"NR" "L_p" "Hb" "DR_p_SLS" "FR_SLS" "FR_NT,SLS" "kr_BU" "t_bot">; FRWTSLS := <"NR" "Fwind_g" "Fwind_py" "F_WA" "F_FC" "F_Htop">; FRWTULS := <"NR" "Fwind_g" "Fwind_py" "F_WA" "F_FC" "F_Htop">; LULSV := <"NR" "Fwind_tot,ULS" "Fwater_tot,ULS">; </pre>	<pre> <FRWTSLS, FRW_{p,1,scat,SLS}, FRW_{p,2,scat,SLS}, FRW_{p,3,scat,SLS}, FRW_{p,4,scat,SLS}, FRW_{p,5,scat,SLS}, FRW_{p,6,scat,SLS}, FRW_{p,7,scat,SLS}, FRW_{p,8,scat,SLS}, FRW_{p,9,scat,SLS}, FRW_{p,10,scat,SLS}, FRW_{p,11,scat,SLS}>; </pre>

(25)

"NR"	"Fwind_g"	"Fwind_py"	"F_WA"	"F_FC"	"F_Htoip"
1	733.34	24.243	19.2	631.59	1408.4
2	1477.0	121.41	19.2	746.60	2364.2
3	1617.0	224.92	19.2	786.58	2647.7
4	1689.4	325.84	19.2	833.32	2867.8
5	1713.3	419.88	19.2	872.44	3024.8
6	1824.9	504.59	19.2	916.71	3265.5
7	1879.4	578.36	19.2	950.83	3427.8
8	1902.8	640.10	19.2	1000.2	3562.4
9	1896.0	689.05	19.2	978.24	3582.5
10	1859.9	724.67	19.2	1058.9	3662.7
11	4144.7	844.08	19.2	1223.7	6231.7

$\langle LSLSN, seq(LSLN_{p,i}, i = 1..11) \rangle$

(26)

"NR"	"Fwind_tot,SLS"	"Fwater_tot,SLS"
1	757.5	650.8
2	1598.	765.8
3	1842.	805.8
4	2015.	852.5
5	2133.	891.6
6	2330.	935.9
7	2457.	970.0
8	2543.	1019.
9	2585.	997.4
10	2585.	1078.
11	4989.	1243.

To create some margin for the design of the superstructure, the wind load will be multiplied by a factor 1.2 and the load due to the water is multiplied by 1.1:

$\langle LSLSMN, seq(LSLN_{p,i, mult}, i = 1..11) \rangle$

(27)

"NR"	"Fwind,m,SLS"	"Fwater,m,SLS"	"Total Fx,m"
1	909.1	716.0	1625.0
2	1918.	842.4	2760.6
3	2210.	886.4	3096.7
4	2418.	937.8	3356.2
5	2560.	980.8	3540.8
6	2796.	1029.	3825.0
7	2949.	1067.	4016.4
8	3052.	1121.	4172.9
9	3102.	1097.	4199.4
10	3102.	1186.	4287.5
11	5987.	1367.	7353.8

$\langle FRWTULS, FRW_{p,1, scaa, ULS}, FRW_{p,2, scaa, ULS}, FRW_{p,3, scaa, ULS},$

$FRW_{p,4, scaa, ULS}, FRW_{p,5, scaa, ULS}, FRW_{p,6, scaa, ULS}, FRW_{p,7, scaa, ULS},$

$FRW_{p,8, scaa, ULS}, FRW_{p,9, scaa, ULS}, FRW_{p,10, scaa, ULS}, FRW_{p,11, scaa, ULS} \rangle$

(28)

"NR"	"Fwind_g"	"Fwind_py"	"F_WA"	"F_FC"	"F_Htoip"
1	1087.0	44.565	28.846	1167.4	2327.8
2	2219.2	223.18	28.846	1382.9	3854.2
3	2429.5	413.47	28.846	1457.3	4329.2
4	2538.3	598.98	28.846	1544.1	4710.2
5	2574.3	771.86	28.846	1616.8	4991.7
6	2742.0	927.57	28.846	1698.8	5397.2
7	2823.8	1063.2	28.846	1762.0	5677.9
8	2859.0	1176.7	28.846	1853.3	5917.8
9	2848.8	1266.7	28.846	1813.2	5957.5
10	2794.6	1332.1	28.846	1961.7	6117.3
11	6454.6	1551.7	28.846	2270.1	10305.


```
<LULSN, seq(LULS_{p,i}, i = 1 ..11)>
```

"NR"	"M_traffic,SLS"	"M_traffic,ULS"
1	13915.	20873.
2	21000.	31500.
3	21000.	31500.
4	21000.	31500.

```
<LULSN, seq(LULS_{p,i}, i = 1 ..11)>
```

"NR"	"Fwind_tot,ULS"	"Fwater_tot,ULS"
1	1132.	1196.
2	2442.	1412.
3	2844.	1486.



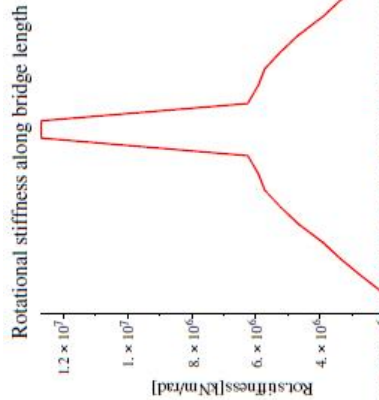
Pontoon Rotational Spring

```
<MTR, seq(MTRAF_{p,i}, i = 1 ..11)>
```

"NR"	"Fwind,m,ULS"	"Fwater,m,ULS"	"Total Fx,m"
1	1357.	1316.	2673.7
2	2931.	1553.	4483.7
3	3412.	1635.	5046.3
4	3765.	1730.	5495.0
5	4015.	1811.	5825.6
6	4403.	1901.	6303.9
7	4665.	1970.	6634.3
8	4843.	2070.	6913.1
9	4939.	2026.	6964.8
10	4952.	2190.	7141.6
11	9608.	2529.	12136.

(30)

```
PKRBU := poinplot((1, 2, 3, 4, 5, 6, 7, 8, 9, 10, 11, 12, 13, 14, 15, 16, 17, 18,
19, 20, 21, 22))((kr_{x,BU,1}, kr_{x,BU,2}, kr_{x,BU,3}, kr_{x,BU,4}, kr_{x,BU,5}, kr_{x,BU,6},
kr_{x,BU,7}, kr_{x,BU,8}, kr_{x,BU,9}, kr_{x,BU,10}, kr_{x,BU,11}, kr_{x,BU,12}, kr_{x,BU,13}, kr_{x,BU,14},
kr_{x,BU,15}, kr_{x,BU,16}, kr_{x,BU,17}, kr_{x,BU,18}, kr_{x,BU,19}, kr_{x,BU,20}, kr_{x,BU,21},
kr_{x,BU,22})), style = line, title = "Rotational stiffness along bridge length",
titlefont = ["calibri", 14], color = red, labels = ["Pontoon",
"Rot.stiffness[kNm/rad]"], labelfont = ["calibri", 12], labeldirections
= ["horizontal", "vertical"]):
display((PKRBU))
```



```

arm_pyl,i := evalf3(bb + cc) ;
end do;

```

Leverarm to node where wave load is acting on is 20 meters for every pontoon.

Leverarm to node where current load is acting on:

```

for i from 1 to 22 do
  gvdz := piecewise(i ≤ 5, 11, 5 < i ≤ 10, 10, 10 < i ≤ 12, 9, 12 < i ≤ 17, 10, 17
  < i ≤ 22, 11) ;

```

```

arm_kr,i := -1 * evalf3(Z_Fc,i,α (gvdz) - z_a) ;
end do;

```

Leverarm to node where the wind load is acting on the bridge girder:

```

for i from 1 to 22 do

```

$$aa := \frac{h_{gp,i}}{2} + \frac{fz(s_{p,i})}{2}; bb := \frac{fz(s_{p,i})}{2} + fr_{p,i,SLS}; cc := z_a;$$

```

arm_krBU,i := (aa + bb + cc) ;

```

```

arm_krBU,i := evalf3(arm_krBU,i) ;
end do;

```

$$\frac{h_{gp,11}}{2} + fz(s_{p,11})$$

75.58826000

(32)

Leverarm to node where wind load is acting on the pylons:

```

for i from 1 to 22 do

```

$$aa := \frac{h_{gp,i}}{2} + \frac{fz(s_{p,i})}{2}; bb := \frac{fz(s_{p,i})}{2} + fr_{p,i,SLS}; cc := z_a;$$

```

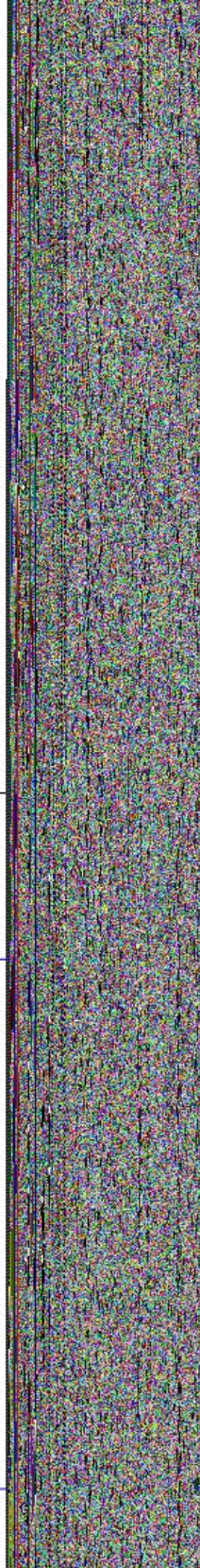
(( #P , , 1, z, 3, 4, 5, 6, 7, 8, 9, 10, 11, 12, 13, 14, 15, 16, 17, 18, 19, 20, 21,
22)) ({"leverarm", "wind BG", arm_krBU,1' arm_krBU,2' arm_krBU,3' arm_krBU,4'
arm_krBU,5' arm_krBU,6' arm_krBU,7' arm_krBU,8' arm_krBU,9' arm_krBU,10'
arm_krBU,11' arm_krBU,12' arm_krBU,13' arm_krBU,14' arm_krBU,15' arm_krBU,16'
arm_krBU,17' arm_krBU,18' arm_krBU,19' arm_krBU,20' arm_krBU,21' arm_krBU,22})
({"leverarm", "wind pyl", arm_pyl,1' arm_pyl,2' arm_pyl,3' arm_pyl,4' arm_pyl,5'
arm_pyl,6' arm_pyl,7' arm_pyl,8' arm_pyl,9' arm_pyl,10' arm_pyl,11' arm_pyl,12' arm_pyl,13'
arm_pyl,14' arm_pyl,15' arm_pyl,16' arm_pyl,17' arm_pyl,18' arm_pyl,19' arm_pyl,20'
arm_pyl,21' arm_pyl,22}) < "leverarm", "current", arm_kr,1' arm_kr,2' arm_kr,3'
arm_kr,4' arm_kr,5' arm_kr,6' arm_kr,7' arm_kr,8' arm_kr,9' arm_kr,10' arm_kr,11'
arm_kr,12' arm_kr,13' arm_kr,14' arm_kr,15' arm_kr,16' arm_kr,17' arm_kr,18' arm_kr,19'
arm_kr,20' arm_kr,21' arm_kr,22}) ({"kr_BU", "(MINI/rad)", kr_x,BU,1' kr_x,BU,2'
kr_x,BU,3' kr_x,BU,4' kr_x,BU,5' kr_x,BU,6' kr_x,BU,7' kr_x,BU,8' kr_x,BU,9' kr_x,BU,10'
kr_x,BU,11' kr_x,BU,12' kr_x,BU,13' kr_x,BU,14' kr_x,BU,15' kr_x,BU,16' kr_x,BU,17'
kr_x,BU,18' kr_x,BU,19' kr_x,BU,20' kr_x,BU,21' kr_x,BU,22})

```

(36)

2372.9

"#P"	"leverarm"	"leverarm"	"leverarm"	"kr_BU"
" "	"wind BG"	"wind pyl"	"current"	"(MNm/rad)"
1	28.7	25.9	6.3	734.29
2	41.8	32.5	0.3	1989.6
3	52.9	38.1	-2.2	2687.1
4	62.8	43.1	-5.5	3350.8
5	71.6	47.5	-8.4	3926.8
6	79.2	51.4	-11.9	4652.9
7	85.6	54.7	-14.7	5227.7



(34)

$$evalf_5(\text{add}(G_{p,i,SLs} \ i=1..22)) + evalf_5(\text{add}(G_{ballast,i,SLs} \ i=1..22))$$

(35)

$$evalf_5(\text{add}(L_{p,i} \ i=1..22))$$

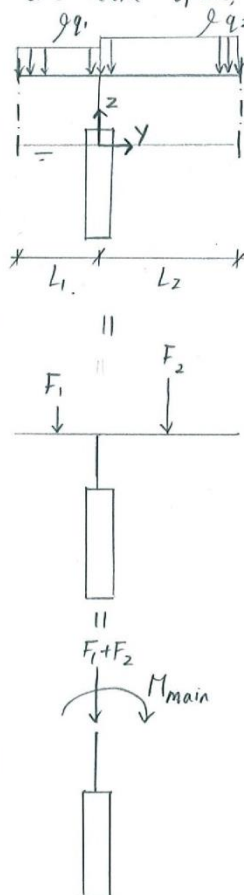
ANNEX T: ROTATIONAL STIFFNESS ALONG BRIDGE GIRDER

Project : Buoyancy Bridge Sognefjord
 Part : Rotational stiffness along bridge girder



Introduction

All spans of the buoyancy bridge are equal, besides the main span. All side spans are 200 meters, and the main span is 465 meters. Moreover, the estimated self-weight of the superstructure is also larger for the main span. This leads to a bending moment load on the pontoons adjacent to the main span, as shown in Fig.1



It is assumed that the bending moment in Fig.1, which is caused by the facts that $L_2 > L_1$ and $q_2 > q_1$, can be compensated by a bending moment due to eccentric ballasting. In this sub study, it will be roughly checked whether sufficient ballast is present to compensate the bending moment at the main span.

Calculations:

$$L_1 = \frac{1}{2} \cdot 200 \text{ m} = 100 \text{ m}$$

$$L_2 = \frac{1}{2} \cdot 465 \text{ m} = 232,5 \text{ m}$$

$$q_1 = 265 \text{ kN/m (self-weight bridge girder)}$$

$$q_2 = 350 \text{ kN/m (self-weight bridge girder + traffic load)}$$

Fig. 1 Bending Moment due at Main span

Name: Christine Yip

Date: 8-5-2015 Page: 1/4

Rev:

Project : Buoyancy Bridge Sognefjord

Part : Rotational stiffness along bridge girder



$$F_1 = q_1 \cdot L_1 = 265 \text{ kN/m} \cdot 100 \text{ m} = 26\,500 \text{ kN}$$

$$F_2 = q_2 \cdot L_2 = 350 \text{ kN/m} \cdot 232,5 \text{ m} = 81\,375 \text{ kN}$$

$$F_1 + F_2 = 26\,500 + 81\,375 = 107\,875 \text{ kN}$$

$$M_{\text{main}} = (F_1 + F_2) \cdot y_{\text{main}}$$

$$y_{\text{main}} = \frac{(F_1 \cdot -\frac{1}{2}L_1) + (F_2 \cdot \frac{1}{2}L_2)}{F_1 + F_2}$$

$$= \frac{(26\,500 \cdot -50) + (81\,375 \cdot 116,25)}{26\,500 + 81\,375}$$

$$= 75,41 \text{ m}$$

$$= 75,41 \text{ m}$$

$$M_{\text{main}} = 107\,875 \text{ kN} \cdot 75,41 \text{ m} = 8\,135 \text{ MNm}$$

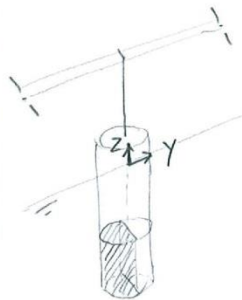


Fig. 2. Eccentric ballasting in y-z plane

$$y_{\text{ballast}} = \frac{\frac{4}{3}\pi}{\pi}$$

The pontoon ballast can be applied eccentrically in the y-z plane as illustrated in Fig. 2. If all ballast is concentrated at one side of the pontoon as illustrated, then, the bending moment caused by the ballast is approximately:

$$G_{\text{ballast},11} = \text{ballast present in pontoon 11 of the proposed substructure} \\ = 1193\,000 \text{ kN}$$

$$R_{\text{pontoon},11} = 26 \text{ m}$$

$$t_{\text{side}} = 2,23 \text{ m}$$

Name: Christine Yip

Date: 8-5-2015

Page: 2/4

Rev:

Project : Buoyancy bridge Sognefjord

Part : Rotational Stiffness along bridge girder



$$R_{ballast} = 26 - 2,23 = 23,77 \text{ m}$$

$$y_{ballast} = -\frac{4}{3} \cdot \frac{R_{ballast}}{\pi} = 10,09 \text{ m}$$

$$\begin{aligned} M_{ballast} &= G_{ballast,II} \cdot y_{ballast} \\ &= 1193800 \text{ kN} \cdot 10,09 \text{ m} \\ &= 12043 \text{ MNm} \end{aligned}$$

Conclusion

The bending moment caused by eccentric ballasting ($M_{ballast} = 12043 \text{ MNm}$) is larger than the bending moment caused by the large loads at the main span ($M_{main} = 8135 \text{ MNm}$). Therefore, it is assumed for now that M_{main} can be solved by eccentric ballasting in the z-y plane (see Fig. 2)

This is however not further taken into account in the pontoon design. Since eccentric ballasting is also applied in the x-z plane to compensate the asymmetric self-weight of the anchoring cables (see chapter 3.4.3), the ballast distribution within the pontoon is different than initially assumed (no eccentric application of ballast). Eccentric ballasting will influence the center of gravity of the pontoons and therefore also the metacentric height and rotational stiffness. For this preliminary study however, the feasibility of the

Name: Christine Yip

Date: 8-5-2015 Page: 3/4

Rev:

Project : Buoyancy Bridge Sognefjord

Part : Rotational Stiffness along Bridge Girder



buoyancy bridge will be further investigated while using the pontoon properties, which are obtained by a simplified representation of the pontoons (without eccentric ballasting).

After this feasibility study in further design stages, the pontoon properties will then have to be calculated more detailedly and accurately.

For now, it is sufficient to know the order of magnitude of the pontoons and to know whether the buoyancy bridge concept is feasible.

Name: Christine Yip

Date: 8-5-2015

Page: 4/4

Rev:

ANNEX U: LOAD CASES

To check the capacity, the bridge structure is subjected to several load cases with wind load, wave load, current load, traffic load, self-weight and temperature load. These loads were calculated in ANNEX N: Estimating External Loads: Calculation File. In to , the different directions and the magnitude of the wind and water loads are shown. The load cases are shown below.

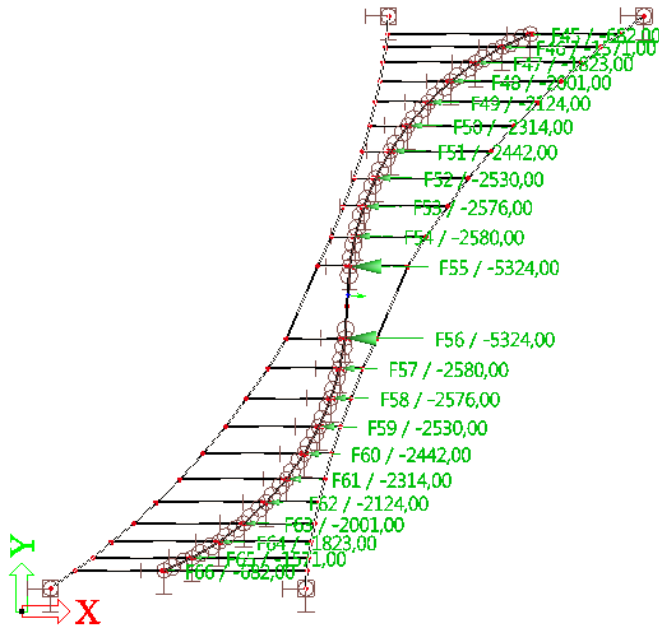


FIGURE U-1 CONCENTRATED WIND LOAD [kN] ACTING ON THE TOP OF THE PONTOONS IN NEGATIVE X-DIRECTION

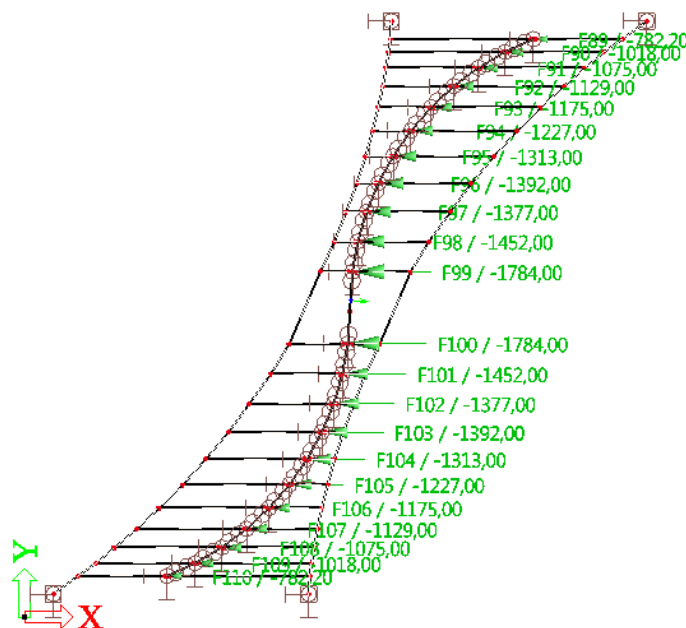


FIGURE U-2 CONCENTRATED WATER LOAD [kN] ACTING ON THE TOP OF THE PONTOONS IN NEGATIVE X-DIRECTION

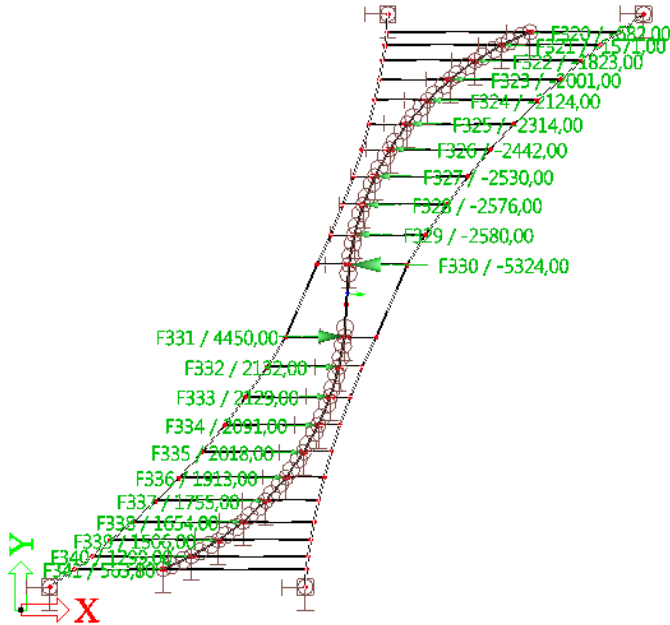


FIGURE U-3 ASYMMETRIC CONCENTRATED WIND LOAD [KN] ACTING ON THE TOP OF THE PONTOONS

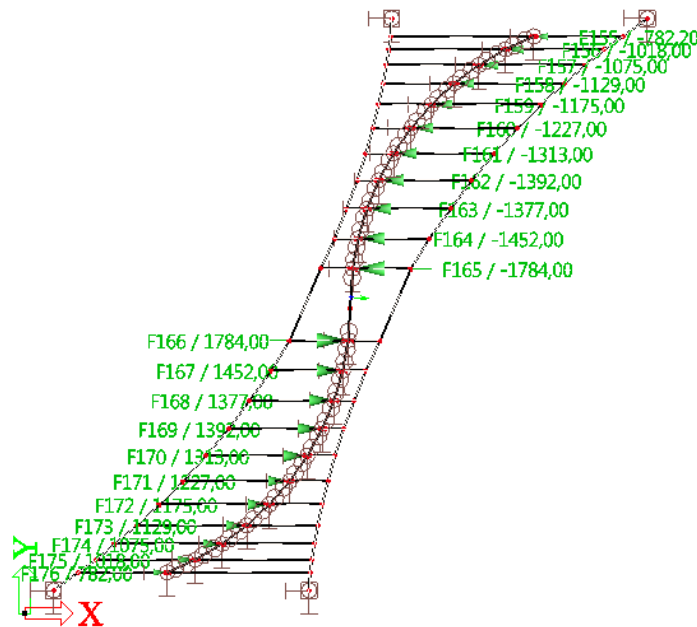


FIGURE U-4 ASYMMETRIC CONCENTRATED WATER LOAD [KN] ACTING ON THE TOP OF THE PONTOONS

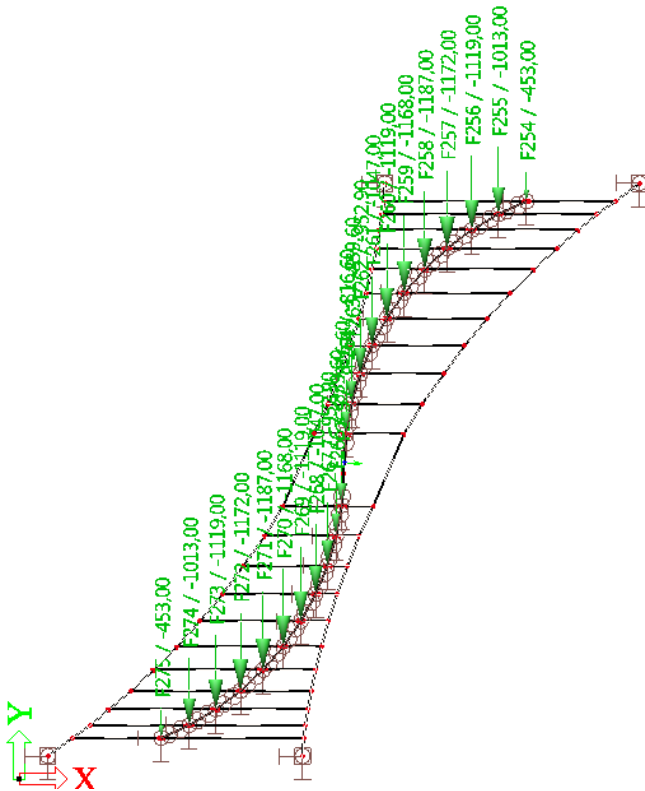


FIGURE U-6 CONCENTRATED WIND LOAD [KN] ACTING ON THE TOP OF THE PONTOONS IN NEGATIVE Y-DIRECTION

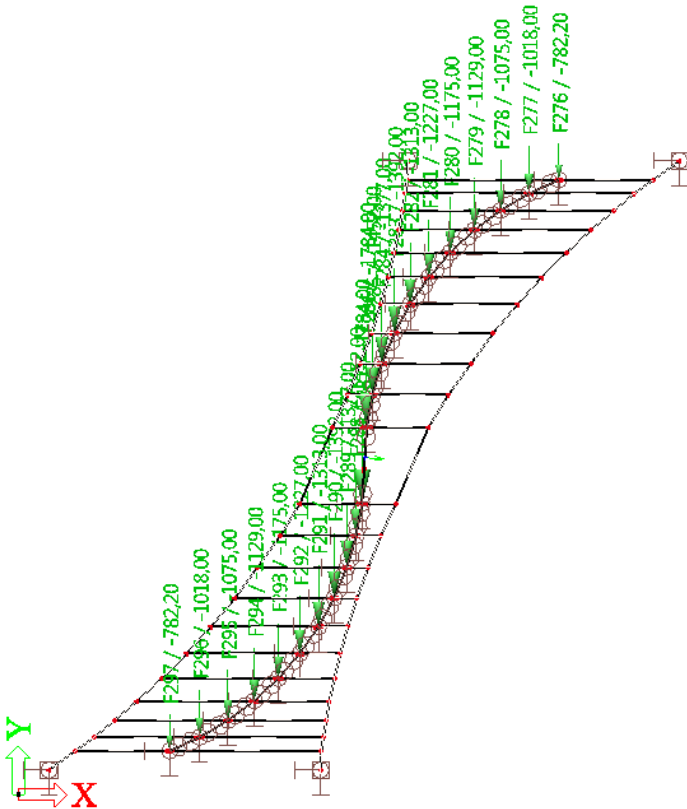


FIGURE U-5 CONCENTRATED WATER LOAD [KN] ACTING ON THE TOP OF THE PONTOONS IN NEGATIVE Y-DIRECTION

Load Case 1 – Self-weight only

Total self-weight

Load Case 2 – Maximum displacements in x-direction

Total self-weight

Full traffic load active on the whole bridge

Wind load (all in negative x-direction)

Water load (all in negative x-direction)

Load Case 3 – Asymmetric water load

Total self-weight

Full traffic load active on the whole bridge

Wind load (all in negative x-direction)

Water load (asymmetric, the top half in negative x-direction and the bottom half in positive x-direction)

Load Case 5 – Maximum displacements in y-direction

Total self-weight

Full traffic load active on the whole bridge

Wind load (all in negative y-direction)

Water load (all in negative y-direction)

Load Case 6 – Self-weight and traffic load

Total self-weight

Full traffic load active on the whole bridge

Load Case 7 – Extreme situation with hurricane

Total self-weight

Full traffic load active on the whole bridge

Wind load (asymmetric, the top half in negative x-direction and the bottom half in positive x-direction)

Water load (asymmetric, the top half in negative x-direction and the bottom half in positive x-direction)

Load Case 8 - Temperature load

Total self-weight

Full traffic load active on the whole bridge

Temperature load of 20° C

ANNEX V: AESTHETICAL DESIGN GUIDELINES FROM THE ARCHITECTS

The design guidelines for the superstructure from the architecture firm Zwarts & Jansma Architects are shown below.


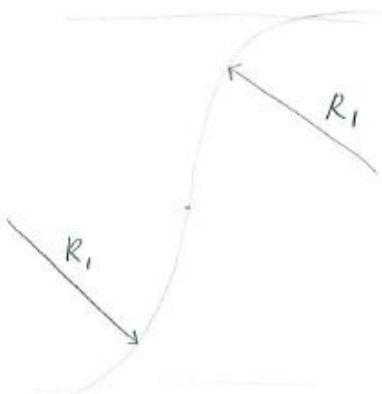

Concept of Rhythm, elegance and Fluidity

- Create a **consistent** visual and **perceptual rhythm** for those traveling on the bridge, and almost like a “**singular, dynamic clean line**” for viewers on land or water who are looking at the bridge.
- Rhythm along the piers is based primarily on **seamless continuity** of longitudinal factors like girders.
- The pontoons radii will be used as the parametric unit on which the architectural girder widths and sizes will be based on to create **dynamic progressive sections** morphing, expanding, shrinking into one **coherent gesture**.
- All the elements throughout the bridge should be **closely tied to the structural systems** .
- Views of fjord and the surrounding landscape will be dramatic from the bridge and it should be accentuated creating 360 degree **unobstructed vistas** all along it.
- Superstructure elements should contribute to the **overall light and airy appearance** of the bridge.
- Floating bridge pier and girder systems shall be a reflection of the form and character.
- Hybrid box girder without any arching element is preferred but needs to be **re-invented** since this bridge has segmented hinged girder sections unlike Viaduct Echinghen.

SOGNEFJORD BUOYANCY BRIDGE - PIERS

- The pier should have sense of robustness, transparency and lightness.
- The pier and pontoon floating devices can be combined into a unibody geometry.
- The geometry corresponds to the girder geometry.
- Has a very elegant vocabulary when seen as a collective.
- Geometry avoids growth of marine life and ice deposition (if necessary).
- Pier and girders meeting point at a hinge must be well thought of and resolved.
- Due to large pontoon sizes at the middle of the bridge, the girder and deck might need to be bifurcated into two.

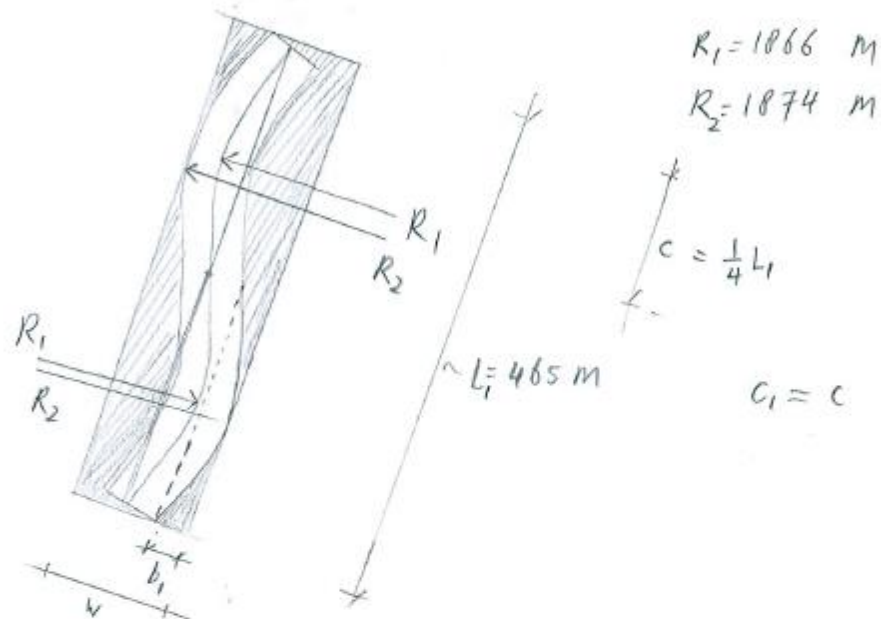
ANNEX W: REQUIRED BRIDGE DECK WIDTH

Project	: Buoyancy Bridge Sognefjord	
Part	: Required width of straight bridge girders	
<p><u>Question:</u></p> <p>Which width is needed in case straight bridge girder segments are used?</p> <p><u>Top view:</u></p> <div style="display: flex; justify-content: space-between; align-items: flex-start;"> <div style="text-align: center;">  </div> <div style="margin-left: 20px;"> <ul style="list-style-type: none"> • $R_1 = 1066 \text{ m}$ • longest bridge girder length = 465 m • required bridge deck width (by R.T.H. Hermans (2014)) = 16 m </div> </div>		
<div style="display: flex; justify-content: space-between;"> <div style="width: 45%;"> <p><u>Calculation rules:</u></p>  $R = \frac{1}{2} \cdot \frac{b^2 + c^2}{b}$ $b = \frac{b^2 + c^2}{2R}$ </div> <div style="width: 45%;"> <p><u>Calculations:</u></p> </div> </div>		
Name:	Christine Yip	Date: 27-5-2015
Page:	1/3	Rev:

Project : Buoyancy Bridge Sognefjord
 Part : Required width of straight bridge girders



Exaggerated top view of longest bridge girder segment:



$$b_1 = \frac{b_1 + C_1}{2R_2} = \frac{3,6^2 + \left(\frac{465}{4}\right)^2}{2 \cdot 1874} = 3,6 \text{ m}$$

$$w_1 \approx 16 + 2 \cdot b_1 = 16 + 2 \cdot 3,6 = 23,2 \text{ m}$$

Name: Christine Yip

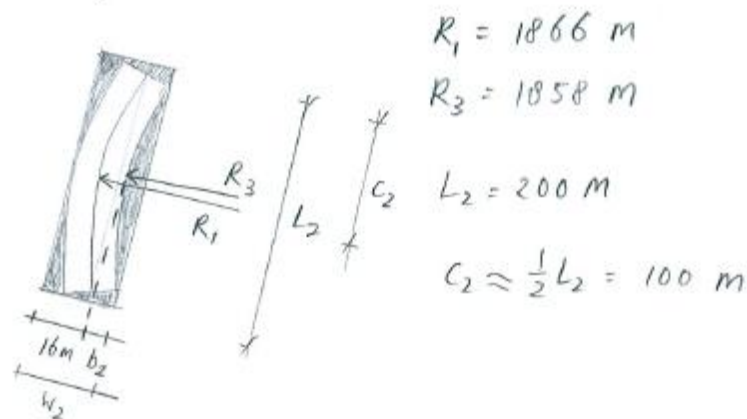
Date: 27-5-2015 Page: 2/3

Rev:

Project : Buoyancy Bridge Sognefjord
 Part : Required width of straight bridge girder



Exaggerated top view of other (shorter) bridge girder segments:



$$b_2 = \frac{b_2^2 + c_2^2}{2 R_3} = \frac{2,7^2 + 100^2}{2 \cdot 1858} = 2,7 \text{ m}$$

$$w_2 = 16 + 2,7 = 18,7 \text{ m}$$

Conclusion and Recommendation :

In case straight girder segments are used, the required minimum width for the bridge deck is 23,2 m at the ferry passage (465m) and 18,7 m at the other spans.

Since horizontally curved bridge segments will induce torsional stress and other complications, it is recommended to use straight bridge girder segments.

Name: Christine Yip

Date: 27-5-2015

Page: 3/3


Rev:

ANNEX X: INTERNAL FORCES AND ROTATIONS OF SUPERSTRUCTURE

In this section, it is shown how the loads on the superstructure are determined. This information can be found on the next pages.

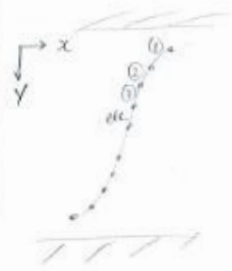
Project : Bouyancy Bridge Sognefjord

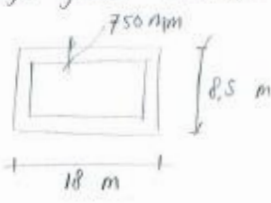
Part : Superstructure : Internal forces and rotation



Assumptions

- pontoons connected to each other by a simple bridge girder
- Bridge girder not connected to the shore yet
- Bridge girder section:






Effects:

- Normal Force

LCS: - wind load
- water load
- traffic




$$N_{max} = -6217 \text{ kN @ BG (6) LC5}$$

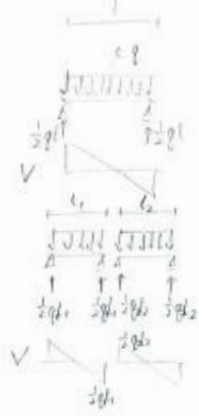
$$-422 \text{ kN @ BG (11) LC8}$$

$$+6400 \text{ kN @ BG (5) LC5}$$

$$+900 \text{ kN @ BG (1) LC7}$$

- Shear force





$$V_{x,max} = 3162 \text{ kN @ BG (11)}$$

$$= \frac{1}{2} q l = \frac{1}{2} \cdot 13.6 \cdot 465 \text{ main span}$$

$$= 1336 \text{ kN @ BG (10)}$$

$$V_{z,max} = \frac{1}{2} q l = \frac{1}{2} \cdot 350 \cdot 465$$

$$= 81375 \text{ kN @ BG (11)}$$

$$= \frac{1}{2} q l = \frac{1}{2} \cdot 300 \cdot 200$$

$$= 30000 \text{ kN @ BG (10)}$$

Name: Christine Yip

Date: 25-5-2015

Page: 1/5

Rev:

Project : Buoyancy Bridge Sognefjord

Part : Superstructure: Internal forces and rotations



Bending Moment

M_y



$$M_{y,max} = \frac{1}{8} \cdot q \cdot L^2 = \frac{1}{8} \cdot 350 \cdot 465^2$$

$$= 9\,459\,844 \text{ kNm @ BG (11)}$$

$$M_{y,max} = \frac{1}{8} \cdot q \cdot L^2 = \frac{1}{8} \cdot 300 \cdot 200^2$$

$$= 1\,500\,000 \text{ kNm @ BG (10)}$$

M_z



$$M_{z,max} = \frac{1}{8} \cdot q \cdot L^2 = \frac{1}{8} \cdot 13,6 \cdot 465^2$$

$$= 367\,583 \text{ kNm @ BG (11)}$$

$$M_{z,max} = \frac{1}{8} \cdot 9,7 \cdot 200^2$$

$$= 48\,500 \text{ kNm @ BG (10)}$$

M_x



$$M_x = GI_p \cdot \theta$$



θ :

LC7 (assym. win) : 91,8 mrad = 5,26°

LC5 (150°) : 18,37 mrad = 1,05°

LC3 (assym. water) : 7,55 mrad = 0,433°

Name: Christine Ylp

Date: 25-5-2015

Page: 2/5

Rev:

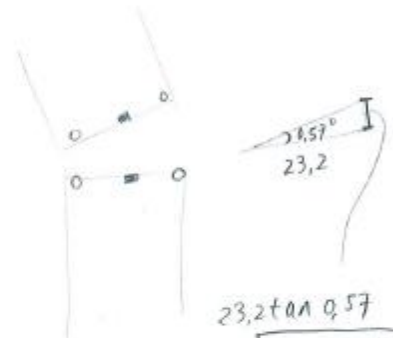
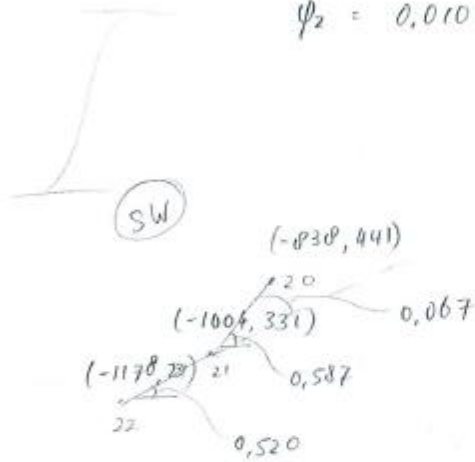
Project : Buoyancy Bridge Sognefjord

Part : Internal forces and rotations of super-structure



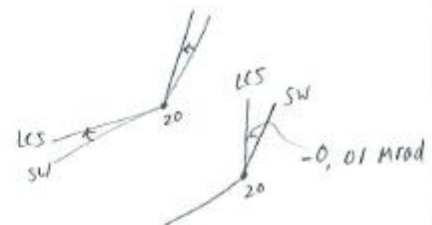
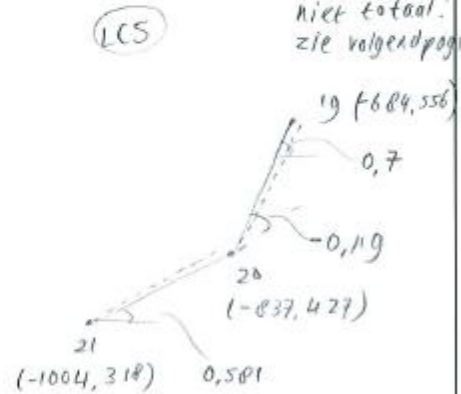
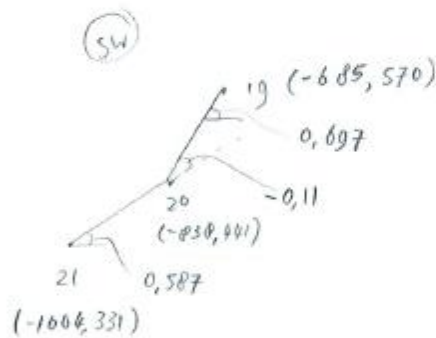
Hoek verdraaiingen due to loads tov SW position

$$\psi_2 = 0,010 \text{ rad} \approx 0,57^\circ$$



$$23,2 \tan 0,57 = 231 \text{ mm}$$

↑
niet totaal!
zie volgende pagina



Global displacement at gap between 2 girders due to ψ_2 : 231 mm

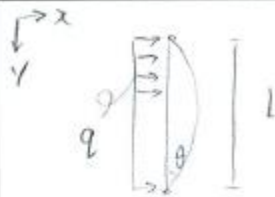
Name: Christine Yip

Date: 25-5-2015 Page: 3/5

Rev:

Project : Buoyancy Bridge Sognefjord

Part : Superstructure: Internal forces and rotations



$$\theta = \frac{q l^3}{24 EI}$$

Local rotation: ψ_2

Main span:

Side span:

$$\psi_{2,ms} = \frac{13,6 \cdot 465\,000^3}{24 \cdot 210\,000 \cdot I}$$

$$\psi_{2,ss} = \frac{9,7 \cdot 200\,000^3}{24 \cdot 210\,000 \cdot I}$$

$$= \frac{2,7 \cdot 10^{11}}{I}$$

$$= \frac{1,54 \cdot 10^{10}}{I}$$

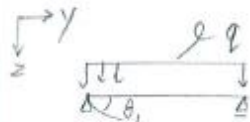
Name: Christine Yip

Date: 25-5-2015 Page: 4/5

Rev:

Project : Buoyancy Bridge Sognefjord

Part : Superstructure: Internal forces and rotations



Local rotation φ_x

$$\theta_1 = \frac{q l^3}{24EI}$$

Main span :

$$\varphi_{x,ms} = \frac{350 \cdot 465000^3}{24 \cdot 210000 \cdot I}$$

$$= \frac{6,98 \cdot 10^{12}}{I}$$

Side span :

$$\varphi_{x,ss} = \frac{300 \cdot 200000^3}{24 \cdot 210000 \cdot I}$$

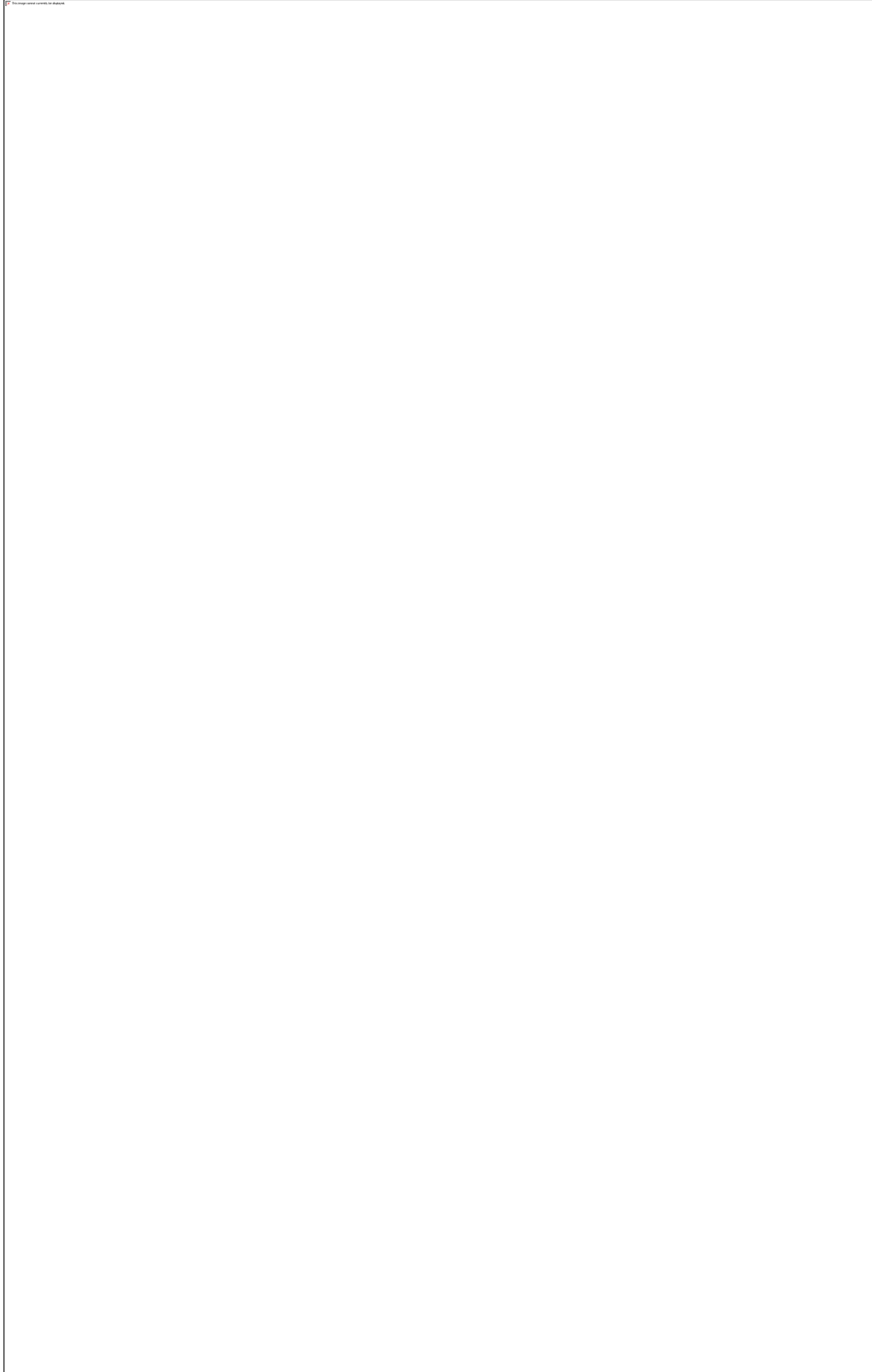
$$= \frac{4,76 \cdot 10^{11}}{I}$$



Name: Christine Yip


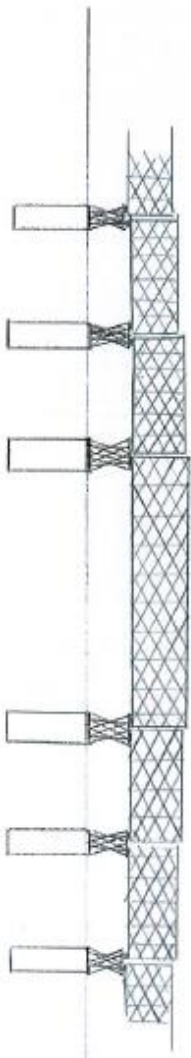
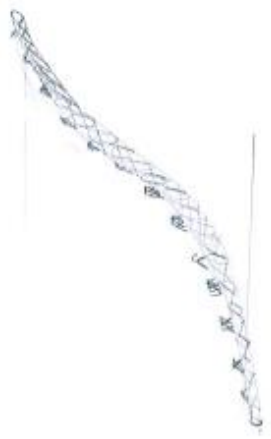
Date: 27-5-2015 Page: 5/5

Rev:

ANNEX Y: SKETCHES WITH HEIGHT ESTIMATION OF DIFFERENT SUPERSTRUCTURE TYPES



Project :			
Part :			
			
<i>Box Girder with girder height 16 m at main span.</i>			
Name:	Date:	Page:	Rev:

<p>Project :</p> <p>Part :</p>			
			
<p>netkous: $d = 10\text{ m}$ $L = 40\text{--}50\text{ m}$ $w = 50\text{--}50\text{ m}$</p> <p>$L = 465\text{ m}$ $d = 103\text{ m}$</p>			
			
Name:	Date:	Page:	Rev:

Project :

Part :



Arch: $\frac{H}{L} \approx 7$ (steel bridges, H4.1.1)
 H main span = 66 m
 H side span = 29 m


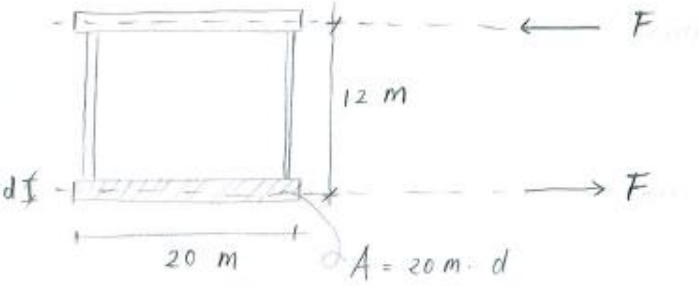
Name:

Date:

Page:

Rev:

ANNEX Z: FOR ARCHITECTS - FEASIBILITY BRIDGE GIRDER HEIGHT OF 12 METERS

Project	: Buoyancy Bridge Sognefjord	
Part	: Bridge girder height estimation	
<p><u>Question</u></p> <p>Does a height of 12 meters suffice for the section of the bridge girder at the main span ($L = 465 \text{ m}$) ?</p> <p><u>Example section:</u></p> <div style="text-align: center;">  </div> <p><u>Calculation:</u></p> <p>Total vertical load (self-weight + traffic) : $q = 350 \text{ kN/m}$</p> <p>Maximum bending moment : $M_{\text{main span, max}} = \frac{1}{8} \cdot q \cdot l^2$</p> $= \frac{1}{8} \cdot 350 \cdot 465^2$ $= 9,5 \cdot 10^6 \text{ kNm}$ $F = \frac{M_{\text{main span, max}}}{12 \text{ m}} = 788 \cdot 10^3 \text{ kN}$ <p>Assume allowable stress of $300 \text{ N/mm}^2 \rightarrow \sigma = \frac{F}{A}$</p> <p>Then :</p> $A = \frac{F}{\sigma} = \frac{788 \cdot 10^6 \text{ N}}{300 \text{ N/mm}^2} = 2\,627\,734 \text{ mm}^2$		
Name:	Christine Yip	Date: 26-5-2015
		Page: 1/2
		Rev:

Project : Buoyancy Bridge Sognefjord

Part : Bridge girder height estimation



Required flange height d is then:

$$d = \frac{A}{12 \text{ m}} = \frac{2\,627\,734}{20\,000} = 131 \text{ mm}$$

The self-weight of the two flanges in the cross-section drawn on page 1:

$$\begin{aligned} q_{G, \text{flanges}} &= 2 \cdot \rho \cdot g \cdot A \\ &= 2 \cdot 7850 \text{ kg/m}^3 \cdot 9,81 \cdot 2,627\,734 \\ &= 405 \text{ kN/m} \end{aligned}$$

Conclusion:

A height of 12 meters between the flanges of the bridge girder will lead to a self-weight of the superstructure ($> 405 \text{ kN/m}$) which is larger than the capacity of the substructure (350 kN/m).

A larger height between the flanges of the bridge girder is recommended. (More efficient)


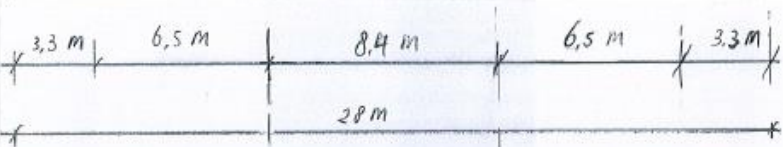
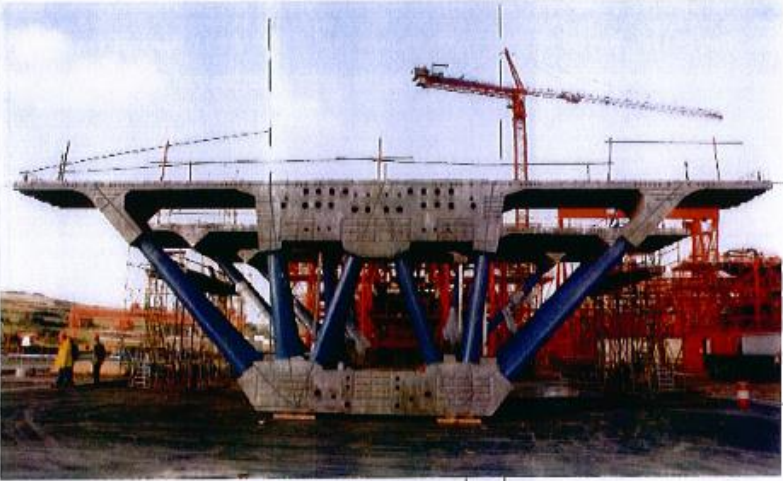
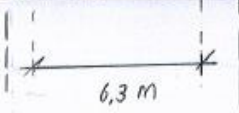
Name: Christine Yip

Date: 26-5-2015 Page: 2/2

Rev:

ANNEX AA: FOR ARCHITECTS - FEASIBILITY COMPOSITE BOX GIRDER

The architects prefer a composite box girder with concrete bottom and top flanges and steel lattice structures at the sides. However, structurally, this is not an efficient solution for the buoyancy bridge. This is explained in the following.

Project	: Buoyancy Bridge Sognefjord	
Part	: Box Girder Section	
Echtinghen viaduct main span = 110 m		
		
		
		
<p>Weight reinforced concrete flange:</p> $G_{flange} = \text{Preint. concrete} \cdot g \cdot A_{flange}$ $= 2500 \text{ kg/m}^3 \cdot 9,81 \text{ m/s}^2 \cdot 8,4 \text{ m} \cdot 1,5 \text{ m}$ $= 309 \text{ kN/m}$		
Name:	Christine Yip	Date: 4-6-2015
Page:	1/2	Rev:

Project : Buoyancy Bridge Sognefjord
 Part : Box Girder Section



Weight of concrete bottom flange of Viaduc
 Echingen ($L=110\text{m}$) : 309 kN/m

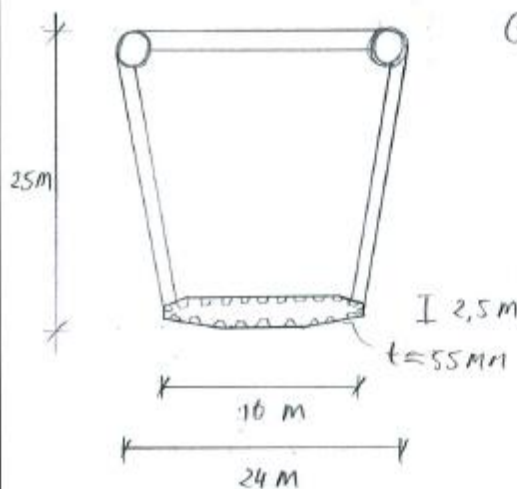
Reserved weight for the main span of the floating
 bridge of Sognefjord ($L=465$) : 350 kN/m

Conclusion

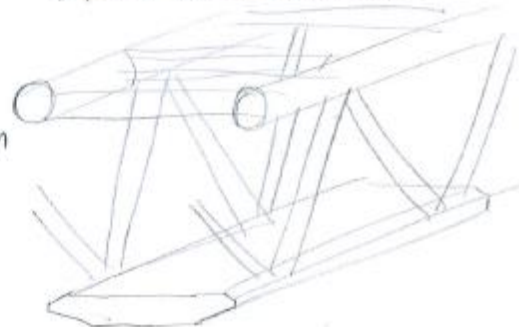
For the floating bridge of Sognefjord, a much more
 efficient solution must be found

Reconnendation : Replace concrete bottom flange
 with flat steel box girder

$G_{\text{steel box girder}} \approx 136\text{ kN/m}$



Smooth bottom surface:



Name: Christine Yip

Date: 4-6-2015


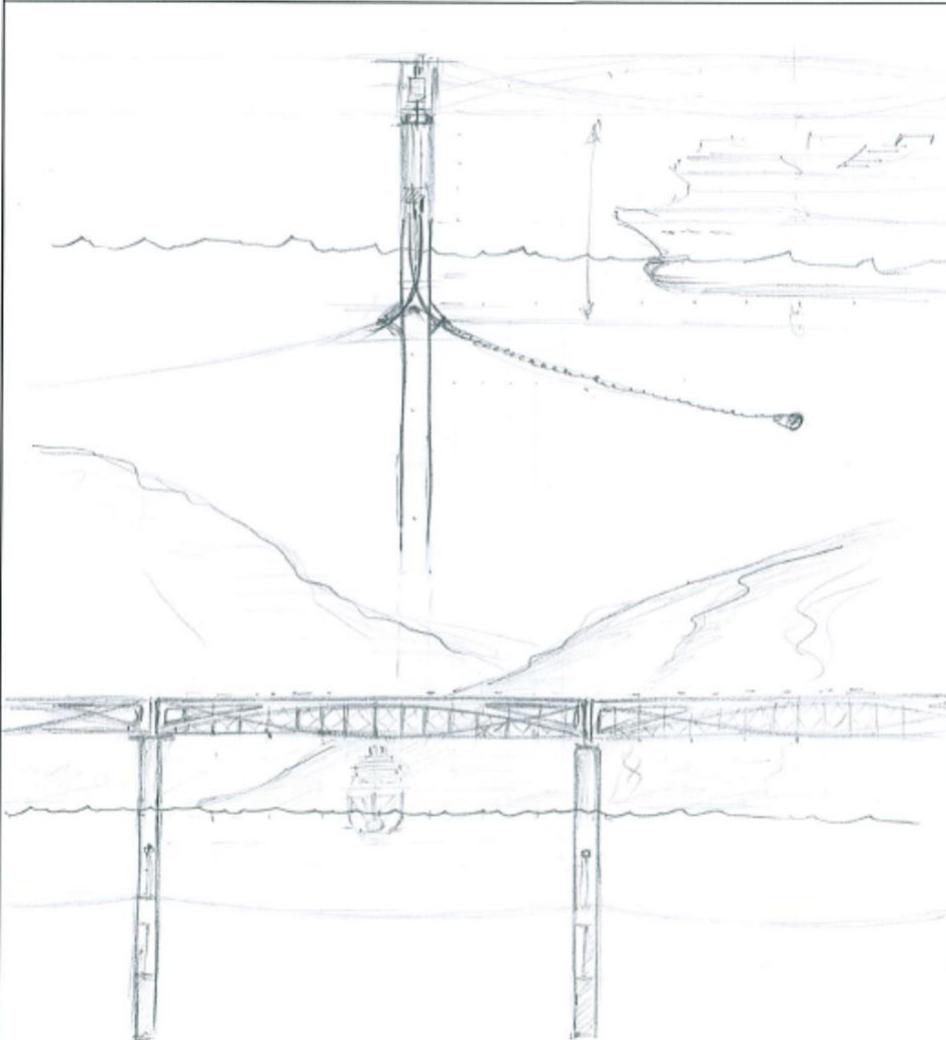
Page: 2/2

Rev:

ANNEX BB: SKETCHES OF POSSIBLE SUPERSTRUCTURES

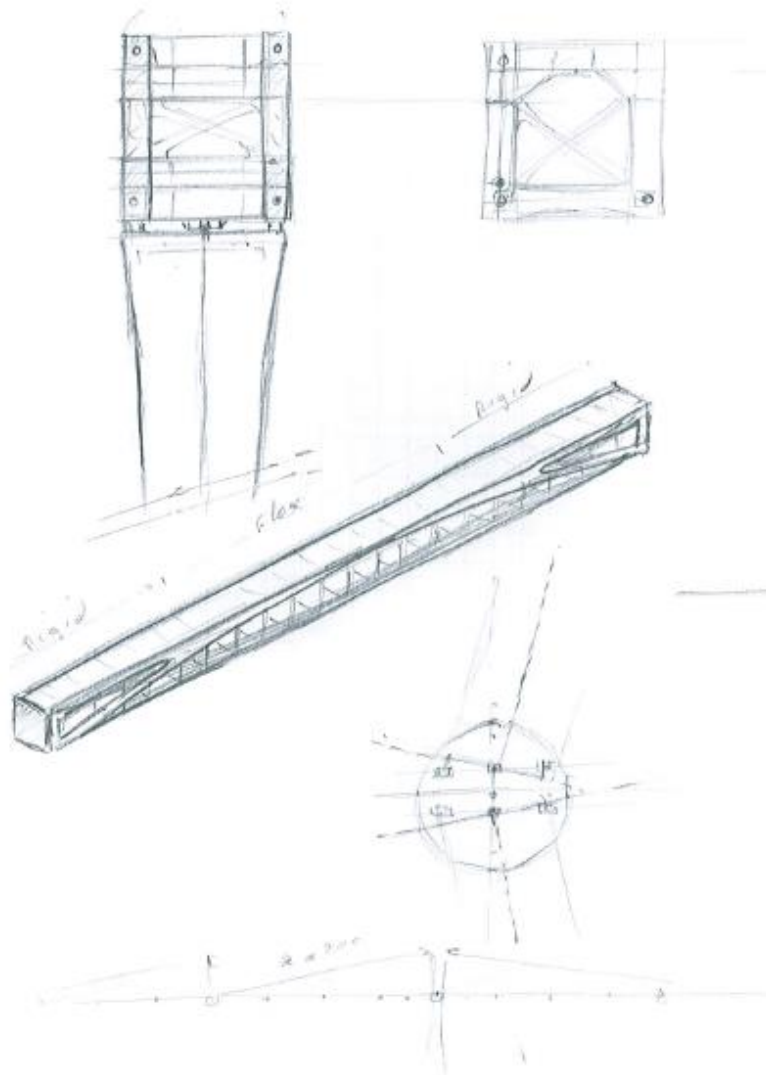
Close cooperation with the architecture firm Zwarts & Jansma lead to a structurally and aesthetically competitive bridge concept.

To develop a competitive bridge concept, there was a continual exchange of ideas with the architects. In this annex, several sketches of different superstructures are shown, which were proposed to the architects.

Project	: Buoyancy Bridge Sognefjord	
Part	: Sketch - Possible Superstructure 1 : Double Arch	
		
<p style="font-family: cursive; font-size: small;"> out for 4m/m x 1000 → 1000m → 1000m 3.2m → 270.22m ≈ 175m/m 10150m/m → 150m </p>		
Name:	Wouter Visser	Date:
		Page: 1/2
		Rev:

Project : Buoyancy Bridge Sognefjord

Part : Sketch - Possible Superstructure 1: Double Arch



Name: Wouter Visser

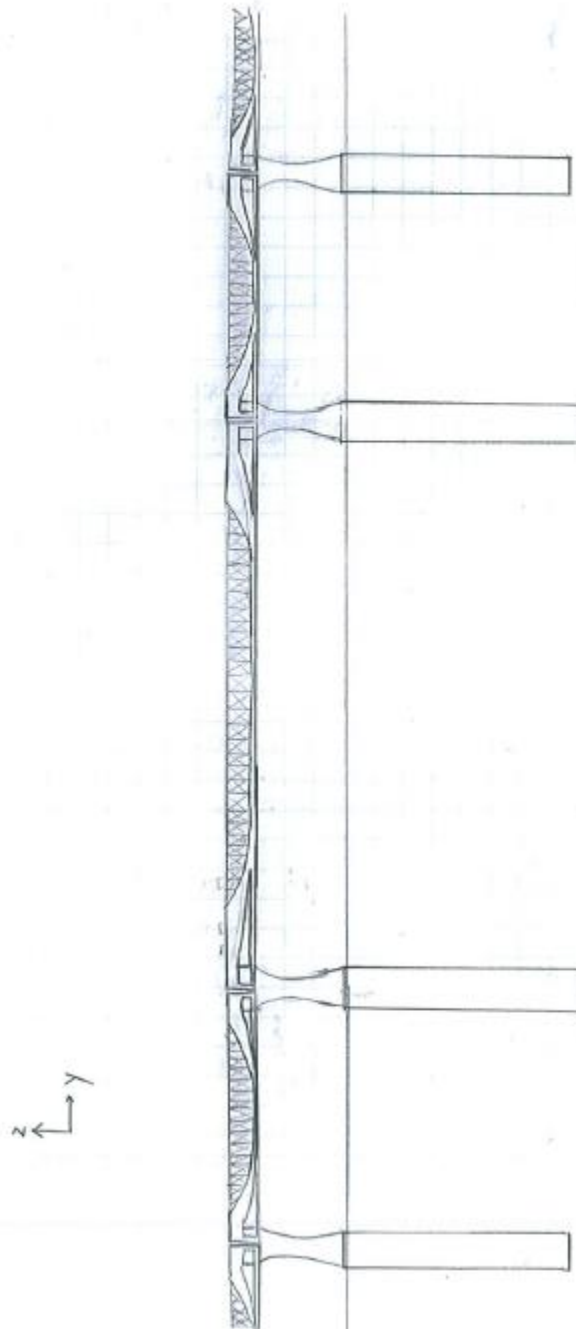
Date:

Page: 2/2

Rev:

Project : Buoyancy Bridge Sognefjord

Part : Proposed Superstructure



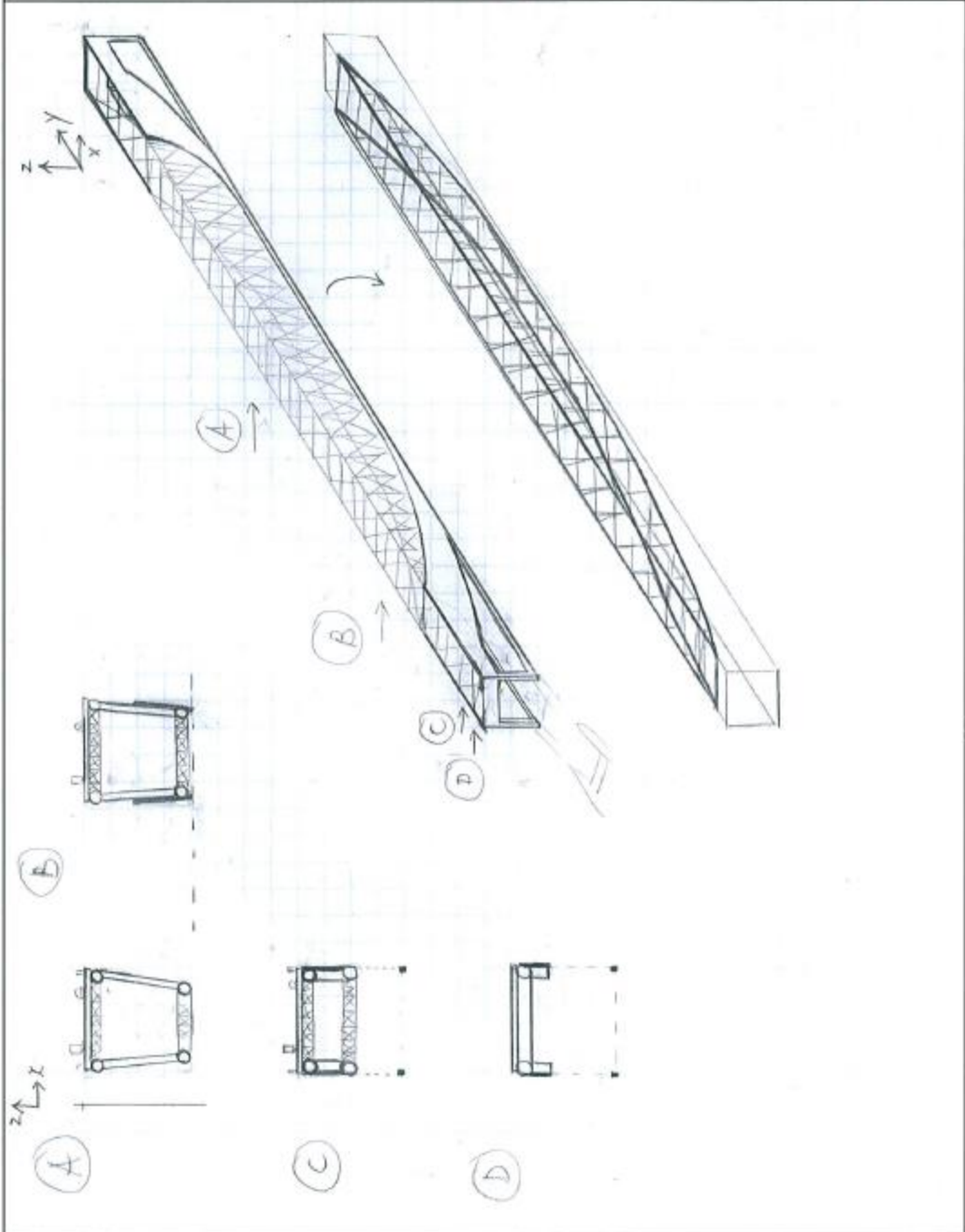
Name: Christine Yip

Date: 1-6-2015 Page: 1/3

Rev:

Project : Buoyancy Bridge Sognefjord

Part : Proposed superstructure



Name: Christine Yip

Date: 1-6-2015 Page: 2/3

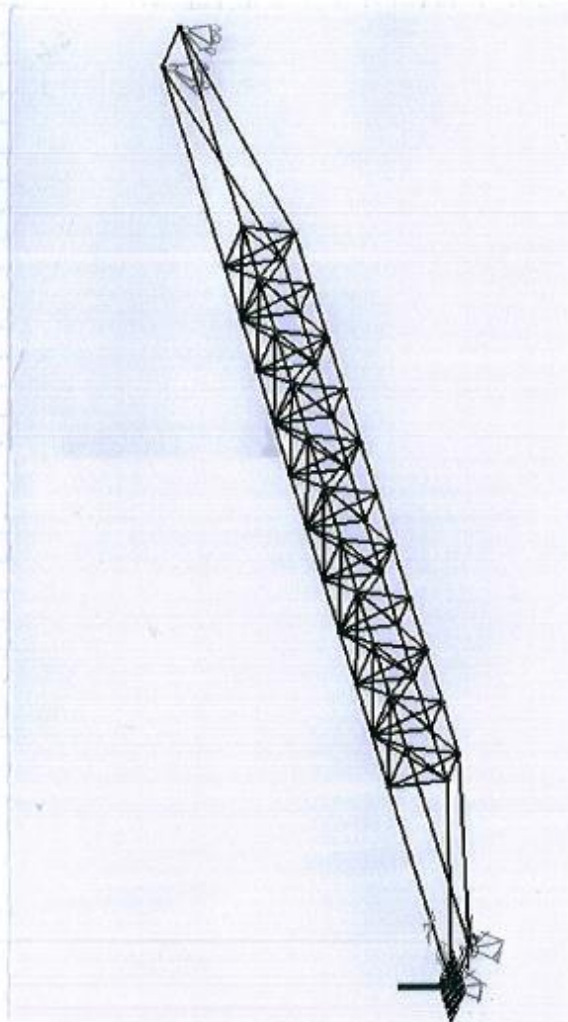
Rev:

Project : Buoyancy Bridge Sognefjord

Part : Proposed Superstructure



Simplified :


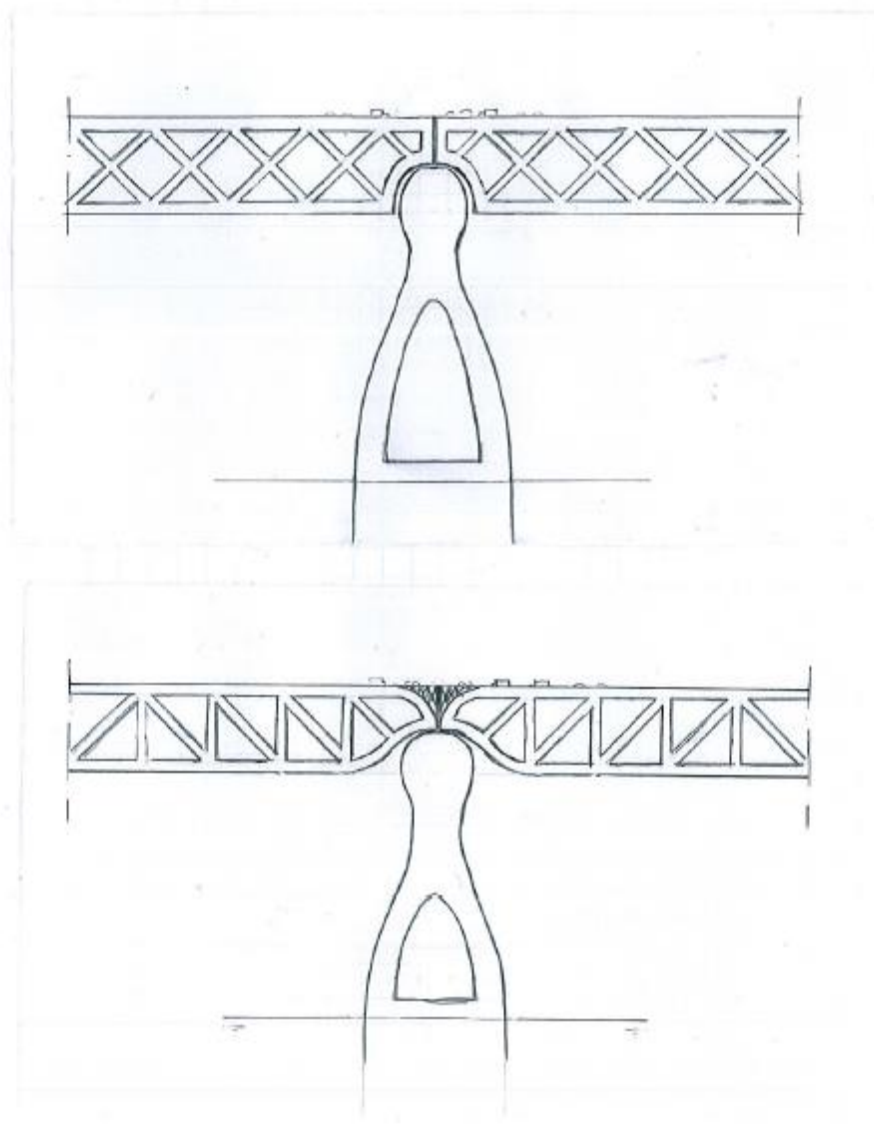



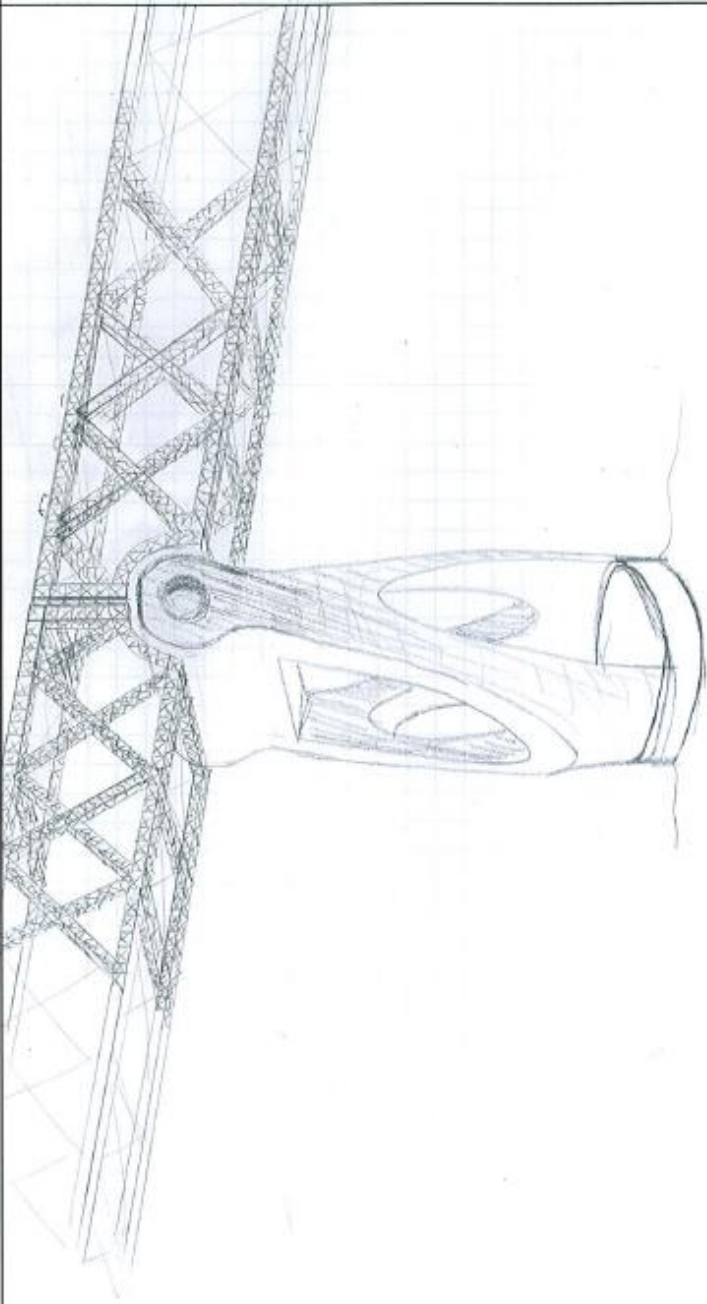
Name: Christine Yip


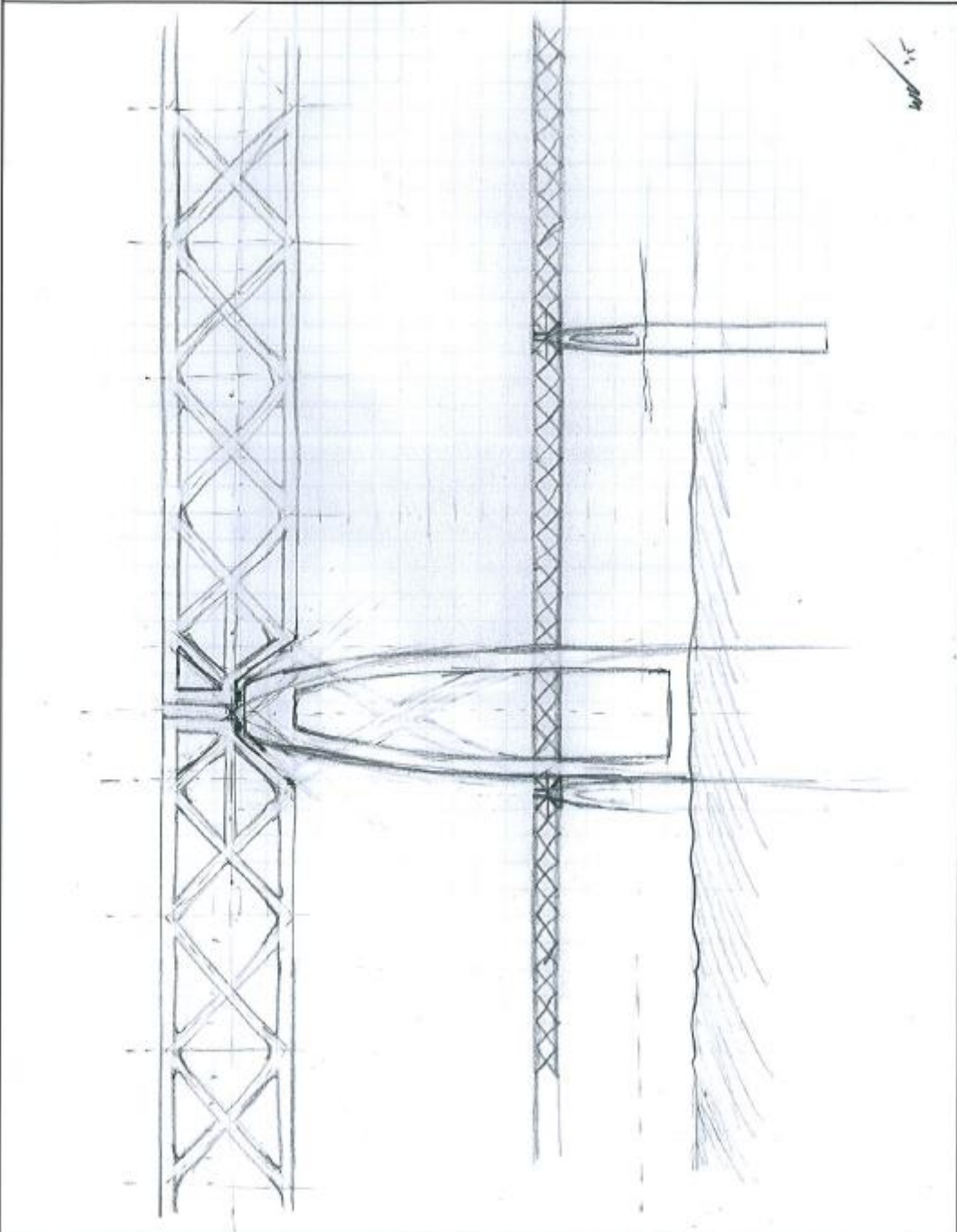
Date: 1-6-2015

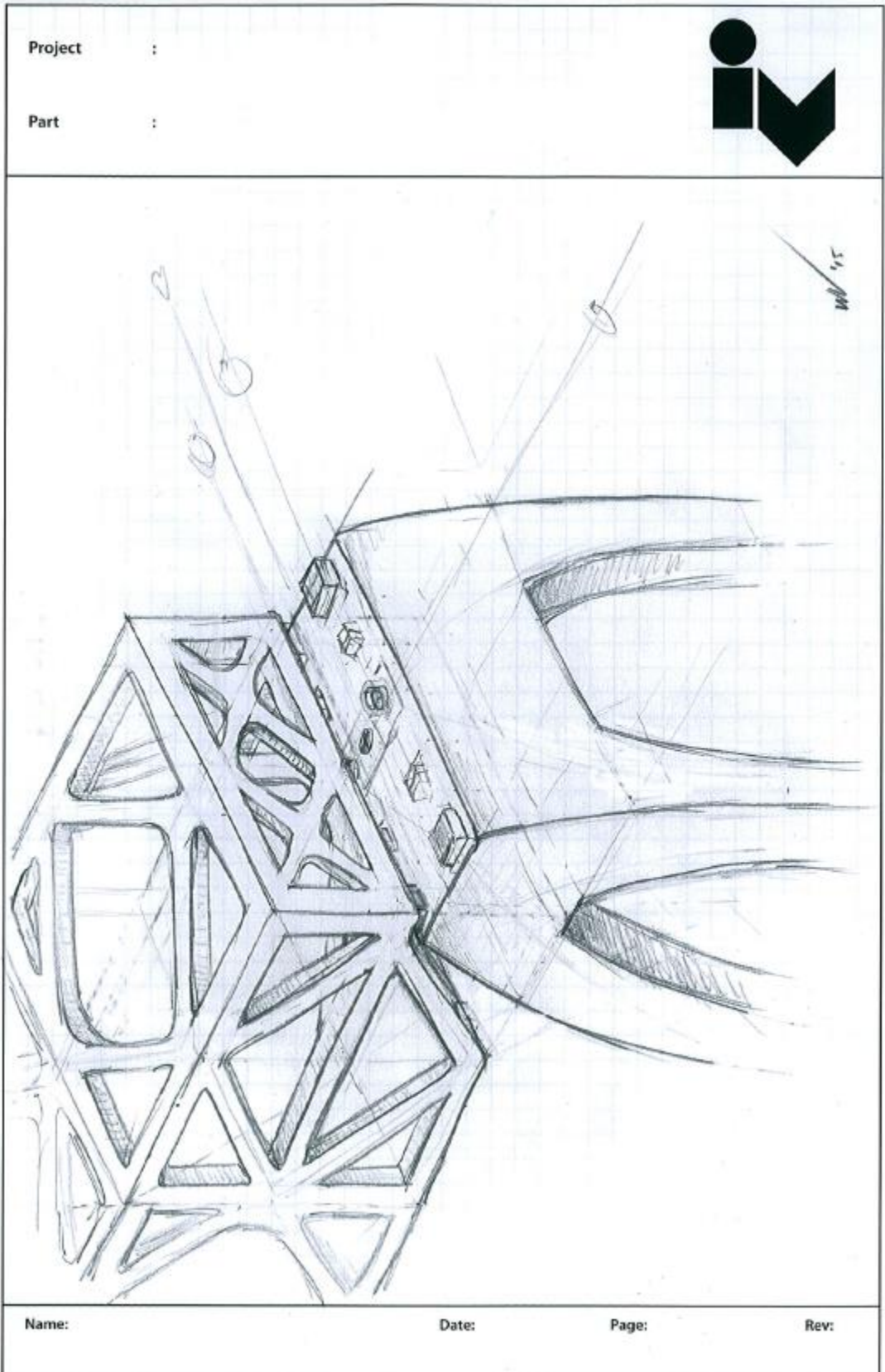
Page: 3/3

Rev:

Project :		
Part :		
		
Name:	Date:	Page: 2/2 Rev:

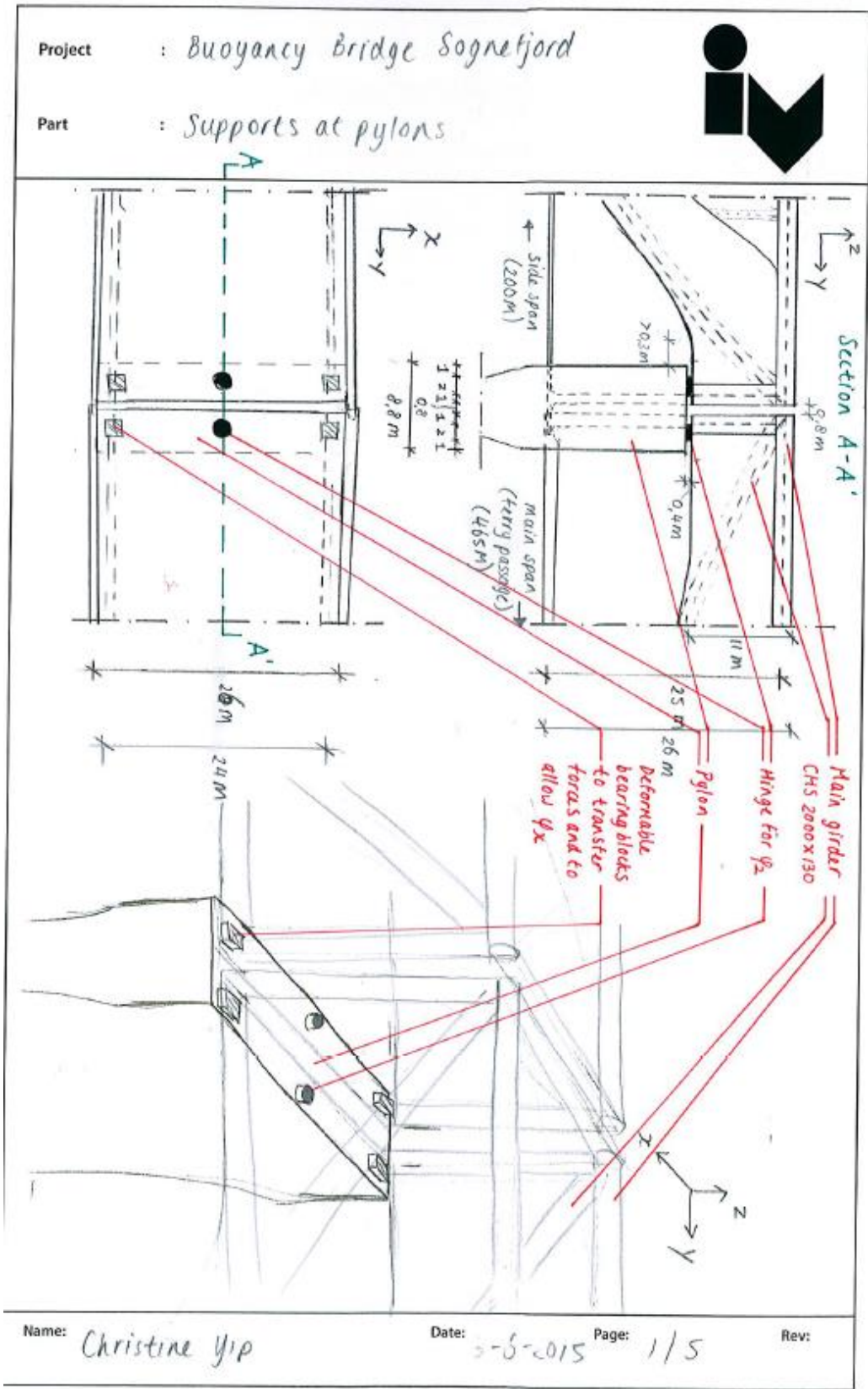
Project :		
Part :		
		
Name:	Date:	Page: 1/2
		Rev:

Project :			
Part :			
			
Name:	Date:	Page:	Rev:



ANNEX CC: SUPPORTS AT BRIDGE PIERS/PYLONS – DIMENSIONS AND DISPLACEMENTS (FIRST ESTIMATION)

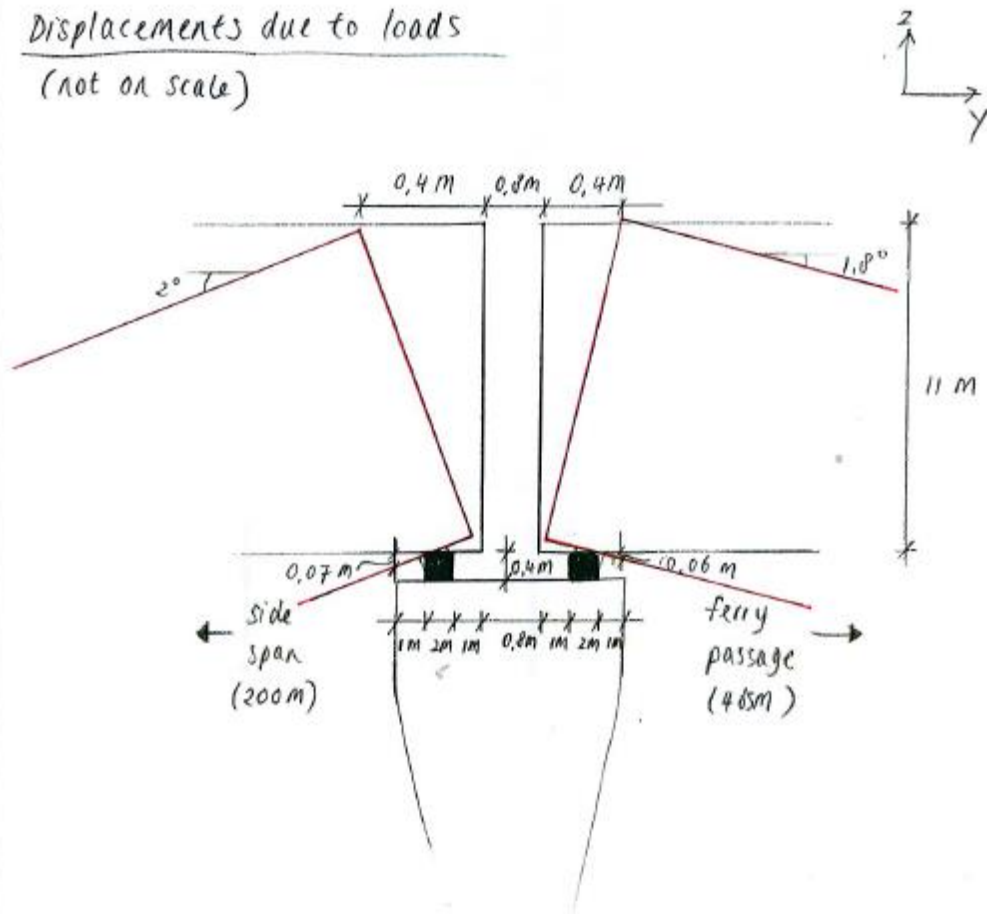
In the next pages, the first estimations for the supports are shown.



Project : Buoyancy Bridge Sognefjord
 Part : Supports at pylons - displacements



Displacements due to loads
 (not on scale)



Name: Christine Yip

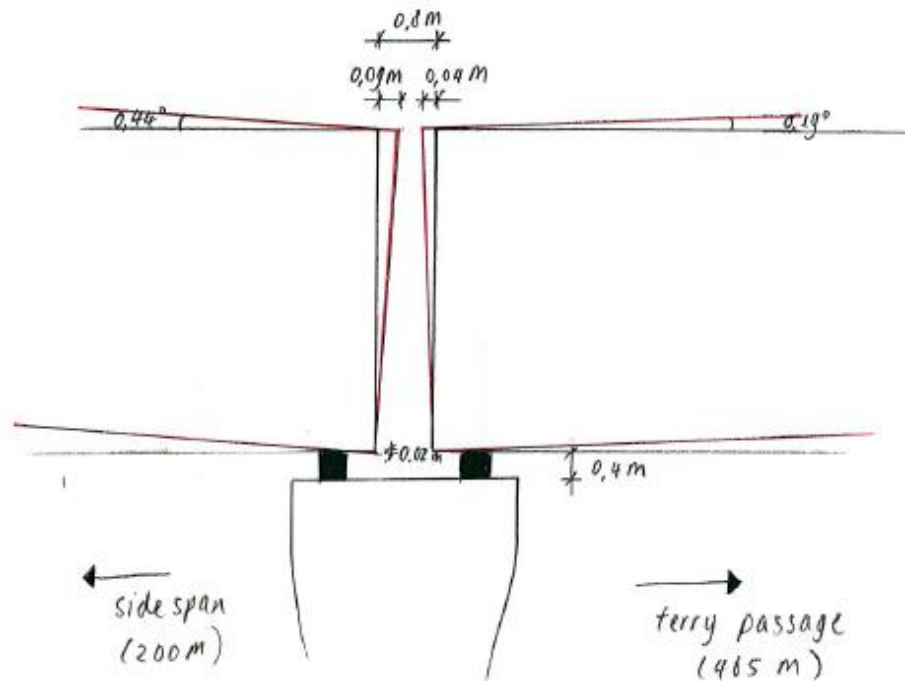
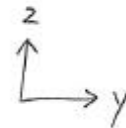
Date: 3-6-2015 Page: 2/5

Rev:

Project : Buoyancy Bridge Sognefjord
 Part : Supports at pylons-displacements



Displacements due to loads
 (not on scale)



Name: Christine Yip

Date: 3-6-2015

Page: 3/5

Rev:

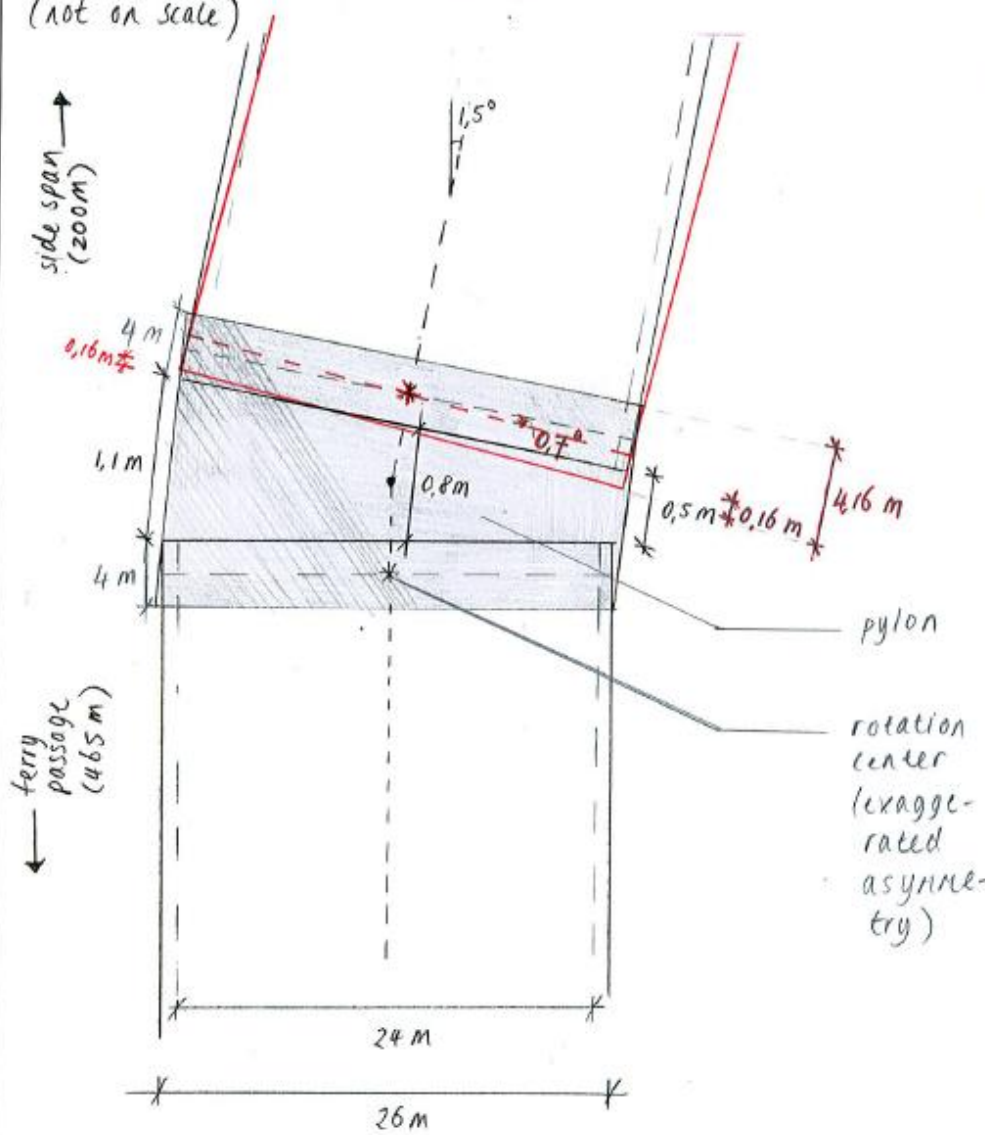
Project : Buoyancy Bridge Sognefjord

Part : Supports at pylons-displacements



Displacements due to loads

(not on scale)



Name: Christine Yip

Date: 3-6-2015

Page: 4/5

Rev:

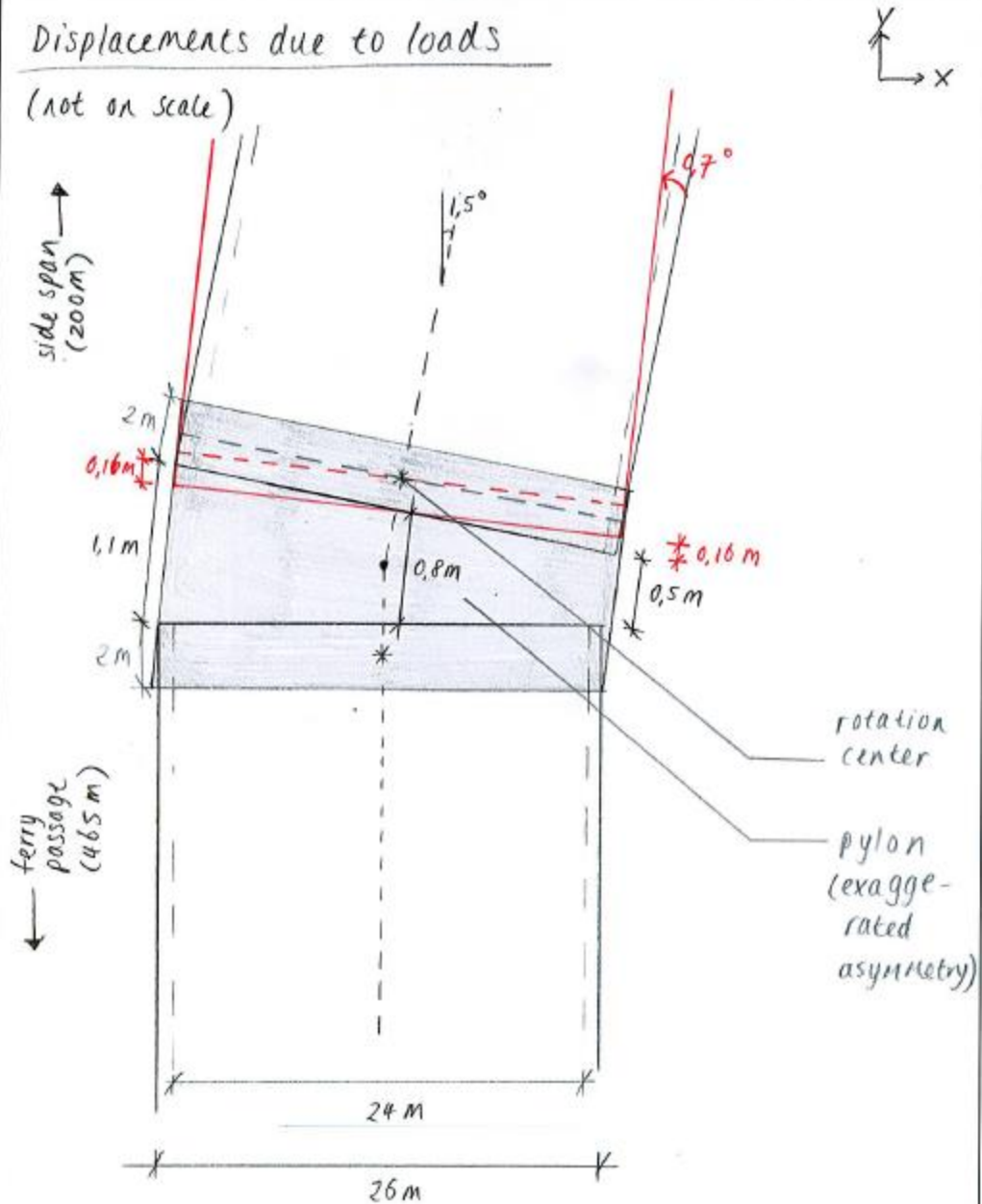
Project : Buoyancy Bridge Sognefjord

Part : Supports at pylons - displacements



Displacements due to loads

(not on scale)



Name: Christine Yip

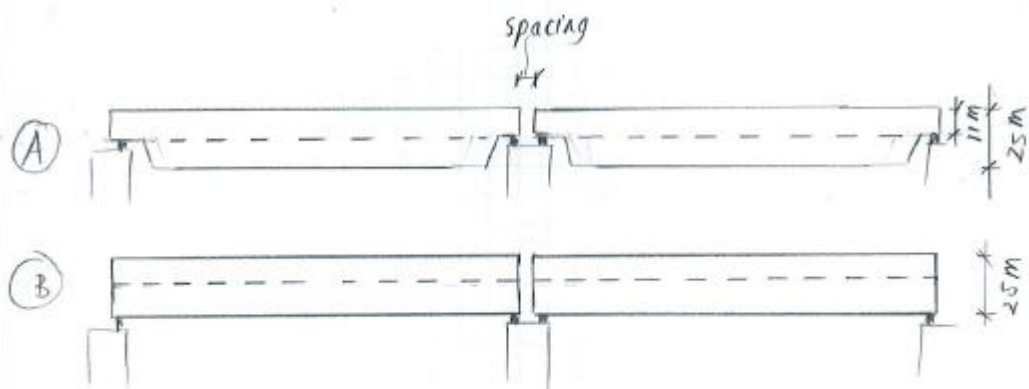
Date: 3-6-2015

Page: 5/5

Rev:

Project : Buoyancy Bridge Sognefjord

Part : Support height influences required spacing



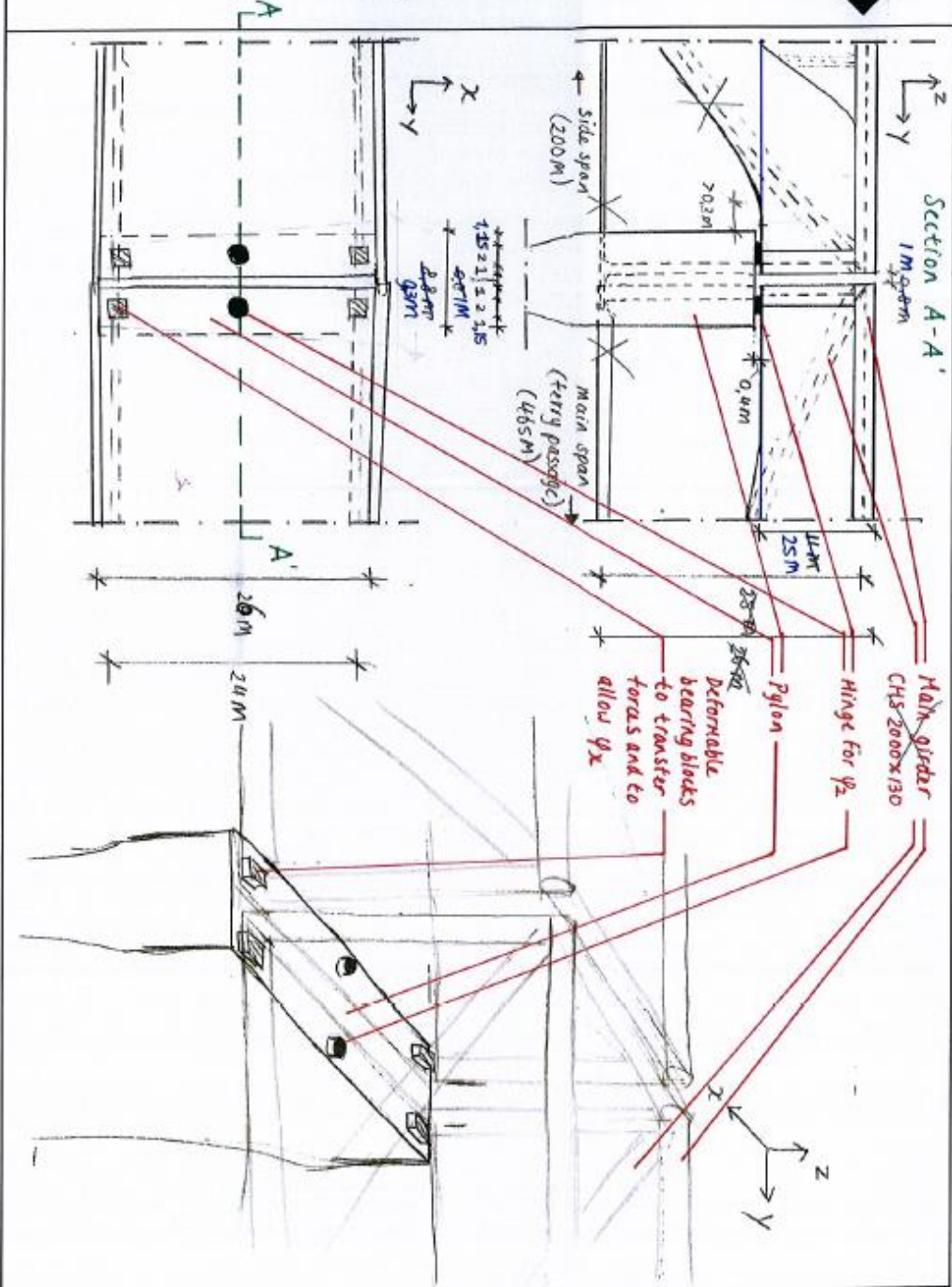
Name: Christine Yip

Date: 4-6-2015 Page: 1/6

Rev:

Project : Buoyancy Bridge Sognefjord

Part : Supports at pylons



Supports :

Name: Christine Yip

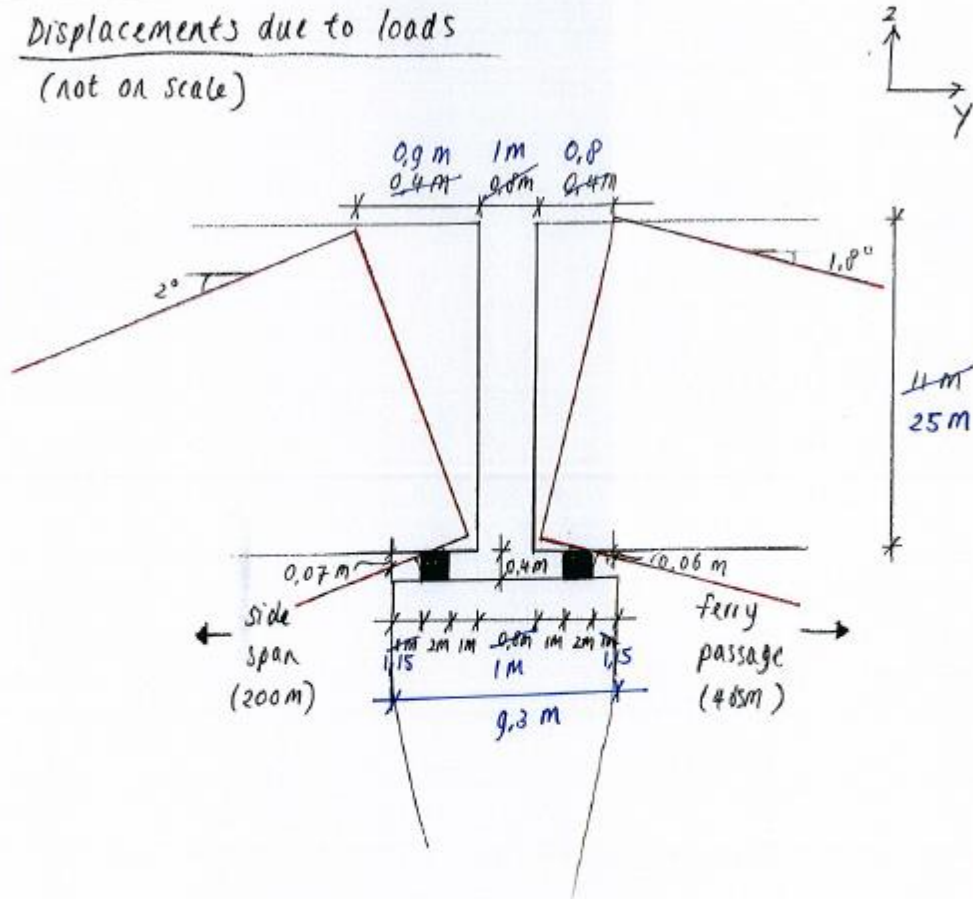
Date: 4-6-2015 Page: 2/6

Rev:

Project : Buoyancy Bridge Sognefjord
 Part : Supports at pylons - displacements



Displacements due to loads
 (not on scale)

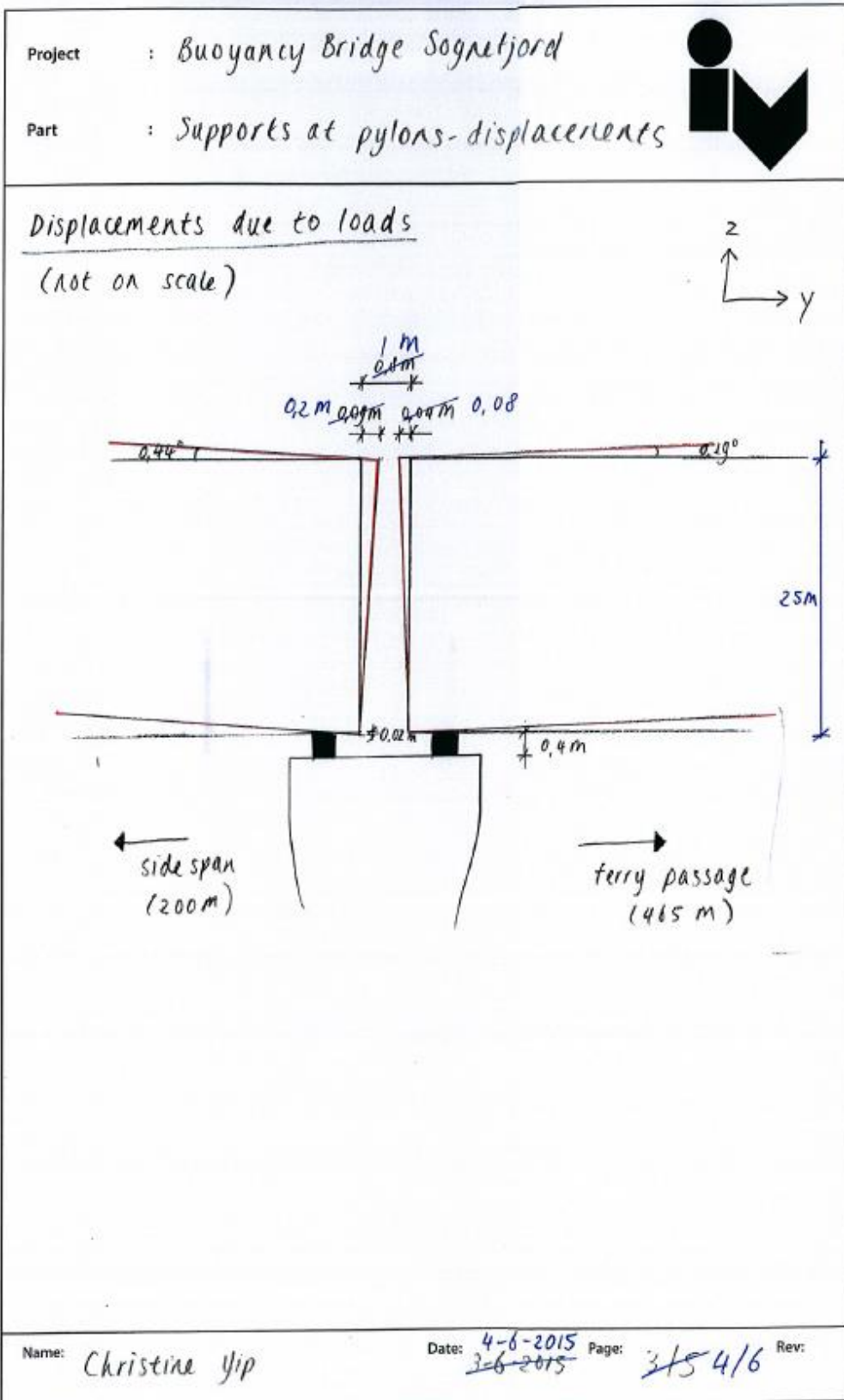


Name: Christine Yip

Date: 4-6-2015
 3-6-2015

Pages: 215 3/6

Rev:



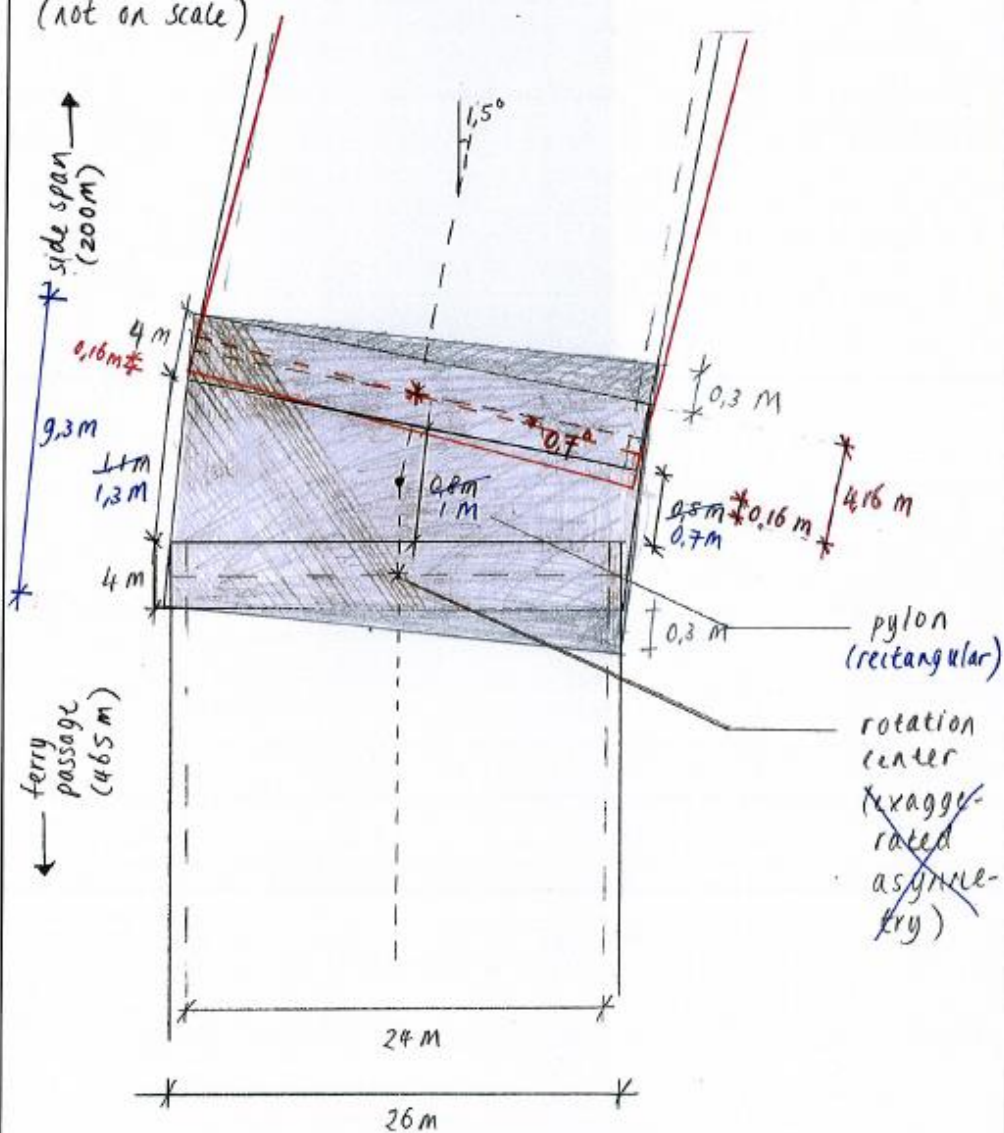
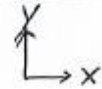
Project : Buoyancy Bridge Sognefjord

Part : Supports at pylons - displacements



Displacements due to loads

(not on scale)



Name: Christine Yip

Date: 4-6-2015
2-6-2015

Page: 4/5 5/6

Rev:

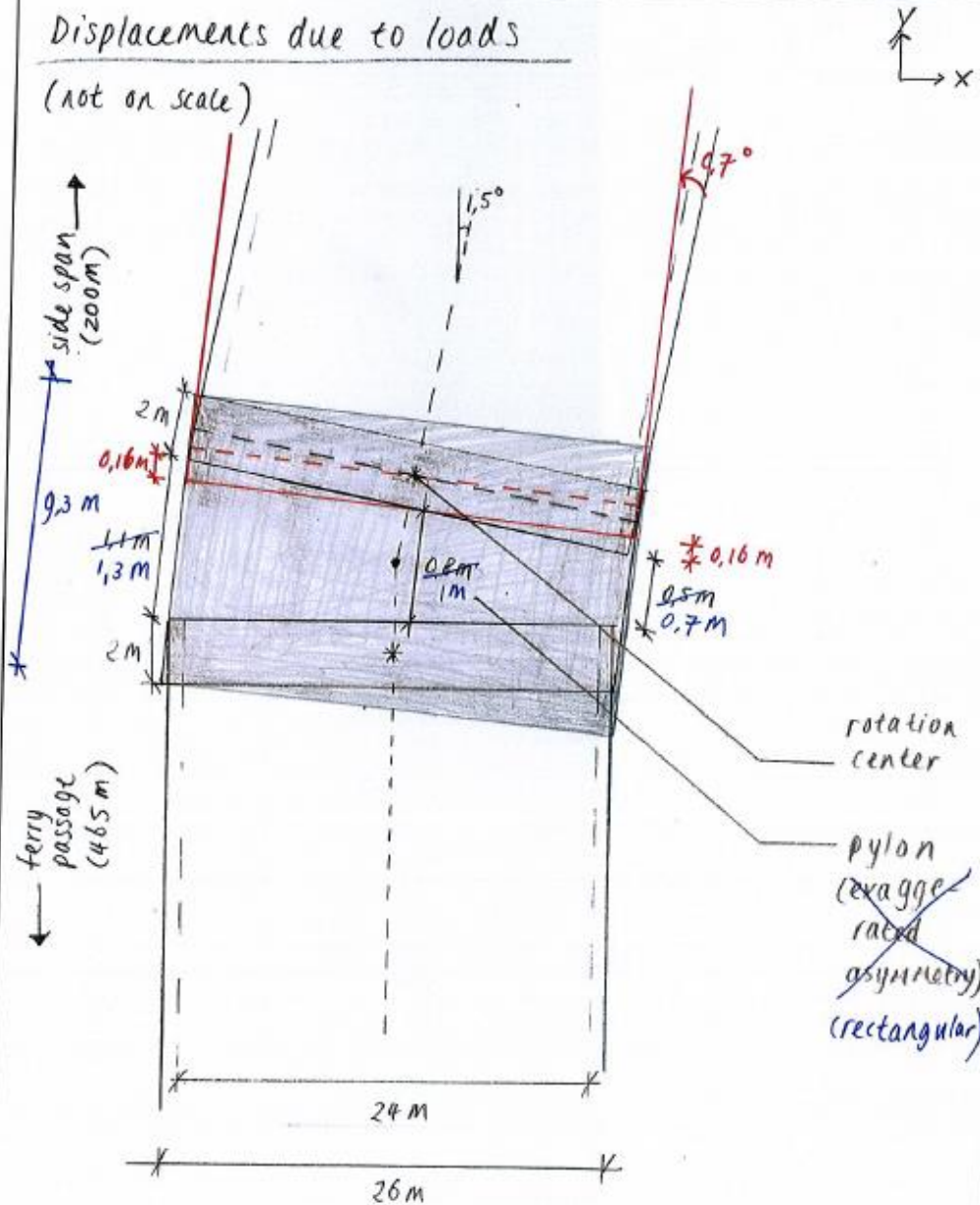
Project : Buoyancy Bridge Sognefjord

Part : Supports at pylons - displacements



Displacements due to loads

(not on scale)



Name: Christine Yip


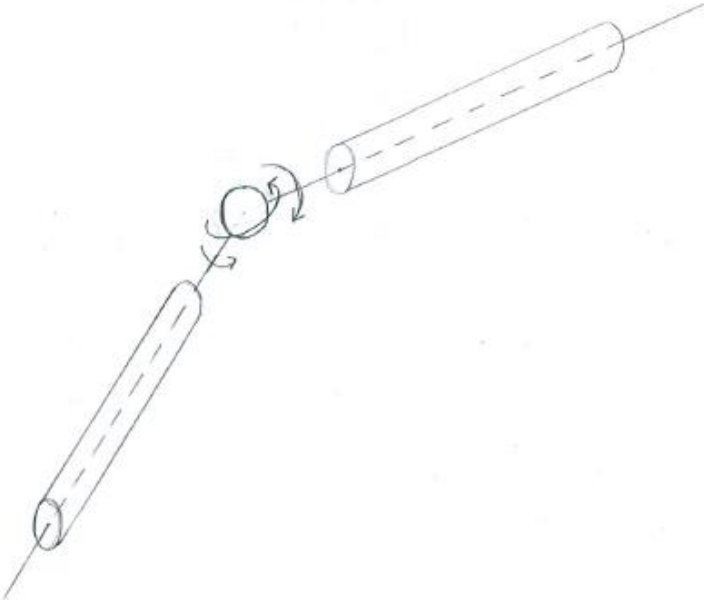
Date: 4-6-2015
3-6-2015

Page:

5/5 6/6

Rev:

ANNEX DD: FOR ARCHITECTS – RECOMMENDATION SUPPORTS (LOCATION AND DIMENSIONS)

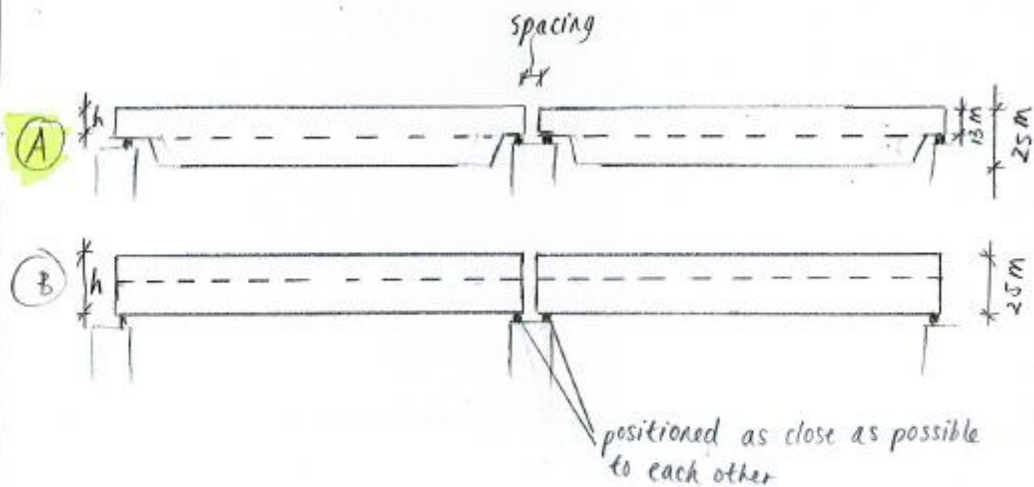
Project	: Buoyancy Bridge Sognefjord	
Part	: Joint	
<p>For a flexible 'chain' of bridge segments, the best position for the joint is at the intersection of the axes of the bridge segments:</p> 		
Name:	Christine Yip	Date: 7-6-2015 Page: 1/8 Rev:

Project : Buoyancy Bridge Sognefjord

Part : Spacings of joint at main span



Support height influences the required spacing



(A) : Hinge in axis of the bridge

$h_A = 13\text{ m}$ ← most suitable for a flexible floating bridge

(B) : $h_B = 25\text{ m}$

Hinge is outside the bridge axis.

Name: Christine Yip

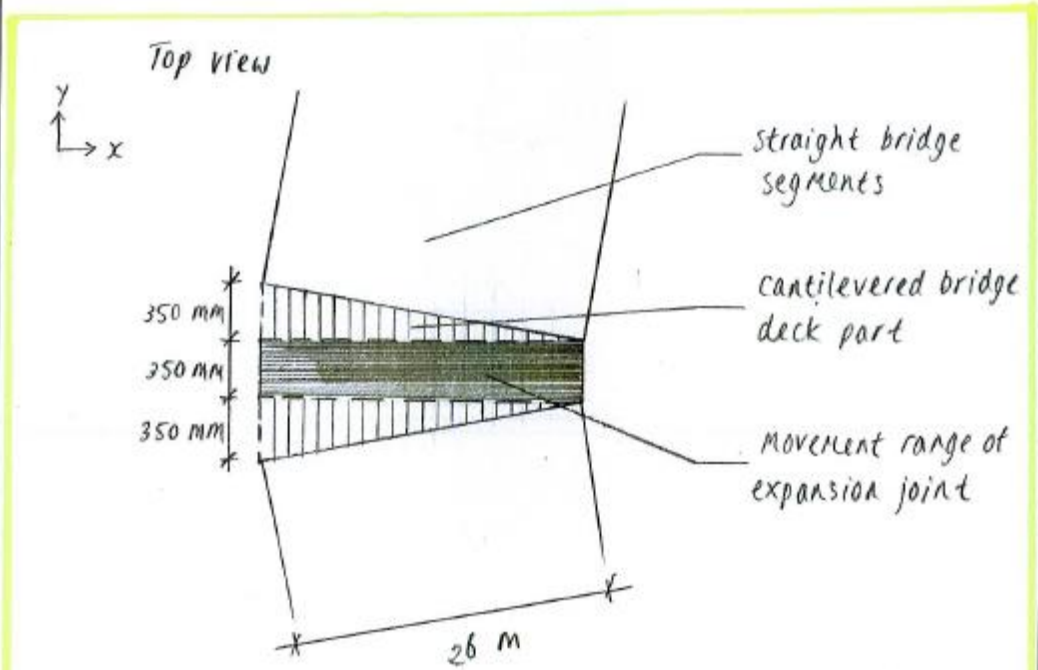
Date: 7-6-2015 Page: 2/8

Rev:

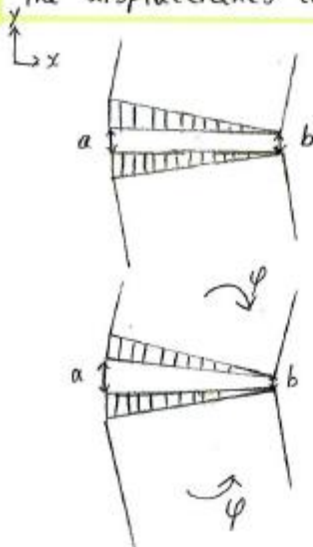
Project : Buoyancy Bridge Sognefjord
 Part : Spacings of joints at main span



Recommendation: $h_{(A)} = 13 \text{ m}$. Then :



The displacements can be found below and on the next pages.



minimum distance at b : 118 mm
 due to loads

maximum distance at a : 573 mm
 due to loads

Name: Christine Yip

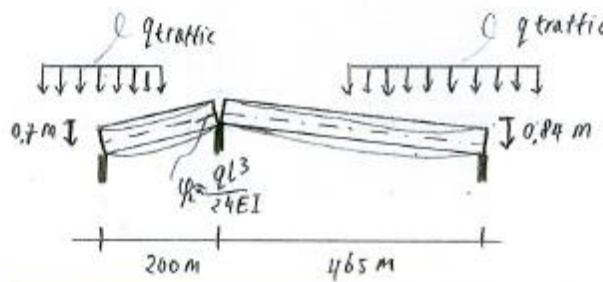
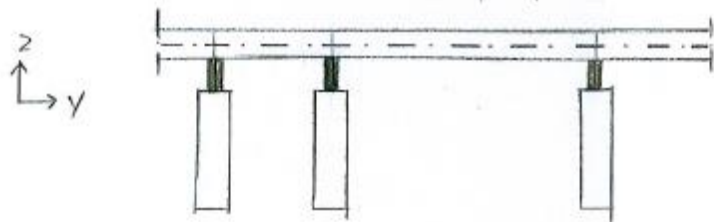
Date: 7-6-2015 Page: 3/8

Rev:

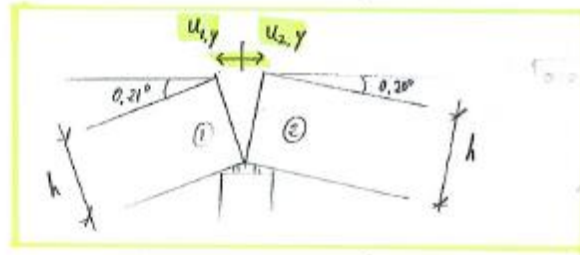
Project : Buoyancy Bridge Sognefjord
 Part : Spacings of joints at main span



Vertical plane :



$q = 35 \text{ kN/m}$
 $E = 210 \cdot 10^6 \text{ kN/m}^2$
 $I = 405 \text{ m}^4$



$$u_{1,y} = h \cdot \tan 0,21^\circ$$

$$u_{2,y} = h \cdot \tan 0,20^\circ$$

maximum 'opening' due to this load case



* If $h = 25 \text{ m}$:

$$u_{1,y} = 92 \text{ mm}$$

$$u_{2,y} = 89 \text{ mm}$$

$$u_{1,y} + u_{2,y} = 181 \text{ mm}$$

* If $h = 13 \text{ m}$:

$$u_{1,y} = 48 \text{ mm}$$

$$u_{2,y} = 46 \text{ mm}$$

$$u_{1,y} + u_{2,y} = 94 \text{ mm}$$

Name: Christine Yip

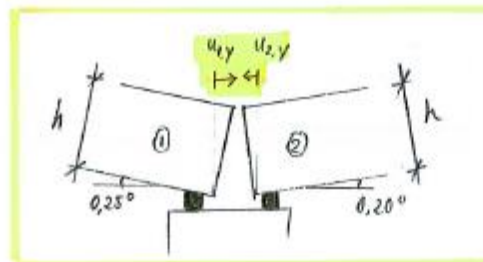
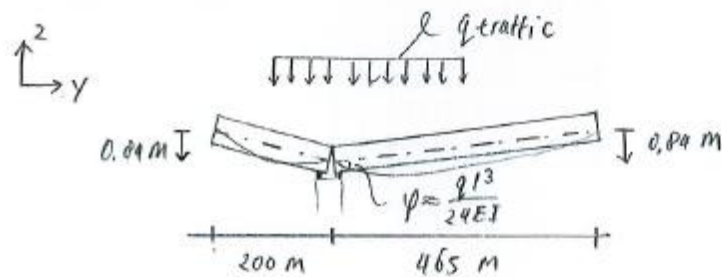
Date: 7-6-2015 Page: 4/8

Rev:

Project : Buoyancy Bridge Sognefjord
 Part : Spacings of joints at main span



Vertical Plane:



$$u_{1,y} = h \cdot \tan 0,25^\circ$$

$$u_{2,y} = h \cdot \tan 0,20^\circ$$

* if $h = 25 \text{ m}$:

$$u_{1,y} = 109 \text{ mm}$$

$$u_{2,y} = 88 \text{ mm}$$

$$u_{1,y} + u_{2,y} = 197 \text{ mm}$$

* if $h = 13 \text{ m}$:

$$u_{1,y} = 57 \text{ mm}$$

$$u_{2,y} = 46 \text{ mm}$$

$$u_{1,y} + u_{2,y} = 103 \text{ mm}$$

↑
 required spacing for this
 load case

Name: Christene Yip

Date: 7-6-2015

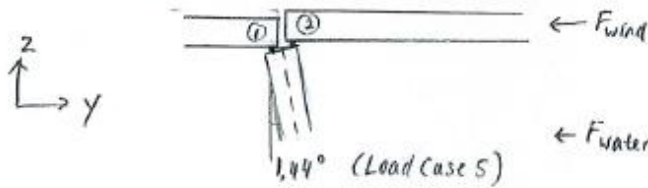
Page: 5/8

Rev:

Project : Buoyancy Bridge Sognefjord
 Part : Spacings of joints at main span



Vertical Plane :



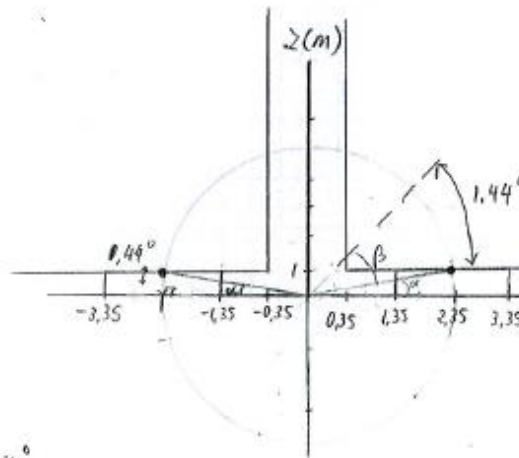
$$R = \sqrt{2.5^2 + 1^2} = 2.7$$

$$\alpha = \tan^{-1}\left(\frac{1}{2.5}\right) = 21.8^\circ$$

$$\beta = 21.8 + 1.44 = 23.2^\circ$$

$$y_\beta = R \cos 23.2^\circ = 2.47 \text{ m}$$

$$z_\beta = R \sin 23.2^\circ = 1.064 \text{ m}$$

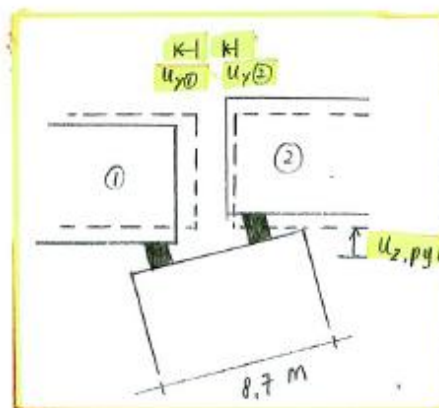


$$\gamma = \alpha - 1.44^\circ = 21.8^\circ - 1.44^\circ = 20.4^\circ$$

$$y_\gamma = R \cos \gamma = 2.53 \text{ m}$$

$$z_\gamma = R \sin \gamma = 0.941 \text{ m}$$

required spacing for this load case:



$$u_{y(1)} = 31 \text{ mm}$$

$$u_{y(2)} = 26 \text{ mm}$$

✓ no problem (smaller than required spacing for load case on previous page)

$$u_{z,pyl} = \frac{8.7}{2} \sin 1.44^\circ = 4.35 \sin 1.44^\circ = 109 \text{ mm}$$

Name: Christine Yip

Date: 7-6-2015 Page: 6/8

Rev:

Project : Buoyancy Bridge Sognefjord

Part : Spacings of joints at main span



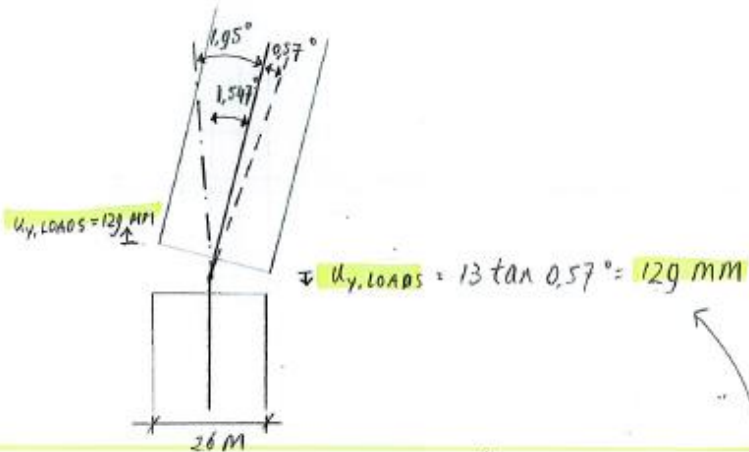
Horizontal plane:



Before placing of the deck: -----

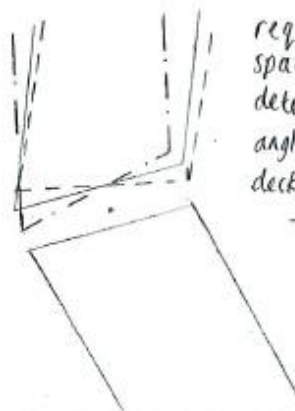
After placing of the deck (total SW): -----

Due to external loads: -----



Option 1:

Using tapered bridge girders:



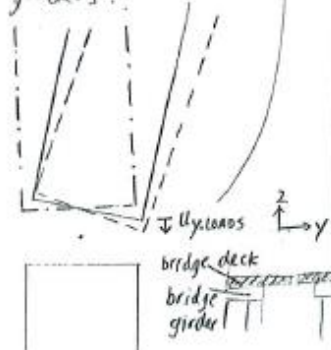
required spacing determined by angle due to deck placing

$$s \geq 13 \tan 1.95^\circ$$

$$s \geq 443 \text{ mm}$$

Option 2:

Using straight, symmetrical bridge girders:



Bridge deck will have tapered shape and placed on top of straight bridge girders (cantilevered)

Name: Christine Yip

Date: 7-6-2015

Page: 7/8

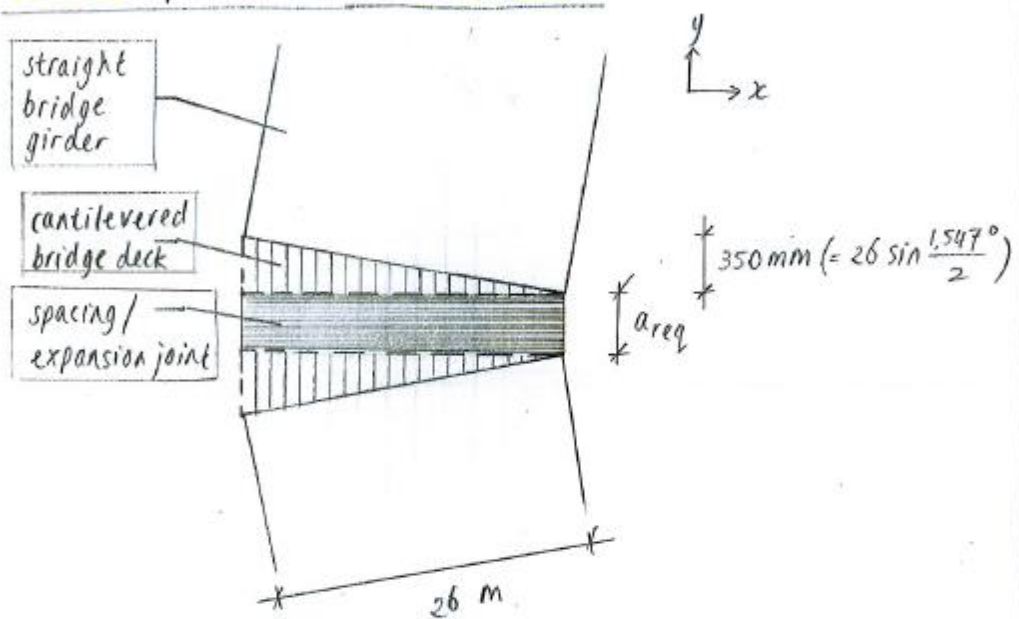
Rev:

Project : Buoyancy Bridge Sognefjord
 Part : Spacings of joints at main span



Recommendation:

Choose option 2 with $h = 13 \text{ m}$



	$h = 25 \text{ m}$	$h = 13 \text{ m}$
a_{req}	326 mm	232 mm

\curvearrowright 29% \uparrow
 most favourable

Name: Christine Yip

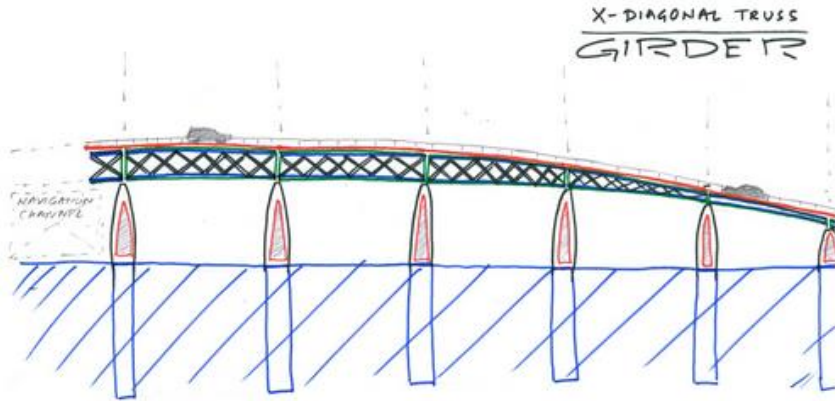
Date: 7-6-2015

Page: 8/8

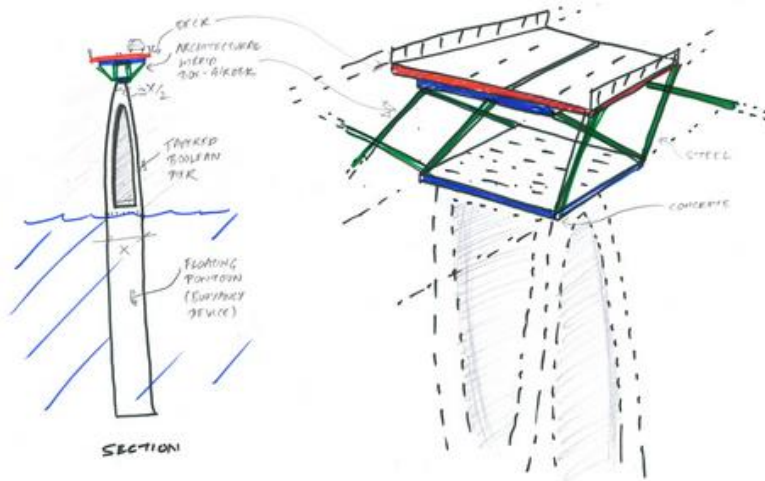
Rev:

This sketch is from the architects:

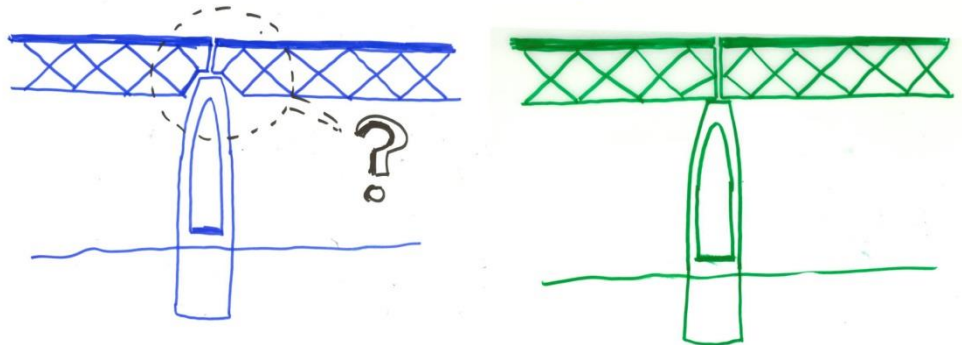
781: SOGNEFJORD BUOYANCY BRIDGE



ELEVATION (CONCEPTUAL)



PIER GIRDER CONNECTION
- WHY CANT IT BE SIMPLE STRAIGHT GIRDERS?

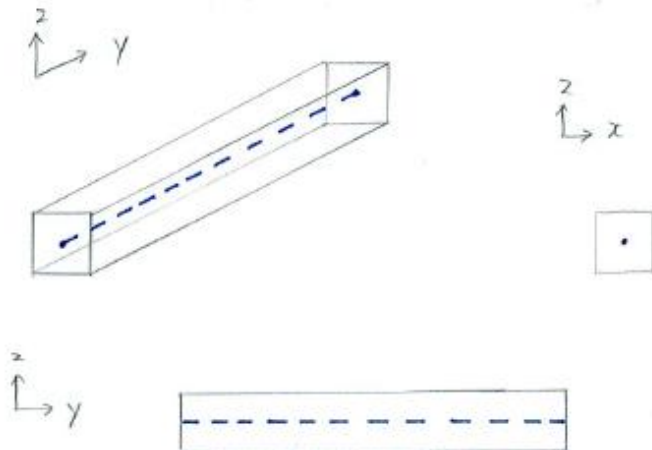


Project :

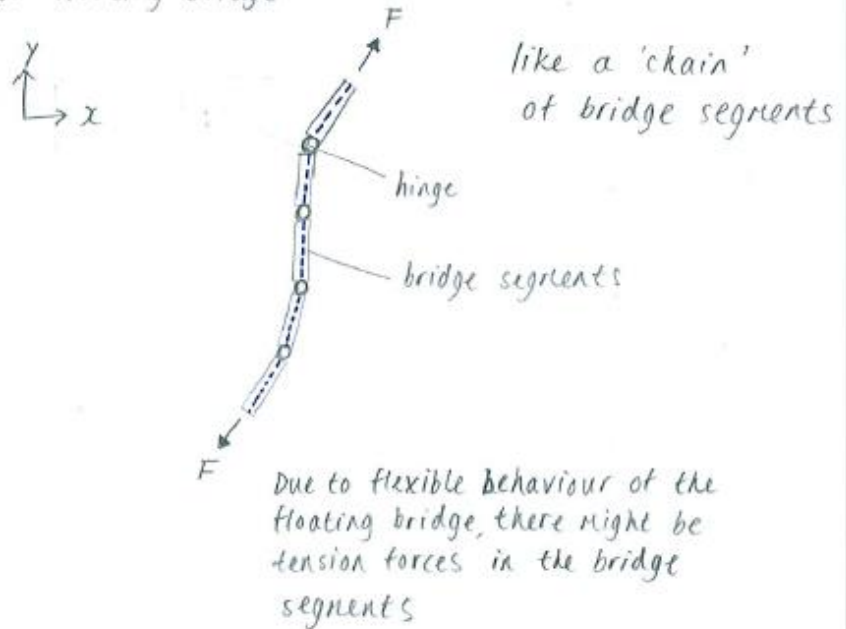
Part :



Bridge girder axis:



Plan view of floating bridge:



Name:


Date:

Page:

Rev:

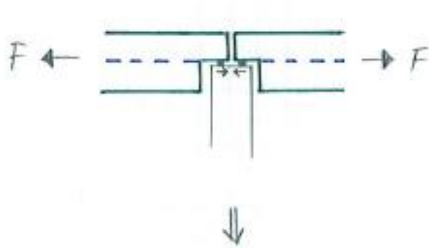
Project : _____

Part : _____

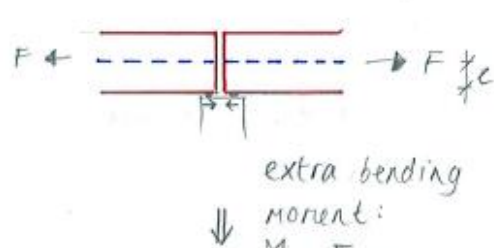


Bridge girders supported

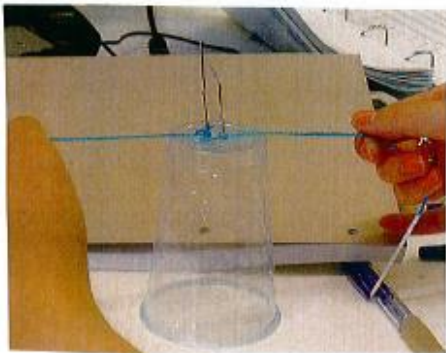
= in axis :



= eccentrically :



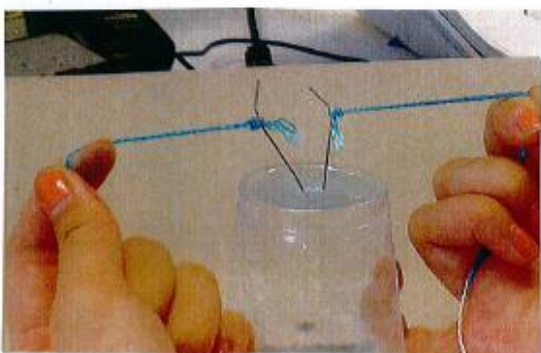
extra bending moment:
 $M = F \cdot e$



↓

✓

most favourable position



↓

✗

unfavourable effects
due to eccentricity
(extra bending moments)

Name: _____


Date: _____

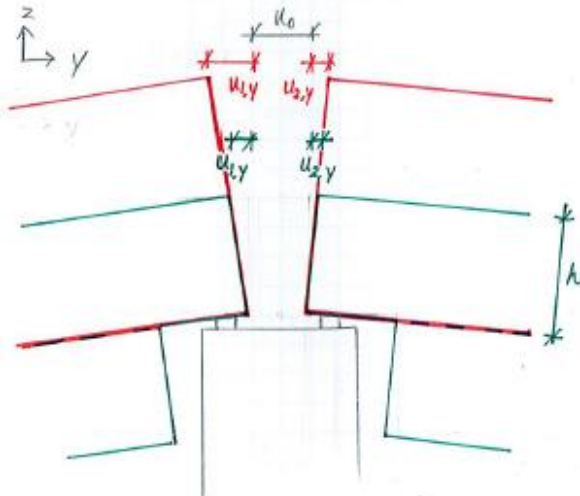
Page: _____

Rev: _____

Project : _____

Part : _____





Displacements

$$u_{1,y} = h \cdot \tan 0,21^\circ$$

$$u_{2,y} = h \cdot \tan 0,20^\circ$$

$h = 13 \text{ m}$	$h = 25 \text{ m}$
$u_{1,y} = 48 \text{ mm}$	$u_{1,y} = 92 \text{ mm}$
$u_{2,y} = 46 \text{ mm}$	$u_{2,y} = 89 \text{ mm}$

↑↑
needs also twice
as much flexibility
in the joint

Name: _____

Date: _____

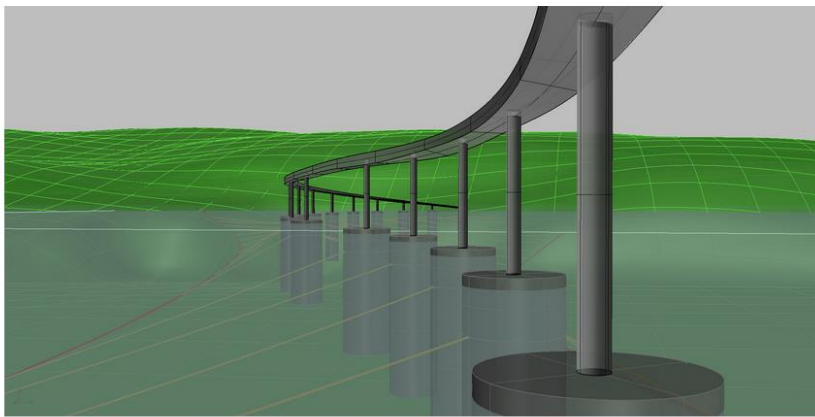
Page: _____

Rev: _____

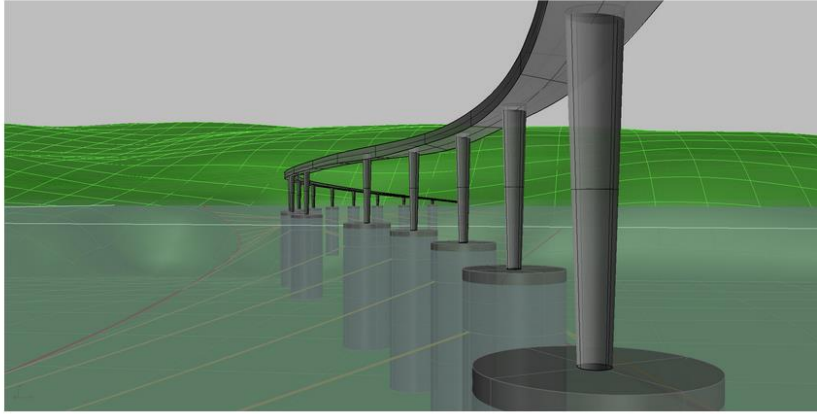
ANNEX EE: IDEA EXCHANGE WITH ARCHITECTS - SUPERSTRUCTURE

Close cooperation with the architecture firm Zwarts & Jansma lead to a structurally and aesthetically competitive bridge concept.

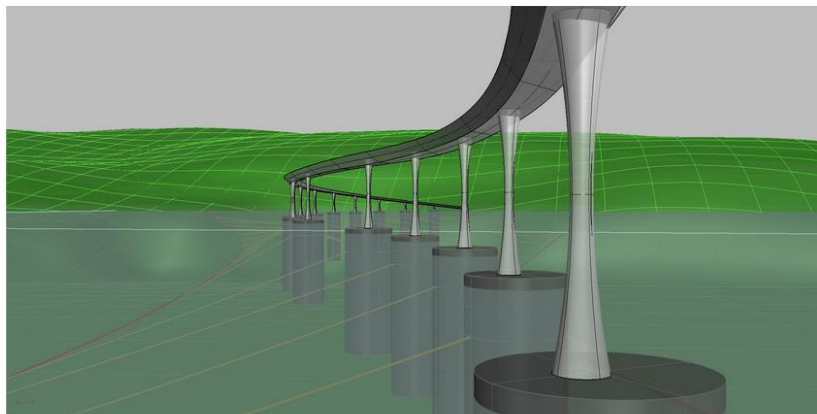
To develop a competitive concept, there was a continual exchange of ideas with the architects. In this annex, the idea exchange about the superstructure is shown.



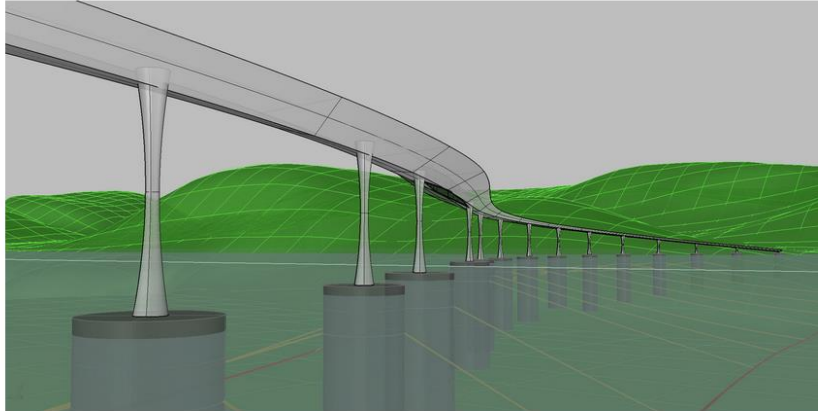
SOGNEFJORD BUOYANCY BRIDGE



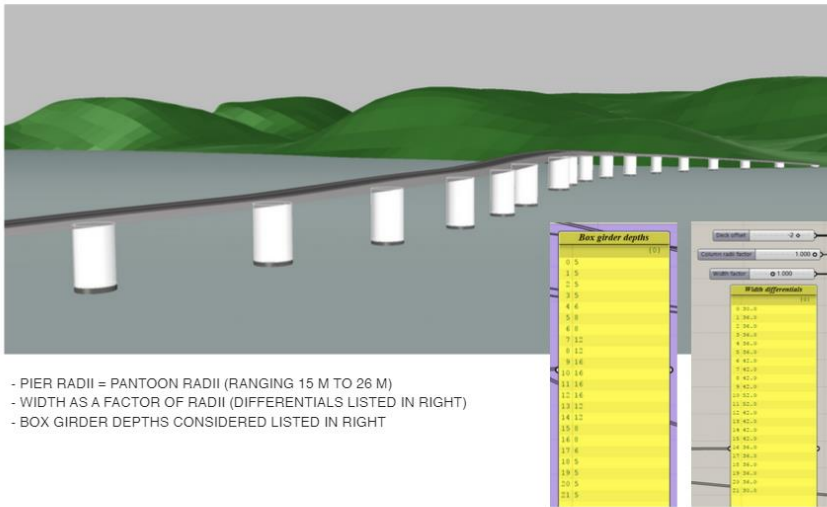
SOGNEFJORD BUOYANCY BRIDGE



SOGNEFJORD BUOYANCY BRIDGE



01 BOX GIRDER

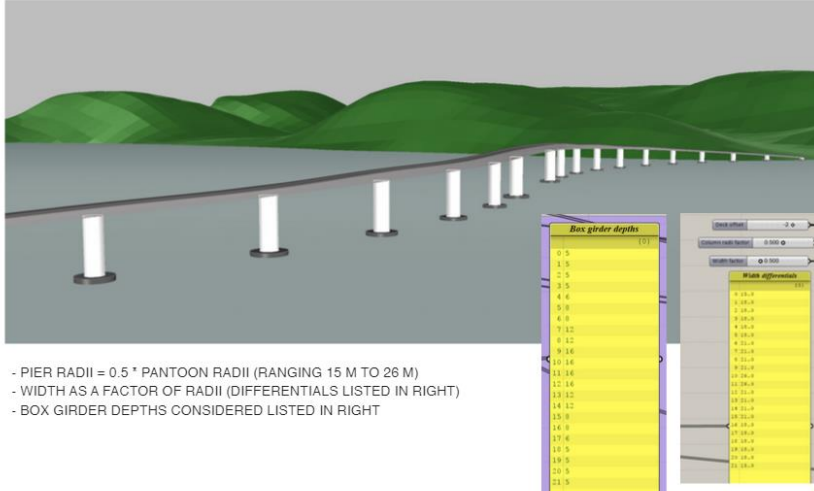


- PIER RADII = PANTOON RADII (RANGING 15 M TO 26 M)
- WIDTH AS A FACTOR OF RADII (DIFFERENTIALS LISTED IN RIGHT)
- BOX GIRDER DEPTHS CONSIDERED LISTED IN RIGHT

Box girder depths	Pier differentials
0.5	10.70
1.5	12.34
2.5	13.98
3.5	15.62
4.4	16.26
5.8	17.90
6.8	19.54
7.12	20.18
8.12	21.82
9.16	22.46
10.16	24.10
11.18	24.74
12.16	26.38
13.12	27.02
14.12	28.66
15.8	29.30
16.8	30.94
17.4	31.58
18.8	33.22
19.5	33.86
20.5	35.50
21.5	36.14

SOGNEFJORD BUOYANCY BRIDGE

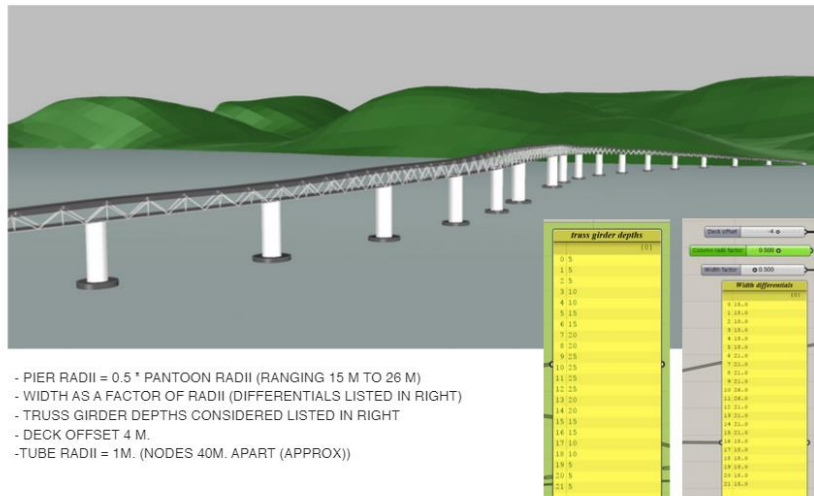
01 BOX GIRDER



- PIER RADII = 0.5 * PANTOON RADII (RANGING 15 M TO 26 M)
- WIDTH AS A FACTOR OF RADII (DIFFERENTIALS LISTED IN RIGHT)
- BOX GIRDER DEPTHS CONSIDERED LISTED IN RIGHT

SOGNEFJORD BUOYANCY BRIDGE

02 TRUSS GIRDER



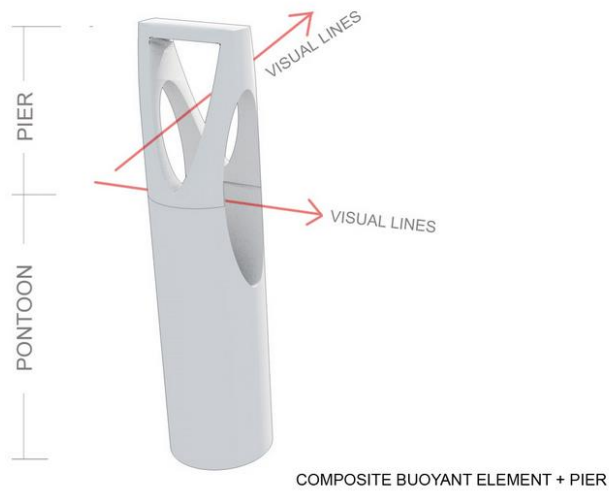
- PIER RADII = 0.5 * PANTOON RADII (RANGING 15 M TO 26 M)
- WIDTH AS A FACTOR OF RADII (DIFFERENTIALS LISTED IN RIGHT)
- TRUSS GIRDER DEPTHS CONSIDERED LISTED IN RIGHT
- DECK OFFSET 4 M.
- TUBE RADII = 1M. (NODES 40M. APART (APPROX))

SOGNEFJORD BUOYANCY BRIDGE

02 TRUSS GIRDER



01 Elliptical boolean Pier+Ponton geometry

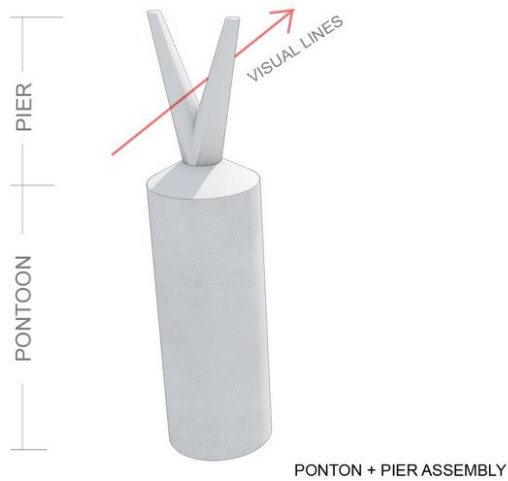


01 Elliptical boolean Pier+Ponton geometry

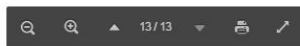


SOGNEFJORD BUOYANCY BRIDGE

02 Branching boolean Pier geometry

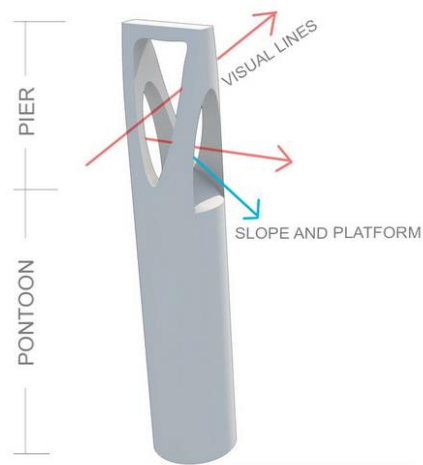


02 Branching boolean Pier geometry



SOGNEFJORD BUOYANCY BRIDGE

01 Elliptical boolean Pier+Ponton geometry V2.0



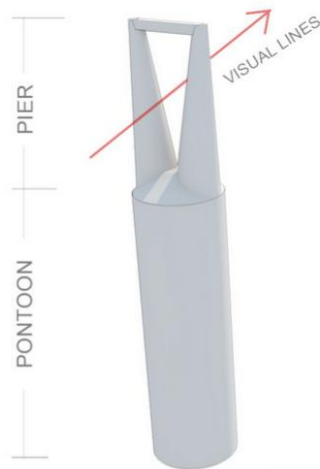
COMPOSITE ELEMENT v2.0 (WITH SLOPE)

01 Elliptical boolean Pier+Ponton geometry V2.0



SOGNEFJORD BUOYANCY BRIDGE

02 Branching boolean Pier geometry V2.0

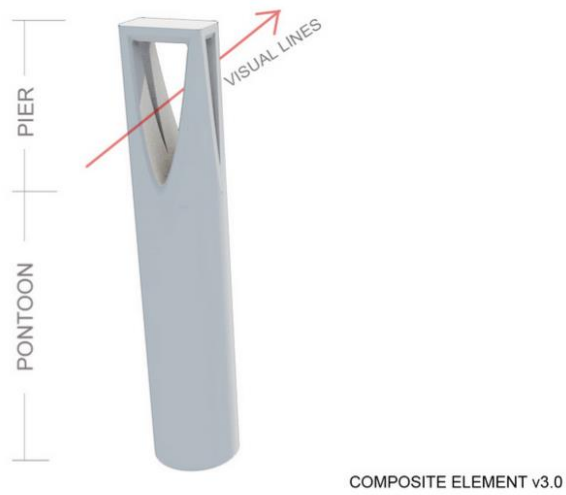


PONTON + PIER ASSEMBLY v2.0

02 Branching boolean Pier geometry V2.0



01 Elliptical boolean Pier+Pontoon geometry V3.0

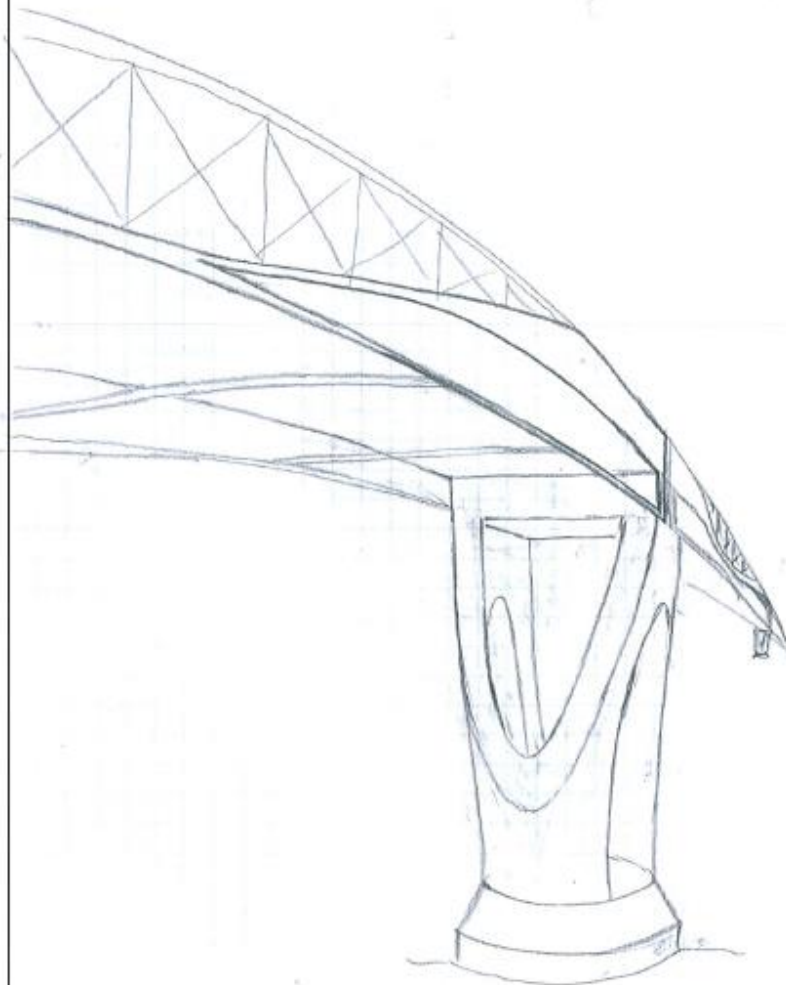


01 Elliptical boolean Pier+Ponton geometry V3.0



SOGNEFJORD BUOYANCY BRIDGE

Project : Buoyancy Bridge Sognefjord
Part : Suggestion for pylons



Name: Christine Yip

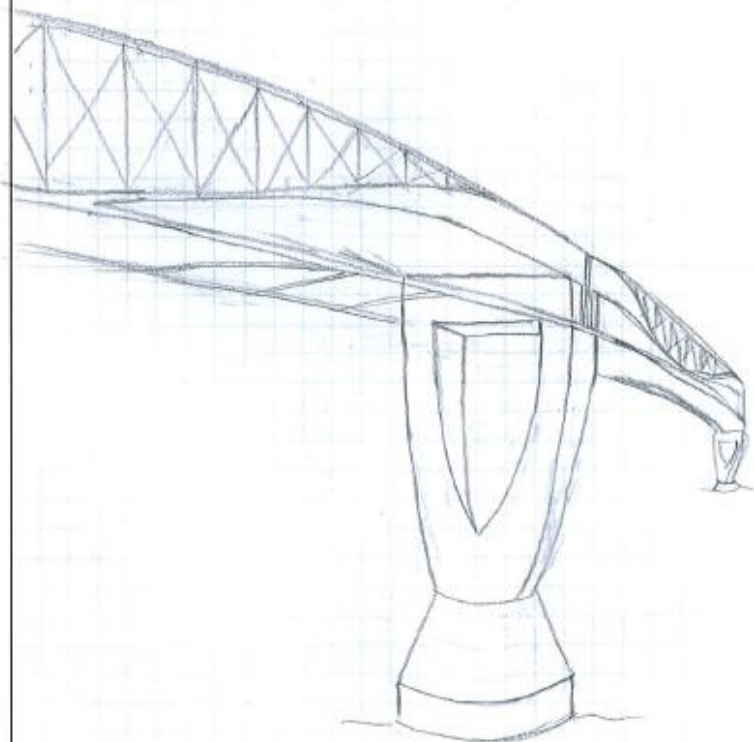
Date: 3-6-2015

Page: 1/2

Rev:

Project : Buoyancy Bridge Sognefjord

Part : Suggestions for pylons

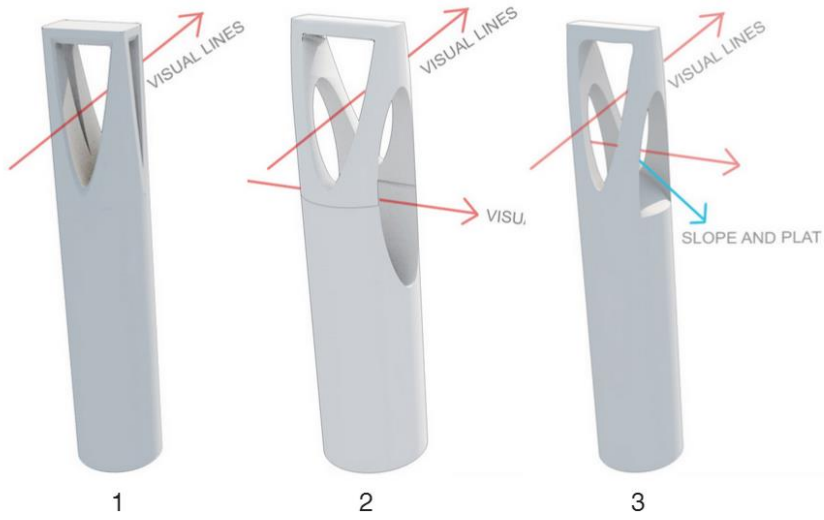


Name: Christine Yip

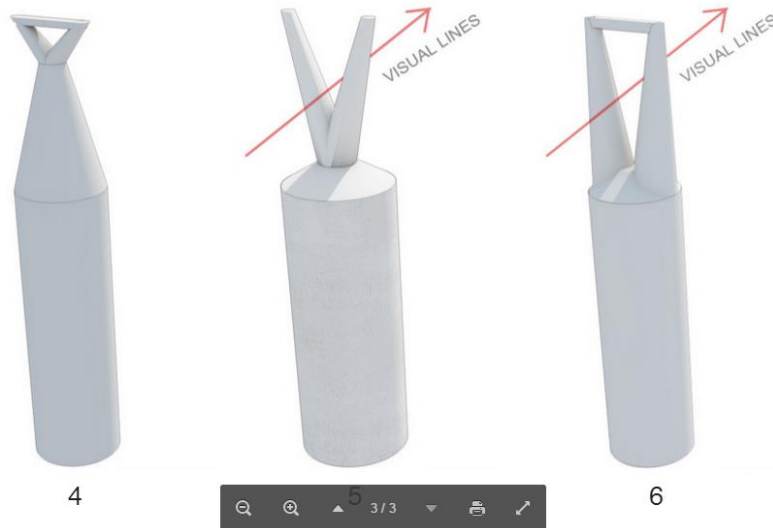
Date: 3-6-2015 Page: 2/2

Rev:

SOGNEFJORD BUOYANCY BRIDGE - CONICAL ELLIPSE VARIANTS

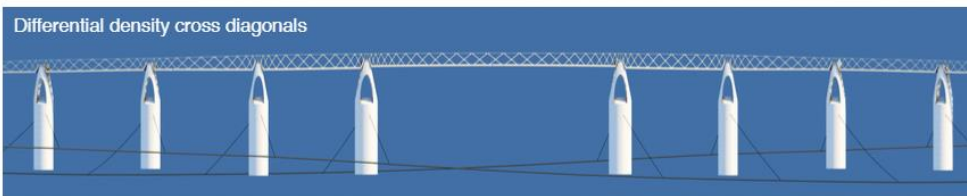


SOGNEFJORD BUOYANCY BRIDGE - BRANCHING VARIANTS



ANNEX FF: SKETCHES FINAL PROPOSED SUPERSTRUCTURE

01 New Axial-supported girder | differential cross diagonals
GIRDER GEOMETRY



SOGNEFJORD BUOYANCY BRIDGE

01 New Axial-supported girder | differential cross diagonals



SOGNEFJORD BUOYANCY BRIDGE

01 New Axial-supported girder | differential cross diagonals
GIRDER GEOMETRY (without deck)



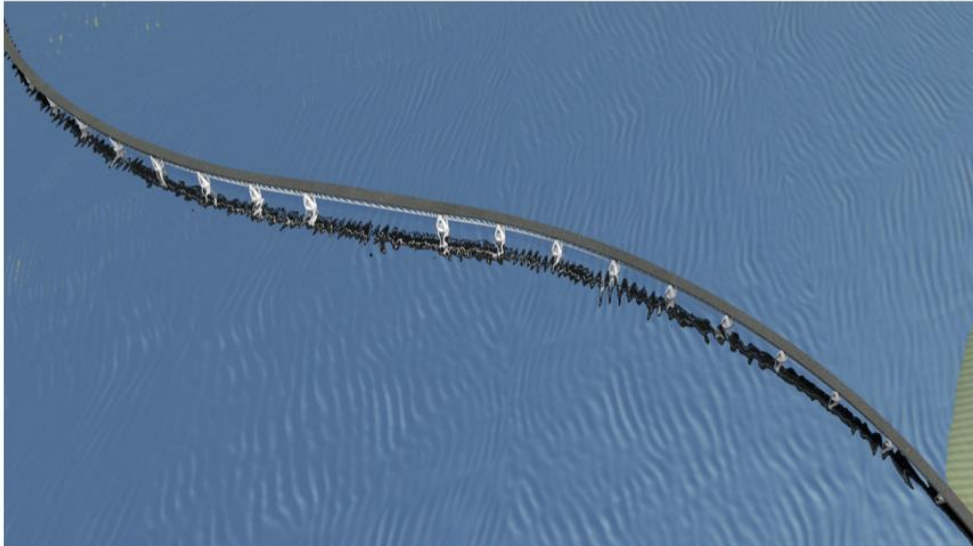
SOGNEFJORD BUOYANCY BRIDGE

01 New Axial-supported girder | differential cross diagonals

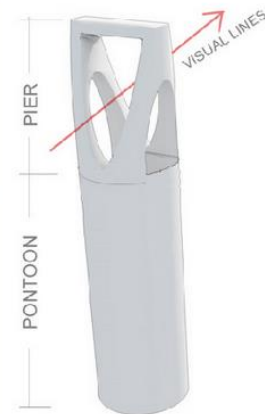


SOGNEFJORD BUOYANCY BRIDGE

01 New Axial-supported girder | differential cross diagonals



SOGNEFJORD BUOYANCY BRIDGE



ANNEX GG: MODELING THE FINAL SUPERSTRUCTURE IN SCIA ENGINEER

After it was decided to use lattice girders for the superstructure, all the members in the girder are designed and checked for their strength and stability. This is done by modeling a girder in Scia Engineer. The modeling and results are shown in this section.

GG.1 Lattice Girder at Main Span Governing

The superstructure consists of 23 lattice girders and 22 piers. No checks will be done for the piers in this study (see chapter 7.8 for explanation). The governing girder is the one in the middle of the fjord, at the main span of 465 meters. It is assumed, that in case a lattice girder can be designed for the main span, then solutions can also be found for the others spans of 200 meters. Therefore, during the modeling, only the lattice structure at the main span is modeled and checked.

GG.2 Input

GG.2.1 Global Dimensions of Lattice Girder

In Figure GG-1, it can be seen that the girder height is 25 meters and the width of the lattice girder is 24 meters at the main span. The span between the piers is 465 meters. However, the lattice girders are supported eccentrically on the pontoons (see Figure GG-1). Therefore, the total length of the lattice girder becomes 460 meters.

Comments

In case in later design phases the design of the support changes, then the length of the lattice girder should be adjusted. This adjustment will however be small compared to the total length, therefore, the assumption of a length of 460 meters is considered sufficient for this feasibility study.

The lattice structure consists mainly of four main circular hollow sections, vertical diagonals, horizontal members and horizontal diagonals. The vertical diagonals in the lattice girder are placed denser at the ends; this can also be seen in Figure GG-2. The distances between the vertical diagonals are shown in Figure GG-3.

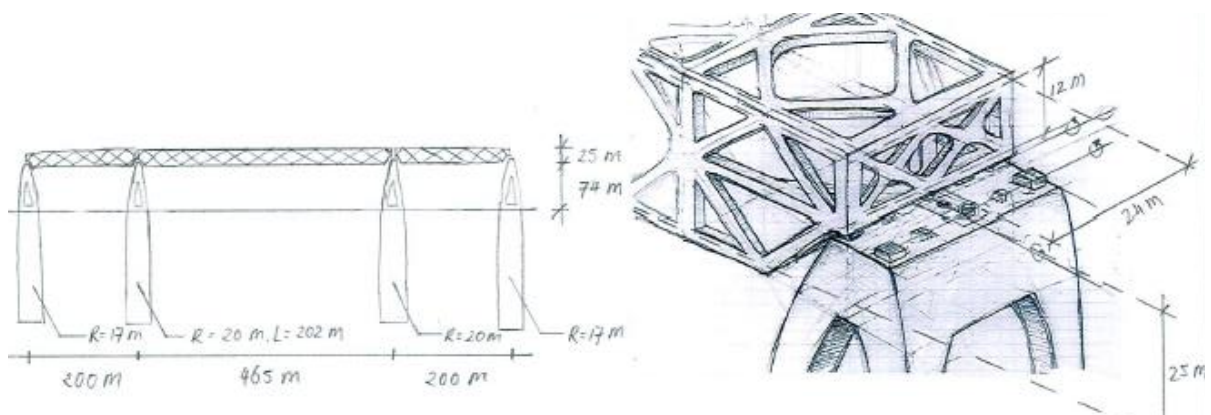


FIGURE GG-1 GLOBAL DIMENSIONS OF THE LATTICE GIRDER

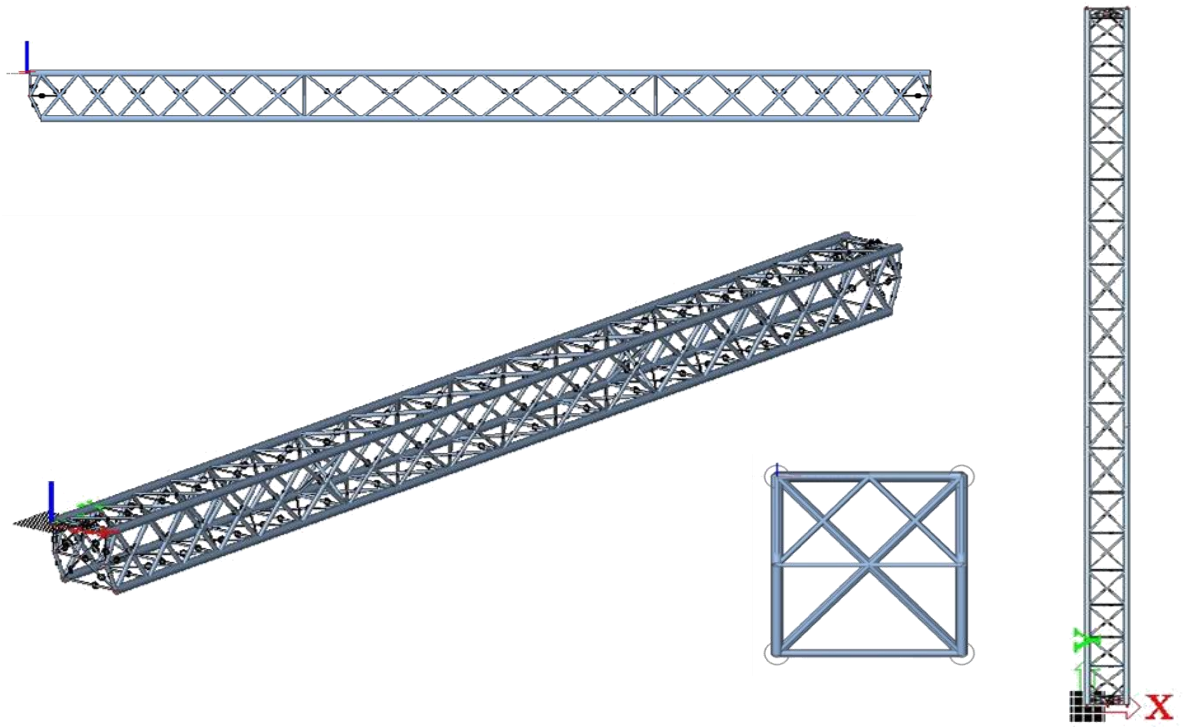


FIGURE GG-2 LAYOUT LATTIC STRUCTURE

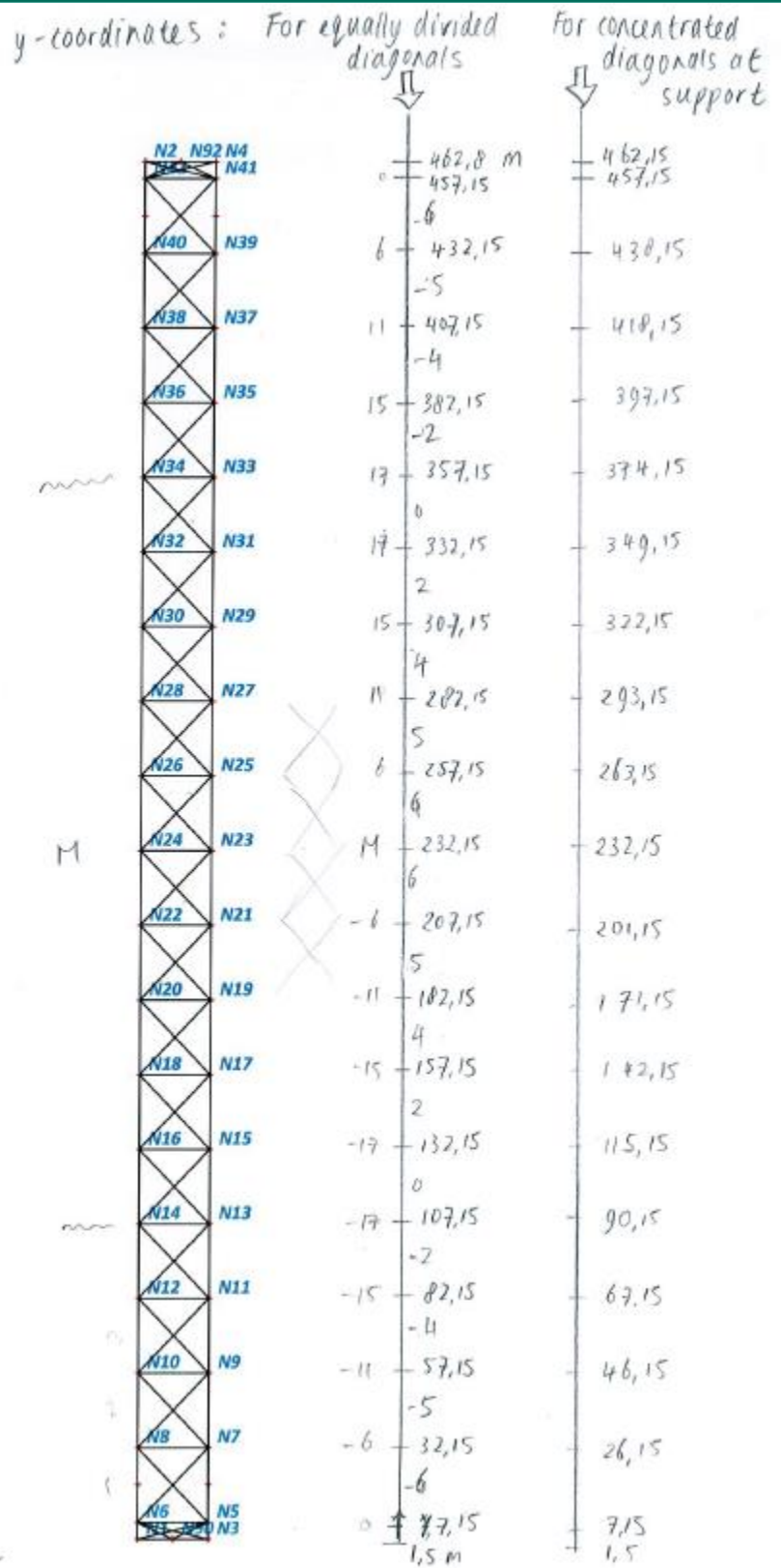


FIGURE GG-3 DISTANCES BETWEEN THE VERTICAL DIAGONALS [M]

GG.2.2 Varying Torsional Rigidity

The torsional rigidity of the girder is not constant. As can be seen in Figure GG-4, the girder parts near the supports are torsional flexible and in the middle, the girder is torsional rigid. This is due to the omitting the bottom horizontal diagonals at the ends of the girder. This can be seen in Figure GG-5, where the main girders and vertical diagonals are hidden to show the horizontal diagonals more clearly. By leaving out the horizontal diagonals at the ends of the girder, the girder section will become an open section with small torsional rigidity, in contrast to closed sections.

This girder is proposed instead of a conventional lattice girder with constant torsional rigidity along its length, because the purpose was to develop a flexible and lightweight bridge structure, which is able to follow the movements due to external loads. A rigid structure would lead to a large, robust and heavy structure, which is not desired for the buoyancy bridge.

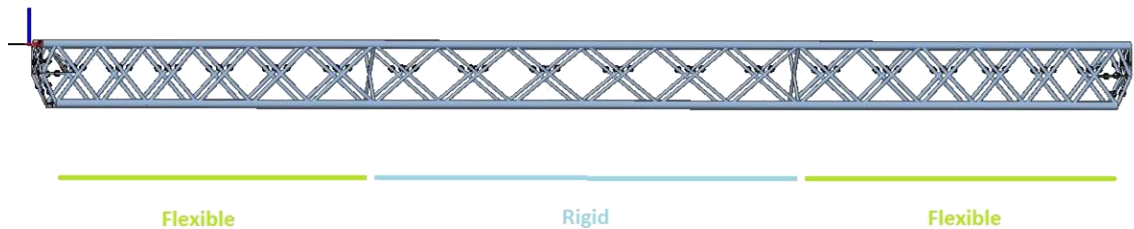


FIGURE GG-4 VARYING TORSIONAL RIGIDITY IN THE GIRDER

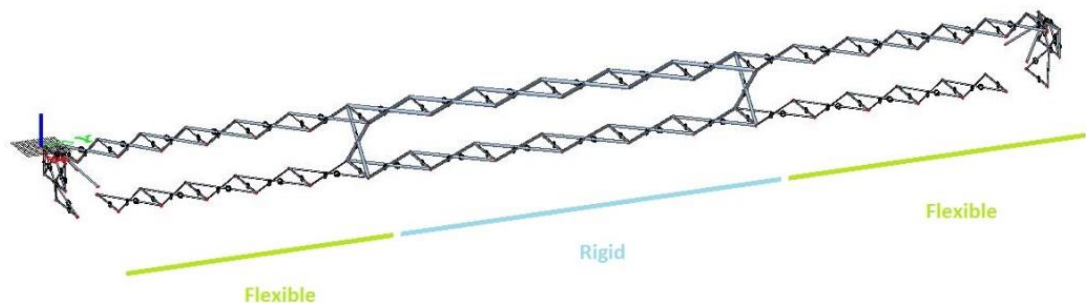


FIGURE GG-5 BOTTOM HORIZONTAL DIAGONALS AT THE ENDS ARE OMITTED TO CREATE MORE TORSIONAL FLEXIBILITY

GG.2.3 Material: High Strength Steel S460

High Strength Steel S460 is used for all members in the lattice structure. Grade S460 is chosen instead of the more regular S235 grade steel to obtain a more favorable strength-self-weight ratio for the superstructure of the buoyancy bridge.

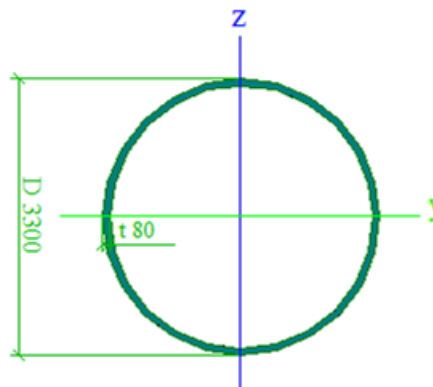
For further studies, the use of even higher strength steel grades can be investigated, for example steel grade S690.

GG.2.4 Member Dimensions

The dimensions of the circular hollow section (CHS) members are first estimated by making rough hand calculations. The dimension of the four main girders is obtained by calculating the required section to resist the global bending moment in the lattice structure. The dimensions of all other members are obtained by calculating the required slenderness ratio i to resist buckling. After these estimations were inputted into the Scia Model, the stresses in the members were reviewed and adjusted until there was sufficient capacity.

The final diameter of the four main girders is 3300 mm and the thickness is 80 mm. Hereafter, the vertical diagonals near the supports are the second largest members, the diameter is 1600 mm and the thickness is 32 mm. For an indication of the size of the other members, see the data from Scia Engineer in Figure GG-6.

Name	main girder
Type	Tube
Detailed	3300; 80
Parameters	
Material	S 460 N/NL
D [mm]	3300
t [mm]	80



vertical diagonals in longitudinal plane - Tube (1300; 26)
vertical diagonals in longitudinal plane 2 - Tube (1600; 32)
horizontal diagonals top support - Tube (1000; 20)
horizontal diagonals top middle - Tube (1500; 30)
horizontal diagonals bottom middle - Tube (1100; 22)
horizontal diagonals bottom support. 2 diag near center - Tube (500; 10)
horizontal diagonals bottom support 3 diag near support - Tube (500; 10)
vertical diagonals in transversal plane size 2 - Tube (1300; 26)
trans girder top middle - Tube (300; 6)
trans girder top center few - Tube (700; 14)
trans girder bottom middle - Tube (1000; 20)
trans girder bottom near support - Tube (700; 14)
trans girder top end - Tube (600; 12)
upright girder - Tube (150; 3)
support tubes top diag - Tube (600; 12)
support tubes horizontal - Tube (300; 6)
support tubes vertical - Tube (600; 12)
support tubes bottom diag - Tube (600; 12)
support tubes horizontal middle - Tube (600; 12)
support tubes vert+angle bottom - Tube (1400; 28)
support diagonals for 150 - Tube (800; 16)

FIGURE GG-6 DIMENSIONS FROM SCIA ENGINEER (DIAMETER; THICKNESS) IN [MM]

GG.2.5 Supports

In Figure GG-7, the modeled supports in Scia Engineer can be seen.

The degrees of freedom are shown below.

For S1 and S3:

$$\begin{array}{ll} u_x = \textit{free} & \varphi_x = \textit{free} \\ u_y = \textit{free} & \varphi_y = \textit{free} \\ u_z = \textit{rigid} & \varphi_z = \textit{free} \end{array}$$

For S2:

$$\begin{array}{ll} u_x = \textit{rigid} & \varphi_x = \textit{free} \\ u_y = \textit{rigid} & \varphi_y = \textit{free} \\ u_z = \textit{free} & \varphi_z = \textit{free} \end{array}$$

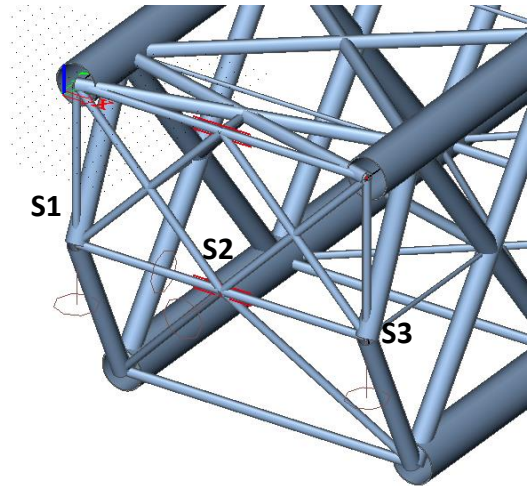


FIGURE GG-7 MODELED SUPPORTS

GG.2.6 Loads

In ANNEX U: Load Cases, the load cases are shown which are considered in this study. The lattice girder is subjected to these load cases as well. In these load cases, the following loads occur, which are applied on the superstructure:

Self-weight – the total self-weight of the lattice structure. The self-weight of the modeled members in Figure GG-2 are taken into account. Furthermore, for the self-weight of the bridge deck (which is not modeled), the deck finishing and the connections, 20 kN/m is taken into account.

Traffic load – a traffic load of 35 kN/m.

Wind load – the wind load in x-direction is estimated to be 19,2 kN/m. The wind load in y-direction is 11,7 kN/m.

Axial load – beside the loads above, the lattice girder is also subjected to an axial load. The axial load is obtained from the Scia Engineer results of the global model of the bridge sub- and superstructure. Due to the external loads and self-weight acting on the bridge, axial loads are present in the bridge girders. This axial load differs for every load case, see Table GG-1.

TABLE GG-1 AXIAL LOADS IN BRIDGE GIRDER

Load case	Axial load (kN)
1	0
2	354
3	689
5	900
6	215
7	900
8	422

Torsion – besides axial loads, also torsion occurs in all load cases. Due to the loads, the pontoons and bridge piers rotate. This causes torsion in the bridge girders. In this modeling, the bridge girder is subjected to a rotation at one end which causes torsion. The angles are given in Table GG-2. These values are obtained from the Scia Engineer results of the global model of the whole bridge structure (substructure and superstructure), in which the bridge was subjected to the loads.

**TABLE GG-2 RELATIVE ROTATION
BETWEEN PONTOONS**

Load case	Rotation (°)
1	~0
2	~0
3	0,433
5	1,050
6	~0
7	5,26
8	~0

Temperature – to get a sense of the influence of temperature change, the lattice structure is subjected to a temperature load of 20° C

Comments

The axial loads are small compared to the other loads. For example, the largest axial load is 900 kN, while the tension in the main girder due to self-weight is already around 200 000 kN. The axial loads are small, because of the chosen erection method, which is described in 3.4.2. Here it is described, that the superstructure is placed on top of the pontoons *after* the substructure is subjected to its self-weight. The weight of the substructure is 91% of the total weight (see Table 5-1). Therefore, by placing the superstructure on top of the substructure after the substructure is already displaced due to its self-weight, then, the effects on the superstructure will be minimized.

However, if the erection method changes in further design stages, then the axial loads in the bridge girders might increase. Subsequently, the capacity of the lattice structure should be checked again.

The self-weight of the bridge deck, finishing and connections is assumed to be 20 kN/m. If in further design stages these weights prove to be larger, then the capacity of the structure should be checked again while taking into account the new self-weights.

The assumed wind load above is an approximation for a certain lattice structure. After it is proven that this bridge concept is feasible and it is decided on the final design of the superstructure, then the accurate wind load can be calculated, while taking into account the shape of the superstructure. For instance, in case rectangular hollow sections will be used instead of circular hollow sections, then the wind load will increase.

GG.3 Results

GG.3.1 Unity Checks

Strength

The unity checks for strength are shown in Table GG-3. For these checks, load factor 1,2 is used for permanent loads and load factor 1,5 is used for variable loads. To see which loads are included in each load case, see ANNEX U: Load Cases.

As can be seen in the table, the largest unity check occurs for the load case with the hurricane. At this extreme situation, the unity check is 0,91. Hereafter, load case 3 is the largest with an unity check of 0,86.

In Figure GG-8, the stresses in the bridge girder due to self-weight are shown.

TABLE GG-3 STRENGTH UNITY CHECKS

Load case	UC (-)	Member	Stress (N/mm ²)
1 : Self-weight only	0,74	bottom main girder	287
2 : Maximum displacements in x-direction	0,85	bottom main girder	369
3 : Asymmetric water load	0,86	bottom main girder	370
5 : Maximum displacements in y-direction	0,82	bottom main girder	319
6 : Self-weight and traffic load	0,82	bottom main girder	319
7 : Hurricane	0,91	bottom main girder	363
8 : Self-weight, traffic load and temperature load	0,83	bottom main girder	322

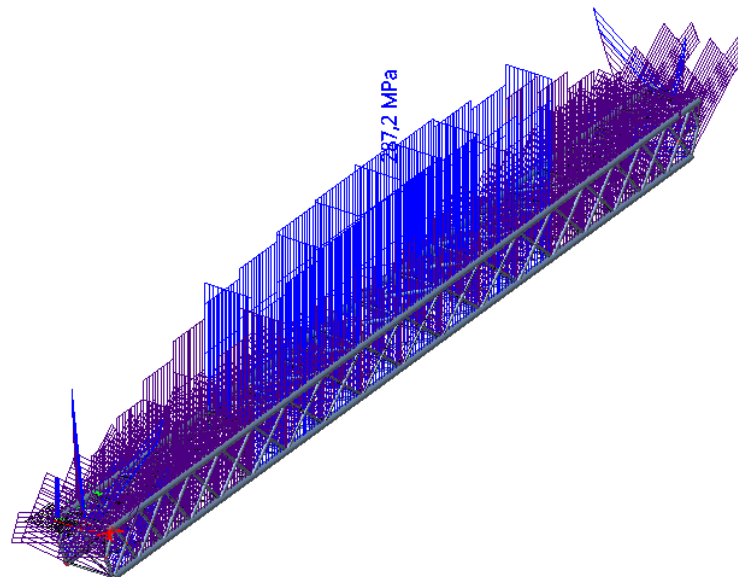


FIGURE GG-8 STRESSES IN THE BRIDGE GIRDER DUE TO LOAD CASE 1

Stability

The unity checks for stability are shown in Table GG-4. For these checks, also load factor 1,2 is used for permanent loads and load factor 1,5 is used for variable loads. The load cases are explained in ANNEX U: Load Cases.

As can be seen in the table, the largest unity check occurs again for the load case with the hurricane. At this extreme situation, the unity check is 0,91. Hereafter, load case 3 and 4 are the largest with unity check of 0,90.

In Figure GG-8, the stresses in the bridge girder due to self-weight are shown.

TABLE GG-4 STABILITY UNITY CHECKS

Load case	UC (-)	Member
1 : Self-weight only	0,69	bottom lateral girder at main span
2 : Maximum displacements in x-direction	0,90	top main girder
3 : Asymmetric water load	0,90	top main girder
5 : Maximum displacements in y-direction	0,79	vertical diagonal near midspan
6 : Self-weight and traffic load	0,77	bottom lateral girder at main span
7 : Hurricane	0,91	top horizontal diagonal near midspan
8 : Self-weight, traffic load and temperature load	0,77	bottom lateral girder at main span

Comments

The unity checks for strength and stability are both the largest for the extreme load case, in which a hurricane occurs. The unity check is then 0,91.

However, it should be noted that very favorable load factors are used ($\gamma_G = 1,2$ and $\gamma_Q = 1,5$). According to the Eurocode, bridges belong to consequence class 3. The load factors should then even be multiplied with 1,1. Therefore, the unity checks will be larger in case the correct load factors are used.

When regarding the strength capacity, in every load case, the capacity of the bottom main girder is governing. In further studies, higher strength steel can be considered for the bottom main girder. Then, the unity checks for the strength capacities will be lower.

When regarding the stability, the second largest unity check after load case 7 with the hurricane is for load cases 2 and 3. In both cases, the top main girder is governing. In reality, this unity check may be lower. In this model, the bridge deck is not modeled. However, the bridge deck can have a beneficent effect on the stability of the top main girders, if these are connected to the bridge deck. This can be taken into account in further stages, when more detailed and accurate modeling will be done.

In case in future, more accurate modeling, the unity checks for strength appear to be larger than the unity checks for stability, then the use of high strength steel can be considered for the whole structure. (This is only applicable in case the displacements are not governing.) The use of high strength steel will require less material for the structure, i.e. smaller self-weight, which in turn results in smaller required strength capacity of the structure to carry its own self-weight. Then a lighter and more efficient superstructure will be possible.

These checks should also be done again in later design phases when the self-weight of the bridge deck, finishing and connections are known. For now, 20 kN/m is assumed. In case the self-weight proves to be larger, then the strength and stability should be checked again.

It is also important to note that only first order checks are done in this feasibility study. For further design stages second order effects, eccentricity, etc. should be checked as well. Also, the strength and stability checks are only done for the members in the lattice structure. The connections between the members are not checked.

GG.3.2 Displacements

Vertical Deflection

Due to the total self-weight (load case 1) the maximum displacement is **2617 mm** at midspan, as can be seen in Figure GG-9. In this study, it will be assumed that the lattice girder will be precambered by 2617 mm. This way, the bridge girder will be straight after being loaded due to its own self-weight. This is also desired for the aesthetics.

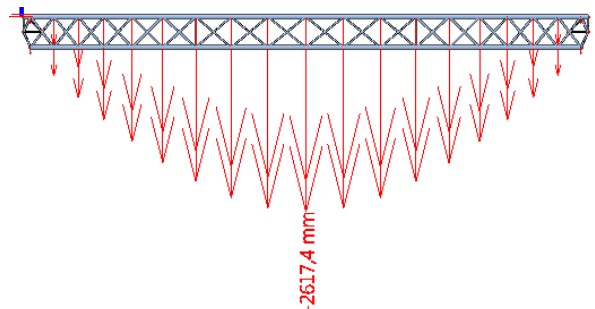


FIGURE GG-9 VERTICAL DISPLACEMENTS DUE TO SELF-WEIGHT

Comments

No calculations or checks are done in this study for the precambering. This should be done in later design phases, as precambering might influence the stresses in the members.

When the structure is also subjected to external loads, the displacements are the largest for load case 3 (see ANNEX U: Load Cases for explanation about the load cases). The total displacement due to self-weight and loads is **3395 mm** in load case 3. If it is assumed that a precambering of 2617 mm is used, then the deflection at midspan will be $(3395 - 2617 =) \mathbf{778 \text{ mm}}$.

The limit for vertical deflection is $L/350 = \mathbf{1329 \text{ mm}}$ (see Table 2-7). This means that the requirement for vertical deflection is met.

Horizontal Deflection

Horizontally, there are almost no displacements due to self-weight. Therefore, no horizontal precambering is needed.

The largest horizontal displacement occurs also for load case 3. At the bottom main members, the largest displacement occurs near the ends of the lattice girder, instead of at midspan (which is more common). The exaggerated deformed structure can be seen in Figure GG-10. Near the supports, the displacement is **1749 mm**. However, the deflection limit is for the serviceability, for the cars on the freeway at the top of the lattice girder. The largest deformation at the bridge deck level is **712 mm** at midspan (load case 2). This is smaller than the deflection limit (1329 mm).

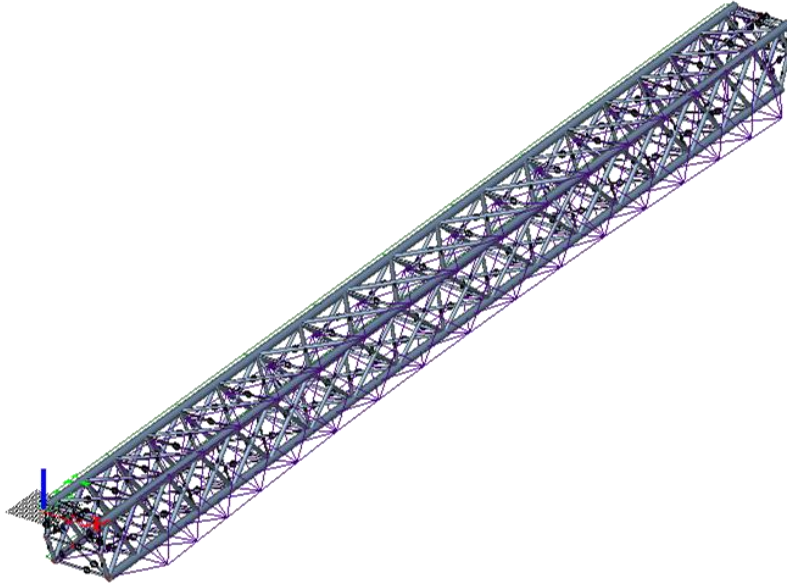


FIGURE GG-10 DEFORMED STRUCTURE DUE TO LOAD CASE 3

Rotations

Rotation in the bridge girder mainly occurs due to rotation of the pontoons. The maximum rotation that occur during the considered load cases are applied in the model. The purpose was to apply the rotations and to design a superstructure, which has to capacity to follow these rotations. The applied rotations are within the serviceability limits. (This is logical, since the substructure was designed in such a way that the rotations would be within the limits).

GG.3.3 Total Self-Weight of Lattice Structure

The total self-weight of all the members in the lattice structure is 158 565 kN. This is approximately 341 kN/m.

GG.4 Conclusion and Evaluation

Results of this preliminary study show that this lattice girder for the buoyancy bridge has sufficient capacity regarding strength and stability. Also the deformations are within limits. These results should be interpreted as an encouragement for further investigation and development of the concept. This is because of the fact that more effects should be investigated before this structure can be deemed reliable. Important effects to investigate in next studies are:

- second order effects
- eccentricity
- design of connections
- fatigue
- self-weight check of bridge deck, finishing and connections (Is it the same as assumed self-weight or larger?)

- unity checks by using the correct load factors according to the Norwegian codes
- investigate the consequences of precambering the girder 2617 mm
- once it is decided on the final layout of the superstructure, the wind load should be determined more accurately (adjust drag coefficients)
- the erection method of the buoyancy bridge influences the axial loads in the superstructure. Check whether these results are still reliable, in case it is decided on a different erection method than was assumed in this study.

The displacements are not governing for the design. Furthermore, by also taking into account the bridge deck (which was not modeled), the resistance against buckling of the members at the top of the lattice girder will increase and stability will also not be governing for the design. Then using higher strength steel can be a good option to make the lattice girder lighter and more efficient.

So topics for further investigation to optimize the design are:

- take into account the contribution of the bridge deck against buckling
- consider high strength steel

It can be concluded from this study, that the proposed concept is promising and it is recommended to further investigate and develop this concept.